N72-31810-56

NASA SP-310

THE SCIENTIFIC RESULTS FROM THE ORBITING ASTRONOMICAL OBSERVATORY (OAO-2)

CASE FILE COPY

A symposium held at
AMHERST, MASSACHUSETTS
August 23-24, 1971

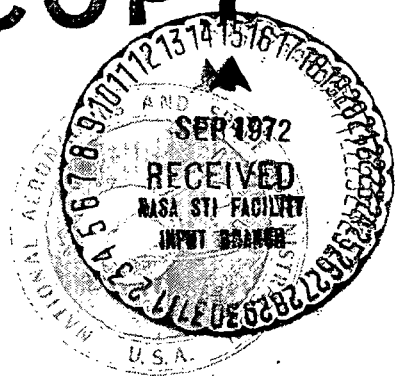

NATIONAL AERONAUTICS AND SPACE ADMINISTRATION

NASA SP-310

THE SCIENTIFIC RESULTS FROM THE ORBITING ASTRONOMICAL OBSERVATORY (OAO-2)

Edited by

ARTHUR D. CODE

Proceedings of a symposium
sponsored by the
National Aeronautics and Space Administration
and the American Astronomical Society
held in Amherst, Massachusetts
August 23–24, 1971

Scientific and Technical Information Office 1972
NATIONAL AERONAUTICS AND SPACE ADMINISTRATION
Washington, D.C.

For sale by the National Technical Information Service
Springfield, Virginia 22151
Price $6.00
Library of Congress Catalog Card Number 72-600185

FOREWORD

In the 1950's, as plans were being made for project Vanguard, Dr. Lloyd Berkner sent a telegram to a number of scientists asking for expressions of interest in the scientific use of small satellites. Four of those responses, from Drs. Code, Goldberg, Spitzer and Whipple suggested astronomical experiments, but each required a heavier satellite than that planned for Project Vanguard. Except for some work at Princeton University supported by the Air Force, little was done until the formation of the National Aeronautics and Space Administration (NASA) late in 1958. At that time, astronomy appeared likely to benefit greatly from the possibility of making observations from above the atmosphere and, early in 1959, the four people who had responded to Dr. Berkner's message with the suggestion of an astronomical satellite were invited to meet with NASA to discuss the possibilities further.

It was apparent immediately that almost any astronomical satellite would require a rather sophisticated stabilization system, the development of which would represent a significant advance in the then current state of the art. Hence, it was decided that it was preferable to develop a single spacecraft which would accommodate each of the instruments in turn, rather than design a separate spacecraft instrument for each type of instrument. In early 1959, NASA was planning to develop a Vega rocket which would have a diameter of ten feet and would comfortably accommodate a one-meter astronomical telescope in its spacecraft. Hence, the original planning was based on these sizes. It became apparent early in the studies that the thermal problems for a solar payload were so different from those for stellar instruments that it would be difficult, although not impossible, to use the same spacecraft design. Therefore, a separate series of satellites was designed for solar observations.

The remaining three experiments plus a three-meter telescope proposed by Dr. Kupperien of the Goddard Space Flight Center (although the center had still not been named at the time) were planned for a series of Orbiting Astronomical Observatories (OAO). Since the instruments proposed by Dr. Code and those proposed by Dr. Whipple were small, it was decided that several of each could fit in the same spacecraft with Dr. Code's and Dr. Whipple's viewing from opposite ends of the satellite. These instruments, planned for the first of the OAO series, are those which finally flew on OAO-2 in December 1968 and are the means for the observations reported in this compendium.

The cancelling of the Vega rocket and the subsequent need to adapt the spacecraft to the Atlas were only the first of many problems which the project had to overcome. The development of the star trackers needed to point the instruments was a source of

worry until they proved themselves in orbit; in general, the accurate stabilization of a large spacecraft proved much more difficult than anyone had conceived ten years before the launch of OAO-2.

The performance of this satellite has completely vindicated the early planners and has rewarded not only Drs. Code and Whipple but the entire astronomical community with many exciting new discoveries and much important data to aid in the unravelling of the secrets of the stars. The papers which follow are ample evidence of the value of such a satellite for astronomy.

Nancy G. Roman
Chief of Astronomy
Physics and Astronomy

PREFACE

This volume contains the texts of the papers presented at the first symposium on "The Scientific Results from the Orbiting Astronomical Observatory," held in Amherst, Massachusetts on August 23 and 24, 1971. This symposium was co-sponsored by the American Astronomical Society and the National Aeronautics and Space Administration.

During the two-day session, 41 papers were presented by 52 authors from 22 different institutions. In view of the diversity of topics covered, the symposium was organized around four sessions. The first session, on Solar System Studies, was chaired by Dr. William Irvine; Dr. Donald Osterbrock chaired the second session on Interstellar Matter; Dr. George Herbig chaired session three on Stellar Observations; and the final session, on Galactic and Extragalactic Systems, was chaired by Dr. Hugh Johnson. The symposium was concluded by a summary of the scientific highlights by Dr. Lyman Spitzer.

Initially we had planned to include a session on the Spacecraft and Experiment performance and operation. As the program developed it became clear that a two-day symposium did not provide enough time to include all of the papers proposed. It was therefore decided to defer the instrumentation description and concentrate on the results from the scientific data analysis. Since the Orbiting Astronomical Observatory is a unique national facility, it was felt that the published volume should contain the engineering and operation descriptions that were not included during the symposium presentations. The first section of this volume, therefore, provides this background against which the scientific discussions following can be more fully understood and appreciated.

The scientific papers were based upon observational data provided by the Smithsonian Astrophysical Observatory's Celescope experiment and by the University of Wisconsin's spectrophotometric instrumentation. The observations have been carried out primarily by personnel from the Smithsonian Astrophysical Observatory, the University of Wisconsin and the Goddard Space Flight Center, and have been ably supported by the OAO project staff under the direction of Mr. Joseph Purcell. Many astronomers from outside these institutions have participated either through the NASA Guest Investigator Program or through less formal channels. It is this wider participation that makes OAO-2 a National Observatory of unique proportions.

The symposium presented many new observations, discoveries and ideas. It also posed new problems and evoked controversy and debate. This, I believe, made OAO more real to the participants. It was clear that the reduction and analysis of the high quality data is a subtle affair, and despite the automation, require all the care and judgment that have been traditional in ground-based astronomy.

I wish to express my appreciation to the participants of this symposium for their cooperation and the general excellence of their presentations. The task of preparing this publication has been lightened by the able assistance of Dr. Blair Savage and Dr. Robert Bless. I am particularly grateful to Mrs. Helen Hay who has typed, edited and assembled the papers with care and competence.

Arthur D. Code
University of Wisconsin
Madison, Wisconsin

CONTENTS

SPACECRAFT AND OPERATIONS PAGE

Ultraviolet Television Data from the Orbiting Astronomical Observatory. I. Instrumentation and Analysis Techniques for the Celescope Experiment.
R. J. Davis, W. A. Deutschman, C. A. Lundquist, Y. Nozawa and Shelby B. Bass 1

Engineering Report on the OAO-2 Wisconsin Experiment Package
Curtis B. Bendell 23

The University of Wisconsin OAO Operating System
Harry C. Heacox and John F. McNall 39

SOLAR SYSTEM STUDIES

Measurements of the Earth's Airglow in the Vacuum Ultraviolet
C. R. Waters and E. S. Fishburne 51

Terrestrial Atmospheric Composition from Stellar Occultations
P. B. Hays, R. G. Roble and A. N. Shah 61

A Comparison of Surface Brightness Measurements from OAO-2 and OSO-6
F. E. Roach and C. F. Lillie 71

The Temporal Characteristics of the Terrestrial Radiation Belt
John F. McNall 81

Ultraviolet Photometry of the Moon with the Celescope Experiment on the OAO-2
I. A. Ahmad and W. A. Deutschman 87

OAO-2 Observations of the Zodiacal Light
Charles F. Lillie 95

PAGE

Ultraviolet Observations of Comets
Arthur D. Code, Theodore E. Houck and Charles F. Lillie 109

Observations of Venus, Mars, Jupiter and Saturn Longward of 2000 Å
L. Wallace, J. J. Caldwell and Blair D. Savage . . . 115

Minor Constituents in Planetary Atmospheres: Ultraviolet Spectroscopy from the Orbiting Astronomical Observatory
Tobias Owen and Carl Sagan 139

INTERSTELLAR MATTER

Stellar Ultraviolet Colors and Interstellar Extinction
Eric Peytremann and Robert J. Davis 159

Interstellar Extinction in the Ultraviolet
Robert C. Bless and Blair D. Savage 175

Diffuse Galactic Light in the 1500-4200 Å Region
Adolf N. Witt and Charles F. Lillie 199

The Ultraviolet Spectrum of the Crab Nebula
Hugh M. Johnson 207

Ultraviolet Photometry of the Eclipsing Variable CW Cephei
Stanley Sobieski 215

Ultraviolet Photometry of Planetary Nebulae
Albert V. Holm 229

A Survey of Local Interstellar Hydrogen from OAO-2 Observations of Lyman Alpha Absorption
Blair D. Savage and Edward B. Jenkins 237

Preliminary Results on Interstellar Reddening as Deduced from Filter Photometry
Michel Laget 283

Collective Excitations and Dust Particles in Space
D. P. Gilra 295

STELLAR OBSERVATIONS PAGE

The Celescope Catalog of Ultraviolet Observations
Robert J. Davis 321

Absolute Ultraviolet Spectrophotometry of Alpha Canis Majoris, Gamma Orionis, Kappa Orionis and Alpha Leonis
Dennis C. Evans 347

Absolute Calibration of Ultraviolet Filter Photometry
R. C. Bless, T. Fairchild and A. D. Code 361

The Near Ultraviolet Spectrum of B and A Type Main Sequence Stars
Anne B. Underhill 367

Theoretical Effect of Various Broadening Parameters on Ultraviolet Line Profiles
Eric Peytremann 377

An Unusual Absorption Feature in the Far Ultraviolet Spectrum of Early-Type Supergiants
A. B. Underhill, D. S. Leckrone and D. K. West . . . 393

Energy Distributions and Spectra of Orion B Stars
Rudolph E. Schild and Frederic Chaffee 405

Photometry of Late Type Stars
Lowell R. Doherty 411

HD 50896 and the Composition of Wolf-Rayet Atmospheres
Lindsey F. Smith 429

OAO-2 Observations of C III] 1909 Å Line in Gamma^2 Velorum
Donald K. West 441

Metal Line Blanketing and Opacity in the Ultraviolet of Alpha^2 Canum Venaticorum
Michael R. Molnar 449

Comparison of Celescope Magnitudes with Model Atmosphere Fluxes for A, F and G Supergiants
Sidney B. Parsons 461

Mg II 2800 Å Emission in Late Type Stars
Lowell R. Doherty 465

PAGE

Ultraviolet Observations of Beta Canis Majoris and Beta Cephei
D. Fischel and W. M. Sparks 475

Spectrophotometry of Beta Lyrae
Theodore E. Houck 479

OAO-2 Observations of Beta Lyrae and a Provisional Interpretation
Yoji Kondo, George E. McCluskey, Jr. and Theodore E. Houck 485

Balmer Continuous Emission and Polarization in Be Stars
George V. Coyne, S. J. 495

Preliminary Results of Ultraviolet Photometry of Shell Stars
Robert L. Bottemiller 505

Ultraviolet Observations of Weak-Helium Stars
P. L. Bernacca and Michael R. Molnar 515

Ultraviolet Photometry of Nova Serpentis 1970
Arthur D. Code 535

GALACTIC AND EXTRAGALACTIC SYSTEMS

Ultraviolet Photometry of Globular Clusters
G. A. Welch and A. D. Code 541

Preliminary Results of OAO Ultraviolet Photoelectric Photometry of Galaxies
A. D. Code, G. A. Welch and T. L. Page 559

Possibility that the Far Ultraviolet Excess in M31 is Due to Main Sequence Stars
Beatrice M. Tinsley 575

The Extragalactic Component of the Ultraviolet Sky Brightness
Charles F. Lillie 583

ULTRAVIOLET TELEVISION DATA FROM THE ORBITING ASTRONOMICAL OBSERVATORY. I. INSTRUMENTATION AND ANALYSIS TECHNIQUES FOR THE CELESCOPE EXPERIMENT

R. J. Davis, W. A. Deutschman, C. A. Lundquist and Y. Nozawa
Smithsonian Astrophysical Observatory
Cambridge, Massachusetts

Shelby D. Bass
EMR Telemetry Division of
Weston Instruments, Inc.
Sarasota, Florida

ABSTRACT

The Celescope Experiment consists of two major subassemblies installed in OAO-2: an optical package containing four 12-inch Schwarzschild telescopes using Westinghouse Uvicons to produce television pictures (2° square) of star fields; and an electronics package, installed in OAO Bay E-4, to control the operation of the Uvicons and to encode the television pictures into digital signals for transmission to the spacecraft and thence to the ground. The only significant failure during 16 months of orbital operation was destruction of one of the four Uvicons by overexposure to daylight during two different types of operation. The other three cameras obtained more than 7400 scientifically useful pictures and provided useful ultraviolet data on more than 5000 stars. Sensitivity decreased significantly during our 16 months of operation (see Figure 8); this decrease was our primary reason for discontinuing operation of the Celescope experiment in April 1970.

Our data-analysis system consists of a combination of computer programs and manual reviews. The system required extensive modification after launch in order to compensate for differences between our pre-launch expectations and the actual data. The final data-analysis system not only transforms the incoming tele-

vision pictures into identifications, positions and ultraviolet brightnesses for the observed stars but also provides an improved set of calibration tables and an accurate curve of sensitivity change for use in that transformation.

This paper describes the Celescope instrumentation and data-analysis system, summarizes the major problems that we encountered during orbital operation, and lists a few major problems that we anticipated but did not encounter.

I. INTRODUCTION

This description of the Celescope experiment is an abridgment of two more detailed discussions: Performance Evaluation of the Celescope Experiment (Celescope Staff 1971) and The Celescope Experiment (Davis 1968).

The principal objective of the Celescope experiment is to measure the ultraviolet magnitudes of very many stars in a statistically significant fraction of the sky (see, e.g. Whipple and Davis (1960); Davis (1968)). During its operational life in the Orbiting Astronomical Observatory (OAO-2), the four ultraviolet-sensitive television cameras carried by the experiment indeed achieved the desired statistical sky survey by recording some 8500 television pictures of stellar fields, each 2°×2°, covering a total of 10% of the sky (see, e.g. Davis (1970)). The stellar data will soon be cataloged in other documents. Recorded here are descriptions of the design and performance of the Celescope experiment and the techniques used for analyzing its data, in the hope that this information will be helpful to later experimenters and to users of the scientific results.

The design, fabrication and operation of the Celescope experiment manifest its astronomical objectives. Because the objective is observation of a significant fraction of the sky, image tubes that view an adequate area at each exposure were the natural choice for detectors on the telescopes. But there were no ultraviolet-sensitive television camera tubes in existence when Celescope was initiated in 1959, and there was no design of a system to use them in a laboratory photometer, let alone a stellar photometer for space-flight. Nor was there an Orbiting Astronomical Observatory with well-defined characteristics into which the photometer must fit. Thus, the engineering experience of Project Celescope started from scratch, evolved through most of the first decade of the space age, and culminated in OAO-2.

Within the sky area observed, magnitude measurement of some several thousand stars is a reasonable statistical sample. Be-

cause stars become increasingly more numerous with decreasing apparent brightness, the television cameras must record stars 10^4 times dimmer than the brightest ultraviolet stars. This requirement sets the sensitivity threshold and the dynamic range required and satisfied by the Celescope hardware.

The sensitivity is achieved by specially produced ultraviolet-sensitive television tubes that employ the secondary electron conduction (SEC) principle in an electron-image storage target. The development of these Westinghouse Uvicon tubes from a starting point where the SEC principle was a new laboratory discovery, to final successful flight operation, is a technological triumph of Celescope.

As a stellar photometer, the Uvicon with its electronics derives its remarkable dynamic range from the property that the brightness of a star is registered on the target as an electron image that increases in both charge density and spatial extent as a function of the brightness of the star. Thus, in its digitized format, the image of a star is a matrix of charge-density values. The brighter the star, the more elements the matrix contains.

The digitization of the television picture requires special circuitry because the OAO spacecraft systems cannot accommodate rapid transmission of a television picture. This design consideration is satisfactorily met by a technique labeled superscan by the EMR Telemetry Division of Weston Instruments, Inc., in which the readout electron beam is off the remaining image most of the time. When the system is ready for data input, the beam is swiftly deflected to the next image point to be sampled, the charge is measured for a small region around the point, and the beam swings back off the image to wait for the next cycle.

The arithmetic sum (Sigma) of the values above background for the matrix elements of a star image is taken as the primary Celescope measure of the ultraviolet magnitude of the star. The processing of the Celescope observations then requires that the correspondence between Sigma and stellar magnitude be accurately known as a function of image position on the camera photocathode and target, of time, and of temperature and other system parameters.

The correspondence between Sigma and ultraviolet magnitude is far from linear. An initial mathematical model for it was generated from extensive laboratory measurements made before the OAO launch. When the experiment was in orbital operation, most parameters in the model were redetermined, and their temporal evolution derived from the stellar observations themselves. For this purpose, the telescopes were periodically directed toward standard star areas. Procedures for improvement of model parameters were implemented with the condition that multiple observations of the same star at different epochs, at different exposure times, and at different positions on the

television picture should yield the same magnitude within expected system accuracies.

These mathematical procedures not only generate the parameters needed for data processing but also yield retrospective engineering information on the time dependence of system sensitivity. The photometric sensitivity decreases with time, as was generally anticipated before launch.

The most useful indication of the accuracy of the processed stellar data comes from the scatter in the magnitude values for multiple observations for each of some 1500 stars. For the different cameras and spectral bands, the standard deviation of this scatter ranges between 0.1 and 0.2 mag. This is in substantial agreement with the 0.1 mag accuracy goal established early in the Celescope design.

Image focus might have profoundly degraded this accuracy but did not. A change in the optical or electronic focus affects the image size in a way that can generate inconsistent Sigma values and magnitudes. That this does not happen appreciably is a validation of the mechanical and thermal design of the telescope systems.

The Celescope experiment incorporates many engineering concepts to enhance reliability. Much of the electronic circuitry is quad-redundant at the component and module level; these systems were still operating normally when they were turned on again and rechecked 26 months after launch. The high-voltage power supplies in the flight package give no indication of arcing problems; the adopted design and potting procedures can be recommended for future uses. Although there are four telescopes in the experiment and four ultraviolet spectral bands to be covered, these are not related in a one-to-one fashion. Instead, a filter configuration bisects the camera field so that each half responds to a different spectral band; thus, for redundancy each spectral band is observed by two camera tubes. However, this concept is not an unqualified success, because star images overlapping the dividing line cannot be used.

The most troublesome problem involving reliability concerns protection of the Uvicon target from accumulating a charge of such size that electrostatic forces puncture or rupture the target material. (Fortunately, recent SEC tube designs avoid this phenomenon.) The Celescope project had to use tubes susceptible to this limitation and therefore had to compensate for it by circuitry design and operational procedures. Even so, one tube suffered target damage early in orbital operations. Although this caused a decrease in operational efficiency, no qualitative loss resulted. Because of the redundant filter configuration, data continued to be taken in all four spectral bands until observations were discontinued.

After 16 months of operation (40% longer than the nominal objective), Celescope sensitivity reached a level below which

further routine observations were unjustified. On April 26, 1970, Celescope was turned off, while still in operable condition. It was turned on again briefly on February 2, 1971, and found to be in the same condition as 9 months earlier. At the time of this writing, Celescope can still be operated and take further data if objectives arise for which its sensitivity is adequate.

The subsequent sections of this paper relate further details about those aspects of Celescope design, engineering and performance that seem most significant to the authors. § II includes a short description of the Celescope instrument. It also addresses some engineering problems and their solutions. § III describes briefly the data-processing procedures implemented for Celescope operations.

If still further detail is needed, the reader is referred to two comprehensive documents from which this paper has drawn much of its material: The Celescope Experiment (Davis 1968) and Performance Evaluation of the Celescope Experiment (Celescope Staff 1971).

The latter document tabulates conclusions from experience with the Celescope experiment, as follows.

1. Optical, mechanical and thermal design of the telescopes proved fully satisfactory in terms of image quality and stability.

2. Contamination-control procedures during ground operations were fully successful.

3. Positional stability of star images in the final television pictures was not completely satisfactory, and careful attention to factors affecting it, such as magnetic fields, is necessary.

4. The lack of an opaque shutter as opposed to the electronic shutter we employed prevented us from using a significant number of dark experimentation periods.

5. High-voltage power supplies, ion traps and associated circuitry (anti-arcing) performed perfectly.

6. Quad-redundancy design in Celescope produced a reliable operation of the electronic package, but at the cost of some increase in power and weight.

7. Superscan readout performed well.

8. The calibrator lamps proved to be valuable for providing a record of Celescope performance from the time the flight telescopes were first assembled, through all phases of subsystem and system testing, to well after launch.

9. The calibrator lamps carried initial calibration data into orbit, but did not provide thereafter sufficient data for accurately establishing the time dependence of the photometer response.

10. Protection against target-material breakdown (crossover) is a critical requirement. The Celescope techniques proved to

be satisfactory for three of our four cameras.

11. For some methods of preventing target-material breakdown and, in particular, the method used in Celescope, the output signal becomes critically dependent on the focus of a stellar image on the target. (This did not become a problem in Celescope but does represent a potential problem for future similar experiments.)

12. Uvicon sensitivity during orbital operations decreased with time. Nevertheless, the useful life of the Celescope experiment significantly exceeded the pre-launch goal of one year in orbit for gathering scientific data.

13. Scattered sunlight severely limited Celescope's opportunities for daylight observations. The most important scattering sources were the sunlit earth and the spacecraft itself.

14. Geocorona seriously interfered with Celescope measurements in the spectral band that includes 1216 Å.

15. Calibration of the Uvicons in orbit was possible and necessary.

16. Photometric accuracy, after orbital calibration, is better than 0.2 mag.

17. The use of two filters on each camera, one for each half of the field of view, provided useful redundancy but posed significant data-reduction problems. It also required rejection of many stars that were observed near the dividing line.

18. Excessive manual intervention in the data-reduction system was necessary because the housekeeping data were on a different data channel from the video data and the camera number was not included with the video data.

Our overall conclusion is that the Celescope experiment system successfully demonstrated the capability of a versatile and precise, space-borne astronomical television photometer.

II. CHARACTERISTICS OF THE CELESCOPE TELEVISION PHOTOMETER

The SAO experiment (Celescope) consists of two major integrated packages: The Celescope Optical Package and the Bay E-4 electronic module assembly.

The Celescope Optical Package contains four Schwarzschild telescopes, each of which images a star field onto the ultraviolet-sensitive photocathode of a special-purpose image tube (Uvicon)(Doughty 1966). In turn, the photoelectrons emitted by the photocathode are imaged on a target where the image is integrated and stored as an electrical-charge pattern for readout at the desired time. The video signal developed by the readout of the image tubes is amplified and supplied to an electronic data-processing system (Bay E-4 module assembly) for data processing in the manner prescribed by a preselected operating mode. Figure 1 illustrates how the Celescope was

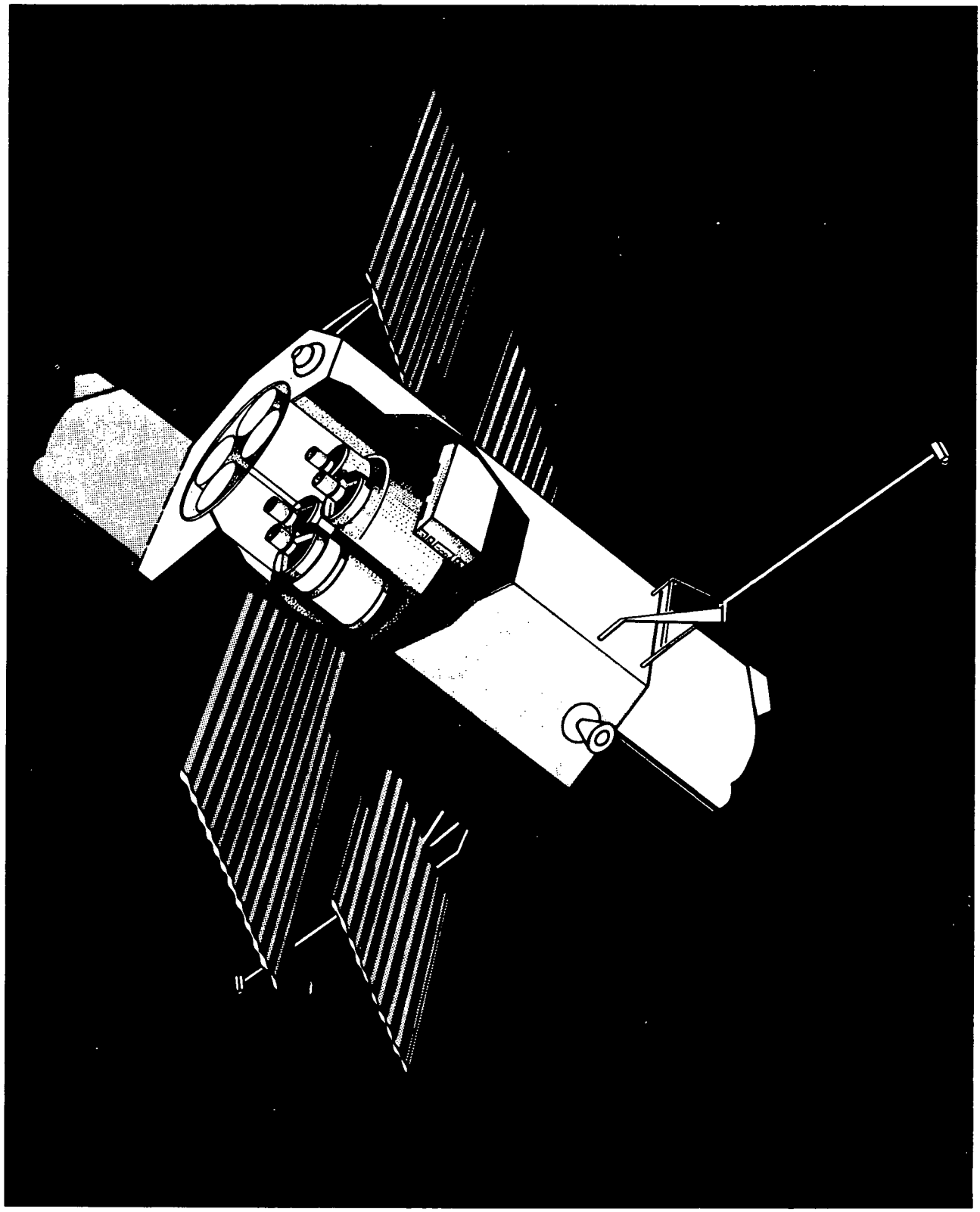

Figure 1.—OAO spacecraft with cutaway showing the Celescope experiment.

mounted in the OAO.

Each Schwarzschild-configured telescope has a diameter of 12.5 in. A telescope assembly is illustrated in Figure 2. The secondary mirror obscures an area of 6.5-in diameter of each aperture. The light is reflected by the primary mirror (hyperboloidal) and brought to focus at a point beyond the plane of the intercepting secondary mirror. The secondary mirror (oblate ellipsoidal), in conjunction with the Uvicon faceplate lens, focuses the light at a surface coincident with the photocathode surface of the faceplate of the Uvicon camera tube.

The field of view of each telescope is determined by the active area of the image-tube photocathodes and is nominally square with an equivalent angular area of 2°×2°. Each telescope tube is designed to compensate passively for optical defocusing caused by thermal expansion and contraction. The use of titanium as tube material, in conjunction with an aluminum

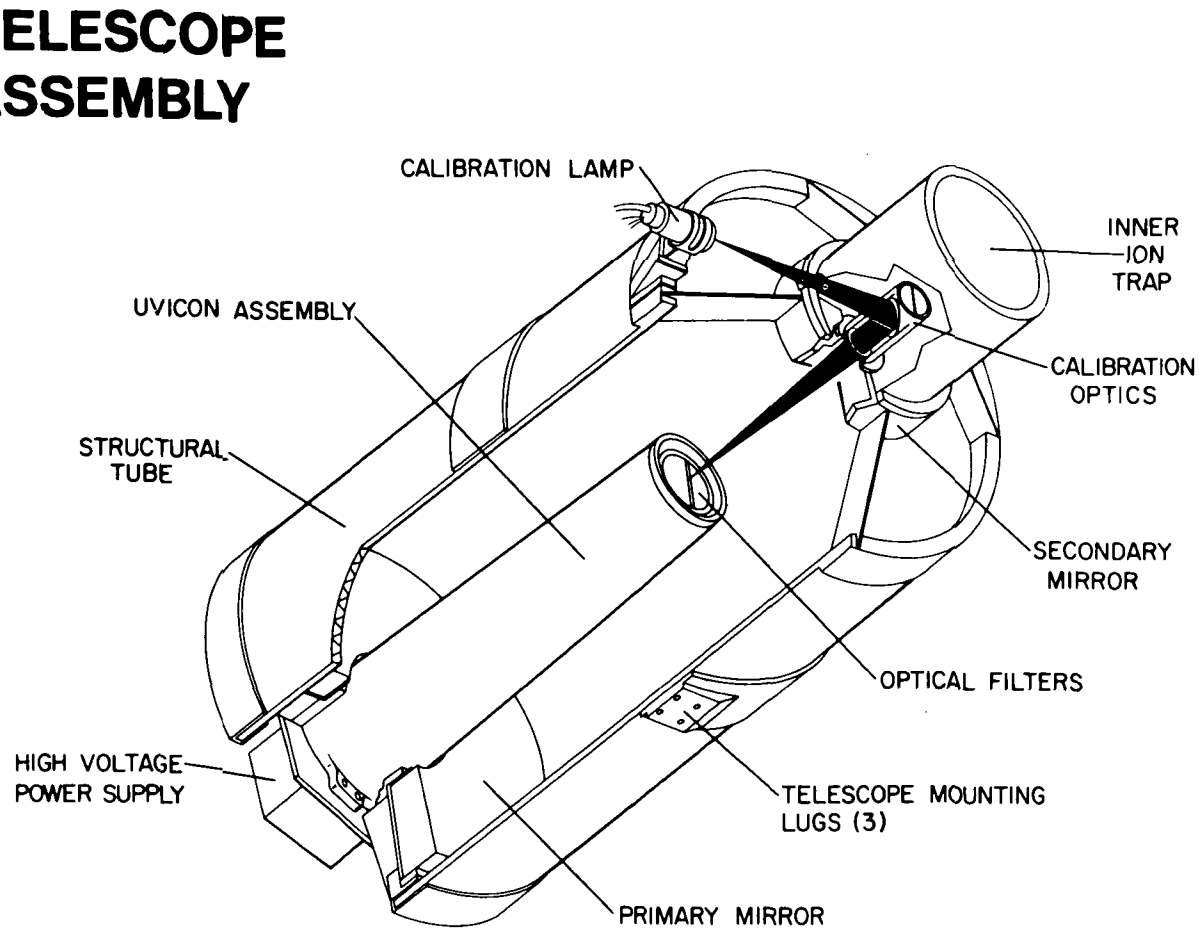

Figure 2.—Cutaway of the telescope assembly.

alloy for the camera-tube housing, compensates for defocusing effects over a 100°C temperature change. To reduce the loss of spacecraft heat to outer space, each telescope was heavily insulated on the outside of the titanium tube and the mounting lugs were designed for minimum contact area.

The field of view of each Uvicon is optically split into two areas of different sensitivity by mounting two different semicircular filters in the focal plane of the photocathode. Further spectral selectivity is achieved by the use of two types of Uvicon: A and D. They differ only in their photoemissive surfaces. The type-A is sensitive between 1050 and 3200 Å, and the type-D between 1050 and 2000 Å. The resulting spectral responses can be seen in Figure 3.

The calibration optics of the optical subsystem consist of a calibration lamp (with controlled and calibrated emission characteristics), apertures (to simulated star point sources of ultraviolet intensity), and a mirror and lens located in the aperture of the secondary mirror of each telescope. The point source of light from the calibration lamp and aperture

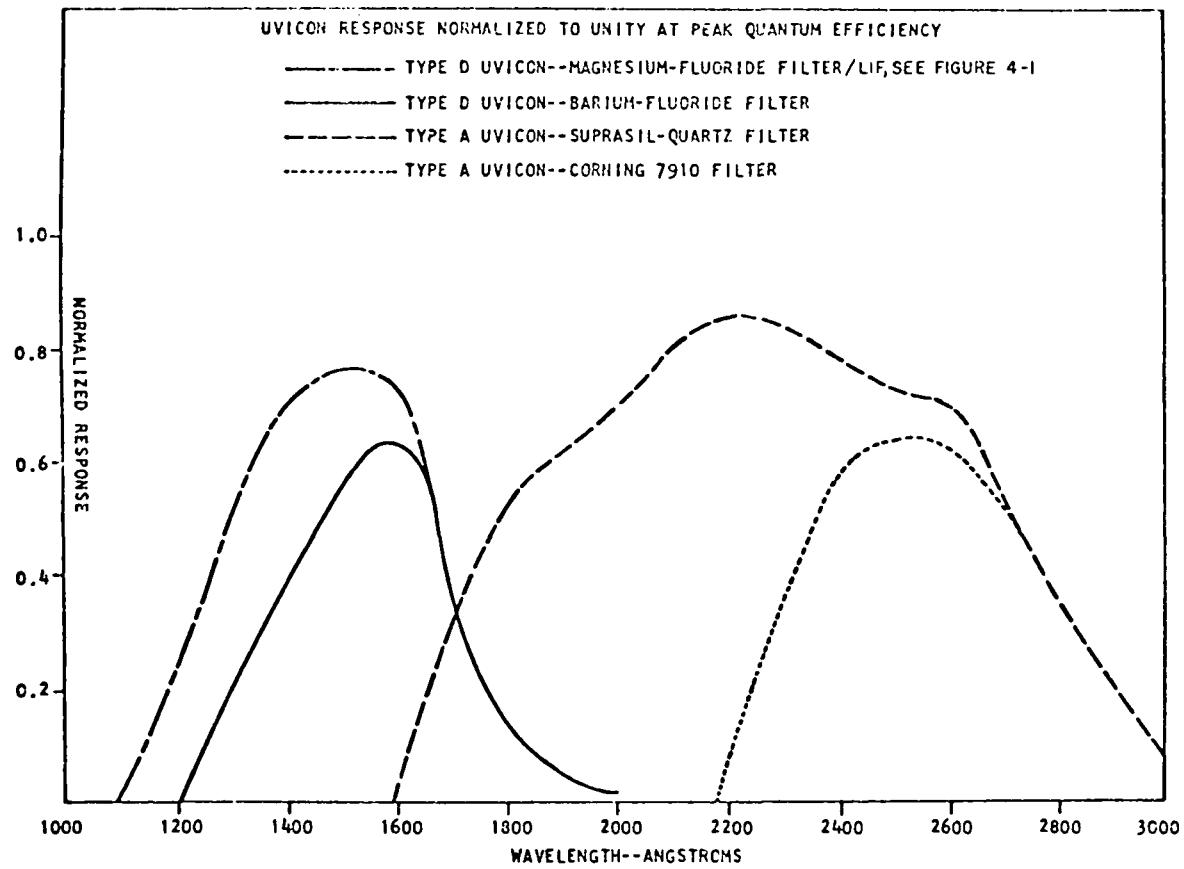

Figure 3.—Typical spectral response characteristics of Uvicons.

is reflected by a mirror, 45° off the plane normal to the optical axis of the telescope, through a lens that brings the light from the simulated stars to focus at the plane of the faceplate lens.

The electronic subsystem of the SAO experiment incorporates command and control functions for the operation of the SAO experiment. No command functions are incorporated into the system for mechanical adjustment or operation, as the design of the SAO experiment is such that the telescopes remain in satisfactory focus under the anticipated environmental conditions. The television camera tubes are effectively exposed to ultraviolet energy only when high voltage is applied to the imaging section of the tube; thus, no mechanical shutter is required.

In this system, exposure to ultraviolet light and scanning of the target are never performed simultaneously. As exposure is controlled by high-voltage on-off commands, the sensitivity of the system can be adjusted by varying the exposure time (the time during which high voltage is applied to each camera). The high-voltage commands energize three high-voltage potentials from 7 to 8 kV. These voltages are tailored for each Uvicon to produce optimum image-section focus. Each camera module is provided with its own high-voltage power supply.

As a result of an exposure interval, an electrical-charge (star-image) pattern is built up on the target of the Uvicon camera. To convert the star image on the target into a video signal, the target must be scanned (read out) by an electron beam. The readout mechanism involves replacement of electrons on the charged areas of the target.

The target can be damaged and effectively destroyed if the potential on the target exit surface (scanned surface) is allowed to increase indiscriminately. Certain conditions of operation can cause the emission from a target element of more electrons than are deposited by the readout beam. This condition, known as crossover, if allowed to continue, will further increase the surface potential at discrete points on the target to the level where electrical breakdown will occur between the exit surface and the backplate of the target, and holes will be punctured into the target.

During orbital operations, we encountered target-material breakdown (also called destructive crossover) four times. Three of these instances occurred in camera 2 and could be traced directly to differences in manufacturing techniques between it and the other three tubes. Camera 2 ceased operation in March 1969, apparently as a result of poor vacuum induced by overexposure to light in December 1968. Two types of overexposure were encountered: overexposure to ultraviolet light (Lyman alpha radiation in the daytime) and overexposure to visible light from the illuminated earth during the waiting per-

iod between exposure and readout. These modes of operation did not damage the other three tubes, primarily because they had higher crossover potentials. Neither daytime operation nor long waiting periods between exposure and readout were necessary, and such operations were not performed after December 1968, except for engineering evaluation.

The fourth instance of target-material breakdown induced two pinholes in the target of camera 4. That instance was brought about by a temporary interruption of ground communication with the satellite, caused by a computer hardware error on the ground; it did not degrade the scientific usefulness of camera 4.

Camera 3 began to show signs of incomplete priming in August 1969 but remained operable. Camera 4 also showed some signs of incomplete priming in December 1969, but modifications in the operating procedures eliminated the symptoms. In both cases, the symptoms consisted of a broad high-background ring in the outer region of the picture.

The most significant change in camera operations was a secular decrease in sensitivity (see Figure 8, § III below). This decrease was satisfactorily represented in our data-reduction program as a gain change dependent only on time and camera number, and not on signal level nor position. The signal from the calibrator lamps decreased faster than would be indicated by the gain change derived from stellar observations, indicating that the primary mechanism for inducing the gain change may be long-term exposure of the target to light. Secondary contributing factors may have been decreasing beam current from the thermionic cathodes and darkening of the lithium fluoride faceplates from exposure to the radiation belts.

The Uvicon is very sensitive to optical focus and to magnetic fields. Defocusing by 0.002 in would have resulted in photometric gain changes considerably larger than the upper limit we were able to place on this effect. The only spacecraft system that interfered with our data-gathering ability was the magnetic unloading system, which blurred the images and changed the gain characteristics. That system was routinely turned off during Celescope data-gathering operations. The earth's magnetic field shifted the television images but did not distort the pictures. The maximum excursion of the center of the raster relative to the optic axis was about 15 arcmin and did not interfere with our operations.

The video signal from the electron-beam readout is in the microampere range, and a video preamplifier is used to condition this signal for transmission outside the camera package. The video preamplifier provides low-noise high-gain amplification of direct Uvicon output signals. Further amplification of the video signal to a level necessary for digital encoding or sync mixing is accomplished in the video amplifier.

The scanning beam can be deflected in either an analog or a digital mode. The analog scan is a 300-line raster with a 1.6 msec sweep duration and a total 0.48-sec scan time. The digitally swept beam is functionally more complex than the analog; however, the readout process at the target is the same. The digital deflection initiates a digitally indexed scanning beam equivalent to an element-by-element scan, 256 elements per line and 256 lines, and a total scan time of 10.5 sec. A unique unblanking technique known as superscan was employed in this experiment. The beam is positioned well into the previously readout area for all but the short period of time (less than 10 μsec) during which the video is being sampled.

The resultant video signal (in either mode) is then transferred to the Bay E-4 module assembly for processing in either ANALOG, PCM or STORE mode before transmission (or storage) by the OAO spacecraft data-handling system.

In the ANALOG mode, the signal from the Uvicon is amplified and mixed with synchronization signals (resulting in a composite video output) for transmission. In both PCM and digital STORE modes, readout is accomplished in digital sweep mode in the Uvicons. In the PCM mode, the video output of the camera is sampled and encoded to 7-bit accuracy. The entire data train is transmitted in real time as PCM telemetry data. In the STORE mode, only data that exceed a preselected threshold are encoded.

Only PCM signals were analyzed for scientific purposes. The other modes were tested and found to work according to specifications; however, no failure occurred that required modifying our plans for using PCM as the primary mode for acquisition of scientific data.

During 16 months of active operation, and an additional 9 months in orbit not operating, Celescope experienced no change in operating characteristics other than the secular decrease in Uvicon sensitivity and the failure of the Uvicon in camera 2. There were no effects that could be directly attributable to space radiation; pictures taken in the South Atlantic Anomaly had the same characteristics as those taken elsewhere.

III. REVIEW OF CELESCOPE DATA-PROCESSING PROGRAMS AND CALIBRATION PROCEDURES

Before discussing the main topics of this section, we should like to show some typical examples of our television pictures. One must remember that we are interested in photometry, not positional astronomy. The shape and size of the images are more than adequate for our purposes.

Figure 4 shows one of these pictures. Note the target ring in each corner of the picture. Each frame consists of 256 scan lines designated by the number k, with each line contain-

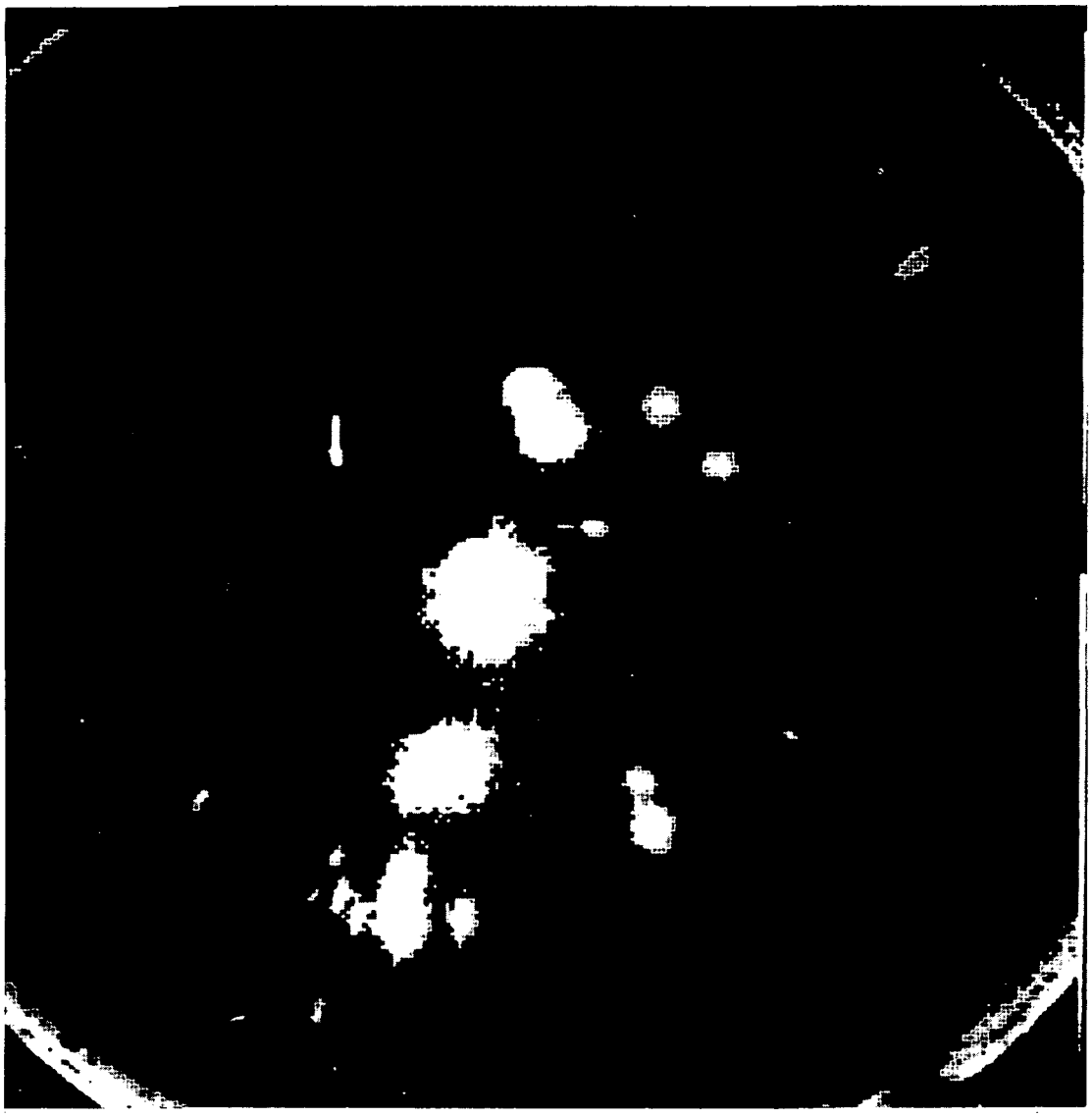

Figure 4.—Stars in Orion.

ing 251 pixels designated by the number ℓ, making a total of 64,256 intensity points $I(k,\ell)$. Lines 1 to approximately 115 have one spectral range; lines 115 to 141 have a composite response from both filters; lines 142 to 256 have a second spectral range. Most spacecraft pointings had exposures from three cameras. Figure 5 shows a montage of pictures from three cameras and a ground-based photograph. The stars in the television pictures range from 6 to 12 mag. The diffuse radiation in the U4 filter of camera 4 is the Lyman alpha radiation from the geocorona.

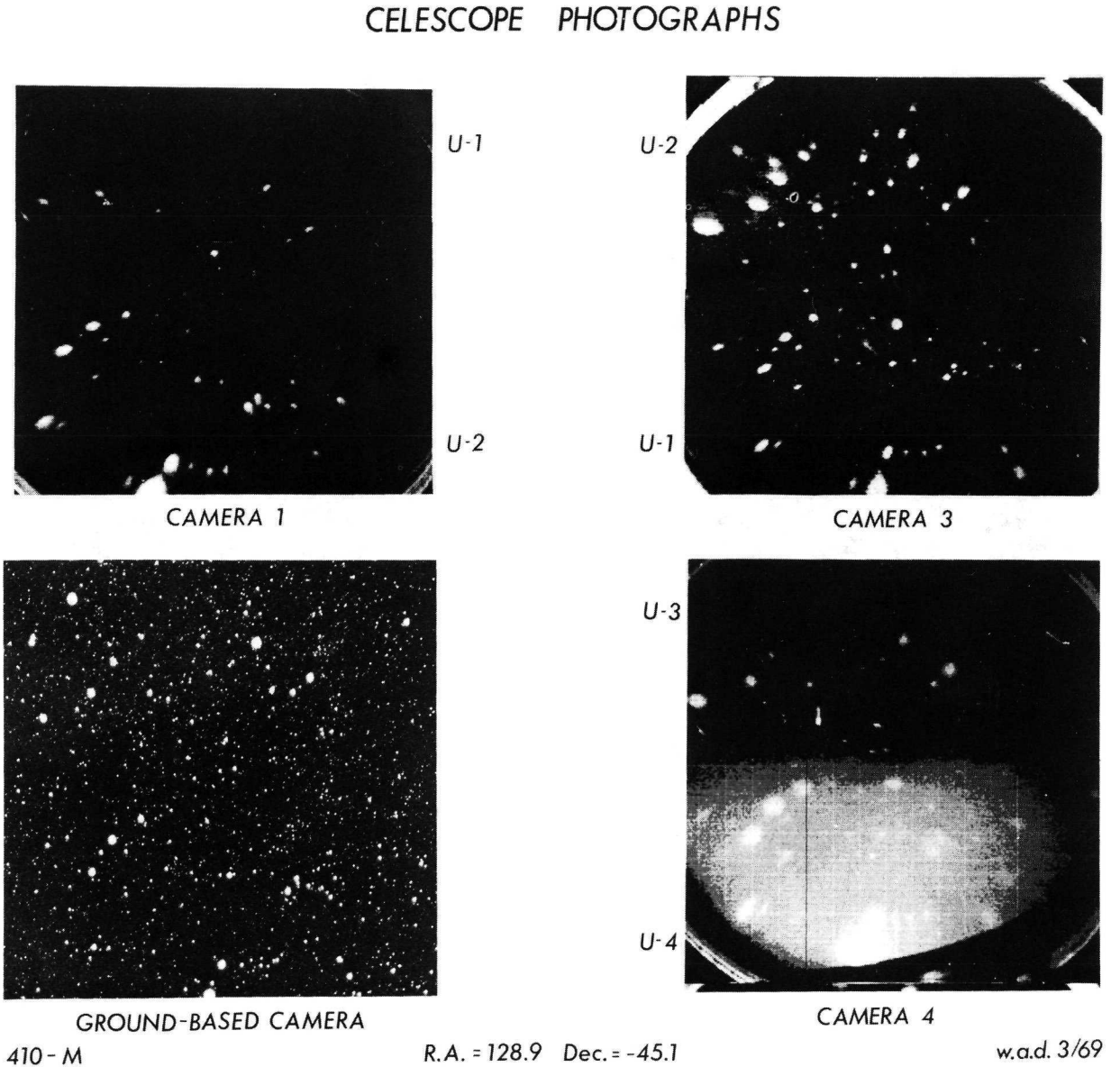

Figure 5.—A composite picture in the Vela region.

The information in a television picture can be expressed and analyzed mathematically as a matrix in which the coefficient represents the signal amplitude for the kth television scanning line and the ℓth television-picture element. As the input signal increases in strength, the matrix image increases in both width and amplitude.

Figure 6 is a block diagram showing the basic design of the Celescope equipment and the various steps by which this equipment transforms the input information into the appropriate output video signal. At the top of Figure 6 are summarized the steps by which the Celescope instrument transforms starlight of intensity I and position α,δ into the matrix A; at the bottom are given the equations by which the data-reduction system inverts that transformation to recover the intensity and position.

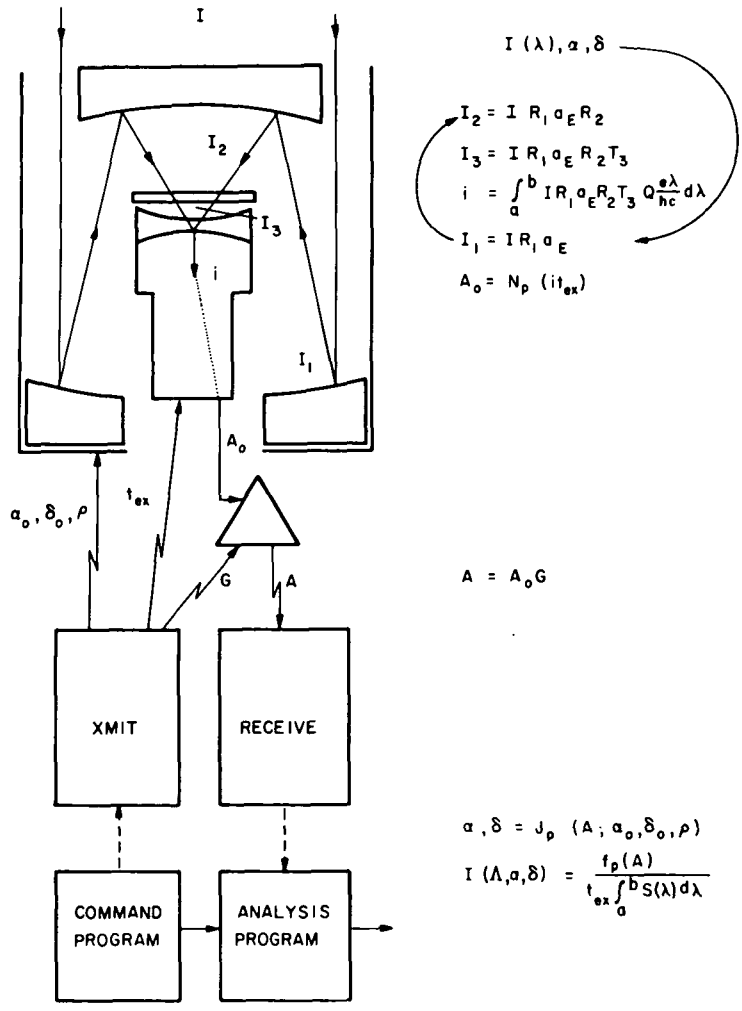

Figure 6.—Block diagram and information flow in the Celescope system.

The data-processing system that evolved during the project deserves some philosophical comment. In spite of extensive pre-launch preparations for data reduction, we were not well prepared for noisy data (streaks, parity errors and partial frames), nor were we ready to handle the Lyman alpha geocorona radiation in cameras 2 and 4.

We received a large number of television pictures from the experiment. Some of them were troublesome because of parity errors originating in the transmission link or in the data-handling equipment. We found that a quick and accurate quality check of the data was mandatory. They were hand carried from the data-processing section to our operations team at the OAO Control Center and immediately evaluated.

The final data-reduction system has a feature that we consider worthy of special attention: a composite observation file, which consists of composite observation records. Each record contains space for all the information that we ever expect to know about an object.

Each object in a picture starts as an empty record with locations for all the information that the data system generates. Subsequent programs read the information from and add information to the record. Each piece of data has an existence bit that tells if the information is in the record; therefore, the availability of information in the record can be determined without unpacking all the data. Sufficient blank spaces are reserved for information that may be added later. The advantages of common input and output routines are self-evident. In addition, the data can easily be used and sorted.

The data system shown in Figure 7 consists of four main programs: Phases 0, 1, 3 and 5. (Phases 2, 4, 6 and 7 existed but either have been absorbed by the existing phases or were dropped.) The temperatures and pointing information are checked at the Phase 0 level. Some data were missing or incorrect on a significant number of the pictures because the necessary data were on four separate data channels and were merged after they were received at GSFC.

The frames then proceed to Phase 1, the heart of the data system. It is the program that finds all the stars in each frame and all the intensities $I(k,\ell)$ associated with each star. We assume that the stars are relatively sharp spikes on a smooth background and that we can fit a general cubic equation, $A + Bk^3 + Ck^2 + Dk + Ek^2 + Fk + Gk^2 + H + I^2 + J^3$, to the background. Any intensity points that are 2.5 standard deviations above the fitted background are regarded as parts of stars.

The program has three distinct parts: the first section fits the background; the second decides which points are signal and to which star they belong; and the third prints the output of the stars for any necessary manual review and creates an output tape for the remaining stages of processing.

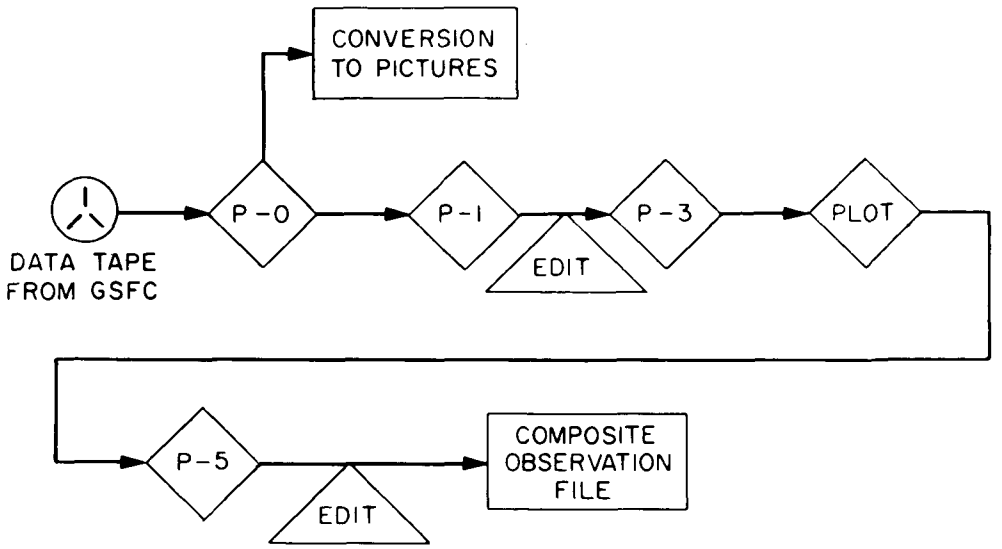

Figure 7.—Schematic diagram of the data-processing system.

Phase 3, the intensity reduction program, uses the raw input intensity calculated by Phase 1, the instrument temperatures, and the calibration data to calculate the intensity of the star. It also eliminates the known positional distortion in the frame and calculates the angular position of each object relative to the center of the frame. To do this it needs to calculate the target gain at any position on the target.

Phase 5 matches the stars in each frame with the Celescope catalog of stars, using a configuration match between the stars in the frame and those in the catalog. The program will correctly match the frame with the catalog even if the input center for the frame is 30 arc min from the actual center. The automatic identification program worked satisfactorily for most of our data. The frame must be manually matched if there are fewer than four stars common to both the frame and the catalog. A review of all frames for correct star identification follows.

Before we launched the experiment, we realized the need for in-orbit calibration and planned to take data for it. The least we could expect was a decay in sensitivity with time, but because of the two years between component calibration and the launch, we also planned to check the calibration in orbit. In addition, we felt strong pressure to acquire quickly a statistically significant amount of scientific data. The apparent conflict between the two goals of gathering calibration data and gathering scientific data in the initial orbits was

not easy to resolve. We pushed on to gather early scientific data at the expense of early calibration data. After the first month of operation, we began systematically to gather data for this task. They are listed below and are discussed in order:

1. A regular grid of stars or star fields; observations with a separation of 10 to 30 arc min between pointings.
2. Repeated observations of the same stars at regular time intervals.
3. Multiple exposures at the same pointing with different exposure times.
4. Repeated observations at the beginning and at the end of every standard slew sequence.
5. Multiple exposures at the same pointing and exposure time.

In order to map the camera sensitivities, each camera observed a number of stars of different intensity with two or more exposure times at each of 40 positions. Whenever possible, we used areas containing many stars so that the frames contained many calibration stars at the same time.

We observed the first regular grid, which was a compromise between calibration and data collection, from orbits 400 to 490. During this period, many stars were observed six times to obtain calibration data as well as scientific data. Later orbital periods were devoted entirely to this type of operation, and they provided data for the calibration-improvement program. Data from these grids were essential for the calibration of the experiment.

The time decay of the system is most easily determined if the same stars are observed at the same positions on the target at regular intervals. Because of sun, power and thermal constraints, this was impossible with our experiment, but we did observe a number of standard star fields as often as practical. Three star fields were used as primary calibration areas. We observed one as long as possible and then observed one of the other two fields as a standard until it was no longer available. Thus, we continually observed one of the three primary standard fields at least once during every operating period. These three areas, along with any chance repeat observations more than 20 orbits apart, provided the data that were used to determine the time decay for each camera-filter combination.

Identical exposures test the repeatability of the instrument. Each of our standard 36-exposure patterns started and ended at the same point for a quick check on the stability of the instrument's sensitivity. Twice, we took approximately ten consecutive exposures of several different stars to determine the repeatability of the observations. Magnitudes determined from these sets of observations varied by less than 0.2

mag.

The calibration data were used to determine

1. An exposure time correction.
2. The decay characteristics of the cameras.
3. The change in the area sensitivity of the target gain from initial calibration until launch.

All the data require an exposure-time correction, but it is only important for short exposure times. We deduced the correction by determining the additional increment of time that gave the best agreement in magnitudes between consecutive exposures of 1, 5, 15, 30 and 60 sec of the same stars.

The time-decay history of each camera-filter combination was determined by fitting a power series to the star data with a least squares technique. Each star must have a unique magnitude at time zero. Its magnitude calculated from measurements at any other time will increase if the system decays. Magnitudes are defined as -2.5 log (power); hence, lower power signals have larger magnitudes. We therefore assumed that

$$M(t=0) = M(t_1) - \sum_1^n A_n t_1^n \quad .$$

If a star was observed twice,

$$M(t=0) = M(t_1) - \sum_1^n A_n t_1^n = M(t_2) - \sum_1^n A_n t_2^n \quad ,$$

and hence the equation

$$M(t_1) - M(t_2) = \sum_1^n A_n (t_1^n - t_2^n)$$

when solved for all pairs of stars defines the coefficients A_n in the decay equation for the system. Note that this is a linear correction; that is, every magnitude receives the same additive correction.

The standard calibration-area data and all chance repeats greater than 20 orbits apart were used in these fits. Other data were not used, because they reflect area sensitivity changes and isolated frame shifts rather than time decays. The curves determined with this program are shown in Figure 8. Each curve stops at the last reliable data point.

We used a Fletcher-Powell optimization technique to refine the target-gain curves. The input data were selected from the regular calibration grids and any other data that were appropriate. All marginal data and data that were contaminated by the filter discontinuity were eliminated from these runs.

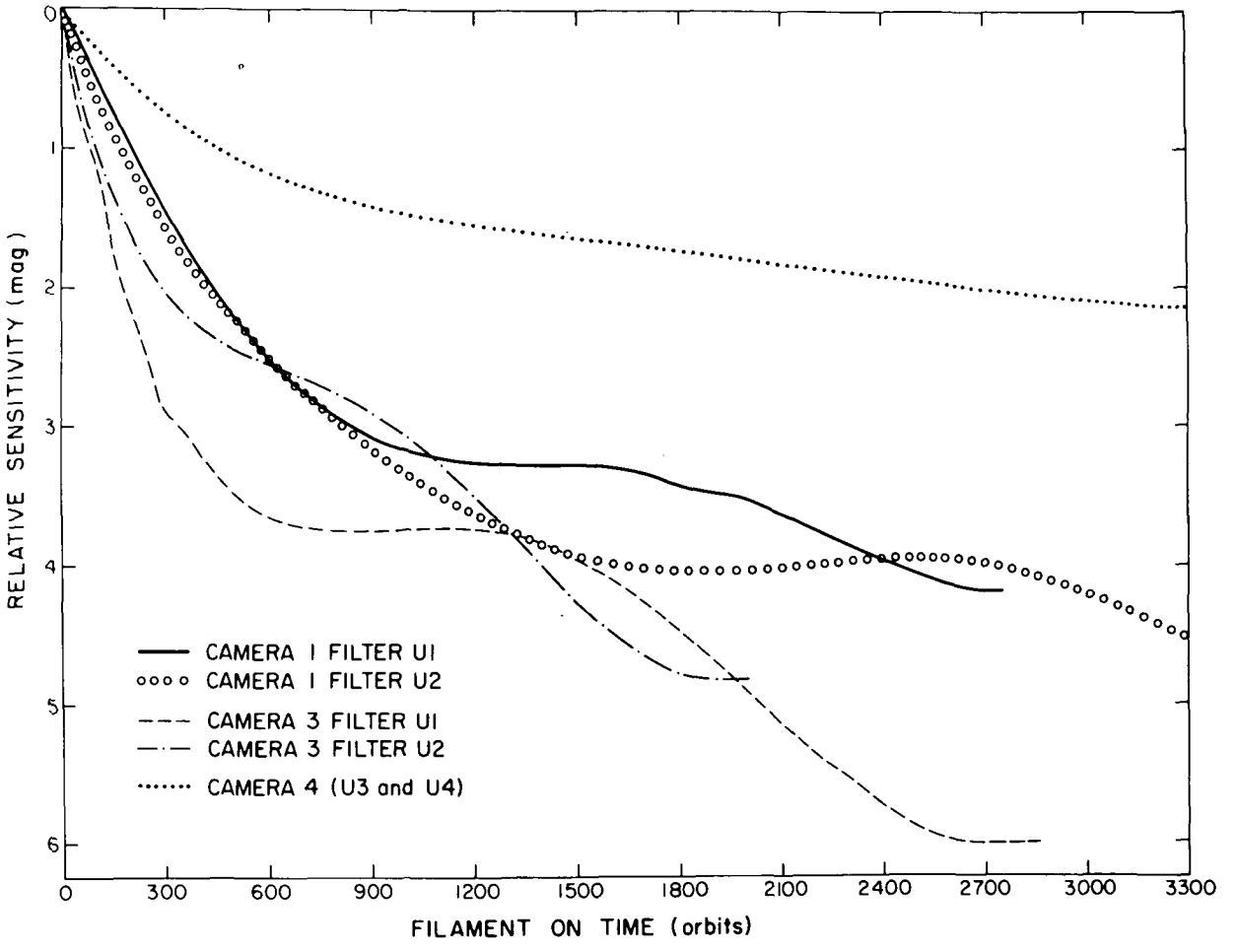

Figure 8.—Celescope sensitivity curves.

The program uses pairs of stars observed at different positions on the target. It computes the required gain change for each grid point that will minimize the RMS magnitude deviation of all pairs of stars. Since we assume that reciprocity holds for our tubes, we also use data at different exposure times. A series of laboratory tests on similar tubes showed no reciprocity failure.

The procedure for calibration improvement went as follows. Each camera was treated separately, and the stars in one filter were not compared with the stars in the other. First, the decay program calculated a decay curve for each filter. These curves provided a first-order correction to the magnitude calibration, and then the optimization program improved the gain curves. These curves were then used to calculate new magni-

tudes. Next, we calculated a new set of decay curves. The iteration between these two techniques continued until the results converged. The resulting gain curves showed only slight variations from the curves determined from the pre-flight data.

A short comment about the amount of data is included here because insufficient data may produce misleading results. All the programs had sufficient data for a meaningful solution. The decay equation contained six coefficients for camera 1 and five for cameras 3 and 4. At least 320 data points were used for the least squares fit. The gain-curve optimization program has 500 parameters and a minimum of 1500 data points.

Table 1 lists the final result of the magnitude-improvement procedure.

Table 1. Final RMS magnitude discrepancies

Camera	RMS discrepancy (mag)
1	0.17
3	0.20
4	0.19

The success of a project as large as Celescope depends upon significant contributions from a very great number of individuals. We wish to acknowledge especially the guidance and support of Dr. Fred L. Whipple, Director of the Observatory and Principal Investigator on Project Celescope; Dr. Nancy G. Roman, Head of Astronomy at the National Aeronautics and Space Administration; Mr. Robert T. Ayer, Project Manager for Celescope; Mr. John J. Burke, Project Manager for Celescope during the time the instrumentation was being built and tested; Dr. Gerhard Goetze, camera-tube engineer for the Westinghouse Electric Corporation; Dr. Mario D. Grossi, electronics engineer, Smithsonian Astrophysical Observatory; Mrs. Katherine L. Haramundanis, who is responsible for the Celescope data-reduction system; Mr. Joseph Purcell, OAO Project Manager for NASA; and Dr. James E. Kupperian, OAO Project Scientist for NASA.

Project Celescope was supported by Contract NAS 5-1535 from the National Aeronautics and Space Administration.

REFERENCES

Celescope Staff 1971, Performance Evaluation of the Celescope Experiment. Report to the National Aeronautics and Space Administration, Contract NAS 5-1535, July.

Davis, R. J., ed. 1968, The Celescope Experiment, Smithsonian Astrophys. Obs. Spec. Rep. No. 282, 132 pp.

_____ 1970, Ultraviolet photometry of stars obtained with the Celescope experiment in the Orbiting Astronomical Observatory, in IAU Symp. No. 36, Ultraviolet Stellar Spectra and Ground-Based Observations, ed. L. Houziaux and H. E. Butler (Dordrecht: D. Reidel Publ. Co.), pp. 109-119.

Doughty, D. D. 1966, Ultraviolet sensitive camera tubes incorporating the SEC principle, in Advances in Electronics and Electron Physics, vol 22, ed J. D. McGee, D. McMullan and E. Kahan (New York: Academic Press), pp. 261-271.

Whipple, F. L. and Davis, R. J. 1960, Proposed stellar and interstellar survey, Astr. J. 65, 285-290.

ENGINEERING REPORT ON THE

OAO-2 WISCONSIN EXPERIMENT PACKAGE

Curtis B. Bendell
University of Wisconsin
Madison, Wisconsin

ABSTRACT

The continued useful operation of the OAO-2 Wisconsin Experiment Package (WEP) for almost three years after its December 1968 launch is evidence of a superior engineering accomplishment. Reliability features of the experiment concept and design which have contributed to its long life are presented. Data anomalies and partial failures are summarized along with conclusions regarding their causes. The thermal, vacuum and radiation effects of the space environment are shown to be minimal and quite localized within the WEP.

I. INTRODUCTION

The purpose of this document is to provide an engineering report on the performance of the Wisconsin Experiment Package (WEP), one of two major experiment equipments which were launched into a circular orbit as a part of the Orbiting Astronomical Observatory (OAO-2) in December 1968. At the time of this writing the WEP is in its third year of operation with the OAO spacecraft. The scientific achievements of this program are unparalleled in the field of ultraviolet astronomy. The continued experiment operation and collection of valuable scientific data over such a long time period is evidence of a superior engineering accomplishment.

This document presents the scope of the WEP engineering accomplishments, the WEP data anomalies and partial failures which have occurred, the observed effects on the WEP of the space environment and other orbital and spacecraft parameters. A summary of observed photometry and filter variations and their causes is presented. It is anticipated that the infor-

mation presented will be useful to astronomers in analyzing their recovered data and also useful to engineers and designers of future space experiments. A functional description and general performance have been reported by Code et al. (1970).

II. ENGINEERING OBJECTIVES

The objective of the engineering effort was to design and fabricate the seven telescopes and associated electronics, optics, structures and mechanisms within the space, weight, environment and power constraints imposed, while still providing for a one year life in orbit. The 15 watt average power constraint alone dictated pulsed or stepping filter, aperture and grating drive mechanisms as well as unique (to the 1961-1965 design period) designs for analog amplifiers, digital electronics and high efficiency power supplies. The space vacuum and thermal constraints required extreme care in selection of materials and lubricants of exposed components and materials. The 500 pound weight limitation ruled out brute force techniques for maintaining structural integrity and the precise optical alinements necessary for telescope construction and mounting.

Despite all of these interesting and challenging design problems, it was readily evident that the most difficult task would be the accomplishment of the reliability goal of one year of operational life in orbit.

III. RELIABILITY FEATURES

The basic scientific concept provided for parallel and redundant means of collecting spectral intensity information on celestial objects. Certain optical filters of the four stellar photometers were used redundantly in adjacent instruments so that the loss of a single stellar photometer would not cause a spectral gap to exist in the data. Similarly, the nebular filters redundantly covered much of the stellar spectral range. Further, Scanning Spectrometer No. 1 covers the approximate wavelength band of 1000-2000 Å while Spectrometer No. 2 covers from 2000 to 4000 Å. Thus, the ultraviolet spectral range is again covered redundantly by these instruments.

Since the instruments contained measuring redundancy, it was possible and profitable from a reliability viewpoint to make their control and data collection electronics independent of one another to the maximum extent possible. Thus, command control data entry is in series form only at the spacecraft command line input isolation point. The WEP internal command storage is by means of parallel input registers rather than serial type shift registers. Also, separate exposure time generators exist for each stellar, and the nebular, as well as

one for the two spectrometers. Filter command decoding circuits and drive circuits are all separate for each stellar and the nebular. While it was not practical to provide a separate power supply for each instrument, two supplies of each of the ±10 volt, ±15 volt and high voltage supplies were provided. These are changeable on command from the ground. Further, it was made possible to collect analog data if the ±10 volt supplies failed or digital measurement data if the ±15 volt supplies failed. The ±10 and ±15 volt power supply line to each instrument in the PIP package was fused so that a short on one line for one photometer would not disable other photometers. High resistance (3.3 meg or 91.1 megohm) series isolation resistors were used in the high voltage line to each phototube, so that short circuits or heavy saturation of one tube would not seriously affect the output from other tubes.

All the standard reliability techniques of the time relative to "worst case" designs, component selection, screening, derating, high vacuum sample, testing etc. were utilized. Extremely detailed qualification tests on the prototype and acceptance tests on the flight models were made at both the manufacturer's site and at Goddard Space Flight Center. Any failures known to occur were diligently followed up to determine the cause and rectify the problem. Rescheduling of tests was closely followed and coordinated by GSFC project and test personnel in cooperation with the WEP group. Given this professional concept and design program, it was the dedication of people (scientists, engineers and administrators alike) to the idea of reliability which ultimately paid off in equipment performance.

IV. INTERNAL WEP ANOMALIES AND FAILURES

a) General

This section presents the WEP anomalies and failures which have occurred, and the analyzed cause and effect of the observed "happenings".

b) HVPS Loading

Saturation of certain of the instrument detector tubes loads the high voltage power supply (HVPS) to an extent that other instruments' sensitivity may be affected. The loading effect is illustrated by the higher than normal HVPS status indicating lower than normal HVPS output voltage. One can project from the WEP data an incident light level having a potential 100 μa Stellar 1 tube current (a 100-fold increase over 1 μa at E1 for full saturation). However, the use of the series 91.7 megohm resistor in both the Stellar 1 and 2 and

Spectrometer No. 1 high voltage power line provided self-limiting of the photomultiplier tube current at about 6 microamps. This self-limiting feature has saved the tubes from deterioration or destruction due to the extremely high incident light levels which occur when the WEP views the sunlit earth. The self-limiting also reduces the dark current recovery time following the high light level exposure.

c) HVPS Arcing

It has been concluded that WEP HVPS arcing took place between 2130 on January 16, 1969 and 1530 on January 17, 1969, about 1-1/2 months after launch. This time period also coincided with a spacecraft loss of control and recovery and recharge of spacecraft batteries. Manually reduced WEP data showed high voltage status variations beyond that attributable to HVPS loading. Uncommanded aperture changes, a collimation status change and filter wheel position changes all occurred during this period. It was also at this time that both the nebular filter wheel and the nebular aperture became permanently stuck, apparently from a blown fuse in the -10 volt power line to the nebular. Data immediately following this time period indicated that the HVPS had switched itself (without command) to the redundant high voltage power supply. The new (different manufacturer) HVPS has performed admirably since that time and no commands have been sent to try the original supply.

It is theorized that the WEP HVPS arcing caused radiative pickup in the aperture, collimation and filter wheel drive monostables of the WEP Prime Instrument Package (PIP), resulting in the erroneous (uncommanded) mechanism status indications. One of the strong radiative transients probably blew the 10 volt fuse to the nebular. The lack of significant changes of the WEP Control Electronics Package (CEP) controlled exposure time status compared to mechanism changes indicates a localization of the fault to the PIP rather than erroneous commands being issued by the spacecraft through the CEP. HVPS arcing could cause conductive pulsing of the WEP-PIP internal 28 volt dc power line which could cause status changes similar to those detected. However, one would expect to notice ±10 and ±15 volt dc internal supply changes with strong conductive pulsing and these changes did not occur. The RFI filters in the +28 volt line and return to the spacecraft provide good isolation of WEP conductive pulsing back into the spacecraft +28 volt dc line.

The cause of HVPS arcing is attributed to the PIP entrapment of some of the spacecraft gas being fired during loss of spacecraft control and subsequent orientation corrections. Current procedures call for WEP power to be turned off when

spacecraft control or power problems occur. Improved OAO spacecraft recovery techniques now require little or no gas ejection.

d) Second Half of Data Storage

Analog WEP data on occasion has been noted to be erroneous on words 1, 4, 7, 10 and 13. Some of the stellar digital data is also erroneous at the same time. The cause of these errors has been traced to bit errors occurring during readout of the WEP data from the second half of the spacecraft data storage. GSFC has been able to verify these bit errors. The +15 volt status (word 10) drops suddenly by 0.16 volts from its normal very steady value. The Control Electronics Temperature status (word 13) also drops by 0.16 volts. The normally .00 Stellar 4 analog data (word 4) will occasionally go to 0.16 volts. Stellar 1 and Spectrometer No. 2 analog measurements vary radically. Command programming and data reduction techniques avoid the use of the second half of spacecraft data storage whenever possible.

e) Stellar 1 Digital Count

Digital counting of Stellar 1 data occasionally is erroneous. During the time periods of this anomaly, data counts show up as one, or one plus only one other binary stage. Thus, while the count one predominates, counts of 1, 17, 33, 65 and 129 often appear to the exclusion of other non-binary plus one count data. This anomaly is easily detectable on manual comparison of stripped data to analog data, but the anomaly may not be so obvious when computer averaged data are presented.

The cause of this anomaly is attributed to the first stage of the Stellar 1 data output counter in the Control Electronics Package being stuck in a binary ONE condition. This prohibits the normal flow of counts from triggering the next stage (2 level) because of the lack of a full one to zero transition. It has been noted in ground testing that attempts to cause the correct transition by incoming data pulses may result in occasional small pulses being amplified by the 2, 4, 8, and succeeding level stages until a sufficient pulse transition causes one downstream binary stage to flip. Thus, all data outputs have the one level count, and occasionally one binary stage well away from one is activated.

The anomaly is quite rare, but exists at least from the beginning of week 31-1 starting on January 21, 1970 and then clears itself up on January 25, 1970. This slow rate of change is indicative of a thermal or thermal transient basic cause for the sticking flip-flop. Weekly CEP thermal status plots did show a greater than normal 10°C thermal variation during

mid-January but these changes steadied out on January 22, 1970.

f) Stellar Filter Wheel Anomalies

(i) General

The stellar filter wheel control circuit operates as a closed loop servo. A filter wheel command is entered in a digital register and the filter wheel steps at a 1 pulse per second rate until a feedback commutator detects that the digital status agrees with the registered command. Redundant codes are used such that all possible bit combinations of each four bit filter wheel command will result in one of the five filter position commands. Thus, a single "noisy" or random command cannot cause the filters to continuously step. Also, any one of the four bit command register stages can fail, and all filter positions can still be commanded.

(ii) Commutator Failure and Wear

Stellar 2 has been noted to have an occasional poor commutator status pickup in the filter 4 calibration slide status position. Typical data for filter 4 E2 or 1 second exposure results in the six mode A data sets being separated by two seconds. The Stellar 2 filter position status for the six measurements were 0, 1, 3, 5, 2 and 0. This is exactly the status which would result if the wiper of the commutator were not making proper contact with the fixed printed circuit board commutator coder on position No. 4. The recurrence of this anomaly was noted only four times in the 20 to 30 Stellar 2 F4 commands during the week 42-3 and was not noted on other positions or stellars during four sample weeks of 1970 data. During late 1970 and early 1971 the Stellar 2 filter wheel had become stuck and then unstuck. It is currently being left at the useful F5 position. The progression of both the Stellar 2 filter wheel conditions is indicative of mechanical wear nearing the end of filter stepping life.

(iii) Filter Cycling

During 1969, filter cycling commands were occasionally sent which should cause the six filter status readings for all stellars to be 1, 2, 3, 4, 5, 1 successively. This command promotes a noisy mechanical and electrical response which increases the probability of the Stellar 2 described anomaly occurring in other stellars. This command also reduces the data accuracy by eliminating the potential for six point averages at each reading. The filter cycling command is limited to single exposure settings which could result in a saturated

reading for the calibration slide or one of the other filters. The recovery time from saturated readings may affect the first sample of the following filter reading. For all of these reasons, the filter cycling command is no longer being used.

(iv) Charge Capacitor Fusing

The power for the filter stepping drive mechanism is derived from the regulated 28 volts provided by the spacecraft. In order to isolate high current stepping transients from the spacecraft power lines, separate energy storage capacitors are used for each photometer along with charge current limiters between the power source and the capacitor. Fusing of the current limited line was done to preclude capacitor or drive circuit shorting failures from drawing continuous current from the spacecraft 28 volts. Test failures of fuses in system tests at GSFC resulted in resistor by-passing of the fuses to a degree such that a storage capacitor could still charge if a fuse were blown, but that the charge time would be longer. The increased charge time is of the order of 16 seconds for satisfactory charge with the fuse blown as versus much less than 1 second with a good fuse. It is not clear whether some of the fuses have blown at the time of this writing. However, commands are being typically issued for only one sequential step (of all four stellars if desired) at a time. This technique conserves the energy stored on a capacitor, and reduces the recharge time.

V. PHOTOMETER PARAMETER CONSISTENCY

Each of the seven WEP instruments uses a photomultiplier tube to convert its input optical signal to an output electrical signal. Each photon of tube input light intensity is converted to an electrical pulse by the photomultiplier tube and its attached pulse preamplifier. The pulses are fed to two parallel detection circuits. One is a digital detection and six stage binary precounter, followed by an eight stage binary digital output measurement counter. The other parallel chain integrates the detected pulses and presents an analog current to an analog amplifier which produces an analog output measurement voltage.

The digital measurement counter output count represents the sum of pulse counts due to light photons on the tube, plus the tube dark current count, plus tube external noise counts, plus an average digital offset of 0.5 count. The tube dark current count plus the tube external noise count are generally lumped together as a total "dark" count. Due to the six stage binary precounter each output signal plus dark count represents 64 photo-electron pulse counts detected by the photomultiplier

tube for any given filter and exposure time. A full scale digital output measurement count is 2^8 minus 1 or 255 units of digital output data which is available for each of the four programmable exposure times. The precounter receives continuous pulses from the detector tube, whereas the input to the output counter is reset and gated on by the start of an exposure time and off at the end of the exposure. If the precounter last stage is in a ONE condition when the output counter is gated on, a one count offset is introduced to the output. Since the precounter is in the ONE condition 50% of the time, a 0.5 count average offset is taken from all digital measurements regardless of exposure. Experience has shown that spacecraft day, viewing the sunlit earth, or passing through the South Atlantic Radiation Anomaly, often contributes sufficient dark count to mask out the actual star signal. Command programming is such that useful digital and analog data is taken only during spacecraft night and when not in a predetermined South Atlantic Anomaly location. There is no digital overflow indicator so it is well to avoid digital overflows by good programming. One technique of measurement when a question regarding overflows is likely, is to program at least two different adjacent exposures for the same object and same filters. Another technique is to predetermine an analog voltage per digital overflow ratio, then determine overflows from the analog voltage measured by the same instrument. Still a third technique is to relate another instrument reading to the measurement count in question. The ground data reduction programs incorporate the best methods of establishing overflows for each instrument.

The analog measurement circuitry is composed of a dc operational amplifier with relay controlled sensitivity ranges. The operational amplifier has a balanced electrometer tube pair input stage followed by a transistorized amplifier. The selectable sensitivity ranges are 10^{-6}, 10^{-7}, 10^{-8} and 10^{-9} amperes full scale. These commanded gain changes are automatically accomplished with the 1/8, 1, 8 and 64 second exposure time commands used for the pulse measurement circuitry. As these amplifiers are used for integrating, specific time constants are provided for each range. These are 1/4 of the associated exposure time: i.e., 1/32, 1/4, 2 and 16 seconds.

The measured analog output voltage consists of the sum of the analog signal due to incident light on the tube, an analog tube dark current signal combined with external noise effects, and an analog offset voltage. The spacecraft day and radiation effects which contribute to digital noise also contribute to analog noise. The gain of each analog amplifier is linear to about 0.5% over each sensitivity range. The linearity at zero input does not correspond to zero output volts, which gives rise to the fixed analog offset for all sensitivi-

ty ranges. Taking two measurements on the same object with the same filters but different exposures within about 5 minutes of time allows one to consider dark currents constant and thus to calculate analog offset. These calculated offsets are averaged over about one week of time and fixed values used as inputs to data reduction programs. The offsets may be positive or negative, and each amplifier offset may vary significantly over more than a one week period.

The digital measurement count has proven to be generally more consistent and valuable than the analog voltage output. The digital sensitivity is higher and consequently it registers significant output for less of a filtered light input to the tube. The resolution of both channels is limited to one part in 256 for a given gain setting. This is because of the 8 binary bit limitation on available digital data output counts and the 8 binary bit analog to digital converter used on the analog channels for data transmission. Thermal and long time variations in the photometer analog and digital outputs have been noted on repeated measurements of calibration slide outputs. The thermal induced variations are of the order of 15% maximum on analog outputs and about 3% maximum on digital outputs. The linear time related variations may run from a maximum of 40% on the analog outputs to 8% maximum on the digital outputs. The variations are highest on the most active tubes (i.e. Stellar 1 which generally observed high light levels) and lowest on the least active far ultraviolet sensitive tubes (Bendell 1971). These thermal and time variations are of little consequence to the stellar photometers since the calibration slide data is used to normalize the measurement data in the data reduction programs. The spectrometers have no built-in calibration source. Consequently, the thermal and aging effects on these units must be obtained from examination of repeated scans, widely separated in time, of reference stars. Preliminary results show significant effects may exist on Spectrometer No. 1. However, Figure 1 plots raw Spectrometer No. 2 digital data on a reference star along with the difference in raw counts over a complete scan separated by a time period of 1-1/2 years. The difference plot shows less than 1% or ±1 count difference in the raw data. Spectrometer No. 1 digital sensitivity was known to increase during late 1969 and early 1970, possibly due to a stuck bit in the precounter, such as that which was previously described as an anomaly for the measurement counter of Stellar 1. This sensitivity variation is slow enough in occurring that it has no effect on the examination of a scan for relative peaks and valleys, indicating emission or absorption spectral lines. It happens that the result of a stuck bit in the precounter is to yield a much higher resolution of peaks and valleys in the data in the measurement

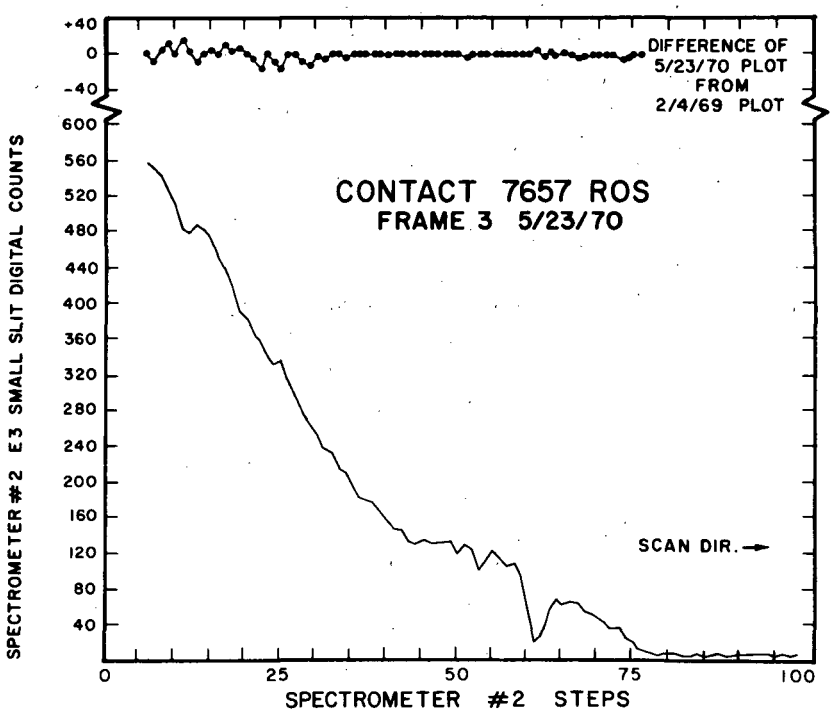

Figure 1.—Spectrometer No. 2 Eta UMa scan.

counter. Consequently, the fault has yielded some excellent data on relatively dim stars.

VI. FILTER CONSISTENCY

a) General

Given the relative consistency of the photometers coupled with the ability to compensate for thermal and time related variations in the photometers, the tools are available to analyze the consistency of the parameters in the optical path; namely the optical filters and mirrors. As will be subsequently shown, there are no major degradations of data taken on repetitive measurements of reference stars for most of the optical filters. One can thus conclude that the reflecting optics have suffered no degradations, and analyze the individual filter data in terms of the filter consistencies.

Table 1 summarizes the nature of the individual WEP filters and all elements within each Stellar affecting detected optical bandwidth. The table and all further comments regarding filters and filter degradation are derived from a letter by Dr. A. D. Code of the University of Wisconsin Space Astronomy

Table 1. WEP - Filter System Characteristics

Instrument	Filter	Type	$\bar{\lambda}$ Å	$\bar{\lambda}$BW	λ_{eff}
EMI 6256B CsSb(1700-6000)					
S1	F1	I.F.+UG11	3317	540 Å	3357±20
	F3	BG12+GG13	4252	840	4290±35
	F4	I.F.+F.Q.	2985	420	3075±25
EMI 6256B CsSb(1700-6000)					
S2	F1	I.F.+F.Q.	2035	480	2249±50
	F2	I.F.+F.Q.	2945	440	3062±25
	F5	I.F.+F.Q.	2386	330	2493±35
ASCOP 541F CsTe(1050-3500)					
S3	F1	I.F.+F.Q.	1913	260	2107±20
	F2	I.F.+F.Q.	2462	380	2589±30
	F5	I.F.+CaF_2	1679	260	2217±50
ASCOP 541G CsI(1050-1950)					
S4	F1	I.F.+CaF_2	1554	240	1662±15
	F3	I.F.+CaF_2	1430	240	1601±30
	F4	I.F.+LiF_2	1332	200	1556±50

Laboratory. Stellar 1 and Stellar 2 employ EMI 6256 Cs Sb photomultipliers with a sensitivity from about 1700 Å to 6000 Å. Stellar 3 employs an ASCOP-541F Cs Te photomultiplier with a cleaved LiF_2 window and a sensitivity from about 1050 Å to 3500 Å. Stellar 4 uses an ASCOP-541G CsI tube with a response from 1050 Å to about 1950 Å. The interference filters (I.F.) are first order filters deposited on a glass, fused quartz (F.Q.) suprasil, CaF_2 or LiF_2 substrate as indicated by Table 1. The wavelength $\bar{\lambda}$ is the constant energy wavelength for the preflight interference filter curves and λ_{eff} is the effective wavelength for a solar energy distribution neglecting the effects of the transmission due to pinholes. $\bar{\lambda}$BW is an indicator of the half power interference filter bandwidth around $\bar{\lambda}$.

The particularly useful filters for late type celestial objects are S1F1 (3317 Å), S3F2 (2462 Å), S3F1 (1913 Å) and S4F1 (1554 Å). Figure 2 illustrates the band passes for the S1F1 filter along with the bandwidth properties of the substrate and photomultiplier response. The S1F1 spectral characteristic is defined by the UG11 as well as the interference filter. It can be shown that the S4F1 is also defined by the ASCOP tube response and the CaF_2 substrate. Should the interference filter vanish, the bandpass would still be at about the same effective wavelength with an increase in width of about 100 Å. S3F2 and S3F1 are not as tightly defined but the suprasil substrate and ASCOP tube definitely eliminate the effects of Lyman alpha leaks on the low wavelength end and red leaks on the high end.

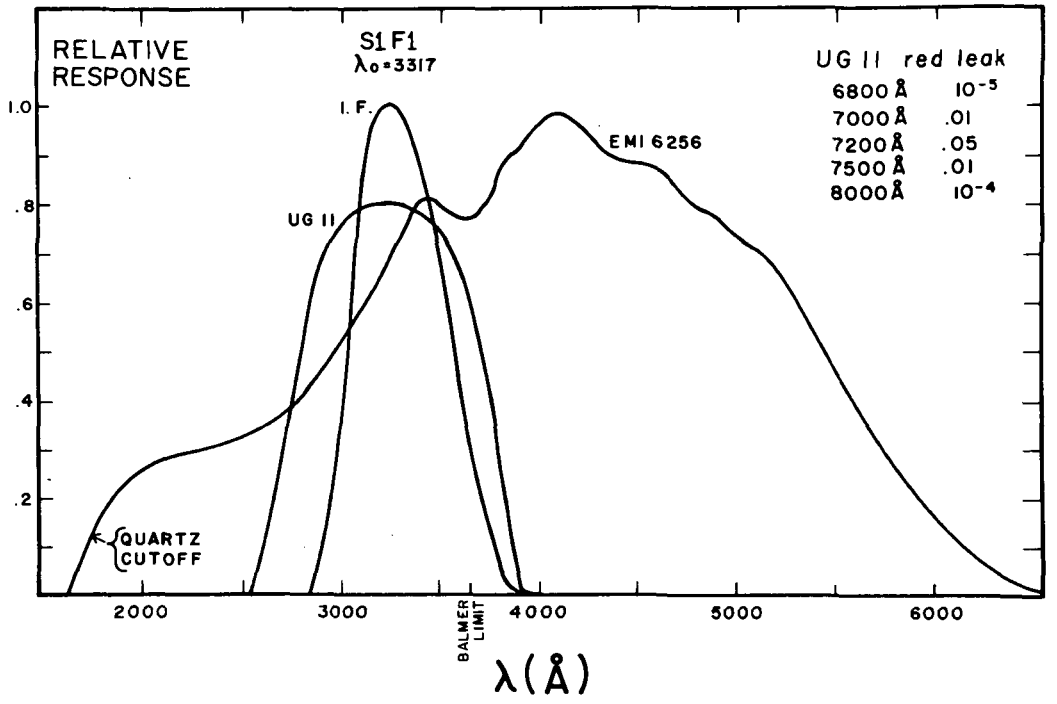

Figure 2.—Stellar 1 Filter (S1F1) optical element response versus wavelength.

b) Pinholes in the Interference Filter

The transmission longward of the maximum for a perfect filter would be determined by the transmission of the aluminum layers of the interference filter except as limited by tube and substrate bandwidth. The perfect filter longward transmission is of the order of 10^{-4} for the layer thickness employed. Pinholes which develop in the filter increase the transmission.

Laboratory tests have shown that longward filter transmissions after abrasion were 1.2×10^{-3} at 4037 Å and 9×10^{-4} at 5210 Å. It is assumed that these transmissions represent a worst case for any flight interference filter. Pinholes in Stellar 2 interference filters would have little effect towards the short wavelength end because of the EMI tube and fused quartz cutoff characteristics. However, pinholes on the S2F5 (2386 Å) filter having a longward wavelength "red leak" of the order of 10^{-3} could produce equal response from red leak as from the normal filter bandwidth for solar type stars. This is because these stars have a high concentration of red energy relative to the filter bandwidth energy. Just such a situation appears to have occurred for the S2F5 (2386 Å) filter. To a lesser degree the red leak has affected the S2F2 (2945 Å) filter and to a greater degree the S2F1 (2035 Å) filter. Red leaks have little effect on Stellar 1 because its interference filters are located at high energy red wavelengths. Red leaks have little effect on Stellar 3 and 4 because of bandwidth limitations of the ASCOP tubes.

The cause of pinholes has not been traced to the space environment since no time related degradation has as yet been found. The S2F1 (2035 Å) filter as was noted has been giving unreliable results on late type stars. Tests were made using a bright red giant star object while offsetting the WEP bore sight. These tests indicated that one half the filter transmits about 10 times the radiation that the other half does. This effect is not noticeable on early type stars and therefore suggests that it is the red leak that is variable across the filter surface. Perhaps a part of this filter has an abrasion or finger print that increased the transmission in the red tail.

c) Fluorescence and Calibration Slide Leaks

The only material that appears to fluoresce significantly is CaF_2. This affects S3F5 (1679 Å) but does not affect the CaF_2 substrate filters in Stellar 4 because the CsI photocathode is not sensitive to the wavelengths at which fluorescence occurs.

Two runs with the OAO spacecraft sun shade closed have allowed us to determine the effects of the Cerenkov source on filter biases. These dark count filter biases are summarized in Figure 3 for Stellar 3 and 4. When Stellar 3 F3 calibration is in front of the photomultiplier tube, we get approximately 16000 E4 counts primarily due to Cerenkov radiation with a small part due to Beta particles. When moved from F3 position to F4 the counts are due to Beta particles passing through shielding and hitting the photomultiplier window. Assume there are 6.8 E4 counts measured on dark above dark

noise. When moved further from window to F5 the Beta particles going to the photomultiplier window drop the count to 1.0 E4 counts; however, the CaF_2 substrate fluorescence with radiation detected by the photomultiplier produces an additional 33.8 counts. In position F1 the effect of the calibration position on the photomultiplier tube produces 0.5 counts. Finally when the calibration position is again adjacent to the window in F2 the counts rise to 5.3 E4 counts.

Stellar 4 is similarly interpreted with the same small asymmetry. When the calibration position is in F2, we get 8960 counts. Since this photomultiplier is not sensitive to radiation longward of about 1800 Å the Cerenkov radiation which comes from suprasil is very weak and the effect is mainly from Beta particles. It was necessary to use a much stronger radioactive source in this photometer for that reason. When the source is moved from the F2 position to F3 we get 10.8 counts from Beta particles on the photomultiplier window. When moved to F4 this drops to 2.0 counts. At the dark position F5 we assume 1 count is registered. Finally in position F1 the counts return to 10.4 E4 counts. Stellar 4 contains two interference filters with CaF_2 substrates; since the photomultiplier is not sensitive to radiation longward of 1800 Å the fluorescence is probably not measurable. There is also reason to believe according to notes made in testing that S3F5 has the interference coating out away from the photomultiplier. This may not be the case for the Stellar 4 filters. It was intended to insert all filters with the interference layers inward.

Figure 3.—E4 dark counts as function of calibration position.

d) Time Related Degradation

Only one filter shows a serious degradation with time; this is the Lyman alpha filter S4F4. A plot was made which shows filter data of several Orion stars taken over 10,000 orbits or 1.9 years. The relative magnitude of the S4F1 data is quite consistent over this period of time which bodes well for the consistency of all the optical elements used in this most ultraviolet sensitive photometer. The S4F4 filter output, however, has linearly decreased by a factor of 2.4 over this time period. This filter is the only filter with a

lithium fluoride substrate and has apparently developed color centers (F centers) from particle bombardment. Both Stellar 3 and 4 have cleaved LiF_2 windows and Stellar 3 has a polished LiF_2 Fabry lens, but apparently these LiF_2 components are protected by the filter wheel and structure from damage from particles. This degradation, being linear, is predictable and therefore usable for time related corrective constants on past and future observations with this filter. The continued reduction of filter sensitivity only limits its usefulness for dim objects.

VII. STATUS AND CONCLUSIONS

A general WEP status in mid-1971 (2-1/2 years after launch) is that reliable photometry can be obtained on faint late type objects with all 12 stellar filters except S2F1 (2035 Å), S2F5 (2386 Å) and S3F5 (1679 Å). Stellar 2 filter is becoming stuck more often than not, but may be left in a useful filter position. The nebular photometer is useful only for calibration slide data, and the Spectrometer No. 1 digital sensitivity has become unreliable. The Spectrometer No. 1 analog is fair, and the Spectrometer No. 2 analog and digital continue to provide extremely valuable original data and backup data for stellar readings. The digital sensitivity is proving to be a most valuable and accurate tool for faint type objects. The system response is constant enough that if careful dark and sky readings are taken, then photometry accurate to ±1 output count on E4 is possible at night well out of the South Atlantic Anomaly. Conservative estimates for total operations to mid-1971 based on reduced data are summarized below.

40,000 steps of each Stellar filter wheel drive motor;
30,000 gain changes involving an estimated 20,000 operations of each of the two gain relays in each Stellar photometer;
260,000 steps of each of the two scanning Spectrometer stepping motors;
1,000,000 data points from the four Stellars in Mode A;
500,000 data points from the two Spectrometers in Mode C.

This status and these quantities of mechanical operations and data observations achieved far outstrip the accepted standards used for evaluation of reliability prior to launch.

The conclusions which may be drawn from the WEP performance are many. The provision of a multiplicity of independent telescopes with overlapping spectral coverage has contributed to the long and continuing useful life of the WEP.

The space vacuum has produced <u>no</u> recognizable deterioration in WEP performance. While the WEP design avoided the use of known outgassing type materials, to the date of writing there have been no catastrophic failures of the unsealed mechanisms,

no positive degradation of the coated optics traceable to the space vacuum, and continued operation of the current layer by layer potted HVPS. The space vacuum would seem to have contributed to the usefulness of mechanisms far beyond their anticipated operational life. Thermal variations are known to affect photometry sensitivity and may contribute to aging but both effects are detectable from the calibration slide data and therefore are removable from both short and long term relative observational data. Thermal excursions probably contributed to some of the anomalies noted.

The space radiation of the South Atlantic Anomaly continues to limit the orbital time during which good data may be collected. The space radiation may also contribute to the aging process noted in calibration slide sensitivity degradation. The space radiation is the likely cause for the S4F4 lithium fluoride interference filter degradation. However, these short and long term effects are predictable and removable from the observed data.

Dr. A. D. Code, Dr. J. McNall and Dr. T. E. Houck of the University of Wisconsin Space Astronomy Laboratory have contributed significantly to this engineering report with facts, advice and encouragement. The work has been performed from support under NASA contract NAS 5-1348 to the University of Wisconsin.

REFERENCES

Boose-Allen Applied Research, Inc., June 1962, in "A Reliability Assessment of the University of Wisconsin Astronomical Experiment Package."

Bendell, Curtis B., June 1971, "Engineering Report on the Orbiting Astronomical Observatory Wisconsin Experiment Package." An internal University of Wisconsin Space Astronomy Laboratory document.

Code, A. D. et al. 1970, Ap. J. 161, 377.

THE UNIVERSITY OF WISCONSIN

OAO OPERATING SYSTEM

Harry C. Heacox and John F. McNall
The University of Wisconsin
Madison, Wisconsin

I. INTRODUCTION

In a volume dealing with the results and accomplishments of the Orbiting Astronomical Observatory OAO-2, it seems appropriate to consider also the problems connected with operating the spacecraft. This paper presents the Wisconsin OAO Operating System which consists of two parts: a computer program called HARUSPEX, which makes possible reasonably efficient and convenient operation of the Wisconsin Experiment Package (WEP) and the Wisconsin Ground Operations Equipment (GOE) which provides real-time status monitoring, commanding and a "quick-look" at the data.

II. THE CONTROL PROBLEM

OAO-2 is essentially a 24-hour-a-day observatory requiring considerable effort if it is to be used to the full extent of its capabilities. In the course of a single day's operation, WEP may observe as many as 20 targets (stars and sky background) though normally the number would be closer to 10. Each of these targets may require five to ten separate observing commands for a complete observation.

In addition to the obvious problems of choosing interesting objects for viewing, the astronomer must contend with certain restrictions. Observations must be scheduled so that they do not interfere with ground contacts. The high level of background illumination during the time when the spacecraft is in direct sunlight makes it desirable to avoid observing during these periods. The effects of the South Atlantic radiation anomaly are even more pronounced. Data taken in the anomaly are unusable and observations must not be scheduled at that time. There are physical restrictions on spacecraft motions and pointing. In moving from one target to another, no single slew may be longer than 30 degrees. Also, large slews take a

correspondingly longer time, which must be taken into account in the observing schedule. To protect the experiment optics, the spacecraft may not point within 45 degrees of the sun or anti-sun, even during a slew. Finally, targets must be chosen so that the solar paddles may be oriented to ensure adequate power input.

In view of the problems mentioned above, it is clear that spacecraft operation is a formidable task under the best of conditions. Of course, spacecraft degradation, particularly in the control and stability systems, makes the problem even more difficult. In order to cope with the task, some computer help is necessary. For this reason, HARUSPEX was written.

III. THE PROGRAM

HARUSPEX is a large, complex computer program intended for use by personnel who are not primarily computer-oriented. The emphasis throughout is on ease, simplicity and convenience of use. To this end, inputs to HARUSPEX are usually free-field, except where external considerations dictate use of a specific format for the input cards. Further, many of the parameters used in HARUSPEX and its subroutines can be assigned standard values. These parameters need to be entered into the program only when the user wishes to assign non-standard values. Also, many of the inputs, such as a request for punched output, are optional and need be entered only when desired. Finally, the sequence of input cards for a particular task is usually rather arbitrary. This approach has greatly reduced the frequency of trivial deck-structure and format errors.

On the output side, heavy use has been made of graphic output, in the form of printer plots rather than printed tables. Such plots, while of limited accuracy, are easier to read and interpret. Since the Support Computer Programming System (SCPS), to which the proposed WEP observing list is submitted, does very precise checking, any lack of accuracy due to the coarseness of a printer plot is not of great importance.

HARUSPEX resembles a very simple computer monitor system. The mainline program plays the part of the executive while major tasks are accomplished by means of large subroutines which are used in much the same way that a person might execute a FORTRAN compiler. In addition, HARUSPEX contains an extensive library of routines for "housekeeping," trigonometric manipulations, and other utility functions.

IV. THE SUBROUTINES

To give some idea of the large range of tasks which must be handled by HARUSPEX, a list of those subroutines which are most frequently used is given below, with a brief description

of each.

SORT allows the astronomer to search a catalog of more than 10,000 stars, selecting those entries which meet a given combination of user-specified criteria. Possible search criteria include the star's position in celestial coordinates, its position with respect to the sun, and various properties of the star, such as magnitude and spectral type. Stars meeting the given criteria may be printed out, punched on cards, written in a disk file, or any combination of these output modes. Typically, the astronomer uses SORT to narrow down the field and makes his final target selections by hand.

Subroutine MAP is used as an aid in scheduling observations. Given a list of stars, MAP produces a time based printer plot showing the following conditions:

(1) time and duration of ground contacts,
(2) time and duration of spacecraft night,
(3) time and duration of passage through the South Atlantic anomaly,
(4) period of time when each star is visible to the spacecraft, along with indications of whether the bore-sighted star tracker may be used, and whether the line of sight to the star intersects the sunny or dark earth when the star is occulted.

Plots begin at ETA for ground contacts at Rosman, Quito or Santiago and extend for 120 minutes. The user specifies the first contact to be plotted and the number of plots desired. An example of MAP output is given in the appendix.

Subroutine BLOTS is designed to aid the astronomer in choosing available areas of the sky for observing. It produces printer plots of the sky showing those areas which are occulted by the sun, moon, anti-sun and earth. The occulted areas are plotted as blocked-in regions, each with a different symbol. BLOTS also shows the areas at the poles of the orbit which are never occulted by the earth. Finally, the star tracker guide stars are plotted, each one denoted by the number assigned to it by SCPS.

In BLOTS, the user may specify the angular radii of the occulting objects, if desired. The time of the first plot, the time interval between plots, and the number of plots to be generated are also user-specified. An example of BLOTS output is given in the appendix.

Subroutine SLEW allows the user to evaluate proposed sequences of objects to be observed. Given a list of objects, SLEW takes them pairwise (i.e. the first and second, second and third, etc.) and computes the possible sequences of motions which will move the spacecraft from one to the other. Each sequence is checked to see that it does not approach too near the sun or anti-sun. The legal sequence, if any, with the shortest

total distance slewed is chosen and printed out.

At the destination, i.e. the second position of each pair, SLEW prints out the positions of the ends of the spectrometer slits, to aid in avoiding contamination of scans due to unwanted stars in the field of view. It also gives the spacecraft's orientation with respect to the sun, which gives the astronomer information concerning the power input to the solar arrays. At both origin and destination SLEW assumes that the spacecraft's orientation is optimum for power input.

Subroutine SATAN produces a latitude-longitude plot showing the position of the sub-satellite point as a function of time. The plot also gives the locations of the South Atlantic anomaly and the ground stations. SATAN plots up to five orbits per page. Each orbit begins at the ascending node. Points are plotted at user-specified time intervals from the node crossing. Digits are plotted for the daylight portions of the orbits and 'N' for the night portions. An example of SATAN output is given in the appendix.

Subroutine TRACK is used to give the astronomer information about the availability of tracker guide stars for a proposed orientation of the spacecraft. The output can be obtained as a printer plot or as a table. In the plot mode, an example of which is shown in the appendix, TRACK produces a plot of the sky showing the limits of the available field for each star tracker, plus the positions of the OAO guide stars. In print mode TRACK produces a table giving the zenith position of each tracker, the guide stars available to it, the rise and set times of each star, and the gimbal angles necessary to set the tracker on each star.

In addition to the astronomical routines, HARUSPEX contains several file-manipulating routines. These subroutines enable the user to build, sort, merge, edit and concatenate card-image disk files. Input from cards is also permitted in these operations. The presence of these routines makes it possible for the astronomer to create and modify observing programs without the handling of large card decks, thus greatly decreasing the probability of error. The disk files so constructed can, for example, be used as input to SORT, MAP, SLEW and TRACK, as well as to the subroutine which translates the observing program into binary codes and writes the tape which is submitted to the SCPS.

V. USING HARUSPEX

The fundamental task of HARUSPEX is the creation of the experimenters' target list (ETL), the proposed observation schedule. This is written on magnetic tape by subroutine TWERP and submitted to the SCPS for final checking. Since SCPS testing is much more detailed and extensive than that

afforded by HARUSPEX, the proposed ETL may be rejected, necessitating correction and re-processing. However, the basic sequence of events in HARUSPEX is quite simple.

The first step is to use MAP, SLEW and BLOTS to determine general sky conditions for a full week. This gives the astronomer some idea of which areas of the sky will be available (i.e. stable, unocculted, good power input, etc.) during the week. SORT gives a large list of stars located in these areas.

In the second step, the astronomer decides which stars should be observed and the sequence in which they will be viewed. The file-manipulating routines are then used to place these stars and appropriate command sequences in a data file. Commands are usually taken from a file of standard sequences, depending upon the magnitude and spectral type of the star. Non-standard commands can be entered from cards. MAP is then used to determine specific times for the various motions and command sequences. These are entered in the schedule using the file-handling routines. SLEW and TRACK are then run to check for gross violations of spacecraft constraints.

In the final phase, any re-ordering, time changes, etc., indicated by the MAP, SLEW and TRACK runs are made. Finally, TWERP is used to write the proposed ETL, which is then submitted to the SCPS.

VI. THE MONITOR REQUIREMENT

The results of the command and control system (HARUSPEX) will be reflected in the spacecraft motions and data collected. Status having to do with the spacecraft itself is monitored by the main control center equipment while experiment data is handled by the experimenters' equipment. It is necessary to know that all requested commands were executed properly since correct observatory operation builds on the past sequence of events. It is also desirable that the astronomer have a quick look at his data since it may influence his future planning.

VII. THE SYSTEM

In order to satisfy these requirements, the Wisconsin GOE was constructed. The heart of the system is a small computer, a PDP-8, with a 32,000 word disk for storage of data. As shown in Figure 1, this machine has a number of peripheral devices attached to it. The data input is from a serial-to-parallel converter driven by telemetry bit synchronizers. This allows the computer to read each spacecraft word as it is received in the NASA control center. The status display panel is used to show the latest equipment status received. This display, used in conjunction with the predicted status panel, gives an immediate check on the gross functioning of

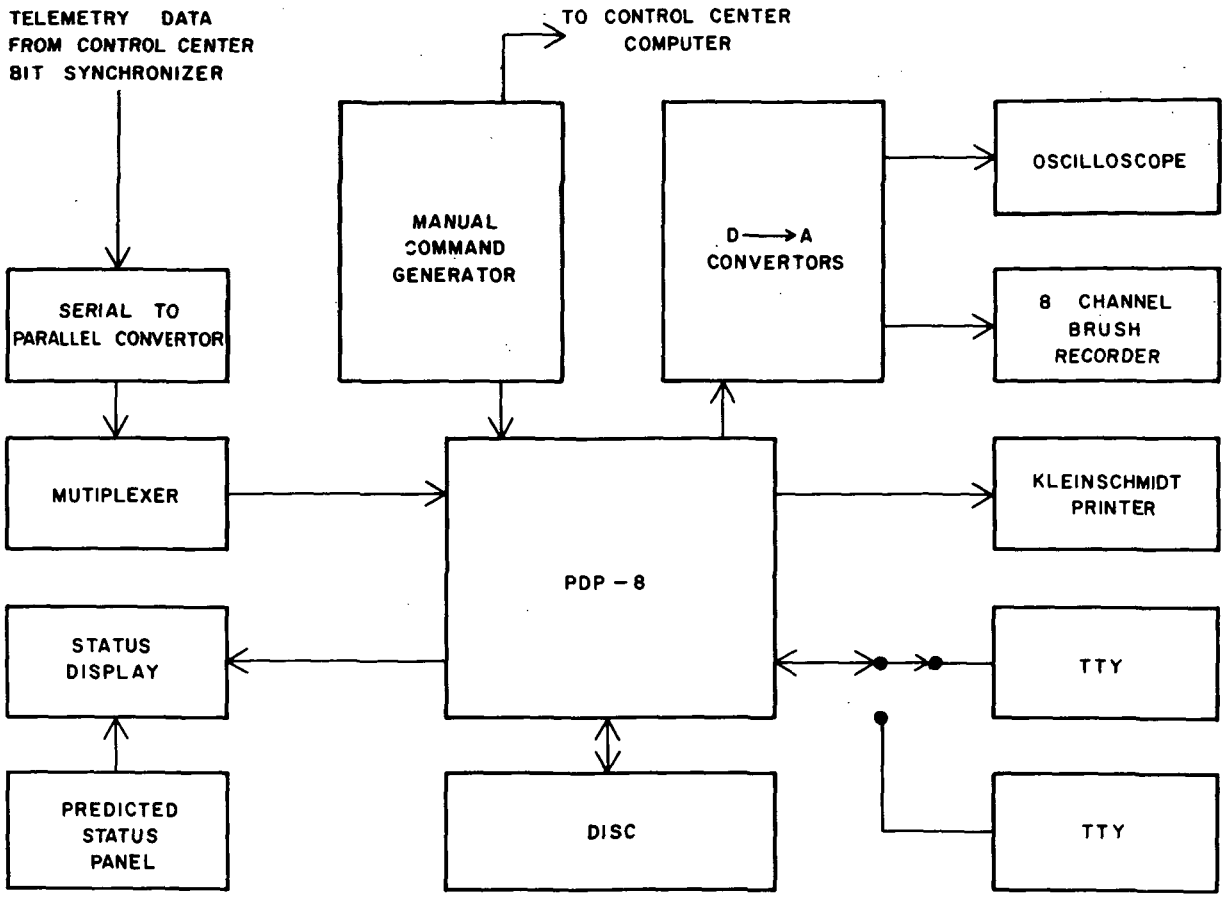

FIGURE 1. GOE BLOCK DIAGRAM

the equipment.

The recorder provides a permanent record of data signals and status voltages while the printer gives a hard copy of the data that was stored in the spacecraft memory and is temporarily stored on the PDP-8 disk. The teletype is used by the console operators to call in various phases of the processing and to override automatic processing that may be going on.

There is also a manual command generator whose function is to allow commands for the Wisconsin experiment to be generated and executed by the spacecraft on a real-time basis. This is used only in emergencies but is very valuable when needed.

VIII. THE PROGRAM (REPTILE)

The operating program for the GOE was written by Mr. Terrel L. Miedaner and is built around a flexible monitor system operating under interrupt control. Several different types of data may come down from the spacecraft and the program must recognize the pertinent experiment data from the structure of the telemetry frame. This is done and all real-time status frames are displayed and sent to the chart recorder while any data storage dump is stored on the disk for later processing.

The teletype and command generator are monitored constantly while data analysis and printout are taking place if a data storage dump has been received. The monitor allows the operator to call for reprocessing of the data, reassignment of chart recorder channels, replay of data to try other possible formats, and various logging and time correlation functions.

The programs necessary to perform the service requested by any particular interrupt are rolled in from disk to the small core of the PDP-8 making this system a time-shared control computer system. The telemetry handling programs are resident in core necessitated by the high speed of data input (50KC).

It should be noted that all of the components of the spacecraft control center are represented here but in a very parochial sense in that we are concerned only with the experiment equipment on the spacecraft and therefore can concentrate on a small portion of the total monitoring problem just as the OAO control center does not concern itself with other satellites.

On a project as large as the OAO it is difficult to make judgments about the value of parts of a system but it is clear that the OAO observatory could not have functioned successfully without both the HARUSPEX control program and the Wisconsin GOE including REPTILE.

The authors would like to thank Carol S. Burkhalter, who wrote TWERP, and Terrel L. Miedaner who wrote REPTILE and parts of MAP and SLEW.

REFERENCE

Heacox, H. C. 1970, M. S. Thesis, University of Wisconsin.

APPENDIX

```
..RUN PLOTS  NOAPORT
COMMENT     ************************************************************
COMMENT     * PLOTS RUN TO SHOW SKY CONDITIONS AT BEGINNING AND END OF *
COMMENT     * NIGHT FOR MIDDLE OF WEEK.                                 *
COMMENT     * LEGEND:                                                   *
COMMENT     *     E = DARK EARTH                                       *
COMMENT     *     / = SUNNY EARTH                                      *
COMMENT     *     . = SUN                                              *
COMMENT     *     ~ = ANTI-SUN                                         *
COMMENT     *     ) = MOON                                             *
COMMENT     *     P = CIRCLES ABOUT POLES OF THE ORBIT WHICH ARE NEVER  *
COMMENT     *         OCCULTED BY THE EARTH                            *
COMMENT     * GUIDE STARS ARE INDICATED BY THEIR ASSIGNED NUMBERS,     *
COMMENT     * WITH THE RIGHT-MOST DIGIT MARKING THE STARS' POSITIONS.  *
COMMENT     ************************************************************
BEGIN AT    263 04 02
DELTAT           1
MAX NUM         32
NUM SETS    1
RADII       45.0   74.0   10.0
START
```

```
..RUN MAP
COMMENT     ************************************************************
COMMENT     * THE NEW FILE IS USED AS INPUT TO MAP, WHICH IS RUN FOR   *
COMMENT     * THE ENTIRE DAY.  THE OUTPUT CAN THEN BE USED FOR MANUAL  *
COMMENT     * SCHEDULING OF OBSERVATIONS.                              *
COMMENT     * LEGEND:                                                  *
COMMENT     *     N = SPACECRAFT NIGHT                                 *
COMMENT     *     ~ = SPACECRAFT DAY OR STAR OCCULTED BY DARK EARTH    *
COMMENT     *     A = SOUTH ATLANTIC ANOMALY                           *
COMMENT     *     / = STAR OCCULTED BY SUNNY EARTH                     *
COMMENT     *     G = STAR UNOCCULTED AND BORE-SIGHT TRACKER USABLE    *
COMMENT     *     X = STAR UNOCCULTED AND BORE-SIGHT TRACKER NOT USABLE *
COMMENT     *     R = ROSMAN GROUND CONTACT (GROUND CONTACT LINE)      *
COMMENT     *     O = ORRORAL GROUND CONTACT                           *
COMMENT     *     M = MADAGASCAR GROUND CONTACT                        *
COMMENT     *     Q = QUITO GROUND CONTACT                             *
COMMENT     *     S = SANTIAGO GROUND CONTACT                          *
COMMENT     ************************************************************
FILE IN     20
INITIAL      1
START
```

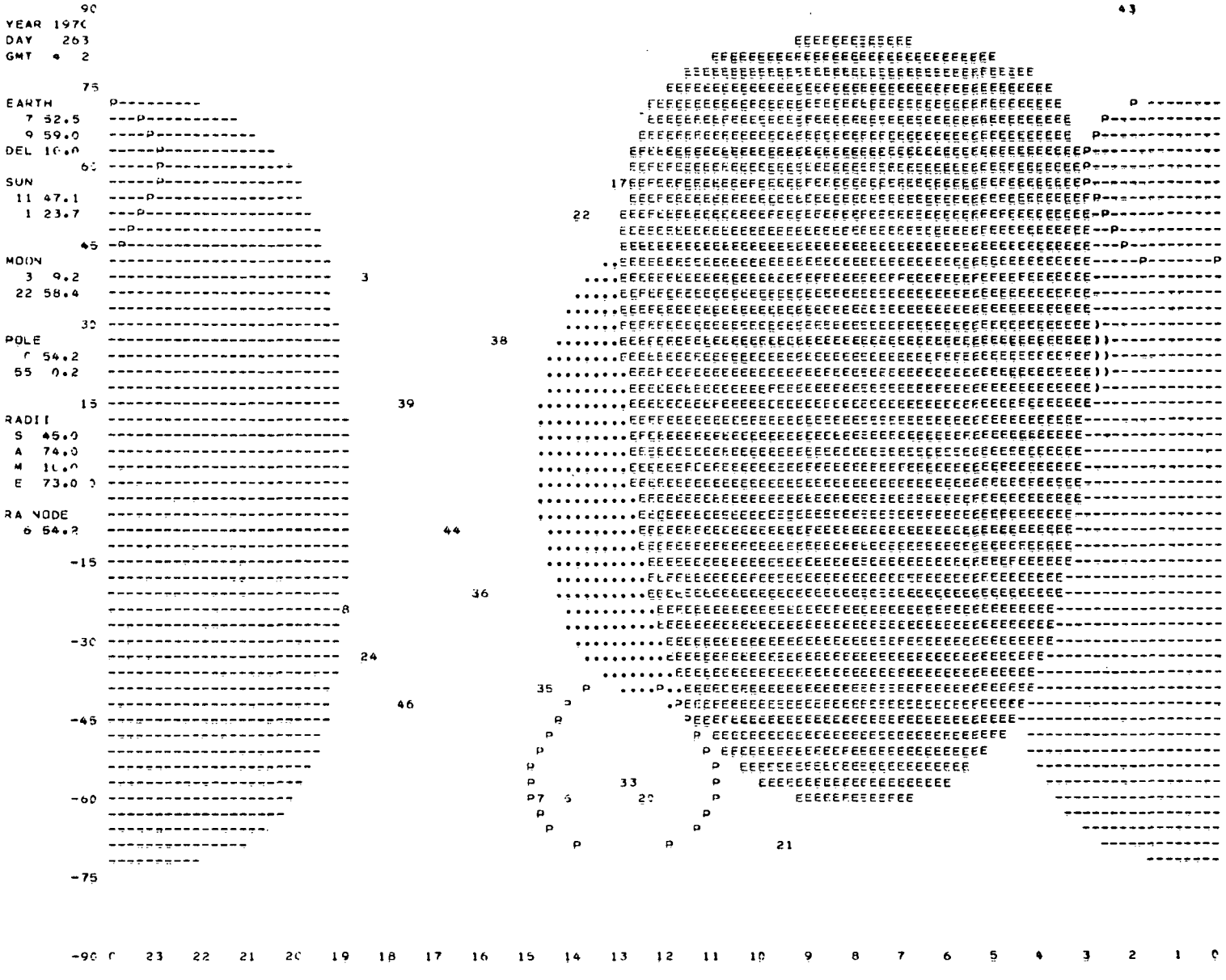
90
YEAR 1970
DAY 263
GMT 2
75
EARTH
7 52.5
9 59.0
DEL 10.0
60
SUN
11 47.1
1 23.7
45
MOON
3 9.2
22 58.4
30
POLE
6 54.2
55 0.2
15
RADII
S 45.0
A 74.0
M 10.0
E 73.0
RA NODE
6 54.2
-15
-30
-45
-60
-75
-90
0 23 22 21 20 19 18 17 16 15 14 13 12 11 10 9 8 7 6 5 4 3 2 1 0
43
38
39
44
36
24
46
35
33
22
21
17

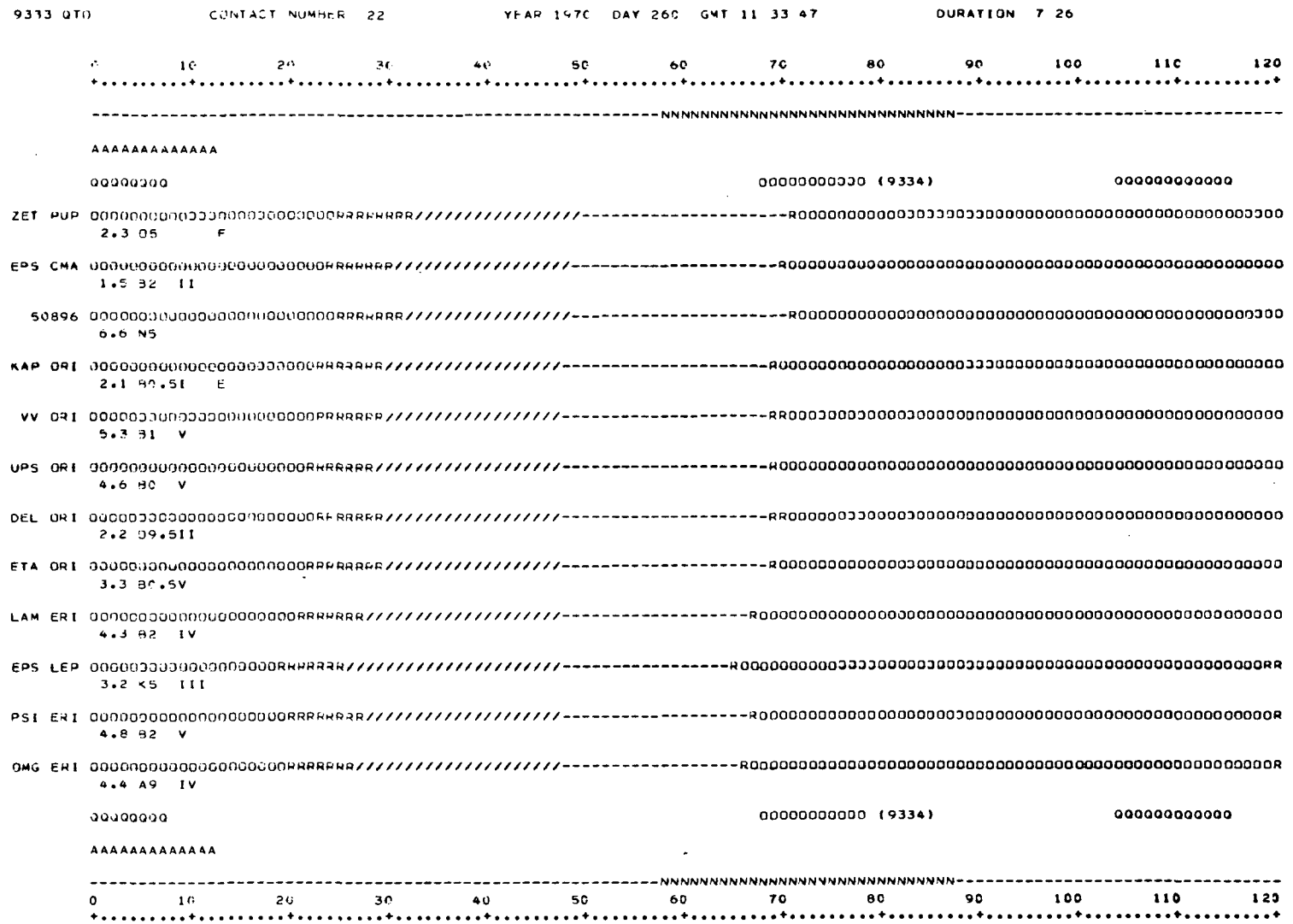
9333 QTO CONTACT NUMBER 22 YEAR 1970 DAY 260 GMT 11 33 47 DURATION 7 26
0 10 20 30 40 50 60 70 80 90 100 110 120
ZET PUP
2.3 05 F
EPS CMA
1.5 32 II
50896
6.6 N5
KAP ORI
2.1 80.5I E
VV ORI
5.3 31 V
UPS ORI
4.6 80 V
DEL ORI
2.2 09.5II
ETA ORI
3.3 80.5V
LAM ERI
4.3 82 IV
EPS LEP
3.2 <5 III
PSI ERI
4.8 82 V
OMG ERI
4.4 A9 IV
(9334)
(9334)

S EPS CMA
6 50.7
-28 53.9
R -32.607
YEAR 1970
DAY 260
GMT 1 21
TRACKER 1
6 57.0
-29 53.9
TRACKER 2
18 56.4
28 51.9
TRACKER 4
2 5.7
28 9.2
TRACKER 5
10 28.4
47 33.7
TRACKER 6
22 28.5
-47 26.5
90
75
60
45
30
15
0
-15
-30
-45
-60
-75
-90
0 23 22 21 20 19 18 17 16 15 14 13 12 11 10 9 8 7 6 5 4 3 2 1 0

SATAN PLOT FOR ORBITS 9330 THROUGH 9334.

KEY TO ORBIT NUMBERS

SYM	ORBIT	TIME AT ASC NODE	SUNSET	SUNRISE
1	9330	1970 260 5 1 44	260 5 50 19	260 6 20 59
2	9331	1970 260 6 41 51	260 7 30 26	260 8 1 7
3	9332	1970 260 8 21 59	260 9 10 34	260 9 41 15
4	9333	1970 260 10 2 6	260 10 50 41	260 11 21 22
5	9334	1970 260 11 42 14	260 12 30 49	260 13 1 30

LONGITUDE SCALE IS 3 DEGREES PER COLUMN, LATITUDE SCALE IS 3 DEGREES PER LINE.
POINTS ARE PLOTTED AT INTERVALS OF 2.0 MINUTE(S) FROM EACH ASCENDING NODE, WITH THE FIRST POINT AT THE NODE.

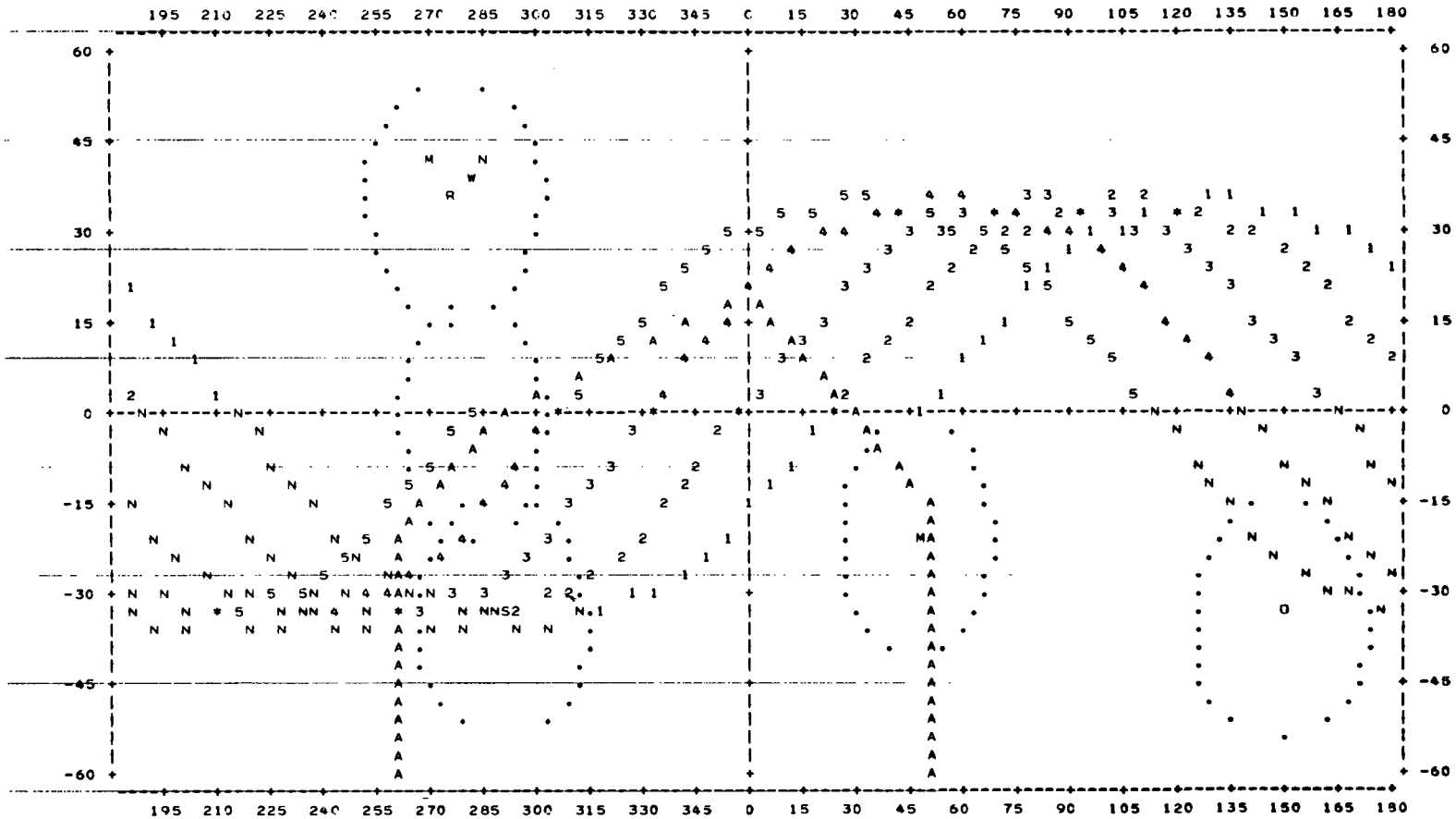

MEASUREMENTS OF THE EARTH'S AIRGLOW IN THE VACUUM ULTRAVIOLET

C. R. Waters and E. S. Fishburne
Grumman Aerospace Corporation
Bethpage, L. I., New York

ABSTRACT

A valuable by-product of the OAO-2 Astronomy Mission has been the first extensive set of measurements of the earth's airglow between 1000 and 3000 Å. These measurements, made with the Wisconsin Experiment Package, provide clues to the structure and chemistry of the upper atmosphere. The most significant results from these observations are (1) the detailed altitude profile of the emissions from the dark and sunlit earth limb and (2) the confirmation of recent theories concerning the source of the dayglow radiation between 1350 and 1700 Å.

I. INTRODUCTION

The term "airglow" has commonly been used to describe the non-thermal upper atmospheric emissions not correlated with magnetic disturbances. The study of this radiation provides information on the nature of the upper atmosphere and gives clues to the physical processes occurring there. The spectral region below 3000 Å is one of the most informative wavelength intervals, but because of the opacity of the atmosphere in this part of the spectrum, knowledge of these ultraviolet emissions can only be obtained by rocket and satellite observations. To obtain more information about the earth's airglow in the ultraviolet, measurements were made of the dark and sunlit earth using the photometers of the OAO-2's Wisconsin Experiment Package (WEP). These measurements used the 2980, 2380, 1920, 1500, 1380 and 1250 Å filters of WEP Stellar Photometers 3 and 4. The highly accurate pointing capability and the small field of view of the WEP photometers have made it possible to define precisely the measurement geometries. This

unique capability has produced a set of unique measurements of the earth limb.

This paper describes how the measurements were made and gives some of the reduced results in terms of the earth's radiance and emission profiles for both the sunlit and dark atmosphere. These results are shown to be in good agreement with other experiments and help to substantiate recent theories on the sources of the ultraviolet airglow.

II. VIEWING GEOMETRY AND INSTRUMENTATION

WEP measurements of the earth's airglow were made at several different times during the 1970-1971 year. The bulk of the measurements were made over a three day period (June 10 through June 13, 1970) on 27 different orbits. Additional measurements were made whenever possible during times when the astronomy mission would not be impacted. The experiment was operated in two basic modes. In Mode C, used in most of the observations, the scanning spectrometer controlled the data sampling interval, 9 seconds, and enabled us to make a series of 188 exposures which covered a time period of approximately one half hour. The exposures were of either 1/8, 1 or 8 second duration. The EDHE Cyclic Store Mode was used to obtain detailed measurements of the earth limb. In this mode, the data is sampled every 1/2 second and up to 2-1/2 minutes of continuous measurements can be stored.

All observations were made by inertially fixing the OAO pointing and exposing during the time the desired portion of the earth moved through the field of view. The position of the OAO relative to the earth during a typical measurement sequence is depicted in Figure 1. The three positions of the OAO shown in the figure correspond to the position at the beginning, middle and end of a half hour measurement sequence. Note that the measurements are initially of the dark earth, then the sunlit earth and finally of the sunlit limb. Also note that the amount of sunlit atmosphere being viewed increases as the earth moves across the field of view. Figure 2 indicates the ground track for this same orbit. The shaded area indicates the portion of the earth in darkness. The short dark path across the terminator indicates the ground track of the OAO field of view during the measurement period. This viewing situation is typical of those made during the first set of observations.

III. DATA ANALYSIS

The variation of the received radiation as the viewing area scans across the earth during a typical measurement sequence is shown in Figures 3-5. In each of these sequences, the OAO field of view initially moves across the dark earth onto the

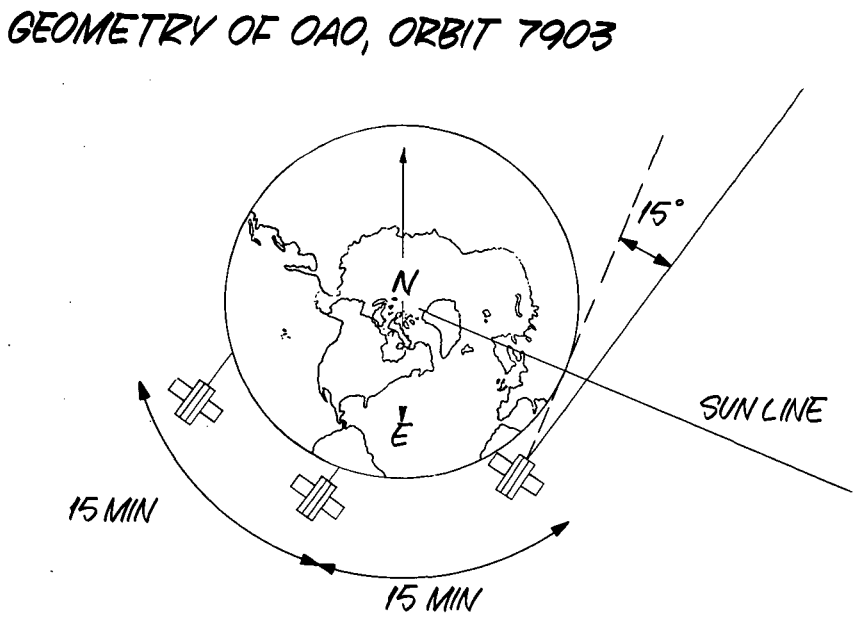

Figure 1.

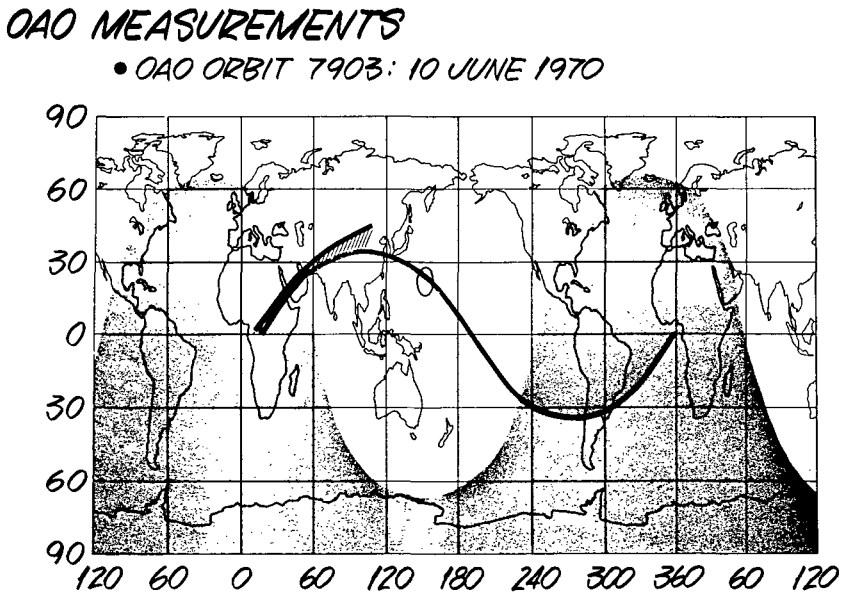

Figure 2.

sunlit earth and then off the earth through the sunlit limb and onto the star. Figure 3 indicates the radiation received by the 1250 Å photometer and Figure 4 represents that received by the 1920 Å photometer during the measurement sequence. These two curves provide an interesting comparison. Radiation in the 1250 Å region appears to reach a maximum value after the field of view has left the surface of the earth. This peak occurs at a tangent altitude of about 210 kilometers. On the other hand, the 1920 Å photometer indicates that as the field of view moves away from the earth's surface, the radiation begins to decrease rapidly. Figure 5 shows the radiation received by the 1500 Å photometer during a later orbit. This radiation also peaks at a tangent altitude of about 210 km.

These measurements have been reduced to the case where both the viewing and the sun lie along the local zenith. Figure 6 shows this reduced data in terms of earth's radiance as well as the results of other experiments. Also shown is our calculation of the expected radiance based on a Rayleigh scattering model. Obviously, the only measurements that agree with the Rayleigh scattering prediction are those in the 1920 Å spectral band which also agree with earlier measurements by others (Barth and Mackey 1969, Elliott et al. 1967). Of particular interest is the spectral region covered by the 1500 Å filter. The measurements in this spectral region agree with the data from the NRL experiment on OGO IV and clearly indicate that the "large dip" in the earth's radiance predicted by Rayleigh scattering does not exist.

The high level of radiation in the 1500 Å region is believed to be the result of electronic excitation of molecular nitrogen by high energy photoelectrons. These photoelectrons are produced from the ionization of high altitude atmospheric constituents by the extreme ultraviolet solar radiation. The principal emissions are from the Lyman-Birge-Hopfield, Birge-Hopfield and Vegard-Kaplan bands of N_2 and cover the spectral region from 1350-1800 Å. This mechanism was first considered theoretically by Barth and Green (1964), Dalgarno et al. (1969) and later refined by Prinz and Meirer (1971) of NRL. Their calculations predict radiation levels that are in general agreement with the data. They also indicate that a peak in the volume emission rate of the atmosphere should exist near 180 km. Results of the detailed measurements of the sunlit limb, shown in Figure 7, indicate that the received radiation in the 1500 Å wavelength region reached a maximum value when the tangent altitude was approximately 210 km. This implies that the volume emission rate also peaks at about 210 km. Note also in this figure that the radiation in the 1900 Å region shows no peak as a function of tangent altitude. The 1250 Å filter also shows a peak at 210 km which may partially be caused by the molecular nitrogen emissions. At present

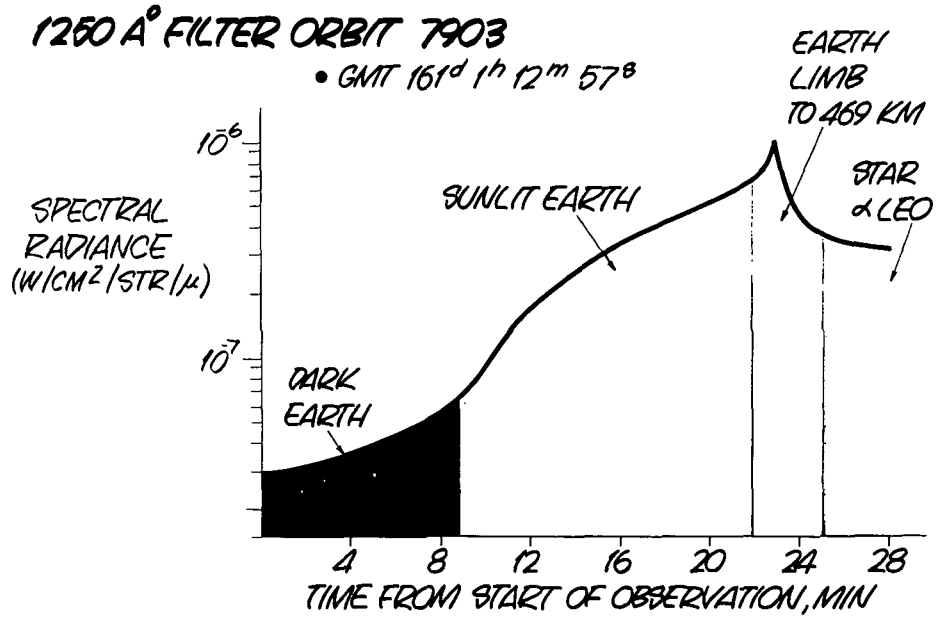

Figure 3.

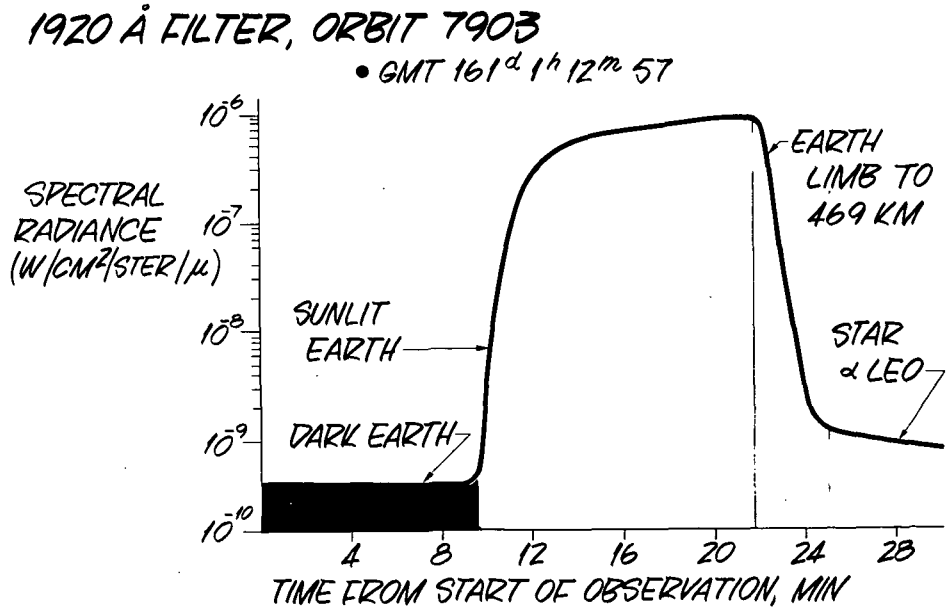

Figure 4.

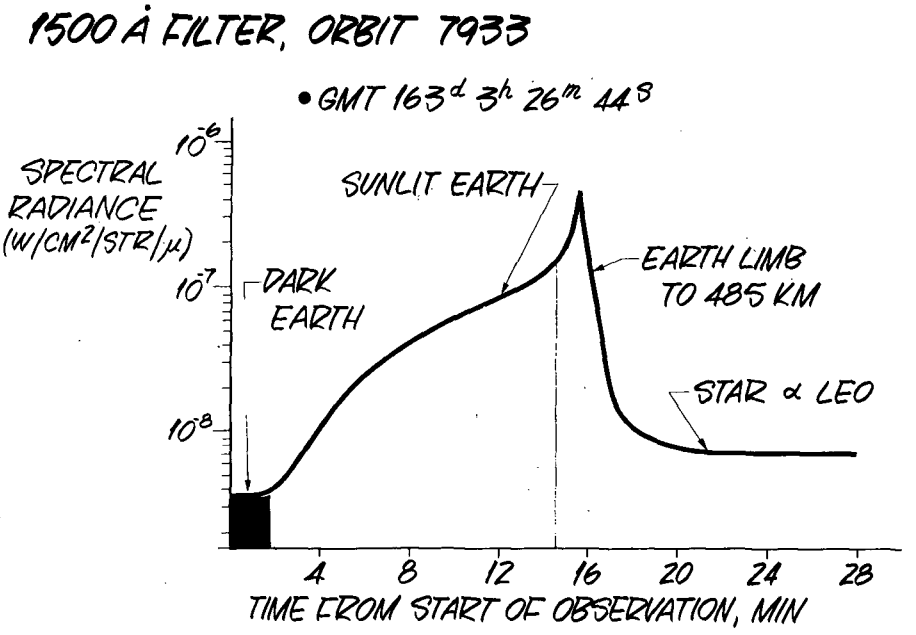

Figure 5.

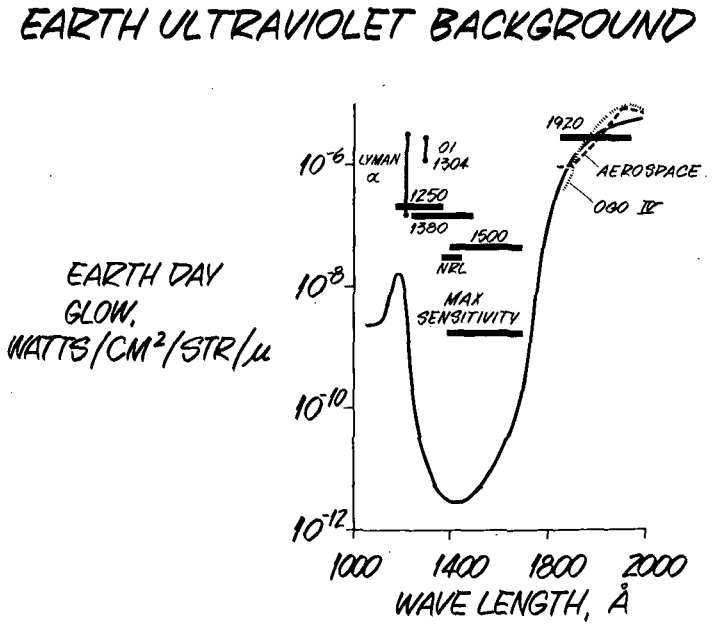

Figure 6.

these measurements are being reduced to terms of volume emission rates. Also being investigated are the implications of the emission peak being at an altitude that is higher than expected.

The tangent altitude profiles of the received radiation from the dark limb are shown in Figure 8. The radiation measured by the 2980 Å filter shows a sharp peak in emission at an altitude of approximately 100 km. The level and peak of the radiation agrees well with that measured by Stecher (1965) and Hennes (1966) and can be attributed to the Herzberg band system of molecular oxygen and the trans-auroral line of O I at 2972 Å. The 2380 Å filter also shows the peak occurring in the same region and is therefore probably measuring the same emissions from O_2. From this figure we also see that the radiation in the 1900 Å region peaks near 70 km. The source of this radiation is currently being investigated.

The radiation measured by the 1250 Å filter shows no variation with altitude and has an equivalent earth's radiance of approximately 10^{-8}w/cm^2-ster-μ. The radiation in the 1500 Å region was at or below the noise level of the detector.

IV. CONCLUSIONS

The OAO measurements indicate the magnitude and altitude profile of dayglow emissions between 1000 and 2000 Å. These measurements tend to support the theory that the radiation between 1300 and 1700 Å is produced by photoelectron excited molecular nitrogen. The nightglow measurements show no detectable emissions between 1700 and 1300 Å and a low level intensity at 1200 Å which is independent of altitude. The prominent feature in the ultraviolet nightglow appears to be the emissions of the Herzberg bands of O_2 in the 2000-3000 Å region.

The OAO results provide a unique part of the picture that describes the earth's ultraviolet airglow. The accurate pointing capability of the OAO spacecraft and the small field of view of the WEP provide the detailed resolution previously not available. The small field of view limits the size of the atmospheric area from which radiation is being received. The diameter of this area is 8 km at the 200 km tangent altitude point and decreases in size the closer the line of sight is to the local zenith. Thus it is possible to measure the spatial variations of the atmospheric emissions with a resolution far better than any previous experiment. The accurate pointing capability of the OAO results in an uncertainty in the tangent altitude of less than 1 km. This pointing capability, in addition to the small FOV, makes it possible to obtain volume emission rates from scans of the earth limb. Other experimenters could not do this confidently. It is hoped that further measurements can be made that will give information on the effects

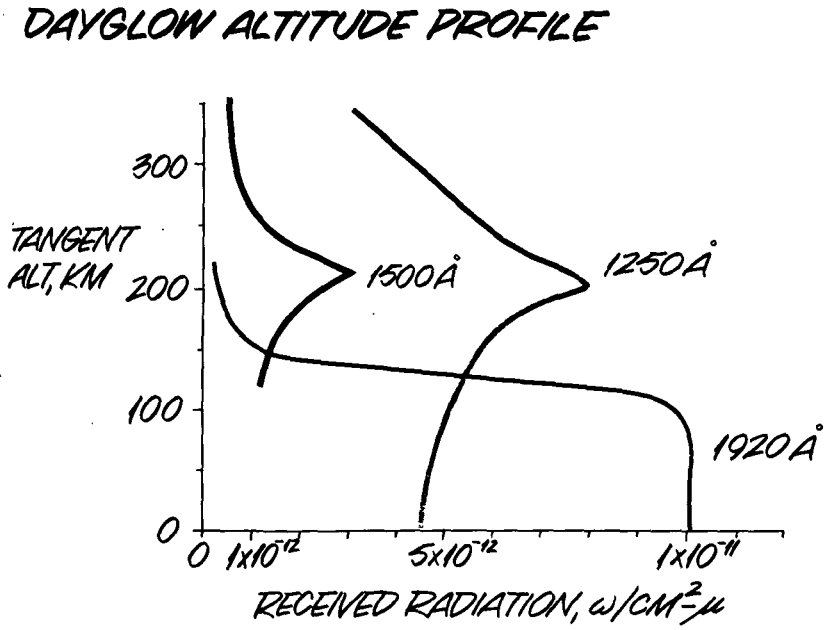

Figure 7.

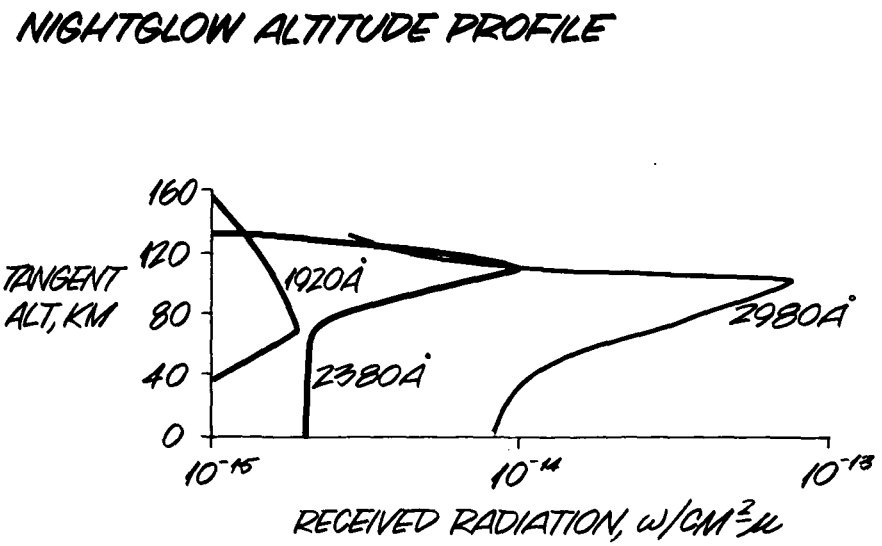

Figure 8.

of solar activity and seasonal variations.

We greatly appreciate the opportunity afforded us by the National Aeronautics and Space Administration Headquarters, NASA Goddard Space Flight Center, and the University of Wisconsin in making this data available. We would especially like to thank Mr. J. Purcell, Dr. A. D. Code, Dr. T. Houck, Dr. M. Molnar and Dr. A. Holm for all their help and cooperation.

REFERENCES

Barth, C. A. 1964, J. Geophys. Res. 69, no. 15, 3301.
Barth, C. A. and Mackey, E. F. 1969, IEEE Trans. Geo. Elec. vol. G.E-7, no. 2, 114.
Barth, C. A. and Schaffner, S. 1970, J. Geophys. Res. 75, no. 22, 4299.
Chamberlain, J. W. 1961, Physics of the Aurora and Airglow (New York: Academic Press).
Chubb, T. A. and Hicks, G. T. 1970, J. Geophys. Res. 75, no. 7, 1290.
Dalgarno, A., McElroy, M. B. and Stewart, A. I. 1969, J. Atmos. Sci. 26, 753.
Elliott, D. D., Clark, M. A. and Hudson, R. D. 1967, Aerospace Report No. TR-1058 (3260-10).
Fastie, W. G., Crosswhite, H. M. and Heath, D. F. 1964, J. Geophys. Res. 69, no. 19, 4129.
Green, A. E. S. and Barth, C. A. 1967, J. Geophys. Res. 72, no. 15, 3975.
Green, A. E. S. 1967, The Middle Ultraviolet; Its Science and Technology (New York: John Wiley and Sons).
Green, A. E. S. and Wyatt, P. J. 1965, Atomic and Space Physics (Reading: Addison-Wesley).
Hennes, J. P. 1966, J. Geophys. Res. 71, no. 3, 763.
Rawcliffe, R. D. and Elliott, D. D. 1966, J. Geophys. Res. 71, no. 21, 5077.
Prinz, D. K. and Meirer, R. R. 1971, J. Geophys. Res. 76, no. 19, 4608.
_____ 1971, private communication.
Stecher, T. P. 1965, J. Geophys. Res. 70, no. 9, 2209.
Winter, W. and Chubb, T. A. 1967, J. Geophys. Res. 72, no. 21, 4405.

Page intentionally left blank

TERRESTRIAL ATMOSPHERIC COMPOSITION FROM STELLAR OCCULTATIONS

P. B. Hays
University of Michigan
Ann Arbor, Michigan

R. G. Roble
National Center for Atmospheric Research[1]
Boulder, Colorado

A. N. Shah
University of Michigan
Ann Arbor, Michigan

ABSTRACT

Stellar ultraviolet light transmitted through the upper mesosphere and lower thermosphere of the earth's atmosphere is primarily affected by the photoabsorption processes of ozone and molecular oxygen. The stellar ultraviolet photometers aboard the OAO-2 satellite have measured the intensity changes of several stars during occultation of the star by the earth. The measurements of the relative intensity change in certain atmospheric absorption bands are used to recover the vertical number density profiles of the absorbing species. Using the OAO-2 occultation data, we have obtained the vertical number density profiles of molecular oxygen in the 100-200 km altitude region and ozone in the 60-100 km altitude region.

I. INTRODUCTION

In the earth's upper atmosphere, stellar ultraviolet light is strongly absorbed in the Schumann-Runge continuum of molecular oxygen and the Hartley continuum of ozone. By monitoring

[1]The National Center for Atmospheric Research is sponsored by the National Science Foundation.

the intensity of ultraviolet starlight in these continuum regions, as the star is occulted by the earth (Fig. 1), we are able to obtain information on the number density distribution of molecular oxygen in the lower thermosphere and ozone in the upper mesosphere (Hays and Roble 1968a,b). In this paper, we describe the technique used to obtain the number density distributions from stellar occultation measurements. The data were obtained by the Wisconsin Stellar photometers aboard the Orbiting Astronomical Observatory (OAO-2) satellite.

We discuss the inversion process and also show the molecular oxygen and ozone distributions determined from a typical occultation scan.

II. OCCULTATION TECHNIQUE

The occultation technique utilizes the principles of classical absorption spectroscopy to determine the number density distribution of the absorbing species in the upper atmosphere. This is illustrated in Figure 1, where the star is a source of ultraviolet light and the OAO stellar photometers are the detectors with the atmosphere between acting as the absorption cell.

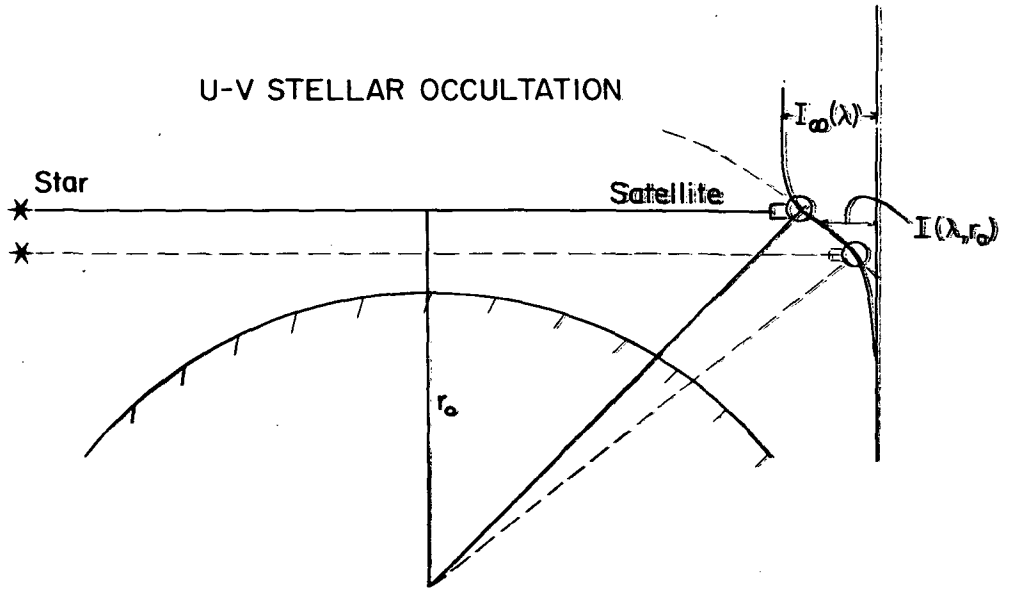

Figure 1.—Geometry of ultraviolet stellar occultation.

The occultation occurs when the air mass between the detector and the star increases such that ultraviolet light is relatively absorbed in spectral regions where molecular oxygen and ozone have large absorption cross-sections. The intensity of

the transmitted ultraviolet light is related to the tangential column number density of the absorbing species by Beer's law,

$$I(\lambda, r_0) = I_\infty(\lambda) \exp\left[-\sum_i \sigma_i(\lambda) \cdot N_i(r_0)\right] \quad (1)$$

where $I_\infty(\lambda)$ is the unattenuated intensity of the star, at wavelength λ, above the atmosphere, $\sigma_i(\lambda)$ is the absorption cross-section of the i^{th} absorbing species, $N_i(r_0)$ is the tangential column number density of the i^{th} absorbing species at a tangent ray height, r_0. The intensity of the star is measured using the OAO ultraviolet spectrometer. By also knowing the absorption cross-section, one can relate the tangential column number density to the intensity of the transmitted ultraviolet light. Ideally, the best results are obtained if the ultraviolet wavelength is chosen such that a single species dominates the absorption process.

Once the tangential column number density of the absorbing species is known, then it is a simple problem to invert the data and obtain the vertical number density distribution of the absorbing species. A simple geometrical argument shows that the tangential column number density for a spherically stratified atmosphere can be written as

$$N_i(r_0) = 2 \int_{r_0}^{\infty} \frac{n_i(r)\ r\ dr}{\sqrt{r^2 - r_0^2}} \quad (2)$$

where $n_i(r)$ is the number density of the i^{th} absorbing species at radius r. Equation (2) is an Abel integral equation (Hays and Roble 1968a,b) easily inverted to give the number density of the absorbing species at tangent ray height r,

$$n_i(r) = \frac{d}{dr}\left\{-\frac{1}{\pi}\int_r^{\infty} \frac{r}{r_0} \frac{N_i(r_0)\ dr_0}{\sqrt{r_0^2 - r^2}}\right\} . \quad (3)$$

Thus, the stellar occultation technique can be used to obtain the vertical density distribution of any absorbing atmospheric species which can be spectrally isolated.

Hays and Roble (1968b) calculated the tangential ultraviolet transmission of the earth's upper atmosphere. Their results show that the strong absorption of O_2 in the Schumann-Runge continuum near 1500 Å and of O_3 in the Hartley continuum near 2500 Å are both spectrally isolated regions where the stellar ultraviolet absorption is primarily due to a single species. The absorption cross-section of both molecular oxygen and ozone at these wavelengths has a peak of around 10^{-17} cm^2. Therefore, we are able to determine the distribution of these species near

altitudes where the tangential column number density is approximately $N_i \sim 10^{17} cm^{-2}$. If a spectral region away from the peak cross-section is utilized, one is able to observe higher tangential column number densities or equivalently measure the number density at lower altitudes within the atmosphere. In order to illustrate the altitude regions applicable, the tangential transmission of stellar ultraviolet light is shown in Figure 2 for the earth's atmosphere at various tangent ray heights (Hays and Roble 1968b). Here a black body energy distribution was assumed and the unattenuated energy spectrum is shown as the upper curve in Fig. 2. The CIRA 1965 model atmosphere was assumed to represent the vertical number density distributions of the various atmospheric species and the ozone density is assumed to be that calculated by Hunt (1966). The ultraviolet light in the wavelength interval 1400-1600 Å is absorbed primarily by molecular oxygen in the 130-230 km altitude range. In the wavelength interval 2400-2600 Å, the ultraviolet light is absorbed primarily by ozone in the 60-100 km altitude range.

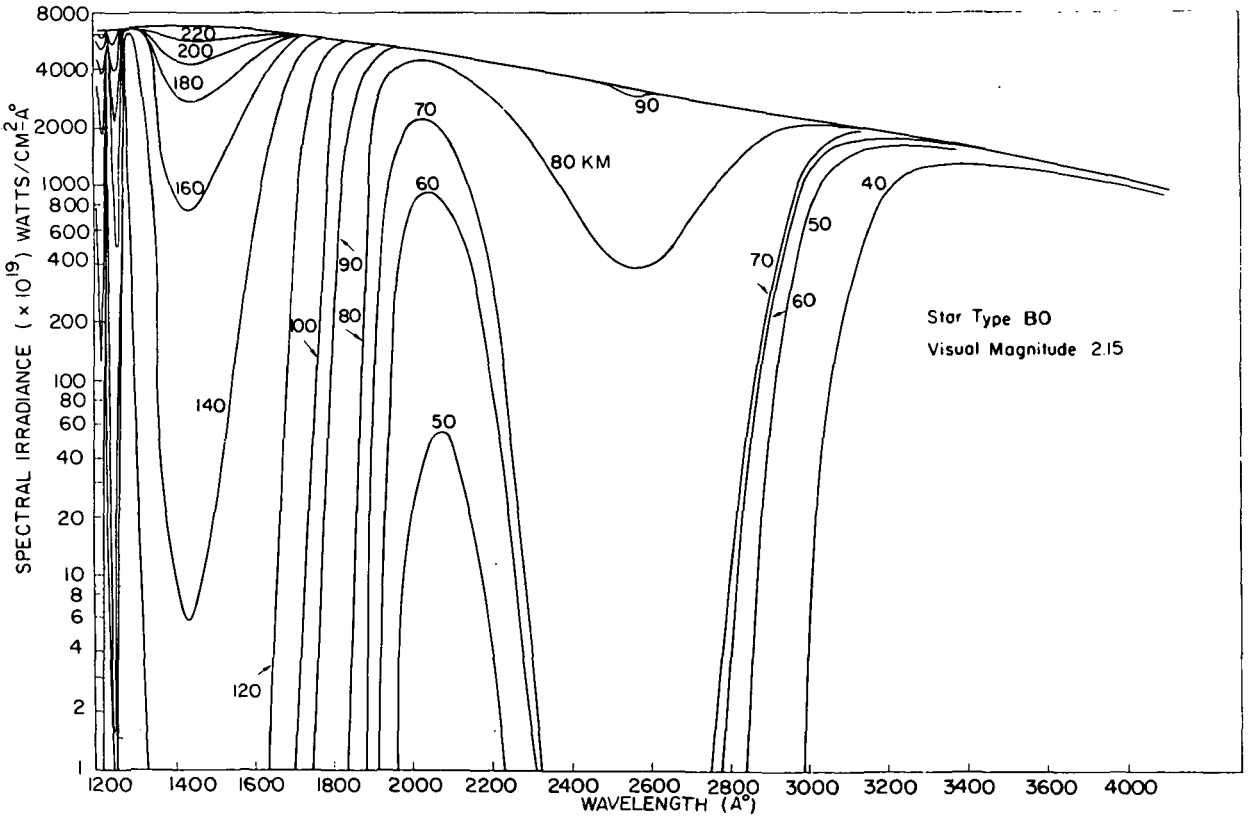

Figure 2.—Ultraviolet stellar spectra for a class B0 star at various tangent ray heights during occultation. Attenuation due to molecular oxygen absorption, ozone absorption, and molecular scattering (Hays and Roble 1968b).

III. OBSERVATIONS

The OAO-2 satellite has tracked several occulting stars, monitoring the intensity change of the star with the Wisconsin stellar photometers. The filters of interest in the Wisconsin package are those located in the Schumann-Runge continuum of molecular oxygen near 1500 Å and the Hartley continuum of ozone near 2500 Å. Figure 3 shows the normalized intensity data obtained during a single occultation from three stellar photometers having filters centered at 1500, 1920 and 2380 Å. The normalized intensity in this figure is plotted as a function of time; however, by knowing the star's position and the satellite orbital elements, we are able to relate time to the tangent ray height of the occulting star. The normalized intensity in the molecular oxygen channel is seen to decay first due to absorption at a high altitude. Next, the intensity in the 1920 Å channel decreases; however, it is difficult to utilize the data

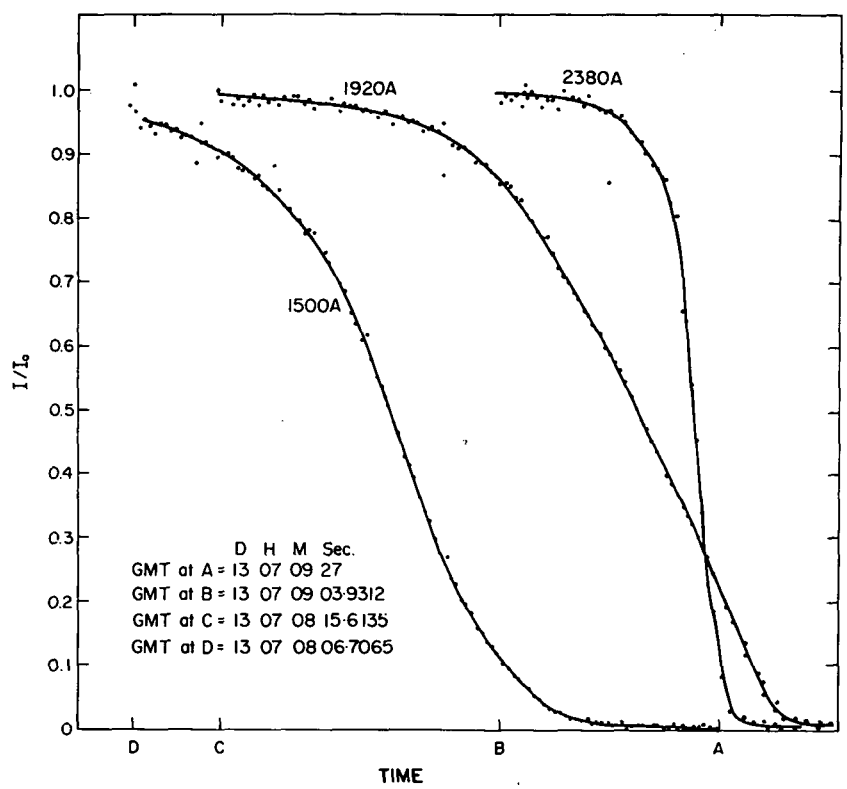

Figure 3.—Normalized intensity of a star during occultation as a function of time. The curves correspond to the intensity measured in the 1500, 1920 and 2380 Å channels of the Wisconsin stellar photometers aboard the OAO-2 satellite.

in this channel to obtain information on the atmospheric composition because of the complex absorption in the Schumann-Runge band system. Lastly, the intensity in the 2380 Å channel decays rapidly in the altitude region where ozone absorption becomes important. The quality of the data obtained by the OAO-2 stellar photometers is excellent allowing detailed structure to be obtained. The data in the 1500 Å channel were inverted and the results are shown in Figure 4 where the molecular oxygen number density profile is shown as a function of height. In addition, the molecular oxygen distributions for the average and low exospheric temperature models of Colegrove et al. (1966) are shown for comparison. The data obtained on 13 January 1970 agree

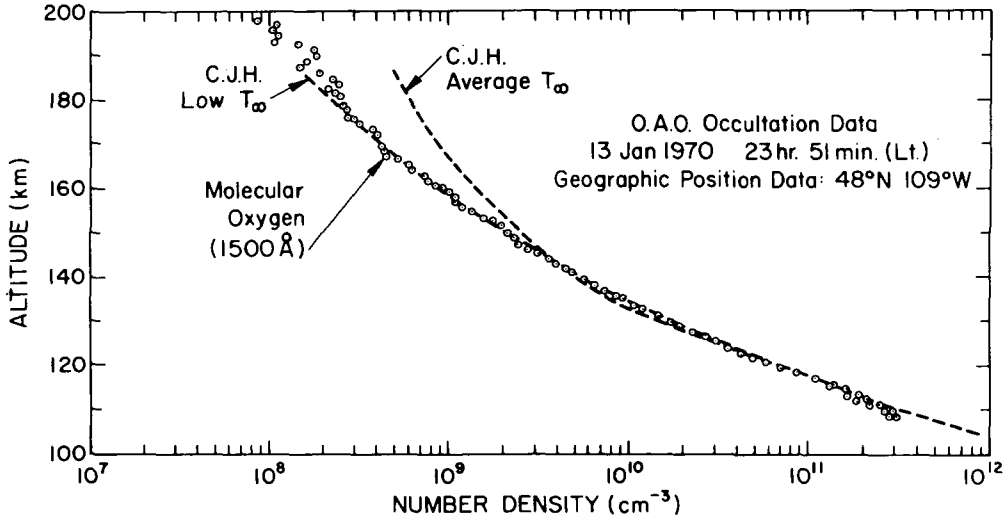

Figure 4.—The number density distribution of molecular oxygen determined from stellar occultation measurements. The models used for comparison are discussed in the text.

with the low exospheric temperature model. The temperature distribution in the lower thermosphere computed from the molecular oxygen number densities, assuming diffusive equilibrium, is shown in Figure 5. The data are compared to the high and low exospheric temperature models as determined by Colegrove et al. (1966). These data are only a sample of the approximately 20 stellar occultation scans which have been reduced thus far and they illustrate the quality of the data which is obtained from the occultation measurements.

Most of the ozone scans obtained with the 2380 and 2460 Å filters aboard the OAO-2 satellite have a normalized intensity scan which is similar to the one shown in Figure 6. In this figure, the intensity of the star in the 2380 Å channel is

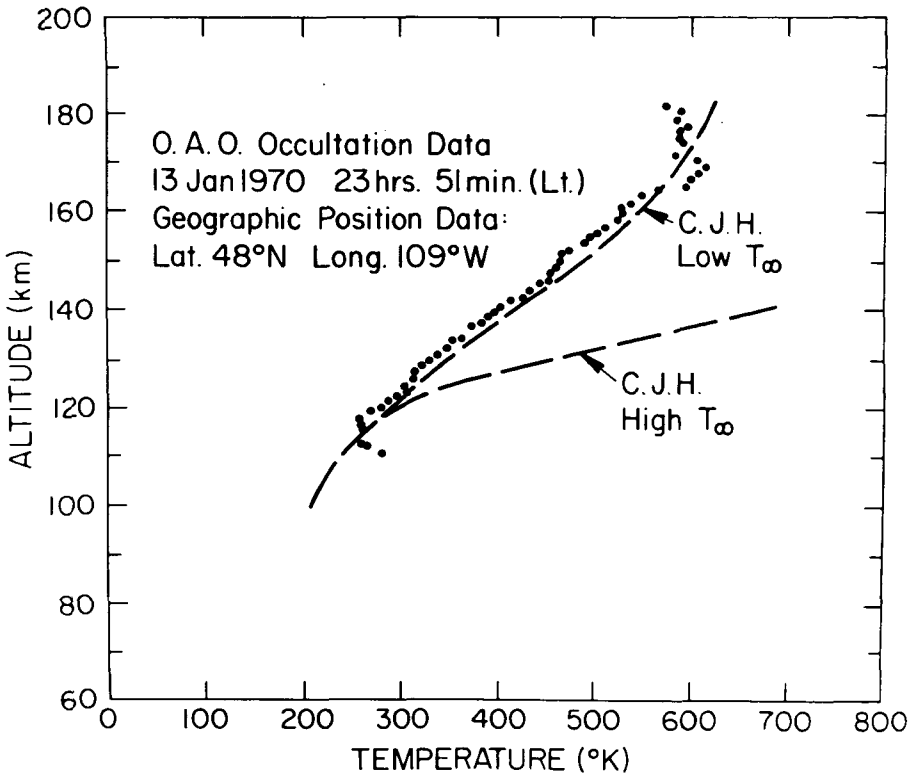

Figure 5.—The temperature distribution in the lower thermosphere determined from the molecular oxygen number density distribution assuming diffusive equilibrium.

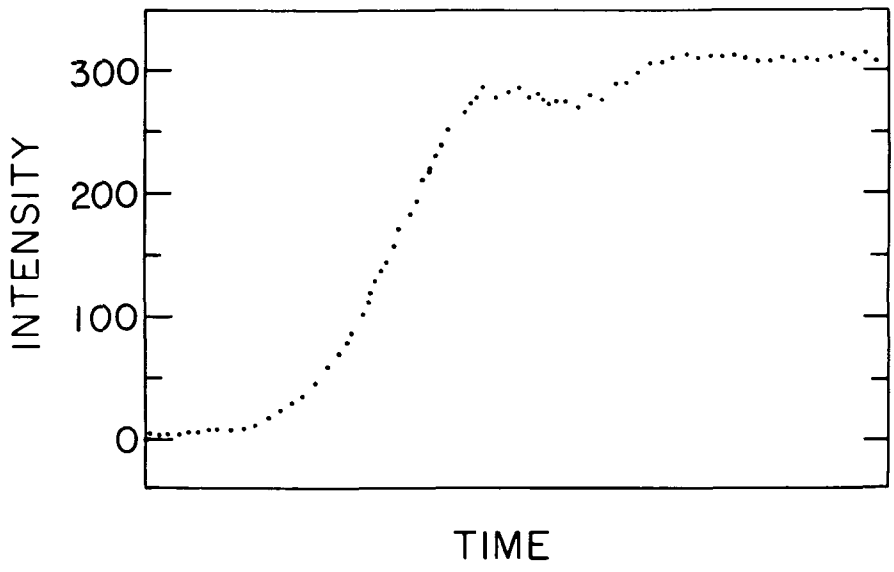

Figure 6.—The measured intensity in the 2380 Å channel of the Wisconsin stellar photometer as a function of time for a star rising from occultation.

plotted as a function of time, or equivalently tangent ray height, for a star rising from occultation. The signal increases as the star rises above the atmosphere until a dip in the intensity curve occurs at a tangent ray height near 90 km. These data, when inverted, give the number density distribution of ozone which is shown in Figure 7. The dip in the measured intensity curve is caused by a bulge in the nighttime ozone number density distribution with the peak occurring near 90 km and a minimum of near 80 km for this particular scan. The stellar occultation measurements clearly define the structure of the nighttime ozone distribution at high altitudes where no previous

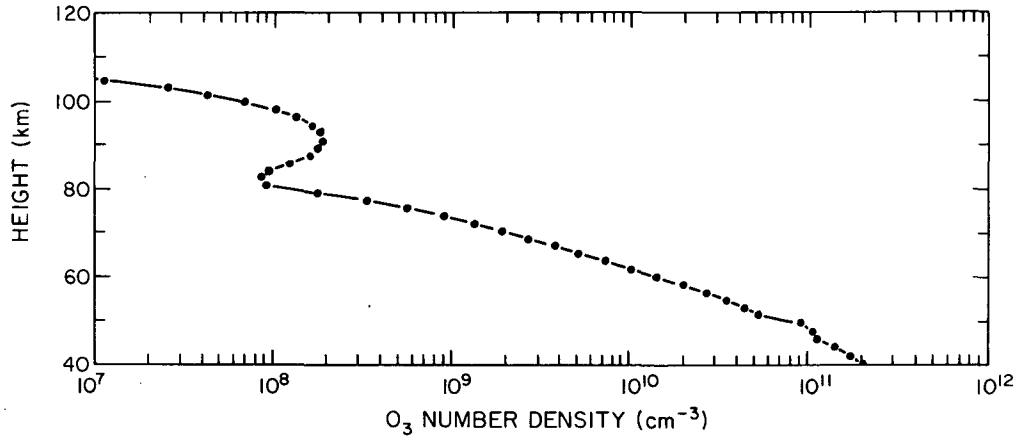

Figure 7.—The ozone number density distribution determined from the intensity scan shown in Figure 6.

measurements existed. These data are important in the study of the ozone photochemistry in the upper mesophere.

IV. DISCUSSION

The OAO-2 occultation data obtained with the Wisconsin stellar photometers have been used to obtain high quality data on the nighttime distribution of molecular oxygen and ozone in the earth's lower thermosphere and upper mesosphere. So far, the feasibility of the stellar occultation technique in obtaining information on atmospheric composition has been demonstrated. However, with the growing number of occultation scans, we are beginning to analyze the scans for information on seasonal variations, geomagnetic storm effects and latitudinal and longitudinal variations. With the stellar occultation data, a considerable amount of information will be obtained about the earth's own upper atmosphere in addition to the prime OAO mission of determining the ultraviolet properties of stars.

REFERENCES

Colegrove, F. D., Johnson, F. S. and Hanson, W. B. 1966, J. Geophys. Res. 71, 2227-2235.
Hays, P. B. and Roble, R. G. 1968a, Planet. Space Sci. 16, 1197-1198.
_____ 1968b, J. Atmos. Sci. 25, 1141-1153.
Hunt, B. G. 1966, J. Geophys. Res. 71, 1385-1397.

Page intentionally left blank

A COMPARISON OF SURFACE BRIGHTNESS MEASUREMENTS FROM OAO-2 AND OSO-6

F. E. Roach
Rutgers University and
Battelle Pacific Northwest Laboratories

C. F. Lillie
University of Colorado
Boulder, Colorado

ABSTRACT

A comparison of surface brightness measurements of the night sky from the OAO-2 and OSO-6 satellites with ground observations shows good agreement between the space experiments but a systematic error in the zero point of the ground observations, indicating an additional atmospheric source of radiation.

I. INTRODUCTION

Ground-based measurements of the surface brightness of the night sky are complicated by extinction and scattering by the troposphere and airglow emissions from the ionosphere. Observations from space vehicles avoid these difficulties but may, in turn, be complicated by sunlight scattered into the instrument and by a time-dependent radiation-belt induced dark current.

In this paper we compare surface brightness measurement of the same sky regions obtained from space with the Wisconsin Experiment on OAO-2 and the Rutgers Experiment on OSO-6. Such a comparison serves as a check on the performance and calibration of each instrument, and, by virtue of the independence of the readings, adds confidence in the combined result.

This preliminary study is based on a few such measurements near the galactic center.

II. INSTRUMENTATION

The two instruments and the spacecraft which support them vary greatly both in design and mode of operation. Their one common feature is the ability to record the surface brightness of the sky background from above the earth's atmosphere. Their characteristics are summarized in Table 1.

Table 1. Summary of Experiment Characteristics

Characteristic	OAO-2	OSO-6
Orbital Information		
Launch Date	December 7, 1968	August 9, 1969
Mean Altitude	776 km	528 km
Period	100.13 min	95.1 min
Eccentricity	0.00073	0.00475
Instrument		
Angular Field	10 arc min	2 degrees
Field Area	0.0218 sq. deg	3.14 sq. deg
Filters	12 in interval 4250-1050 Å	4000, 5000, 6100 Å (±200 Å)
Polarization Measurement	No	Yes
Measurements Made	During satellite night	During satellite day

The Wisconsin experiment (Code et al. 1970) was designed for the photometry of bright stars at twelve wavelengths in the 1000-4000 Å spectral region. It is carried by the OAO-2 spacecraft which is stabilized in three-axes and can be pointed to a discrete region of the sky with an accuracy of ±1 arc minute. The OAO has no capability for continuous sweeps across the sky.

The Rutgers experiment was designed for precise polarimetry of the zodiacal light at 4000, 5000 and 6000 Å. It is located in the wheel section of the OSO-6 spacecraft which is spin-stabilized at 30 rpm with its axis of rotation nearly perpendicular to the ecliptic plane. As the wheel turns, the sky brightness is measured at five degree intervals from 180° to

±10° solar elongation. In the course of a year, a band of sky along the ecliptic several degrees wide is swept by the OSO photometer.

The two instruments complement each other in the sense that one scans the sky continuously in a narrow band around the sky while the other obtains single point measurements over the entire sky. The instruments have a bandpass in common at 4000 Å and, for sky regions which both have observed, provide continuous wavelength coverage from 1050 to 6300 Å.

III. OBSERVATIONS

a) The OAO-2 Photometer

The observing program for the Wisconsin experiment is controlled by an astronomer on the ground who selects discrete objects for study and programs the spacecraft to obtain the appropriate measurements. Most of the observing time has been devoted to spectrophotometry and multi-color photometry of stars, planets and galaxies. Surface brightness measurements have been made (1) as off-sets from the stars to determine the sky background correction, (2) by observations of the Kaptyen Selected Areas and (3) by observations of particular regions of the sky such as the ecliptic and galactic poles.

A typical observing sequence with one of the four stellar photometers consists of nine measurements: two dark readings, a calibration reading and two measurements with each of the photometer's three interference filters. The sequence requires from 24 to 32 minutes depending on the integration times used and takes up a complete spacecraft night.

b) The OSO-6 Photometer

The Rutgers photometer is automatically programmed to make a sequence of readings from which the brightness, degree of polarization, plane of polarization and degree of ellipticity of the sky background light can be determined at 4000, 5000 and 6100 Å. During a given rotation of the satellite wheel sky readings are made for a given arrangement of filter and analyzer wheels at three solar elongations (i.e., -195°, -190°, -185°). After five rotations the analyzer-filter combination is changed and another set of readings is obtained. Ninety wheel rotations or about three minutes are required to record data for all 18 combinations of filter and analyzer settings (three filter and six analyzer positions). This procedure is then repeated for three new elongations (i.e., -180°, -175°, -170°). For elongations ±60° to ±10° the filter-analyzer combination is changed every rotation. The photometer continues to make observations all around the orbit, as long as the

satellite is in daylight. In one orbit a total of 5256 sky readings are made. To date more than 11,000 orbits have produced about 58 million sky observations. In this report we concentrate on some 950 individual readings from 95 orbits selected for the purpose of effecting a general comparison between the OSO and OAO instruments.

III. THE SKY REGION UNDER STUDY

The problem of the intercomparison of the two sets of observations is illustrated in Figure 1. The solid line represents the ecliptic in galactic coordinates in the general vicinity of the galactic center (galactic latitude, $b_{II} = 0$; galactic longitude, $l_{II} = 0$). OSO-6 observations are made along the ecliptic (at an elongation of 180°) as the sun moves approximately one degree per day and, since, further, there are about 15 orbits per day, there are 150 individual readings between the 10-day markers in Figure 1. The parallel dashed lines represent the region raked over by four other solar elongations during 1970. We note that elongation 175° involves an observational sweep across the galactic center direction.

The circles on Figure 1 indicate regions of the sky which have been included in the OAO program, usually as sky background measurements near planets. On the scale of the figure, the OAO field (1/6°) is approximately equal to the thickness of the ecliptic line; the OSO field is about twice the size of the circles.

Figure 2 illustrates the nature of the seasonal variation in surface brightness along the ecliptic for observations made in the anti-solar (gegenschein) direction. The gegenschein itself may be considered as a constant background superimposed on which is the highly variable contribution from the integrated starlight. The plot was made on the basis of published ground observations, omitting any contribution from airglow. During May, June and July (orbits 4000 to 5500 for OSO-6 during 1970) the bright region of the Milky Way in the vicinity of the galactic center is traversed. Thus a natural photometric band of variable brightness is at our disposal for comparing (a) the separate experimental results against the published ground data and (b) the two experimental results against each other.

IV. A COMPARISON OF GROUND AND SPACE OBSERVATIONS

The relationship between pairs of some ground observations of sky brightness and space observations of the same regions are shown in Figure 3. In the upper diagram the 5000 Å data from OSO-6 has been compared with the expected sky brightness due to the zodiacal light (Smith et al. 1965) plus integrated

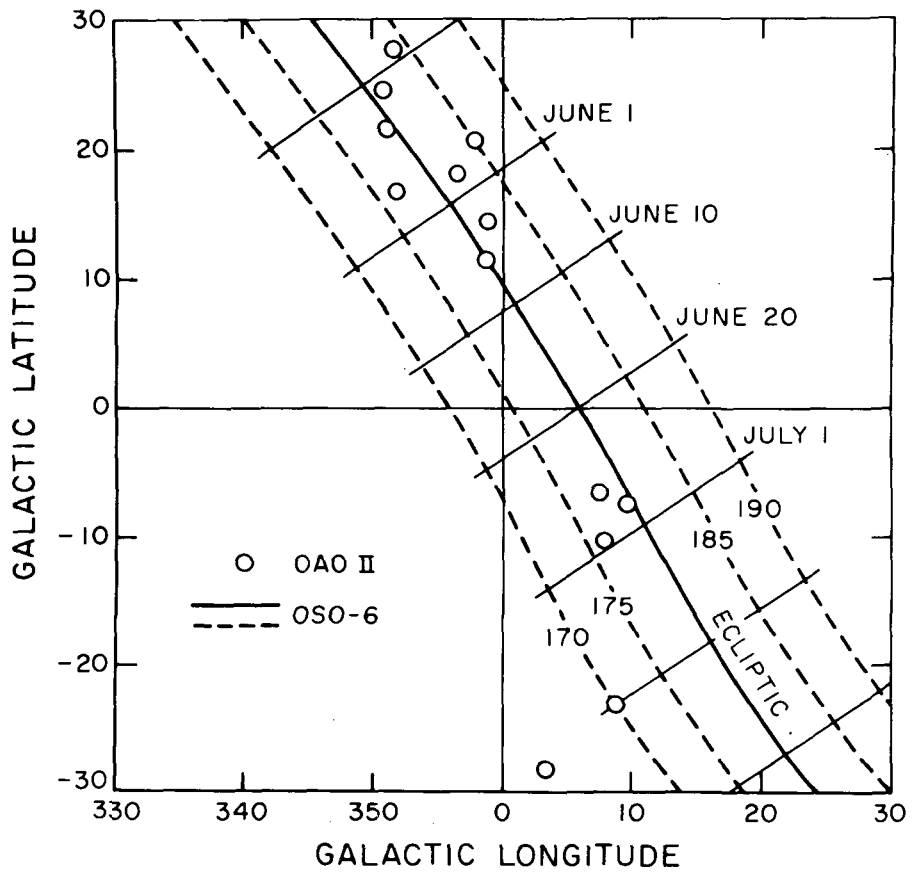

Figure 1.—The sky regions observed by OSO-6 and OAO-2 in galactic latitude and longitude.

starlight (Roach and Megill 1961) at 5300 Å. In the lower diagram the 4250 Å data has been compared with the sky brightness predicted by the zodiacal light observations of Smith, assuming $S_{10}(B) = S_{10}(V)/1.69$ (Roach and Smith 1964) and the GR 43 star counts for the Kapteyn Selected Areas (Van Rhijn 1925), assuming $S_{10}(B) = 0.903\ S_{10}(pg)$.

An examination of the data reveals a linear relationship between the ground and space observations with a scatter which probably represents real fluctuations in the star background intensity. The slopes of the lines provide a check on the instrumental calibration. For both instruments the slope is in excellent agreement with that predicted from star observations and the nominal field of view.

In both cases the intercept is such that ground-based photometry shows a residual sky brightness when the satellite measurements go to zero. This is consistent with previous

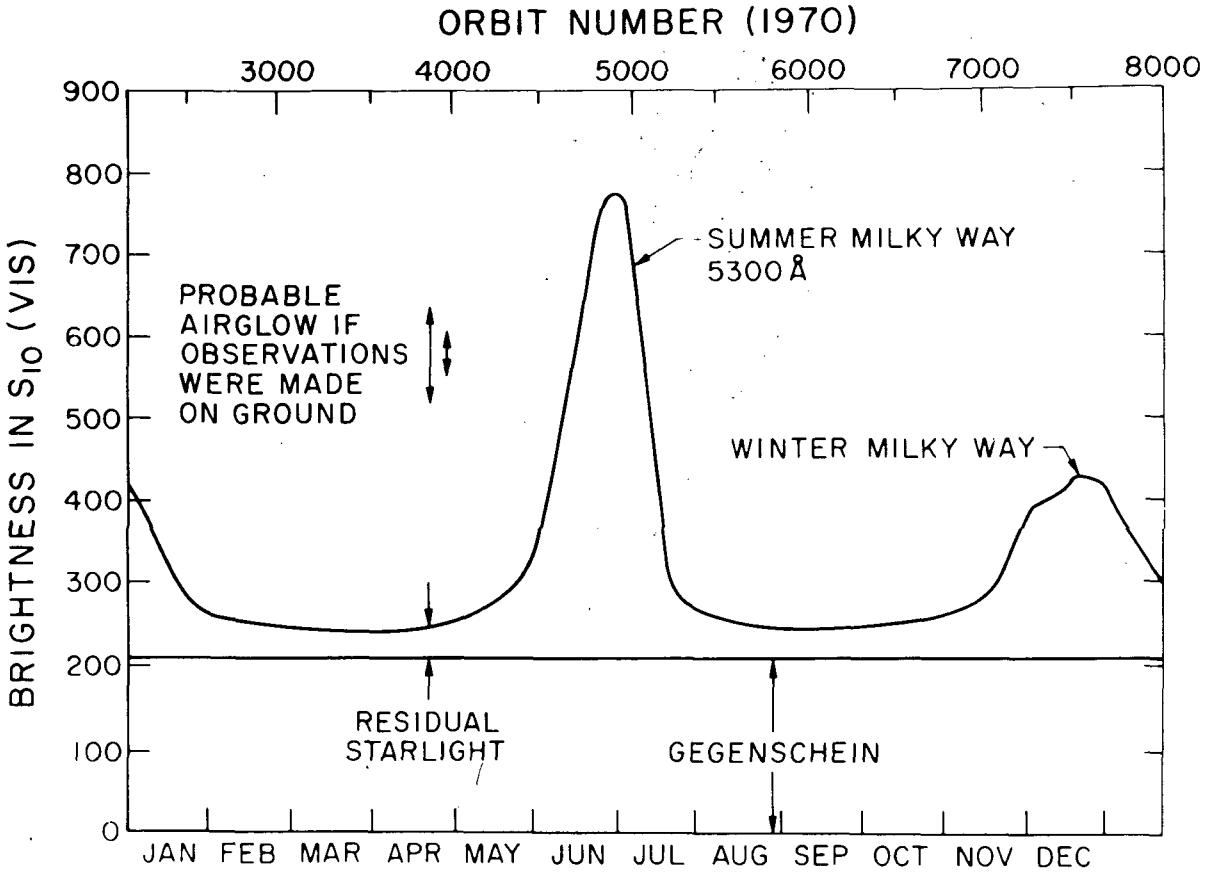

Figure 2.—The brightness of the night sky due to starlight and zodiacal light in the anti-solar direction as a function of time.

rocket and satellite measurements of the sky brightness (Lillie 1969), (Sparrow and Ney 1968) which indicate ground-based observations suffer from a systematic error, perhaps from scattering in the earth's atmosphere. Also, there is no suggestion of scattered light in the OAO or OSO data.

V. COMPARISON OF OBSERVATIONS FROM THE TWO SPACE EXPERIMENTS

A comparison of OAO-2 and OSO-6 results for the region of the galactic center is shown in Figure 4. In this diagram we plot the sky brightness at 4000 Å in the anti-solar direction as measured by OSO-6 versus time, orbit number and galactic latitude. (This is the scan path labeled "ecliptic" in Figure 1.) The data is for the time span May 3 to July 26, 1970 (orbital span 4050 to 5325 and galactic latitude span +39° to

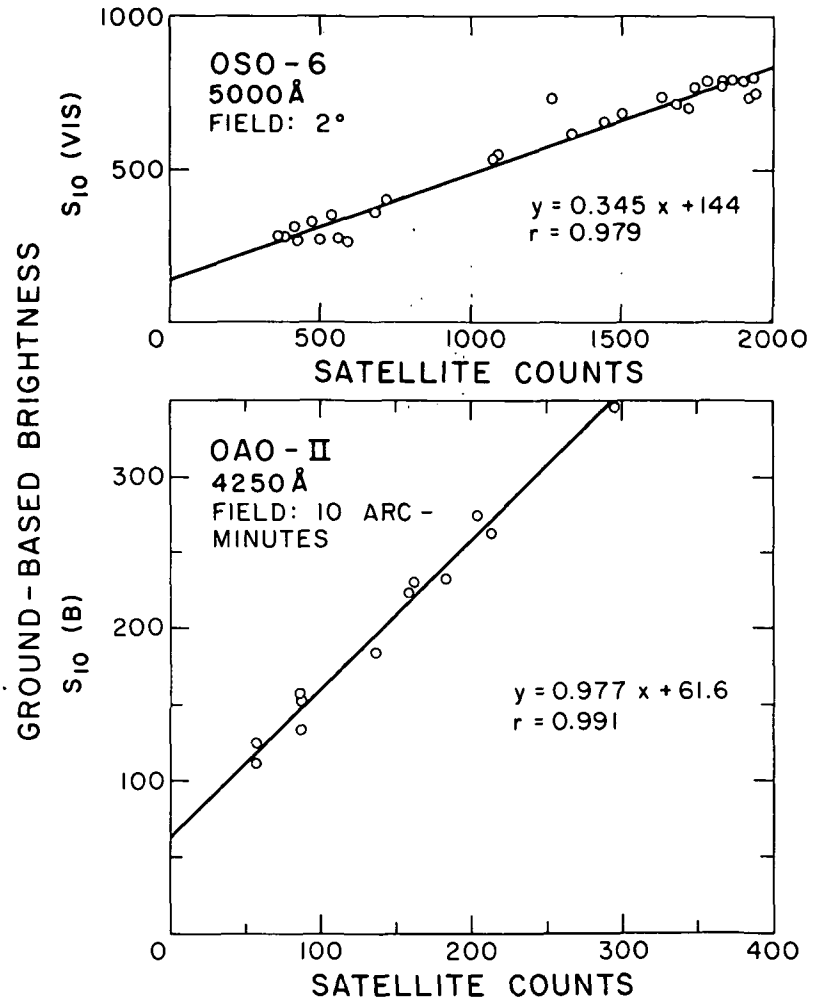

Figure 3. A comparison of the OAO-2 and OSO-6 observations with sky brightness due to starlight and zodiacal light from ground-based observations.

-27°). The ordinate is in units of stars of brightness B = $10^{m}.0$ per square degree [$S_{10}(B)$].

(Note that Figure 2 and the upper part of Figure 3 are in S_{10}(vis) units which are numerically about twice the S_{10}(blue) values.)

The circles in the figure are 4250 Å observations made with the OAO-2 photometer in twelve specific regions near the ecliptic plane. As shown in Figure 1, the OAO observations were not always at points within the OSO field of view and they have been plotted for the orbit of "nearest approach" to the OSO scan path. The OAO observations have been given the

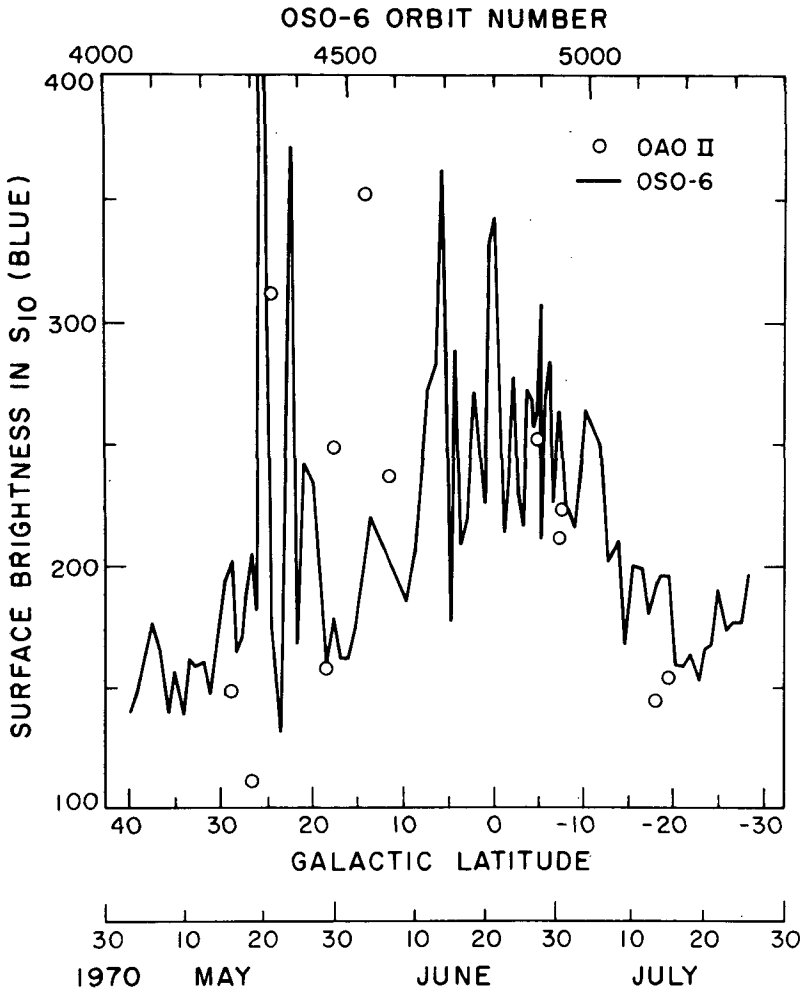

Figure 4.—A comparison of observations from the two space experiments in the region of the galactic center.

gegenschein zodiacal light intensity by first removing the contribution of the measured signal due to zodiacal light (Lillie 1970) and then adding 100 S_{10}(B), which is close to the value of the gegenschein brightness found by Lillie (1969) in a rocket experiment.

Examining Figure 4, we note the following:

a) there is a pronounced maximum in the OSO observations at 0° galactic latitude;

b) there is pronounced scatter in the OSO observations;

c) the general level of the two independent sets of observations is similar; and

d) the scatter of the OAO results is consistent with the scatter in the OSO observations and with the probability that

one or more stars of magnitude 10 or fainter may have been in the field of view.

VI. SUMMARY

In this paper we have compared sky brightness measurements from two independent space experiments with each other and with ground-based observations. We find good agreement between the space experiments, considering the difference in their fields of view.

We agree with ground observations as far as variations in sky brightness are concerned but disagree with the zero point. The ground observations are systematically too bright at both 4250 Å and 5000 Å, suggesting a light source in the earth's atmosphere for which the ground observations are not being corrected.

REFERENCES

Code, A. D., Houck, T. E., McNall, J. F., Bless, R. C. and Lillie, C. F. 1970, Ap. J. 161, 377.
Lillie, C. F. 1969, Bull. Am. Astron. Soc. 1, 198.
_____ 1970, Bull. Am. Astron. Soc. 2, 328.
Roach, F. E. and Megill, L. R. 1961, Ap. J. 133, 228.
Roach, F. E. and Smith, L. L. 1964, NBS, Tech. Note, No. 214.
Smith, L. L., Roach, F. E. and Owen, R. W. 1965, Planet. Space Sci. 13, 207.
Sparrow, J. G. and Ney, E. P. 1968, Ap. J. 154, 783.
van Rhijn, P. J. 1925, Publ. Astr. Lab. Groningen 31, 1.

Page intentionally left blank

THE TEMPORAL CHARACTERISTICS OF THE TERRESTRIAL RADIATION BELT

John F. McNall
University of Wisconsin
Madison, Wisconsin

I. INTRODUCTION

In considering the terrestrial radiation belt and its measurement, one must first note the effect of this radiation on the detectors in the Wisconsin equipment. The lowest dark count rate observed in orbit, compared with that measured in the Thermal Vacuum test on the ground, shows no measurable difference for the solar blind ASCOP 541-F photomultiplier tubes while the EMI-6256B tubes show an increase in minimum dark count of a factor of from 20 to 150 times that observed on the ground. All instruments are perturbed when in the South Atlantic Anomaly, but the EMI tubes are by far the most sensitive to it. Indeed, the effect never goes away. Stellar 1 is the most sensitive so its data will be used for this first analysis.

II. THE OBSERVATIONS

When we plot the raw observed counts per second versus time for Stellar 1, in its dark configuration, at night, and outside of the South Atlantic Radiation Anomaly, we obtain Figure 1. Two gross features are visible at once; first, that from time to time there are large increases in the observed count rate, and second, that there is a quiescent or "normal" count rate between 10 and 30 counts per second. We shall examine the large variations first.

It can be argued that the peaks could be accounted for if the spacecraft happened to be closer to the South Atlantic Anomaly when the high count rates occur. This is not the case since a detailed investigation shows that high count rates occur at the same sub-satellite points as low count rates.

If we expand the time scale in the vicinity of a particularly sharp increase in counts, say, the area near day 320 on Figure 1 (21 November 1969), we get the result shown in Figure

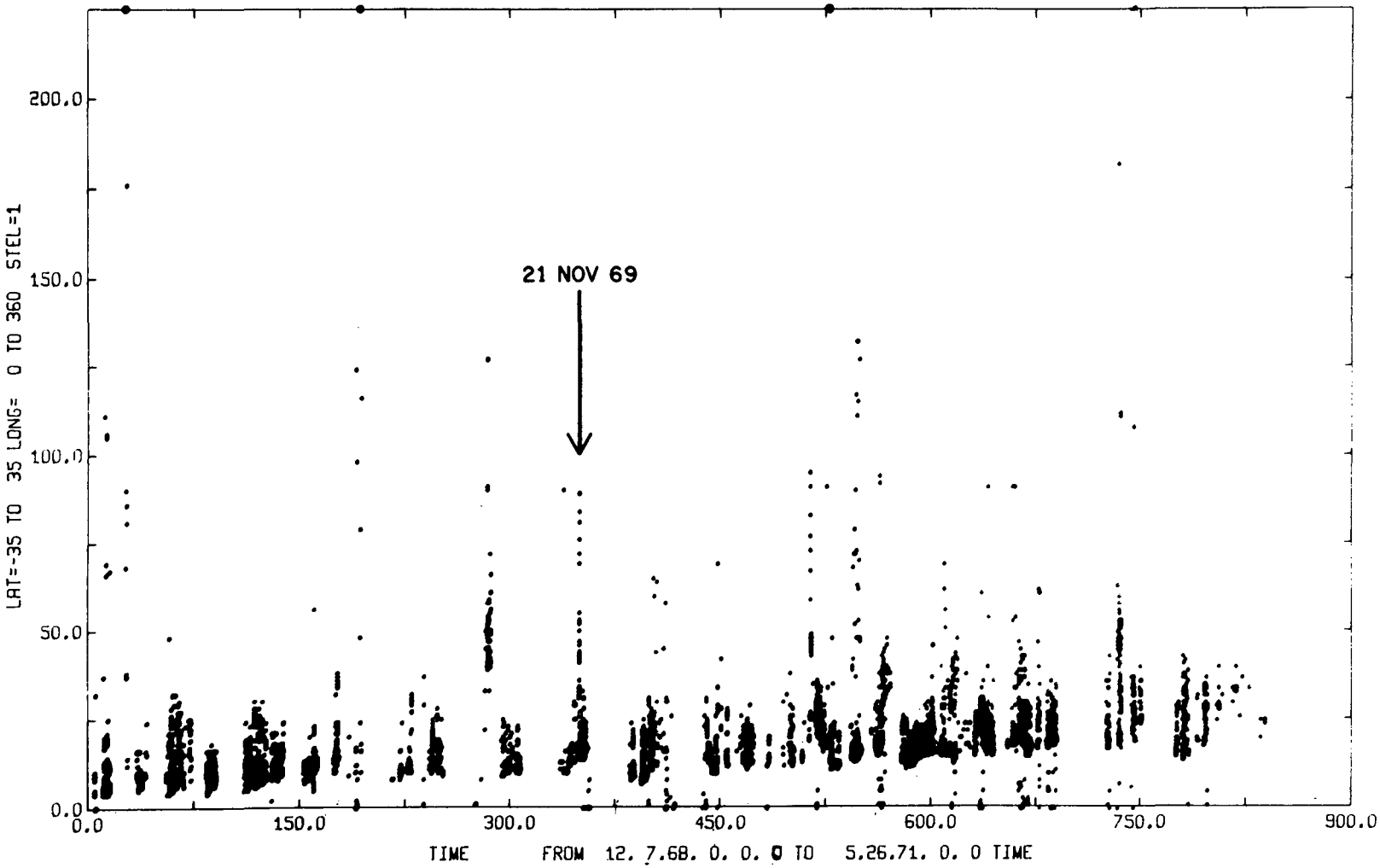

Figure 1.—Photometer dark counts for Stellar 1 at night, outside the anomaly, versus time in days after launch.

2. We observe a sharp increase of counts followed by a fairly rapid decay with, perhaps, a long tail. At 0900 GMT on the 21st of November 1969 the background seemed normal, while at 1021 GMT on the 21st an increase of counts of a factor of 3 to 4 was observed. The sawtooth structure at low count rates is typical of "normal" background data reflecting a one-day periodicity and a slope depending upon how recently the spacecraft has been in the South Atlantic Anomaly. Each point on the curve represents the data obtained from one orbit.

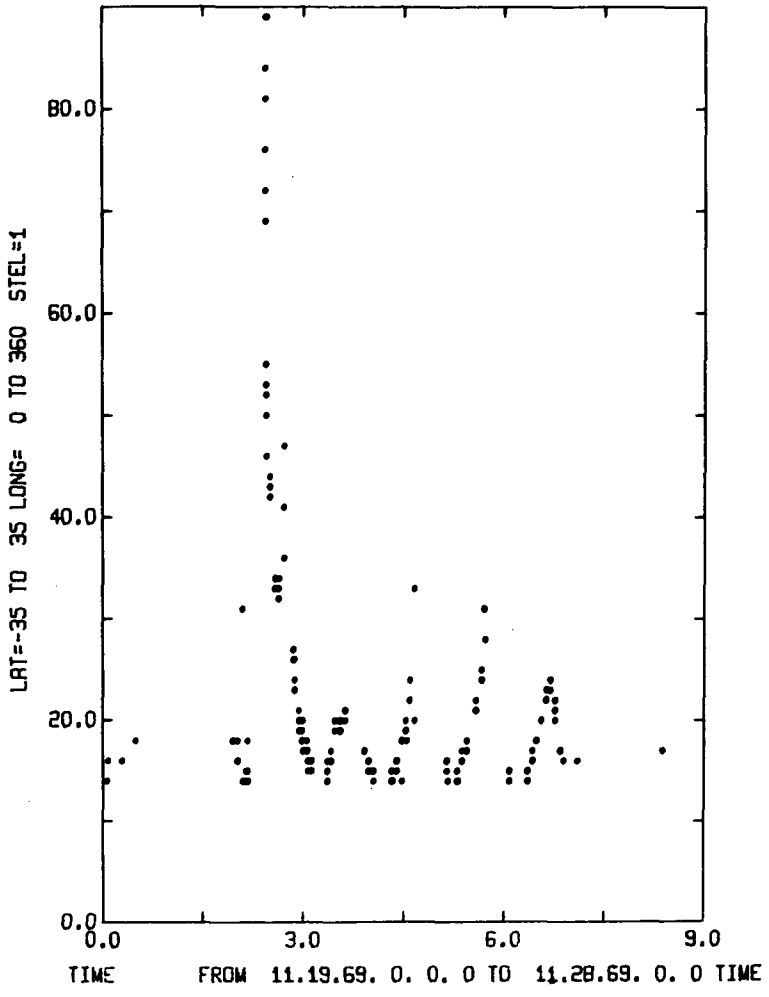

Figure 2.—Expansion of Figure 1 for the period 19 November to 29 November 1969.

To ensure that this increase in counts is due to something real we may place the count rate for the nine-day period of Figure 2 on a Latitude-Longitude plot shown as Figure 3. The South Atlantic Anomaly is in the lower half of the plot near 0°

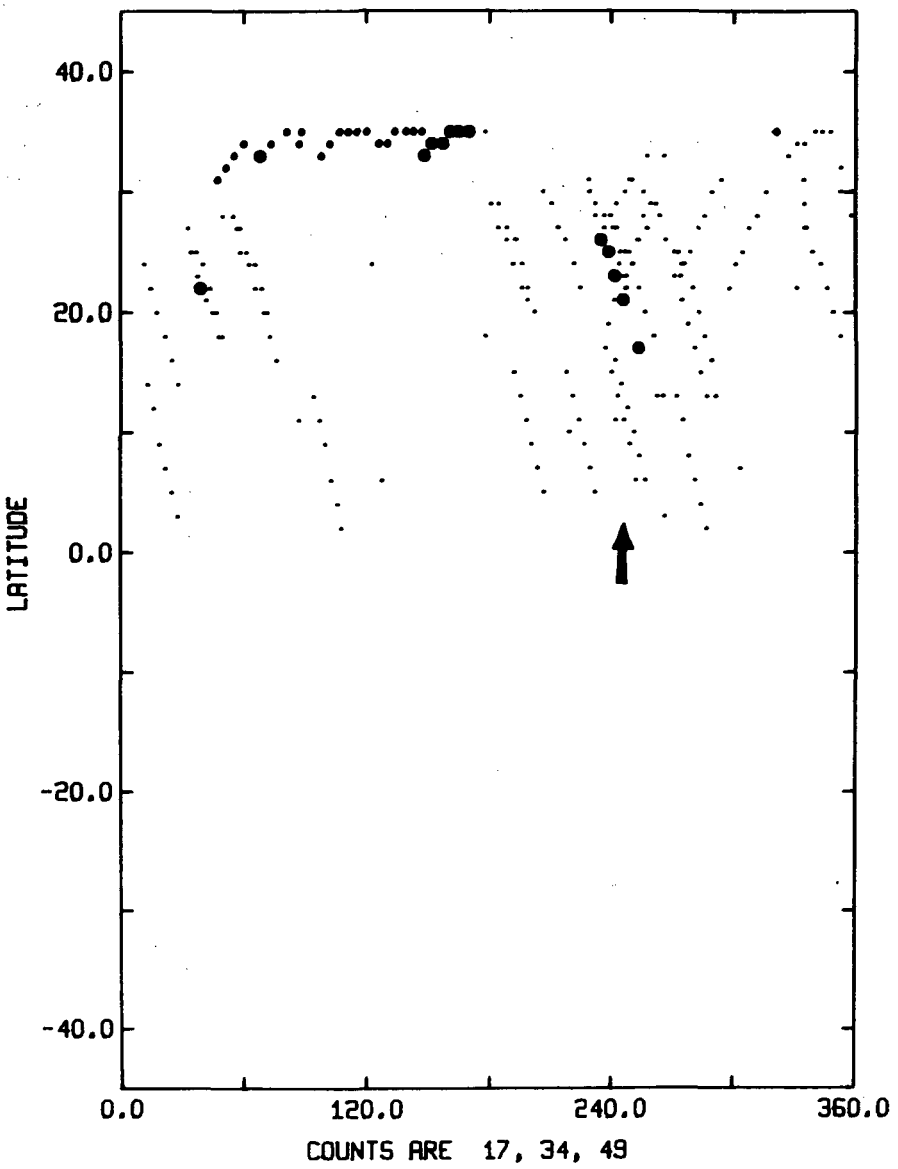

Figure 3.—Dark counts from Figure 2 plotted on a Latitude-Longitude plot, showing increase due to solar activity.

and 360° with its center at Long. 320° Lat. -30°. Orbital motion is left to right and upwards or downward depending upon daily phase. Of particular interest is the area near Long. 240° and Lat. +20°. This area will have the lowest "normal" count rate since the spacecraft has not been in the anomaly for a long time or is skirting around it. The normal count rate for this area is on the order of 20 counts per second. However, it

is seen that there are some data points that show a count rate in the range of 50 per second and more. These points are the peak data points shown on Figure 2.

We now have the picture that each peak time represents a real increase in background count rate due most likely to trapped radiation. It is noted that in this particular case there was a proton flare on the 19th of November allowing for particle transit time—the 21st for this event is reasonable. Indeed, all increased count periods correlate with solar activity (particularly proton flares), and all quiet times are during no flare activity.

Let us now consider the "normal" or low count rate periods. One feature is that there is a net increase in the normal background with time. This amounts to about ten counts per second per year. The second thing that is evident after detailed plots have been examined is that there is an increase in the normal background when the spacecraft has been in the Anomaly recently over times when the orbits skirt around it. If we look at an area near Long. 150° and Lat. +20° (near the anti-anomaly) we see a difference of a factor of two between going south (about 30 counts per second, having been in the Anomaly) and going north (about 15 counts per second skirting the Anomaly). This difference accounts for the spread in observed low count rates. The minimum count rates are seen for orbits that cross Long. 0° and Lat. 35° since the spacecraft has not been near the anomaly in several orbits. The orbital period results in approximately 23° of earth motion per orbit. Therefore, the spacecraft must be in the Anomaly twice a day which accounts for the sawtooth curve seen in Figure 2.

III. DISCUSSION

One can see then that there are two decay mechanisms in the data: first, the actual decay of the radiation belt from high levels due to solar flare activity down to equilibrium levels, and second, the noise decay time of each photomultiplier detector after having been exposed to extreme radiation levels in the South Atlantic Anomaly. The 10 count per second upward trend may be explained by a net increase in tube noise due to a decay time of the order of 1/2 day so that the detectors never get a chance to recover before being subjected to intense radiation again. The multiplier tube decay must be removed before a correct interpretation of the actual spatial contribution of the radiation belt can be made. At present, it is felt that there is enough data to allow a determination of these two decay times but more work remains to be done.

Regardless of the decay mechanisms, it is seen that our most sensitive EMI tube has variations of ±10 counts where the radiation belt is quiet and may increase by a factor of 10 or more

during solar storms. In order to obtain real dark count rates one must multiply the above numbers by 64 since the Wisconsin pulse counters have a precounter of length 6 bits. This gives a "normal dark" count of about 1200 counts per second for Stellar 1 and about 200 counts per second for Stellar 2 (a less sensitive instrument).

IV. CONCLUSION

It is felt that most of the low background observed is inherent tube dark count from having been in the radiation anomaly and not a measure of the real radiation away from the anomaly. If one argues that the noise is due to protons with energy levels on the order of 5 to 10 MEV then it is difficult to explain the background count rate on the basis of these particles at the place observed, since Stassinopoulos (1970) reports fewer than 10 such protons per second per square centimeter. One might suggest that the EMI tubes (sensitive to visible light) are seeing fluorescence of their envelopes due to cosmic rays. There appears to be enough cosmic ray flux to cause this background. However, this does not explain the large count during periods of increased solar activity.

Increased count rates are correlated well with solar activity in all cases. The long term upward drift is probably due to the instrument decay parameter and not a real increase in background.

REFERENCES

Heath, D. F. 1971, Observations of the Solar Long Term Variability and Irradiance in the Near and Far Ultraviolet, NASA X-651-71-116 (Preprint).

I. A. U. Quarterly Bulletin on Solar Activity.

Stassinopoulos, E. G. 1970, World Maps of Constant B, L and Flux Contours, NASA SP-3054.

ULTRAVIOLET PHOTOMETRY OF THE MOON WITH THE CELESCOPE EXPERIMENT ON THE OAO-2

I. A. Ahmad and W. A. Deutschman
Smithsonian Astrophysical Observatory
Cambridge, Massachusetts

ABSTRACT

Thirteen television frames of the Moon taken in the wavelength regions of 1350-2150 Å by filter U_3 and 1050-2150 Å by filter U_4 of the Smithsonian Astrophysical Observatory's Celescope experiment are discussed. The data include phase angles from -81° to -26°. The brightness dependence on phase angle differs slightly from that of visual observations. The brightness dependence on selenographical longitude is compared with the theoretical photometric function derived by Hapke.

I. INTRODUCTION

Many people have studied the photometric properties of the Moon in the infrared, visual, and near-ultraviolet ranges at wavelengths longer than 1900 Å. In the summer of 1969, we lowered this range to 1050 Å with the data gathered by a television photometer whose field of view was divided in half by broadband filters. The effective wavelengths are 1600 Å for filter U_3 and 1500 Å for U_4. Figure 1 gives the transmission for each filter.

Figure 2 shows two representative television pictures of the Moon. Thirteen such pictures were used in this study; eight were taken with the U_4 filter, and five with the U_3. The Moon's phase angle ranged from -81° to -26°, permitting us to examine the Moon's phase law as well as its normal reflectivity. We were unable to obtain smaller phase angles because of spacecraft constraints.

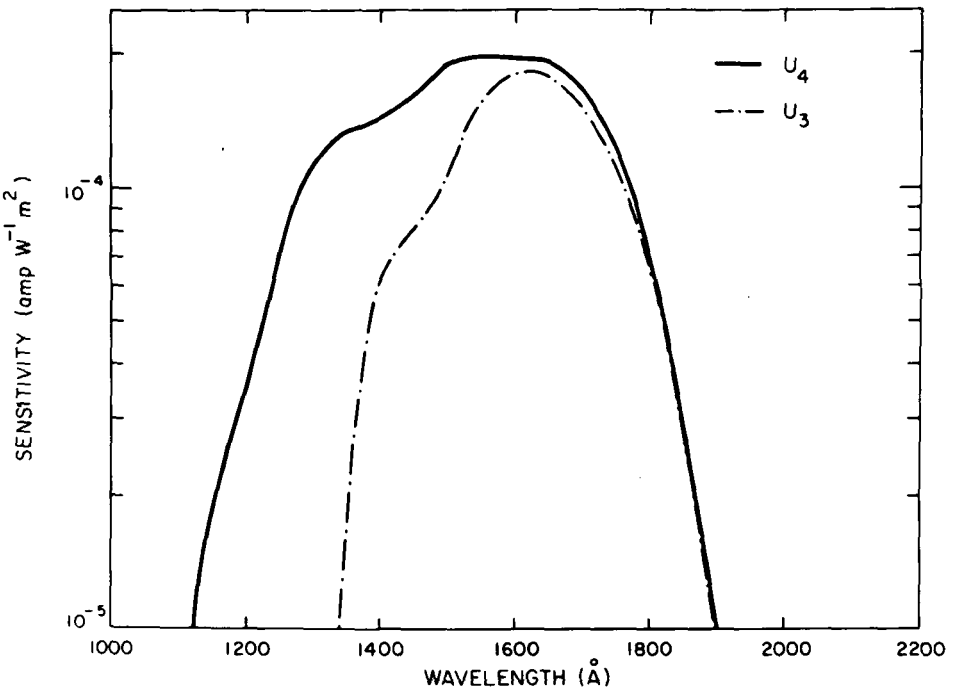

Figure 1.—Transmission of Celescope filters.

II. THE MOON'S PHASE LAW

The phase law of the Moon at intermediate phase angles is

$$I_0 = I(\theta) - \beta\theta \qquad (1)$$

where $I(\theta)$ is the intensity of the Moon measured at phase angle θ, and β is the phase coefficient. At small phase angles, this relationship does not hold; however, our observations were at phase angles large enough to lie wholly in this linear region. We determined with a least-squares fit that the best coefficient is $\beta = 0.04$ mag/deg. This value is 0.012 mag/deg larger than the phase coefficient in the visual range.

Figure 3 shows our values of β plotted with those from the visual range (Gehrels et al. 1964). They appear to fall on a straight line over the entire range.

III. THE NORMAL REFLECTIVITY OF THE MOON

The normal reflectivity of the Moon is given by

Orroral 2851
16:37 UT 23 June 69

MOON

R.A. $12^h\ 28^m\ 01^s$
DEC. $-4^o\ 40'\ 08''$

5 sec. exp.
Camera 4

Madagascar 2853
19:44 UT 23 June 69

MOON

R.A. $12^h\ 33^m\ 25^s$
DEC. $-5^o\ 58'\ 07''$

15 sec. exp.
Camera 4

Figure 2.—Celescope pictures of the ultraviolet Moon.

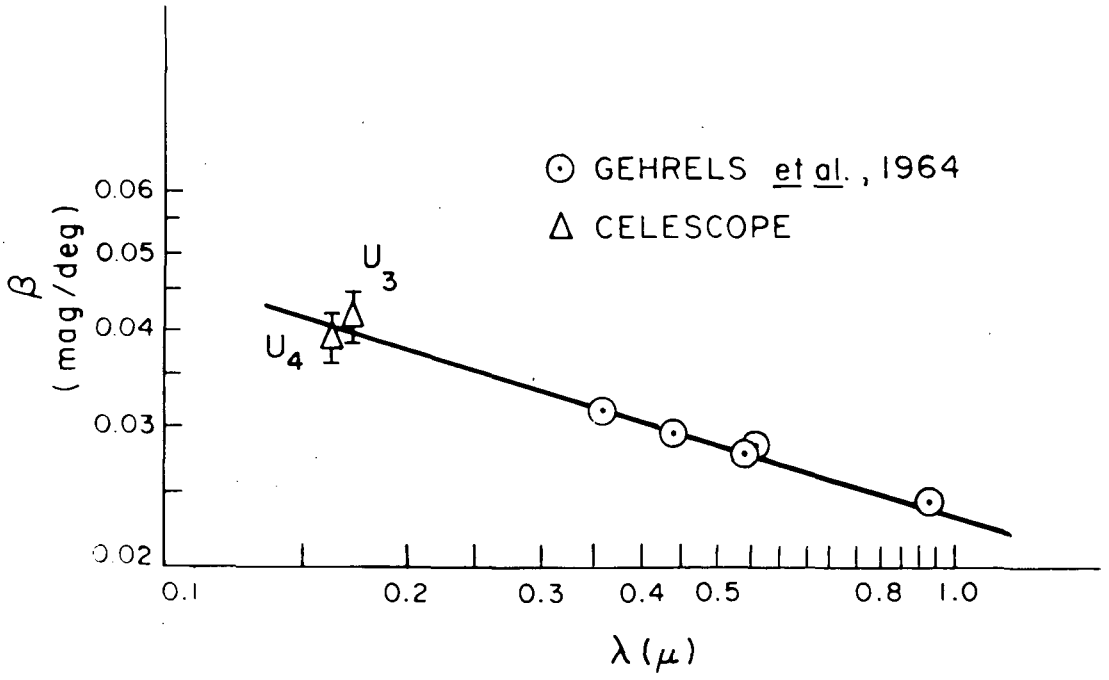

Figure 3.—Moon's phase coefficient vs. wavelength.

$$\frac{I_{\leftmoon}}{I_{\odot}} \left(\frac{a}{r}\right)^2 \qquad (2)$$

where $I_{\leftmoon}$ is the intensity of the Moon at zero phase, $I_{\odot}$ is the intensity of the Sun that would be measured by Celescope, a is the semidiameter of the Moon, and r is the Moon-Sun distance. We use the phase coefficient derived in equation (1) to extrapolate to the brightness of the Moon at zero phase. Obtaining the solar intensity needed in these calculations presents problems. There is some question as to what the Sun's intensity is at Celescope wavelengths. The values published earlier by NRL (Widing et al. 1970) are higher than those of Parkinson and Reeves (1969) by a factor of 3 at 1600 Å and of 2 at 1800 Å. However, a calibration problem caused a zero-point error in the NRL data; its discovery makes the discrepancy even larger, for the corrected NRL intensities are 40% higher than the published values at these wavelengths (Widing 1970). Figure 4 shows the normal reflectivities from earlier studies at short wavelengths and the Celescope reflectivities derived from two different intensity measurements. The one marked NRL uses the revised NRL solar intensities for

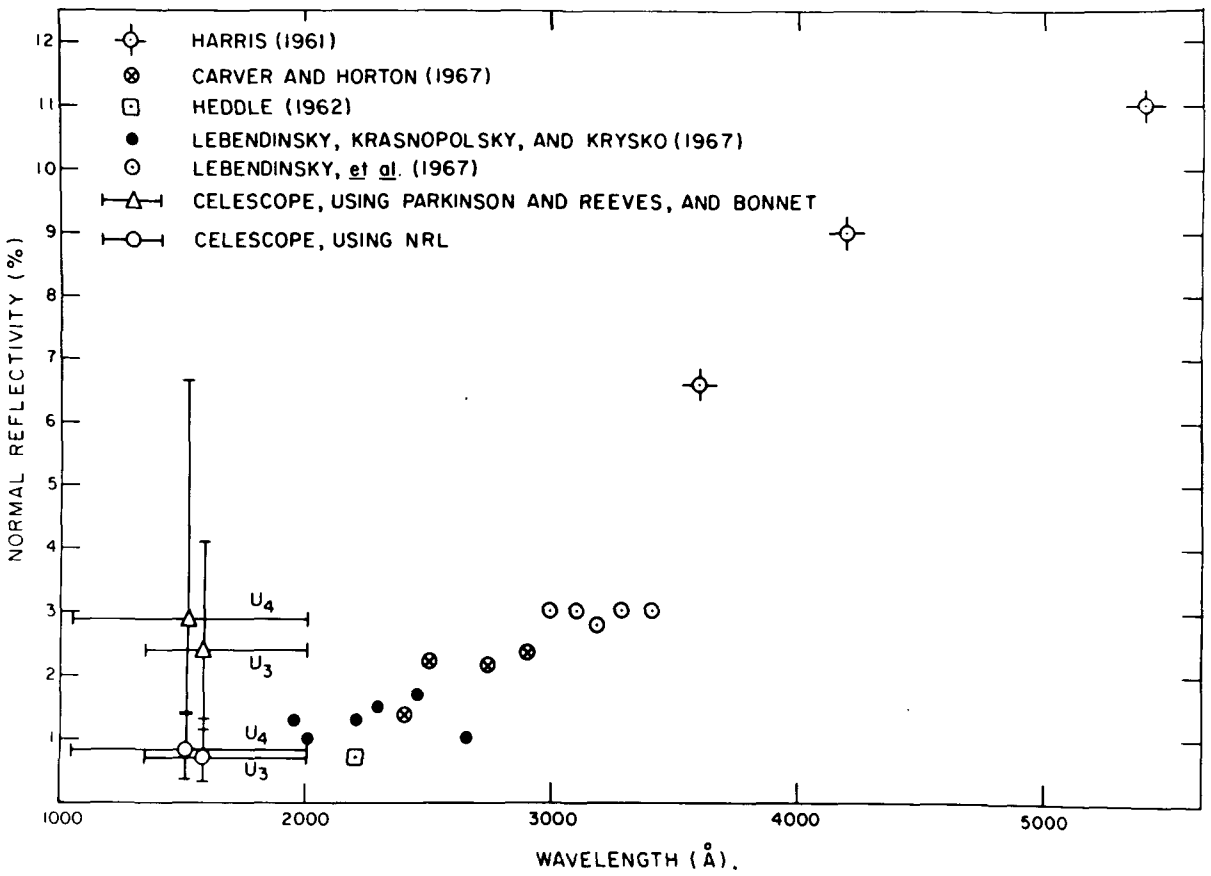

Figure 4.—Normal reflectivity of the Moon.

$\lambda \geq 1400$ Å, the OSO-IV intensities for $\lambda < 1400$ Å (Parkinson 1970), and the intensity of Lyman alpha from Hinteregger (1965). The one marked Parkinson and Reeves-Bonnet uses the Parkinson and Reeves data for 1400-1850 Å and the findings of Bonnet at 1900 Å (Parkinson 1970), the OSO-IV intensities for $\lambda < 1400$ Å (Parkinson 1970), and the intensity of the Lyman alpha line from Hinteregger (1965). The reflectivity from these measurements depends not only on the absolute value of the solar flux but also on the absolute value of the Celescope data. Our instrument is calibrated for point sources, not area sources. We have indicated the worst-case effects of the error on the reflectivity. If the Parkinson and Reeves values are correct, the Moon's reflectivity is leveling off or increasing in the 1000-2000 Å range covered by the Celescope filters even if the minimum reflectivity values allowed are used.

IV. THE ULTRAVIOLET PHOTOMETRIC FUNCTION

Bruce Hapke (1963,1966) devised a model for the Moon's photometric function, $\phi(\lambda,\alpha)$, defined as

$$\phi(\lambda,\alpha) = \frac{B(\lambda,\delta,\alpha)}{B(\lambda,\delta,0°)} , \qquad (3)$$

where $B(\lambda,\delta,\alpha)$ is the brightness of a unit region of the Moon at longitude λ, latitude δ, and phase angle α — that is, the change of brightness with the selenographic longitude and phase angle. Figures 5 and 6 show Celescope data points plotted along with a Hapke curve. For these points, ϕ has been computed from the formula

$$\phi(\lambda,\alpha) = \frac{\zeta(\alpha)\ B(\lambda,\delta,\alpha)}{\zeta(0°)\ B(62°,0°,\alpha)} , \qquad (4)$$

where $\zeta(\alpha) = \phi(\lambda,\alpha)$ as defined by the Hapke theory, and $\zeta(\alpha)/\zeta(0°)$ serves as a normalizing factor to fit the Celescope points to the Hapke curve. The photometric function from the ultraviolet data at -25° shown in Figure 6 is very similar to that of Herriman et al. (1963); they derived theirs from the

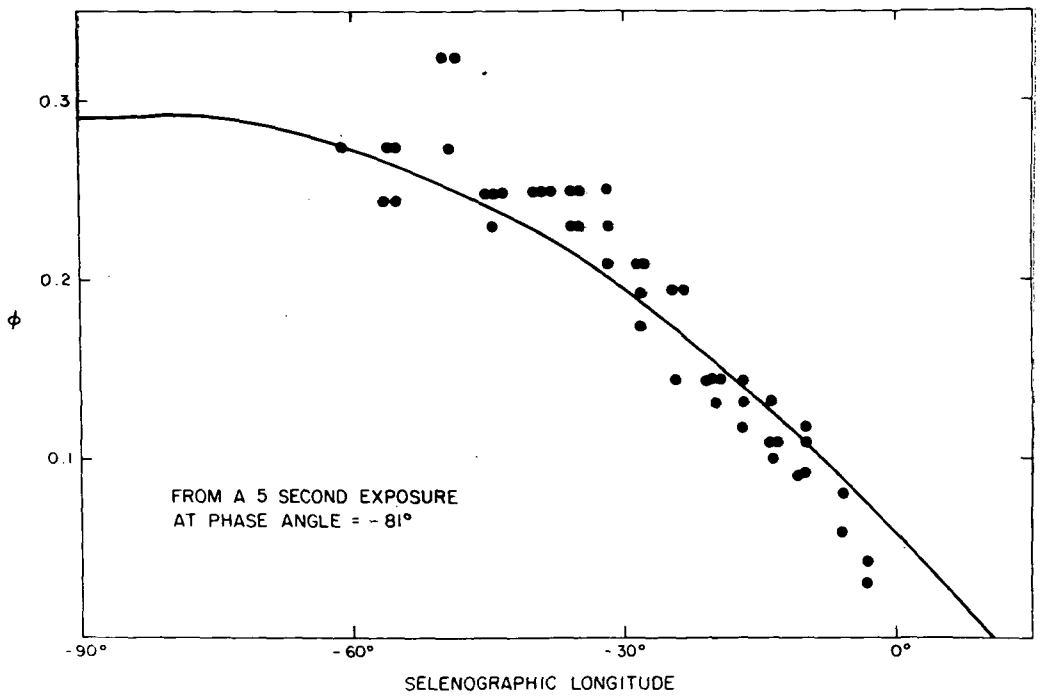

Figure 5.—Celescope data (points) vs. theoretical Hapke function.

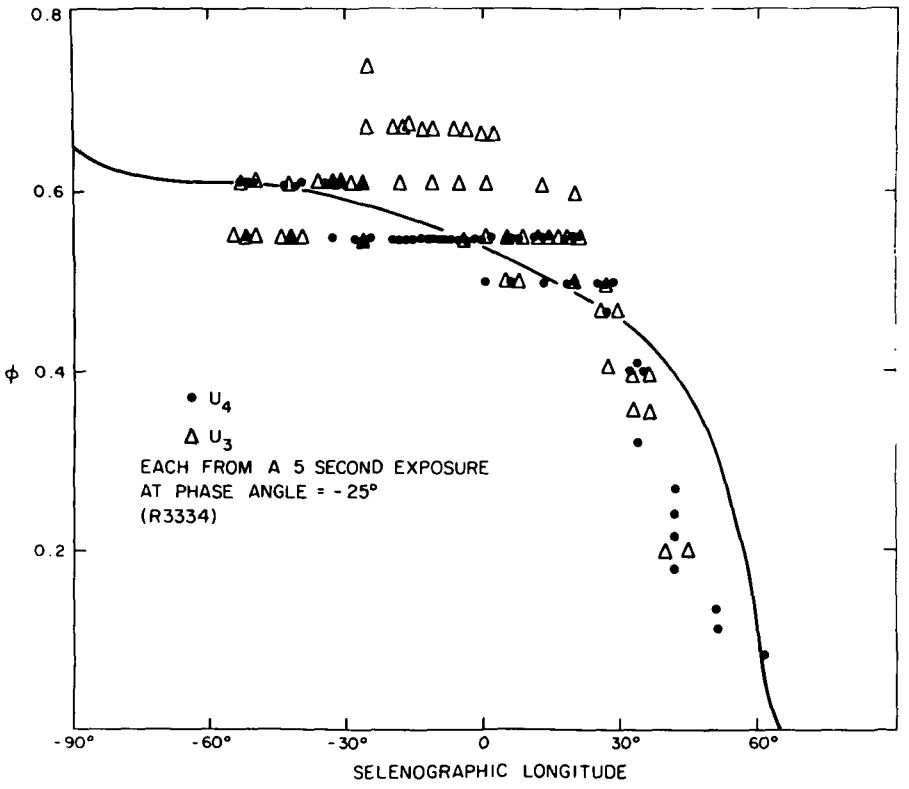

Figure 6.—Celescope data (points) vs. theoretical Hapke function.

data of Fedoretz (1952) as reported by Hapke (1966); theirs is reproduced here in Figure 7. Our ultraviolet measurements also fall under the curve in the 30-60° region.

We conclude that the phase coefficient β is larger in the ultraviolet than in the visual, that the normal reflectivity is leveling off or perhaps increasing, and that the Hapke photometric functions predict our results as well as they do the visual results.

We wish to acknowledge the support of NASA Contract NAS 5-1535. We thank all the Celescope personnel who have helped us with this analysis and all Grumman ground-support personnel who helped us obtain these data.

REFERENCES

Carver, J. H. and Horton, B. H. 1967, Proc. Astron. Soc. Austral. 1, 11.
Fedoretz, V. 1952, Publ. Kharkov Obs. 2, 49.
Gehrels, T., Coffen, T. and Owings, D. 1964, A. J. 69, 826.

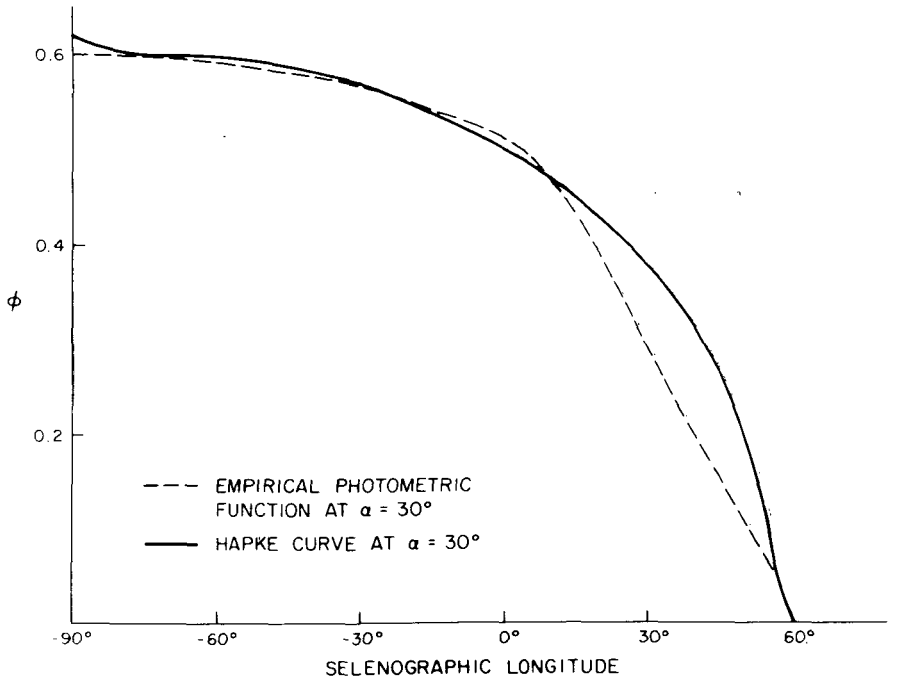

Figure 7.—A comparison of the visual Moon with the Hapke photometric function.

Hapke, B. 1963, J. Geophys. Res. 68, 4571.
_____ 1966, A. J. 71, 333.
Harris, D. L. 1961, Planets and Satellites, ed. G. P. Kuiper and G. M. Middlehurst (Chicago: University of Chicago Press), chapter 8.
Heddle, D. W. O. 1962, Nature 193, 861.
Herriman, A., Washburn, H. and Willingham, D. 1963, J.P.L. Lab. Tech. Rept. No. 32-384 (Rev.).
Hinteregger, H. E. 1965, Space Sci. Rev. 4, 461.
Lebendinsky, A. I., Krasnopolsky, V. A. and Krysko, A. A. 1967, Moon and Planets, ed. A. Dollfus (Amsterdam: North-Holland Publ. Co.), p. 59.
Lebendinsky, A. I., Aleshin, G. M., Dozenus, V. A., Krasnopolsky, V. A., Selivanov, A. S. and Zasetsky, V. V. 1967, Moon and Planets, ed. A. Dollfus (Amsterdam: North-Holland Publ. Co.), p. 65.
Parkinson, W. H. 1970, personal communication.
Parkinson, W. H. and Reeves, E. M. 1969, Solar Phys. 10, 342.
Widing, K. G. 1970, personal communication.
Widing, K. G., Purcell, J. D. and Sandlin, G. D. 1970, Solar Phys. 12, 54.

OAO-2 OBSERVATIONS OF

THE ZODIACAL LIGHT

Charles F. Lillie
The University of Colorado
Boulder, Colorado

ABSTRACT

Photometric measurements of the night sky brightness have been obtained at twelve wavelengths between 1000 Å and 4300 Å from above the earth's atmosphere. A preliminary analysis of the data reveals a component of the sky brightness with ecliptic symmetry and an intensity distribution similar to that of the zodiacal light.

At wavelengths greater than 2500 Å this component is significantly redder than the sun and has the energy distribution of a G8 star. At wavelengths shorter than 2500 Å this component is bluer than the sun and has the energy distribution of an early B-star.

At the longer wavelengths the zodiacal light isophotes have a shape similar to those obtained from ground-based observations by Smith, Roach and Owen (1965). At shorter wavelengths the isophotes tend toward radial symmetry with respect to the sun.

The ultraviolet spectrum of the zodiacal light can be closely approximated with a two component model in which one component has an albedo proportional to the wavelength (λ) and the other component has a scattering efficiency proportional to $\lambda^{-1.9}$.

The observations at 4250 Å indicate a zodiacal light intensity of 30 ± 3 stars of magnitude B = 10.0 per square degree [$S_{10}(B)$] at the north ecliptic pole. This ecliptic pole intensity is about 35 $S_{10}(B)$ fainter than that indicated by ground-based observations, but is in good agreement with the balloon measurements of Gillette (1966) and the satellite observations of Sparrow and Ney (1968). The source of this discrepancy is unknown.

I. INTRODUCTION

Ground-based observations of the zodiacal light are hampered by the low light levels involved and by emission, scattering and absorption in the earth's atmosphere. These highly variable atmospheric sources contribute 30-40% of the zenith sky brightness at 5300 Å (Roach 1964). Thus it is not surprising that the absolute brightness of the zodiacal light is uncertain by more than a factor of two (Wolstencroft and Roach 1969, Roosen 1971). The same difficulties have produced measurements of the color of the zodiacal light which vary from spectral type F5 to G8 (Peterson 1967).

In the past decade it has become possible to measure the surface brightness of the night sky from above the earth's atmosphere with rocket and satellite-borne instruments and to extend these measurements into the ultraviolet region of the spectrum.

In this paper we report a preliminary analysis of observations of the zodiacal light in the 1600-4300 Å spectral region obtained with the Wisconsin Experiment Package of the Orbiting Astronomical Observatory (OAO-2).

II. THE OBSERVATIONAL MATERIAL

a) Instrumentation

The Wisconsin Experiment Package (WEP) has four 8-inch photometric telescopes which can be used to measure the surface brightness of the sky at twelve wavelengths in the 1050-4250 Å region of the spectrum. The instrumentation and operation of this package has been described in detail by Code et al. (1970). Briefly, each 8-inch telescope has a photometer with a five-position filter wheel containing three medium-band filters, a dark slide and a Cerenkov radiation calibration source. Using the 10-arc minute diameter field-of-view, it is possible to measure the surface brightness of the night sky at all wavelengths with a 64-second integration time.

b) Observing Sequence

A typical observing sequence consists of eleven readings with each photometer: two dark readings, a calibration reading and eight (3-2-3) filter readings. The filter readings are made at different gain settings to avoid ambiguities in the digital data. A complete sequence lasts from 24 to 32 minutes and takes an entire spacecraft night. Since orbit 3000, the dark readings have been made at the beginning and end of the sequence to determine the time dependence of the

radiation-belt induced dark current.

c) Observations

OAO-2 can point to discrete regions of the sky with an accuracy of ±1 arc-minute, but it has no capability for continuous sky scans. The sky brightness data for this program have been obtained in two ways:

1) During routine photometry of discrete objects such as stars, planets and galaxies, it is necessary to measure and remove the contribution of the sky background. Thus, a large number of sky observations have been obtained near specific targets.

2) In addition, a number of observations of sky background areas selected for known star counts or uniform distribution in galactic and ecliptic coordinates have been obtained.

III. RESULTS

a) Shape

We have identified the zodiacal light component in our data in two ways:

1) by selecting observations obtained in a short period of time at high galactic latitudes which cover a large range of ecliptic coordinates and assuming the variations in sky brightness are due to zodiacal light; and

2) by selecting observations of the same sky region obtained over a period of weeks or months and identifying the component which varies with time with the zodiacal light.

An example of the first method is shown in Figures 1 and 2. We plot net digital counts at four wavelengths versus ecliptic latitude and longitude ($\lambda - \lambda_o$). The data were obtained on February 17, 1969 by measuring sky brightness along the ecliptic at 10° intervals from 50° to 80° from the sun and at ±15° and ±30° ecliptic latitude at 50° ecliptic longitude. The sky areas were selected to exclude all stars brighter than $10^{m}.0$ and all areas have galactic latitudes $b_{II} < -40°$ except the (50°, 30°) area at $b_{II} = -25°$.

At 4250 Å the sky brightness contours show a strong ecliptic symmetry. When these data are plotted against the 5300 Å zodiacal light brightness predicted from the tables of Smith, Roach and Owen (1965) [SRO] one finds a linear relationship with no deviation greater than 3% from a straight line. This suggests there are no large differences between the intensity distribution of the zodiacal light at 4250 Å and that at 5300 Å which is consistent with neutral scattering by the interplanetary dust particles.

The observations at 3330 and 2980 Å also show brightness

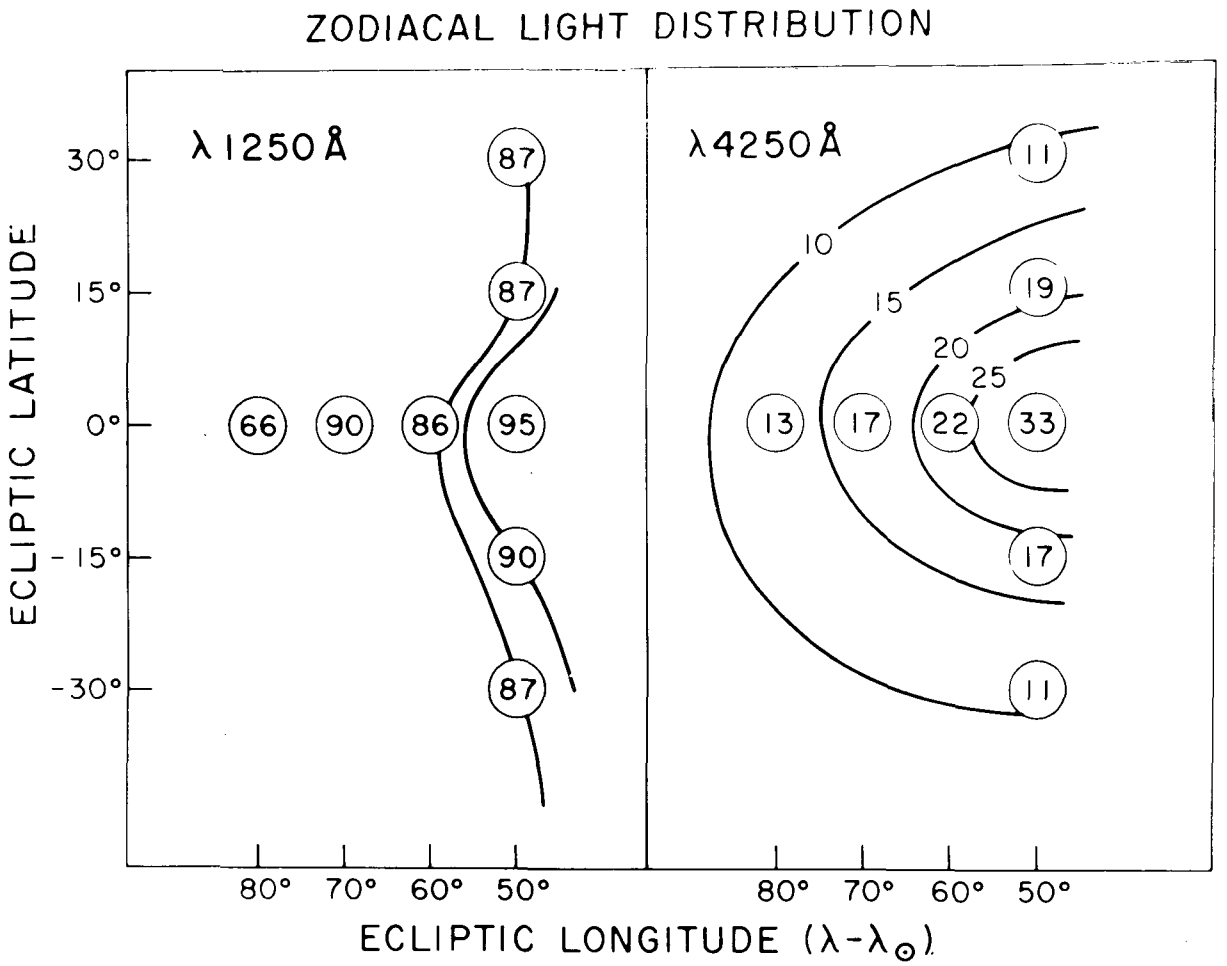

Figure 1.—The sky brightness at 4250 Å and 1250 Å is plotted vs. position in ecliptic coordinates. The brightness data is in digital counts and includes the contribution of stars fainter than 10th magnitude and the geocorona.

contours with ecliptic symmetry and agree well with the 4250 Å data. There is, however, a tendency toward less elliptical, more circular contour lines with decreasing wavelength. This trend seems to continue for data at 2500 and 2200 Å.

The observations at 1250 Å include a strong contribution from L_α emission in the geocorona which may amount to 80% of the measured sky brightness (Thomas and Krassa 1971). One can see an ecliptic symmetry in the data, but further interpretation will require a detailed model of the geocorona.

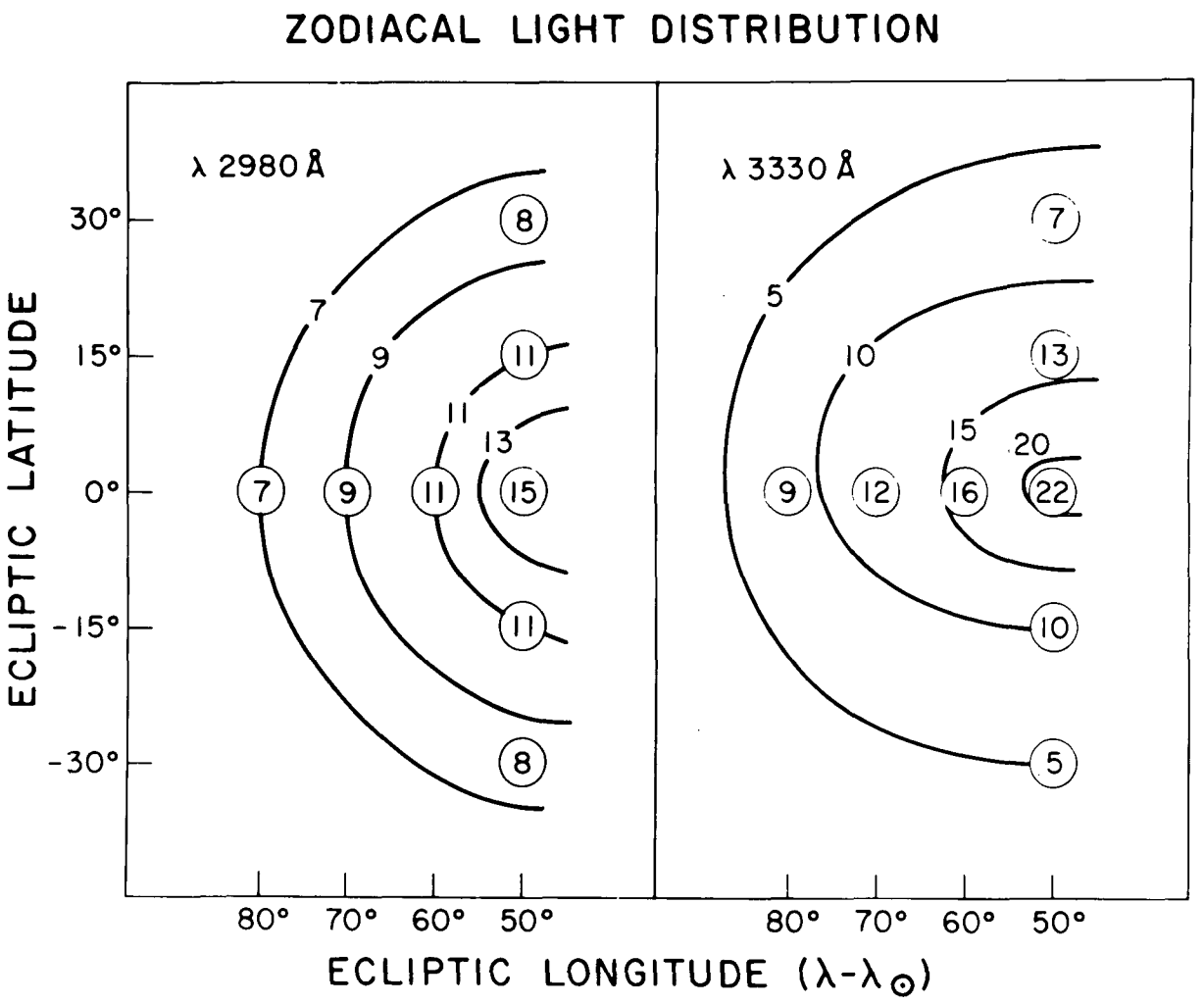

Figure 2.—The sky brightness at 3330 Å and 2980 Å is plotted vs. position in ecliptic coordinates.

b) Color

An example of the second method is shown in Figure 3 which presents observations of the sky near Nova Serpens 1970 obtained over a period of seven weeks in February and March of 1970. We plot net digital counts versus the zodiacal light intensity predicted by ground-based observations at 5300 Å [SRO] in units of stars of magnitude B = $10^{m}.0$ per square degree [$S_{10}(B)$]. Here we assume

$$1\ S_{10}(V) = 1.69\ S_{10}(B)$$

(Roach and Smith 1964).

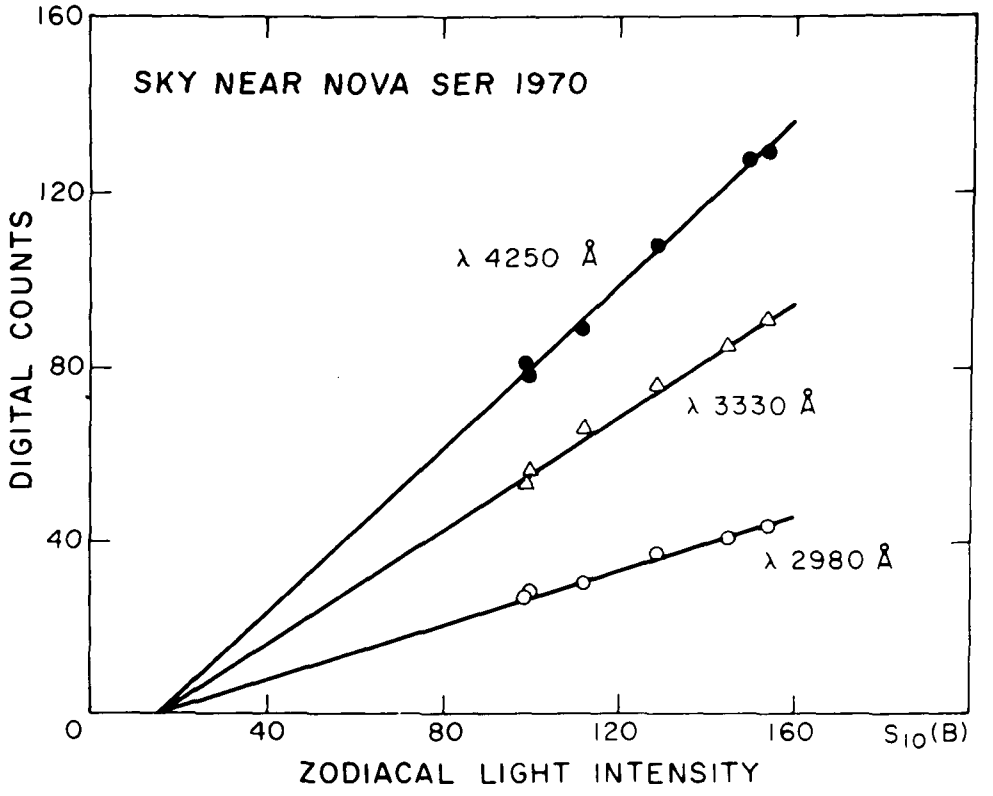

Figure 3.—Observations of the sky brightness near Nova Serpens 1970 for a period of seven weeks are plotted against the zodiacal light intensity predicted from the observations of Smith, Roach and Owen (1965). Digital counts are plotted vs. the number of stars of magnitude B = 10^{m}.0 per square degree.

Here again, we find a linear relationship between ground and space observations. From the slope of these lines we can find the number of digital counts to be expected at each OAO wavelength for a given zodiacal light intensity. If we then divide by the number of digital counts observed for some comparison star, we have a spectrum of the zodiacal light in the instrumental system of the spacecraft. The results of this calculation are shown in Figure 4. We have chosen an Al V star, θ Lep, for a comparison standard, because it is not too bright to be observed with Stellar 1 and its ultraviolet energy distribution is nearly constant with wavelength. We also show curves for several other stars compared to θ Lep.

The zodiacal light data for Figure 4 are average values for three separate series of observations. The data is listed in

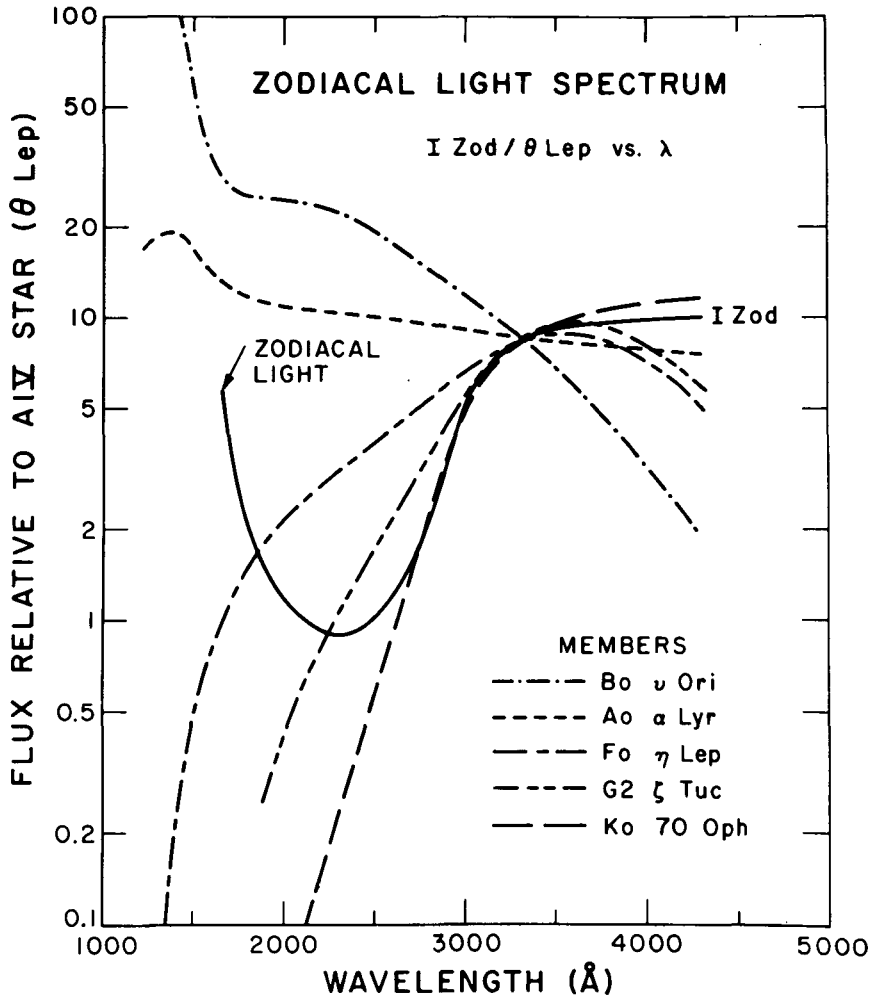

Figure 4.—The flux ratio of the zodiacal light, relative to θ Lep, an A1 V star, is compared with the flux ratios of a grid of main sequence stars. The curves are normalized to an arbitrary value at 4250 Å.

Table 1 in which we give the slope of the relationship between the OAO net digital counts at gain E4 versus zodiacal light intensity predicted from SRO in S_{10}(B). The estimate of probable error is based on the internal consistency of the data. The next two columns give the net digital counts observed for θ Lepus and β Hydrus, the comparison stars for Figures 4 and 5. The last column gives the ratio of the zodiacal flux at each wavelength to that from β Hyi, normalized to 4250 Å.

From an examination of Figure 4 it is apparent that the zodiacal light is redder than the sun in the 2500-4300 Å region

Table 1. Zodiacal Light Spectrum

λ	Slope	P.e.	θ Lep	β Hyi	$F_z/F_{\beta Hyi}$
4250 Å	52.45*	4.5%	343,380†	983,800†	1.00
3330	4.75	7.6	36,650	111,100	0.766
2980	2.18	2.2	29,500	53,250	0.729
2940	0.907	13.0	15,380	27,970	0.580
2380	0.119	18.8	6,400	2,300	0.919
2040	0.275	18.7	4,880	3,070	1.613
2460	0.140	10.0	9,600	3,890	0.638
1920	0.106	31.2	2,110	126	15.0
1680	0.0251	73.2	357	22	203.

*Digital counts at gain E4 per S_{10}(B)

†Net digital counts less sky at gain E4

with an energy distribution similar to that of a star of spectral type G8. Below 2500 Å the zodiacal light is much bluer than the sun, approaching an early B-star in its energy distribution.

The flux ratio of the zodiacal light relative to the sun is shown in Figure 5. The results obtained earlier by Lillie (1968) with data from an Aerobee rocket are presented for comparison, as well as a rocket measurement due to Sudbury and Ingham (1970). The "sun" for the OAO data is β Hyi, a G2 IV star [B - v = $0^m.62$] whose energy distribution is quite similar to that of the sun in the ultraviolet (Code 1971). The agreement between the observations is quite good, considering the low light levels involved and the difficulty in removing the contribution of starlight to the rocket data.

Earlier reports of an upturn in the zodiacal light intensity below 2500 Å (Lillie 1968) are confirmed by the OAO measurements and extended to shorter wavelengths. It is interesting to note that the zodiacal light spectrum can be reproduced by a two component model of the interplanetary dust cloud in which one component has an albedo proportional to the wavelength, λ, while the other component has a scattering efficiency proportional to λ to the -19th power.

The reason for this upturn is unknown. It does not seem to be a phase effect, since the rocket observations are for the entire night sky and the OAO data is the average for several points at elongations from 50° to 120° from the sun. And the wavelength dependence is too high for small particle scattering.

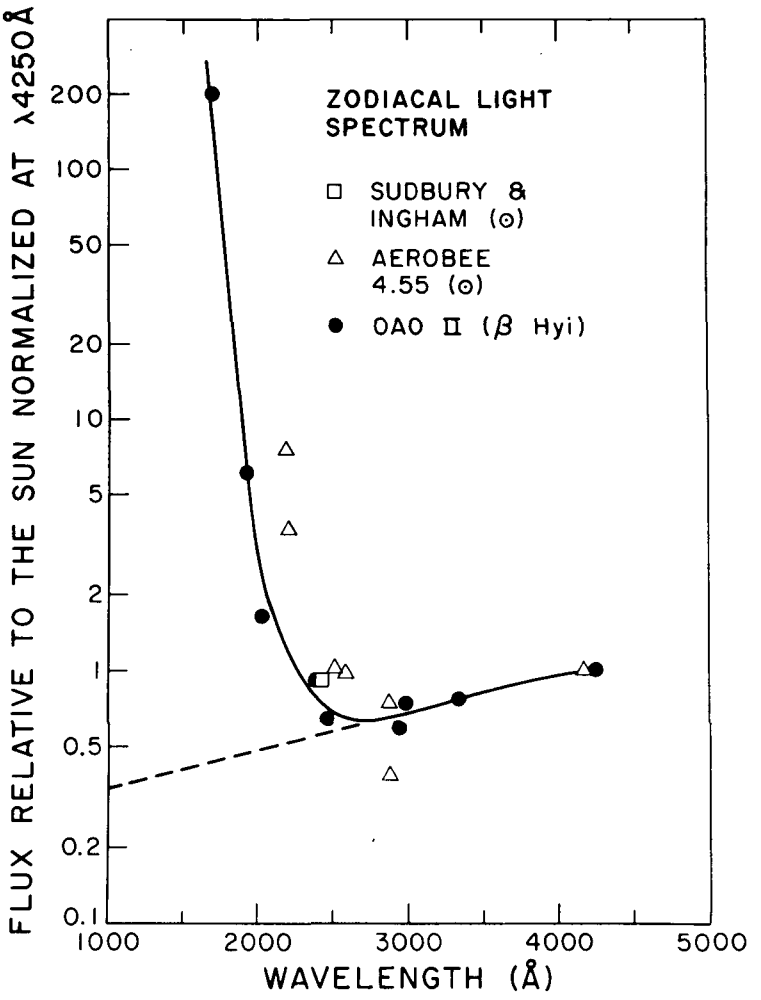

Figure 5.—Flux ratios for the zodiacal light relative to the sun from OAO-2 data and data from Aerobee 4.55. The curves are normalized at 4250 Å.

The most likely explanation is that the effect is produced by the plasma oscillations in small particles which Gilra (1972) has suggested to explain the "bump" in the interstellar extinction curve at 2200 Å. This feature in the extinction curve (Bless and Savage 1972) shows a sharp decrease in extinction around 2000 Å with a wavelength dependency of about λ to the -20 to -24. In this interpretation of the data the λ dependency would be due to large (micron-sized) particles, while the λ^{-19} component would be due to very small particles with little or no coating.

It is also of interest to note that the zodiacal light isophotes in Figures 1 and 2 seem to become more radially symmet-

ric below 3000 Å. This would be consistent with a two component model in which large particles of asteroidal origin are found near the ecliptic, while small particles of cometary origin form a spherical halo around the sun.

c) Brightness

(i) General

The difficulty of measuring the absolute brightness of the zodiacal light has been discussed in detail by Wolstencroft and Roach (1969). The principal sources of error in this determination are uncertainties (a) in the absolute calibration of the photometer, and (b) in the subtraction of other sources of background radiation.

The second source of error is not too significant for the OAO observations because atmospheric emission, scattering and absorption can be ignored and the small field of view of the OAO photometers makes it possible to reject the contribution of stars brighter than 10th magnitude. In sky regions at high galactic latitude 90% of the observed background is typically due to zodiacal light.

The usual method of calibrating sky brightness photometers is to observe stars whose energy distribution is known as they drift through the field of view (Roach and Smith 1964). This provides a test for vignetting and a measurement of the photometer's absolute sensitivity.

(ii) OAO Data

Extensive tests with the OAO photometers indicate a uniform response ±5% across the field of view for Stellars 1-3, and ±10% for Stellar 4. The choice of a star for calibration at 4250 Å is complicated by the broad band-pass of the filter (860 Å) and the uncertain spectrum of the sky background. The relationship between (B - V) and (m_{4250} - V) is non-linear and corrections range up to $0^m.26$ for late-type giant stars. (The correction for main sequence stars is much smaller, however.) The adopted calibration

$$1 \text{ digital count at Gain E2} = 1.18\ S_{10}(B)$$

is based on the average transformation from m_{4250} to B for six main sequence stars ranging in spectral type from B2 V to G2 V. This average agrees within $0^m.01$ with the transformation for 70 Oph, a K0 V star, whose energy distribution closely resembles that of the zodiacal light in the 3000-4500 Å region, as shown in Figure 3.

The results of applying this calibration to five sky back-

ground areas of particular interest are shown in Table 2. In successive columns we list the area designation, its ecliptic latitude, ecliptic longitude, the sky brightness observed by OAO, the contribution due to starlight, the zodiacal light component ($I_{obs} - I_{star} = I_{zod}$) and the zodiacal light according to Smith, Roach and Owen (1965) converted to $S_{10}(B)$ assuming the ratio $S_{10}(V)/S_{10}(B) = 1.69$.

Table 2. Zodiacal Light Brightness

Sky Area	β	$\lambda-\lambda_0$	I_{obs}	I_{star}	I_{zod}	SRO
# 5	0°	50°	312*	11*	301*	454*
7	0	60	208	13	195	302
9	0	70	161	13	148	224
11	0	80	123	12	111	166
NEP	90	0	53	23	30	65

*Brightness in $S_{10}(B)$

The contribution of direct starlight was calculated using the tables of Roach and Megill (1961) for stars fainter than 10th magnitude and converted with the relationship

$$1\ S_{10}(B) = 0.903\ S_{10}(pg)$$

(Wolstencroft and Rose 1967).

The contribution due to diffusely scattered starlight was included by multiplying the star counts by 1.34 (Lillie 1968).

(iii) Comparison in the Ecliptic Plane

The first four entries in Table 2 are for the data points in the ecliptic plane shown in Figure 1.

An examination of the table indicates the factor 1.69 is not correct for the conversion of $S_{10}(V)$ to $S_{10}(B)$; it should be 2.55 for sky areas 5 - 11, i.e., the zodiacal light is much redder than the sun.

We can check this result by assuming both the OAO and SRO observations are correct at 4250 and 5300 Å respectively. Using the absolute calibration of the WEP photometer: 1 E4 count = 2.38×10^{-16} ergs/cm^2-sec-Å from the observation of A0 V

stars and the calibration

$$1\ S_{10}(V) = 1.31 \times 10^{-13}\ \frac{\text{ergs}}{\text{cm}^2\text{-sec-Å}}$$

(Roach and Smith 1964), we find the zodiacal light flux at 4250 Å is 0.59 times the flux we predict from the solar energy distribution and the SRO 5300 Å observations. This compares with the value 0.57 found by Lillie (1968) with rocket observations at 4170 Å.

If we extrapolate the OAO observations in the ecliptic to an elongation of 45°, we find a brightness of 363 $S_{10}(B)$ or 925 $S_{10}(V)$ if 2.55 is the correct conversion factor. This value may be compared with the mean value of 857 ± 147 $S_{10}(V)$ for eight previous investigations (Wolstencroft and Roach 1969).

(iv) Comparison at the Ecliptic Pole

The surface brightness of the zodiacal light at the ecliptic pole provides a sensitive test for models of the interplanetary dust cloud. Ground-based measurements disagree by factors of 2 or more, but space measurements seem to be converging to the value of 30 ± 3 $S_{10}(B)$ which was found in this investigation. The results of previous photoelectric determinations are shown in Table 3.

We note that the result of Sparrow and Ney (1971) would be reduced by 5 or 6 $S_{10}(B)$ if allowance were made for a diffuse galactic light component. Part of the disagreement between observers may be due to the use of the solar color index to convert observations from the visual to the blue photometric system. But there still seems to be an excess of 15 to 20 $S_{10}(B)$ in the ground-based observations over those from space. The source of this discrepancy is not known, but may be scattering by aerosols or airglow from altitudes greater than 200 km.

IV. CONCLUSIONS

The purpose of this paper was to present some preliminary results from the OAO-2 observations of the zodiacal light. The main conclusions which can be drawn at this stage of the investigation are:

1. The surface brightness of the zodiacal light at 4250 Å is equal to 30 ± 3 stars of magnitude B = $10^{m}.0$ per square degree [$S_{10}(B)$]; in the ecliptic at 45° elongation the brightness is 363 $S_{10}(B)$.

2. The color of the zodiacal light is redder than the sun between 4300 and 2500 Å, resembling that of a G8 star. Below 2500 Å the zodiacal light is bluer than the sun, with the col-

or of an early B star.

3. The spectrum of the zodiacal light can be approximated with a two component model, one component having an albedo proportional to λ, the other with a scattering efficiency proportionate to λ^{-19} power.

Table 3. Surface Brightness of Zodiacal Light at the Ecliptic Pole

Author	Brightness	Location†
Elvey and Roach (1937)	40 S_{10}(B)	G
Beggs et al. (1964)	105*	G
Weinberg (1964)	110*	G
Smith, Roach and Owen (1965)	65*	G
Dumont (1965)	41*	G
Wolstencroft and Rose (1967)	92	R
Gillett (1966)	27#	B
Sparrow and Ney (1968)	30	S
Lillie (1968)	30	R
Sparrow and Ney (1971)	35	S
Present Study	30	S

* Value determined from observations in visual assuming $[S_{10}(V)]/[S_{10}(B)] = 1.69$

\# Value extrapolated from balloon observations with model calculations

† G = Ground, R = Rocket, B = Balloon, S = Satellite

REFERENCES

Beggs, D. W., Blackwell, D. E., Dewhirst, D. W. and Wolstencroft, R. D. 1964, M.N.R.A.S. 128, 419.
Bless, R. C. and Savage, B. D. 1972, this volume.
Code, A. D., Houck, T. E., McNall, J. F., Bless, R. C. and Lillie, C. F. 1970, Ap. J. 161, 377.
Code, A. D. 1971, unpublished result.
Dumont, R. 1965, Ann. d'ap. 28, 265.
Elvey, C. T. and Roach, F. E. 1937, Ap. J. 85, 213.
Gilra, D. P. 1972, this volume.
Gillett, F. C. 1966, Thesis, University of Minnesota.
Lillie, C. F. 1968, Thesis, University of Wisconsin.
Peterson, A. W. 1967, The Zodiacal Light and the Interplanetary Medium, ed. J. L. Weinberg, NASA SP-150, p. 23.
Roach, F. E. and Megill, L. R. 1961, Ap. J. 133, 228.
Roach, F. E. 1964, Space Sci. Rev. 3, 512.
Roach, F. E. and Smith, L. L. 1964, N.B.S. Tech. Note, No. 214.
Roosen, R. G. 1971, Rev. Geophys. & Space Phys. 9, 275.
Smith, L. L., Roach F. E. and Owen, R. W. 1965, Planet. Space Sci. 13, 207.
Sparrow, J. G. and Ney, E. P. 1968, Ap. J. 154, 783.
_____ 1971, to be published.
Sudbury, G. C. and Ingham, M. F. 1970, Nature 226, 526.
Thomas, G. E. and Krassa, R. F. 1971, Astron. and Astrophys. 11, 218.
Weinberg, J. L. 1964, Ann. d'ap 27, 718.
Wolstencroft, R. D. and Rose, L. J. 1967, Ap. J. 147, 271.
Wolstencroft, R. D. and Roach, F. E. 1969, Ap. J. 158, 365.

ULTRAVIOLET OBSERVATIONS OF COMETS

Arthur D. Code and Theodore E. Houck
University of Wisconsin
Madison, Wisconsin

Charles F. Lillie
The University of Colorado
Boulder, Colorado

Observations of comets in the ultraviolet have a brief history. It begins with the discussion by Biermann and Trefftz (1964) of resonance fluorescence radiation in the ultraviolet. They predicted that comets should be surrounded by a large exosphere of hydrogen atoms and thus possess a very large luminosity at Lyman alpha. These considerations were further developed by Biermann (1968). The first observations of a comet in the vacuum ultraviolet were obtained on January 14, 1970, when OAO-2 recorded the spectrum of the bright comet Tago-Sato-Kosaka (1969g) (Code et al. 1970, Houck and Code 1970). The observations revealed, among other things, the extensive hydrogen Lyman alpha halo predicted by Biermann and Trefftz. OAO-2 continued to collect spectrophotometric measurements of this comet throughout January of that year. On January 28, Princeton University astronomers obtained a photograph of the nucleus in Lyman alpha revealing finer scale structures (Jenkins and Wingert 1972). In February of 1970, the bright comet Bennet (1969i) became favorable for space observations. On the basis of the OAO discovery, OGO-V made several measurements of comet Bennet with low spatial resolution photometers. Since the OGO spacecraft is above most of the Lyman alpha geocorona and the wide field photometers are more sensitive, it was possible to follow the hydrogen halo out to much fainter isophotes (Bertaux and Blamont 1970). OAO-2 continued systematic observations both at Lyman alpha and in other spectral regions for about two months to follow the temporal changes as well as the spatial distribution of the comet's coma. Comet Enke was detected by OGO in January of 1971 at a large heliocentric distance from its Lyman alpha emission.

Figure 1 shows two spectra of comet Bennet that are typical of the results obtained on both bright comets. The spectrum

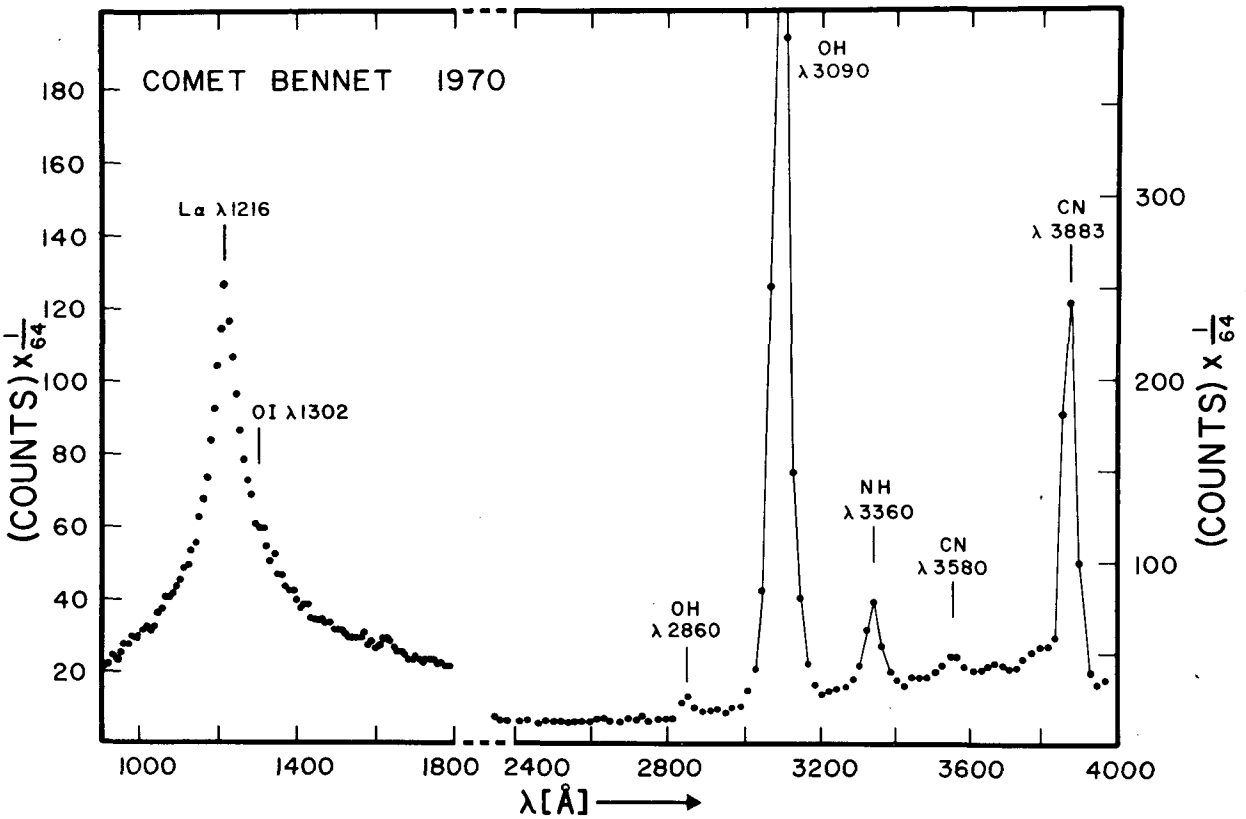

Figure 1.

on the left was obtained with the short wavelength spectrometer and shows the surface brightness in Lyman alpha. The long wavelength spectrometer shows the very strong 0-0 band of OH. The noise in these scans is no greater than the radius of the plotted points and the fine scale features are probably real. Since the spectrometers are objective grating instruments with a slot collimation, a spectral scan of a monochromatic feature represents the surface brightness distribution in a direction parallel to the dispersion. The spatial resolution at Lyman alpha is 1' by 8' in the plane of the sky. One minute of arc corresponds to 10 Angstroms on the spectral scan. The full width at half intensity on the scan illustrated in Figure 1 corresponds to an angular size of 13 minutes for the hydrogen coma, which at the time of observation is about 4.5×10^5 km.

Figure 2 shows Lyman alpha isophotes on April 16, 1970 for comet Bennet obtained by successively scanning the spectrum and offsetting the spacecraft perpendicular to the dispersion. The isophotes are reasonably circular, indicating primarily a radial expansion. The outer isophotes show an elongation in

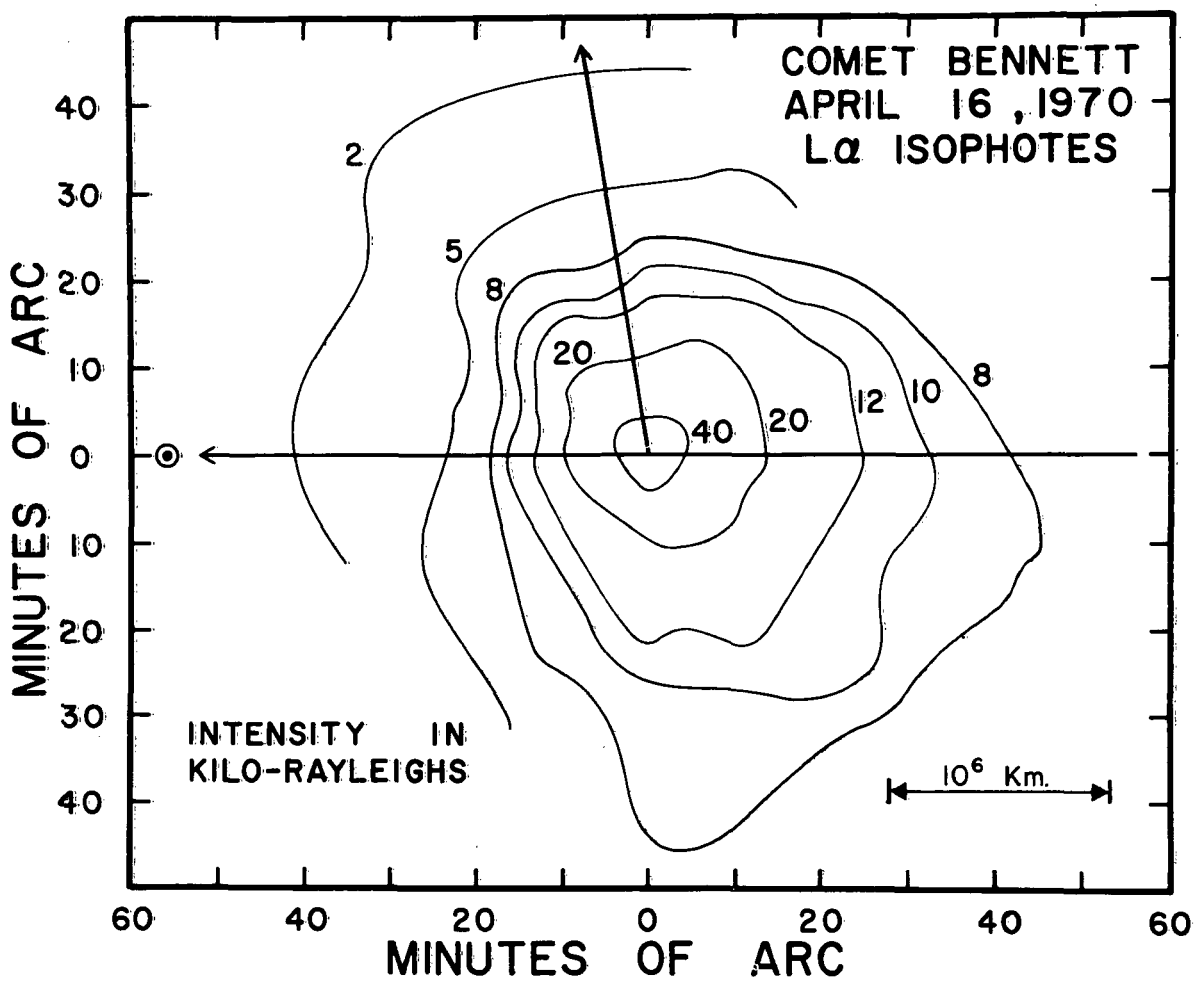

Figure 2.

the anti-sun direction and opposite to the comet motion. This distortion of the isophotes is in reasonable quantitative agreement with calculations of the acceleration produced by Lyman alpha radiation pressure. The isophotes found for April 1 by Bertaux and Blamont (1970) when the radiation flux was twice as great show considerably more elongation.

A lower limit to the number of hydrogen atoms in the coma may be estimated from the integrated brightness. The total number of Lyman alpha photons inferred from the April 16, 1970 isophotes is approximately 3.6×10^{32} photons/sec. Hunten (1970) gives the g-factor for Lyman alpha as $g(L\alpha) = 2.1 \times 10^{-3}$ sec^{-1} which corresponds to 3.2×10^{-3} sec^{-1} at .809 astronomical units. Hence for an optically thin coma the number of hydrogen atoms would be 1.1×10^{35} or 1.9×10^{11} grams. Ber-

taux and Blamont adopted a g-factor of 10^{-3} sec^{-1}, which would yield a mass of 3.8×10^{11} grams, on April 16th. From their measurements on April 1 they found a mass of approximately 2×10^{12} grams. Comparison of these results would suggest that the production of hydrogen varies approximately as r^{-4}. Another source of information bearing on this problem is provided by the variation of reduced surface brightness with heliocentric distance. Both H and OH vary approximately as the inverse 6th power. Delsemme (1972) interprets this result to imply a three-step process involving the evaporation of water ice, the photodissociation of H_2O and the resonance fluorescence of the hydrogen and hydroxyl radical, where each step follows approximately an inverse square law dependence on solar flux. Since the lifetime of H_2O is given as 20 hours by Potter and Del Ducca (1964), virtually all the H_2O would be expected to dissociate well within the coma. In this case the inverse square dependence of the dissociation should not affect the observed surface brightness. The interpretation of these observations is therefore probably more complex than that described by Delsemme. From the above discussion one should have to invoke a different two-step process for the production of hydrogen, possibly the release of ice particles and the subsequent evaporation of a fraction of them. There was, however, a much stronger particle tail for comet Bennet than for comet Tago-Sato-Kosaka although both comets exhibited rather similar hydrogen envelopes.

A variety of circumstantial arguments have suggested that among the cometary ices of Whipple's comet model (Whipple 1950) water ice was the most abundant. Delsemme and Miller (1970) have indicated how the formation of clathrate hydrates on water snow can adequately account for the other observed constituents of cometary spectra. The conclusion that water is a major constituent of comets and that the hydrogen envelope must be primarily due to the photodissociation of H_2O is strongly supported by the OAO observations. The relatively great strength of the OH emission shown in Figure 1 indicates abundances comparable to that of hydrogen and greatly in excess of other gases. The OH emission is about 3 times as strong as the strong 0-0 band of CN at 3883 Å, despite the fact that the solar spectrum is only 1/3 as bright at 3090 Å as it is at 3883 Å and the f-number for CN is about 24 times that of OH. Thus OH should be more than 200 times as abundant. The lifetime for the OH radical should be relatively short (of the order of 10^5 seconds) and dissociate into H and OI (^3P). All OAO scans show a feature corresponding to a few digital counts centered at about 1300 Å on the wings of the Lyman alpha profile. This has been identified on Figure 1 as the OI resonance line at 1302-4-6. Hunten (1970) gives the ratio of g-factors for Lyman alpha relative to OI (^3P-^3S) as 21. The

spectrometer is 1.47 times as sensitive at 1304 Å as it is at Lyman alpha. Therefore, the ratio of counts is

$$\frac{\text{OI counts}}{\text{Ly}\alpha \text{ counts}} = .07 \frac{N_{OI}}{N_H} .$$

If we take the abundance of H to be twice that of OI and assume the same spatial distribution, then we would expect 3.5 counts for OI to correspond to the 100 net counts observed in Lyman alpha. If we compare OI with the intensity of Lyman alpha where the OH intensity has fallen to a few percent, we obtain about 2 counts. Thus, the identification of OI is consistent with the assumption that the parent molecule for H, OH and O is H_2O and is several hundred times as abundant as other constituents.

The assumption that the coma is optically thin in Lyman alpha is probably not valid in the inner 10 minutes of arc. Although this fact would have little effect on the total masses discussed above, it would significantly modify the variation of surface brightness with radius in the inner coma. Using the value of 5.1 ergs cm^{-2} sec^{-1} given by Detwiler et al. (1961) for the solar flux in Lyman alpha at one astronomical unit, we find a photon flux of 5.33×10^{11} photons cm^{-2} sec^{-1} at 0.772 a.u. If complete scattering over the line width of the comet emission is assumed, then the surface brightness would be 42 KiloRayleighs for a width 8 percent of the solar Lyman alpha line. This width is consistent with the measurements described below. This result indicates that the envelope must be optically thick in the inner isophotes. Even the peak intensity found by Bertaux and Blamont of 24 KR with their 40' resolution implies an optical depth greater than 0.5. If the intensity gradient is similar to the OAO results, then the OGO observations with 40' resolution would correspond to a peak surface brightness within 2 minutes of arc of 72 KR.

Optical depths greater than unity within 10 minutes of arc of the nucleus are not in contradiction with the bright core found by Jenkins and Wingert (1972). This is because the comet was observed nearly perpendicular to the direction of incident solar radiation. In this case solutions of the appropriate radiative transfer problem indicate a peak in the intensity slightly in front of the comet nucleus proper.

The width of the comet emission line has been determined by measurements during perigee where the telluric absorption reduces the intensity of the comet emission. The residual hydrogen above the satellite corresponds to an optical depth of the order of 0.6 and thermal doppler width of about 1000°K. As comet Tago-Sato-Kosaka passed through perigee the telluric absorption moved across the comet emission line at about 50 milliangstroms per day.

An upper limit to the width of the comet emission is given by the fact that no absorption was detected until the velocity difference between the earth and the comet was less than 10.4 km/sec or a doppler shift of 0.042 Å. Now the telluric absorption corresponds to a thermal width of the order 1000°K; thus the comet emission if Maxwellian would be less than 3000°K. A more detailed analysis of the decrease in Lyman alpha intensity during perigee passage yields a thermal doppler width for the emission in comet 1969g of 1600°K.

Comet 1969g was observed during the time in which its coma occulted the star π Psc and comet 1969i when it occulted σ Cas. Preliminary analysis of these data indicates absorption of starlight in the center of the OH band for comet 1969g.

REFERENCES

Bertaux, J. L. and Blamont, J. 1970, C. R. Acad. Sci. Paris 270, *1581.*
Biermann, L. 1968, JILA Report 93, University of Colorado.
Biermann, L. and Trefftz, E. 1964, Z. Astrophys. 59, *1.*
Code, A. D., Houck, T. E. and Lillie, C. F. 1970, I.A.U. Announcement Card 2201.
Delsemme, A. H. 1971, Science 172, *1126.*
Delsemme, A. H. and Miller, D. C. 1970, Planet Space Sci. 18, *717.*
Detwiler, C. R., Garret, D. L., Purcell, J. D. and Tousey, R. 1961, Am. Geophys. 17, *263.*
Houck, T. E. and Code, A. D. 1970, Bull. Amer. Astron. Soc. 2, *321.*
Hunten, D. M. 1971, The Radiating Atmosphere, ed. B. M. McCormac (Dordrecht: Reidel Publ. Co.).
Jenkins, E. B. and Wingert, D. W. 1972, Ap. J., in press.
Potter, A. E. and Del Ducca, B. 1964, Icarus 3, *103.*
Whipple, F. L. 1950, Ap. J. 111, *375.*

OBSERVATIONS OF VENUS, MARS, JUPITER AND SATURN LONGWARD OF 2000 Å

L. Wallace
Kitt Peak National Observatory
Tucson, Arizona

J. J. Caldwell and Blair D. Savage
University of Wisconsin
Madison, Wisconsin

ABSTRACT

A number of high quality spectra of Mars, Jupiter, the combined disk and rings of Saturn, as well as lower quality spectra of Venus, have been obtained with an objective grating spectrometer of the Wisconsin Experiment Package of OAO-2. An intercomparison of the Mars, Jupiter and Saturn spectra has failed to disclose any discrete planetary absorptions. Continuous albedos have been derived for the four planets by using OAO-2 observations of G-type stars for $\lambda > 2700$ Å and a new photoelectric solar spectrum by A. L. Broadfoot for $\lambda < 2700$ Å. The geometric albedo of Mars shows a steady increase below 3500 Å which appears to be due to Rayleigh scattering combined with a decreasing surface reflectivity. The albedos of Venus, Jupiter and Saturn show a maximum in reflectivity in the region of 2500 Å.

I. INTRODUCTION

The second Orbiting Astronomical Observatory (OAO-2) was launched in December 1968. At the time of writing (~2-1/2 years later) the Wisconsin Experiment Package in OAO-2 is still successfully obtaining high quality ultraviolet astronomical data. The observatory has been used for making ultraviolet observations of stars, gaseous nebulae, interstellar matter, star clusters, galaxies, diffuse background radiation, and solar system objects such as comets, planets and the zodiacal

light. Thus far the planets Venus, Mars, Jupiter, Saturn, Uranus and Neptune have been observed with either broadband photometers or low-resolution spectral scanners. In this paper we present the results of observations of Venus, Mars, Jupiter and Saturn longward of about 2000 Å.

The Wisconsin Experiment Package has been described by Code et al. (1970). The package contains four 8-inch broadband ultraviolet photometers, one 16-inch broadband photometer, which failed before planetary observations were made, and two objective grating scanning spectrometers. One spectrometer operates between 1050 Å and 2000 Å with a nominal resolution of 10 Å. The other spectrometer operates between 1800 Å and 3600 Å with a nominal resolution of 20 Å. This paper considers the scanner and photometry data on the brighter planets longward of 2000 Å. These data have been used to derive geometric albedos over the spectral region 2100-3600 Å. Observations at shorter wavelengths with the scanners have not revealed measurable planetary fluxes.

In § II we discuss some aspects of the data reduction and in § III we discuss the method of determining the continuous albedos. In § IV we present the results of an unsuccessful search for absorption features which are narrow enough to be undetected in the continuous albedos obtained in § III. In § V we compare the OAO data with previous observations and in § VI we discuss the results.

II. DATA REDUCTION

The longer wavelength spectrometer scans between 1800 Å and 3600 Å in discrete steps of approximately 20 Å. The exit slit width is 20 Å and the integration time used for the planetary observations was 8 seconds per step position except for a single scan of Saturn with a 64-second integration time. With the 8-second integration time the spectrum from 1800 Å to 3600 Å was scanned in about 13 minutes. Typically a planet was scanned twice in one night period of the satellite's orbit.

Table 1 lists the various scans that were analyzed in this paper along with data concerning the planets at the time of observation. Other scanner observations were attempted but those data were judged to be of poor quality because of various observing problems. The data on Venus listed in Table 1 are of lower quality than those on Mars, Jupiter and Saturn. When the Venus observations were attempted the digital counter was inoperative, so that only an analog signal of lower quality was recorded. Restrictions on the pointing of OAO-2 close to the sun prevented us from obtaining additional Venus data.

Repeated observations of objects with the long wavelength spectrum scanner have shown that the count rate at any given

Table 1. OAO Spectral Scans Used in the Analysis

Planet	Orbit & Data Frame Number of Scan	Date (1969)	Hour (U.T.)	Phase Angle (Degrees)	Comments
Venus	1029(1) 1029(3)	February 16	21 h	103.0	
Mars	1608(2) 1608(4) 1610(1) 1610(2)	March 29	5 h	34.5	Longitude of Central Meridian (LCM) = 120°
	1966(12)	April 23	1 h	26.8	LCM = 200°
Jupiter	2316(23) 2317(3) 2317(4)	May 17	12 h	9.3	LCM (System II) = 123°
	2510(2) 2510(3)	May 31	17 h	10.3	LCM (System II) = 64°
Saturn	2782(23) 3124(1)	June 19	20 h	6.2	Ring Parameters B=17.8 B'=15.9
	3125(5)	July 12	17 h	6.0	B=18.4 B'=16.2

wavelength varies by about ±30% over periods of several days. This problem is due to difficulties in the discriminator circuit of the scanner. The observed spectral distributions are, however, highly reproducible (±2 to 4%) (Bless and Savage 1972). Because of the discriminator problem, planetary albedo curves have been determined by using the scanner data to set the relative run of the albedo while OAO broadband photometry data and ground-based photometry data were used to set the absolute level of the albedo.

A. D. Code (private communication) has provided the spectrometer calibration curve which allows the counts to be converted into relative flux units. This curve has been derived from a combination of (1) a laboratory calibration performed one year before the flight; (2) OAO observations of early-type stars compared to models; (3) OAO observations of α CMa compared to Stecher's (1970) calibrated photometric measurements of this star. Calibration curves based on all the above methods agree to within 15% over the region 1800-3600 Å. We believe that the spectrometer relative calibration curve used here is accurate to ±10%.

Figure 1 gives a typical scan of Mars on a linear signal scale. It is apparent that below 1900 Å, where the solar flux is falling off rapidly, the signal remains constant. For the planets fainter than Jupiter this signal is at approximately the dark level but shows some variation which is due to the influence of the Earth's radiation belts and background light accepted by the objective grating instrument. A larger short-wavelength signal from Jupiter (which was about five times brighter than Mars) is due to scattering of the Jupiter light internal to the instrument. From scans of the sky with the long wavelength spectrometer it was found that the sky background typically increases from about 5 counts to 9 counts when scanning from 1800 Å to 3600 Å (one OAO count corresponds to 64 photoevents). Thus to correct the OAO scans of the planets fainter than Jupiter, we have assumed that the background is sky background and made a correction in which the observed level at 1800 Å increased linearly by 4 counts to 3600 Å. In the case of the Jupiter scans, we have assumed the scattered light contribution to the background to be the same at longer wavelengths as it was at 1800 Å. In all cases the uncertainty introduced by the background correction is small longward of 2300 Å because of the large increase of the planetary signal. In § III we will discuss the possible uncertainties introduced into the measurements by these background corrections.

Because the spectrometer has no entrance slit the wavelengths of the data points are subject to uncertainties due to pointing errors in the attitude control system and to errors in the predicted target position. Consequently, it was neces-

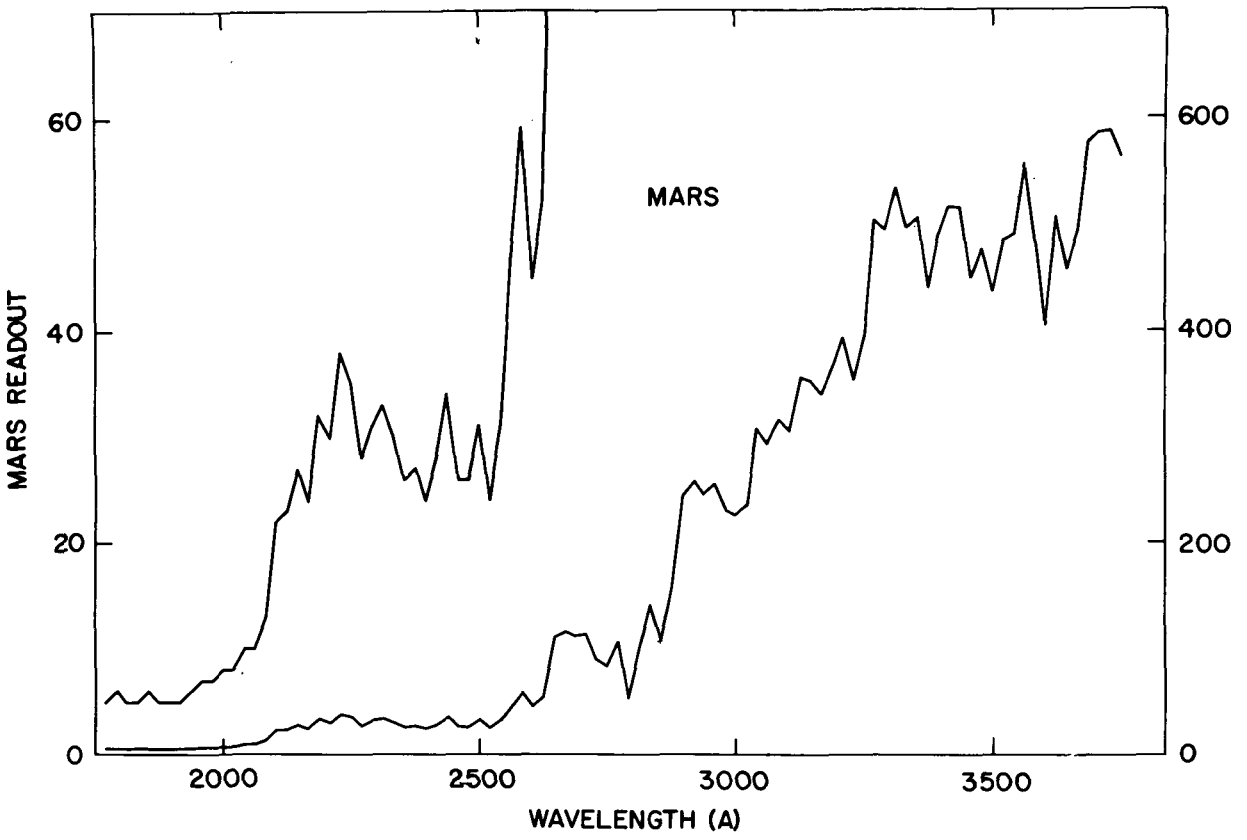

Figure 1.—OAO-2 spectral scan of Mars. The data points, connected with straight line segments, are given on two scales differing by a factor of 10. The telemetered readout is the photo event count divided by 64.

sary to establish the wavelength scale for each spectrum by comparison with a synthetic solar spectrum. We generated this synthetic spectrum from the digitized version of the NRL solar material given by Brinkmann, Green and Barth (1966) for wavelengths less than 2990 Å, and the digitized version mainly of Brückner's (1960) material given by Furukawa, Haagenson and Scharberg (1967) for wavelengths greater than 2990 Å, smeared to the resolution of the instrument. The wavelength determinations appeared accurate to the order of 1 Å in the region of 2800 Å and perhaps as uncertain as 3 Å at other wavelengths.

III. CONTINUOUS ALBEDOS

Preliminary OAO albedo curves were discussed by Wallace (1970) and Caldwell (1971). Solar data used to obtain those

curves were taken from Brinkmann et al. (1966) for wavelengths less than 2990 Å and from Furukawa et al. (1967) for longer wavelengths. When the OAO albedos were joined to ground-based albedos at 3600 Å, all the curves showed an abrupt change in slope at 3600 Å. Since it was physically unreasonable to expect all planets to exhibit this unusual feature, it was concluded that these preliminary curves were in error because of uncertainties in the solar ultraviolet data.

As a result of these problems, we have developed a reduction method that avoids using the ultraviolet solar data cited above. Two fortunate circumstances have made possible a significant improvement over the preliminary curves. First, Broadfoot (1972) has made available to us before publication his recent photoelectric measurements of the sun in the ultraviolet. Second, Caldwell (1971) has demonstrated that OAO observations of late-type stars similar to the sun can be used to obtain accurate planetary albedos down to a wavelength of about 2700 Å. This second procedure has the advantage that albedos can be derived which are independent of the sensitivity curve of the scanner and a solar spectrum measured by another instrument. Caldwell (1971) found that, for unreddened late-type stars of luminosity classes V and IV, their (B-V) colors are excellent indicators of the stars' ultraviolet energy distributions. For a detailed discussion of OAO late-type star photometry see Doherty (1972). To take advantage of this correlation of flux distribution with color, it is necessary to know $(B-V)_\odot$. However, it is extremely difficult to measure this parameter precisely. $(B-V)_\odot$ has been determined through several indirect means to be 0.65 ± 0.01 by van den Bergh (1965). More recent determinations by Fernie et al. (1971) of 0.628 ± 0.011, by Alexander and Stansfield (1966) of 0.663 ± 0.008, and by Spite (1966) of 0.68 bracket the result of van den Bergh. For this paper, we used the value 0.65. This is also the value of $(B-V)_\odot$ generally used for interpolating among standard star observations to obtain albedos in the visible region of the spectrum (Young and Irvine 1967; Irvine et al. 1968a,b). An uncertainty of ±0.02 in $(B-V)_\odot$ will introduce an uncertainty into albedo determinations of ±10% at 3600 Å, ±20% at 2600 Å, and ±30% at 2200 Å. Because of this increasing uncertainty toward shorter wavelengths and because OAO scanner observation of G stars are generally unreliable below 2500 Å, we proceeded to generate albedo curves as follows: (1) We used OAO scanner data for the G star ζ Her (B-V = 0.65) to obtain relative albedo curves down to 2700 Å. Interpolation among G stars having (B-V) colors from 0.55 to 0.75 to a (B-V) of 0.65 produced a spectrum essentially identical to that of ζ Her for $\lambda > 2500$ Å, so that it is expected that the relative shapes of the albedo curves in this region are very accurate. (2) At wavelengths less than 2700 Å, we

used Broadfoot's (1972) photoelectric solar spectrum. (3) The long and short wavelength sections of the albedo curves were joined in the region 2650-2700 Å. (4) The absolute level of the OAO albedo curves was determined by OAO broadband filter photometry in those cases where it was available; otherwise the data were scaled to the ground-based photometry of Irvine's group. This procedure was made necessary by the previously mentioned sensitivity changes of the scanner. Since each broadband OAO photometer has a Cerenkov calibration source, absolute sensitivity changes of the OAO photometers (which proved to be small) could be accounted for. The OAO broadband filters used for this purpose have effective wavelengths (for G2 stars) and full widths at half intensity of 3075 Å (FW = 420 Å) and 3062 Å (FW = 440 Å).

To calculate geometric albedos from OAO broadband filter data, photometry of ζ Her was used. The photometric data for this star are: V = 2.81, (B-V) = 0.65, (U-B) = 0.21 (Johnson et al. 1966). For the sun, we used: $V_\odot$ = -26.74 (Johnson 1965), $(B-V)_\odot$ = 0.65 (van den Bergh 1965), $(U-B)_\odot$ = 0.14 (Fernie et al. 1971). All ζ Her photometry was scaled to the sun by adjustment of the U magnitude (ΔU = 29.62). Planetary radii were taken from Dollfus (1970) and planetary distances were taken from The American Ephemeris and Nautical Almanac. Good OAO broadband photometry, taken within a few hours of the respective scans, exists for Mars (at phase angle 26.8°), for Jupiter and for Saturn. For the other OAO scanner data it was necessary to normalize the OAO observations to ground-based photometry because in these cases the OAO photometry observations were not successful.

The OAO geometric albedos for Venus, Mars (at two phase angles), and Jupiter are plotted in Figures 2, 3, 4 and 5. These geometric albedos are defined as the ratio of the observed brightness to the brightness of a Lambert disk at the same distances and of the same size as the planet, but observed at zero phase angle. For Saturn (disk plus rings) we give, in Figure 6, the ratio of the measured brightness compared to that of the sun. In these figures we also give the corresponding ground-based measurements. The curves were evaluated for 100 Å averages of the ratio planet/ζ Her for $\lambda > 2700$ Å, and the ratio planet/sun for $\lambda < 2700$ Å. The two Venus scans (see Table 1) were combined and represent the planet at a phase angle of 103°. The curves for Mars for the two phase angles are presented separately because the change in phase angle was large. The four scans at the phase angle of 34.5° were combined. Since the five independent Jupiter scans all exhibited the same spectral variation, they were combined to represent the planet at a phase angle of 10°. Similarly, the three Saturn scans were combined to represent the planet at a phase angle of 6° and ring inclinations of B = 18° and B' =

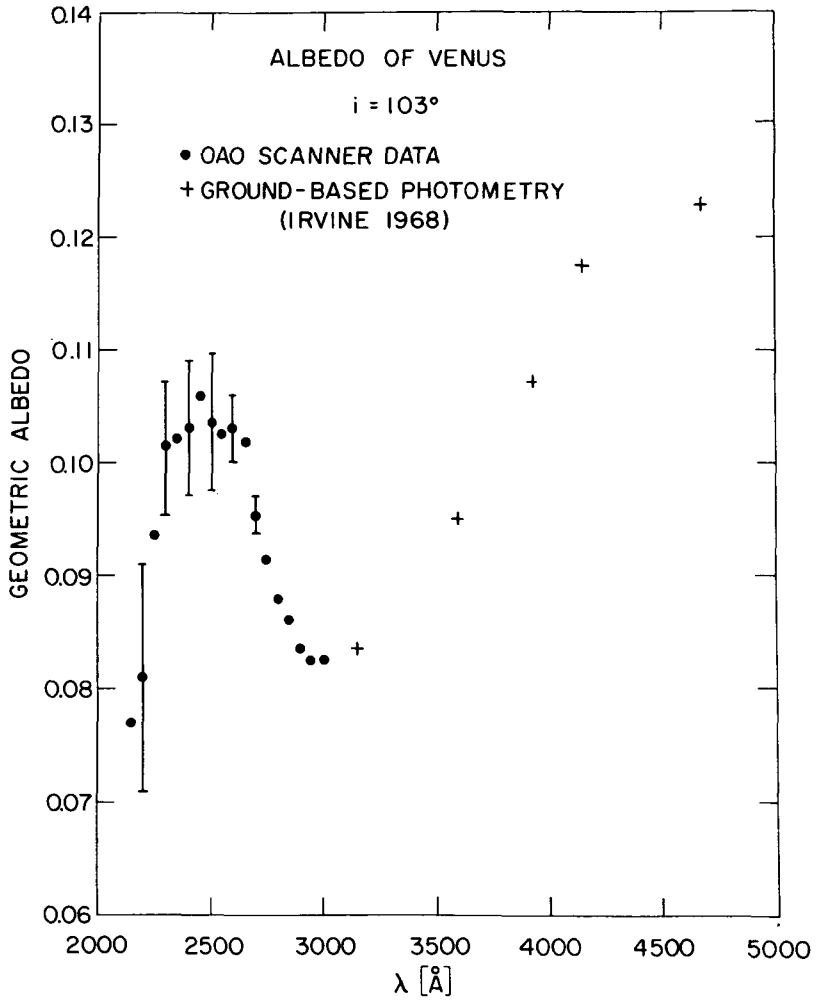

Figure 2.—Continuous geometric albedo of Venus at a phase angle of 103°. The error bars indicate the possible error due only to the uncertainty in the background correction. The absolute level of the OAO curve has been adjusted to smoothly join onto the ground-based data of Irvine (1968).

16°. As was the case for Jupiter, there was no indication of any change in spectral detail, so that no information was lost by combining scans.

The ground-based photometric data plotted in Figures 2, 3, 4, 5 and 6 were taken from the results of various papers reporting on the data of the Harvard College Observatory planetary photometry program. For Venus, albedos for the phase angle of 103° were obtained from the data of Table I of Irvine (1968). The data of Irvine et al. (1971) were used to calcu-

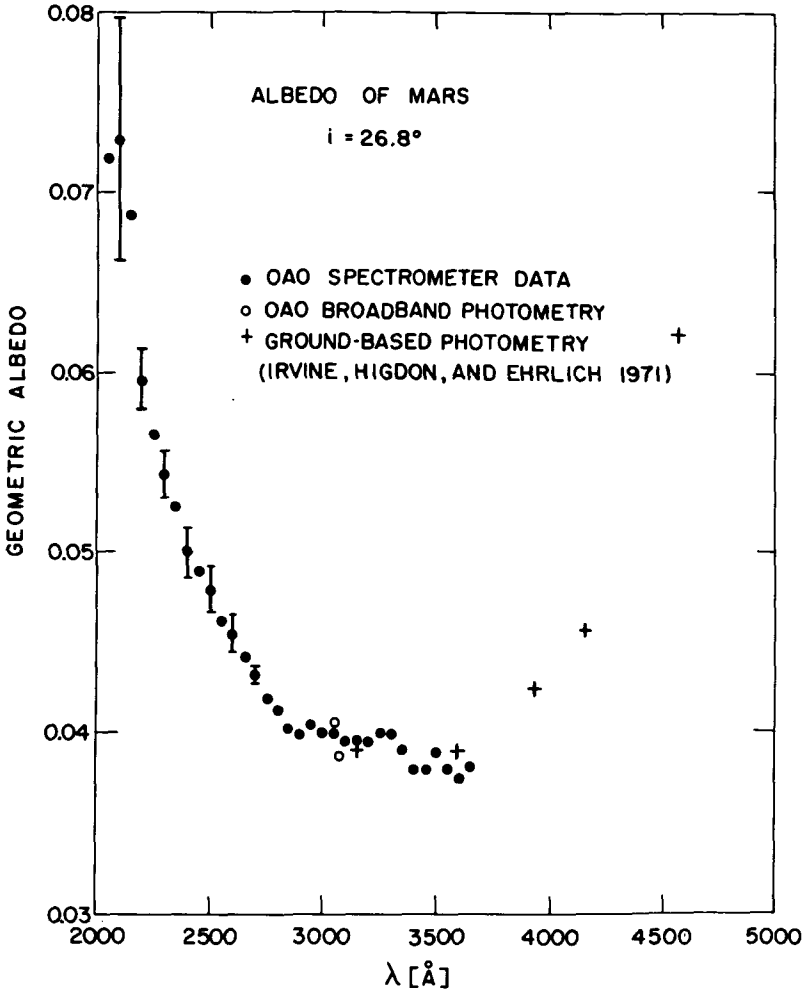

Figure 3.—Continuous geometric albedo of Mars at a phase angle of 26.8°. The error bars indicate the possible error due only to the background correction. The absolute level of the OAO curve has been set by the OAO broadband photometry. The ground-based data from Irvine, Higdon and Ehrlich (1971) are for the phase angle of the OAO observation.

late geometric albedos for Mars for phase angles of 34.5° and 26.8°. The magnitudes and phase coefficients derived by Irvine et al. (1971) using data only from phase angles greater than 15° were used here, that is, columns two and three of their Table I. These authors made this restriction because their observations at smaller phase angles are affected by the zero-phase anomalous brightening. Since the zero-phase effect is not important for the OAO observations, the comparable ground-

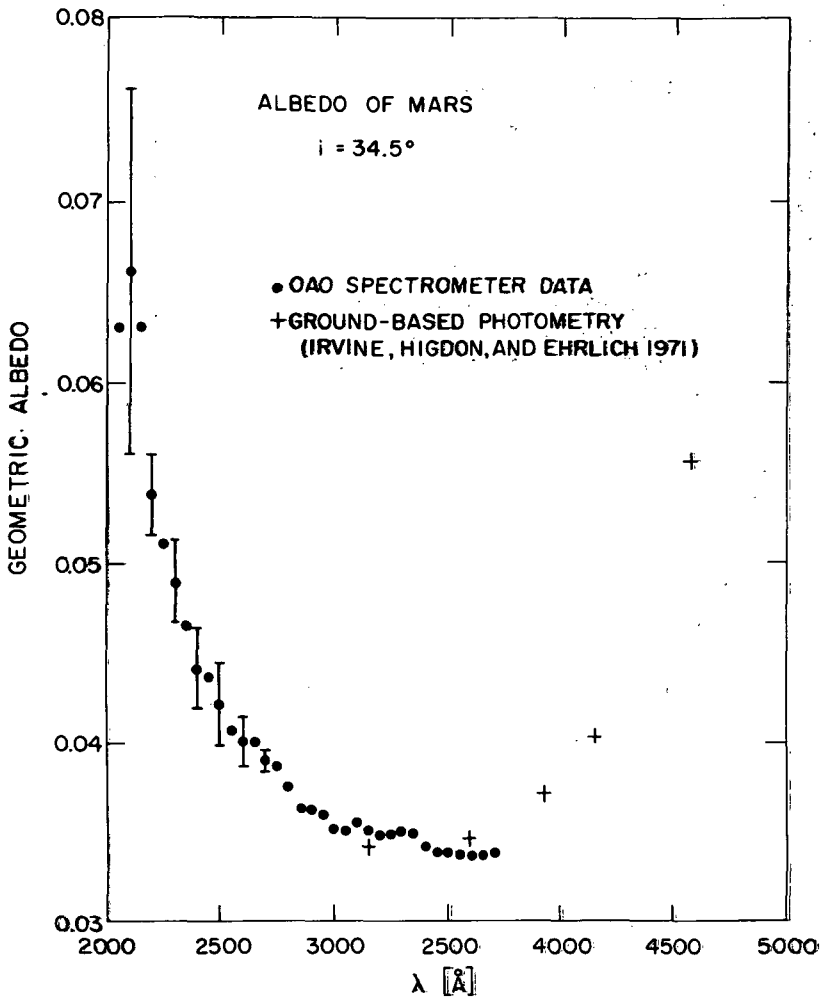

Figure 4.—Continuous geometric albedo of Mars at a phase angle of 34.5°. The error bars indicate the possible error due only to the background correction. The absolute level of the OAO curve has been adjusted to the ground-based data of Irvine, Higdon and Ehrlich (1971) for the phase angle of the OAO observation.

based data excluding it were used here. For Jupiter, Hopkins and Irvine (1971) present albedo calculations for three different apparitions (their Table II). For the present paper, these results were averaged, and a phase coefficient of 0.005 magnitudes per degree (Irvine et al. 1968b) was used to derive geometric albedos at a phase angle of 10°. For Saturn, the data of Irvine and Lane (1971) were used. Average phase coefficients were computed from their Table I for each of their fil-

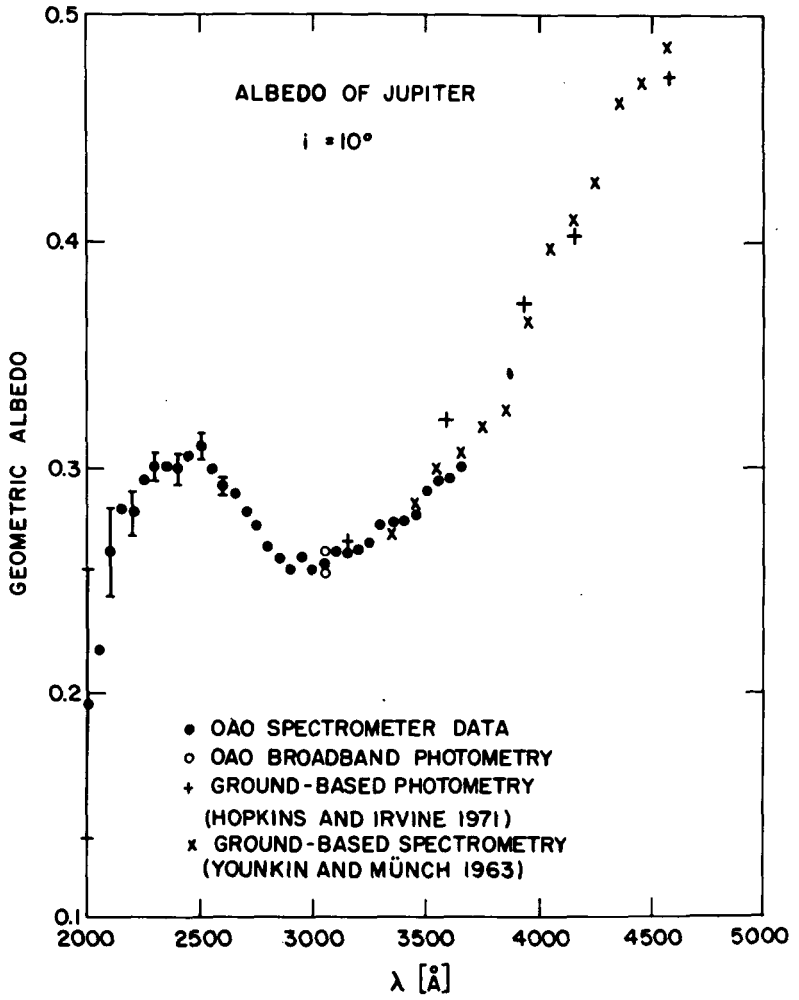

Figure 5.—Continuous albedo of Jupiter at a phase angle of 10°. The error bars indicate the possible error due only to the background correction. The absolute level of the OAO curve has been set by the OAO broadband photometry data at 3062 Å. The ground-based data of Hopkins and Irvine (1971) for a phase angle of 10°, as well as the relative ground-based data of Younkin and Münch (1963) adjusted to the data of Hopkins and Irvine, are also shown.

ters, and these were used with their values of m_{nr}, a and a' (presented in their Table III) to calculate total brightness (rings and planet) for the phase angle of 6° and ring inclinations B = 18° and B' = 16° at which Saturn was observed by the OAO. For Saturn (see Figure 6) we have also indicated the contributions from the planet alone as calculated from the data

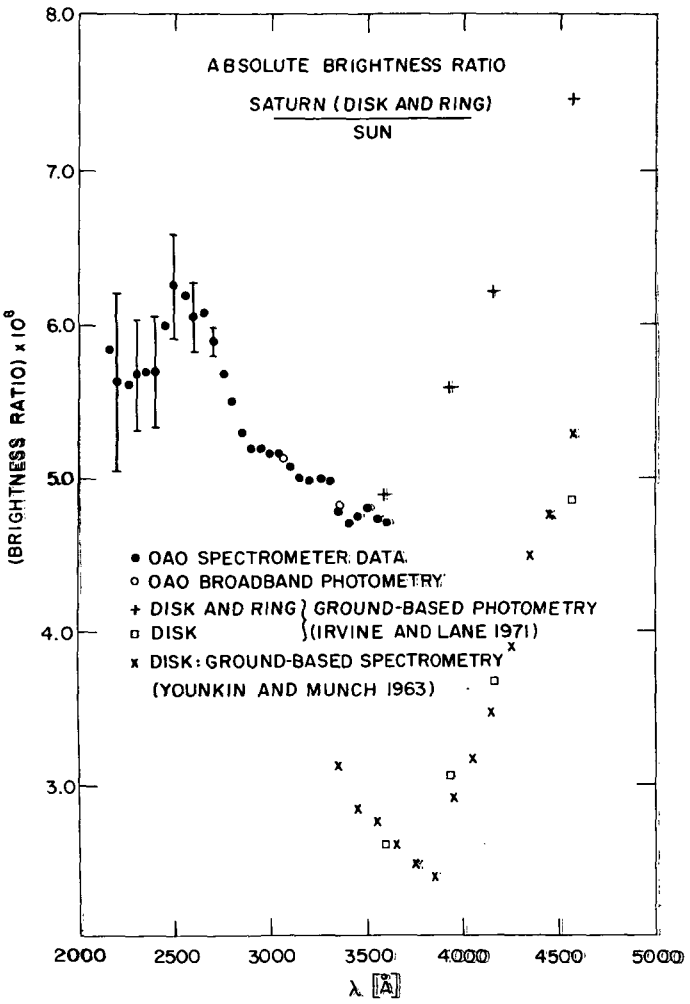

Figure 6.—Absolute brightness ratio of Saturn (disk plus ring). The phase angle was 6° and the ring inclinations B = 18° and B' = 16°. The error bars indicate the possible error due only to the background correction. The absolute level of the OAO curve has been set by the OAO broadband photometry data at 3062 Å and 3590 Å. The ground-based data of Irvine and Lane (1971) for the disk and rings together and disk alone are shown for the phase and inclinations of the OAO data. The relative ground-based data of Younkin and Münch (1963) adjusted to the data of Irvine and Lane are also shown.

of Irvine and Lane (1971). Since the rings contribute a major part of the observed light from the planet, and since we have

no data on the variation of brightness with ring inclination in the ultraviolet, the Saturn curve is represented as an absolute ratio of planet (disk plus rings) to solar brightness, rather than as a geometric albedo. For all planets, calculated ground-based albedos were adjusted for the values of $V_\odot$ (-26.74) and planetary radii (Dollfus 1970) used here, which are slightly different than those used by Irvine and his group.

The error bars in the geometric albedo curves show the uncertainty due to possible errors in the background correction. These errors depend on the quality of the data and were judged to range from 20% of the background correction in the best cases to 40% in the worst cases. Over the region 2100-2700 Å, further sources of possible error are: (1) OAO calibration curve errors and (2) errors in Broadfoot's (1972) photoelectric solar spectrum. The combined effects of these two sources of error lead to an uncertainty that is unlikely to exceed 15%. Over the region 2100-2700 Å Broadfoot's (1972) solar spectrum used here was very similar (±10%) to the NRL spectrum except for the region 2400-2700 Å where the difference became as large as 20%. In the region 2700-3600 Å, the uncertainty of $0^m.02$ $(B-V)_\odot$ introduces an uncertainty of about 10% in the albedo determinations. In summary, over the region 2100-3600 Å, the relative accuracy of these albedo curves is probably about ±10 to 15%.

As can be seen from Figure 2, the absolute normalization of the OAO observations of Venus is less certain than for the other planets because there is no planetary broadband OAO photometry, and the scanner data do not overlap with the ground-based observations. The absolute level of the albedo shortward of 3000 Å depends on the assumption that there are no spectral features in the gap from 3000 Å to 3150 Å. Longer wavelength scanner data were lost because the signal recorded for Venus was saturated.

IV. NARROW ABSORPTION FEATURES

We have made a detailed intercomparison of the planetary spectra in order to detect narrow absorption features which would have gone unnoticed in the continuous albedos derived in § III. Small photometric errors and uncertainties in the instrumental profiles make the use of the solar spectrum for this purpose very unprofitable (cf. Anderson *et al.* 1969). The chance coincidence of a trace absorber common to the two planets being compared would, of course, lead to a negative result. However, the physical natures of the planets under consideration are different enough that such coincidences are unlikely.

Since the continuous albedos of the planets are significantly different, only short strips of spectra of the different

planets 50 Å to 100 Å long, could be compared at a time. This comparison showed no differences significant to within the scatter of the data. We have also constructed Jupiter/Mars ratios at 100 Å intervals using 100 Å strips of the data and used these ratios to scale the Mars spectra to Jupiter. The result of this process is given in Figure 7. Again there do not appear to be any significant differences.

The peak-to-peak scatter in the data of Figure 7 is given in Figure 8. The general increase in scatter from long wavelengths to short is due to the decreasing signal. In addition, an increase in the scatter is apparent where the signal level changes rapidly. Below about 2175 Å the signal-to-noise ratio decreases rapidly so that the data contain essentially no information on narrow features. Figure 9 gives the result scaling the Saturn spectra to Mars, again showing no significant features. The corresponding peak-to-peak scatter is about 1.2 times greater than that given in Figure 7. The Venus spectra were not good enough to warrant a similar comparison.

The scanner obtained only one data sample per 20 Å slit width instead of the three or more per slit width usually obtained with such instruments. In addition, the data points for the Jupiter spectra occur in 4 Å wide clusters separated by about 16 Å gaps; those for Mars occur in 10 Å wide clusters centered in Jupiter gaps. This character is apparent in Figures 7 and 9 and is presented in more detail in Figure 10. The mean wavelengths of the Jupiter sampling points are given in Table 2.

To investigate how much narrow absorption could be hidden between two successive data points we have constructed a series of synthetic profiles. The instrumental profile was taken as the convolute of a square wave 20 Å wide, representing the exit slit, and a uniform disk 6 Å wide, representing the disk of Jupiter. We then convolved this profile with a series of absorptions of Gaussian shape, zero residual intensity, and a range of half widths. Finally, these synthetic profiles were compared with a grid of sampling points separated by 21 Å to establish as a function of position between grid points and the peak-to-peak noise in the data, how large an absorption could be hidden. For a profile centered on an observed wavelength this was taken as the product of the percentage peak-to-peak noise and the 20 Å wide slit. The results are given in Figure 11. As the center of the profile is displaced from an observed wavelength the maximum equivalent width remains constant since the profile, for small absorptions, retains a flat bottom in the central region. Displacements beyond that point indicate that rapidly increasing amounts of absorption could be hidden, becoming a maximum when the profile is centered between two observed wavelengths. Other approximations, including a planetary disk of zero width and a square absorption

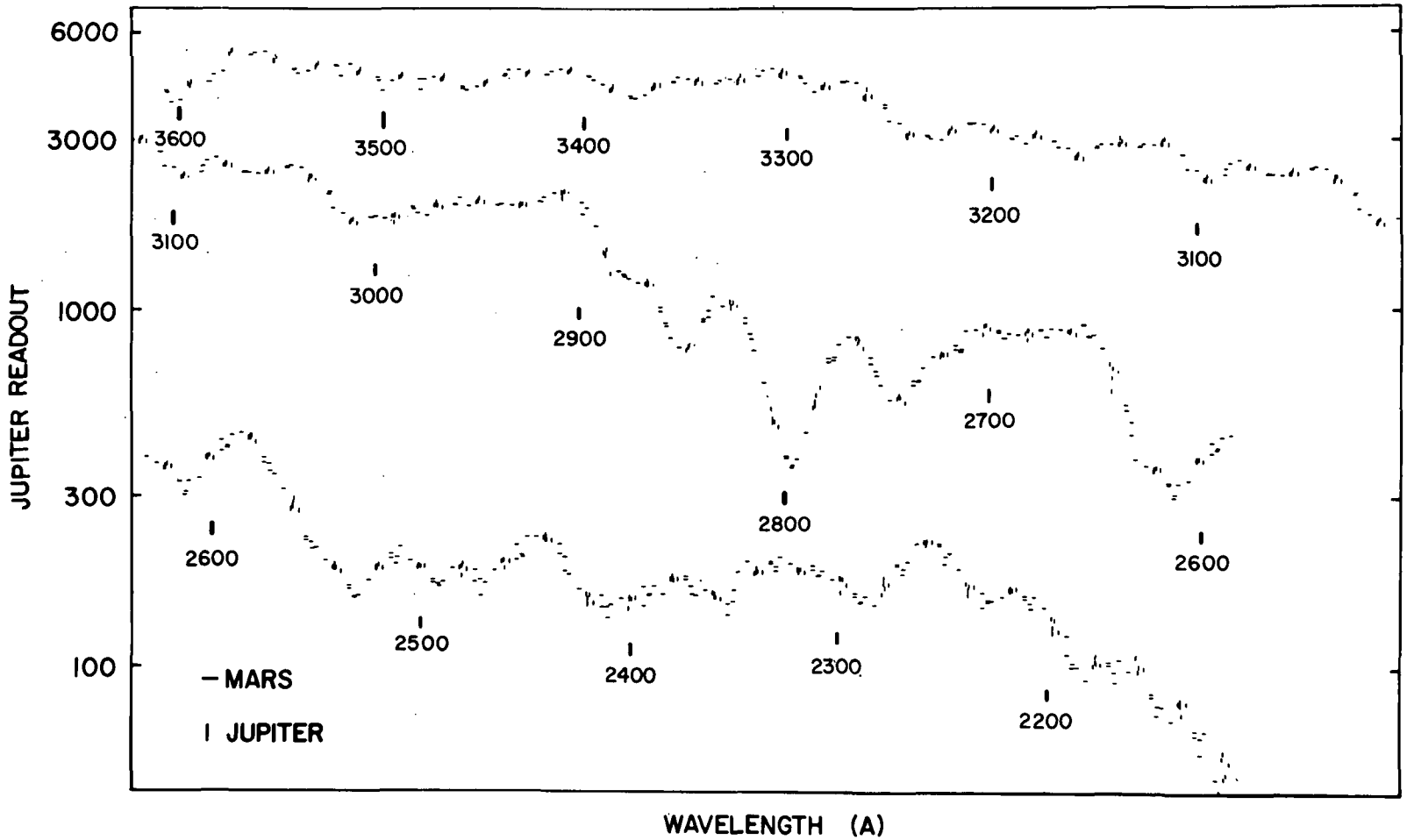

Figure 7.—A comparison of the Jupiter spectrum with adjusted spectrum of Mars. The adjustment, at 100 Å intervals, compensated for the difference in continuous albedos. The lack of significant residual differences between the two spectra indicates that there are no significant narrow absorption features in either spectrum.

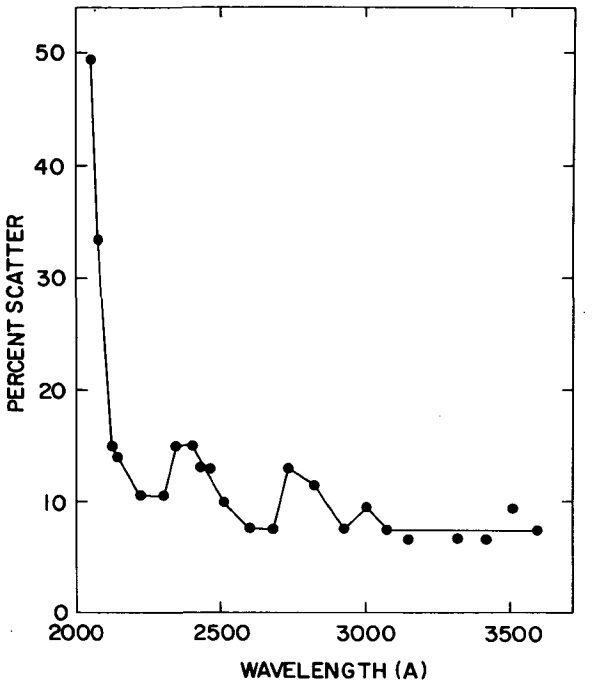

Figure 8.—Peak-to-peak scatter in units of the signal level of the combined Jupiter-Mars spectrum of Figure 7.

with zero residual intensity yield essentially identical results. Consequently, we believe the estimates given in Figure 11 are conservative. Since the results are very insensitive to the size of the planetary disk, as long as it is small compared to the slit width, they can be used equally well for Mars, Jupiter and Saturn.

The equivalent width of a potential feature can be estimated by obtaining the wavelength displacement from Figure 10 and Table 2, the peak-to-peak noise from Figure 8, and then the equivalent width from Figure 11.

V. COMPARISON WITH PREVIOUS OBSERVATIONS

The present results longward of about 2300 Å are superior to those previously reported. The spectra are inherently cleaner and we have been able to use an improved solar reference synthesized from observations of solar-type stars obtained with the same instrument for $\lambda > 2700$ Å, while for $\lambda < 2700$ Å we have made use of an improved photometric solar spectrum. The remarkable agreement between the OAO albedos and the independently derived ground-based albedos seen in Figures 3, 5 and 6 gives an indication of the quality of these new data.

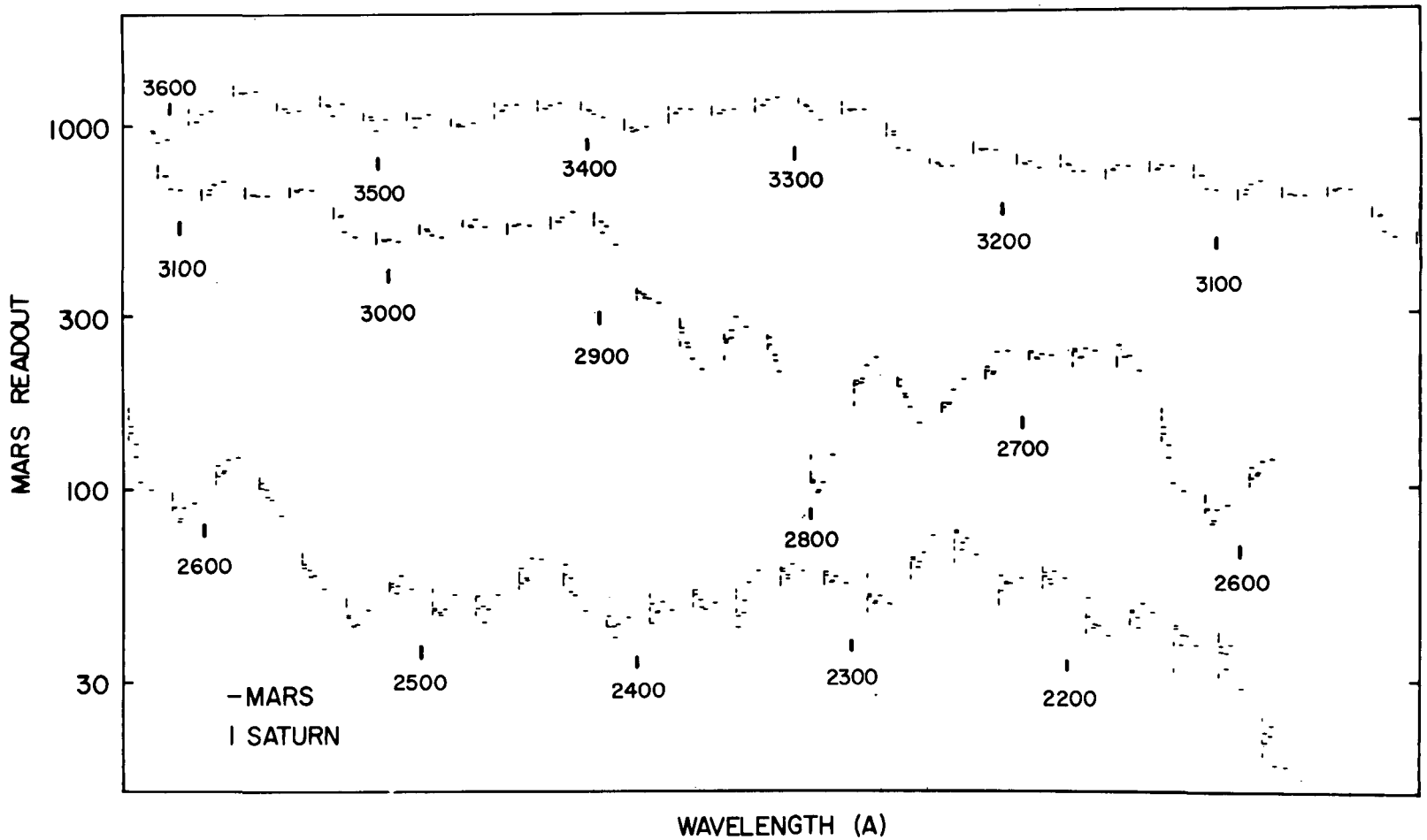

Figure 9.—A comparison of the Mars spectrum with the adjusted spectrum of Saturn. See caption to Figure 7.

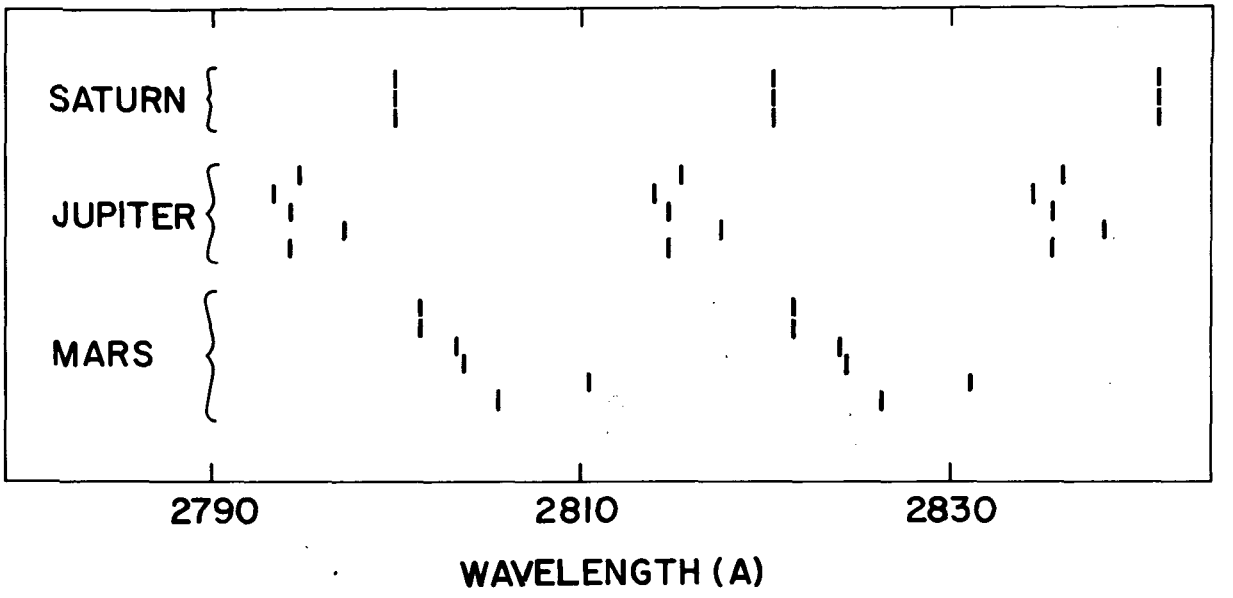

Figure 10.—Wavelengths sampled near 2820 Å in the spectra of Mars, Jupiter and Saturn.

The data of Anderson et al. (1969) for Venus do not show as pronounced a hump at ~2500 Å as our data but they do extend to shorter wavelengths and exhibit a cutoff due to CO_2 absorption beginning at about 2100 Å. The less well-defined data of Jenkins, Morton and Sweigart (1969) suggest a hump at ~2400 Å similar to what we have observed. The broad minimum in the albedo at ~2600 Å suggested by the results of Evans, Boggess and Scolnik (1965) and Evans (1967) has not been verified by the subsequent observations. Possible narrow absorptions at about 2174 Å suggested by Jenkins et al. (1969) and at 2145 Å suggested by Anderson et al. (1969) do not appear to be real.

Evans' (1965) determination of the Mars albedo disagrees only slightly with the OAO determination, since the OAO material is almost included within his error estimates (0.07 to 0.20 at 2400 Å). Broadfoot and Wallace (1970) reported a Mars albedo flat to within about 5% from 3200-2500 Å whereas our results show a 20% increase over the same region. The difference may be due to the different solar reference spectrum. Similarly the dip in the Mars albedo at 2500 Å reported by Wallace (1970) and Caldwell (1971) on the basis of the same planetary spectra used here, does not appear in the present reduction because of the different solar reference spectrum. Barth and Hord (1971) have reported ultraviolet spectra and albedos obtained with Mariners 6 and 7. Since they were ob-

Table 2. Mean Wavelengths of Jupiter Sampling Points

2094	2618	3113
	39	33
2115	60	54
35	81	74
56		94
77	2702	
98	23	3215
	43	35
2219	64	55
40	85	76
61		96
82	2805	
	26	3316
2303	46	37
24	67	57
45	88	78
66		98
87	2908	
	29	3418
2408	49	39
29	70	59
50	91	79
71		
92	3011	3500
	31	20
2513	52	40
34	72	61
55	92	81
76		
97		

tained at high spatial resolution they are not directly comparable to our results. We can only note that their curve for desert regions shows a factor of 2 increase in reflectivity going from 3500 to 2700 Å, at variance with both the present results and those of Broadfoot and Wallace (1970) obtained in integrated light. Of more importance is their ratio of polar cap spectra to desert spectra which show a broad minimum of about 30% depth entered at ~2500 Å which could be due to ozone absorption. Such a characteristic does not contradict our data because at the time of the OAO observations the projected areas of the north polar cap and southern hood were only 2% and 17% that of the disk.

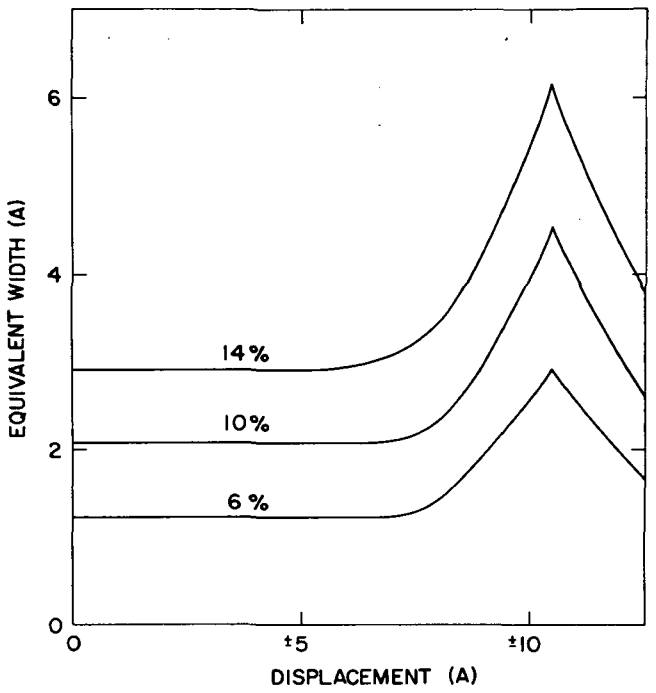

Figure 11.—Maximum equivalent widths of narrow features as a function of peak-to-peak scatter in the data and the difference between wavelength of the features and the wavelength of a point observed.

The Jupiter albedos given by Stecher (1965) and by Evans (1967) are very uncertain and, except for a broad absorption feature at 2600 Å, are consistent with the OAO albedo. Their feature at 2600 Å has not been confirmed by any of the subsequent observations. As with Venus, the Jupiter albedo given by Anderson et al. (1969) does not show as large a hump at 2500 Å as does the OAO data. Their data is better defined shortward of about 2200 Å. Kondo's (1971) Jupiter albedo from 2200-3600 Å differs from ours by no more than 5 or 10% in spite of his use of the Brinkmann-Furukawa version of the solar spectrum. The narrow absorption at 2165 Å mentioned by Anderson et al. (1969) does not appear to be real.

The measurements of Saturn (disk and rings) by Bless, Code and Taylor (1968) at 2450 Å, 2800 Å and 2950 Å are less certain than the OAO data but indicate the same trend.

VI. DISCUSSION

A detailed analysis of the albedos is not presented here since the results of such a process are highly model dependent.

This has been illustrated by Anderson et al. (1969) in their attempts to interpret the ultraviolet albedos of Venus and Jupiter. The general features are, however, worth discussion in view of the fact that any systematic errors that exist in our determinations of the continuum albedos are common to all four of the planets. As we noted earlier, these errors could amount to ~15% and would be more likely to occur shortward of 2700 Å since longward of 2700 Å the use of ζ Her as the solar reference makes the albedos independent of instrumental calibrations.

In order to intercompare the shapes of the albedos we have replotted them on a logarithmic scale in Figure 12. This shows fairly clearly that Venus, Jupiter and Saturn have humps of similar magnitude at ~2500 Å which do not appear in Mars. In previous reductions of these data using the Brinkmann version

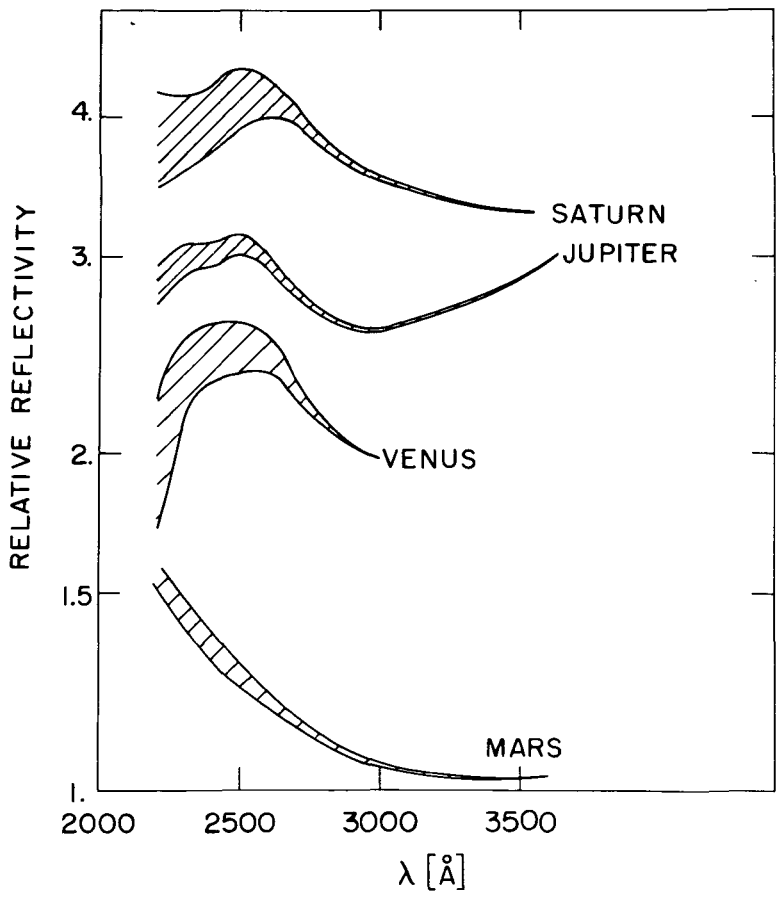

Figure 12.—Relative reflectivities of Venus, Mars, Jupiter and the disk and rings of Saturn. The hatched area at short wavelengths is a measure of the uncertainty of the background correction.

of the solar spectrum instead of Broadfoot's (Wallace 1970; Caldwell 1971) these humps were less pronounced and a depression having at least some of the characteristics of an ozone absorption appeared in the Mars albedo.

To explain the Jupiter hump, Axel (1971) has suggested that the rise in the albedo from ~3000 to ~2500 Å could be due to the increasing importance of Rayleigh scattering. Some absorption beginning at ~2500 Å and increasing to shorter wavelengths could then offset the further increase due to Rayleigh scattering.

The hump in the Venus albedo could have a similar explanation in which HCl might be a candidate for the absorber. CO_2 absorption appears to be responsible for the sharp cutoff below 2100 Å (Anderson et al. 1969) but in view of its lack of influence on the Mars albedo and the discrepancy between different measures of its absorption coefficient above 2000 Å (Shemansky 1972; Ogawa 1971), it is probably not connected with the hump.

The Mars albedo, in contrast to that of Venus, can be explained nicely in terms of Rayleigh scattering by the generally accepted amount of CO_2 (~80 m atm) combined with a general decrease in surface albedo (Caldwell 1971).

The hump in the Saturn reflectivity presents more of a problem since the ground-based observations of Irvine and Lane (1971) given in Figure 6 indicate that longward of about 3600 Å the rings contribute about as much to the reflectivity as the disk and might well contribute more at shorter wavelengths. If that were the case and if the reflectivity of the rings were essentially featureless, any hump in the albedo of the disk would have to be more pronounced than it is in Jupiter in order to show through in the total reflectivity. H_2O crystals now appear to be the best candidate for the ring material (Pilcher, Chapman, Lebofsky and Kieffer 1970), but published measurements of the reflectivity of such crystals (Dressler and Schnepp 1960) do not rule out a hump at the required wavelength. Also, the ground-based spectrometric observations of Younkin and Münch (1963) of Saturn's disk indicate an abrupt upturn in reflectivity at ~3800 Å (see Figure 6) which does not appear to be in conflict with the Irvine and Lane data. The abruptness of the upturn is hard to understand but difficult to dismiss since Jupiter, Uranus and Neptune, observed by Younkin and Münch as part of the same program, show no upturn and their Jupiter results given in Figure 5 are in good agreement with other determinations. Thus it is possible that the disk does dominate over the rings below 3000 Å.

We wish to thank Dr. A. D. Code for making available to us the OAO-2 planetary data and for many helpful suggestions throughout this research. In addition we thank Drs. T. E. Houck, J. F. McNall, R. C. Bless and C. F. Lillie for their

help in obtaining the OAO planetary data. J. J. C. and B. D. S. were supported by NASA contract NAS 5-1348. Kitt Peak National Observatory is operated by the Association of Universities for Research in Astronomy, Inc., under contract with the National Science Foundation.

REFERENCES

Alexander, J. B. and Stansfield, R. 1966, R. Obs. Bull., No. 119, E325.
Anderson, R. C., Pipes, J. G., Broadfoot, A. L. and Wallace, L. 1969, J. Atmos. Sci. 26, 874.
Axel, L. 1971, submitted to Ap. J.
Barth, C. A. and Hord, C. W. 1971, Science 173, 197.
Brinkmann, R. T., Green, A. E. S. and Barth, C. A. 1966, JPL Technical Report No. 32-951.
Bless, R. C., Code, A. D. and Taylor, D. J. 1968, Ap. J. 154, 1151.
Bless, R. C. and Savage, B. D. 1972, Ap. J., in preparation.
Broadfoot, A. L. 1972, in preparation.
Broadfoot, L and Wallace, L. 1970, Ap. J. 161, 303.
Brückner, G. 1960, Photometric Atlas of the Near Ultraviolet Solar Spectrum (Göttingen: Vandenhoeck and Ruprecht).
Caldwell, J. J. 1971, Ph. D. Thesis, University of Wisconsin.
Code, A. D., Houck, T. E., McNall, J. F., Bless, R. C. and Lillie, C. F. 1970, Ap. J. 161, 377.
Doherty, L. R. 1972, Ap. J., in preparation.
Dollfus, A. 1970, Surfaces and Interiors of Planets and Satellites, Ed. A. Dollfus, (London: Academic Press).
Dressler, K. and Schnepp, O. 1960, J. Chem. Phys. 33, 270.
Evans, D. C. 1965, Science 149, 969.
Evans, D. C. 1967, The Moon and Planets, ed. A. Dollfus, (Amsterdam: North Holland Publishing Co.) pp. 135-149.
Evans, D. C., Boggess, A., and Scolnik, R. 1965, Astron. J. 70, 321.
Fernie, J. D., Hagen, J. D., Hagen, G. L. and McClure, L. 1971, Pub. A. S. P. 83, 79.
Furukawa, P. M., Haagenson, P. L. and Scharberg, M. J. 1967, NCAR Technical Note 26.
Hopkins, N. B. and Irvine, W. B. 1971, Proc. IAU Symp. No. 40 on Planetary Atmospheres, ed. C. Sagan, T. Owen and H. Smith (Dordrecht: D. Reidel Publ. Co.) p. 349.
Irvine, W. M. 1968, J. Atmos Sci. 25, 610.
Irvine, W. M., Higdon, J. C. and Ehrlich, S. J. 1971, Proc. IAU Symp. No. 40 on Planetary Atmospheres, ed. C. Sagan, T. Owen and H. Smith (Dordrecht: D. Reidel Publ. Co.), p. 141.
Irvine, W. M. and Lane, A. P. 1971, Icarus, in press.

Irvine, W. M., Simon, T., Menzel, D. H., Charon, J., Lecomte, G., Griboval, P. and Young, A. T. 1968a, Astron. J. 73, 251.
Irvine, W. M., Simon, T., Menzel, D. H., Pikoos, C. and Young, A. T. 1968b, Astron. J. 73, 807.
Jenkins, E. B., Morton, D. C. and Sweigart, A. V. 1969, Ap. J. 157, 913.
Johnson, H. L. 1965, Comm. Lunar and Planetary Lab. No. 53, 3, 73.
Johnson, H. L., Mitchell, R. I., Iriarte, B. and Wisniewski, W. Z. 1966, Comm. Lunar and Planetary Lab. No. 63, 3, 99.
Kondo, Y. 1971, Icarus, 14, 269.
Ogawa, M. 1971, J. Chem. Phys. 54, 2550.
Pilcher, C. B., Chapman, C. R., Lebofsky, L. A. and Kieffer, H. H. 1970, Science 167, 1372.
Shemansky, D. E. 1972, submitted to J. Chem. Phys.
Spite, F. 1966, quoted by Alexander and Stansfield (1966).
Stecher, T. P. 1965, Ap. J. 142, 1186.
_____ 1970, Ap. J. 159, 543.
van den Bergh, S. 1965, J. R. A. S. C. 59, 253.
Vodar, M. B. 1948, J. Phys. Radium, Ser. 8, 9, 166.
Wallace, L. 1970, Bull. A. A. S. 2, 240.
Young, A. T. and Irvine, W. M. 1967, Astron. J. 72, 945.
Younkin, R. L. and Münch, G. 1963, Mém. Soc. Roy. Sci., Liège, Series 5, 7, 125.

MINOR CONSTITUENTS IN PLANETARY ATMOSPHERES: ULTRAVIOLET SPECTROSCOPY FROM THE ORBITING ASTRONOMICAL OBSERVATORY

Tobias Owen
State University of New York at Stony Brook
Stony Brook, L. I., New York

Carl Sagan
Cornell University
Ithaca, New York

ABSTRACT

Orbiting Astronomical Observatory data between 2000 Å and 3600 Å, obtained by the Wisconsin Experimental Package objective grating scanning spectrometer, are used to set upper limits to the abundances of many minor constituents in the atmospheres of Mars, Jupiter, Saturn, and Venus.

I. INTRODUCTION

Because of the large absorption cross-section of electronic transitions, ultraviolet spectroscopy has considerable appeal for the study of planetary atmospheres, providing an opportunity to search for trace constituents with abundances of one ppm or less. On the other hand, because of the increase of Rayleigh scattering towards short wavelengths, the effective penetration of ultraviolet photons into the planetary atmosphere may not be very deep, resulting in ultraviolet sampling of only the outer parts of the planetary atmospheres. In the present paper we present the results of a search for such trace constituents in the atmospheres of Mars, Jupiter, Saturn and Venus from observations carried out for this purpose by the Wisconsin Experimental Package (WEP) of the Orbiting Astronomical Observatory OAO-2.

The data were obtained with an objective grating scanning spectrometer, providing usable data between 2000 and 3600 Å.

A description of the instrumentation has been published by Code et al. (1970). A treatment of the planetary observations and their reduction, used in the following analysis, has been presented and discussed in general terms by Wallace, Caldwell and Savage (1972). Our analysis takes their results and derives specific upper limits on atmospheric constituents and some further interpretation of the observations in terms of simple atmosphere models, a division of labor agreed upon during our association as guest investigators on OAO/WEP. The albedo curves are reproduced here as Figures 1 and 2 for Mars at two different phase angles; Figure 3 for Jupiter; Figure 4 for Saturn (this is a brightness ratio of Saturn to the Sun rather than a geometric albedo); and Figure 5 for Venus. The reliability of this observational material is discussed in the above-cited article. The resolution achieved by the WEP scanner between 2000 and 3500 Å was slightly better than 25 Å. Wallace et al. (1972) describe the necessary modifications of this resolution required in cases where there were gaps in the data resulting from non-overlapping scans. Most of the gases in which we are interested exhibit continuous rather than discrete absorptions, in which case such refinements are unnecessary. We assume throughout that a 20% deviation from the continuum would be readily detectable ($\tau \simeq 0.1$). Accordingly any gas producing an absorption with a total equivalent width ~3 Å should be easily detectable at these wavelengths. Under these assumptions, abundance upper limits are readily derived with an absorption model and a systematic culling of the literature on absorption cross-sections. In all cases we have adopted a simple reflecting layer formalism. We feel that greater sophistication is unjustified and unnecessary at present (Regas and Sagan 1970a, 1970b; Sagan and Regas 1970).

II. MARS

In Figures 1 and 2 are displayed the OAO data on the Martian geometric albedo as a function of wavelength for two phase angles, with representative probable errors also shown. The spectra seem to be in good agreement with the ground-based photometry of Irvine, Higdon and Ehrlich (1971). The results of two measurements made by the WEP broad band photometers are also indicated. While there is a bare hint of structure in the 3200 to 3600 Å region, there is no convincing evidence of absorption anywhere in the spectrum. The data are consistent with a pure Rayleigh atmosphere of carbon dioxide at a surface pressure of about 5.5 mb — or somewhat lower pressures if there is a significant aerosol component to the scattering. However, the Rayleigh component alone does not provide useful compositional information. An earlier indication (Wallace 1970) of a 2600 Å OAO absorption feature, ascribed to ozone,

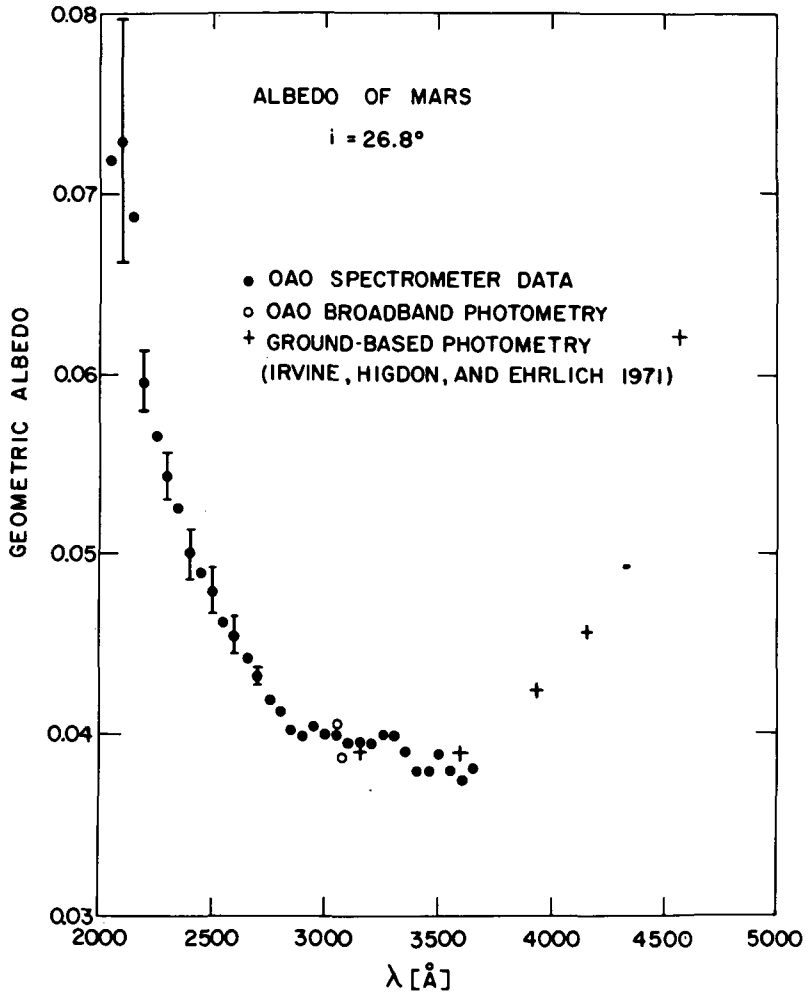

Figure 1.—Geometric albedo of Mars as a function of wavelength, at phase angle 26.8°, as determined by the Wisconsin Experimental Package of OAO-2. The large increase in reflectivity to short wavelengths is consistent with Rayleigh scattering by a CO_2 atmosphere of 5.5 mb surface pressure. Observational details of this and the following figures are discussed by Wallace, Caldwell & Savage (1972).

has disappeared in the present photometric reduction. Since the OAO observations are made of the integrated planetary disc the present observations neither confirm nor deny the report by Barth and Hord (1971) that ozone absorption is present preferentially over the south polar cap.

Upper limits in cm-atm to the abundances of a number of gases of interest are shown in Table 1. Our OAO upper limits,

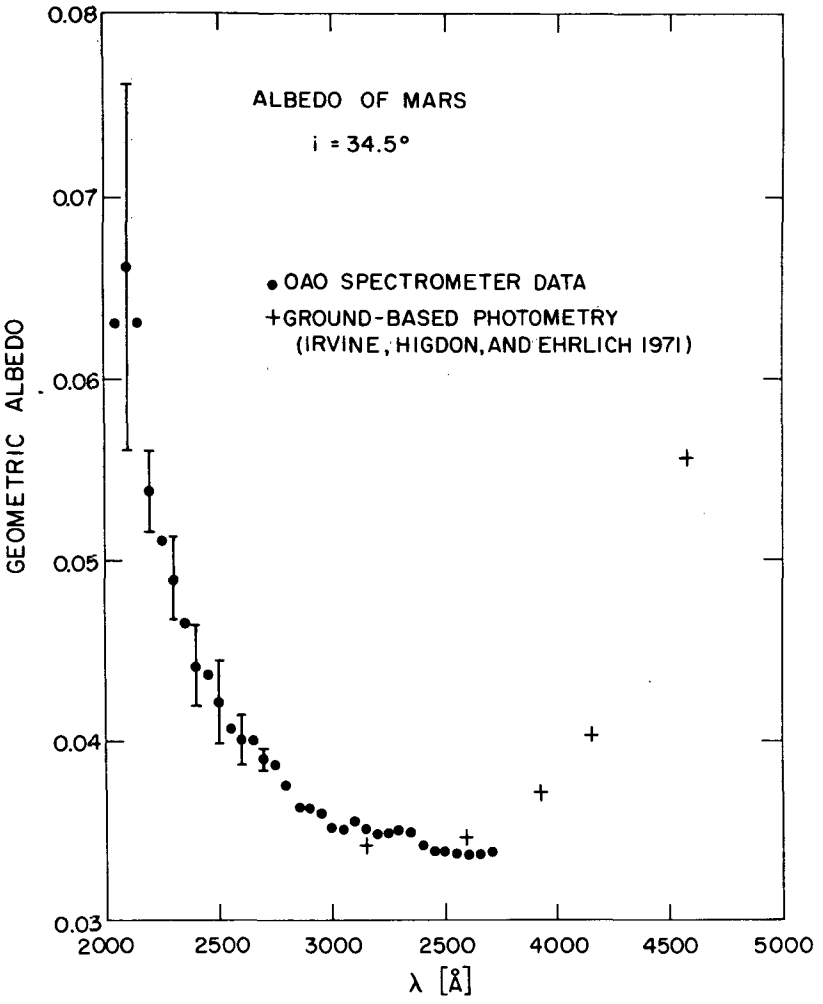

Figure 2.—Geometric albedo vs. wavelength of Mars at 34.5° phase angle.

based on a model atmosphere composed entirely of 80 m-atm of CO_2, are there compared with limits set by other techniques. The last column is our best estimate on abundance upper limits from all methods. We stress that values we report here are very conservative, corresponding to a 20% deviation from continuum reflectivities. For some materials such as H_2S the ultraviolet upper limits are much below infrared upper limits because of the large ultraviolet absorption coefficient. In other cases, for example HCl and especially O_2, our ultraviolet wavelength range does not extend to short enough wavelengths, and infrared results are more sensitive.

As in the case of the Earth, the low upper limits on such

Table 1. Upper Limits on Minor Constituents in the Martian Atmosphere

Molecule	OAO	Other Methods	Best Limit
O_3	2×10^{-4} cm-atm	3×10^{-3} cm-atm	(1)
			(2) 0.025 ppm
O_2	500	20	(3) 2500
C_3O_2 monomer	1×10^{-2}	3×10^{-3}	(1) 0.5
		2×10^{-2}	(4)
COS	1×10^{-2}	4×10^{-3}	(1) 0.6
		2×10^{-1}	(4)
SO_2	1×10^{-3}	4×10^{-3}	(1) 0.1
H_2S	1×10^{-3}	27	(1) 0.1
		3	(4)
NO	1×10^{-1}	5×10^{-3}	(1) 0.7
NO_2	1×10^{-3}	2×10^{-3}	(1) 0.1
		2×10^{-2}	(4)
		8×10^{-4}	(5)
N_2O_4	3×10^{-3}	4×10^{-2}	(4) 0.4
N_2O		1×10^{-2}	(1) 18
NH_3	1×10^{-3}	3×10^{-3}	(1) 0.1
HCN		4×10^{-1}	(1) 50
CH_4		3×10^{-2}	(1) 4
C_2H_2		4×10^{-1}	(1) 50
		2	(4)
C_2H_4, C_2H_6		4×10^{-2}	(1) 6
Benzene and its derivatives	1×10^{-3}	4×10^{-2}	(1) 0.1
HCHO	1×10^{-1}	5×10^{-3}	(4) 0.6
CH_3CHO and higher aldehydes	1×10^{-1}	7×10^{-2}	(4) 0.8
$(C_2H_5)_2S_2$ etc.	1×10^{-1}		12
CH_3COCH_3 and higher ketones	1×10^{-1}		12
Purines, pyrimidines and their derivatives	3×10^{-4}		0.03
HCl	1×10^{-1}	4	(1) 0.1
		1×10^{-3}	(4)

Upper limits for other gases, largely halides, are set in Ref. (1).

References for Table 1
(1) Horn, McAfee, Winer, Herr, and Pimentel (1972)
(2) Barth and Hord (1971)
(3) Margolis, Schorn, and Young (1971)
(4) Beer, Norton, and Martonchik (1971)
(5) Marshall (1964)

potential volcanic effluents as H_2S and SO_2 might be particularly interesting in view of the extent of geologically recent volcanic activity reported by Mariner 9 (Masursky et al. 1972). However, the rate of ultraviolet photodissociation of H_2S and SO_2 on Mars is such that these results place no useful limits on the possibility of a few sites of contemporary volcanism on the planet. The Mariner 9 ultraviolet spectrometer (Barth et al. 1972), which is able to obtain comparable ultraviolet spectra, but in the vicinity of the observed calderas, may be able to shed more light on the problem. Somewhat more stringent upper limits than shown in Table 1 on the abundance of oxides of nitrogen on Mars can be set from the photochemistry (Sagan, Hanst and Young 1965).

The upper limits on formaldehyde, acetaldehyde and other aldehydes are of some interest. Such materials were first suspected on Mars from infrared spectroscopy in the 3.5 μ region (Sinton 1957, 1961; Colthup 1961), but subsequent investigations show that the reported absorption features are almost certainly spurious (Rea, O'Leary and Sinton 1965; Beer, Norton and Martonchik 1971). However, Hubbard, Hardy and Horowitz (1971) have found formaldehyde and acetaldehyde to be among the products synthesized by long wavelength ultraviolet irradiation of simulated Martian atmospheres above a silicate substratum. From the results reported by Hubbard et al. (also Hubbard 1971, private communication), a quantum yield of several times 10^{-6} results. The ultraviolet photon flux at Mars, capable of synthesizing aldehydes in this way, is very roughly 5×10^{15} cm^{-2} sec^{-1}, implying a production rate $\sim 10^{10}$ molecules cm^{-2} sec^{-1}. The photolytic photon flux is approximately the same with an absorption cross-section for photolysis of the order of 3×10^{-20} cm^2. The mean time to photolysis of an aldehyde molecule is then $\sim 10^4$ sec, or a few hours. The expected steady state concentration is therefore $\sim 10^{15}$ molecules cm^{-2}, several orders of magnitude below the OAO limit exhibited in Table 1. With even the OAO upper limit on aldehyde abundance, the ultraviolet optical depth of these molecules is less than 0.1, implying no self protection against ultraviolet photolysis. The short aldehyde lifetime in the Martian solar ultraviolet radiation flux implies that,

like H_2S, it cannot be found very far from its site of production. The quantum yields, while large by ordinary photochemical standards, are still so small that there does not appear to be any prospect for an immediate ultraviolet test of the production of aldehydes on Mars by the mechanism of Hubbard et al. (1971). However, the possibility of large quantities of aldehydes in the Martian surface material does seem to be excluded: each time a molecule leaves the surface it is photolyzed, producing a situation not unlike evaporation into a vacuum. We have also listed in Table 1 abundance upper limits on some other organic molecules, such as alkyl sulfides and acetone, materials much less likely than aldehydes on a priori ground to be present on Mars.

Our upper limits on the abundances of the carbon suboxide monomer permits us to comment on the suggestion by Plummer and Carson (1969) that the carbon suboxide polymer $(C_3O_2)_n$ may be a principal coloring material of the Martian surface. The monomer vapor has been studied in the ultraviolet by Bell et al. (1966), who found that an effective path of the order of 0.25 cm-atm led to detectable absorption at 2600-2700 Å. The results of Smith et al. (1963) suggest ~0.4 cm-atm. The absence of this feature in our OAO data suggests an upper limit of 30 ppm for the monomer. A more sensitive upper limit of 200 μ-atm (2.5 ppm with our model) has been set by Beer et al. (1971) from their infrared interferometry and of 30 μ-atm by Horn et al. (1972) from the Mariner 1969 infrared spectrometer. This independent confirmation of the low upper limit on the abundance of the monomer unfortunately has little direct bearing on the fundamental question of whether the polymer is present in large abundance on the Martian surface. The molecular structure of the polymer is not a simple repetition of the monomer. Accordingly the vapor pressure of monomer above polymer should be very low and may follow a temperature dependence different from the usual reciprocal exponential law. From our literature survey, no definite detection of the monomer above the polymer could be found, but recent experiments place an upper limit to the C_3O_2 mixing ratio above ultraviolet-irradiated polymer under Martian conditions at $\sim 10^{-5}$ (Khare, Khare and Sagan 1972), or $\sim 10^{-4}$ mb. The upper limits on the monomer abundance found by Beer et al. (1971) correspond to a partial pressure $\sim 2 \times 10^{-5}$ mb, and by Horn et al. (1972) $\sim 3 \times 10^{-6}$ mb. We must conclude that the vapor pressure above the polymer on Mars will be below the observational limits given. Accordingly spectroscopic searches for the monomer are poor indices of the existence of the polymer. Such tests also must take account of the ultraviolet photolysis of the monomer, following arguments similar to those presented above for the aldehydes. The residual reflection spectrum of the planet in the ultraviolet, after the contribu-

tion of the atmosphere is removed, could also be used to provide information on surface materials. However, many samples of $(C_3O_2)_n$ do not show the characteristic 2600 Å absorption feature of the monomer, and the ultraviolet reflectivity of the polymer appears to be strongly dependent on its mode of formation (Smith et al. 1963, Khare et al. 1972). The absence of an absorption feature in these wavelength regions is not a convincing demonstration of the absence of carbon suboxide polymer on the surface. The monomer absorption at 2600 Å mimics moderately closely the absorption in the same wave length region of ozone; accordingly it is barely possible that the results of Barth and Hord (1971) apply to C_3O_2, and not to O_3.

Another gas of some interest is HCl. Here again (Table 1), our data complement those of Beer et al. (1971) who find an equivalent upper limit of 0.1 ppm, an order of magnitude more sensitive than our results. These limits are of significance because HCl has been detected on Venus (Connes et al. 1967) where the mixing ratio is quoted as 0.6 ppm. Thus the present detection threshold for this gas in the Martian atmosphere is comparable to the abundance which is identified in the atmosphere of Venus, especially because of the chance that substantial quantities of CO_2 reside in the north polar cap of Mars. The Martian atmosphere may be deficient in HCl relative to Venus. However, because of the possibility of the preferential trapping of HCl and its compounds both as condensates and as clathrates in the Martian polar caps, and as chlorides in the epilith, such a discrepancy cannot yet be considered established. Since both atmospheres were presumably formed by an outgassing process similar to that which occurred on Earth, real differences in composition provide clues to differential planetary atmospheric evolution. For this reason it seems especially worthwhile to attempt an improvement in the HCl detectivity.

III. JUPITER

The OAO Jupiter spectrum is displayed in Figure 3 where the spectrophotometric and broad band photometric results are compared with the ground-based spectroscopy of Younkin and Münch (1963), and the ground-based photometry of Hopkins and Irvine (1971). The decline from long to short visible wavelengths, corresponding to the generally reddish or yellowish coloration of Jupiter, is reversed at about 3000 Å. The spectrum exhibits a slight rise to about 2500 Å and a falloff towards shorter wavelengths. The general decline from long visible wavelengths to 3000 Å is due to chromophores, probably not in the gas phase, whose identification is still under discussion (see, e.g., Sagan 1971a). The general rise from 3000

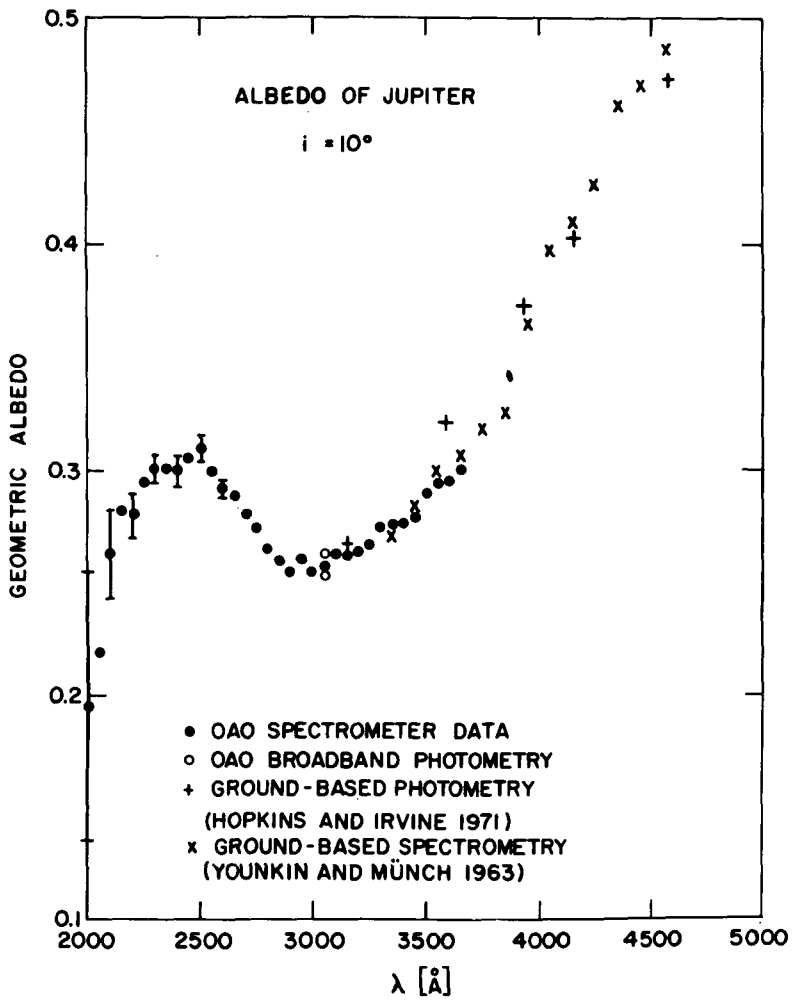

Figure 3.—Geometric albedo vs. wavelength of Jupiter at phase angle 10°. The increase in reflectivity short of 3000 Å is attributed to 5 km-atm of H_2; the decline shortward of 2500 Å to ~50 μ-atm of NH_3.

to 2500 Å is consistent with Rayleigh scattering by ~5 km-atm of H_2. The decline shortward of 2500 Å is consistent with absorption by ~50 μ-atm of NH_3. But these quantitative estimates must be regarded as quite uncertain, and even such qualitative attributions as the decline at short wavelengths to absorption by ammonia must be regarded as conjectural. What seems quite well established, however, is that the solar radiation reflected in the near ultraviolet from Jupiter arises from a much higher atmospheric level than the radiation observed at long visible and infrared wavelengths, a conclusion in agreement with previous interpretations of such spec-

tra (see, e.g., Greenspan and Owen 1967; Anderson et al. 1969).

Vapor pressure limitations furnish our principal reason for attributing the 2100 Å absorption feature to NH_3, other than the fact that we know this gas to exist on Jupiter. We still lack the spectral resolution to distinguish NH_3 from H_2S absorption at these wavelengths, and we cannot be completely certain of the relative importance of solid and gaseous NH_3 in causing the observed absorption, the solid being especially likely to contribute at the shorter wavelengths (Dressler and Schnepp 1960).

A conceivable alternative interpretation of this spectrum is that, superposed on a broad general decline in reflectivity from visible to ultraviolet wavelengths, is a broad absorption feature centered at 2900 Å. In this interpretation we look so high in the atmosphere in the ultraviolet that the Rayleigh scattering contribution is dominated by the broad absorption feature. But this model runs into serious difficulties precisely because at such high altitudes and therefore low temperatures there are no likely candidate absorbers to produce the broad absorption feature. The most successful category of such absorbers would be the aldehydes; roughly 1 mm-atm of formaldehyde, plus the same quantity of acetaldehyde, could produce a broad absorption feature of this sort, but the vapor pressure and ultraviolet photolysis time scale, as presented above for Mars, as well as the absence of the aldehyde precursor molecule, water, at these altitudes, makes this hypothesis quite unlikely. Accordingly, we opt for an explanation in terms of Rayleigh scattering and short wavelength absorption.

Except for the short wavelength decline, here attributed to ammonia, no other absorption features are in evidence. In Table 2 are compared the OAO ultraviolet upper limits on constituents, relative to 5 km-atm of H_2, with ground-based infrared upper limits on a number of molecules, based on the work of Owen (1969) and Cruikshank and Binder (1969), as related to 80 km-atm of H_2 by Sagan (1971a). The differences in ammonia mixing ratios, like the differences in H_2 abundances, reflect the smaller depth of penetration of ultraviolet compared to infrared photons into the Jovian atmosphere. Alkyl sulfides are produced in simulated Jovian environments if initial H_2S is present (Sagan and Khare 1971). The upper limits for benzene and its derivatives derived here are of the same order as the abundance of benzene predicted under conditions of quenched thermodynamic equilibrium in the Jovian atmosphere (Lippincott et al. 1967). Since the molecules are expected to be produced under non-equilibrium conditions, it is not implausible that they should be secularly variable with abundances hovering around 10^{-8} - 10^{-9}. A similar remark probably applies to purines and pyrimidines. Because many of these constituents are readily photolyzed in the ultraviolet

Table 2. Mixing Ratios for Minor Constituents on Jupiter

Molecule	OAO UV	Ground-Based IR
CH_4		$\sim 6 \times 10^{-4}$
NH_3	$\sim 1 \times 10^{-8}$	1.2×10^{-4}
H_2O		6×10^{-7}
H_2S	$< 6 \times 10^{-9}$	$< 3 \times 10^{-6}$
C_2H_2		$< 5 \times 10^{-7}$
C_2H_4		$< 2 \times 10^{-5}$
C_2H_6		$< 3 \times 10^{-5}$
HCN		$< 6 \times 10^{-7}$
HCHO	$< 2 \times 10^{-7}$	
CH_3CHO and higher aldehydes	$< 2 \times 10^{-7}$	
$(C_2H_5)_2S_2$, etc.	$< 2 \times 10^{-7}$	
CH_3COCH_3 and higher ketones	$< 2 \times 10^{-7}$	
Benzene and its derivatives	$< 5 \times 10^{-10}$	
Purines, pyrimidines and their derivatives	$< 2 \times 10^{-10}$	
HCl	$< 6 \times 10^{-8}$	

we would not expect to see them in significant abundance at these high altitudes. In addition, simple atmospheric models suggest temperatures on the order of 115°K or less at the base of the atmospheric region probed in these ultraviolet wavelengths. Such low temperatures place serious constraints on the presence of vapor phase complex molecular constituents. Studies of the constituents expected at thermodynamic equilibrium (Greenspan and Owen 1966; Lippincott et al. 1967; Lewis 1969) show no molecules other than hydrogen, helium, methane and ammonia expected in this region of the atmosphere. Likely non-equilibrium products, such as simple hydrocarbons and nitriles (Sagan and Miller 1960; Lippincott et al. 1967; Woeller and Ponnamperuma 1969; Sagan and Khare 1971) do not absorb at these ultraviolet wavelengths. When water vapor is introduced into such experiments, aldehydes are produced (Sagan and Miller 1960; Sagan and Khare 1971), but no water vapor is expected at the altitudes probed at these ultraviolet frequencies. The upper limits on aldehyde abundances ~several ppb are consistent with these expectations.

The best hope of more useful ultraviolet spectroscopic determinations of minor constituents in the Jovian atmosphere is from a flyby or orbiter ultraviolet spectrometer able to resolve the disc of Jupiter. The non-uniform distribution of optical frequency chromophores across the Jovian disc should continue to be characteristic of the planet in the ultraviolet. A variety of evidence suggests that the disturbance re-

sponsible for the Great Red Spot propagates very high into the Jovian atmosphere and that the chromophores responsible for its characteristic coloration may be located at least in part at high altitudes (Sagan 1962; Owen and Mason 1969; Sagan 1971b). It would be most interesting to determine whether characteristic ultraviolet absorption features are associated with the GRS, but a firm test of this hypothesis requires good spatial resolution. It is a remarkable curiosity that none of the ultraviolet spectra of the integrated disc of Jupiter to date have been obtained when the GRS is near the planet's central meridian. Our best hope in detecting disequilibrium products and simple organic molecules at the low temperatures which apply to the ultraviolet is when they are entrained in solid particles — presumably ammonia — circulating up from greater depth. The fact that we do not see a very large increase in reflectivity towards shorter wavelengths, as expected from the near infrared abundances of hydrogen, indicates that the ultraviolet reflectivity is indeed dominated by such cloud particles. It is exactly such a situation which may be responsible for the color of the GRS.

The absence of absorption features other than the general decline short of 2500 Å is consistent with other recent data (Kondo 1971; Anderson et al. 1969), and inconsistent with the early reports of a discrete absorption feature near 2600 Å in rocket spectra by Stecher (1965) and by Evans (1965). This absorption is of particular interest because the two categories of molecules proposed to explain it — benzene and its derivatives (Greenspan and Owen 1966; Owen and Greenspan 1968) and purines and pyrimidines and their derivatives (Sagan 1968) — are organic molecules whose presence in the Jovian atmosphere would have important implications. The difference in results of the 1965 work from that of more recent workers may be due to problems with the solar spectral calibrations employed, but it is at least barely possible that all observations are valid and that the feature is a true secular variable (Sagan 1971b).

IV. SATURN

Here again a significant degradation of the data occurs because of the limited angular resolution of the OAO spectrometers. For Saturn we are forced to observe the rings and the disc together. Because of the difficulty in separating these two components we do not learn much about either. This is a special pity since we know that the Equatorial Belt darkens in the near ultraviolet, and limb brightening along the belt also occurs at these wavelengths (Marin 1968). Furthermore, extension of observations of the rings to shorter wavelengths might help to better define the composition of its constituent par-

ticles. We already have evidence that at least two components (of which water ice is certainly one) are present (Lebofsky et al. 1970).

Unresolved ultraviolet observations of Saturn have been reported by Bless et al. (1968). Three filters were used to isolate 300 Å bandpasses centered at 2800, 2500 and 2100 Å. If the rings are black in the ultraviolet, an upper limit of 25 km-atm for the H_2 abundance in the planetary atmosphere was obtained. The present OAO data are consistent with this interpretation, and the general pattern of the Saturnian ultraviolet spectrum is very reminiscent of that of Jupiter. There is some hint of absorption features at 3000, 3200 and 3400 Å, but we do not believe the reliability of the data warrants any attempt to search for candidate absorbers. If we accept 25 km-atm of H_2, the resulting upper limits are those listed in Table 2 for Jupiter, but with upper limits on mixing ratios reduced by a factor of 5.

The increase of reflectivity short of about 3600 Å is very likely due to Rayleigh scattering; a similar feature appears in the ground-based spectrometry of Younkin and Münch (1963), where the contribution from the ring was very small. The alternative explanation in terms of increased ultraviolet reflectivity by the rings towards short wavelengths seems unlikely, in view of the results of Lebofsky et al. (1970) which indicate a sharp decrease in reflectivity towards the blue and the ultraviolet. While the error bars are large, there does seem to be a marginally significant decrease in reflectivity below 2500 Å. By analogy with Jupiter, we might again anticipate the presence of ammonia absorption. While equivocal results have been obtained, the best recent evidence suggests that ammonia is not detectable on Saturn in the near infrared (Owen 1965). The near infrared upper limit would be ~1-2 m-atm. The amount of ammonia required to account for our ultraviolet absorption is extremely small — 10 to 20 μ-atm, an amount not inconsistent with the vapor pressure curve of ammonia if the relevant regions of the upper atmosphere of Saturn are not below 100°K. In the lower atmosphere of Saturn, ammonia is expected on cosmic abundance grounds, and indeed the microwave spectrum gives a rather clear indication of ammonia absorption (Gulkis et al. 1960; Wrixon and Welch 1970). Uniform mixing ratios $\sim 10^{-4}$ NH_3 in the lower atmosphere, implied by the microwave data, would also be consistent with abundances of a few tens of μ-atm of ammonia in the upper atmosphere under the temperature boundary conditions mentioned above.

Concerning the ring spectrum, pure ammonia ice is, from observations in the 1 to 2.5 μ region (Pilcher et al. 1970), not a significant constituent of the ring particles. Water ice does not significantly absorb in the 2000 to 2500 Å region

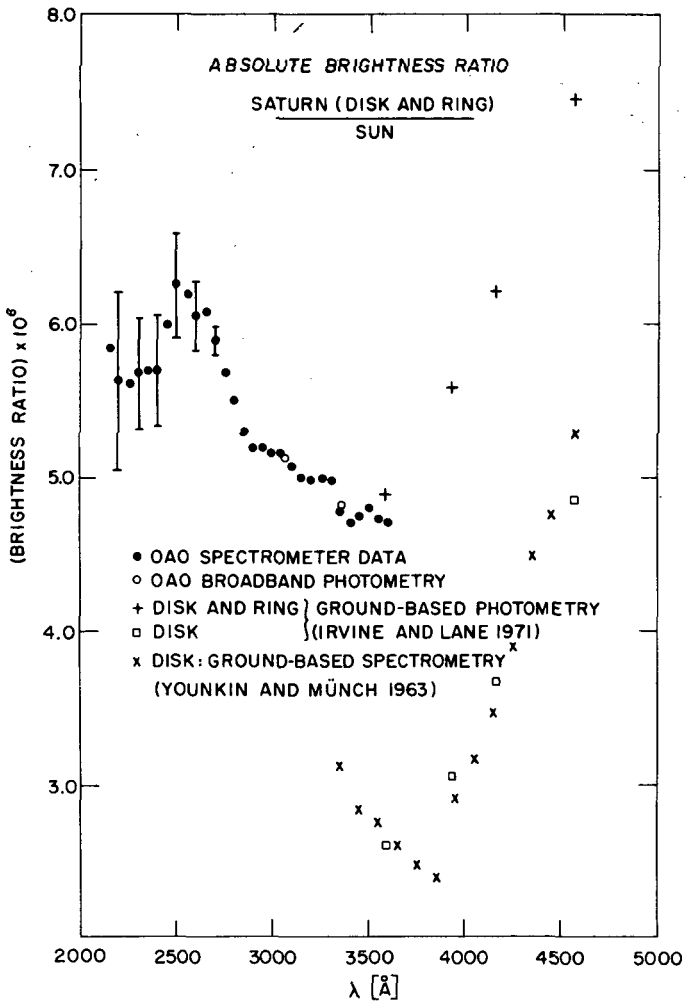

Figure 4.—Absolute brightness ratio of disc plus rings of Saturn as a function of wavelength. The increase in reflectivity shortward of 3500 Å is consistent with Rayleigh scattering by several tens of km-atm of H_2; the decline shortward of 2500 Å is consistent with absorbtion by a few tens of μ-atm of ammonia.

(Dressler and Schnepp 1960). Other conceivable components of the ring such as NH_4OH might absorb in this region, but the atmosphere will dominate the ring spectrum below 2500 Å; accordingly, ring absorption features should have little effect on the overall spectrum. Separate ultraviolet spectra of the disc and rings — as, for example, obtained by a Saturn flyby — would be of considerable interest.

V. VENUS

Of the OAO data presented in the present paper those for Venus are most uncertain. They have been presented as geometric albedo vs. wavelength in Figure 5 where they have been made to join smoothly to the ground-based photometric results of Irvine (1968). The general character of the spectrum is again similar to that of Jupiter and Saturn. The general decline from long visible wavelengths to 3000 Å is a quantita-

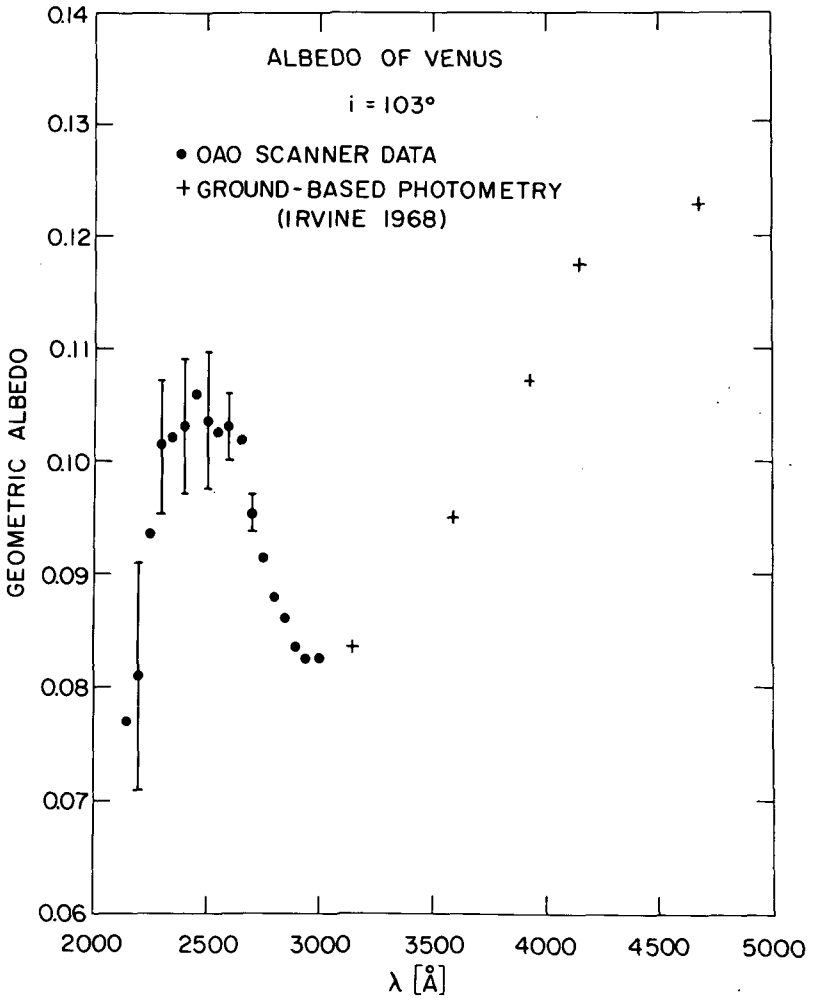

Figure 5.—Geometric albedo of Venus as a function of wavelength at phase angle 103°. The increase in reflectivity short of 3000 Å is consistent with ~1 km-atm of CO_2 Rayleigh scattering. The decline in reflectivity shortward of 2500 Å is due to an as yet unidentified absorber.

tive indication of the pale lemon yellow color of Venus. The nature of the chromophores — probably in the Venus clouds — responsible for this absorption remains in dispute. The most natural explanation of the increase in reflectivity between 3000 and 2500 Å is Rayleigh scattering by atmospheric carbon dioxide. Very roughly several km-atm of CO_2 would be required — the correct order of magnitude of the effective amount above the visible clouds. In this interpretation, an additional absorber, operating at wavelengths shortward of 2500 Å would be required.

In the case of Jupiter, we have discussed an alternative explanation, namely, that, in the ultraviolet spectrum, we are looking sufficiently high that no strong Rayleigh component remains. A similar alternative exists for Venus, where we would be observing a broad absorption feature centered at about 2950 Å. Sulfur dioxide has an absorption spectrum of this sort; $\sim 5 \times 10^{-3}$ cm-atm would produce a dip of approximately the observed extent. In some models of atmospheric chemistry decoupled from gas-mineral equilibria (Lippincott et al. 1967), SO_2 is expected to be the principal sulfur-containing molecule. But again because of the ultraviolet lability of this molecule (and vapor pressure problems?) we believe the Rayleigh scattering interpretation is more likely to be correct.

In this case upper abundance limits on a number of constituents can be set from the OAO scanner data and are displayed in Table 3. As in the case of Mars, the low upper limits found on the monomer of carbon suboxide and on the aldehydes may again have little to do with the possible presence of carbon suboxide polymer or paraformaldehyde, this time as significant constituents of the Venus clouds. It is of interest that the upper limit for the HCl abundance set by OAO is of the same order as the abundance detected by Connes et al. (1967) in the near infrared. However, again because of the vapor pressure and ultraviolet photolysis arguments, it is likely that the HCl mixing ratio as observed in the ultraviolet will be less than that observed in the infrared.

The short wavelength decline in geometric albedo begins in the OAO spectra several hundred Å longward of that implied by the rocket ultraviolet spectrum of Anderson et al. (1969). But whether the difference is due to the 27° difference in phase angles between the two observations, to a secular variation in cloud reflectivity, or to undiagnosed observational errors is not known at the present time. Observations at an intermediate phase angle by Jenkins et al. (1969) also show the cut-off at shorter wavelengths, thereby weakening the first alternative. Anderson et al. attribute their short wavelength absorption edge to CO_2 and HCl. If the OAO data are accurate, CO_2 cannot be responsible for an absorption beginning at 2500 Å although it can play a role in diminishing

Table 3. Upper Limits on Minor Constituents in the Cytherean Atmosphere
(OAO Estimates Based on ~1 km-atm CO_2)

Molecule	OAO Upper Limit	Previous Estimates (1)
O_3	0.003 ppm	0.03 ppm
C_3O_2	0.1	1.
COS	0.1	0.2
SO_2	0.01	0.05
H_2S	0.1	0.3
NO	1.	
NO_2	0.01	0.8
N_2O_4	0.04	
HCHO	1.	
CH_3CHO and higher aldehydes	1.	
CH_3COCH_3 and higher ketones	1.	
HCl	1.	1.
NH_3	0.1	

(1) Tabulated by Anderson et al. (1969)
Further upper abundance limits are tabulated by Marov (1972).

the reflectivity at the shortest wavelengths we observe. Possible time-variable contributors to the short wave cut-off include Cl_3^- and HOCl, complexes suggested by Lewis (1972) as likely constituents in an HCl-H_2O cloud system. Further integrated-disc ultraviolet spectroscopy of Venus would clearly be a great help in checking these points.

We are grateful to A. D. Code, L. V. Wallace and B. D. Savage for assistance in interpretation of the OAO instrumentation, calibration, and data reliability when we were Guest Investigators on the Wisconsin Experimental Package of OAO. We thank Brian O'Leary for his efforts in the earliest stages of our participation in this mission, Dennis Ward and Thomas Scattergood for useful literature searches of ultraviolet absorption coefficients, and Charles Barth for a constructive reading of the manuscript. This research was supported in part by NASA Grant NAS 1-9683.

REFERENCES

Anderson, R. C., Pipes, J. G., Broadfoot, A. L., and Wallace, L. 1969, J. Atmos. Sci. 26, 874.
Barth, C. A., Hord, C. W., Stewart, A. I. and Lane, A. L. 1972, Science 175, 309.
Barth, C. A. and Hord, C. W. 1971, Science 173, 197.
Beer, T., Norton, R. H. and Martonchick, J. V. 1971, Icarus 15, 1.
Bell, S., Varadarajan, T. S., Walsh, A. D., Warsop, P. A., Lee, J. and Sutcliffe, L. 1966, J. Mol. Spec. 21, 42.
Blake, A. R., Eeles, W. T. and Jennings, P. P. 1964, Trans. Faraday Soc. 60, 691.
Bless, R. C., Code, A. D. and Taylor, D. J. 1968, Ap. J. 154, 1151.
Code, A. D., Houck, T. E., McNall, J. F., Bless, R. C. and Lillie, C. F. 1970, Ap. J. 161, 377.
Colthup, N. B. 1961, Science 134, 529.
Connes, P., Connes, J., Benedict, W. S. and Kaplan, L. D. 1967, Ap. J. 147, 1230.
Cruikshank, D. P. and Binder, A. B. 1969, Ap. and Space Sci. 3, 347.
Dressler, K. and Schnepp, O. 1960, J. Chem. Phys. 33, 270.
Evans, D. C. 1967, in The Moon and Planets, ed. A. Dollfus (Amsterdam: North-Holland Publ. Co.), p. 135.
Greenspan, J. A. and Owen, T. 1967, Science 156, 1489.
Gulkis, S., McDonough, T. R. and Craft, H. 1969, Icarus 10, 421.
Hopkins, N. B. and Irvine, W. M. 1971, I.A.U. Symp. No. 40, p. 349.
Horn, D., McAfee, J. M., Winer, A. M., Herr, K. C. and Pimentel, G. C. 1972, Icarus 16, in press.
Hubbard, J. S., Hardy, J. P. and Horowitz, N. 1971, Proc. Nat. Acad. Sci. 68, 574.
Irvine, W. M. 1968, J. Atmos. Sci. 25, 610.
Irvine, W. M., Higdon, J. C. and Ehrlich, S. J. 1971, I.A.U. Symp. No. 40, p. 141.
Khare, B. N., Khare, M. and Sagan, C. 1972, in preparation.
Kondo, Y. 1971, Icarus 14, 269.
Lebofsky, L. A., Johnson, T. V. and McCord, T. B. 1970, Icarus 13, 226.
Lewis, J. S. 1969, Ap. J. 171, L75.
Lippincott, E. R., Eck, R. V., Dayhoff, M. O. and Sagan, C. 1967, Ap. J. 147, 753.
Marin, M. 1968, J. des Obs. 51, 179.
Marov, M. Y. 1972, Icarus, in press.
Masursky, H. et al. 1972, Science 175, 294.
Owen, T. 1965, Ap. J. 142, 782.

_____ 1969, Icarus 10, 355.
Owen, T. and Greenspan, J. A. 1968, Science 159, 449.
Owen, T. and Mason, H. P. 1969, J. Atmos. Sci. 26, 870.
Pilcher, C. P., Chapman, C. R., Lebofsky, L. A. and Kieffer, H. H. 1970, Science 167, 1372.
Plummer, W. T. and Carson, R. K. 1969, Science 166, 1141.
Rea, D. G., O'Leary, B. J. and Sinton, W. M. 1965, Science 147, 1286.
Regas, J. and Sagan, C. 1970a, Comments Astrophys. Space Phys. 2, 116.
_____ 1970b, ibid., 138.
Sagan, C. 1962, Proc. XI Intern. Astrophys. Colloq. Liège, p. 506.
_____ 1968, Science 159, 448.
_____ 1971a, Space Sci. Rev. 11, 827.
_____ 1971b, Comments Astrophys. Space Phys. 3, 65.
Sagan, C., Hanst, P. and Young, A. T. 1965, Planet. Space Sci. 13, 73.
Sagan, C. and Khare, B. N. 1971, Ap. J. 168, 563.
Sagan, C. and Miller, S. L. 1960, Astron. J. 65, 499.
Sagan, C. and Regas, J. 1970, Comments Astrophys. Space Phys. 2, 161.
Sinton, W. M. 1957, Ap. J. 126, 231.
_____ 1961, Science 134, 529.
Smith, R. N., Young, D. A., Smith, E. N. and Carter, C. C. 1963, Inorg. Chem. 2, 829.
Stecher, T. P. 1965, Ap. J. 142, 1186.
Wallace, L. 1970, Bull. A. A. S. 2, 240.
Wallace, L., Caldwell, J. J. and Savage, B. D. 1972, Ap. J. 172, 755.
Woeller, F. and Ponnamperuma, C. 1969, Icarus 10, 386.
Wrixon, G. T. and Welch, W. J. 1970, Icarus 13, 163.
Younkin, R. L. and Münch, G. 1963, Mém. Soc. Roy. Sci., Liège, Series 5, 7, 125.

Page intentionally left blank

STELLAR ULTRAVIOLET COLORS AND INTERSTELLAR EXTINCTION

Eric Peytremann and Robert J. Davis
Smithsonian Astrophysical Observatory
Cambridge, Massachusetts

ABSTRACT

In this paper, we study a sample of Celescope results. Most of the sample stars belong to the Orion and Vela regions. We first compare measurements by Celescope filter U3 with the m1500 of Weber et al. (1971). (The U3 filter has an average wavelength of about 1600 Å.) Second, we select stars with visual excess E(B-V) less than 0.05 in order to derive relationships of intrinsic color index versus spectral type. We compare the resulting intrinsic color-color relations with existing blanketed and unblanketed model calculations. Finally, we utilize the preceding intrinsic relations to derive some results on interstellar extinction. Owing to the rather large scatter in the Celescope data (0.2-mag standard deviation for multiply observed stars), the Vela stars give the more significant results because their visible excess E(B-V) is, in general, larger than that for the Orion stars. We find somewhat less ultraviolet extinction than do other authors, although their results lie within 1 standard deviation of our values.

I. INTRODUCTION

In this paper, we study a sample of results from The Celescope Catalog of Ultraviolet Observations (Davis 1972). In addition to the results for the Vela region already published in the preliminary catalog, we have used data for several hundred stars in the Orion and southern Scorpio regions.

For this preliminary interpretation of these Celescope results, we have selected only those stars for which we know

the photoelectric V magnitude and B-V color index, the spectral type, and at least one Celescope ultraviolet magnitude. There are 166 stars in the resulting sample; most of them are B and early A-type stars.

In addition to the derivation of some specific relationships from our sample data (e.g., intrinsic color versus spectral type, or ultraviolet color excesses versus visible-light color excesses), one purpose of this work is to show what sort of properties we can deduce from a broad survey such as the Celescope Catalog. We restrict ourselves to those properties that show a significant effect on ultraviolet broad-band colors. To do this, we must compare the expected size of these effects to the size of the observational errors. Because the Celescope Catalog contains a very large number of observed stars, we can determine statistical properties with considerably more accuracy than we can determine the properties of individual stars. A study of our observational errors, based on repeated observations of individual stars, indicates a standard deviation of slightly less than 0.2 mag for an individual observation of normal weight. The scatter in our color-spectrum relationships (§ III) is compatible with a standard deviation of such a size. The scatter in our comparison with the results of Weber, Henry and Carruthers (1971) (§ II) can most easily be attributed to a standard deviation exceeding that amount for their observations.

We shall divide the rest of this paper into three parts. The first compares Celescope results with those of Weber et al. (1971) and discusses the accuracy of the Celescope results. In the second, we derive intrinsic relationships (i.e., no interstellar extinction) of color versus spectral type and of different colors against each other. And in the third, we derive ultraviolet color excesses arising from interstellar extinction.

Here we summarize the basic features of the Celescope broad-band measurements. One of us (Davis 1968) has described the observational system. A shorter description, which also includes a brief account of our data-analysis procedure, appears elsewhere in these proceedings (Davis, Deutschman, Lundquist, Nozawa and Bass 1972).

The Celescope photometric system consists of four band passes, designated by U1, U2, U3 and U4. (Only the results for the U1, U2 and U3 filters will be considered here.) The corresponding magnitudes are also designated by the same symbols or, more generally, by U_i (i = 1,2,3,4). The mean wavelengths λ_{0i} of each filter i are defined by

$$\lambda_{0i} = [\int_0^\infty S_i(\lambda)\lambda\, d\lambda]/[\int_0^\infty S_i(\lambda)\, d\lambda], \quad i = 1,2,3,4 ,$$

where $S_i(\lambda)$ are the sensitivity functions of the system as a function of the wavelength λ.

Table 1 lists average wavelengths, λ_{0i}, and the total bandwidths, $\Delta\lambda_i$, at half the maximum sensitivity ($\Delta\lambda_i = \max\{S_i(\lambda)\}/2$).

Table 1. Average wavelengths λ_{0i} and total bandwidths $\Delta\lambda_i$ for the Celescope filters.

Celescope filter designation U_i	Average wavelength λ_{0i} (Å)	Total bandwidth $\Delta\lambda_i$ (Å)
U1	2582	550
U2	2308	850
U3	1621	325
U4	1537	450

II. COMPARISON WITH OTHER OBSERVATIONS

Weber et al. (1971) have measured a number of ultraviolet electronographic magnitudes. Their effective wavelength is about 1500 Å, and their band pass covers the wavelength range 1230-2100 Å. These heterochromatic magnitudes are therefore very similar to Celescope's U3 magnitudes. This means that if we compare the magnitudes of stars measured in both systems, they should be identical, provided that both magnitude scales have been given the same zero point. In all, 51 resolved stars have been measured by both experiments; the comparison of both sets of results is displayed in Figure 1, with Weber's m(1500) magnitudes plotted against Celescope's U3 magnitudes. (Weber's m(1500) magnitude was computed by adding his tabulated V magnitude to his tabulated m(1500)-V color.) Also shown on Figure 1 are three reference lines for comparing the calibrations: (1) the solid line, of slope 45°, corresponds to no scale error in either magnitude system; (2) the dashed line, departing from the solid line at m(1500) = 1.8, corresponds to the dashed line in Weber's Figure 12 and indicates a possible correction to his magnitude scale for magnitudes brighter than that; and (3) the dotted line corresponds to the best least-squares fit between the two magnitude systems. The dotted line corresponds to the situation where one or both of the magnitude systems may have a zero point error and a scale

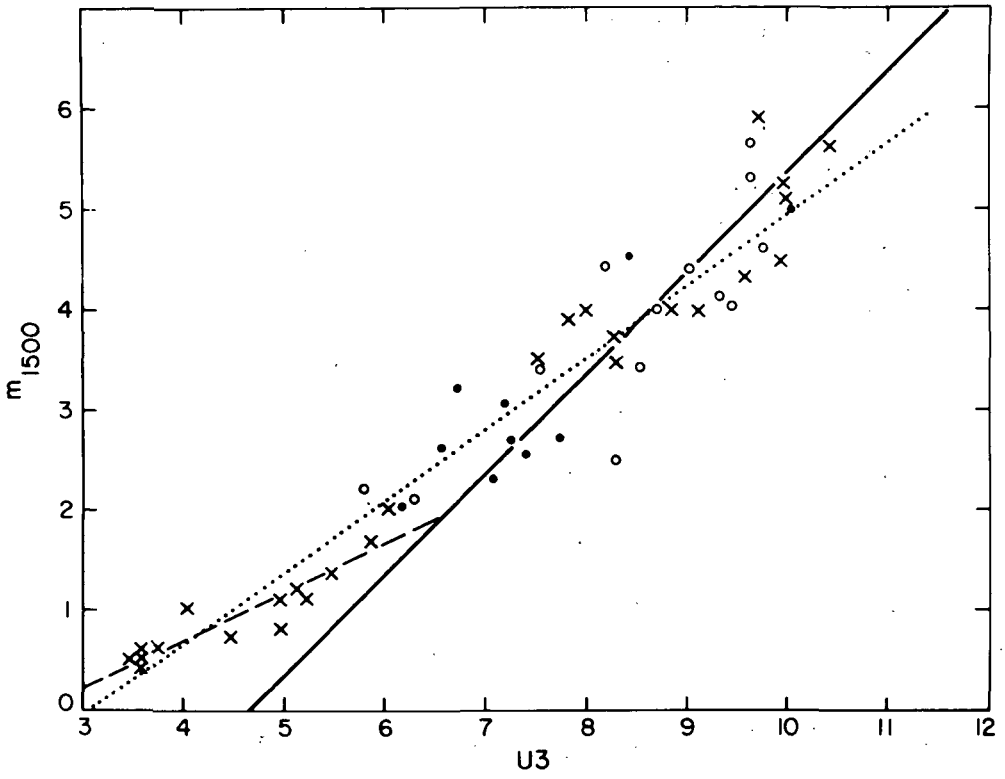

Figure 1.—Comparison of the ultraviolet magnitudes m_{1500}-V by Weber et al. (1971) with the U3-V magnitudes of the Celescope Catalog. Open circles (○), dots (●), and crosses (×) represent, respectively, B3 V stars, B1 V stars, and other spectral types. The solid line (——) indicates the relationship the two systems would have if there were no scale error. The dashed line (- - -) indicates Weber's suggested revision of his magnitude scale for bright stars. The dotted line (· · ·) indicates the best least-squares linear fit between the two systems.

error.

The standard deviation of the scatter between the two magnitude systems is about the same, 0.5 mag, whether we use the dotted line or the combination of dashed line and solid line in making the comparison. If the errors in both systems are the same size, this comparison would indicate standard deviations of about 0.35 mag for each system. We ran an independent check on the standard deviation of magnitudes in our system. Based on about 1500 observations in each color band, of the 500 stars we observed more than once, our standard deviation is slightly less than 0.2 mag. For the purposes of this

paper, it does not matter whether we take our standard deviation to be 0.2 or 0.35 mag, since our sample is sufficiently large to enable us to derive average properties quite accurately in either case. We therefore postpone a more detailed discussion of our observational errors to a later paper.

The results presented in the next two sections have thus been obtained from data whose analysis had revealed scatters on the order of 0.3 to 0.4 mag in the color-color, or color-spectrum, diagrams. We could have attempted to explain these scatters in terms of properties of the stars or the interstellar medium. However, the comparison we have made in this section tells us that it is probably not justified to interpret observed effects in terms of peculiarities of individual stars unless these effects are larger than, say, 0.5 mag; we have confined this paper to a discussion of the statistical properties of our observed stars and of the interstellar medium.

III. INTRINSIC COLOR-SPECTRUM RELATIONSHIPS

In what follows, we shall call "intrinsic" all those properties that are proper to the observed stars before encountering the interstellar medium. To derive these intrinsic properties, we selected stars whose color excess E(B-V) due to interstellar extinction is less than 0.05. The intrinsic $(B-V)_0$ indices have been taken from Schmidt-Kaler (1965). This limit was chosen as a compromise between (1) as little interstellar reddening as possible and (2) the need for a rather large sample of stars. The underlying assumption is that there is no unknown extinction component in the ultraviolet or, in other words, that E(B-V) near zero implies that the ultraviolet interstellar extinction is also approximately zero.

For each spectral class, we then computed the average ultraviolet colors Ui-V (V being the photoelectric magnitude in the UBV system). Stars of various luminosity classes within the same spectral class were lumped together. The results for the colors U1-V, U2-V and U3-V are plotted in Figures 2, 3 and 4, respectively. The dots and crosses represent averages for Orion stars and Vela stars, respectively. The number of stars in each spectral class ranges from 1 (B0, A7, A8, F0, F2) to 14 (B8) and 16 (B9). We do not indicate the standard deviations for each color and each spectral class. In general, for a given number of stars, the standard deviation is smallest for the U3 color and largest for the U1 color. As can be seen from Figures 2, 3 and 4, the scatter between adjacent spectral classes gives a fair idea of the internal errors or of the individual peculiarities or of both, because we do not expect such drastic and random changes between plus or minus one spectral class, as they appear on the various graphs. On the basis of what we have seen in § II, it could well be that much

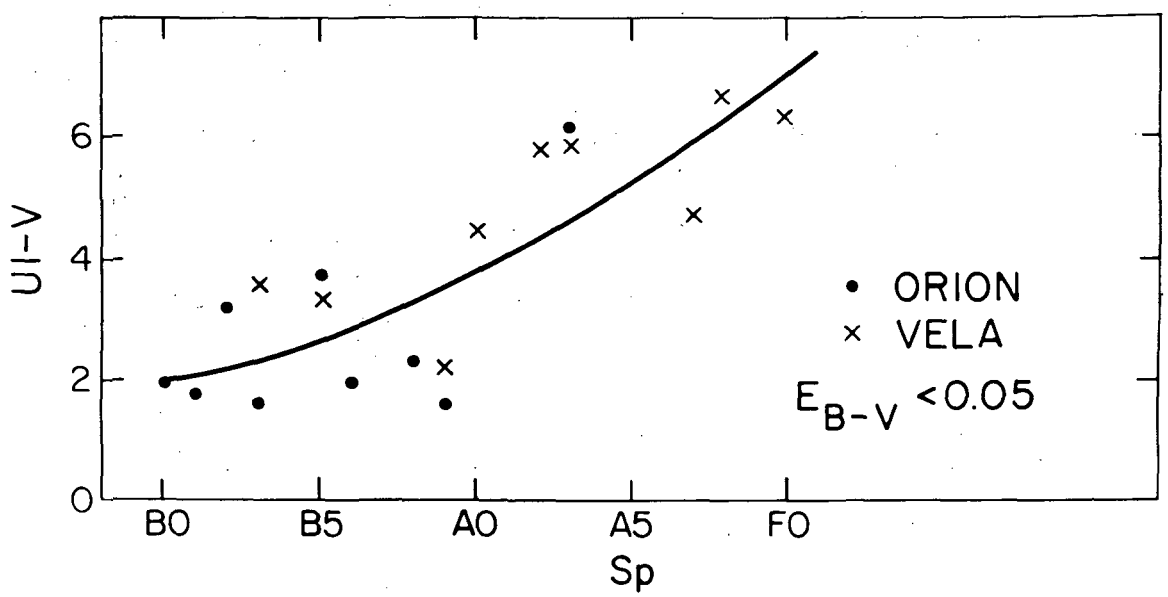

Figure 2.—Ultraviolet color index U1-V versus spectral type. The dots (●) (Orion) or crosses (×) (Vela) are average colors for each spectral type. Only stars with visual color excess E(B-V) < 0.05 have been selected. The solid line represents a tentative relation between intrinsic color index and spectral type.

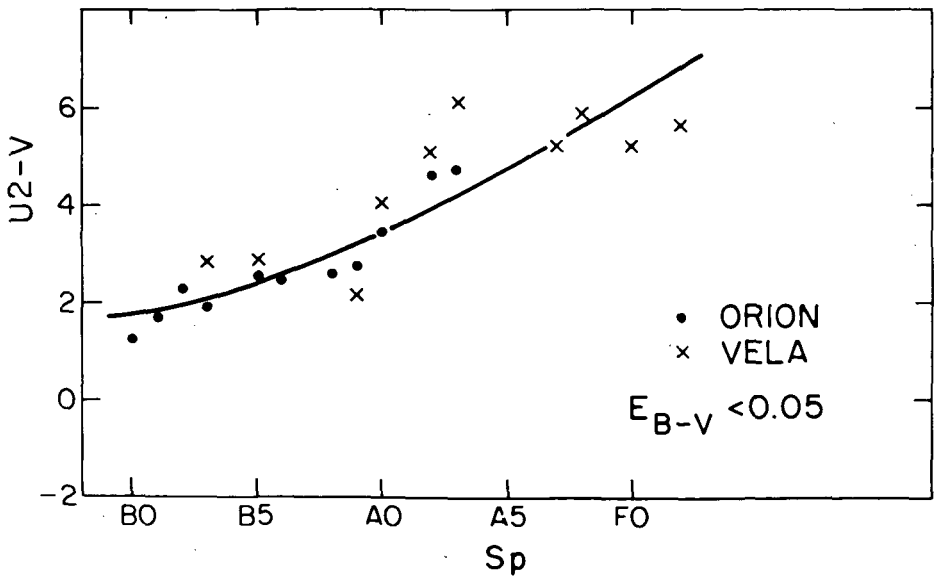

Figure 3.—Same as Figure 2, for color U2-V.

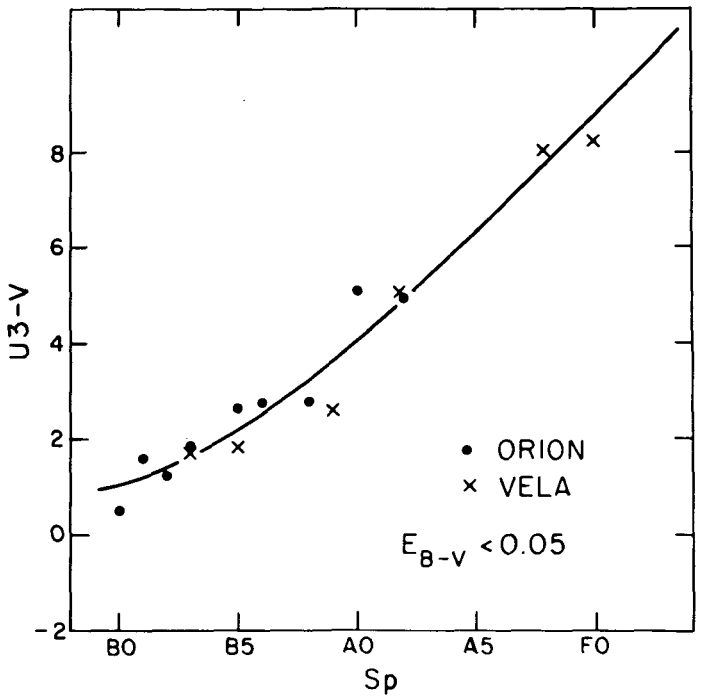

Figure 4.—Same as Figure 2, for color U3-V.

of this scatter is due to observational errors. Some is also most certainly due to our use of Henry Draper spectral types for stars having no MK classification; as shown by Schild and Chaffee (1971), significant differences exist between the HD and the MK classifications for stars having HD spectral types of B8 and B9. Nevertheless, we can try to derive average relations between the observed colors (U_i-V) and the spectral types. These relations are shown by solid lines. It is questionable whether the curvature of our fitted curves corresponds to reality. The fitting is best for the U3-V color; it is not so good for U1-V and U2-V.

From the set of relations (U_i-V) = f(Sp), where Sp stands for the spectral type, we can now derive a set of color-color relations

$$U_i\text{-}V = g_{Sp}(U_j\text{-}V) \ , \qquad j,i = 1,2,3;\ i \neq j \ ,$$

with the spectral type Sp as a parameter. The relations U3-V versus U1-V and U3-V versus U2-V are represented by solid lines in Figures 5 and 6, respectively. These lines are broken for spectral types later than about A3, because the scarcity of the data gives them less reliability for those later

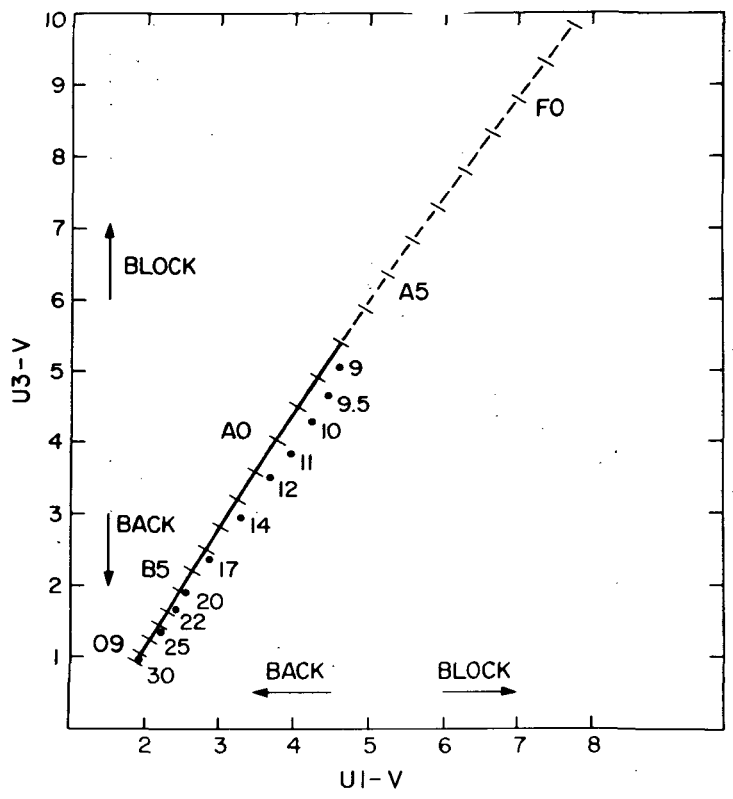

Figure 5.—Intrinsic color indices U3-V versus U1-V. The line labeled with spectral types is deduced from observations. The dots, labeled with $T_{eff} \times 10^{-3}$, represent colors computed from model atmospheres. Arrows show in which direction pure backwarming or pure blocking would displace the theoretical colors.

types. We can see that within a given spectral type range, the change in ultraviolet color is larger for the U3-V color than for U2-V or U1-V. Also, the change in color index per unit spectral type is smaller for early spectral types than for later spectral types. This is a direct consequence of the curvature of the lines in Figures 2, 3 and 4 and could therefore be modified, although we do not believe that straight lines would be a good fit for the $(U_i\text{-}V) = f(Sp)$ relations. It is interesting to note that the observed color-color relations

$$(U_i\text{-}V) = g_{Sp}(U_j\text{-}V)$$

can be represented by straight lines (there is only a very slight curvature).

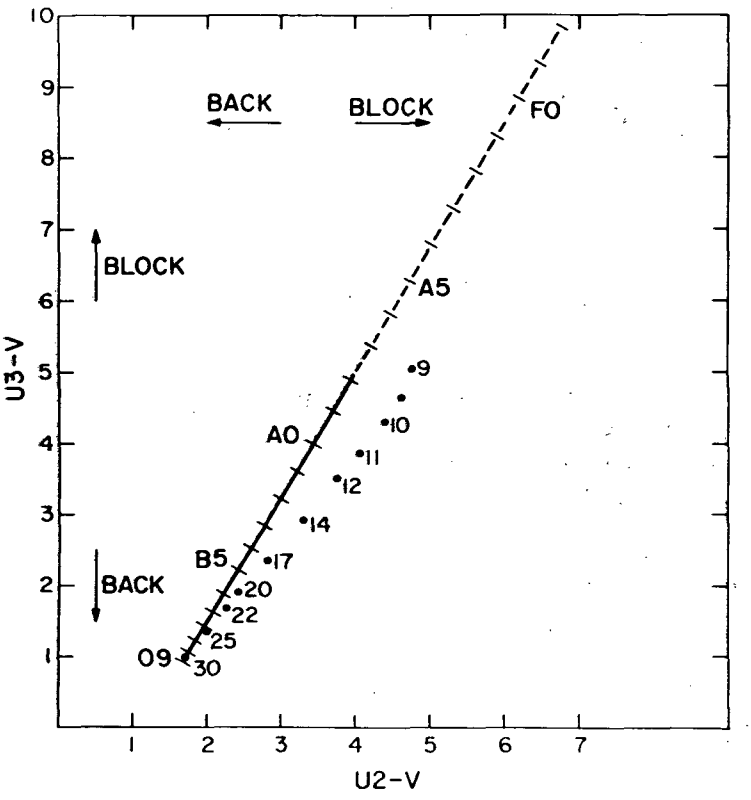

Figure 6.—Same as Figure 5, but U3-V versus U2-V.

To this point, we have derived all our intrinsic relationships from observed quantities only, without the aid of any theoretical models. This allows us now to make an independent comparison of the observed intrinsic relationships with the same relationships derived from model calculations. Weber et al. (1971) could not do so, because they used the theoretical colors to establish their calibration.

The theoretical colors $m_i - m_j$ $(i \neq j)$ are calculated quite generally (for spherically symmetric stars) according to the formula

$$m_i = -2.5 \log(E_i/\phi_i) + C_i + C \quad , \qquad (1)$$

where i stands for a given band pass, C_i are constants that should be equal to zero if the sensitivity functions $S_i(\lambda)$ had been calibrated absolutely; C is a constant that stands for all quantities independent of the wavelength λ, such as the radius or the distance of the star. If the C_i's were equal to zero, the theoretical color indices $m_i - m_j$ would be directly comparable to the observed indices as defined in the Celescope

experiment. However, as we shall see, these constants C_i have to be adjusted, as is generally the case for photometric systems. Next, we define E_i and ϕ_i:

$$E_i = \int_{\lambda_{ai}}^{\lambda_{bi}} F_\lambda(\lambda) \cdot A(\lambda) \cdot S_i(\lambda) \cdot d\lambda \ , \qquad (2)$$

$$\phi_i = \int_{\lambda_{ai}}^{\lambda_{bi}} S_i(\lambda) \ d\lambda \ , \qquad (3)$$

where λ_{ai} and λ_{bi} are the shortest and longest wavelengths of filter i; $S_i(\lambda)$ are again the sensitivity functions; and $A(\lambda)$ represents the monochromatic interstellar extinction at wavelength λ, with $0 \leq A(\lambda) \leq 1$. In this section, we deal only with stars for which the interstellar extinction is negligible; hence, $A(\lambda) = 1$. Finally, $F_\lambda(\lambda)$ is the stellar monochromatic flux per unit wavelength interval at wavelength λ.

The sensitivity function of the filter V has been taken from Azusienis and Straizys (1969). The Celescope sensitivity functions were taken from Davis (1968); see also § I, above.

The theoretical fluxes $F_\lambda(\lambda)$ have been computed by means of the program ATLAS (Kurucz 1969) with hydrogen line-blanketed model atmospheres also calculated by ATLAS. The resulting color indices U_i-V (defined by (1), (2) and (3)) are represented by dots in Figures 5 and 6. The parameter of the theoretical color-color relations is the effective temperature T_{eff} of the models. The representative points are labeled with T_{eff} in thousands of degrees Kelvin. The gravity of the models is equal to log g = 4. Some calculations with models having log g = 3 did not show any significant differences on the U1, U2 and U3 colors. Also, we compare the theoretical indices with average results derived mostly from class V stars, and therefore a gravity log g = 4 seems to be appropriate.

In addition to the ATLAS results, we also calculated a number of color indices with fluxes taken from Van Citters and Morton (1970). It turns out that these models do not show any significant line-blocking effect on the magnitudes U1, U2 and U3. These blanketed models bring about a backwarming effect on these three filters, and hence the net change between these blanketed models and the ATLAS models consists essentially of a shift in effective temperature along the sequence of theoretical colors. However, the theoretical color sequence had to be translated anyway, because the zero point of the theoretical magnitudes was ill defined (constants C_i in (1) not equal to zero). We adjusted the zero point of the theoretical colors so that the model at T_{eff} = 30,000°K has the same colors as do

stars of spectral class between O9 and B0. Once this arbitrary adjustment of the theoretical curve has been made, it is possible to discuss only relative differences between models and observations.

We then notice that the theoretical color-color relations in Figures 5 and 6 are not parallel to the observed relations and that this effect is more pronounced in the U3-V versus U2-V relation. We also see that the cooler models have colors that make them look like stars with spectral types that are too late. For example, the models at 10000°K look like A1 or A2 stars, which, according to Morton and Adams (1968), are too late by about 2 classes for this temperature.

In view of the rather poor fit of the relations of the intrinsic color versus spectral type (Figures 2, 3 and 4), it is difficult to decide whether these differences between models and observations are real. It should first be noted that our models do not include significant line blocking in any of the U1, U2 or U3 magnitudes. Models with a significant number of lines in these filters could modify the actual color-color relationships by a combination of backwarming and blocking effects. We have not yet studied the modified theoretical relations.

On the other hand, if we assume that the models give a good picture of real stars, the differences between models and observations could be explained in the following terms. The change in color per unit spectral class is essentially a function of the slope of the relations of color versus spectral type. A curvature change of these relations would expand or contract the spectral type scale in the color-color relations. The poor fit in Figures 2, 3 and 4 shows that such a change in curvature could explain quite well a difference of 2 to 3 spectral classes in the range 10,000 to 30,000°K.

The second difference between models and observations (i.e. the observed and theoretical color-color relations are not parallel) can be explained as follows. The curvature of the color-color observed relations is essentially due to different curvatures in the relations of color versus spectral type.

By changing any one of these curvatures, one could easily fill the gap between observations and theory in the color-color relations. As stated before, owing to the large scatter in our data, we cannot ignore the possibility of such changes in the fittings of Figures 2, 3 and 4.

Further discussions should be based on the analysis of much larger samples of the Celescope Catalog and on the use of models that include the best possible treatment of line blocking (i.e. very extensive tables of oscillator strengths).

IV. INTERSTELLAR EXTINCTION

In this section, we attempt to derive some results on interstellar extinction. Because our data are broad-band heterochromatic magnitudes, we are not able to present our results in terms of a monochromatic extinction law. Instead, we estimate color excesses in the usual way:

$$E_{i-V} = (U_i-V) - (U_i-V)_0 \ , \qquad (4)$$

where i stands for any one of the Celescope filters, and $(U_i-V)_0$ and (U_i-V) are, respectively, the intrinsic and observed color indices. In addition, we normalize the excesses E_{i-V} so that $E(B-V) = 1$. This requires that for the stars used to calculate the excesses E_{i-V}, we know the spectral type (necessary to define the star's intrinsic color indices), the B-V index, and at least one of the ultraviolet color indices. Furthermore, we need to select stars with an excess E(B-V) as large as possible, for the following reasons: a) because we normalize with respect to E(B-V), E(B-V) must be much larger than its possible errors $\delta E(B-V)$; b) the excesses E_{i-V}, as given by (4), must be larger than the typical standard deviations of the U_i-V indices. As seen previously, these deviations are on the order of 0.3 mag. So we require that

$$E_{i-V} >> 0.3 \ . \qquad (5)$$

With our normalization, the normalized excess E^*_{i-V} is

$$E^*_{i-V} = \frac{E_{i-V}}{E_{B-V}}$$

which, together with (5), gives the condition

$$E_{B-V} >> \frac{1}{E^*_{i-V}} \ .$$

As we shall see later, our results, as well as those of others, indicate that for our filters, $E^*_{i-V} \gtrsim 3$, so that we should like to select stars with

$$E_{B-V} >> 0.1 \ .$$

But only five of our sample stars have $E(B-V) > 0.6$. Of the three in Orion having $E(B-V) > 0.15$, two are supergiants, and the third (HD 37903) has an abnormal spectral energy distribu-

tion, as indicated by its U-B color, by our observations in U2 and U3, and by Weber's observations at 1500 Å.

To derive average ultraviolet excesses for a reasonably sized sample, we adopted the compromise limit of $E(B-V) > 0.4$. This leaves us with samples of 10, 12 and 8 stars for the filters U1, U2 and U3, respectively. The normalized average color excesses are plotted in Figure 7 against $1/\lambda(\mu^{-1})$. In the case of heterochromatic excesses, λ stands for the average wavelength of the band passes. The Celescope results are represented by large dots. The associated scatter bars represent the standard deviations within each of our three samples.

We compare the Celescope results with those of Weber et al. (1971), Smith (1967), Sivan and Viton (1971), Stecher (1965) and Bless and Savage (1972).

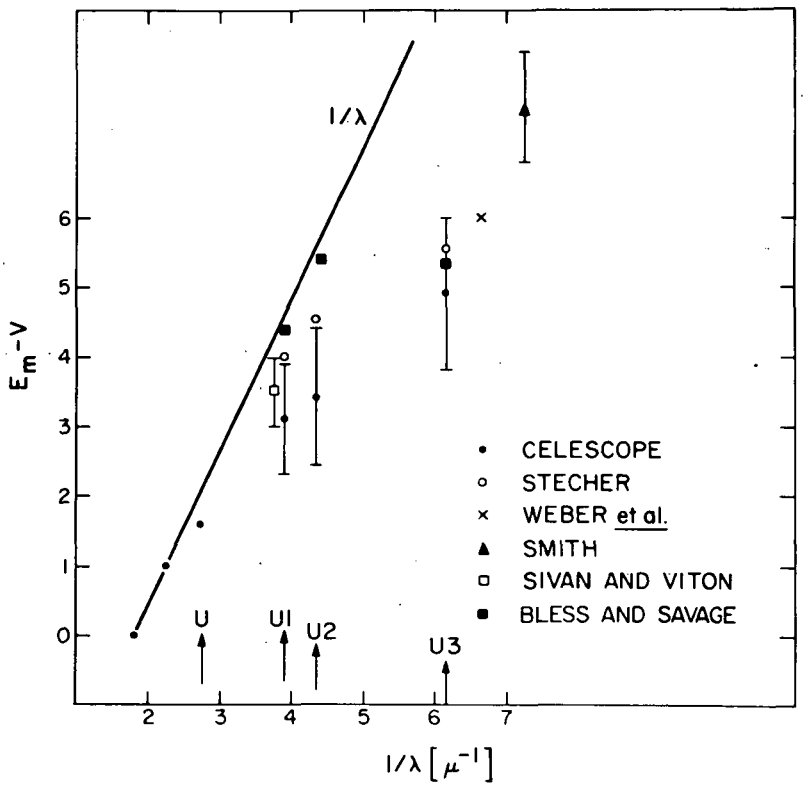

Figure 7.—Heterochromatic color excesses E_{m-V} normalized to $E(B-V) = 1$. The solid line represents a $1/\lambda$ extinction law (λ is the wavelength in μ^{-1}). The vertical arrows show the mean wavelengths of filters U, U1, U2, and U3. Filled circles (●) show Celescope results. Stecher's (○) and Bless and Savage's (■) extinction values have been folded with the Celescope filter response curves. The results by Weber et al. (×), Smith (▲), and Sivan (□) are from broad-band observations.

In the case of monochromatic-extinction curves (Stecher's results and theoretical curves), we calculated heterochromatic excesses according to relations (1), (2), (3) and (4) for filters U1, U2 and U3. The only change with respect to the calculations of § III is that now $A(\lambda) \neq 1$.

Figure 7 shows that the Celescope excesses are smaller than those found by other authors, although those of Sivan and Viton, Weber et al., and Stecher lie within our scatter bars, or very close to them. One cannot exclude the possibility that the interstellar extinction in Vela is not the same as that in other regions of the sky.

Finally, it should be noted that reddening lines in the color-color diagrams (Figures 5 and 6) would be nearly parallel to the intrinsic effective temperature sequence. This means that with our ultraviolet broad-band colors, we are unable to analyze independently the interstellar extinction and the effective temperature. On the other hand, the advantage is that all effects perpendicular to the temperature sequence will be fairly independent of interstellar extinction. In other words, the properties responsible for these effects could be analyzed even if one does not know the exact amount of interstellar extinction.

One of us (EP) wishes to acknowledge that he held an ESRO-NASA International Fellowship while this work was done.

The Celescope program is supported in part by contract NAS 5-1535 from the National Aeronautics and Space Administration.

REFERENCES

Azusienis, A. and Straizys, V. 1969, Soviet Astr. 13, 316.
Bless, R. C. and Savage, B. D. 1972, this volume.
Davis, R. J. 1968, SAO Spec. Rep. No. 282, 132 pp.
Davis, R. J. 1972, this volume.
Davis, R. J., Deutschman, W. A., Lundquist, C. A., Nozawa, Y. and Bass, S. D. 1972, this volume.
Kurucz, R. L. 1969, in Theory and Observation of Normal Stellar Atmospheres, ed. O. Gingerich (Cambridge: M.I.T. Press), p. 375.
Morton, D. C. and Adams, T. F. 1968, Ap. J. 151, 611.
Schild, R. E. and Chaffee, F. 1971, Ap. J., in press.
Schmidt-Kaler, Th. 1965, Landolt-Börnstein, Numerical Data and Functional Relationships in Science and Technology, Gruppe VI, Bd., Astronomie und Astrophysik, ed. H. H. Voigt (Berlin: Springer-Verlag), p. 298.
Sivan, J. P. and Viton, M. 1971, COSPAR Symposium, Seattle, Wash.

Smith, A. M. *1967*, Ap. J. *147*, *158*.
Stecher, T. P. *1965*, Ap. J. *142*, *1683*.
Van Citters, G. W. *and Morton*, D. C. *1970*, Ap. J. *161*, *695*.
Weber, S. V., *Henry*, R. C. *and Carruthers*, G. R. *1971*, Ap. J. *166*, *543*.
Wickramasinghe, N. C. *and Nandy*, K. *1968*, *Nature* *219*, *1347*.

Page intentionally left blank

INTERSTELLAR EXTINCTION IN THE ULTRAVIOLET

Robert C. Bless and Blair D. Savage
University of Wisconsin
Madison, Wisconsin

ABSTRACT

Interstellar extinction curves over the region 3600-1100 Å for 17 stars are presented. The observations were made by the two Wisconsin spectrometers on board the OAO-2 with spectral resolutions of 10 Å and 20 Å. The extinction curves generally show a pronounced maximum at 2175 ± 25 Å, a broad minimum in the region 1800-1350 Å, and finally a rapid rise to the far ultraviolet. Large extinction variations from star to star are found, especially in the far ultraviolet; however, with only two possible exceptions in this sample, the wavelength at the maximum of the extinction bump is essentially constant. These data are combined with visual and infrared observations to display the extinction behavior over a range in wavelength of about a factor of 20. The observations appear to require a multi-component model of the interstellar material.

I. INTRODUCTION

Recent observations of the continua of stars in the spectral region shortward of 3000 Å have shown that the nature of the interstellar extinction curve in the ultraviolet is quite different than had been expected on the basis of observations in the visual region of the spectrum. OAO-2 has observed many stars suitable for extinction determinations; preliminary results were reported by Bless and Savage (1970). In this paper we present additional extinction curves derived from pairs of stars which display the broad range of behavior so far found.

II. INSTRUMENTAL AND OBSERVATIONAL CONSIDERATIONS

The observations reported here were obtained with the two objective grating spectrum scanners in the Wisconsin instrument package on the OAO; one is sensitive over the wavelength range from about 3600-1800 Å, the second over the interval 2000-1050 Å. The effective collecting area of each instrument is 265 cm^2 and the nominal resolution of the long and short wavelength instruments is 20 Å and 10 Å, respectively. To scan the spectrum, the gratings are rotated in increments equal to the instrumental resolution; integration times at each grating position may be 64 or 8 seconds (usually the latter). Both analog and digital readouts of the signal from the photomultiplier detectors are stored in the spacecraft memory and transmitted to the ground on command. For more information concerning the Wisconsin instrumentation and its operation, see Code et al. (1970).

Spectral scans of S Mon and ξ Per over the long wavelength and short wavelength ultraviolet regions are given in Figures 1 and 2, respectively. The scans have not been normalized;

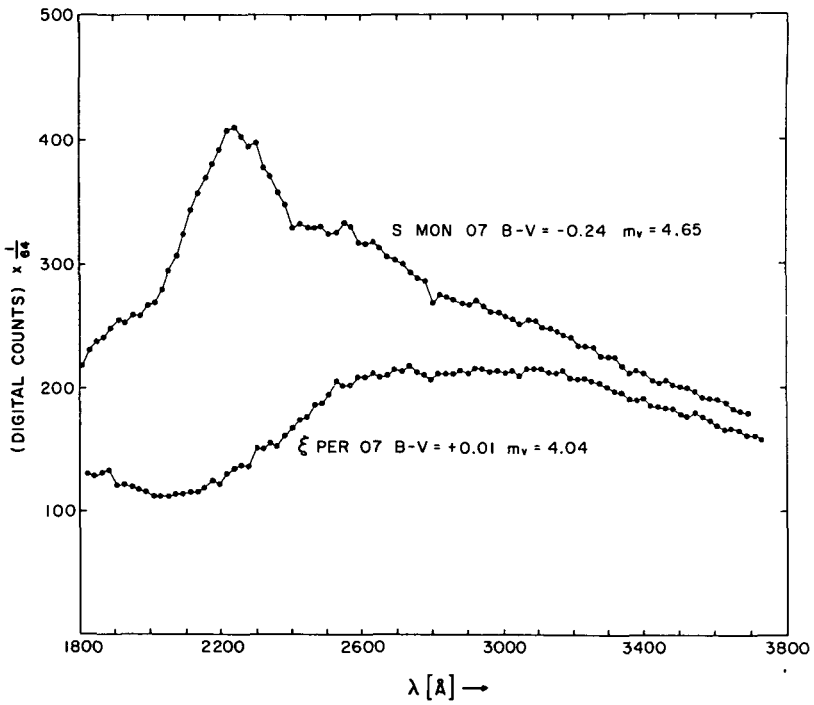

Figure 1.—Spectral scans of S Mon and ξ Per over the region 1800-3700 Å, made by Spectrometer 1 on OAO-2. Note the large extinction effects, especially near 2200 Å. These scans are neither normalized nor corrected for the instrumental sensitivity function.

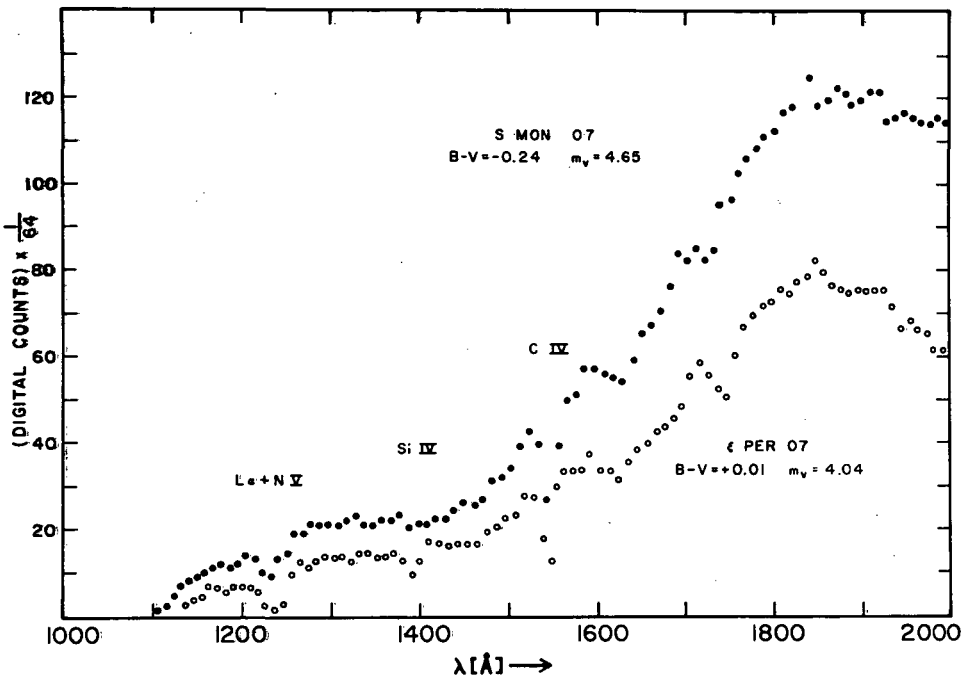

Figure 2.—Spectral scans of S Mon and ξ Per over the region 1100-2000 Å made by Spectrometer 2. As with the curves in Figure 1, these scans are raw data, with only a small, constant background correction made.

note the large extinction effects, especially around 2200 Å, in the reddened star ξ Per. A number of strong lines appear in the spectra of early-type stars shortward of 1800 Å; thus, fitting two scans in this spectral region to a common wavelength scale is straightforward. In the 2000-3000 Å region, however, only the Mg II doublet at 2800 Å appears in the spectra of most early-type stars, and then sometimes only weakly. As a consequence there can be an uncertainty of about ±20 Å in matching two scans over this spectral interval. For our present purposes, however, this uncertainty is of no importance. Sample spectral scans made by these instruments are also given by Code and Bless (1970) as well as in the two papers already mentioned.

The photometric stability of the two scanners is well established. The absolute response of the short wavelength scanner is constant to within 1-2% over a period of many months, whereas the relative response of the longer wavelength instrument is similarly constant. Thus no loss of accuracy whatsoever results in comparing scans made many months apart.

The background count rate of the scanners is primarily due to thermal dark counts, sky light, and scattered light. This background can be determined by observing shortward of the LiF cutoff (1050 Å) of the short wavelength scanner and shortward of the quartz cutoff (1800 Å) of the long wavelength scanner. For early-type stars the background correction is only significant over an interval of a few hundred Angstroms extending longward from 1050 Å; elsewhere the correction is of little consequence.

Since observations of stars made when the OAO is in daylight or traversing the South Atlantic Anomaly of the earth's radiation belt may be affected by extraneous signals and noise, scans which were accidentally made under these circumstances have been rejected.

The field of view of the objective scanners is 8 arc minutes perpendicular to the dispersion and about ±1.5° along the dispersion. Thus, care must be taken to see that stars other than the program star capable of contributing to the ultraviolet flux do not fall within this field. This is routinely checked before an observation is made and, if necessary, the spacecraft is rolled about the scanner optical axis to avoid other stars. In addition, the observations reported here have been checked again; with the exceptions noted in the discussion, only the program stars contribute radiation to the observed flux.

Of obvious importance for ultraviolet extinction determinations is whether or not two stars of the same spectral and luminosity classes and intrinsic visual colors are identical in the ultraviolet. Bless and Savage (1970) gave evidence that such stars do indeed have the same ultraviolet energy distributions; in fact, early B-type stars of the same spectral types and colors, but of any luminosity class II to V, show the same relative flux distribution in the ultraviolet. This characteristic has now been confirmed for many more early-type stars of which a small sample is given in Figure 3, where flux ratios, expressed in magnitudes, are plotted against wavelength. The curves shown were chosen from a series of plots of point-by-point flux ratios made for each pair of stars indicated, each plot in a series for two stars having been shifted slightly in relative wavelength as compared to the next. The particular plots given in Figure 3 were those for which the wavelength scales of the two stars fit best, as indicated by the least scatter of individual points. The longer wavelength scan ratios were then adjusted to fit those over the shorter wavelength region, with the results given in the figure. The sense of the magnitude scale is such that ζ Ori, e.g., is about $0^m.5$ fainter than σ Ori at 1200 Å relative to the V magnitude. Figure 3 also shows that the energy distributions of supergiants is not the same as that of lower luminosity stars of the

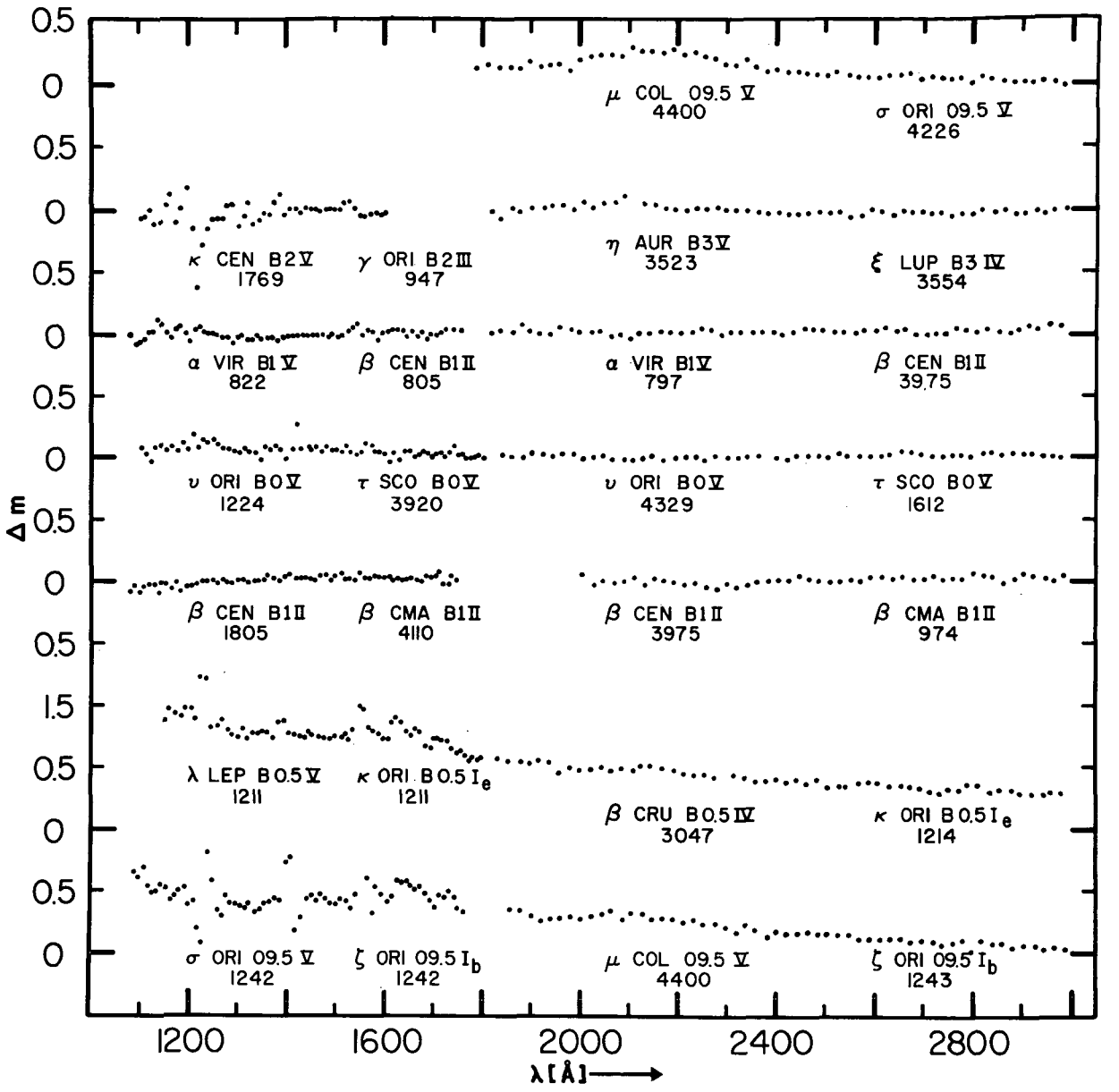

Figure 3.—Ratios, in magnitudes, of ultraviolet energy distributions of little reddened stars of similar spectral types and colors. The data are normalized to the V magnitude and the flux from the star listed on the right of each pair is taken as the numerator in the flux ratio, e.g., F(σ Ori)/F(μ Col). The scatter near Ly α, 1400 Å (Si IV) and 1550 Å (C IV) is caused by differences in these features in the two stars. Note that energy distributions of stars of luminosity classes II to V are essentially identical, whereas supergiants are systematically fainter towards shorter wavelengths as compared with lower luminosity stars.

same spectral type, but that the flux from the former becomes fainter with decreasing wavelength. This effect was first noted by Carruthers (1969) and has been interpreted by Mihalas (1970) as the result of differences in surface gravity and effective temperature between early-type supergiants and dwarfs of the same spectral type. The intercomparison of μ Col and σ Ori in Figure 3 illustrates how ultraviolet energy distributions are modified by only a slight amount of interstellar extinction (σ Ori is $0^m.04$ redder in (B-V) than μ Col).

Calculations have indicated that very rapid rotation should significantly affect the far ultraviolet energy distributions of early-type stars (Collins 1965, Hardorp and Strittmatter 1968). We have looked for such rotation effects by comparing the ultraviolet continua of two stars similar in every way except for their projected rotational velocities. For example, comparison of the energy distributions of δ Lup, α Leo, and ϕ Per ($v \sin i$ = 350 km/sec, 370 km/sec, and 480 km/sec, respectively) with those of a range of stars of similar spectral types and (B-V) colors, but with low rotational velocities, showed no significant differences which could be attributed to rotation. These comparisons were made in the 1050-1800 Å region where the effects are predicted to be greatest. However, we have found that Be stars with strong emission lines in the visual do radiate more energy longward of 2000 Å than do normal stars of the same spectral type. This excess radiation from the Be stars is most likely Balmer continuum emission, similar to that reported by Bohlin (1970) for γ Cas. These same shell stars, however, have normal continua in the spectral region shortward of 2000 Å.

In addition to this fairly detailed search for rotation effects in the continua of a few stars, a cruder search was carried out for about 60 stars with (B-V) color excesses less than $0^m.1$ by plotting their $(1700\text{Å}-V)_o$ colors against their $(B-V)_o$ colors (see Figure 4). To obtain intrinsic colors a small reddening correction was applied using a mean extinction curve (see § IV). As can be seen in the figure, there is no significant difference attributable to rapid rotation, at least at a level important for extinction determinations. The results concerning rotational effects summarized here will be discussed in greater detail in a later paper. For our present purposes we will not use observations in the 2000-3000 Å spectral region of stars which show strong Be characteristics; otherwise we assume that rapid rotation does not significantly distort the continuous spectrum of a star.

Figure 4 also shows that for this sample, unreddened stars of similar intrinsic colors do not differ appreciably in the far ultraviolet; all of the observational points fall within $0^m.25$ of a mean curve. Since the slope of the color-color plot

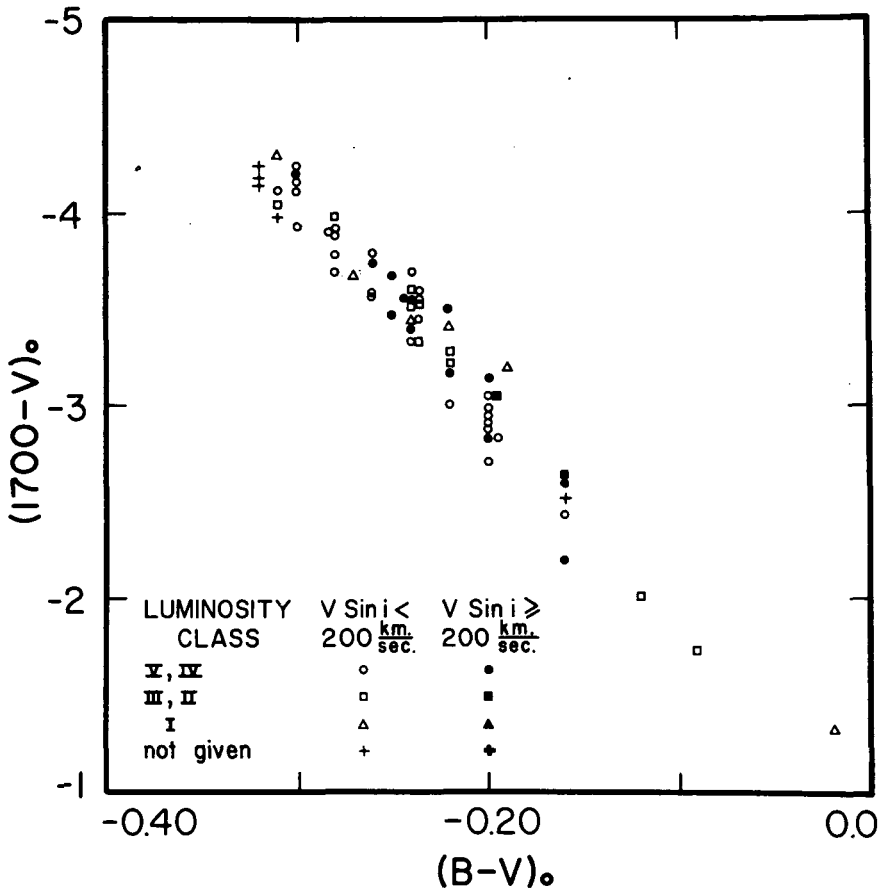

Figure 4.—Color-color diagram for 60 stars with E(B-V) ≤ 0.1, and of a variety of spectral types, luminosity classes, and rotational velocities. Ultraviolet extinction was corrected for by means of the "average" extinction curve shown in Figure 6. No prominent rotational effects are apparent.

of Figure 4 is so large much of the $0^{m}.25$ scatter can probably be explained as small errors in the $(B-V)_o$ determinations. In this diagram, supergiants do not appear systematically fainter in the ultraviolet since their ultraviolet colors are plotted against their visual colors rather than against their spectral types.

In conclusion, the discussion above indicates that one can derive extinction curves by intercomparing reddened and unreddened early-type stars of the same spectral type and of any luminosity class, II through V, or by intercomparing supergiants of the same spectral type. Furthermore, one can intercompare rapidly rotating stars with slowly rotating stars provided Be stars are avoided in the region 2000-3600 Å.

III. THE OBSERVATIONS

Table 1 lists the stars used in this paper for extinction determinations. Wherever possible, photometric data for northern stars were taken from Iriarte et al. (1965) and for southern stars from Cousins and Stoy (1962). Spectral types are those given by Lesh (1968) or by Hiltner, Garrison and Schild (1969) for northern and southern objects, respectively. Intrinsic colors used to form the (B-V) excess are those given by Johnson (1963). Projected rotational velocities (Boyarchuk and Kopylov 1964) are given for stars with v sin i $\geq$ 200 km/sec.

We thought it useful to display all available extinction data for the stars listed in Table 1. For this purpose we used Johnson's (1966) infrared and visual colors for the more heavily reddened star of each pair. Since infrared measurements are not available for several of our comparison stars, we used for the colors of these objects Johnson's (1968) mean values for the appropriate spectral types and luminosity classes. In nearly all of those instances which could be checked, the mean infrared colors well represent the colors of the individual objects.

The procedure by which the infrared, visual and ultraviolet observations were fitted together was straightforward. Differences between the program and comparison stars in their infrared and visual colors were adjusted to $\Delta(B-V) = 1\overset{m}{.}0$ and the V magnitude point set equal to zero. The values so found were plotted as circles in Figures 5a, b, c and d. Flux ratios were formed for the ultraviolet scanner data in the manner previously described for the comparisons of the unreddened stars, and then adjusted to $\Delta(B-V) = 1\overset{m}{.}0$. The longer wavelength data were fitted to Johnson's measurement at 3600 Å ($1/\lambda = 2.78\ \mu^{-1}$) and the shorter wavelength scanner data joined to the longer in the 2000 Å region. Generally, this procedure was satisfactory and only in a few instances was any judgment required to join the scans.

A rather sharp spike appears on some of the curves in Figure 3 and Figures 5a-d, especially near Ly α, but also at 1400 Å (Si IV) and 1550 Å (C IV). This is simply the result of incomplete canceling of the line profile in the two stars in question due either to differences in the profile or to a slight wavelength discrepancy. Such points are not representative of the real observational scatter, which is considerably smaller. It is difficult to make a precise assessment of the errors in these curves, but an estimate can be obtained from the scatter in the curves shown in Figures 3 and 4. Generally the observational error in the longer wavelength region is small, but it increases towards shorter wavelengths pri-

Table 1. Data for Stars Used in Extinction Determination

Star*	V	S. T.	(B-V)	Remarks
ξ Per	4.06	O7.5	+0.01	v sin i = 211 km/sec
15 Mon }	4.66	O7	-0.24	Multiple system; comb. mag. and color; S Mon brightest member
15 Mon }				
ζ Oph	2.57	O9.5 Vnn	+0.02	v sin i = 400 km/sec
μ Col	5.16	O9.5 IV	-0.29	
σ Ori	3.83	O9.5 V	-0.24	Multiple system; composite; mag. and color for A, B, and C
β^1 Sco	2.55	B0.5 V	-0.08	
β Cru }	1.25v	B0.5 III	-0.24	Double, Δm = 10; β CMa variable
β Cru }				
σ Sco	2.89v	B1 III	+0.14	Sp. bin.; primary β CMa type
β Cen	0.60	B1 III	-0.22	Sp. bin.; double
α Vir	0.96	B1 IV	-0.25	Sp. bin.
ρ Oph	4.63	B2 IV/V	+0.22	Multiple system; brightest components B2 and B3; v sin i = 280 km/sec
γ Ori }	1.64	B2 III	-0.21	
γ Ori }				
HD 48099	6.37	O5.5	-0.04	
15 Mon	4.66	O7	-0.24	See ξ Per

Table 1, continued

Star*	V	S. T.	(B-V)	Remarks
19 Cep	5.10	O9.5 Ib	+0.07	Double; $\Delta m = 6$
ζ Ori	1.74	O9.5 Ib	-0.21	Double; O9.5 Ib($2^m.05$) + B3($4^m.2$) comb. mag. and color
HD 47129	6.06	O8f	+0.05	Sp. bin.; companion probably same type; Plaskett's star
λ Ori	3.39	O8	-0.18	Double with Oe5 ($5^m.6$); comb. mag. and color
λ Cep	5.04	O6f	+0.23	
15 Mon	4.66	O7	-0.24	See ξ Per
ζ Per	2.86	B1 Ib	+0.10	Multiple system
β Cen	0.60	B1 III	-0.22	See σ Sco
β CMa	1.98	B1 II/III	-0.24	
$\theta^{1,2}$ Ori	3.98	O8.5	-0.03	Composite color, mag., and s.t.
15 Mon } 15 Mon }	4.66	O7	-0.24	See ξ Per
δ Sco	2.33	B0.5 IV	-0.10	
τ Sco } τ Sco }	2.82	B0 V	-0.25	

Table 1, concluded

Star*	V	S. T.	(B-V)	Remarks
κ Aql	4.95	B0.5 IIIn	0.00	v sin i = 280 km/sec
β Cru	1.25v	B0.5 III	-0.24	See β^1 Sco
χ^2 Ori	4.63	B2 Ia	+0.29	
γ Ori	1.64	B2 III	-0.21	
ω^1 Sco	3.99	B1 V	-0.04	
β Cen	0.60	B1 III	-0.22	See σ Sco
139 Tau	4.83	B1 Ib	-0.07	
β Cen }	0.60	B1 III	-0.22	See σ Sco
β Cen }				
α Cam	4.29	O9.5 Ia	+0.03	
ζ Ori }	1.74	O9.5 Ib	-0.21	See 19 Cep
ζ Ori }				

*The first star of a group is the reddened object; the second and third are the comparison stars observed by Spectrometer 1 and 2, respectively.

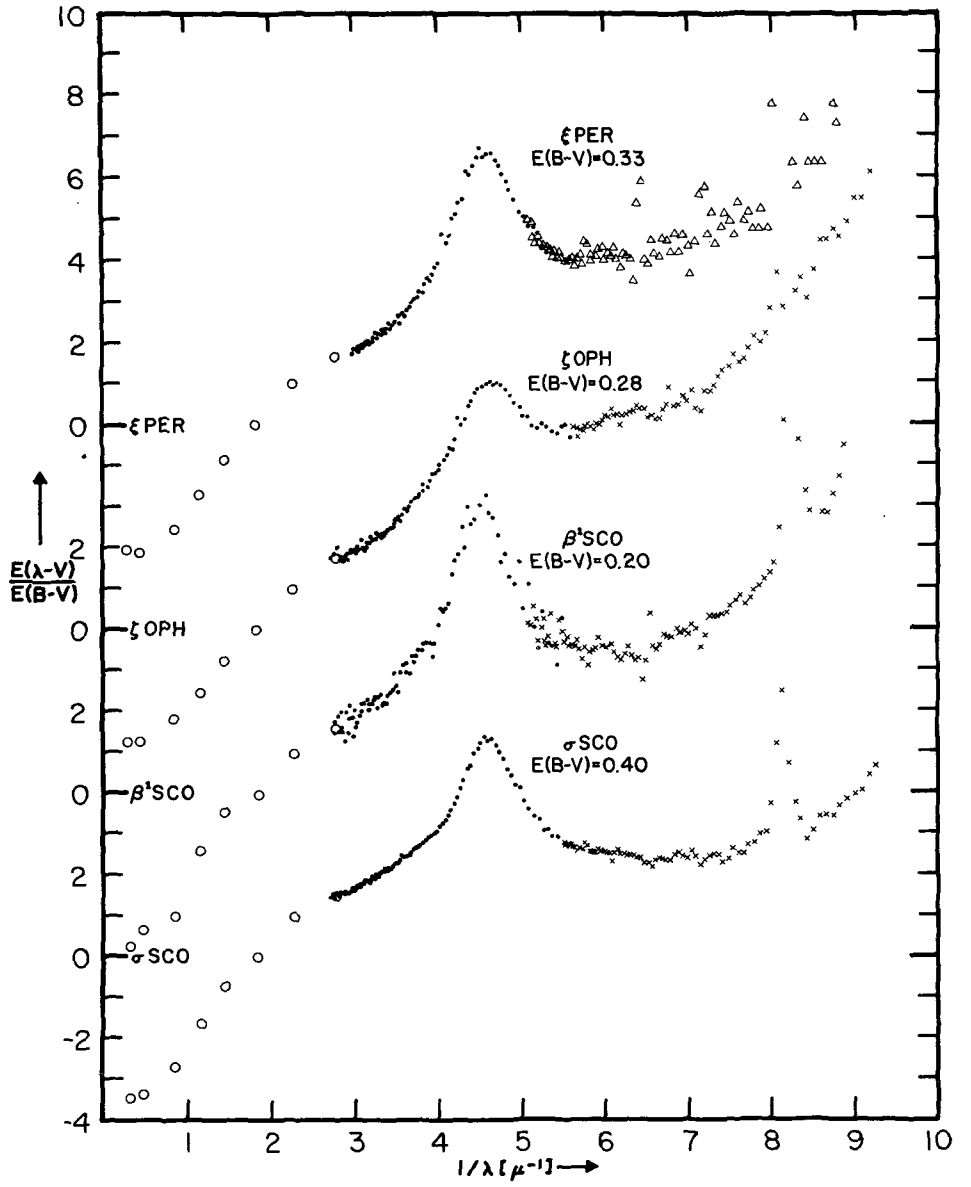

Figures 5a, b, c, d.—Interstellar extinction curves for 17 stars. Data for these stars as well as for the comparison stars are given in Table 1. The dashed lines in the diagrams for 139 Tau, χ^2 Ori, and ζ Per indicate the extinction curve after an approximate correction was applied for the systematically smaller intrinsic ultraviolet flux from a supergiant as compared with that from a lower luminosity star. See the text (§ III) for comments concerning the observational scatter. Extinction curves for β^1 Sco and δ Sco in the 3600-1800 Å region were derived from analog rather than digital data, and are, therefore, of lower quality.

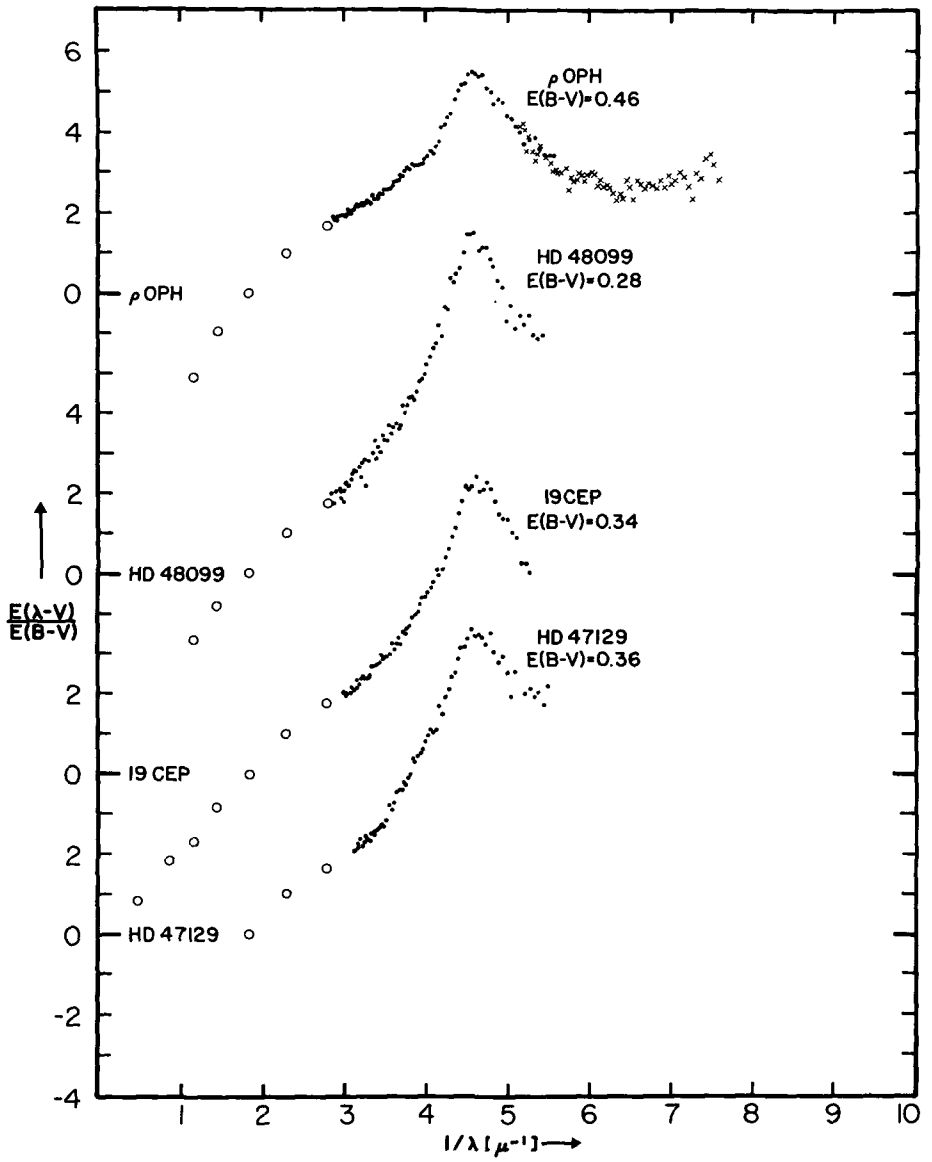

Figure 5b.—See caption for Figure 5a.

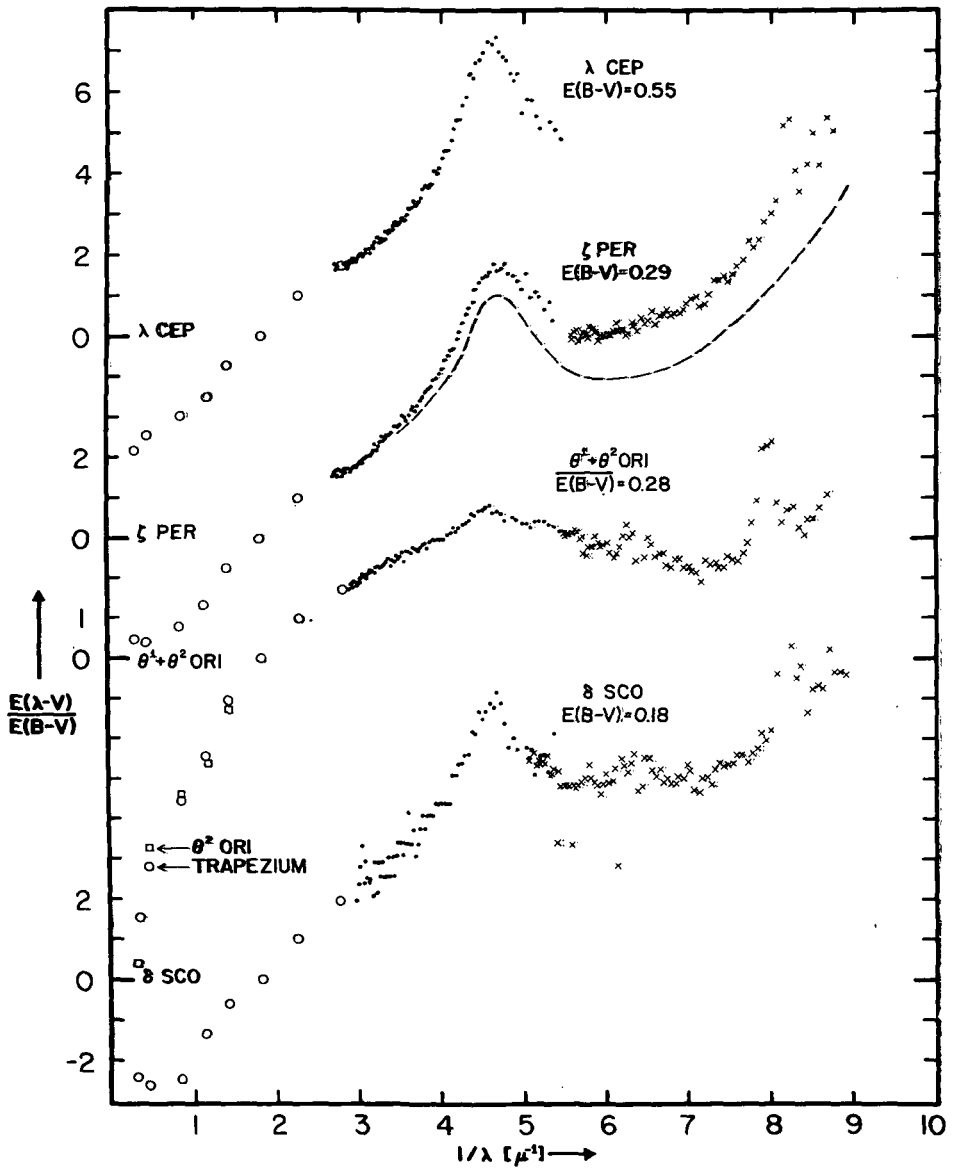

Figure 5c.—See caption for Figure 5a.

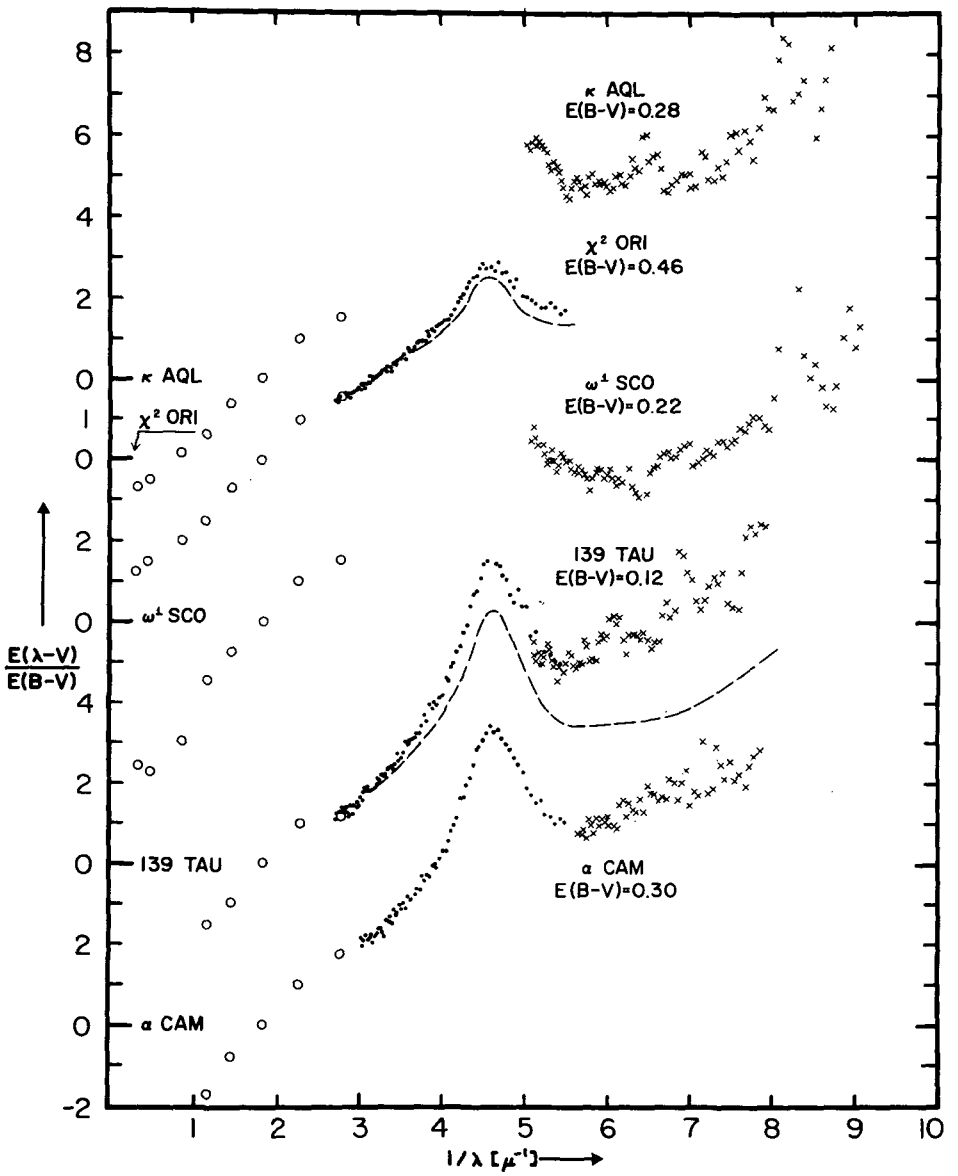

Figure 5d.—See caption for Figure 5a.

marily because of the decrease in instrumental sensitivity. The scatter is not sufficient, however, to mask the overall trend of the points. The precision of the extinction curves depends not only on the accuracy of the ultraviolet observations, but also on that of the (B-V) measurements. Wherever possible, we have used, for a given pair of stars, (B-V) observations made by the same observer in order to minimize systematic errors. For the average Δ(B-V) of the stars used here, about $0^m.30$, a (B-V) error of $0^m.01$ or $0^m.02$ is negligible, but when Δ(B-V) is as small as $0^m.12$ (139 Tau) such an error is significant and the resulting extinction curve uncertain, especially at the shortest wavelengths.

Extinction curves derived from five supergiants are included here. Two of these, α Cam and 19 Cep, were compared with another supergiant, ζ Ori. However, three stars, 139 Tau, χ^2 Ori and ζ Per were compared with less reddened objects of luminosity classes II or III with the consequence that the resulting extinction curves need a slight modification to reflect the previously mentioned intrinsic differences between supergiants and less luminous stars of the same spectral types. A precise correction for the systematic decrease in flux with decreasing wavelength in supergiants as compared to stars of lower luminosity is not possible at this time. A crude correction, however, to the curves for ζ Per, 139 Tau and χ^2 Ori, shown in Figures 5c and d, can be made by decreasing the values of $E(\lambda-V)/E(B-V)$ monotonically so that they are lower at $\lambda^{-1} = 9$ than at $\lambda^{-1} = 3$ by 1.9, 4.0 and 1.2 respectively. These corrections were obtained by applying the observed difference between λ Lep (B0.5 V) and κ Ori (B0.5 Ie) (see Figure 3) to the three supergiants. We have assumed here that the ultraviolet brightness differences for the B1 supergiants (139 Tau and ζ Per) and B2 supergiant (χ^2 Ori) are the same as for B0.5 supergiants.

No serious ambiguities in the data are produced by flux from other stars in the field of view, such stars most often being too faint to contribute more than a few percent to the ultraviolet flux of the program star, or else being of about the same spectral type as the program star, thereby not significantly changing its relative energy distribution.

Generally, the same comments apply in the case of multiplicity of the program or comparison stars themselves. In a few instances, however, lack of information on the nature of the components makes it difficult to determine their effect, so these systems were compared with other objects having, as nearly as possible, identical colors and spectral types. It was found that the colors and spectral types given in Table 1 well represent their ultraviolet spectra. The particularly interesting systems, $\theta^{1,2}$ Ori, σ Sco and ρ Oph will be discussed in the next section.

IV. DISCUSSION

The characteristic features of the ultraviolet extinction curves are: (1) the pronounced bump at about $\lambda^{-1} = 4.6\ \mu^{-1}$; (2) the minimum in extinction which occurs in the region $\lambda^{-1} \simeq 5.5$ to $7.5\ \mu^{-1}$; (3) the rapid rise in extinction in the far ultraviolet; and (4) the large variations in ultraviolet extinction from object to object, these variations being greatest in the far ultraviolet. The extinction bump has been detected in every extinction curve derived thus far (in addition to the curves presented in this paper the bump has been observed in about 30 other slightly or moderately reddened stars). The wavelength of maximum extinction at the bump is rather well defined with nearly all maxima falling at $\lambda^{-1} = 4.6 \pm 0.1\ \mu^{-1}$ (2175 Å ±25); ζ Oph and ζ Per apparently deviate from this behavior with their maxima falling at $\lambda^{-1} = 4.75 \pm 0.1\ \mu^{-1}$ (2105 Å ±25). It has not been established if this difference is due to real differences in the interstellar extinction or rather to peculiarities of the energy distributions of these two stars over the near ultraviolet. (Before it was recognized that continuous Balmer emission significantly modifies the near ultraviolet spectra of early-type emission line stars, extinction curves derived for Be stars also showed peculiar extinction bumps.) The use of various other unreddened comparison stars for the derivation of extinction curves for ζ Oph and ζ Per produced curves nearly identical to those shown in this paper.

Large variations from object to object occur in the ultraviolet extinction curves. These are illustrated in Figure 6 where we have plotted a number of extinction curves which show the range of behavior in the ultraviolet and infrared extinction. The spread in extinction is greatest in the far ultraviolet, although in a few cases the bump is significantly modified ($\theta^{1,2}$ Ori for example). Incidentally, this variation in extinction requires that, as was the case in this paper, comparison stars be little reddened since otherwise one could be comparing two stars having markedly different ultraviolet extinction characteristics, giving a misleading extinction curve.

Table 2 gives an "average" ultraviolet extinction curve we suggest for general use when more detailed information is not available. The values given in the table do not represent the mean through the envelope of extinction curves given in Figure 6. Rather, since the extinction in the direction of $\theta^{1,2}$ Ori, σ Sco and ρ Oph does not appear to occur commonly, the curve given in the table is the average of all stars except these three and represents our estimate of the most likely extinction to be encountered. Obviously, the applicability of this

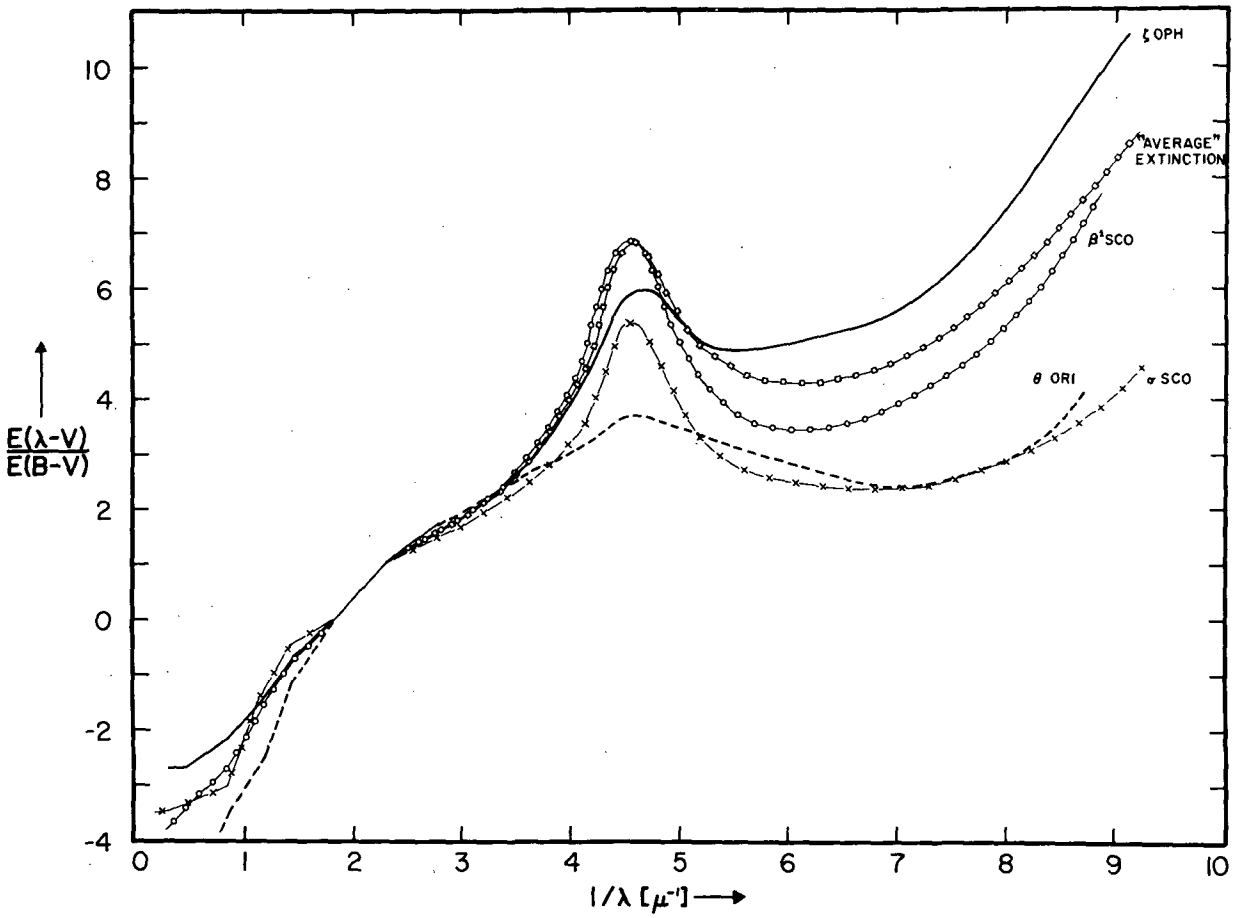

Figure 6.—Interstellar extinction curves which generally define the envelope of all such curves so far obtained. The "average" curve represents the most probable extinction behavior derived from all the extinction data presented in this paper except that for σ Sco, ρ Oph, and $\theta^{1,2}$ Ori.

average curve will depend on the use to which it is put.

The stars $\theta^{1,2}$ Ori, σ Sco and ρ Oph deserve some comment since their extinction curves differ markedly from the majority of those so far found. All three of these stars are multiple: $\theta^{1,2}$ Ori includes six stars ranging from O6 to B3 which have a weighted mean spectral type of O8.6 and a (B-V) color of $-0^{m}.03$, and so a color excess of $+0^{m}.28$. ρ Oph consists of five stars, the brightest two of which are B2 IV and V stars and provide most of the system's radiation; the next brightest, 2 magnitudes fainter, is a B3 star, whereas the faintest two stars contribute little radiation to the system. σ Sco is the simplest of these systems, being the brighter

Table 2. "Average" Ultraviolet Extinction Curve

$\lambda^{-1}(\mu^{-1})$	$E(\lambda-V)/E(B-V)$
3.0	1.9
4.0	4.1
4.6	6.8
5.0	5.6
6.0	4.3
7.0	4.7
8.0	6.0
9.0	8.4

component of a single line spectroscopic binary and having another companion, 7 magnitudes fainter; σ Sco itself is a β CMa star. Though these are complex systems, it seems to us that the composite colors and spectral types taken for these objects represent their ultraviolet flux without error significant for our purposes. In particular, the multiplicity of these objects is not responsible for their peculiar extinction curves. There would seem to be three possible alternatives: the energy distributions of the stars are peculiar; a large amount of flux is scattered into the line of sight by dust grains near the star; the extinction properties of the surrounding medium are abnormal.

The first alternative implies that the extinction suffered by these objects is "normal" and that the observed curves are a consequence of the abnormally large flux radiated by these stars between 2500 and 1100 Å, as compared with normal objects of similar spectral type and color. At $\lambda^{-1} = 4.5$, this additional flux amounts to about $0^m.45$, $0^m.50$, $0^m.75$; at $\lambda^{-1} = 6.0$, $0^m.65$, $0^m.70$ and $0^m.40$; at $\lambda^{-1} = 8.0$, $1^m.0$, $1^m.3$ and $0^m.9$, for ρ Oph, σ Sco and θ Ori, respectively. Now since it is in the ultraviolet that these stars radiate most of their energy, these extra fluxes imply a very large increase in the total energy they emit. Opacity sources for early-type atmospheres would seem to be well understood; it is difficult to see how models based on these sources could successfully predict fluxes in the visual and at the same time be wildly incorrect in the ultraviolet. The contention by Weber et al. (1971) that some unreddened stars are abnormally bright in the ultraviolet should be considered with caution; the relatively low photometric accuracy of their data seems to us to vitiate such a conclusion especially in view of the results on 60 stars presented in Figure 4.

Since all three of these systems are embedded in nebulosity, the possibility exists that associated dust scatters radiation into our line of sight. Such a possibility cannot be ruled out with the data presently available. Simple theoretical calculations of Code (private communication) indicate, however, that under the assumption of spherical geometry and isotropic scattering, grain albedos of nearly one would be required to produce the modifications observed.

The most plausible explanation of these curves seems to us to be that the effect is at least primarily one of anomalous extinction produced by material near the star whose radiation field has modified the grain size distribution and perhaps the composition of the dust. Destruction of the small particles responsible for the far ultraviolet extinction would tend to make the extinction here grey, as is observed. ρ Oph and σ Sco are located in the same association; their extinction curves are similar. In the far ultraviolet they show much the same behavior as $\theta^{1,2}$ Ori, whereas they differ markedly from $\theta^{1,2}$ Ori near the extinction peak. This, along with the anomalous infrared extinction for these three objects, would seem to be more naturally explained by a multi-component model of interstellar grains, such as Gilra (1971) has recently described.

Although the sample of stars is small, we have looked for possible systematic behavior in the variations found in the extinction curves. A convincing systematic effect is that the stars $\theta^{1,2}$ Ori, σ Sco and ρ Oph, all of which have less than normal ultraviolet extinction, also show a large E(V-I)/E(B-V). Apparently, large variations in the ultraviolet extinction are related to variations in the infrared. The characteristics of the extinction bump do not appear to be simply related with infrared extinction. However, one might note that in the two cases where the bump occurs at $\lambda^{-1} = 4.75\ \mu^{-1}$ rather than at $4.6\ \mu^{-1}$, there is also a large far ultraviolet extinction. One possible explanation is that the material responsible for the large far ultraviolet extinction has disturbed the extinction in the region of the bump to such an extent that the bump has been shifted toward shorter wavelengths. If this is the case, however, it is difficult to understand why the star, α Cam, exhibits a "normal" bump and large far ultraviolet extinction. In the data we have presented, there exists a weak inverse correlation between the normalized extinction at the bump and the (B-V) color excess. However, the small sample of stars and the fact that a number of the most highly reddened stars ($\theta^{1,2}$ Ori, ρ Oph and σ Sco) have abnormal ultraviolet and infrared extinction makes this correlation suspect. The position of the far ultraviolet minimum is related to the amount of far ultraviolet extinction in the sense that the

minimum occurs at shorter wavelengths in those cases where the far ultraviolet extinction is smaller.

The extinction curves presented in this paper are not suitable for carrying out a detailed search for possible new diffuse absorptions in the ultraviolet. For many of the curves illustrated in Figures 5a-d there was not a precise spectral match between the two stars which were compared. As a result, many curves contain spurious spikes near the strong stellar ultraviolet lines. However, a reasonably good spectral match was obtained for σ Sco (see Figure 5a). In this case an upper limit to central depths of possible diffuse absorptions as observed with 20 Å and 10 Å slots is found to be approximately 10%. One should compare this upper limit with the observed central depth for the diffuse feature at 4430 Å in σ Sco of 5.7% (Duke 1951). A later paper will be devoted to a much more careful search for possible new diffuse features and for fine structure in the new extinction curves.

The stars studied in this paper are relatively nearby and are therefore unsuitable for investigating any possible dependence of extinction on local galactic structure.

We will not attempt to present a detailed interpretation of the new extinction curves but rather, will review briefly some of the past work to assess its applicability to these results. Much effort has been concerned with attempts to identify the material responsible for the ultraviolet extinction bump and a large number of suggestions have emerged. For example, Stecher (1969), Bless and Savage (1970), Gilra (1971, 1972) and Wickramasinghe and Nandy (1971) believe graphite particles may be responsible for the bump; Huffman and Stapp (1971) attribute the bump to silicates; Manning (1971) suggested quartz, whereas Graham and Duley (1971) indicated that solid hydrocarbons can produce the ultraviolet bump. While it is fair to say that at the present time a conclusive identification of the material responsible for the bump has not been made, the case for graphite seems to be getting stronger. Wickramasinghe and Nandy (1971b) and Gilra (1972) demonstrated that the suggestion of Huffman and Stapp (1971) that silicates are responsible for the 4.6 μ^{-1} feature is unlikely because of the severe size distribution restrictions required to produce a pronounced bump from silicates. A critical review of all the suggestions and a discussion of the physics of extinction bumps is given by Gilra (1972), who concluded that the most likely cause of the extinction bump is plasma oscillations in small (mean radius $\simeq$ 100 Å), nearly spherical, uncoated graphite particles. If the bump is produced by graphite, the particles must be small and nearly spherical in order to produce a relatively narrow bump at the observed position of 4.6 μ^{-1}. As can be seen in the curves of Bless and Savage (1970) and Gilra (1971), large (radius > 200 Å) spherical graphite particles produce

broad bumps which are centered at much longer wavelengths than observed. This is why Bless and Savage (1970) suggested small graphite particles as a possible explanation of the ultraviolet bump. If the graphite particles are small compared to the wavelength, then the position of the bump becomes nearly independent of the details of the size distribution of the particles. This is an important point because most of the observed bumps occur at $\lambda^{-1} = 4.6\ \mu^{-1}$ and it is unreasonable to expect the interstellar particles to have the same size distribution everywhere. Gilra (1972) also points out that the position of the bump is dependent on the particle shape. It was of great interest to us to note that the pronounced ultraviolet extinction bump may not only provide clues on the kind of material producing the extinction but also on the size and shape of the interstellar particles.

There have been various attempts to explain the entire extinction curve. The most complete description is that of Gilra (1971) who attempted to explain all the existing observational data on interstellar grains in terms of a mixture of particles of graphite, silicates, and silicon carbide; these are the three materials Gilman (1969) predicted would form in the atmospheres of cool stars. Gilra was able to reproduce quite well much of the observational data on interstellar grains with his model, but his proposed mixture does contain many variable parameters. The new extinction data presented in this paper strongly suggests that interstellar grains likely have a variety of compositions. The stars σ Sco, β^1 Sco and ξ Per in Figure 5a all have extinction bumps which are quite similar whereas each has a different amount of far ultraviolet extinction. One obvious explanation for this effect is that the constituent responsible for the far ultraviolet extinction is different from that producing the bump. As mentioned earlier, a similar conclusion is reached if one compares the extinction curves for σ Sco and ρ Oph with that for $\theta^{1,2}$ Ori. In this case the far ultraviolet extinction is similar in the three stars while the bump is nearly absent in $\theta^{1,2}$ Ori.

In attempting to interpret these new data one should consider molecules as a possible source of continuous extinction. Stecher and Williams (1969) suggested that photodisassociation of the H_2+ molecule may be partly responsible for the extinction rise in the far ultraviolet. Using the H_2+ photodisassociation cross-sections of Solomon (1964) one finds that for approximately 4.0×10^{17} H_2 + molecules cm^{-2} in the ground vibrational state the extinction at 1150 Å is 3.0 which is about what is observed by OAO in the star ξ Per (see Figure 5a). Furthermore, ξ Per is the star in which Carruthers (1970) detected an H column density of 1.3×10^{20} molecules cm^{-2}. Therefore if 0.3% of the molecular hydrogen in interstellar

clouds is ionized one could understand the rise in far ultraviolet extinction in ξ Per. However, recent radio searches for H_2^+ (Encrenaz and Falgarone 1971; Jefferts et al. 1970) have failed to detect the molecule.

In addition to reducing more data of the kind presented here, future work will be concerned with the behavior of the extinction bump in a large number of stars with a wide range in reddening, in an attempt to better understand this important feature. Also, the OAO filter photometry data will be reduced for extinction purposes. Many of the stars observed photometrically are considerably fainter than those observed spectrophotometrically so that results pertaining to a larger volume of space will become available.

We would like to thank Dr. A. D. Code and Mr. D. P. Gilra for helpful discussions. This work was supported by the National Space and Aeronautics Administration through NAS 5-1348.

REFERENCES

Bless, R. C. and Savage, B. D. 1970, I.A.U. Symp. No. 36, p. 28.
Boyarchuk, A. A. and Kopylov, I. M. 1964, Isz. Krym. Astron. Obs. 31, 44.
Carruthers, G. R. 1969, Ap. and Space Sci. 5, 387.
_____ 1970, Ap. J. (Letters) 161, L81.
Code, A. D. and Bless, R. C. 1970, I.A.U.Symp. No. 36, p. 173.
Code, A. D., Houck, T. E., McNall, J. F., Bless, R. C. and Lillie, C. F. 1970, Ap. J. 161, 377.
Collins, G. W., II 1965, Ap. J. 142, 265.
Cousins, A. W. J. and Stoy, R. H. 1963, Bull. Roy. Obs., No.64.
Encrenaz, P. J. and Falgarone, E. 1971, Ap. Letters 8, 187.
Gilman, R. C. 1969, Ap. J. (Letters), 155, L185.
Gilra, D. P. 1971, Nature 229, 237.
_____ 1972, in preparation.
Graham, W. R. M. and Duley, W. W. 1971, Nature 232, 43.
Hardorp, J. and Strittmatter, P. A. 1968, Ap. J. 151, 1057.
Hiltner, W. A., Garrison, R. F. and Schild, R. E. 1969, Ap. J. 157, 313.
Huffman, D. R. and Stapp, J. L. 1971, Nature 229, 45.
Iriarte, B., Johnson, H. L, Mitchell, R. I. and Wisniewski, W. K. 1965, Sky and Tel. 30, 21.
Jefferts, K. B., Penzias, A. A., Ball, J. A., Dickinson, D. F. and Lilley, A. E. 1970, Ap. J. (Letters), 159, L15.
Johnson, H. L. 1963, Basic Astronomical Data, Ed. K. Aa.Strand (Chicago: University of Chicago Press), p. 204.
_____ 1966, Comm. Lunar and Planet. Lab. 4, 99.

_____ 1968, Nebulae and Interstellar Matter, Ed. B. M. Middlehurst and L. H. Aller, p. 167.
Lesh, J. R. 1968, Ap. J. Suppl. 17, 371.
Manning, P. G. 1971, Nature 229, 115.
Mihalas, D. 1970, Ap. and Space Sci. 8, 50.
Solomon, P. M. 1964, Ph. D. Thesis, University of Wisconsin.
Stecher, T. P. 1969, Ap. J. (Letters), 157, L125.
Stecher, T. P. and Williams, D. A. 1969, Ap. Letters 4, 99.
Weber, S. V., Henry, R. C. and Carruthers, G. R. 1971, Ap. J. 166, 543.
Wickramasinghe, N. C. and Nandy, K. 1971a, Nature, 229, 81.
_____ 1971b, Nature 230, 16.

DIFFUSE GALACTIC LIGHT

IN THE 1500-4200 ANGSTROM REGION

Adolf N. Witt
The University of Toledo
Toledo, Ohio

Charles F. Lillie
The University of Colorado
Boulder, Colorado

ABSTRACT

Diffuse galactic light has been observed with the four stellar photometers of the OAO-2 in 29 of Kapteyn's selected areas. The data can be understood in terms of a wavelength dependent albedo of the interstellar grains with a pronounced minimum around 2200 Å with a rapid increase towards unity at wavelengths below 2000 Å.

I. INTRODUCTION

The properties of the interstellar particles must be deduced from observational material on their extinction, scattering and polarization of starlight. Uncertainties arise in the interpretation of this data because the observations are not perfectly accurate and because several theoretical models may fit the data.

The success of OAO-2 has made it possible to obtain extensive observations of interstellar extinction and the diffusely scattered galactic radiation in the 1000-4000 Å spectral region. The extinction curve for this region is well-established from rocket and OAO observations (Stecher 1965, Bless and Savage 1972). Since extinction is the sum of scattering and absorption, a measurement of the albedo of the interstellar dust and its change with wavelength permits us to determine the wavelength dependence of the particles' scattering efficiency and absorption efficiency separately. Such information aids significantly in studies of the nature of interstellar

dust grains, their temperatures and the related infrared radiation and in the calculation of the interstellar radiation field.

In this paper we present the results of a program to extend measurements of the diffuse galactic light (DGL) into the ultraviolet using the stellar photometers in the Wisconsin Experiment Package (WEP) on OAO-2. Our approach was to measure the surface brightness of the sky background in Kapteyn's selected areas for which detailed star counts are available. After removing the contributions due to zodiacal light and direct starlight, we find a residual which we identify as diffuse galactic light. We computed the ratio of DGL to direct starlight and compared it with models to find the albedo and asymmetry factor of the interstellar particles. Combining extinction data with our albedo determinations, we then calculate scattering and absorption efficiencies for the interstellar grains.

II. THE OBSERVATIONAL MATERIAL

The instrumentation and operation of the Wisconsin experiment has been described in detail by Code et al. (1970). For this investigation we used the four stellar photometers with the 10-arc-minute diameter field of view to measure the surface brightness of the night sky in 29 of Kapteyn's Selected Areas at twelve wavelengths between 1050 and 4200 Å. In most cases, we centered the central star in the field of view.

A typical observing sequence consisted of eleven measurements with each photometer: two dark readings, a calibration reading and eight readings (3-2-3) with the three medium band filters. It required 24 to 32 minutes to complete, depending on the integration times used.

The reduction of these observations was complicated by a time dependent dark current induced by charged particles trapped in the earth's radiation belts. The dark current was typically 50% of the total signal and care had to be exercised in removing it.

The data reduction procedure consisted of first plotting the dark current readings as a function of time and then interpolating to find the proper correction for each measurement. For stellar photometers 3 and 4 an additional correction was necessary to account for the signal induced by beta-particles from the Cerenkov radiation source used for calibration and for fluorescence in the calcium-fluoride substrate of some filters.

After finding the net digital counts from the sky background in this manner, we then removed the signal attributable to zodiacal light on the basis of a separate study by Lillie (1972). The data were then converted to units of AOV stars of magnitude

$V = 10^{m}.0$ per square degree using stellar observations with the same instruments.

III. CORRECTIONS FOR STARLIGHT

The choice of selected areas as regions to be observed was inspired by the fact that detailed starcounts are available for these areas. In this way we were able to determine relatively reliable corrections for the integrated starlight included in the diaphragms of the photometers. The principal difficulty in using the photographic magnitudes of the starcount data was found to be in the uncertainty of the magnitudes in some of the brighter stars contained in our fields. Consequently, we used a 16-inch telescope at the Kitt Peak National Observatory to determine photoelectric magnitudes and colors in the UBV system for those stars brighter than 11th magnitude which we were able to reach from that location. These measurements were also used to establish a transformation relation between the photographic and the photoelectric B magnitudes, allowing us to eliminate at least systematic effects from the magnitudes of those southern stars which we were not able to observe directly from Kitt Peak.

The integrated light of the fainter stars was determined from the Harvard-Groningen Durchmusterung of Selected Areas and the Mount Wilson Catalogue of Photographic Magnitudes in Selected Areas 1 - 139.

After the total starlight correction in one wavelength bandpass is secured, one faces the additional problem of determining the corresponding starlight correction in the observed ultraviolet wavelength bandpasses where no starcounts are available. This was solved in a two-fold way. The brighter stars, for which colors are available, were transformed individually using photometric data from the OAO for stars of similar spectral characteristics as a guideline. The fainter stars were dealt with collectively, using for transformation the predictions made with the help of a photometric Milky Way model, which was used previously by Witt (1968) and Lillie and Witt (1969). This model utilizes a distribution of stars and interstellar dust in an idealized galaxy, which produces integrated starlight with properties very similar to those derived from actual starcounts in our galaxy. By the use of transformations of the luminosity function into bandpasses of shorter wavelengths, based on OAO photometry, and by appropriate scaling of the interstellar extinction detailed information concerning the integrated star background in the ultraviolet can be generated.

IV. ANALYSIS OF RESIDUAL BACKGROUND RADIATION

The residual obtained after subtracting the corrections for zodiacal light and integrated star background from the measured surface brightness was interpreted as diffuse galactic light (DGL). DGL is assumed to be due to starlight scattered in interstellar space by dust grains. Figure 1 shows the resulting DGL intensity at 4250 Å, plotted against galactic latitude. We have performed sliding averages over three consecutive points in order to demonstrate more clearly the concentration towards the galactic plane. Only part of the scatter is due to uncertainties; largely it reflects the real variation of DGL intensity with galactic longitude. The results at the other OAO bandpasses are very similar.

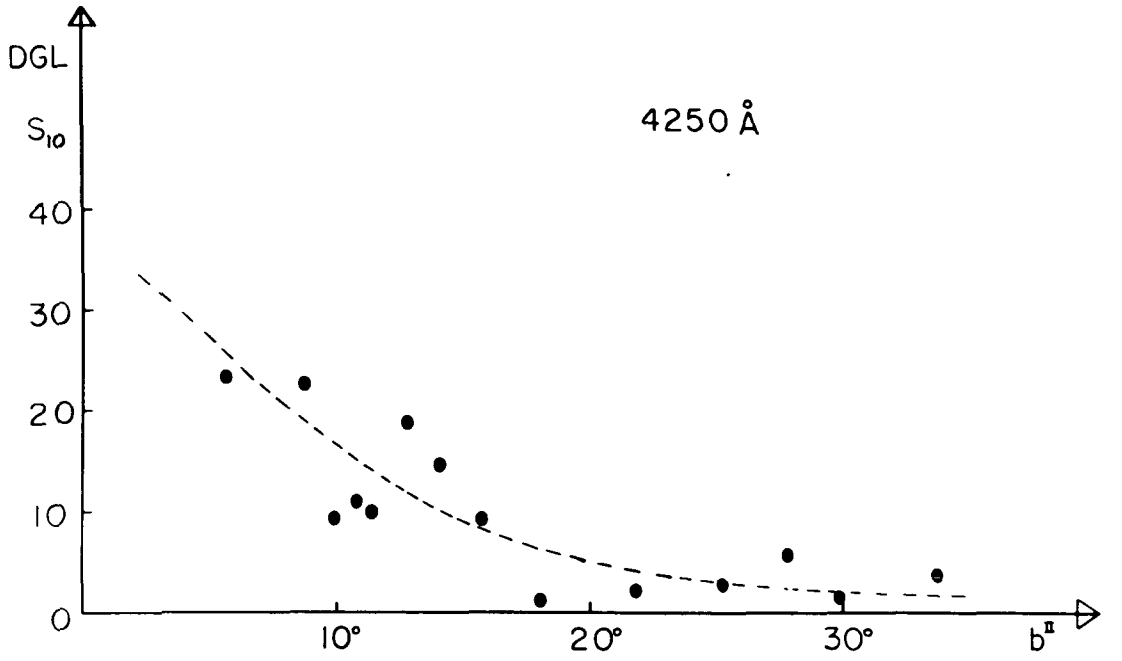

Figure 1.—Residual background radiation as a function of galactic latitude.

For the interpretation of these measurements we used the recent models for the radiative transfer of DGL including multiple scattering which were calculated by van de Hulst and de Jong (1969). From their tables we calculated the ratio of DGL to line-of-sight starlight as a function of galactic latitude, using the albedo, a, of the dust grains and the asymmetry factor, g, of the scattering phase function as free parameters,

to be determined by comparison of the model with the observational data. The line-of-sight starlight for the observed selected areas was obtained by integration of the starcounts in Groningen Publication No. 43. The optical thickness of the galactic layer was taken to be 0.3 at 4250 Å and was assumed to reach 0.4 at 2000 Å.

Ratios of measured DGL to line-of-sight starlight were formed for all observed areas and a best fit was found out of the series of model predictions for each wavelength bandpass. Thus, combinations of a and g were found.

V. RESULTS

Figure 2 shows the albedo, a, as a function of wavelength between 4250 and 1500 Å. The outstanding features are the pronounced decrease in albedo around 2200 Å, which is coincident in wavelength with the "hump" observed in the interstellar extinction curve and the sharp rise of albedo at wavelengths shorter than 2000 Å. The vertical error bars are estimates based on combined uncertainties in the observations and the radiative transfer model; the horizontal error bars reflect the finite width of the filters. The measured points are plotted at the position of the effective wavelength of the filters. Note at this point the striking similarity between

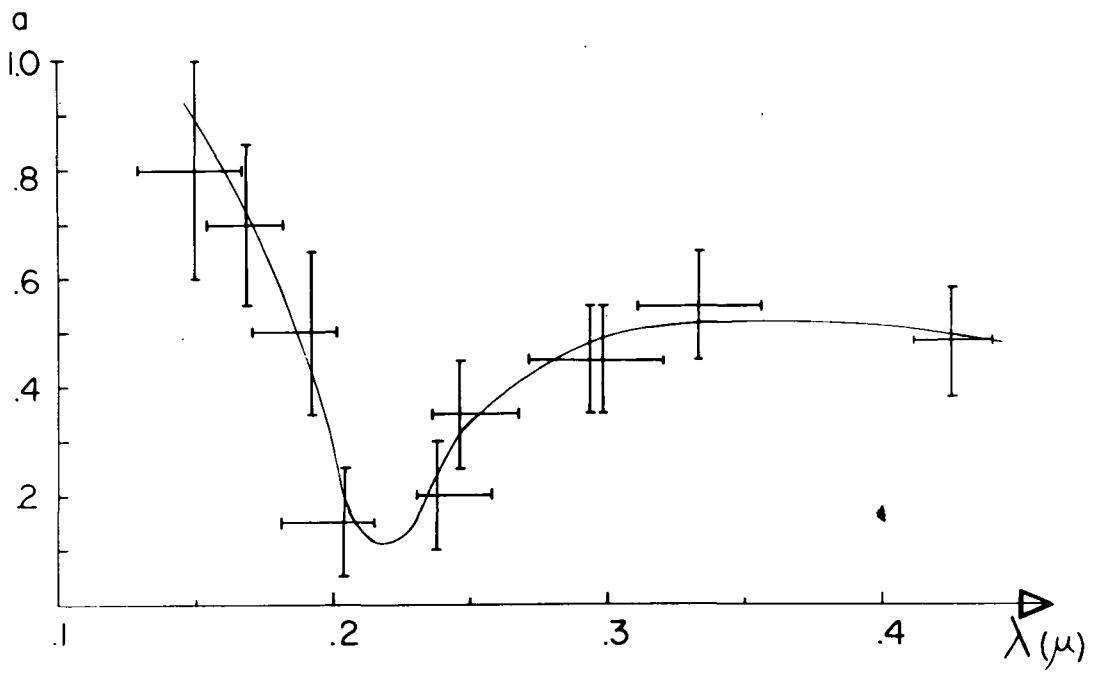

Figure 2.—Albedo of the interstellar particles as a function of wavelength.

the albedo variation of interstellar grains and the curves of the wavelength dependence of the zodiacal light brightness found by Lillie.

One may now attempt to use the results shown in Figure 2 in combination with the interstellar extinction in the ultraviolet, as determined by Bless and Savage, to derive separately the efficiencies for scattering and absorption for the interstellar grains. This becomes possible since extinction is the sum of scattering and absorption and albedo is the ratio of scattering to extinction efficiency. Figure 3 shows the result of such calculations based on the observed wavelength dependence of albedo and extinction. It shows clearly the pure absorption nature of the "hump" in the extinction curve. The low albedo around 2200 Å is caused by this strongly increased absorption efficiency rather than a drastically decreased scattering efficiency. The renewed rise of the extinction curve below 2000 Å seems to be caused by a process of pure scattering.

Care should be applied when comparisons are attempted between theoretical models and our albedo curve or the scattering and absorption efficiency shown in Figure 3. The convolution of the DGL spectrum with the finite filter widths has to be taken into account.

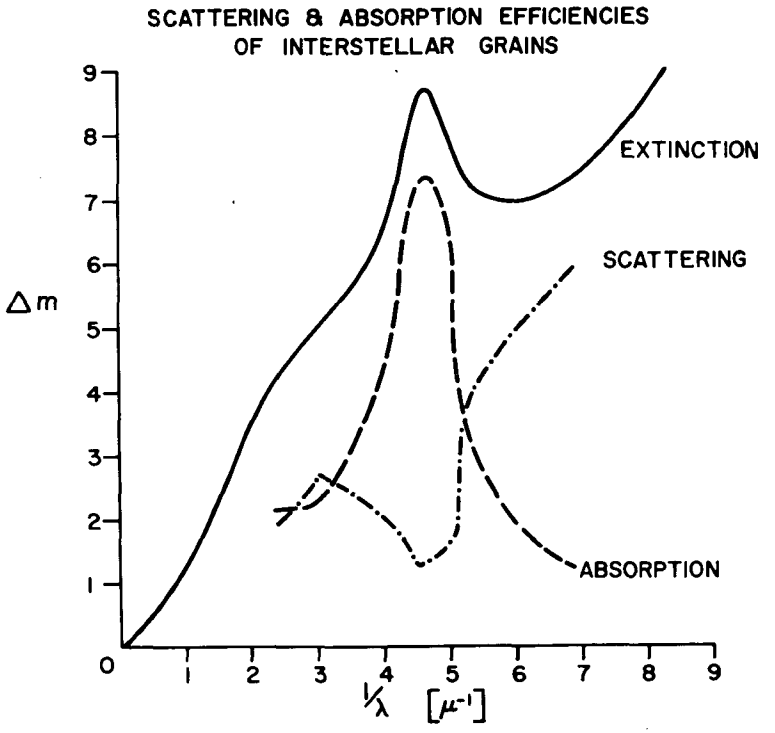

Figure 3.—Wavelength dependence of scattering and absorption efficiencies of interstellar grains. Heavy curve is the extinction curve of Bless and Savage.

The asymmetry factor, g, of the scattering phase function of the interstellar grains may be estimated from the variation of the ratio of DGL to line-of-sight starlight with galactic latitude. The observed ratios for all bandpasses above 1900 Å decrease significantly with increasing galactic latitude, thus indicating a strongly forward scattering phase function, with g = 0.75 representing the average estimate. At 1680 Å and 1500 Å, the DGL appears much less concentrated towards the Milky Way, suggesting a tendency for the phase function towards isotropy.

We feel that this result together with the rapidly increasing albedo in the same part of the spectrum may be indicative that either a new particle component becomes important for wavelengths below 2000 Å or that a new scattering process becomes active in this region.

REFERENCES

Bless, R. C. and Savage, B. D. 1972, this volume.
Hulst, H. C., van de and de Jong, T. 1969, Physica 41, *151.*
Lillie, C. F. and Witt, A. N. 1969, Astroph. Letters 3, *210.*
Lillie, C. F. 1972, this volume.
Stecher, T. P. 1965, Ap. J. 142, *1683.*
Witt, A. N. 1968, Ap. J. 152, *59.*

Page intentionally left blank

THE ULTRAVIOLET SPECTRUM OF THE CRAB NEBULA

Hugh M. Johnson
Lockheed Missiles and Space Company
Palo Alto, California

I. INTRODUCTION

Before the OAO-2 no observations of the Crab Nebula were available between 3210 Å from ground-based photoelectric observations (O'Dell 1962) and one-quarter keV in the soft X-ray region (Fritz et al. 1971; Coleman et al. 1971). This paper reports new observations made under the OAO-2/NASA guest investigator program with the WEP "stellar" photometers described by Code et al. (1970). The 10'-diameter focal-plane diaphragm is ample to accept the 4' × 6' image of the Crab. Figure 1 shows the data of the Crab as processed by the principal investigators of WEP. It gives the logarithm of the integrated relative intensity per wavelength interval, corrected for sky background, and the rms error, from 11 passbands in the range 4250-1380 Å. No correction has been made for polarization of the light. The data are converted to logarithm of the flux density per frequency interval, F_ν, and plotted on scales of log ν (Hz) and of reciprocal microns (μ^{-1}) in Figure 2, with two adjustments. First, the OAO-2 data are normalized to O'Dell's (1962) data in the range 3210-4280 Å, and all of the data including O'Dell's are corrected for interstellar extinction.

II. INTERSTELLAR EXTINCTION AND THE CRAB SPECTRUM

The total extinction at wavelength λ is

$$A_V + E(\lambda-V) = A_V + E(\lambda-V)/E(B-V) \times A_V/R \qquad (1)$$

where A_V is total extinction in the V passband, $R = A_V/E(B-V)$ is its ratio to color excess $E(B-V)$, and $E(\lambda-V)/E(B-V)$ is the ratio of the color excesses at λ and at the B passband. Then $0.4[A_V + E(\lambda-V)]$ is the correction for extinction to the loga-

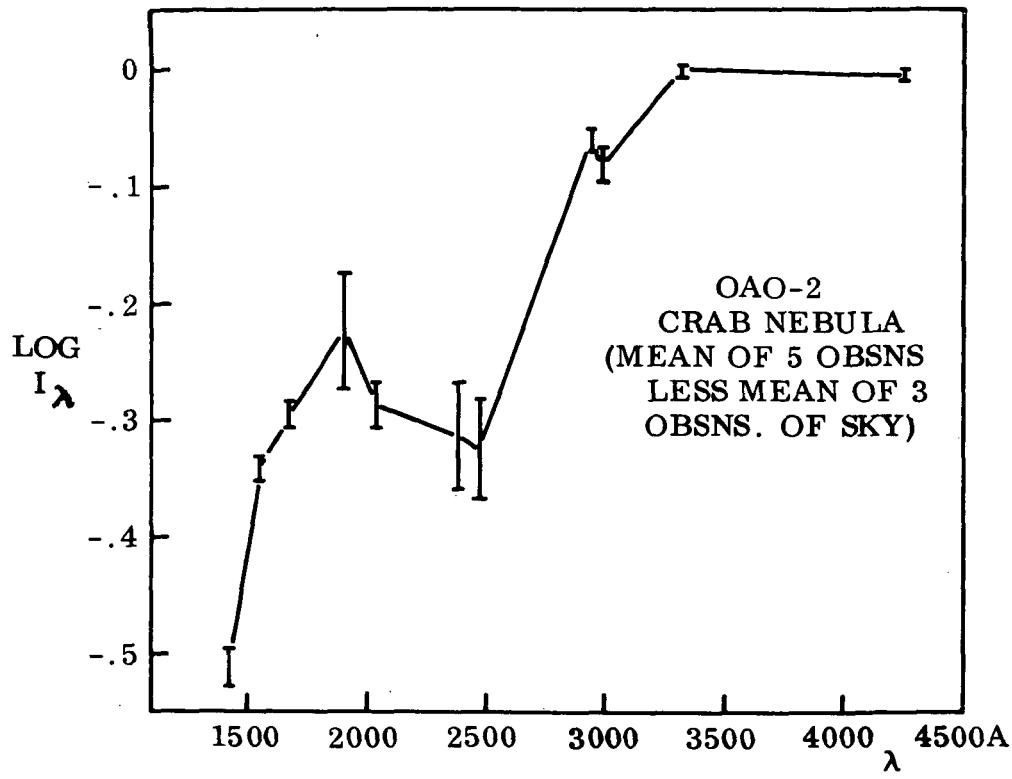

Figure 1.—OAO-2/WEP photometer observations of the Crab Nebula.

rithm of observed intensity. We proceed first with estimates of A_V and R made independently of the OAO-2, and with the OAO-2 observations of $E(\lambda-V)/E(B-V)$ made independently of the Crab by Bless and Savage (1972). Minkowski (1968) estimates A_V = 1.9 mag for the Crab, and Johnson (1968) estimates R = 6 approximately in the direction of the Crab. These values are used in equation (1) for Figure 2. Unfortunately for making corrections to the observed spectrum of the Crab, $E(\lambda-V)/E(B-V)$ is not uniform in the Galaxy and we do not know the preferred function in the line of sight to the Crab. The "average" curve and the "θ Ori" curve of $E(\lambda-V)/E(B-V)$ are both used in Figure 2. Table 1 lists some of the relevant data. Although O'Dell's (1962) optical data are only slightly differently corrected according to the two extinction curves, the OAO-2 data fall into two quite distinct branches according to choice of $E(\lambda-V)/E(B-V)$, keeping A_V = 1.9 mag and R = 6. Both branches are steeper than the spectrum $F_\nu \propto \nu^{-1.0 \pm 0.1}$ which Peterson and Jacobson (1970) have found to hold over the range of 1 - 500 keV in the Crab. The extrapolation of this X-ray spectrum is shown for comparison in Figure 2. The uncertainty in

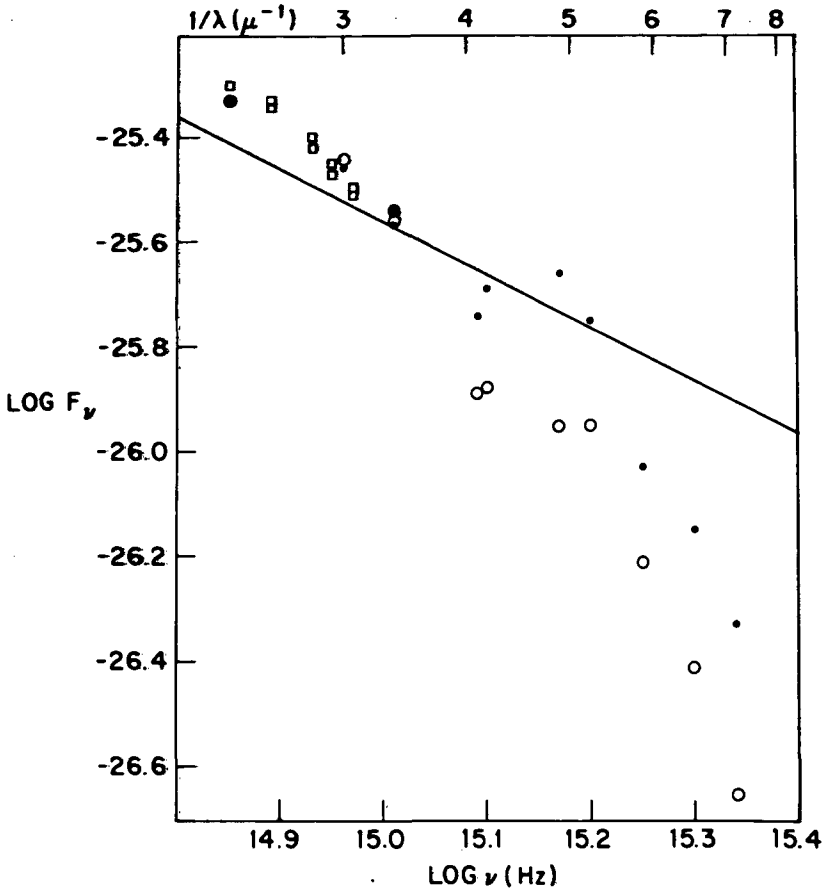

Figure 2.—The solid and open circles are the data of Figure 1 in transformed coordinates and corrected for extinction according to Bless and Savage's (1972) "average" and "θ Ori" curves, respectively. They are normalized to O'Dell's (1962) data (squares). The straight line is an extrapolation of Peterson and Jacobson's (1970) X-ray spectrum of the Crab Nebula, starting at the frequency of 1 keV = 2.42×10^{17} Hz and the flux density of 17.2 photons $cm^{-2}sec^{-1}keV^{-1} = 1.14 \times 10^{-28}$ W $m^{-2}Hz^{-1}$, with the power-law spectral index = -1.

log F_ν corresponding to the uncertainty of ±0.1 in the exponent on ν is about ±0.34 at log ν = 14.97 since the latter differs from log ν (10 keV) by 3.4. It is the observed and corrected slope $dF_\nu/d\nu$ which is significant in a comparison with the extrapolated X-ray spectrum rather than the level of observed and corrected F_ν. The "average" branch also shows an apparent emission hump around $1/\lambda = 4.6\mu^{-1}$, and the "θ Ori"

Table 1. Data of the Crab Nebula for Figures 1 and 2.
F_ν Normalized to O'Dell's (1962) Optical Data.

WEP Photometer Filter	Effective log ν	Relative log I_λ	Relative log I_ν	Average extinction $\frac{E(\lambda-V)}{E(B-V)}$	Average extinction log F_ν ($Wm^{-2}Hz^{-1}$)	θ Ori extinction $\frac{E(\lambda-V)}{E(B-V)}$	θ Ori extinction log F_ν ($Wm^{-2}Hz^{-1}$)
S1F3	14.85	0.00	+0.22	1.14	-25.33	1.14	-25.33
1	14.96	0.00	0.00	1.85	-25.46	1.96	-25.44
4	15.01	-0.08	-0.17	2.31	-25.57	2.34	-25.56
S2F2	15.01	-0.06	-0.16	2.45	-25.54	2.45	-25.54
5	15.10	-0.31	-0.60	4.75	-25.69	3.23	-25.88
1	15.17	-0.29	-0.71	5.85	-25.66	3.54	-25.95
S3F2	15.09	-0.33	-0.59	4.24	-25.74	3.11	-25.89
1	15.20	-0.22	-0.69	4.96	-25.75	3.36	-25.95
5	15.25	-0.30	-0.89	4.32	-26.03	2.89	-26.21
S4F1	15.30	-0.34	-1.03	4.48	-26.15	2.47	-26.41
3	15.34	-0.51	-1.27	4.97	-26.33	2.44	-26.65

branch is inflected in the same vicinity. The emission hump may simply reflect the shape of the extinction curves. All of the curves plotted by Bless and Savage (1972) show an absorption maximum near $1/\lambda = 4.6\mu^{-1}$, but the curve for θ Ori shows it least markedly. If average extinction were overestimated, a false emission hump would appear on a smooth spectrum, while θ Ori-type extinction might not show it.

It may appear simple to select a curve of $E(\lambda-V)/E(B-V)$ and vary the parameters A_V and R until the corrected spectrum is smooth and agrees in slope with the extrapolated X-ray spectrum; it is not known, incidentally, whether R is independent of the shape of $E(\lambda-V)/E(B-V)$. The observed flux densities of the Crab at, say, the extremities $\log \nu = 14.85$ and $\log \nu = 15.34$ differ logarithmically by 1.49, while the extrapolation of the X-ray flux density changes logarithmically by 0.49 in the same interval. Therefore we want to correct the observed spectrum by about 1.00 in $\log F(\log \nu = 14.85) - \log F(\log \nu = 15.34)$ in order to match the slope of the X-ray spectrum. When the values of the average curve of $E(\lambda-V)/E(B-V)$ at these frequencies are used, we find $E(B-V) = 0.65$ and $A_V = 2.0$ mag ($R = 3$) or $A_V = 3.9$ mag ($R = 6$). Similarly for the θ Ori curve of $E(\lambda-V)/E(B-V)$, $E(B-V) = 1.92$ and $A_V = 5.8$ mag ($R = 3$) or $A_V = 11.5$ mag ($R = 6$). Thus it appears that the observed spectrum would be corrected very nearly to the slope of the X-ray spectrum by using Minkowski's (1968) $A_V = 1.9$ mag, but with $R = 3$ rather than $R = 6$ as in Figure 2. Any use of the θ Ori curve of $E(\lambda-V)/E(B-V)$ appears to require excessive visual extinction in order to match the slope of the X-ray spectrum. However, if the average extinction curve is indeed used with $A_V = 1.9$ mag and $R = 3$, the emission hump becomes even stronger than it appears in Figure 2, and the data of the three highest frequencies break into a steep slope. The conclusion is that the OAO-2 data of the Crab cannot simultaneously match the slope of the X-ray spectrum and remain smooth. It is, of course, possible that a recalibration of the WEP photometer efficiencies would alter the conclusion. It is unlikely that a least-squares solution of all of the observed data of the Crab, rather than the present use of the data of the two extreme frequencies, would alter the conclusion.

III. QUESTIONS ABOUT THE CRAB FILAMENTARY NEBULA

There is, of course, no reason to match the observations with the simple extrapolation of the X-ray spectrum of the Crab, except the simplicity of it. Also, the pulsar spectrum or the filamentary spectrum might rise to be a significant contribution in the ultraviolet. The following nebular emissions are predicted (Osterbrock 1963) in the filamentary spec-

trum near the $1/\lambda = 4.6\ \mu^{-1}$ peak: recaptures by He^+ (2^3S series limit at 2600 Å), recaptures by He^{2+} ($n = 3$ series limit at 2051 Å), and the 2-photon continuum with a maximum at 2431 Å. The $n = 3$ series limit of He^{2+} is interesting because the first line of the series, He II 4686, is unaccountably strong in the filament spectrum according to Davidson and Tucker (1970). There are no good candidate line emissions, and one such line would not explain the $1/\lambda = 4.6\ \mu^{-1}$ peak which appears in four separate passbands. We may only conclude, in the absence of a quantitative evaluation, that the filamentary continua may be significantly necessary because of the rather positive conclusion against a featureless continuum in the previous section.

Woltjer (1958) assumed an ultraviolet continuum of the amorphous component to explain the observed excitation conditions in the filaments of the Crab in terms of photoionization and heating. Davidson and Tucker (1970) have specified four alternative models of the high-frequency continuum to investigate these effects on the filaments. The OAO-2 data do not make obvious a choice of any one model, because the power-law spectral index in the observed range of frequencies can be, according to the different extinction curves, either -1.2 or -2 as in the models. This conclusion ignores the $1/\lambda = 4.6\ \mu^{-1}$ hump and the probable curvature of any of the corrected spectra. The theoretical models of Davidson and Tucker do not, in turn, tell how to correct the observed Crab spectrum for extinction because they are ambiguously capable of explaining most of the line spectrum of the Crab filaments, except the high intensity of He II 4686.

This work has been done under NASA contract NASW-1977 for the OAO-2 guest observer program. Many people at NASA Headquarters and in the University of Wisconsin contributed to the result.

REFERENCES

Bless, R. C. and Savage, B. D. 1972, private communication and this volume.

Code, A. D., Houck, T. E., McNall, J. F., Bless, R. C. and Lillie, C. F. 1970, Ap. J. 161, 377.

Coleman, P. L., Bunner, A. N., Kraushaar, W. L. and McCammon, D. 1971, private communication.

Davidson, K. and Tucker, W. 1970, Ap. J. 161, 437.

Fritz, G., Meekins, J. F., Chubb, T. A., Friedman, H. and Henry, R. C. 1971, Ap. J. (Letters) 164, L55.

Johnson, H. L. 1968, in Nebulae and Interstellar Matter, ed. B. M. Middlehurst and L. H. Aller (Chicago: University of

Chicago Press), p. 167.
Minkowski, R. 1968, in Nebulae and Interstellar Matter, ed. B. M. Middlehurst and L. H. Aller (Chicago: University of Chicago Press), p. 623.
O'Dell, C. R. 1962, Ap. J. 136, 809.
Osterbrock, D. E. 1963, Planet Space Sci. 11, 621.
Peterson, L. E. and Jacobson, A. S. 1970, Pub. A. S. P. 82, 412.
Woltjer, L. 1958, B. A. N. 14, 39.

Page intentionally left blank

ULTRAVIOLET PHOTOMETRY OF THE ECLIPSING VARIABLE CW CEPHEI

Stanley Sobieski
National Aeronautics and Space Administration
Goddard Space Flight Center
Greenbelt, Maryland

ABSTRACT

An extended series of photometric observations were made of the eclipsing variable CW Cephei using the Wisconsin instrument on OAO-2. Approximate elements which were derived based solely on the eclipse depths and shape of the secondary are in satisfactory agreement with those found using ground-based observations. However, persistent asymmetries and anomalous light variations, all larger than the expected experimental error, were also found; subsequent ground-based observations show H_α entirely in emission indicating the presence of an extended gaseous system surrounding one or both of the components. Consistent solutions utilizing all data at all wavelengths were not found.

In addition to the light curve analysis, a detailed comparison was made of the flux distribution of the binary relative to that for the nominally unreddened stars δ Pic B1 III and η Aur B3 V to investigate the effects of interstellar extinction. The observations for these comparison stars were obtained near to the time of the binary observations, thereby minimizing spurious results due to instrumental changes. The resultant extinction curves, normalized at 3330 Å, show a relatively smooth increase with decreasing wavelength; no conspicuous hump near 2200 Å is evident. Additionally assuming E(B-V) = 0.68 a smaller amplitude for the curves is found than that for the Perseus region given by Stecher.

I. INTRODUCTION

Starting in mid-April, 1971 the OAO-2 spacecraft began to be stable for extended observing periods while pointed toward the region around Cepheus, and it became feasible to obtain complete ultraviolet light curves of the eclipsing binary CW Cephei. Petrie's (1947) observations of CW Cephei show it to be a double line spectroscopic binary consisting of two early B stars of nearly equal mass but with a differential spectroscopic luminosity $\Delta m = 0.30 \pm 0.03$. It is designated as No. 69 (bright) by Blaauw, Hiltner and Johnson (1959) in their photometric study of the Cep OB 3 association. They list for it B-V = 0.41 and U-B = -0.52; the application of the Q-method results in unreddened colors of $(B-V)_o = -0.27$, $(U-V)_o = -1.04$, and hence a color excess E(B-V) = 0.68. Its revised MK classification is B1.5 Vn according to Garrison (1970), while the intermediate band and β index photometry of Crawford and Barnes (1970) and that of McNamara (1966) leads to a somewhat earlier classification. These later classifications and that based on the earlier photometry are in substantial agreement. Membership in the association appears certain, based on the binary's location in the color-magnitude plane after corrections are made for interstellar absorption using R = 3.0. By implication then, one can expect that the binary is young, i.e. of the order of the expansion age of the association, which is given by de Vegt (1966) to be approximately 1.6×10^6 years. Abrami and Cester (1960) obtained approximate orbital solutions from two color photoelectric light curves. They found that primary eclipse is a partial transit and they confirmed that the components, though quite similar in surface brightness, are distinctly different in size. A complete rediscussion of this system is being prepared by Il-Seong Nha (1971) based on his new multi-color photoelectric observations. Of some interest is his report of finding rapid apsidal motion.

II. DATA REDUCTION

The present observations were made with the four photometers in the University of Wisconsin instrumentation on OAO-2. A total of 49 data points, each being the mean of six separate measurements of the binary, were obtained over 29 orbits. Dark and calibration readings were obtained at least once per orbit for each photometer. In addition, 6 orbits were dedicated to sky measurements distributed over the nine days of observing. The majority of the orbits between #12280 and #12411 were used for this program. The 10 arc-min field aperture was decentered from the nominal position of the binary by 25 arc min in order to avoid photometric contamination by

a nearby fainter B star; sky readings were taken 30 arc min north of this nominal pointing. No attempt was made to obtain data with the shortest wavelength filter and all data from the longest wavelength filter were rejected due to contamination by the unavoidable inclusion of a faint late-type star in the aperture. The other short wavelength data appear to be free of this contamination since the eclipse depths appear to be normal. All data were reduced in the manner suggested by Code (1970). The flux measured through filter "i" with photometer "j" relative to that at λ_{eff} = 3330 Å is given by

$$\log \frac{F_i}{F_{3330}} = \log \left(\frac{(\text{Star}_i - \text{Dark}_j) - (\text{Sky}_i - \text{Dark}_j)}{\text{Calibration}_j - \text{Dark}_j} \right) - \log \left(\frac{(\text{Star}_1 - \text{Dark}_1) - (\text{Sky}_1 - \text{Dark}_1)}{\text{Calibration}_1 - \text{Dark}_1} \right) + \log \Delta_i$$

The correction factors Δ_i are those suggested by Code but as amended by Holm (1971) to allow for the declining sensitivity of photometer #4. Linear interpolation between dark measures gave the dark appropriate at the time of the star or sky measurement. The means for all calibration measurements obtained during the experiment were used to normalize the data from each photometer. Heliocentric orbital phases corresponding to the mean GMT of each observation were computed using Nha's (1971) ephemeris, kindly supplied prior to publication,

$$\text{JD} = 2435373.4487 + 2^{d}.72919396E \pm 0^{d}.0256 \sin (0.07018E - 31^{\circ}.55)$$

where E = 2083 for the observed primary minimum. Approximate times of minima were determined graphically from the data, and they are in excellent agreement with this ephemeris. The observed epochs for primary and secondary eclipses are JD 2441058.270 and JD 2441054.128, respectively.

III. INTERSTELLAR EXTINCTION

In order to investigate the ultraviolet extinction of CW Cep, relative fluxes were found first by forming the means of data taken on April 10 and April 15, 1971 when the system was at maximum light. The approximate effective wavelengths corresponding to each flux measurement, the data for CW Cep expressed in magnitudes, and similar data for two nominally unreddened stars are presented in the first four columns of Table 1. The original data for the two comparison stars were very kindly supplied by the University of Wisconsin, and they were reduced in the same manner as is described above. The stars η Aur, B3 V, and δ Pic, B1.5, were selected to match,

Table 1. Observational Data

Relative Flux (mag)				Extinction			
λ (1)	CW Cep (2)	δPic (3)	ηAur (4)	CW-δPic (5)	CW-ηAur (6)	Bless, Savage (7)	Stecher (8)
3330	0.00	0.00	0.00	0.00	0.00	0.00	0.00
2980	-0.03	-0.46	-0.36	0.63	0.49	0.65	0.8
2940	0.06	-0.12	-0.34	0.26	0.59	0.85	1.0
2460	0.43	-1.16	-0.80	2.34	1.81	2.34	3.0
2380	0.59	-0.96	-1.04	2.27	2.39	2.90	3.4
2040	0.40	-1.26	-1.47	2.44	2.75	4.00	5.5
1920	0.14	-1.93	-1.55	3.05	2.48	3.32	5.2
1680	-0.02	-2.14	-1.68	3.11	2.44	2.48	3.8
1500	-0.83	-2.60	-2.19	2.59	2.00	2.58	4.3
1380	-1.29	-2.75	-2.19	2.14	1.32	3.07	5.2

respectively, the original and the more recent spectral classifications of CW Cep. Just as important, these observations were obtained at approximately contemporaneous epochs, thus minimizing any effects of instrumental variation. The extinction law is defined here as the difference in magnitude at each effective wavelength between the binary and comparison star, normalized to unity color excess. It differs somewhat from the usual representation in that Δ_m is set equal to zero, arbitrarily, at λ = 3330 Å. The differential magnitudes thus formed are listed separately in columns 5 and 6 of Table 1 while the "average" extinction curve found by Bless and Savage (1972) from OAO-2 observations and that found for the Perseus region by Stecher (1969) are given in the last two columns. The data and the two reference extinction curves are shown in Figure 1. It is immediately evident by intercomparing these curves that the shape of the extinction curve for CW Cep differs markedly from that appropriate to the Perseus region. It is also seen that the average extinction fits the observed data only poorly. Most conspicuous is the apparent absence of the $4.6\mu^{-1}$ bump and the turning-down of the curve at the shortest wavelengths. The overall shape resembles that found by Bless and Savage for $\theta^1 + \theta^2$ Ori except that the amplitude, i.e. relative absorption, is greater for CW Cep in the mid-ultraviolet range. No definite explanation can be offered for the unusual shape of this extinction curve. The fact that the photometric colors are consistent with the spectral type, and that the resultant position of the binary in the color-magnitude diagram of the association appears reasonable after the visible wavelength data are corrected for reddening and absorption with the usual relations, suggests that the absorbing medium is normal, at least in regard to its properties at visible wavelengths. In support of this view, spectra of CW Cep, obtained with the GSFC Cassegrain spectrograph and 36-inch telescope, show moderately strong 4430 Å absorption; the estimated equivalent width of 2-3 Å appears consistent with the E(B-V) = 0.68. On the other hand these same spectra show H_α entirely in emission confirming the report of Wackerling (1970). Its strength appears to vary from approximately 3 to 5 Å as a function of the orbital phase. With this evidence for the presence of an extended gaseous system about one or both components one can speculate that the intrinsic flux distribution is abnormal in the sense that overlying Balmer emission could be modifying the observed ultraviolet flux distribution in a way similar to that found for Be stars. However, the net effect of this would be to exaggerate the apparent absorption at the shortest wavelengths where the Balmer emission would be the weakest which, of course, is contrary to what is observed. Furthermore, this emission as opposed to strategically located line emission cannot explain the absence of the

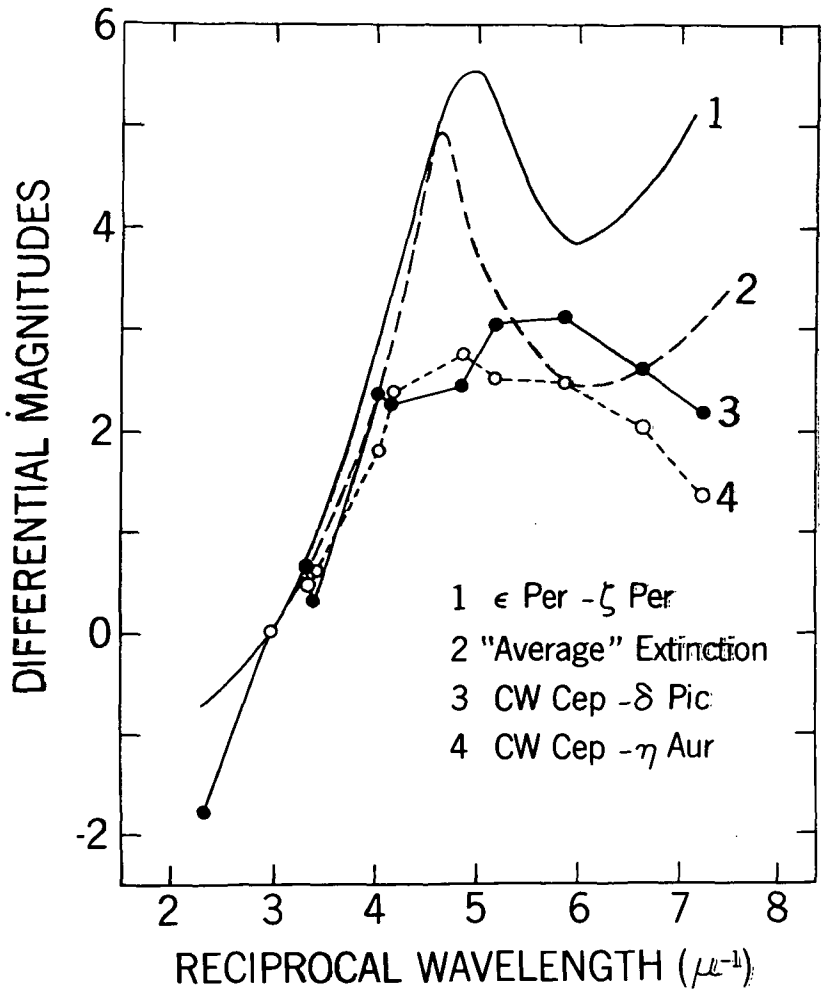

Figure 1.—Ultraviolet extinction curves for CW Cep formed with (1) δ Pic and (2) η Aur, as comparison stars. Curves labelled (3) and (4) refer respectively to the average extinction given by Bless and Savage (1972) and to the extinction in Perseus according to Stecher (1969).

$4.6\mu^{-1}$ bump. It should be noted that spectral scans of θ^1 + θ^2 Ori had not revealed emission at $4.6\mu^{-1}$. It is likely that for CW Cep both conditions obtain, i.e., the ultraviolet flux distribution may well be abnormal, and the interstellar medium or perhaps the immediate stellar environs may be peculiar. Like θ^1 + θ^2 Ori, CW Cep is a multiple system and, additionally, is a member of a young association. It would be of interest to determine if the infrared color excess is unusual as is reported for θ^1 + θ^2 Ori. Of course, data for other members of the Cep OB 3 association would be valuable in elucidating this puzzle.

IV. LIGHT CURVE ANALYSIS

The original objective was to verify the theoretical limb-darkening coefficients by solving the light curves. This could not be done due to instrumental problems which resulted in incomplete coverage and poor phase resolution. Hence, only approximate solutions were possible. Pre-primary maximum is adequately observed as is the entire secondary eclipse, but the egress of primary eclipse is represented by few observations of low weight, and the post-primary maximum is essentially unobserved. Comparison stars were not used as controls, but no systematic differences in light levels were detected for the phases in the pre-primary maximum for which redundant data were available and also for the shallow partial phases of primary ingress.

The light curves, consisting of the highest weight data corresponding to the largest signal to noise cases, are shown in Figure 2 where for simplicity the individual data points have been connected by straight lines. On the basis of visual inspection of the data, rectification in the main appeared unwarranted although some curvature in the maximum of the 1920 Å light curve seems to be present.* The proximity effects, if present, are small but peculiar light variations are evident at the shoulders of both eclipses. Primary eclipse is grossly asymmetric but it must be recalled that egress is only poorly represented. Secondary eclipse changes shape with wavelength. To quantify the shapes of both eclipses, the shape parameter $\chi(n = 0.8)$, as defined by Russell and Merrill (1952) was determined from smooth curves passed through the data for the ingress of primary and the combined data from both branches of secondary. The shape parameters, the observed eclipse depths, and their mean values which are used in a nomographic solution are listed in Table 2. All observational data are tabulated in Appendix I. Because of the paucity of data and the peculiar light variation at the shoulders an uncertainty in the unit light level existed at several wavelengths for data taken during the eclipses. The values of the corrections listed in Table 2, which were applied to all eclipse data, are those which force the light curve to attain unit light near to external tangency. The correction in magnitudes was subtracted from each data point before the corresponding shape parameter was calculated.

The variation in the χ's for secondary eclipse is quite

*One can show that, based on the solution given later in this paper, the effects of reflection and photometric ellipticity should be observed, and one must conclude that the scatter in the present data masks these effects.

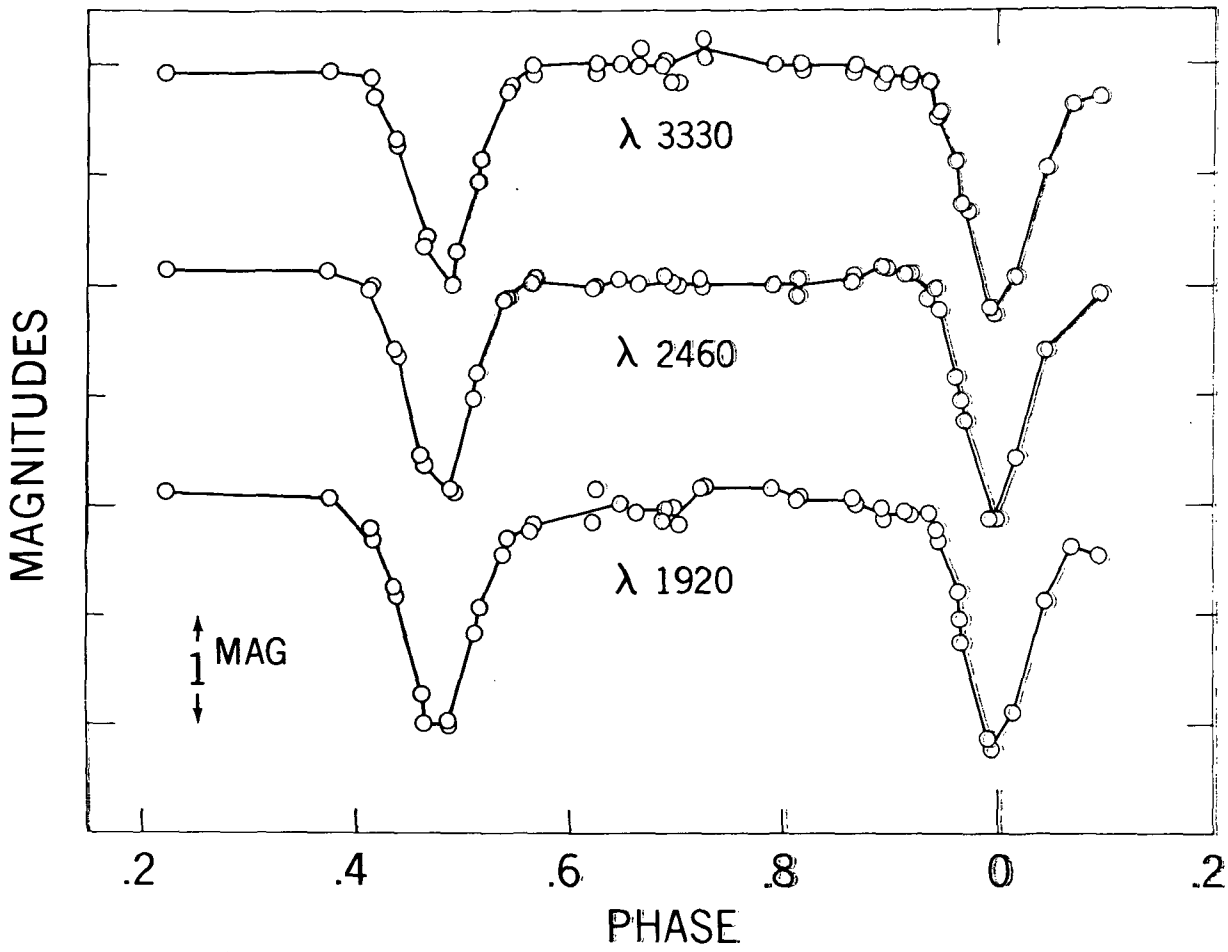

Figure 2.—Representative light curves of CW Cep.

large; the sense of the variation is that the branches steepen with decreasing wavelength. Even if one excludes the case where the corrections were applied, the variation is much larger than can be explained by changing the limb darkening of the eclipsed secondary components.* On the other hand, both the eclipse depths and the shape of primary remain constant. The depths of the eclipses are similar to those found by Abrami and Cester, $\Delta m_{prim} = 0.44$ and $\Delta m_{sec} = 0.37$. This implies that, to a first approximation, the surface brightnesses of the components are alike.

* Although the run of the eclipse is only poorly defined, the data at minimum for the 1920 Å light curve suggest that a total phase may exist.

Table 2. Computed Parameters

	3330 Å			2460 Å		1920 Å		
Eclipse	Pri I	Pri II	Sec	Pri	Sec	Pri	Sec I	Sec II
Depth (mag)	0.473	0.455	0.380	0.454	0.377	0.451	0.395	0.360
Shape χ(n=0.8)	0.274	0.273	0.315	0.251	0.353	0.249	0.398	0.440
Correction (mag)	0	0.025	0	0	0	0	0	0.04

In attempting a nomographic solution, it was found that the depths and line shape relation for primary eclipse yielded no solution at any wavelength, while the secondary eclipse shapes all yielded solutions specifying primary eclipse to be a geometrically deep partial transit. The nomographic solution based on the mean depths and shape of secondary yielded the following elements: ratio of radii = 0.69, radius of primary = 0.26, orbital inclination = 83° and the luminosity of the primary = 0.7. The usual normalizations were adopted, the ratio of surface brightness was set equal to 0.9 (the value used by Abrami and Cester), and a limb darkening of 0.6 was assumed for both components. These elements agree in the main with those found by Abrami and Cester and, in view of the low precision and scarcity of the data, further refinement is considered unwarranted. The computed solutions of Abrami and Cester and that given here during the minima are shown along with the 2460 Å data in Figure 3.

V. DISCUSSION

The system of CW Cep is unusual in many respects. To recapitulate, the ultraviolet extinction is abnormal, emission in H_α is observed, peculiar light variations appear at the shoulders of the minima, and the shape of secondary eclipse varies with wavelength in the ultraviolet. The photometric solution implies an approximate difference in luminosity of $\Delta m = 0.9$, which is inconsistent with that determined spectroscopically. Both components should be well situated on the main sequence if the expansion age of the association applies, since the contraction to the main sequence is given by Iben (1965) for comparable mass stars as 1.5×10^5 years while the main sequence life time is of the order of 10^7 years. And yet from the ratio of the radii or the differential luminosity, either the primary has evolved away from the main sequence or the secondary is a subdwarf. On the basis of the empirical mass-radius relation given by Harris, Strand and Worley (1963), Petrie's spectroscopic solution combined with the photometric results would indicate that the primary is evolved. These questions and particularly the problem of the variation of the eclipse shapes cannot be resolved solely with the present photometric data. If an extended atmosphere exists about either one of the components then one may question the applicability of the Russell-Merrill model and the elements derived thereby. It is easy to show that for a system undergoing eclipses where the geometric depth $p_o = -1.0$, i.e. the case of internally tangent eclipses, a large change can be induced in the shape parameter by moderate changes in the radii. For example, a 10% change in the radius of the secondary star in CW Cep could account for the observed χ variation if the radius decreases

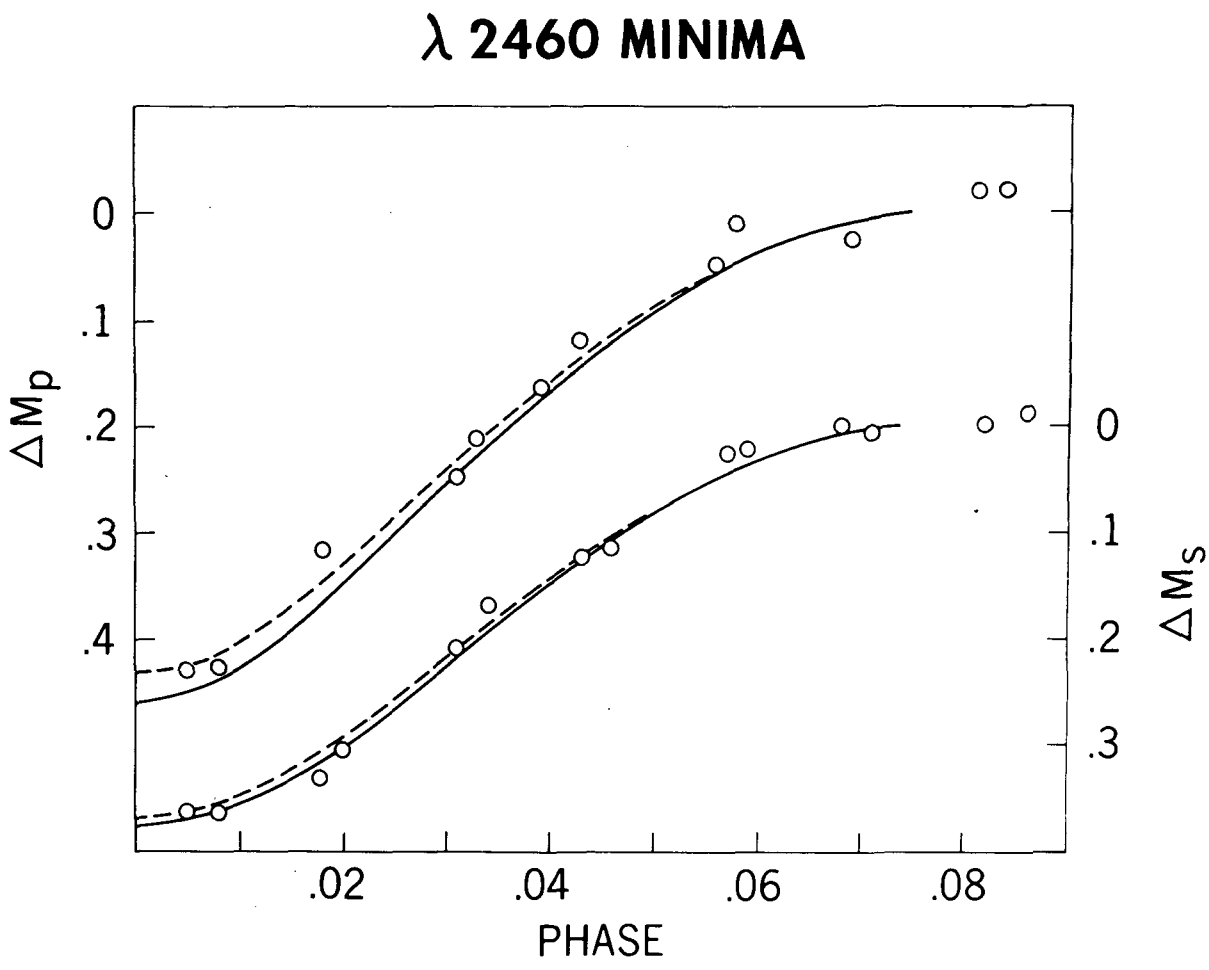

Figure 3.—Computed solutions of Abrami and Cester (1960), represented by the dotted curve, and the present work, given by the solid curve, are shown with the 2460 Å data.

with decreasing wavelength. This situation could obtain if the smaller secondary were surrounded by an optically thin shell which emits a Balmer continuum. An optically thick shell surrounding the larger (and presumably more evolved) star would produce the inverse effect.* Unfortunately this picture of the binary aggravates the already unusual ultraviolet extinction by requiring the true extinction freed of the anomalous shell flux to turn down even more steeply at the shortest wavelengths. Additional observations, particularly

* The phase of external tangency should vary but the photometric difficulties at the shoulders will mask this effect.

scanner measures of the flux distribution, may resolve some of these problems.

I would like to express my appreciation to Dr. Code for making available the large amount of observing time necessary to carry out this research. My thanks also go to Drs. M. Molnar and A. Holm, University of Wisconsin, and to Drs. S. Heap, D. Leckrone and D. West at GSFC for their assistance in preparing the program and for the many useful discussions afterwards.

REFERENCES

Abrami, A. and Cester, B. 1960, Osserv. Astron. Publ. Trieste, No. 300.
Blaauw, A., Hiltner, W. A. and Johnson, H. L. 1959, Ap. J. 130, 69.
Bless, R. C. and Savage, B. D. 1972, this volume.
Code, A. D. 1971, private communication.
Crawford, D. L. and Barnes, J. V. 1970, Astr. J. 75, 952.
De Vegt, Chr. 1966, Zeit. F. Astrop. 64, 268.
Garrison, R. F. 1970, Astr. J. 75, 1001.
Harris, D. L., Strand, K. Aa. and Worley, C. E. 1963, in Basic Astronomical Data, ed. K. Aa. Strand (Chicago: University of Chicago Press), p. 273.
Holm, A. V. 1971, private communication.
Iben, I. 1965, Ap. J. 141, 421.
McNamara, D. H. 1966, in Spectral Classification and Multicolour Photometry, I.A.U. Symp. No. 24, eds. K. Loden, L. D. Loden and U. Sinnerstad (New York: Academic Press) p. 190.
Nha, Il-Seong 1971, unpublished doctoral thesis, University of Pennsylvania.
Petrie, R. M. 1947, Publ. Dominion Astrop. Obs. 7, 305.
Russell, H. N. and Merrill, J. E. 1952, Contr. Princeton No. 26.
Stecher, T. P. 1969, Ap. J. 157, L125.
Wackerling, L. R. 1970, Mem. Roy. Astron. Soc. 73, 153.

Appendix I. Observed Data for CW Cep

Phase	m_λ λ 3330 Å	2980 Å	2460 Å	1920 Å
0.018	0.384	0.349	0.316	0.372
043	191	152	120	167
069	076	070	---	064
094	060	---	019	079
223	016	012	-033	-028
375	010	018	-031	-011
412	020	-012	007	040
415	057	---	000	065
437	133	080	114	147
440	142	122	123	168
463	328	285	306	346
466	305	331	333	401
488	399	350	364	389
491	337	339	366	400
514	210	228	208	237
517	164	173	158	190
539	047	023	026	088
542	037	036	022	060
565	-002	019	-002	047
568	021	031	-014	039
621	-002	-010	005	027
624	014	011	006	027
648	-000	-006	-011	000
662	004	-034	000	018
663	-033	---	004	---
687	003	-014	---	029
689	-010	014	-016	007
698	027	-002	002	005
701	030	011	002	039
723	-050	009	-009	-031
726	-016	-013	000	-030
790	-000	013	003	-033
814	-000	015	019	-007
817	005	006	-010	-014
865	015	013	-001	-006
867	003	021	-015	001
891	035	-015	-028	006
893	016	-020	-030	034
916	035	000	-021	018

Appendix I, continued

Phase	m_λ λ 3330 Å	2980 Å	2460 Å	1920 Å
0.919	0.020	0.013	-0.021	0.017
936	031	034	027	013
942	097	088	011	042
944	082	065	048	071
961	177	184	165	158
967	255	220	214	212
969	269	241	250	247
992	441	421	427	416
0.995	0.453	0.372	0.430	0.437

Note: Heliocentric phases were computed with the ephemeris given in the text for primary minimum.

ULTRAVIOLET PHOTOMETRY OF PLANETARY NEBULAE

Albert V. Holm
University of Wisconsin
Madison, Wisconsin

ABSTRACT

Nine of the planetary nebulae observed by the Wisconsin filter photometers are compared with 15 Monocerotis in the spectral region 1430-4250 Å. The data are corrected for the degradation of the filters of stellar photometer number four with time. Comparisons with simple models indicate that most of the observed nebulae are subject to some interstellar extinction in the far ultraviolet. However, NGC 246 and NGC 1360 appear to be nearly unreddened. Thus far no unexpected features have been found in the observations.

This is a preliminary discussion of ultraviolet photometry of nine planetary nebulae by the filter photometers of the Wisconsin Experiment Package on OAO-2. The observed nebulae were selected on the basis of total brightness and estimated small interstellar absorption. At the present only a small amount of the data has been reduced and compared with a simple model of the nebulae. When the study is complete, I expect to be able to check theories of nebular emission, to find reddening constants for the observed nebulae, and to find lower limits for temperatures of some of the central stars.

There may be some question about the accuracy with which objects as faint as planetary nebulae can be observed with the OAO. One observational problem is that, in many cases, the dark noise is larger than the signal collected by the eight-inch telescopes. Fortunately, if the OAO is not near the South Atlantic Anomaly, the dark noise usually varies smoothly with time (McNall 1971). Therefore, this contribution can be accurately subtracted from the observations if the dark noise

has been measured at the beginning and end of an observational sequence and at some intermediate point. A second problem is the possibility that the 10' field of view of the telescopes will include other faint stars that would confuse the measurements. This is a possible hazard for the measurement of both the star and the sky background. However, the nebulae and their central stars emit more strongly in the far ultraviolet than the average background star. Thus, contamination usually would be limited to the longest wavelength observations. In practice, I have found that even long wavelength measurements can be quite accurate. Observations have been made of peculiar O and B stars as faint as the 12th magnitude. The ratios, in magnitudes, of the measurements of these faint stars to the measurements of brighter stars at 4250 and 3320 Å agree with the differences in ground-based B and U magnitudes. Moreover, at shorter wavelengths the differences in magnitudes between the faint stars and brighter stars with the same B-V and U-B colors agree with the differences in visual magnitudes to $0^m.3$ and usually better. This is good agreement since the spectral types of the faint stars are not well defined and the stars may have abnormal ultraviolet fluxes. Hence, I am convinced that blue objects as faint as the 12th magnitude can be observed meaningfully by the OAO.

Unfortunately, the shortest wavelength filters on OAO, those of stellar photometer 4 (Code et al. 1970), have degraded since launch. Since very short wavelength observations are necessary for the study of planetary nebulae, I have investigated the behavior of these filters as a function of time. In Figure 1 the relative loss of filter sensitivity, in magnitudes, for early type stars is plotted against the number of orbits since launch. This degradation was determined by comparing observations of eleven O and B stars which have been observed repeatedly during the lifetime of the satellite. Filter 1, the 1550 Å filter, has undergone the least amount of change. Filter 3, the 1430 Å filter, has degraded rapidly after orbit 9000. Filter 4, the Lyman alpha filter, has degraded continuously since launch and has suffered the greatest loss of sensitivity. The rate of degradation of filter 3 and of filter 4 has lessened greatly since orbit 13000. The mean deviation of the observations from these curves is $0^m.04$ for filter 1, $0^m.05$ for filter 3, and $0^m.07$ for filter 4. A change in the effective wavelength of these filters has apparently accompanied the loss of sensitivity. The filters have become relatively more opaque to light of shorter wavelengths. Therefore, those stars which emit most of their light at longer wavelengths appear brighter in recent observations than predicted from the curves in Figure 1.

The results of the observations of the nebulae are presented in Table 1. In order to avoid questions of calibration and

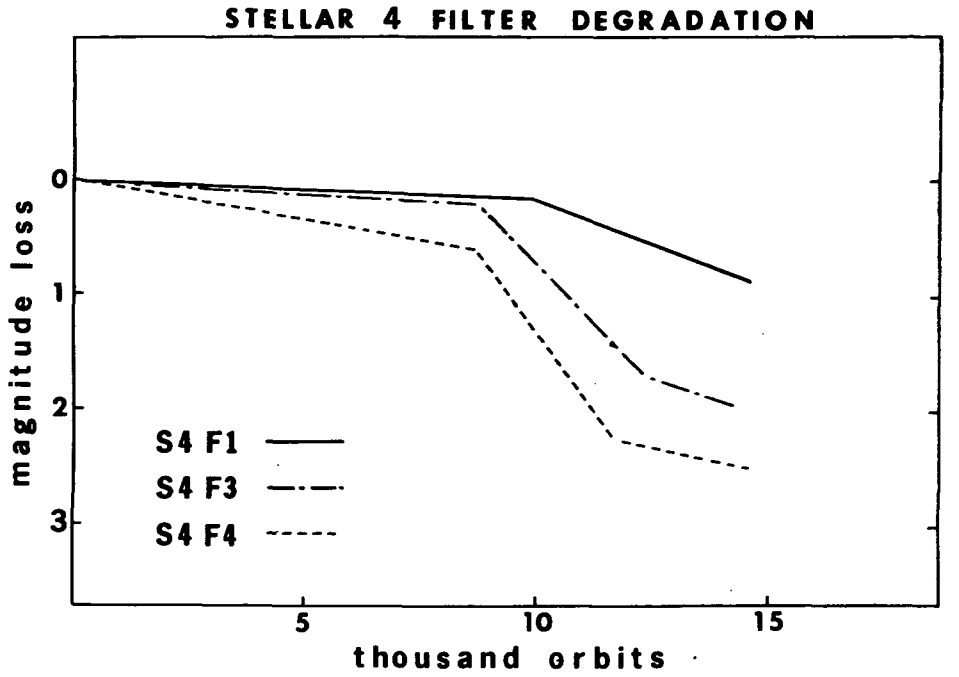

Figure 1.—The loss of sensitivity of the filters of stellar photometer four as a function of time between launch and orbit 15,000. Each orbit is approximately 100 minutes. These curves were derived for O and B stars.

to highlight features of the observations, the results are presented in the form of magnitudes relative to 15 Monocerotis (O7, V = 4.65, B-V = -0.25). These measurements have been corrected to the launch date for the degradation of the stellar 4 filters and for the decay of the ^{90}Sr calibration sources. I have not used the data from the Lyman alpha filter because for that filter the sky background is too bright in comparison to the nebulae. I have not used data from stellar 3 filter 5 because, in recent orbits, the amount of light transmitted by that filter is a function of the position of the star image on the filter. I have not used the data from stellar 2 because red leaks in its filters make sky brightness measurements for planetary nebulae unreliable.

Instead of discussing the details of all of the observations, I will speak mostly about two representative objects, NGC 246 and NGC 6826.

NGC 246 in the far ultraviolet appears to be an unreddened planetary with a moderately bright nebula and central star. It is similar to NGC 1360, but is fainter than that nebula.

Table 1. The ratios, in magnitudes, of the ultraviolet fluxes of the nebulae to those of 15 Mon. The estimated errors in the table refer only to the measurements of the nebulae. No corrections have been made for interstellar extinction.

Nebula	S1F3 4250 Å	S1F1 3320 Å	S1F4 2980 Å	S3F2 2460 Å	S3F1 1910 Å	S4F1 1550 Å	S4F3 1430 Å	*
NGC 40	5.95±0.14	6.88±0.17	7.49±0.26	8.53±0.22	8.53±0.21	8.40±0.50	8.45±0.63	
NGC 246	6.10±0.08	6.19±0.05	6.37±0.05	6.32±0.02	6.27±0.02	5.94±0.04	5.95±0.12	1,2
IC 418	4.93±0.03	5.05±0.03	5.37±0.03	5.77±0.01	6.10±0.02	6.03±0.04	---	1,2
NGC 1360	5.72±0.12	5.96±0.09	5.89±0.08	5.81±0.02	5.70±0.03	5.31±0.06	5.37±0.11	3
NGC 1535	6.29±0.20	6.44±0.15	6.74±0.17	6.94±0.03	7.06±0.07	6.70±0.18	6.66±0.52	
NGC 3587	6.74±0.26	7.53±0.38	8.20±0.62	8.37±0.07	8.54±0.22	8.20±0.60	7.96±2.0	
NGC 6543	4.78±0.05	5.21±0.04	5.64±0.05	---	---	5.93±0.06	6.04±0.06	2
NGC 6826	5.27±0.05	5.45±0.04	5.57±0.03	5.75±0.01	5.81±0.02	5.67±0.07	5.84±0.09	1,2
NGC 7293	5.22±0.07	5.77±0.06	6.34±0.07	6.68±0.05	6.73±0.04	6.60±0.09	6.82±0.12	

*1. Nebula observed twice.
2. Two separate measurements made for sky background.
3. Sky background is the mean of three nearby sky measurements.

Figure 2 shows the photometry of NGC 246 relative to 15 Mon. The data for NGC 246 are the means of two observations and the sky background data are the means of observations of two skys. The observations are compared with a simple model which is derived from the results of ground-based observations. This model uses only the hydrogen two-photon and recombination continuum radiation (Spitzer and Greenstein 1942, Seaton 1960, and Brown and Mathews 1970), the observed relative line fluxes (Minkowski 1942), and the He II 1640 Å flux estimated from the He II 4686 Å line strength. The central star was represented by the model atmosphere #204 (T_{eff} = 200,000°K and log g = 7.0) of Hummer and Mihalas (1970). This atmosphere was adjusted to the B magnitude of Liller and Shao (1968). The Hβ flux was estimated from the 2695 MHz radio measurement of Davies et al. (1967). The relation between the nebular flux and the stellar magnitude was derived using the absolute flux measurement of Vega by Oke and Schild (1970). The nebular temperature was assumed to be 10,000°K. Every hydrogen recombination which entered the n = 2 level for the first time in the 2^2S state

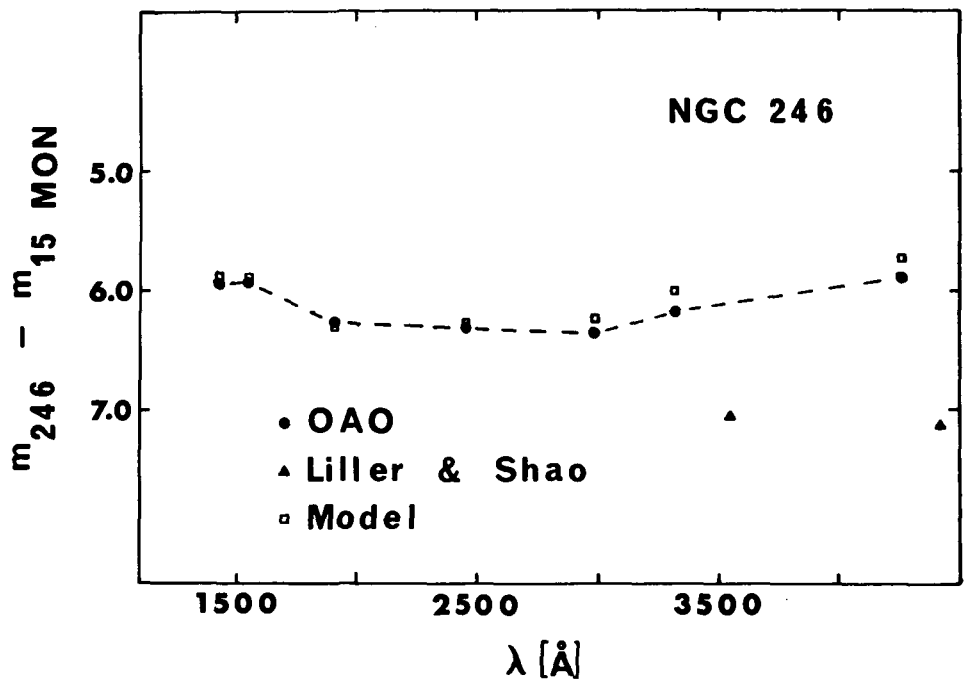

Figure 2.—Filter photometry of NGC 246 relative to 15 Mon. The observations of Liller and Shao (1968) are B and U magnitudes of the central star. The model nebula is described in the text. No corrections have been made for ultraviolet extinction. Note that the observed and model nebulae nearly coincide at wavelengths shorter than 2500 Å.

was assumed to result in two-photon emission. The calculated model was related to the OAO observations by the normalization factors derived by Code (1970) from B3 V models and observations. No reddening corrections were applied. Although a number of approximations were made in constructing the model, the fit with observations is good. In the model most of the radiation at wavelengths longer than 2500 Å is contributed by the nebula. At 1910 Å the model star contributes two-thirds of the flux. The He II 1640 Å emission line causes a small bump at 1550 Å. The agreement between the observations and the unreddened model indicates that this nebula is little reddened. This agrees with Kaler's (1970) estimated reddening constant of 0.0.

NGC 6826 is typical of most other nebulae observed in that the interstellar absorption appears to be significant. Figure 3 shows the photometry of NGC 6826 relative to 15 Mon. The model nebula was generated in the same manner as that of NGC 246. The relative line fluxes are from O'Dell (1963) and the $H\beta$ flux is from Collins, Daub and O'Dell (1961). The magni-

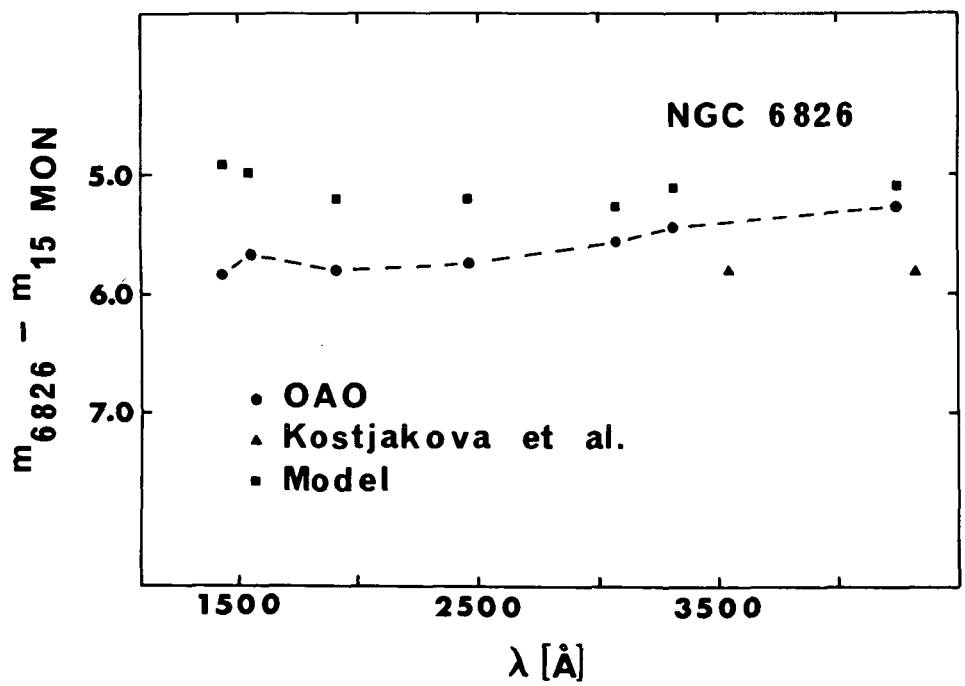

Figure 3.—Filter photometry of NGC 6826 relative to 15 Mon. The observations of Kostjakova et al. (1968) are B and U magnitudes of the central star. Note that the model deviates increasingly from the observed nebula towards short wavelengths. This trend can be removed with the "average" extinction curve of Bless and Savage (1972) if a reddening constant of 0.19 is assumed.

tude of the central star is from Kostjakova et al. (1968). As is seen in the figure, the model nebula increasingly deviates from the observed nebula at short wavelengths. This trend could be eliminated with the average reddening curve of Bless and Savage (1972) if the E(B-V) were 0.14. This color excess corresponds to a reddening constant of 0.19. This reddening constant is consistent with the values of 0.24 given by Osterbrock (1964) and of 0.18 given by Kaler (1970), but it disagrees with the values near 0.0 given by Thompson, Colvin and Stanley (1967) and by Terzian (1968).

NGC 7293 causes special problems because its angular extent is larger than the field of view of the photometers. The observations presented here were centered about 3'.5 north and 1'.5 east of the center of the nebula. There is a possibility that the four telescopes were not perfectly aligned so that the data from different telescopes may refer to different parts of NGC 7293.

In conclusion, the OAO observations of planetary nebulae appear to be good. Thus far no unexpected features have been found. New observations of planetaries and reductions of earlier observations are still being made. With more refined models, I expect to extract more information from the data.

I want to thank Dr. M. R. Molnar, Dr. T. E. Houck, Dr. C. F. Lillie, and Dr. R. C. Bless for assisting in acquiring the data, Dr. A. D. Code and Dr. B. D. Savage who emphasized the importance of the hydrogen two-photon emission in the ultraviolet spectra of planetary nebulae, and Dr. S. R. Heap who made her observations of NGC 1535 available to me. Finally, special thanks are due to the OAO project personnel, the operations crews, and the programmers who are continuing to maintain the OAO as an operating observatory.

REFERENCES

Bless, R. C. and Savage, B. D. 1972, this volume.
Brown, R. L. and Mathews, W. G. 1970, Ap. J. 160, 939.
Code, A. D. 1970, private communication.
Code, A. D., Houck, T. E., McNall, J. F., Bless, R. C. and Lillie, C. F. 1970, Ap. J. 161, 377.
Collins, G. W., Daub, C. T. and O'Dell, C. R. 1961, Ap. J. 133, 471.
Davies, J. G., Ferriday, R. J., Haslam, C. G. T., Moran, M. and Thomasson, P. 1967, M.N.R.A.S. 135, 139.
Hummer, D. G. and Mihalas, D. 1970, JILA Report No. 101.
Kaler, J. B. 1970, Ap. J. 160, 887.
Kostjakova, E. B., Savel'eva, M. V., Dokuchaeva, O. D. and Noslova, R. I. 1968, in Planetary Nebulae I.A.U. Symposium

No. 34, ed. D. E. Osterbrock and C. R. O'Dell (New York: Springer-Verlag), p. 317.
Liller, W. and Shao, C.-Y. 1968, in Planetary Nebulae I.A.U. Symposium No. 34, p. 320.
Minkowski, R. 1942, Ap. J. 95, 243.
O'Dell, C. R. 1963, Ap. J. 138, 1018.
Oke, J. B. and Schild, R. E. 1970, Ap. J. 161, 1015.
Osterbrock, D. E. 1964, Ann. Rev. Astr. Astrophys. 2, 95.
Seaton, M. J. 1960, Rept. Prog. Phys. 23, 313.
Spitzer, L. and Greenstein, J. L. 1951, Ap. J. 114, 407.
Terzian, Y. 1968, in Planetary Nebulae I.A.U. Symposium No. 34, p. 87.
Thompson, A. R., Colvin, R. S. and Stanley, G. J. 1967, Ap. J. 148, 429.

A SURVEY OF LOCAL INTERSTELLAR HYDROGEN FROM OAO-2 OBSERVATIONS OF LYMAN ALPHA ABSORPTION

Blair D. Savage
University of Wisconsin
Madison, Wisconsin

Edward B. Jenkins
Princeton University
Princeton, New Jersey

ABSTRACT

The Wisconsin far-ultraviolet spectrometer aboard OAO-2 observed the wavelength region near 1216 Å for 69 stars of spectral type B2 or earlier. From the strength of the observed interstellar L_α absorption, atomic hydrogen column densities were derived over distances averaging 300 pc away from the sun. Measurements of the equivalent widths of this absorption were found to be inappropriate for deducing column densities because of the blending of nearby strong stellar lines by the 12 Å wide instrumental profile of the OAO. Instead, the OAO data were compared to synthetic ultraviolet spectra, originally derived from earlier higher resolution rocket observations, which were computer processed to simulate the effects of absorption by different amounts of hydrogen followed by the instrumental blending.

An average volume density $n_H = 0.6$ atoms cm^{-3} was derived using all the stars. For stars nearer the sun ($r<140$ pc) we obtained $n_H = 0.25$ atoms cm^{-3}. The fact that no stars were observed much beyond 1 kpc precludes our obtaining any general information on large-scale galactic structure. However there is evidence for a pronounced enrichment of gas toward a number of stars in Scorpius, and a general deficiency seems to exist in the $180° < l^{II} < 270°$ sector. A comparison of L_α column densities

to those derived from observations of 21-cm emission shows a very poor correlation, which demonstrates the importance of the unavoidable differences in sampling geometry. The L_α column densities correlated reasonably well with D line, H and K line and color excess measurements for the respective stars, and the average ratios $\langle N_{NaI}/N_{HI}\rangle = 3.5 \times 10^{-9}$, $\langle N_{CaII}/N_{HI}\rangle = 2.5 \times 10^{-9}$ and $\langle N_H/E(B-V)\rangle = 5 \times 10^{21}$ atoms $cm^{-2}mag^{-1}$ were obtained. For assumed ionization equilibrium constants and a model for the interstellar medium, we find the observed ratios imply the total abundances $\langle Na/H\rangle = 2.3 \times 10^{-7}$ and $\langle Ca/H\rangle = 6.8 \times 10^{-9}$. For a very recent grain model we derive $\langle \rho_{HI}/\rho_{dust}\rangle \simeq 100$ from the $\langle N_H/E(B-V)\rangle$ relation.

I. INTRODUCTION

It has long been recognized that ultraviolet observations from space observatories can provide important new information on the interstellar gas and dust (Spitzer and Zabriskie 1959; Code 1960). The successful launch and operation of the second Orbiting Astronomical Observatory (OAO-2) (Code, Houck, McNall, Bless and Lillie 1970) has demonstrated that stellar space observatories can be designed to yield high-quality astronomical data for long periods of time. OAO-2 was launched on December 7, 1968, and at the time of writing (~2-1/2 years later) continues to collect high-quality scientific data. In this paper we will report on observations of the absorption from the interstellar Lyman alpha (L_α) line of atomic hydrogen at 1215.7 Å made by OAO-2. Other papers have dealt with OAO-2 observations of interstellar dust (Bless and Savage 1970, 1972).

Interstellar L_α absorption was first observed with sounding-rocket instrumentation by Morton (1967) in the far ultraviolet spectra of O and B type stars in Orion (see also Jenkins and Morton 1967). Since that first observation, sounding rockets have recorded the L_α line in approximately 20 stars. Reviews of these rocket observations and their implications have been given by Carruthers (1970a) and Jenkins (1970a). The primary conclusion which has been drawn from these observations is that the local interstellar hydrogen density is of the order of 0.1 atom cm^{-3} instead of the 0.7 atom cm^{-3} generally quoted by 21-cm observers (Kerr and Westerhout 1965). In the case of the rocket data the coverage of the sky has been small and therefore these early observations can not be considered as a general survey of the neutral hydrogen near the sun. However, these data have been very important because they have provided

an independent means of obtaining information on neutral interstellar hydrogen.

The short wavelength spectrometer in the University of Wisconsin experimental package on board OAO-2 has observed a large number of stars of type B2 or earlier in the spectral region 1050-1800 Å. For such stars the stellar L_α line is in most cases narrow enough to reside within the highly saturated core of the interstellar L_α profile. The distribution in galactic latitude and longitude of the stars observed is shown in Figure 6. Most stars are within 1000 pc of the Sun and are located near the plane of the galaxy. These new data provide a fairly representative sample of the local interstellar hydrogen.

A preliminary discussion of the OAO L_α data was given by Savage and Code (1970). In that analysis it was recognized that the relatively low resolution of the spectral scans obtained by the OAO produced a blending of the interstellar L_α line with adjacent stellar lines. The equivalent widths reported by Savage and Code were for the blend of stellar and interstellar lines near 1216 Å. This blend equivalent width was used to obtain an upper limit to the hydrogen column density. For many stars the OAO blended equivalent widths were significantly larger (2 to 3 times) than the reported rocket L_α equivalent widths. In contrast, for other cases there was a fair agreement between the OAO blended equivalent widths and the rocket L_α equivalent widths. Since that preliminary OAO report, a large effort has gone toward trying to understand the apparent differences between the OAO data and the rocket data and toward developing a method which corrects for the line blending in the OAO data. In this paper we present the results of this investigation.

II. OBSERVATIONS

The OAO L_α observations were obtained with an objective grating scanning spectrometer having an effective collecting area of 265 cm^2. Starlight was incident on a plane reflecting grating with 300 lines/mm and the first order dispersed light was focused by a parabolic mirror back through a hole in the center of the grating. Behind the grating, a slit having a width of 10 Å was positioned in front of an EMR 541F photomultiplier which contained a LiF window. The spectrum was scanned by a rotation of the grating in discrete wavelength steps of approximately 10 Å. The integration time at each step position for all the L_α data reported here was 8 seconds. In this integration time an unreddened 3rd magnitude B0 star produces approximately 8000 counts in the region of 1200 Å. Typically it was possible to obtain two spectral scans of a star from 1000-2000 Å during one night period of an orbit.

All observations reported here were made at night since the presence of scattered sunlight made the daytime observational material difficult to interpret. For a more detailed description of the OAO instrumentation and observational problems see Code et al. (1970).

Figure 1 shows some typical OAO-2 scans over the wavelengths 1050-1400 Å. We have plotted spectrometer counts vs. wavelength. An individual scan of an early type star would have the appearance of the plot for π Sco (B1 V + B2, m_V = 2.92). In this scan one can easily see spectral features that are primarily due to C III (1175.7 Å, a multiplet of 6 lines), H I (1215.7 Å), and Si IV (1393.8 and 1402.8 Å). In addition, some weaker lines are apparent at 1300 Å and 1335 Å. The line at 1300 Å is produced by a multiplet from an excited level of Si III (lines between 1294.5 and 1303.3 Å) combined with the weak O I interstellar line at 1302.2 Å. The line at 1335 Å is due to a combination of stellar and interstellar C II (1334.5 and 1335.7 Å). These line identifications were made with reference to higher resolution rocket spectra of the Princeton group (Bohlin 1970).

The wavelength scale for the OAO data was established through a comparison of OAO data and higher resolution rocket data degraded to the OAO instrumental resolution. The presence of the strong stellar lines makes such a comparison possible (see Figure 1). It was found that the number of Angstroms per spectrometer step depended on the direction of the scan (because of mechanical backlash), the wavelength and the incident angle.

When more than one spectral scan was obtained for an object, a detailed spectrum could be produced by combining scans. In Figure 1 we have combined two scans of the star τ Sco (B0 V, m_V = 2.83) and also four scans of the star δ Sco (B0.5 IV, m_V = 2.32). These observations were obtained by utilizing the satellite's bore-sighted startracker. With this startracker it was possible to make a scan, change the incident angle by 0.25 arc min (which corresponds approximately to a 2.5 Å shift in the spectrum), and then make another scan. If this process were continued one could produce a composite spectral scan similar to that for δ Sco shown in Figure 1. However, only a few stars were observed using this technique to fill in the data between the 10 Å stepping interval of the scanner. In general we combined two or more totally independent scans and shifted them in wavelength until a reasonable wavelength alignment was obtained. In fortunate situations this procedure led to a significant gain in information about the detailed shape of the spectrum. In other cases the data points simply all coincided.

The OAO spectrometer records a background signal which is a combination of thermal dark counts, counts due to charged

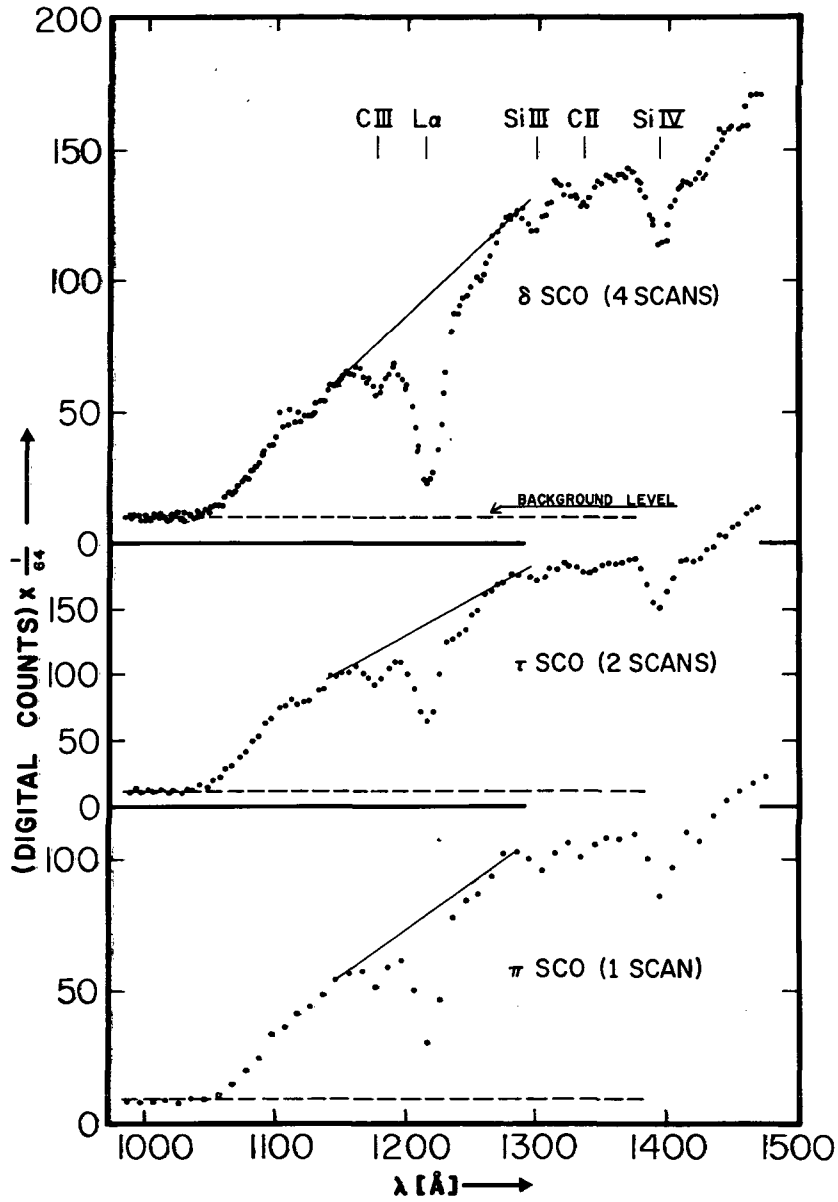

Figure 1.—OAO-2 spectrometer scans of the stars δ Sco (B0.5 IV), τ Sco (B0 V) and π Sco (B1 V + B2). We have plotted raw digital counts vs. wavelength. The 1/64 multiplier for the digital counts is due to a scaler in the OAO electronics. The plot for π Sco illustrates an individual scan. The plots for τ Sco and δ Sco are a composite of 2 and 4 scans, respectively. More frequent sampling than the spectrometer's 10 Å stepping interval was accomplished by controlled offsets in incident angle provided by the spacecraft's bore-sighted startracker. The dashed line represents the extrapolated background level.

energetic particles, sky background light, and scattered light in the optical system. The background due to charged particles from the radiation belts is usually unimportant (for 8-second integration times) except at those times when the satellite passes through the South Atlantic radiation anomaly. In general, astronomical observations were not carried out during this period of time. The scattered light contribution dominates over the other sources of background for O and B type stars brighter than approximately $m_V = 2$. The scattering is undoubtedly from the grating and dust elsewhere in the optical system. The sky background light is mainly resonance scattered L_α from hydrogen in the earth's geocorona. The net background due to all the above mentioned effects can be measured by observing an object shortward of the LiF cutoff of the photomultiplier. In the data illustrated in Figure 1 one can see that for $\lambda<1050$ Å (the LiF cutoff) the counts level off to a constant background level. For the purpose of obtaining L_α line profiles we have assumed that the background level measured at $\lambda<1050$ Å can be extrapolated as a constant background level for wavelengths greater than 1050 Å (see dashed lines in Figure 1). This assumption would have been invalid if some of the various background contributions were wavelength dependent or time dependent. A number of spectral scans of just the dark sky existed which demonstrate that the sky background is essentially constant with wavelength. We feel it is reasonable to assume that the scattered light contribution to the measured background is also wavelength independent. Since for most of the observational material presented in this paper the background is small compared to the observed signal at 1200 Å, the relative uncertainty in the derived intensity will be negligible. However, for stars faint in the ultraviolet the background can be comparable in size to the signal being measured at 1200 Å. Under this situation an uncertainty in the background correction can produce a large uncertainty in the derived intensity. It is this uncertain background correction for faint objects and not counting statistics that limit the instrument for L_α studies to O and B type stars brighter than about $m_V = 5$.

The data in Figure 1 illustrate the reproducibility of the OAO spectrometer observations. In general, spectral scans agree to within an uncertainty governed by photon statistics. Spectral scans of the same objects made two years apart have been compared, and typically they are identical to within 2 to 3%.

Much of the analysis which follows relies upon a detailed fitting of the OAO scanner data to reconstructions of prototype stellar spectra whose resolutions have been degraded. To accomplish this comparison one must know the shape of the

scanner's instrumental slit profile. This profile was derived from OAO observations of zero-order star images and from spectral scans of the relatively narrow He II (1640.4 Å) emission line in the star ζ Pup (O5 f, m_V = 2.25). Rocket observations of this line by one of us (EBJ) show its intrinsic width to be approximately 4 Å. The zero-order image data were used to establish the shape of the instrumental profile while observations of the He II emission line were used to determine width of the profile. A small correction was made for the finite width of the He II line. The derived function has an approximate Gaussian shape with a full width at half intensity of 12 Å. When this function was used to degrade higher resolution rocket spectra, a good agreement was obtained between the OAO scans and degraded rocket observations (see Figure 2). These comparisons will be discussed in detail in § III.

III. DERIVATION OF COLUMN DENSITIES

a) Preliminary Considerations

As mentioned earlier, some equivalent widths reported by Savage and Code (1970) differed significantly from those of the earlier rocket investigators. It was not clear at that time to what degree errors in either case could be attributed to (a) faulty measurements, (b) an improper estimate of the stellar continuum level on either side of 1216 Å or (c) confusion of the L_α profile with nearby stellar absorptions. We shall briefly review our conclusions on these possibilities and show how they influence our approach in the reduction of the OAO data presented here.

In spite of the measurement problems discussed in the previous section, the photometric accuracy of the OAO photoelectric scans is generally more trustworthy than that of the rocket spectra recorded on film. Uncertainties from film grain noise, errors in the film's characteristic curve and ambiguous intensities below the film's threshold must all be recognized as possible sources of error in the raw data from many of the rocket observations. On the other hand, the rocket spectra clearly resolve wavelength intervals significantly smaller than the width of the L_α profile, and we depend upon our ability to see this finer structure to answer questions about the possible sources of error (b) and (c) mentioned earlier.

A necessary (but not sufficient) test of the reliability of the OAO and rocket data is a comparison of the two after the rocket spectra have been convolved with the OAO instrumental profile. It is encouraging to see in Figure 2 that there is a surprisingly good agreement between the independently derived spectra. Figure 2 shows the references where the origi-

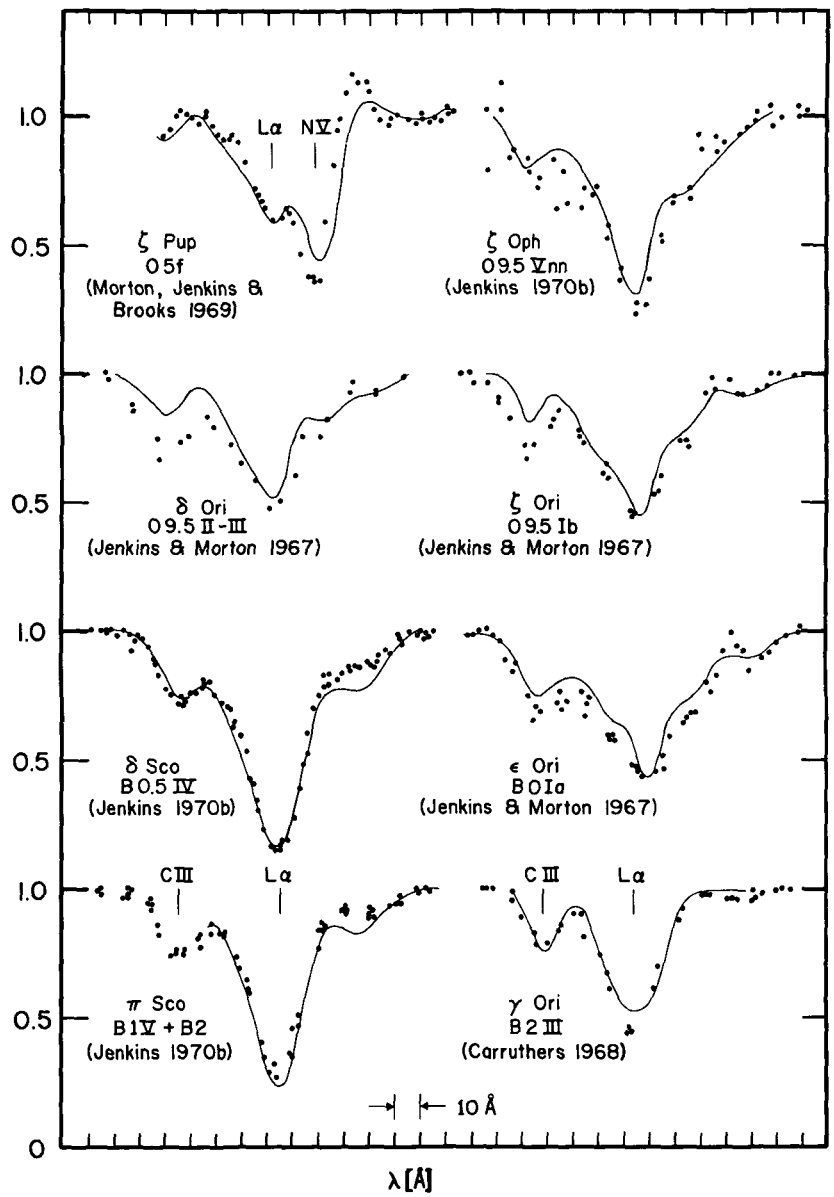

Figure 2.—A comparison of OAO data (dots) with high resolution rocket spectra which have been smoothed by the OAO instrumental profile (curves). Both the OAO and rocket spectra have been renormalized to make the apparent continuum level relatively flat at 1.0 (for the rocket spectrum of δ Sco, this operation is demonstrated in the change from Fig. 4a to 4b).

nal rocket spectra were first recorded. The most serious difference between rocket data and OAO data shown in this figure is seen in ζ Pup. In this case both the emission and absorption components of N V look somewhat different, although the match in the core of the L_α line is good. For this star the rocket intensity calibration may be somewhat in error for the strong emission of the N V line. The slight difference in the core of the L_α line for the γ Ori comparison can probably be understood in terms of too much smoothing of the rocket observation. In the convolution of the rocket data with the OAO slit function we did not allow for the finite resolution of the rocket data. The rocket spectrum of γ Ori was of slightly lower resolution (~3 Å) than the other rocket spectra used. In the case of δ Sco and π Sco it appears that atmospheric O_2 absorption could produce the difference between the OAO and rocket spectra at 1240 Å. One would expect a slightly weaker feature also to occur at 1206 Å (Watanabe, Zelikoff and Inn 1953). The only arbitrary adjustment which was applied to force a correspondence for the profiles in Figure 2 was a multiplication of each spectrum by a smoothly varying function which made the overall height of the continuum nearly level over the complete wavelength span. This renormalization compensated for any sloping trend in the stellar output and differences in each of the instrumental sensitivities versus wavelength. An illustration of this procedure is shown in the transformation of the rocket spectrum of δ Sco between Figures 4a and 4b.

Figure 2 makes it very clear that for these stars previous differences in column densities from OAO and rocket data cannot be attributed to any fundamental disagreement in the recorded information. In trying to explain why many of the rocket investigations revealed significantly lower column densities than their own, Savage and Code (1970) suggested the possibility that their predecessors had failed to account for the depression of the true continuum level by the broad damping wings in the L_α profile, and the rocket equivalent widths were measured under continua drawn systematically too low. Later, Jenkins (1971) reanalyzed the Princeton rocket L_α data for δ, ε and ζ Ori by evaluating the goodness of fit of the observed profiles with theoretical absorption profiles as the hydrogen density and continuum height were both allowed to vary as free parameters. Jenkins pointed out that unless a careful reduction procedure is used, rocket column densities could be subject to errors. Nonetheless, the fact that Jenkins still found much lower column densities for the Orion stars than those of Savage and Code, together with preparations for the work presented here, made it clear that when interstellar column densities were not very large, a principal contribution to the measured equivalent widths in the OAO absorptions recorded

near 1215 Å came from neighboring stellar lines blended in with the L_α absorption.

b) Derivation of N_H

The aforementioned difficulties associated with OAO equivalent width determinations forced us to consider alternate criteria for establishing hydrogen column densities. The following approach was adopted for the analysis of the OAO data. The stars shown in Figures 2 and 3, whose spectra were observed at good resolution by rockets, were selected as prototypes for the analysis of stars of identical or nearly the same spectral type observed by the OAO.

The actual column densities N_a (atoms cm^{-2}) to these stars were either taken from Jenkins' (1971) analysis or evaluated using a somewhat simpler technique suggested in his article. A reconstruction of the appearance of a spectrum in the absence of any absorption by atomic hydrogen was produced by multiplying the observed spectrum by exp $(+\tau)$, where the optical depth τ equaled 4.26×10^{-20} $atom^{-1}$ cm^2 $Å^2$ N_a $(\lambda-\lambda_0)^{-2}$ (Jenkins 1970a, 1971). Near the line core at λ_0, where excessive magnification of small errors would occur, the flux was assumed to be a straight line joining the reconstructed spectrum on either side. Figure 3 shows each prototype spectrum with and without interstellar absorption. One can see in this figure that the nearest strong stellar lines, Si III (1206.5 Å) and N V (1240 Å), are often a major source of line blending for the L_α profile and contribute to varying degrees in the different spectral types exhibited. Occasionally these lines show significant negative velocity shifts. For δ Sco (B0.5 IV), π Sco (B1 V + B2) and γ Ori (B2 III), Si III is the major source of blending, while for ζ Oph (O9.5 Vnn), δ Ori (O9.5 II-III), ζ Ori (O9.5 Ib) and ε Ori (B0 Ia), both Si III and N V contribute to the line blending. N V is a very strong component in ζ Pup (O5 f).

The next step consisted of generating a set of synthetic OAO spectra for these stars for various trial column densities N_t. A substitution of different values for N_t into the equation for τ and multiplication of each spectrum by exp $(-\tau)$ produced high resolution versions of the spectra with various amounts of absorption, and these were subsequently smoothed by the OAO slit function. As a final preparation of the curves for matching with the actual data from other stars, these synthetic curves were renormalized so that they all reached the same height in the vicinity of 1160 Å and 1270 Å. Figure 4 illustrates the various stages described for one of the prototype stars, δ Sco (B0.5 IV).

Figure 5 illustrates how the prototype spectra were used to obtain the adopted hydrogen column densities N_H to each OAO

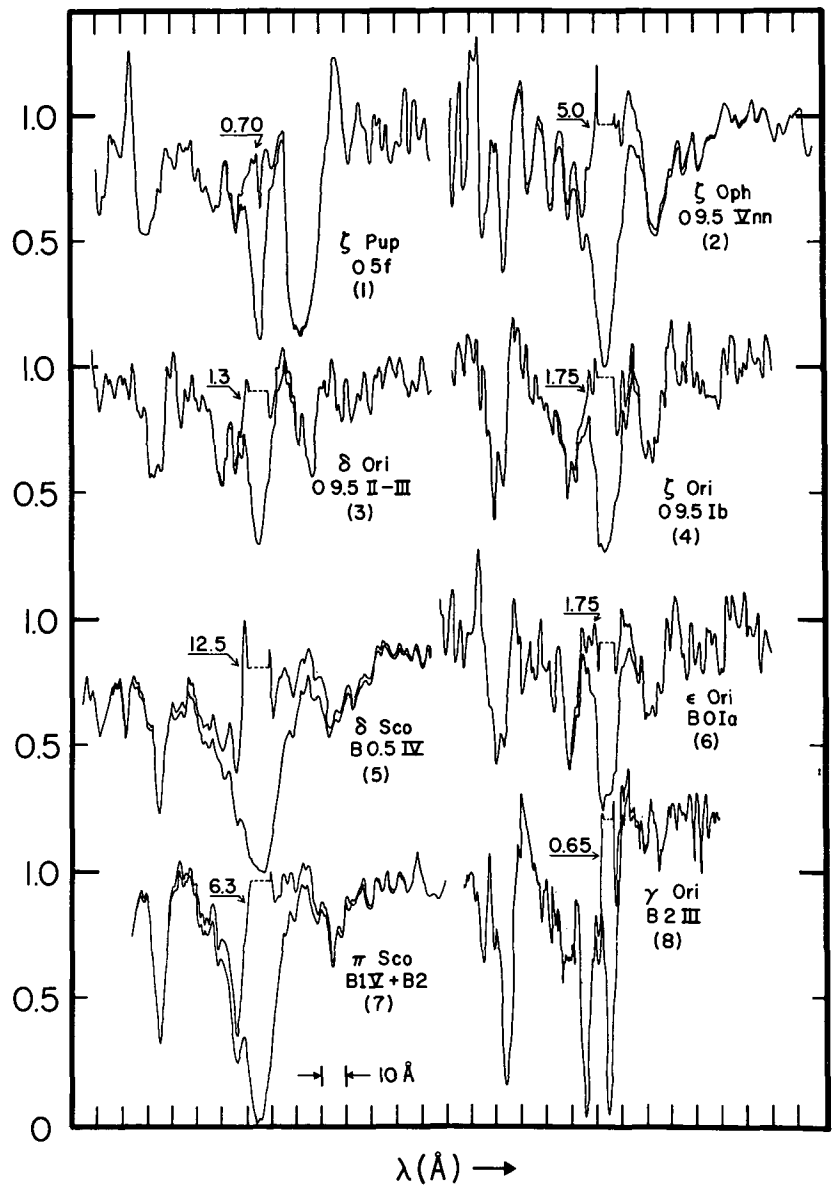

Figure 3.—Eight high resolution (renormalized) rocket spectra chosen for processing into prototype profiles for comparison with the OAO data. The upper curve near L_α represents the original intensity (lower curve) multiplied by exp $[\tau(N_a)]$, where the best estimate for the actual column density N_a to the star is shown in terms of 10^{20} atoms cm^{-2}. The number in parentheses is the code assigned for designating in column 12 of Table 1 which star was used for the derivation of N_H.

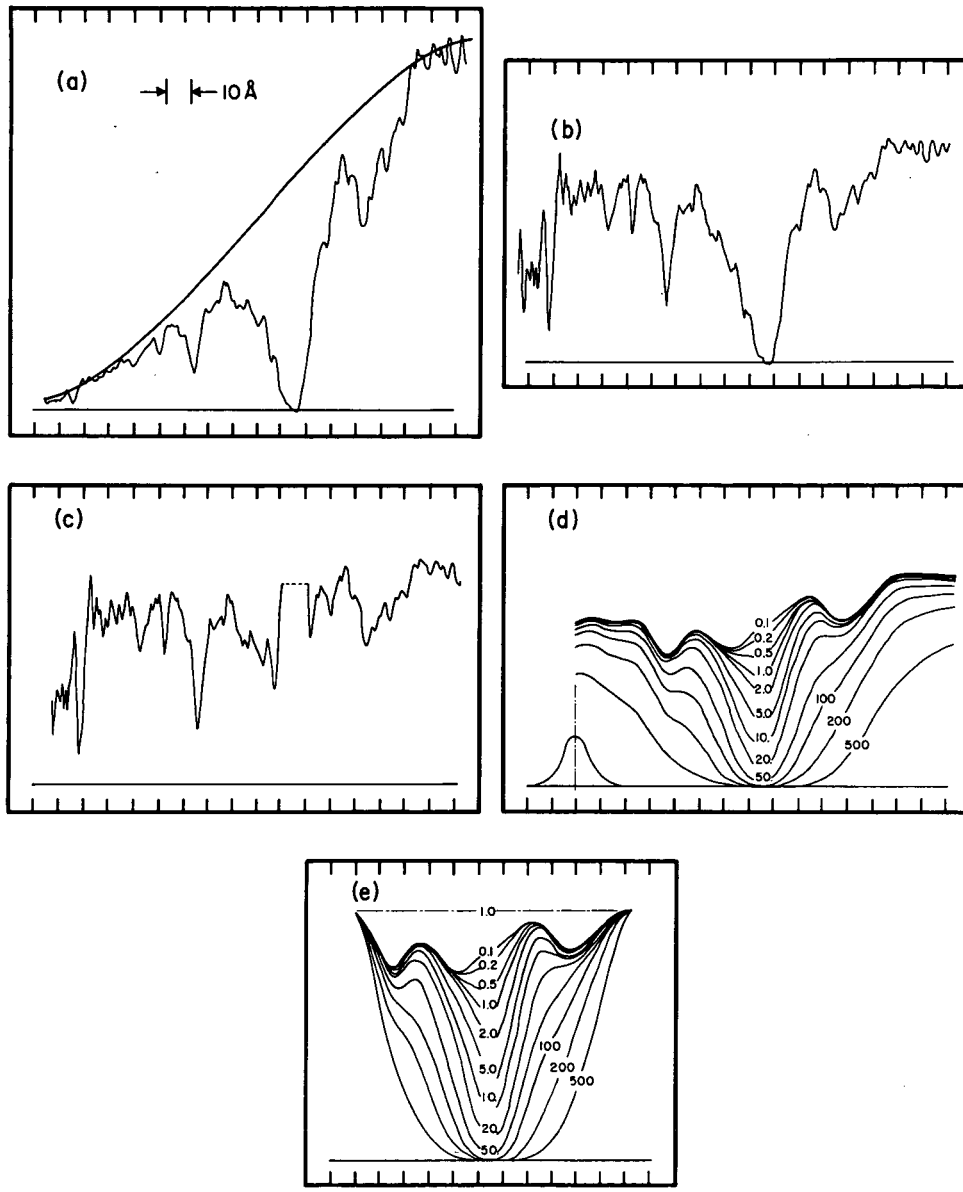

Figure 4.—The steps in preparing a prototype spectrum from an intensity tracing of a rocket spectrum. The spectrum is normalized to the line shown in (a) to give a level spectrum in (b). After multiplication by exp [$\tau(N_a)$], the reconstruction in (c) of the stellar spectrum in the absence of L_α absorption is derived. This profile is multiplied by exp [$-\tau(N_t)$] to simulate the appearance of the spectrum for various column densities N_t. The curves in (d) are the results for the different N_t values (10^{20} atoms cm^{-2}) after a convolution with the instrumental profile shown in the corner of (d). The profiles are ready for comparison with the OAO data after renormalization to a standard height in (e) by a straight line.

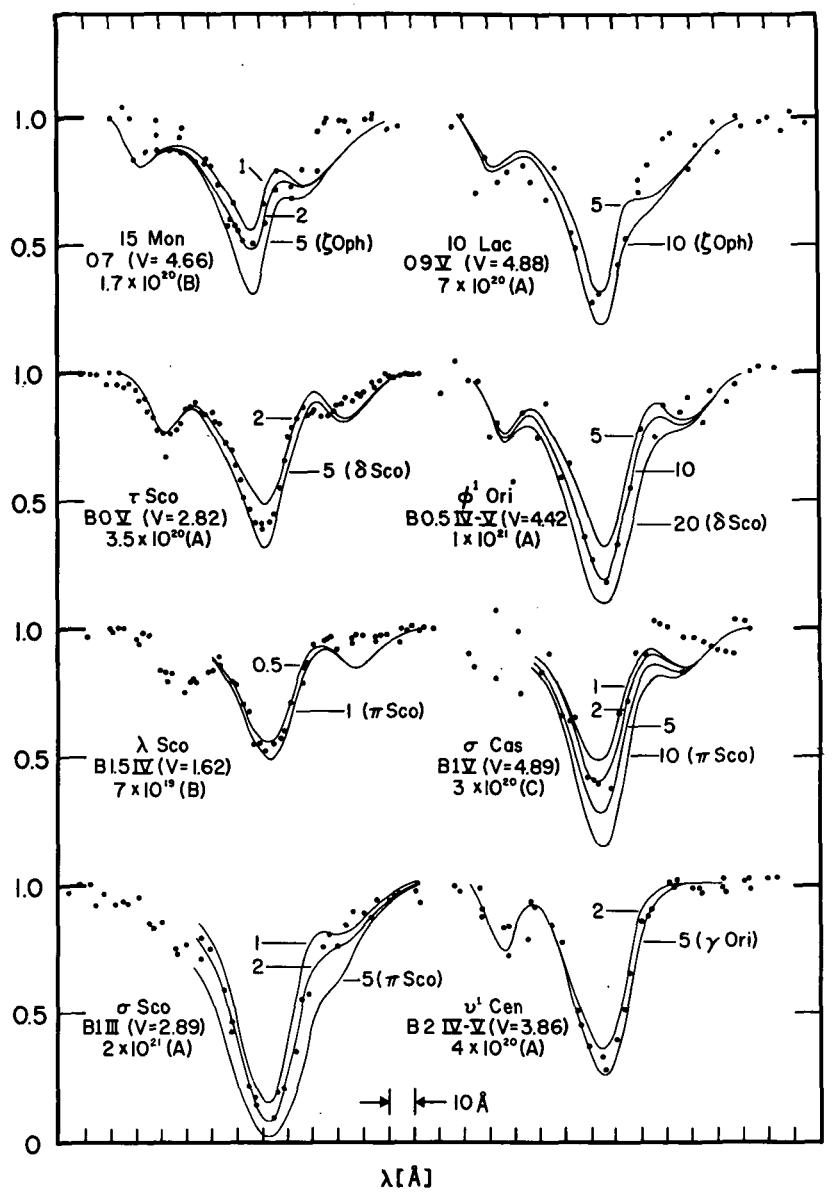

Figure 5.—An illustration of the derivation of hydrogen column densities for eight OAO stars. The dots represent OAO data for the star listed to the left of each profile. The solid lines are prototype spectra for various trial column densities (marked in units of 10^{20} atoms cm^{-2}). The prototype star (indicated in parentheses next to the lowest curve of each set) is the closest match in spectral classification to the OAO star. Below the spectral type and V of each OAO star is shown the adopted N_H and error estimate (A, B or C).

star. The general method of reduction was to choose the prototype star which matched most closely in spectral type and luminosity class the OAO star being analyzed. One then obtained the hydrogen column density by choosing the trial column density that gave the best fit to the OAO data. For example, in the case of the star ϕ^1 Ori (B0.5 IV-V) shown in Figure 5, we used the prototype star δ Sco (B0.5 IV) to obtain the hydrogen column density. As is evident, a trial column density of about 10^{21} atoms cm^{-2} applied to δ Sco would give a good match with the OAO observations of ϕ^1 Ori.

Since in our analysis we employed as prototype spectra only the eight stars shown in Figures 2 and 3, it was not possible always to use a prototype star which matched precisely an OAO star's spectral and luminosity class. For example, in the case of 10 Lac (O9 V) shown in Figure 5 we used the prototype star ζ Oph (O9.5 V) to obtain a column density of 7×10^{20} atoms cm^{-2}. We matched σ Sco (B1 III) with the prototype π Sco (B1 V + B2) to derive $N_H = 2 \times 10^{21}$ atoms cm^{-2}. We shall discuss the possible errors introduced into the final column densities through these unavoidable differences shortly.

The OAO hydrogen column densities as obtained by the above mentioned procedure are contained in Table 1. For each of the stars observed we have listed the following: (1) HD number, (2) name, (3) galactic longitude and (4) latitude (System II), (5) spectral type, (6) V magnitude, (7) B-V color, (8) E(B-V) color excess, (9) distance to star (in pc), (10) OAO hydrogen column density, (11) error and position code (see § IIIc and § IVa), (12) prototype star used to obtain the hydrogen column density (see Fig. 3), (13) mean interstellar space density n_H, (14) 21-cm hydrogen column density N_H (see § IVa), (15) x (see § IVa), (16) simplified model density (see § IVa), (17) Na I and (18) Ca II column densities (see § IVb), and (19) central depth (in percent) of the diffuse feature at 4430 Å. Wherever possible, photometric data for northern stars were taken from Iriarte et al. (1965) and for southern stars from Cousins and Stoy (1963). Spectral types are those given by Lesh (1968) or by Hiltner, Garrison and Schild (1969) for northern and southern objects, respectively. The determination of E(B-V) utilized the intrinsic colors of Johnson (1963). Distances were calculated using the photometric data in the table and absolute visual magnitudes from Blaauw (1963) along with the relation:

$$m_V - M_V = 5 \log r - 5 + 3E(B-V) \quad . \qquad (1)$$

Although there are a number of special cases where other methods could establish more accurate distances, we decided to retain the same system of assigning distances for all our stars in order not to upset the basis for studying regional variations of the hydrogen column density and its correlation

TABLE 1

(1)	(2)	(3)	(4)	(5)	(6)	(7)	(8)	(9)	(10)	(11)	(12)	(13)	(14)†	(15)	(16)	(17)	(18)	(19)
HD	Name	ℓ^{II}	b^{II}	S. T.	V	B-V	E(B-V)	r(pc)	OAO Hydrogen Column Density 10^{20} cm^{-2}	Error Estimate	Comparison Star	Mean Hydrogen Space Density cm^{-3}	21 cm Hydrogen Column Density 10^{20} cm^{-2}	x	Model Density	Na I Column Density 10^{12} cm^{-2}	Ca II Column Density 10^{12} cm^{-2}	Ac (%) λ4430
886	γ Peg	109	-47	B2IV	2.86	-0.21	0.03	180	1.3	B	8	0.23	3.3(1)	0.72	3.0	<0.24(12)		
3360	ζ Cas	121	-9	B2IV	3.66	-0.18	0.06	220	5.0	A	8	0.74		0.24	4.7			3.0(2)
5394	γ Cas	124	-2	B0.5IVe	2.41	-0.11	0.17	180	1.9	B	5	0.34		0.05	3.9	0.21(12)		
10516	φ Per	131	-11	B2Vpe	4.06	-0.04	0.20	160	10.	A	8	2.0	21.(3, 1.0)	0.22	3.4	2.9(4)		
24398	ζ Per	162	-17	B1Ib	2.86	+0.10	0.29	340	12.	A	6, 7	1.1	4.5(4) 9.9(3, 0.6)	0.60	6.3	3.3(4) 2.5(12)	3.2(13)	4.1(2)
24760	ε Per	157	-10	B0.5III	2.89	-0.18	0.10	290	3.0	B	5	0.33		0.35	6.1	1.8(4) 0.6(12)		3.8(2)
24912	ξ Per	160	-13	O7.5	4.06	+0.01	0.33	480	20.	A	1, 2	1.4	9.9(3, 3.5)	0.65	8.6	>7.6(4) 4.1(14) >17.(12)	2.0(13)	3.1(5) 7.2(2)
30614	α Cam	144	+14	O9.5Ia	4.29	+0.03	0.30	830	15.	C	4	0.58	14.(3, 1.5)	0.85	11.			3.4(2)
34816	λ Lep	215	-26	B0.5IV	4.29	-0.25	0.03	540	2.5	V	5	0.15	6.2(1) 8.6(6) 12.(3, 5.4)	0.89	6.0			
35411	η Ori	205	-20	B0.5Vnn	3.32	-0.18	0.10	250	6.0	V	5	0.78	12.(1) 18.(7) 12.(4) 11.(3, 2.7)	0.56	4.8	~3.4(4)		
35439	25 Ori	201	-18	B1Vn	4.95	-0.21	0.05	480	4.0	V	7	0.27	18.(3, 2.3)	0.77	7.3	<0.24(12)		
35468	γ Ori	197	-16	B2III	1.63	-0.21	0.03	110	0.65	V	8	0.19	21.(3, 4.7) 21.(8, 1.4)	0.22	2.4	<0.24(12)	<0.43(12)	
36486	δ Ori	204	-18	O9.5II-III	2.21	-0.21	0.09	340	1.3	V	3	0.12	18.(7) 10.(4) 18.(3, 1.9)	0.63	6.2	0.6(4)		0.2(5) 1.0(2)
36512	υ Ori	210	-19	BOV	4.63	-0.26	0.04	600	3.0	V	5	0.16	8.5(1) 10.(7) 12.(3, 2.1)	0.84	7.8			
36822	ϕ^1 Ori	195	-12	B0.5IV-V	4.42	-0.15	0.13	450	10.	V	5	0.72	24.(3, 0.9) 23.(8, 0.2)	0.60	8.4	2.9(14) 2.8(12)	2.9(13)	
36861	λ Ori	195	-12	O8	3.39	-0.18	0.13	440	11.	V	2	0.81	24.(3, 0.6) 23.(8, 0.5)	0.58	8.3	~4.2(4) 2.6(12) 2.9(14)	2.7(13)	2.0(2)

TABLE 1 (continued)

(1)	(2)	(3)	(4)	(5)	(6)	(7)	(8)	(9)	(10)	(11)	(12)	(13)	(14)†	(15)	(16)	(17)	(18)	(19)
HD	Name	ℓ^{II}	b^{II}	S. T.	V	B-V	E(B-V)	r(pc)	OAO Hydrogen Column Density 10^{20} cm^{-2}	Error Estimate	Comparison Star	Mean Hydrogen Space Density cm^{-3}	21 cm Hydrogen Column Density 10^{20} cm^{-2}	x	Model Density	Na I Column Density 10^{12} cm^{-2}	Ca II Column Density 10^{12} cm^{-2}	Ac (%) λ4430
37022	θ Ori	209	-19	O6p	5.13	+0.04	0.36	870	11.	W	*	0.47	19.(10)	0.86	7.9	1.9(12)	1.8(13)	1.3(9)
-41				O9.5Vp	5.07	-0.09	0.21	650					29.(11)			1.7(12)		1.8(5)
																		7.5(2)
37043	ι Ori	210	-20	O9III	2.76	-0.23	0.08	440	1.5	W	3, 4	0.11	12.(4)	0.76	6.8	<0.74(4)	1.7(13)	0.0(2)
													12.(3, 3.5)			0.54(14)		
																0.65(12)		
37128	ε Ori	205	-17	B0Ia	1.70	-0.19	0.05	360	1.75	W	6	0.16	18.(7)	0.64	6.5	2.1(4)	0.98(13)	-0.1(5)
													14.(4)			1.6(12)		0.0(2)
													18.(3, 3.0)			1.3(14)		
37468	σ Ori	207	-17	O9.5V	3.83	-0.24	0.06	450	5.0	W	2	0.36	18.(7)	0.73	7.3	2.5(4)	0.62(13)	0.0(2)
													18.(3, 4.6)			3.3(14)		
37742	ζ Ori	206	-17	O9.5Ib	1.74	-0.21	0.06	320	1.75	W	4	0.18	18.(7)	0.58	6.0	2.5(4)	0.97(14)	0.5(5)
													18.(3, 4.1)			1.3(14)		1.0(2)
																2.1(12)		
38771	κ Ori	215	-19	B0.5Ia	2.06	-0.18	0.04	470	4.0	W	6	0.28	16.(7)	0.76	7.2	2.3(4)	1.0(14)	2.0(2)
													20.(3, 2.8)			1.5(14)	1.1(13)	
													12.(15, 3.6)			1.4(12)		
40111	139 Tau	184	+1	B1Ib	4.83	-0.07	0.12	1080	8.0	C	6, 7	0.24		0.11	24.		3.6(13)	3.9(5)
																		5.5(2)
44743	β CMa	226	-14	B1II-III	1.98	-0.24	0.00	220	0.2	C	7	0.029	24.(3, 3.0)	0.38	4.6	<0.24(12)		0.4(5)
													20.(8, 1.1)					
47839	15 Mon	203	+2	O7	4.66	-0.24	0.08	900	1.7	B	2	0.061		0.24	19.	0.64(12)		0.9(9)
52089	ε CMa	240	-11	B2II	1.50	-0.21	0.01	180	0.2	C	8	0.036		0.25	3.9			1.0(5)
57060	UW CMa	238	-5	O7f	4.95	-0.15	0.17	910	3.5	A	1, 2	0.12		0.55	18.	3.0(12)	1.6(13)	
66811	ζ Pup	256	-5	O5f	2.25	-0.29	0.03	390	0.7	A	1	0.058		0.23	8.4	<0.24(12)	<0.43(12)	
91316	ρ Leo	235	+53	B1Iab	3.85	-0.13	0.06	750	4.5	A	6, 7	0.19	2.4(1)	1.00	3.8	1.2(4)	1.2(13)	2.8(9)
													5.5(6)			0.76(12)	1.2(14)	2.3(5)
													5.3(15, 1.6)			0.72(14)		
93030	θ Car	290	-5	B0.5Vp	2.75	-0.23	0.05	210	2.5	B	5	0.39		0.13	4.6			
105435	δ Cen	296	+12	B2IVne	2.63	-0.09	0.15	130	1.3	B	8	0.32		0.19	2.8			
106490	δ Cru	298	+4	B2IV	2.82	-0.24	0.00	170	1.5	B	8	0.29		0.08	3.7			
108248	α^1 Cru	300	0	B0.5IV	0.81	-0.25	0.03	110	0.6	C	5, 7	0.18		0.00	2.4			
-49	α^2 Cru			B1V														

TABLE 1 (continued)

(1)	(2)	(3)	(4)	(5)	(6)	(7)	(8)	(9)	(10)	(11)	(12)	(13)	(14)†	(15)	(16)	(17)	(18)	(19)
HD	Name	ℓ^{II}	b^{II}	S. T.	V	B-V	E(B-V)	r(pc)	OAO Hydrogen Column Density 10^{20} cm^{-2}	Error Estimate	Comparison Star	Mean Hydrogen Space Density cm^{-3}	21 cm Hydrogen Column Density 10^{20} cm^{-2}	x-	Model Density	Na I Column Density 10^{12} cm^{-2}	Ca II Column Density 10^{12} cm^{-2}	Ac (%) λ4430
111123	β Cru	302	+3	B0.5III	1.24	-0.24	0.04	150	1.5	B	5	0.32		0.06	3.3			
116658	α Vir	316	+51	B1IV	0.96	-0.25	0.01	100	0.4	B	7	0.13	1.6(1) 6.9(15, 0.5)	0.51	2.0	<0.023(4) <0.062(16)	<0.43(12) 0.040(16)	
118716	ε Cen	310	+9	B1III	2.29	-0.24	0.02	210	0.8	B	7	0.12		0.23	4.5			
120307	ν Cen	314	+20	B2IV	3.40	-0.22	0.02	210	1.2	B	8	0.18	10.(15, 2.5)	0.48	4.2	<0.24(12)		
120324	μ Cen	314	+19	B2IV-Ve	2.97	-0.17	0.07	140	2.0	B	8	0.46	10.(15, 3.0)	0.32	3.0			
121790	υ^1 Cen	315	+16	B2IV-V	3.86	-0.21	0.03	210	4.0	A	8	0.62	6.8(15, 1.8)	0.41	4.3			
122451	β Cen	312	+1	B1III	0.59	-0.22	0.04	90	0.3	C	7	0.11		0.01	2.0			
127381	σ Lup	319	+9	B2III	4.41	-0.20	0.04	380	5.0	A	8	0.43		0.42	7.8			
127972	η Cen	323	+17	B1.5Vn	2.30	-0.21	0.04	110	2.0	B	7	0.59	10.(15, 1.2)	0.23	2.4	<0.24(12)		
129056	α Lup	322	+11	B1.5III	2.29	-0.21	0.04	170	1.5	B	7	0.28	15.(15, 0.8)	0.24	3.6			
132058	β Lup	326	+14	B2III	2.67	-0.21	0.03	170	1.5	B	8	0.28	14.(15, 3.1)	0.29	3.6	<0.24(12)		
132200	κ Cen	327	+15	B2IV	3.12	-0.20	0.04	190	3.0	B	8	0.51	14.(15, 3.8)	0.34	4.0	<0.24(12)		
136298	δ Lup	331	+14	B1.5IV	3.21	-0.22	0.03	230	1.2	C	7	0.17	7.7(15, 2.3)	0.38	4.8	<0.24(12)		
138690	γ Lup	333	+12	B2IV	2.77	-0.20	0.04	150	1.8	B	8	0.39	15. (15, 1.4)	0.22	3.2	<0.24(12)		
141637	1 Sco	346	+22	B1.5Vn	4.69	-0.06	0.16	180	10.	C	7	1.8	8.8(1) 13.(15, 1.0)	0.45	3.6	<2.2(4)		3.4(2)
142669	ρ Sco	345	+18	B2IV-V	3.85	-0.20	0.04	210	5.0	B	8	0.77	15.(15, 3.2)	0.44	4.3			
143018	π Sco	347	+20	B1V, B2	2.92	-0.19	0.06	140	6.3	A	7	1.5	5.8(1) 13.(3, 4.9) 13.(15, 1.0)	0.34	2.9		<0.43(12)	1.8(9)
143275	δ Sco	350	+23	B0.5IV	2.33	-0.10	0.18	170	12.5	A	5	2.4	10.(1) 11.(17) 13.(3, 2.3) 17.(15, 2.3)	0.44	3.4	3.8(4) 1.6(12)	<0.43(12)	1.8(9)
144217	β^1 Sco	353	+24	B0.5V	2.55	-0.08	0.20	160	13.	A	5	2.6	8.8(1) 17.(15, 2.6) 13.(3, 2.3)	0.44	3.3	2.8(4) 1.4(12)	0.70(13) <0.43(12)	4.7(5) 6.7(2)

TABLE 1 (continued)

(1)	(2)	(3)	(4)	(5)	(6)	(7)	(8)	(9)	(10)	(11)	(12)	(13)	(14)†	(15)	(16)	(17)	(18)	(19)
HD	Name	ℓ^{II}	b^{II}	S. T.	V	B-V	E(B-V)	r(pc)	OAO Hydrogen Column Density 10^{20} cm^{-2}	Error Estimate	Comparison Star	Mean Hydrogen Space Density cm^{-3}	21 cm Hydrogen Column Density 10^{20} cm^{-2}	x	Model Density	Na I Column Density 10^{12} cm^{-2}	Ca II Column Density 10^{12} cm^{-2}	Ac (%) λ4430
144470	ω^1 Sco	353	+23	B1V	3.99	-0.04	0.22	240	12.	A	7	1.6	10.(1) 17.(15, 1.6) 13.(3, 2.3)	0.58	4.5	∿2.7(4) 3.3(12)	<0.43(12)	5.6(2)
145502	ν Sco	355	+23	B2V	4.02	+0.04	0.28	140	15.	A	8	3.5	9.0(1) 14.(15, 2.8) 13.(3, 2.9)	0.37	2.9	2.6(4) 3.2(12)		4.8(2)
147165	σ Sco	351	+17	B1III	2.89	+0.14	0.40	160	20.	A	7	4.0	15.(17) 16.(15, 1.0) 16.(3, 1.0)	0.33	3.4	3.4(4) 2.2(12)	0.78(13)	5.7(2)
148703	N Sco	346	+9	B2III	4.23	-0.17	0.07	330	7.0	A	8	0.69	17.(15, 2.4)	0.37	6.9			
149438	τ Sco	352	+13	B0V	2.82	-0.25	0.05	260	3.5	A	5	0.44	17.(15, 1.6) 19.(3, 1.6)	0.40	5.4	<0.60(4)		1.0(9)
149757	ζ Oph	6	+24	O9.5Vnn	2.57	+0.02	0.32	180	5.0	A	2	0.90	11.(1) 18.(3, 4.7) 14.(6) 16.(15, 2.3)	0.48	3.6	3.7(4) 2.6(12) 49.(18)	0.73(18)	1.3(9) 1.6(5) 8.8(2)
151890	μ^1 Sco	346	+4	B1.5IV	3.02	-0.23	0.02	220	3.5	B	7	0.51		0.11	4.8			
157056	θ Oph	0	+7	B2IV	3.27	-0.22	0.02	200	3.0	B	8	0.49		0.16	4.3			
157246	γ Ara	335	-11	B1Ib	3.33	-0.13	0.06	590	8.0	A	6, 7	0.44		0.68	10.			
158926	λ Sco	352	-2	B1.5IV	1.62	-0.18	0.07	100	0.7	B	7	0.23		0.03	2.2			
160578	κ Sco	351	-5	B1.5III	2.41	-0.20	0.05	180	1.5	B	7	0.27		0.11	3.9			
184915	κ Agl	32	-13	B0.5IIIn	4.95	0.00	0.28	580	8.0	B	5	0.45	12.(3, 0.5) 17.(15, 0.5)	0.72	9.5	4.0(14)	3.0(13)	4.0(2)
202904	υ Cyg	81	-10	B2Ve	4.42	-0.10	0.14	200	15.	A	8	2.4	16.(3, 1.3)	0.25	4.3	<0.82(4) 0.58(12)		
203064	68 Cyg	88	-4	O8n	4.98	-0.01	0.30	720	15.	A	3, 4	0.67		0.34	15.	10.(12)	4.6(13)	2.8(9) 2.4(5) 6.2(2)
205021	β Cep	108	+14	B1III	3.23	-0.21	0.05	320	1.0	B	7	0.10	21.(3, 5.3)	0.51	6.3			
214680	10 Lac	97	-17	O9V	4.88	-0.20	0.11	740	7.0	A	2	0.30	11.(3, 5.3)	0.87	8.9	≥3.3(4) ∿5.0(14) 3.0(12)	1.6(14)	1.3(9) -0.4(5) 1.0(6)
224572	σ Cas	116	-6	B1V	4.89	-0.08	0.18	390	3.0	A	7	0.25	16.(3, 5.1)	0.30	8.3	6.2(12)		

Table 1. References

(1) Goldstein and MacDonald (1969)	(10) Muller (1958)
(2) Duke (1951)	(11) Clark (1965)
(3) Takakubo and Van Woerden (1966)	(12) Merrill et al. (1937)
(4) Hobbs (1969, 1971)	(13) Spitzer et al. (1950)
(5) Stoeckly and Dressler (1964)	(14) Routly and Spitzer (1952)
(6) Habing (1968)	
(7) Menon (1958)	(15) McGee et al. (1966)
(8) Linblad (1966)	(16) Dunham (1941)
(9) Wampler (1966)	(17) Howard et al. (1963)
	(18) Herbig (1968)

*Measured from data of Carruthers (1969) by Savage and Code (1970).

†For those 21 cm surveys where the beam was not centered on the star, we have listed after the reference number the angular distance (in degrees) between the star position and radio position.

with other observables. References for the data on Na I, Ca II, 21-cm column densities, and 4430 Å central depths are listed at the end of the table. When more than one prototype star is listed in column 12 we have evaluated column densities by using both stars and then averaging the results. Such a procedure was necessary for certain intermediate spectral types.

c) Error Estimate

For each column density listed in Table 1 we have indicated the uncertainty by a letter classification system. Classification A implies the probable error is such that the true N_H may be 30% lower or 40% higher than the quoted value. Class B corresponds to -40% and +60%, while C is -50% and +100%. For example, the star ϕ^1 Ori (see Fig. 5 and Table 1) has an estimated error of class A and therefore has a column density of $10 \times 10^{20} + 4 \times 10^{20} - 3 \times 10^{20}$ atoms cm^{-2}. These error estimates are based on a consideration of the quality of each OAO spectrometer scan and the degree of confidence we have in the use of the prototype spectra to reduce a particular OAO star.

The varying degrees of uncertainty in the OAO column densities arise from several sources. In a number of cases the OAO line profiles are poorly determined because of a large and uncertain background correction. In these cases an estimate of possible errors has been made by allowing the background correction to vary over permissible limits and determining the corresponding hydrogen column density for each background se-

lected. A source of error common to all the OAO column densities is that of an incorrect allowance for line blending. Errors of this type can occur for a number of reasons. For example, the stellar features in the prototype stars may differ somewhat from the features in the OAO star being analyzed because of (1) a spectral type mismatch, (2) a luminosity class mismatch, (3) large differences in element abundances between the prototype star and OAO star, (4) other differences due to the peculiar nature of certain stars being studied, and (5) possible atmospheric O_2 absorption at 1206 Å in some of the prototype spectra. We estimate the O_2 feature to have an equivalent width no greater than 1 Å and hence this possible feature would be relatively unimportant compared with the much stronger Si III stellar absorption at the same wavelength. We have obtained information on how large errors of type (1) and (2) can be by using several prototype stars to analyze a single OAO star. Our general finding was that when the interstellar hydrogen column densities are large ($N_H > 2 \times 10^{20}$ atoms cm^{-2}) the errors due to spectral class or luminosity class mismatches are small (class A and B errors). This was the consequence of line blending being less important when the interstellar L_α line dominates the stellar lines. In contrast, when the interstellar hydrogen column densities are small ($N_H < 2 \times 10^{20}$ atoms cm^{-2}) the effects of line blending are more important and small mismatches between the OAO star and the prototype star produce larger errors (generally class B and C). For this reason the stars with small hydrogen column densities in Table 1 are usually of class C error while the stars with large column densities are usually of class A error except in those cases where the OAO profiles are poorly determined.

As we saw in Figure 1, for every star observed at L_α the OAO spectrum scanner obtains information on a number of strong ultraviolet stellar lines, and we can verify that the prototype star with the most similar ultraviolet spectrum has been selected. Since the Si III (1206.5 Å) feature is a major source of line blending with L_α in the OAO data, it is particularly instructive to study the relative strengths of the prominent Si III (1300 Å) and Si IV (1400 Å) multiplets. Differences in these two silicon features between the prototype and subject star provides a gauge of the importance of any of the four earlier mentioned dissimilarities in reducing the accuracy of our L_α absorption measurement. For example, in Figure 1 we can see that the stellar lines of Si III and Si IV in τ Sco (B0 V) and δ Sco (B0.5 IV) are of similar strength. This observation gives one confidence that the use of the rocket data on δ Sco as a prototype for the column density determination in τ Sco is valid. Through comparisons of this type we have noted that for stars of spectral type B0 to B2, the spectra of stars of luminosity class V, IV, III and II are quite similar,

while the supergiants have much stronger ultraviolet lines (Bless and Code 1970). We therefore feel we are justified in using, for example, the prototype star γ Ori (B2 III) to analyze other B2 stars of luminosity classes ranging from V through II. For the O type stars the differences among luminosity classes are larger. However, in the case of O9.5 stars we have prototypes for luminosity classes V, II and I.

The column densities reported in Table 1 should in most cases pertain to the interstellar medium. Jenkins (1970a) has considered the possibility that L_α emission from the star or its surroundings might significantly modify derived interstellar column densities. His conclusion was that such modifications are very unlikely. A more relevant problem for the data presented here is that of determining if photospheric absorption at L_α is contributing to the observed hydrogen column densities. As we indicated earlier, stars of spectral types later than B2 were excluded from this paper because in such stars the stellar L_α line is very strong. For all of the stars listed in Table 1, we have plotted N_H vs. spectral type and have found no overall tendency to obtain larger column densities in the cooler stars. It will be apparent from the material presented in § IVc on the gas to dust correlation that for B2 stars the stellar L_α line does not significantly modify the derived interstellar column densities. On the other hand, a reasonable fraction of the L_α absorption could be stellar when the measured N_H is as low as approximately 10^{20} atoms cm^{-2}; hence it is probably wiser to consider these lower values as upper limits for the interstellar N_H.

d) Comparison of OAO and Rocket Column Densities

A comparison of our results with various rocket column densities is given in Table 2. For the prototype stars we have listed the results obtained from measurements different from the ones we have employed for our comparisons. It is reassuring to note that the N_a values we have used do not differ appreciably from the values of the other investigators. In the case of the prototype star γ Ori, our determination of N_a from Carruthers' (1968) data is somewhat larger than his own measurement. The N_H values for the remaining stars in the right hand portion of the table were all derived from the OAO data by the technique discussed in § IIIb. For these stars roughly half show good agreement (γ Cas, ι Ori, α Vir, β^1 Sco, σ Sco and ω^1 Sco) while the rest disagree considerably with the OAO column densities. For η Ori and σ Ori the differences can be understood as due to the low quality of these particular rocket spectra. For β CMa the OAO value has a C error estimate, and in addition, Carruthers' spectrum for this star was of low quality (private communication). With κ Ori, ε Per

Table 2. Comparison of OAO and Rocket Column Densities

Prototype Stars

Star	Spectral Type	N_a 10^{20} cm^{-2}	N_H(rocket)	Reference
γ Ori	B2 III	0.65	$0.39^{+0.19}_{-0.15}$	3
δ Ori	O9.5 II-III	1.3	1.5	1
ζ Ori	O9.5 Ib	1.75	1.5	1
			$1.1^{+0.30}_{-0.26}$	3
			$1.1^{+0.5}_{-0.4}$	5
ζ Pup	O5 f	0.70	$0.59^{+0.17}_{-0.16}$	3
π Sco	B1 V, B2	6.3	$7.5^{+8.}_{-4.}$	6
δ Sco	B0.5 IV	12.5	$12.^{+6.}_{-3.}$	6
ζ Oph	O9.5 Vnn	5.0	4.2	10
			4.6 ± 1.5	

REFERENCES

1. Morton (1967)
2. Jenkins and Morton (1967)
3. Carruthers (1968)
4. Smith (1969)
5. Carruthers (1969)
6. Jenkins, Morton and Matilsky (1969)
7. Jenkins (1970b)
8. Carruthers (1970b)
9. Bohlin (1970)
10. Smith and Stecher (1971)

Table 2, continued

OAO Stars

Star	Spectral Type	N_H(OAO) 10^{20} cm $^{-2}$	OAO Error Estimate	N_H(rocket) 10^{20} cm $^{-2}$	Reference
γ Cas	B0.5 IVe	1.9	B	$1.0^{+1.1}_{-0.3}$	9
η Ori	B0.5 Vnn	6.0	A	$2.7^{+3.3}_{-2.0}$	2
θ Ori	O6p,O9.5 Vp	11.	B	$4.8^{+2.7}_{-2.1}$	5
σ Ori	O9.5 V	5.0	A	$2.7^{+1.5}_{-1.2}$	2
ι Ori	O9 III	1.5	B	$1.5^{+1.2}_{-0.8}$	2
				$0.67^{+0.3}_{-0.24}$	3
				$1.4^{+0.6}_{-0.4}$	5
κ Ori	B0.5 Ia	4.0	A	$0.89^{+0.33}_{-0.28}$	3
β CMa	B1 II-III	0.2	C	$0.57^{+0.48}_{-0.34}$	3
α Vir	B1 IV	0.4	B	<0.4	4
β^1Sco	B0.5 V	13.	A	$14.\pm6.$	7
σ Sco	B1 III	20.	A	$20.\pm3.$	7
ω^1Sco	B1 V	12.	A	$16.\pm4.$	7
ε Per	B0.5 III	3.0	B	1.1 ± 0.3	8
ξ Per	O7.5	20.	A	$4.2^{+1.9}_{-1.5}$	8

and ξ Per the column densities of Carruthers are all significantly lower than the OAO values. We believe the problem for these stars (and also his determination for γ Ori) could be related to that previously discussed by Savage and Code (1970) for θ^1 Ori C, for which it was shown that Carruthers (1969) had underestimated the equivalent width by placing a continuum level too low and by not allowing for the broad damping wings of L_α.

IV. DISCUSSION

a) The Distribution of Hydrogen

Of the 69 stars listed in Table 1, 81% are less than 500 pc away, and all but one are closer than 1 kpc. The proximity of observed stars is simply a manifestation of the magnitude limit for OAO observations of good quality at L_α. Over such a small distance scale, the observed distribution of interstellar atomic hydrogen provides relatively little insight on general features in the structure of our galaxy, such as spiral arms. Moreover, the well known grouping of O and B type stars into associations makes it inevitable that some limited sections of the sky are well sampled while other more extensive regions are left unobserved. In spite of these shortcomings, however, interesting conclusions on significant local excesses or deficiencies of gas from one region to the next may be drawn from the stars in our list. A strong suggestion of this variability came from earlier rocket observations (Jenkins, Morton and Matilsky 1969). We have here a large enough set of observations, all made by the same instrument, to over-rule any earlier misgivings one may have had that the differences in hydrogen densities were attributable to systematic errors arising from the markedly different wavelength resolutions of the separate rocket flights or the differences in spectral types of the stars available.

The information on distance r and average volume density n_H in Table 1 is plotted in Figure 6a in the form of ellipses whose centers are located at the galactic coordinates for the appropriate star. The length of an ellipse's horizontal axis is proportional to r and the vertical axis corresponds to n_H. It follows that the area of each ellipse is proportional to the measured column density N_H. One can immediately see from this plot that the hydrogen gas distribution is not at all uniform. Certain areas of the sky stand out as being characteristically rich or deficient in hydrogen.

In trying to assess the degree of variability in the L_α column density measures, it is helpful to compare the observations with what one would expect to obtain if the hydrogen were perfectly uniform except for a stratification parallel to the ga-

lactic plane. For the z dependence of the volume density n_H we shall adopt the distribution given by Schmidt (1957) scaled to a thickness between half-density points of 220 pc (Schmidt 1957, McGee and Milton 1964). The density is normalized to 0.71 atom cm^{-3} for z = 0, which corresponds to a compromise between the $N_H = 3.5 \times 10^{20}$ csc |b| atom cm^{-2} relation observed somewhat away from the galactic equator by McGee and Murray (1961) and the 2.5×10^{20} csc |b| atom cm^{-2} result of Goldstein and MacDonald (1969). The expected amount of hydrogen the model would give to each star is shown in column 16 of Table 1. The vertical axis of each ellipse in Figure 6b has a length proportional to the L_α N_H, whereas the horizontal axis corresponds to the expected density for the simple distribution. The shape of the ellipses depict excesses or deficiencies of gas, which is basically the same information given in Figures 4 and 5 of the article by McGee and Murray (1961).

With the exception of a few of the Orion stars, the observations indicate a general deficiency of gas in the 180-270° sector of galactic longitude (an average of n_H over all of the stars in this area is 0.27 atom cm^{-3}). Three stars on the order of 1 kpc away and near the galactic plane, 139 Tau, 15 Mon and UW CMa, have n_H equal to 0.24, 0.061 and 0.12 atom cm^{-3}, respectively. This suggests that the lack of hydrogen in this area of the sky may not be confined to only the local few hundred pc distance which is typical of most of the stars covered in our survey. A deficiency in 21-cm emission near ℓ = 240° may be seen in both the plots of integrated brightness temperature of McGee and Murray (1961) and the contours of peak brightness temperature shown by McGee, Murray and Milton (1963) (perhaps best seen in Figure 4 of the latter article). This 21-cm minimum does not appear to extend as far back in longitude as 15 Mon (ℓ = 203°) or 139 Tau (ℓ = 184°), however.

Some of the reduction in N_H for ζ Pup (ℓ = 256°, b = -5°) may be attributed to the ionization of hydrogen within the Gum Nebula which surrounds this star (Gum 1955, Rodgers et al. 1960). The only other line of sight we observed which intersects this nebula is that toward UW CMa (ℓ = 238°, b = -5°), but this star is very distant, and only the outer edge of the nebula is in the way, so the ionization would probably be of negligible importance. Brandt, Stecher, Crawford and Maran (1971) have suggested that ionization of the interstellar gas occurs well outside the apparent boundary of the nebula. They made use of the earlier measured low N_H to ζ Pup and γ Vel, together with an estimate of 0.4 atom cm^{-3} for n_H in the neighborhood of the sun, to argue that the volume of the ionization extended to within 60 pc of the sun. Such an interpretation would appear to be substantiated by our observation that neutral hydrogen seems to be deficient over a very wide angle in

Figure 6a.—Pictorial representation of the distribution of interstellar hydrogen observed by the OAO. In both plots the centers of the ellipses correspond to the galactic coordinates (System II) of the stars observed. In (a) the total length of the horizontal axis of each ellipse is proportional to the star's distance, and the vertical axis is equal to the average volume density of gas along the line of sight. The area of each ellipse therefore is proportional to the column density that was measured.

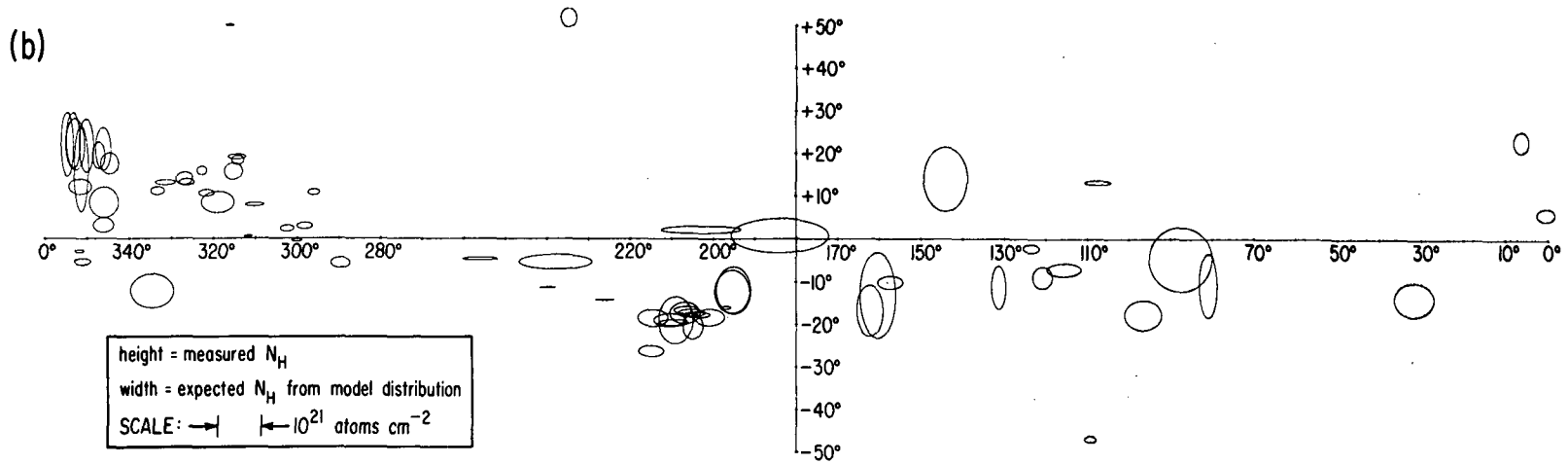

Figure 6b.—A comparison of the measured column density (vertical axis) for each star against what one would expect if the hydrogen were horizontally stratified according to Schmidt's (1957) $n_H(z)$ distribution normalized to 0.71 atoms cm^{-3} at $z = 0$. The dashed boundaries with identifying symbols define groups of stars which are distinguished from one another in the correlation plots (Figures 7, 8 and 9).

this region. On the other hand, it is hard to understand why the dispersion measures of MP 0818 (ℓ = 237°, b = +12°), PSR 0628-28 (ℓ = 237°, b = -17°) and CP 0834 (ℓ = 220°, b = +26°) are significantly less than PSR 0833-45, MP 0835 and MP 0736 located well inside the nebula (Gott and Ostriker 1971). It therefore seems more plausible that the ionization is still confined to the 40° diameter nebula, and that there is simply less interstellar gas in this particular area of the sky.

Another area which is prominent in Figure 6a is a small patch in Scorpius where the gas density is particularly rich. Although there is a spur of 21-cm emission projecting out of the galactic plane in this general neighborhood, details of the emission contours mapped in Figure 1(a) by McGee et al. (1963) do not correlate closely with the variations from one Scorpius star to the next. This might be an indication that these stars are embedded in a cloud complex, with some stars in front and others behind or within the gas cloud. (The properties of the medium in this region have been discussed by Herbig (1968) and Johnson (1970, 1971)).

It would be tempting to use the $L\alpha$ results to actually determine the general behavior of $n_H(z)$ in the solar vicinity since in each case an observation of $N_H \sin|b|$ is an average measure of $\int_0^{z(star)} n_H(z)\, dz$ along the line of sight. Unfortunately the plot of log $N_H \sin|b|$ vs. log z for our observations in Figure 7a shows considerable scatter, and it is difficult for us to define any systematic departures from the concept that n_H does not vary with z. (In this and succeeding figures in this paper, we have plotted the assigned A, B or C error code for each point instead of error bars to eliminate clutter.) Figure 7a, along with displays in Figure 6, helps to emphasize the strong irregularity in the H I gas distribution. We feel, however, that this type of display can be misleading because at high z we cannot avoid preferentially viewing toward isolated enrichments of gas projecting out of the galaxy, since it is precisely in such areas one usually finds young stars. If our sampling of directions were truly random (which it is not), the plot would be more meaningful. Similarly, we feel that any attempt to find some simple distribution which best fitted our data (such as the determination of the plane of the local gas layer in the manner of Goldstein and MacDonald (1969)) will be more a reflection of the irregularity of our sampling procedure, rather than a true generalization on the local distribution of hydrogen gas.

Figure 7a shows that 78% of the stars we observed have an average volume density n_H somewhere between 0.1 and 1.0 atoms cm^{-3} along the lines of sight. An average n_H for all of the stars equal to 0.6 atoms cm^{-3} was obtained over a mean dis-

tance of 300 pc from the sun. The average color excess per unit distance Σ E(B-V)/Σ r for these stars is equal to 0.31 mag kpc^{-1}. On the other hand, an average figure for the general reddening within 1 kpc of the sun is 0.61 mag kpc^{-1} (Spitzer 1968), which is roughly twice our average for the OAO stars. This difference demonstrates that our magnitude limit $V \gtrsim 5$ for L_α scans imposes a bias against the more heavily obscured stars at large distances. Hence, if one were to assume that the ratio of hydrogen to dust is constant everywhere (see § IVc and Fig. 9), a representative figure for the density over all directions would be twice the average n_H we have derived. There are seven stars closer than 140 pc for which the average n_H is 0.25 atoms cm^{-3}. We do not expect these nearby stars to be subject to the aforementioned observational selection.

Figure 6a or 6b reveals that of all the stars observed, a considerable fraction share some characteristic with their neighbors. We have already singled out for discussion the hydrogen-rich Scorpius region and a collection of stars having anomalously low column densities. The stars in Orion are all located within a reasonably confined solid angle, and stars in Crux, Centaurus and Lupus ($\diamond$), although fairly spread out, all have nearly the same distance modulus. It is of benefit to later discussions on the correlations of N_H with other observables to define memberships in groupings, even though the assignments are somewhat arbitrary. We have designated four groups, shown by the dashed perimeters in Figure 6a, and have put the remaining stars into a classification of "other" since they seem to be reasonably heterogeneous with respect to N_H, r and position in the sky. The symbols accompanying the regions in Figure 6a identify the membership of each star in the correlation plots (Figures 7, 8 and 9) and column 11 of Table 1.

In the introduction (§ I) we mentioned that the findings of the sounding rocket observers generally indicated the local hydrogen density was lower than previously suggested by overall surveys of 21-cm emission. More specifically, flights by several investigators clearly demonstrated that only occasionally did one find a L_α measurement yielding a column density as high as that suggested by the 21-cm emission in the same direction. This would not have been surprising for low galactic latitude stars since much of the 21-cm emission would have originated from portions of the galaxy beyond the stars, but a number of stars with $|b| \gtrsim 10°$ exhibited densities a factor of 10 lower than the corresponding 21-cm measures (Jenkins 1970a).

We are now in a position to repeat the comparison with the 21-cm data on a much wider scale. Figure 7b is a logarithmic plot of the L_α N_H against the 21-cm measures listed in column 14 of Table 1 for stars with $|b| > 10°$. For some of the stars we have observed, we could draw upon the results reported by

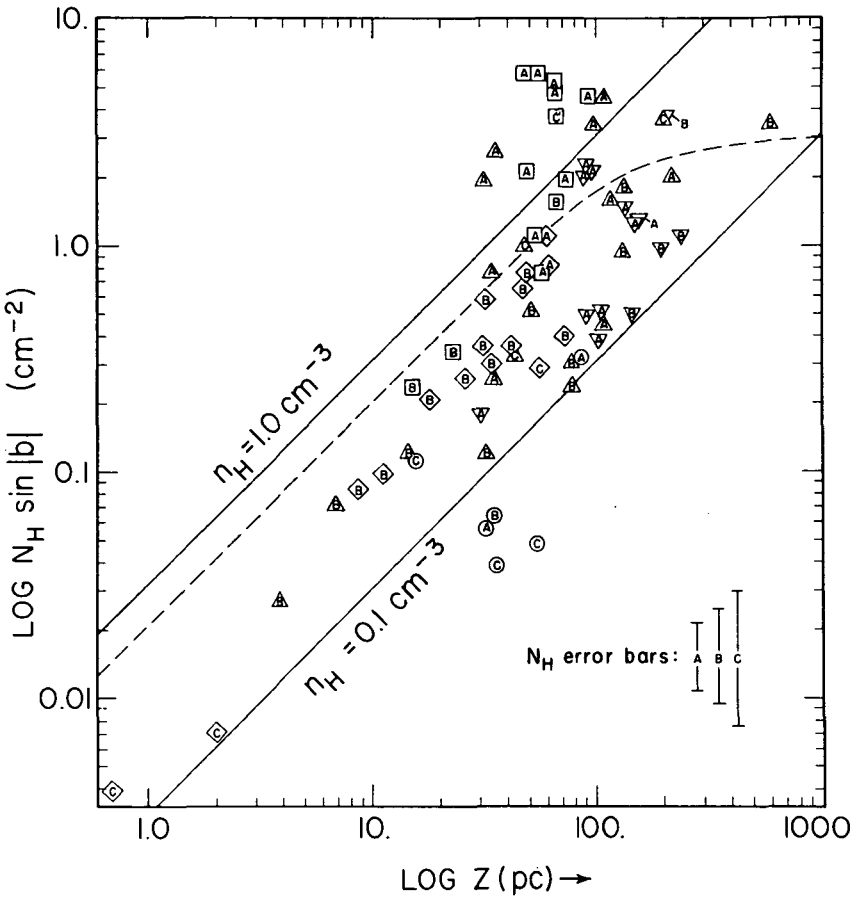

Figure 7a.—N_H sin |b| values plotted are an average measure along the line-of-sight of the amount of hydrogen situated between the z distance of a star and the plane of the galaxy (i.e., $N_H \sin |b| = \int_0^{z(star)} n_H(z)\,dz$ if n_H depends only upon z). The dashed line shows the expected behavior of the measurements if $n_H(0) = 0.71$ atoms cm^{-3} with a decrease in density away from the galactic plane following the distribution given by Schmidt (1957).

Habing (1968), Goldstein and MacDonald (1969) or Hobbs (1971), where the 21-cm emission has been sampled from a small diameter (1/2°) beam centered on the star's position (for the express purpose of comparing 21-cm and visual absorption line data). For many other cases, however, we had to rely on a measurement taken on the nearest grid point in the routine surveys of the other investigators referenced in the table. In each case we have shown in the tabulation the distance of the

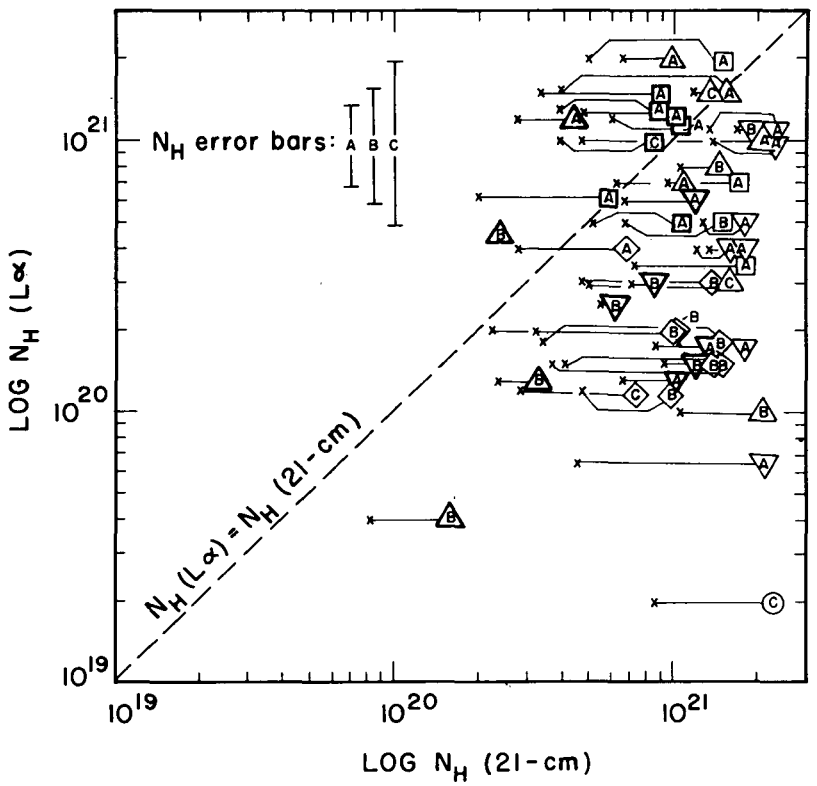

Figure 7b.—A correlation of L_α N_H measurements (at $b > 10°$) against 21-cm emission measurements (see column 14 in Table 1) in the same direction. The lines away from the left of each symbol indicate an estimated downward correction of the 21-cm results to compensate for background emission beyond the stars (see § IVa). The shapes of the plotted points show the star locations as defined in Fig. 6a, and the bolder symbols indicate the small-beam observations directly centered on the stars.

survey point from the star. We expect to have the closest correspondence with the centered observations; for Figure 7b we have chosen these measurements, when available, in preference to the survey values and plotted the symbols more boldly to emphasize their greater relevance to our measurements. For the surveys by Takakubo and van Woerden (1966) and Linblad (1966) we added up the N_H values given for the Gaussian components of optical depth, which were computed under the assumption that the spin temperature equalled 125°K. For all of the other references, we listed N_H simply computed from the integral of brightness temperature over frequency, which invokes the assumption that $\tau_{21\text{-cm}} \ll 1$. The fact that optical depths often

are not negligible means that the column densities computed by the latter method are usually somewhat lower than the true values.

Figure 7b demonstrates that the OAO data show virtually no correlation with the 21-cm emission measurement. A large majority of the column densities deduced from the 21-cm data are higher than those obtained from the L_α absorption measurements. To some degree, one would generally expect to find higher N_H values from the 21-cm data because of the additional contribution from hydrogen beyond the stars we have observed. To obtain a rough estimate of how much the 21-cm N_H should be revised downwards to correct for the background emission, we may resort to the idealized model for $n_H(z)$ discussed earlier and say it is reasonable to multiply each 21-cm result by the factor

$$x = \frac{\int_0^{z(\text{star})} n_H(z)\,dz}{\int_0^{\infty} n_H(z)\,dz} \qquad (2)$$

where the integral to infinity equals 3.0×10^{20} csc $|b|$ atoms cm^{-2}. The factor x is tabulated for each star in column 15 of Table 1, and each point plotted in Figure 7b has a line extending toward the left (ending at an "x") whose length corresponds to the logarithm of the correction factor. Even with the x corrections, however, most of the points still lie well below the diagonal $N_H(L_\alpha) = N_H(21\text{-cm})$ line. For stars above this line, it is likely that saturation of the radio emission is causing us to underestimate the 21-cm N_H.

b) Correlation of H I with Na I and Ca II

Measures of the interstellar D line absorption of Na I and the H and K lines of Ca II have been made for many of the stars in our program, as is evident from the many entries in columns 17 and 18 of Table 1. A comparison of H I to Na I and Ca II column densities should allow us to derive reasonably secure values for the overall abundance ratios in the interstellar medium, as well as to carry out a limited study on how much these ratios fluctuate over the various lines of sight. Past studies of this nature (Lawrence 1956, Howard, Wentzel and McGee 1963, Takakubo 1967, Habing 1968, Habing 1969, Goldstein and MacDonald 1969, Hobbs 1971) have had to contend with the uncertainty of how well the optical column corresponded with the 21-cm beam. We have seen from the results of the previous section that even for small radio beams exactly centered on a star, the 21-cm measurement is not very representative of the column density to the star. The earlier investi-

gators, however, did have the opportunity to use the velocity information in both the 21-cm emission and visible absorption data to help resolve this problem. Interesting conclusions from the earlier investigations on the correlations of specific velocity components cannot, of course, be verified or explored further with the L_α results.

The equivalent widths of both components of the doublets have been obtained by the investigators referenced in the appropriate columns of Table 1, with the exception of Hobbs (1969), who observed with an interferometric, photoelectric scanner and displayed high resolution (0.5 km sec^{-1}) tracings of the D2 line (and also the D1 line when D2 appeared to be saturated). For all but Hobbs' data, we have made use of Strömgren's (1948) Table 2 to derive column densities by the doublet ratio method, except for a revision of the transition f values to those given by Wiese, Smith and Miles (1969) of 0.327 for D1 and 0.344 for H. For the cases where the doublet ratio exceeded 2.0, we used the procedure of Routly and Spitzer (1952) of equating W_{D1} to $(W_{D1} + W_{D2})/3$ and assuming the lines were completely unsaturated. Occasionally, only an upper limit for the equivalent width of one component was available for a particular star. In this situation we derived column density upper limits assuming the line was weak enough that no saturation occurred. The two entries for Ca II in β^1 Sco (HD 144217) exemplify that this assumption may not always be valid and that such upper limits are not entirely trustworthy.

The greater profile accuracy and detail in the sodium data of Hobbs (1969) warrant a treatment which does not rely upon the simplifying assumption on the velocity behavior which is inherent with the doublet ratio method. As long as the residual intensity at the line center is not near zero, we can derive the neutral sodium column density from a straightforward integration of the measured optical depth over frequency,

$$N_{Na\ I} = \frac{mc}{\pi e^2 f_{12}} \int \tau d\nu = \left\{ \begin{matrix} 1.96 \times 10^{11} (D1) \\ 9.8 \times 10^{10} (D2) \end{matrix} \right\} (km\ sec^{-1})^{-1}\ cm^{-2} \int \tau dv \qquad (3)$$

Optical depths τ greater than 3.0 were hard to measure accurately and 4.6 was the maximum value we could include in the reduction. For stars having an absorption much stronger than $\tau = 3$ over a significant fraction of the profile's total velocity spread, the measurements very likely underestimate the true column densities, and hence these values were quoted as lower limits in Table 1. When available, D1 line values were listed in preference to the more saturated D2 line determinations. For some stars, we noticed that a large fraction of the τ_{D2} measurements ranged from 10 to 40% lower than the ex-

pected value of $2\tau_{D1}$ at the same velocity. This effect occurred for τ_{D2} significantly less than 3, and we conclude this may be an indication that for some cases the 0.5 km sec^{-1} resolution was not quite adequate for resolving saturated fine structure in the profiles. Hence it is possible that even some of the determinations not having excessive τ values may slightly underestimate the true Na I column density.

Occasionally, telluric water vapor absorptions appeared along with the D2 profiles. Hobbs pointed out this contamination when it occurred in his data, and in such situations we either totally relied upon the D1 profile (if available) or we eliminated the water peaks from the integration if they were small and separable. At times we could make use of only D2 tracings which had strong water lines blended with the sodium absorption, and in such cases we quoted the Na I column density values as upper limits in Table 1 and Figure 8a without attempting to separate out the spurious absorption since we could not estimate its strength. Stars having both large sodium optical depths and water vapor lines have values designated as approximate ($\sim$) in the table.

When the Na I column density has reached a value well in excess of that necessary to saturate the D lines, the 3302 doublet becomes strong enough to measure. Once again the ratio method can be used to derive a figure for $N_{Na\ I}$ by now comparing the 3302 and D line strengths (Strömgren 1948). Herbig (1968) used this approach to arrive at $N_{Na\ I} = 4.9 \times 10^{13}$ atoms cm^{-2} to ζ Oph (HD 149757). As noted by Herbig (1968) and Hobbs (1971), the doublet ratio method applied to the D lines fails for such large column densities, and it appears that even our value of 3.7×10^{12} atoms cm^{-2} derived from integration of the high resolution data is far lower than Herbig's result. The discrepancy with our method is rather puzzling in view of the fact that Herbig's curve of growth shows the optical depth $\tau_0 = 56$ for the center of the D1 line, whereas the largest τ seen in the D1 tracing of Hobbs (1969) is about 2.4. The residual intensity measured at the bottom of the strong D1 profile seems, by a good margin, to be larger than either the statistical noise or any reasonable uncertainties in subtracting off the parasitic light and dark current contributions described by Hobbs, although the profile does appear to have a slightly flattened bottom which suggests saturation.

In view of the aforementioned disagreement, we are somewhat skeptical of the larger $N_{Na\ I}$ values quoted in Table 1. In deriving a representative average value for the density ratio $\langle Na\ I/H\ I \rangle$ we disfavored the larger $N_{Na\ I}$ measurements as well as those where only upper limits were available. Estimates of 3.5×10^{-9} for $\langle Na\ I/H\ I \rangle$ and 2.5×10^{-9} for $\langle Ca\ II/H\ I \rangle$ were derived from a visual inspection of Figures 8a and 8b, where points in the middle of the sequences were

given the greatest weight. Our value for $\langle$Na I/H I$\rangle$ is in excellent agreement with an average given by Hobbs (1971) of 4×10^{-9}.

A large fraction of the interstellar sodium and calcium atoms are expected to be in the ionization state just higher than that observed, since both Na I and Ca II can be ionized by starlight photons less energetic than the Lyman limit at 13.6 eV. Hence, to deduce representative values for the total element abundance ratios $\langle$Na/H$\rangle$ and $\langle$Ca/H$\rangle$, one must evaluate the equations for ionization equilibrium and accordingly apply large corrections to the observations of Na I and Ca II. In the case of sodium, for any point along the line of sight we may consider the balance of photoionization of Na I against recombinations of free electrons and Na II,

$$\Gamma n_{\text{Na I}} = \alpha n_{\text{Na II}} n_e \quad , \tag{4}$$

and assume all of the sodium has a fixed abundance relative to hydrogen and exists only in neutral or singly ionized form,

$$n_{\text{Na}} = n_{\text{Na I}} + n_{\text{Na II}} = (n_e + n_{\text{H I}}) \langle \text{Na/H} \rangle \tag{5}$$

to arrive at the relation

$$\langle \text{Na/H} \rangle = n_{\text{Na I}} \frac{1 + (\Gamma/\alpha n_e)}{n_{\text{H I}} + n_e} \quad . \tag{6}$$

The above equation may also be recognized for the relation of $\langle$Ca/H$\rangle$ with respect to $n_{\text{Ca II}}$. The accuracy of the ionization calculations, however, is severely limited by our incomplete knowledge about conditions along any path through the interstellar medium, as well as some uncertainties in the ionization and recombination cross sections. Nevertheless it is instructive to evaluate an estimate for total element abundances based on reasonable estimates for the relevant parameters, even if many of the choices seem to be rather arbitrary and hypothetical.

A recent survey by Radhakrishnan, Murray, Lockhart and Whittle (1971) of 21-cm emission and absorption in the direction of 35 extragalactic sources suggests that the hydrogen is about equally divided between cool, dense clouds and a surrounding hotter medium. These observations, together with an interpretation by Hjellming, Gordon and Gordon (1969) on conditions in the direction of three pulsars, suggest that we could adopt the picture that, on the average, about 5% of any line of sight has roughly 5 H atoms cm^{-3} at 60°K and the remaining 95% contains 0.26 atoms cm^{-3} of hydrogen at 1000°K. Pressure balance is maintained in this model, and the overall

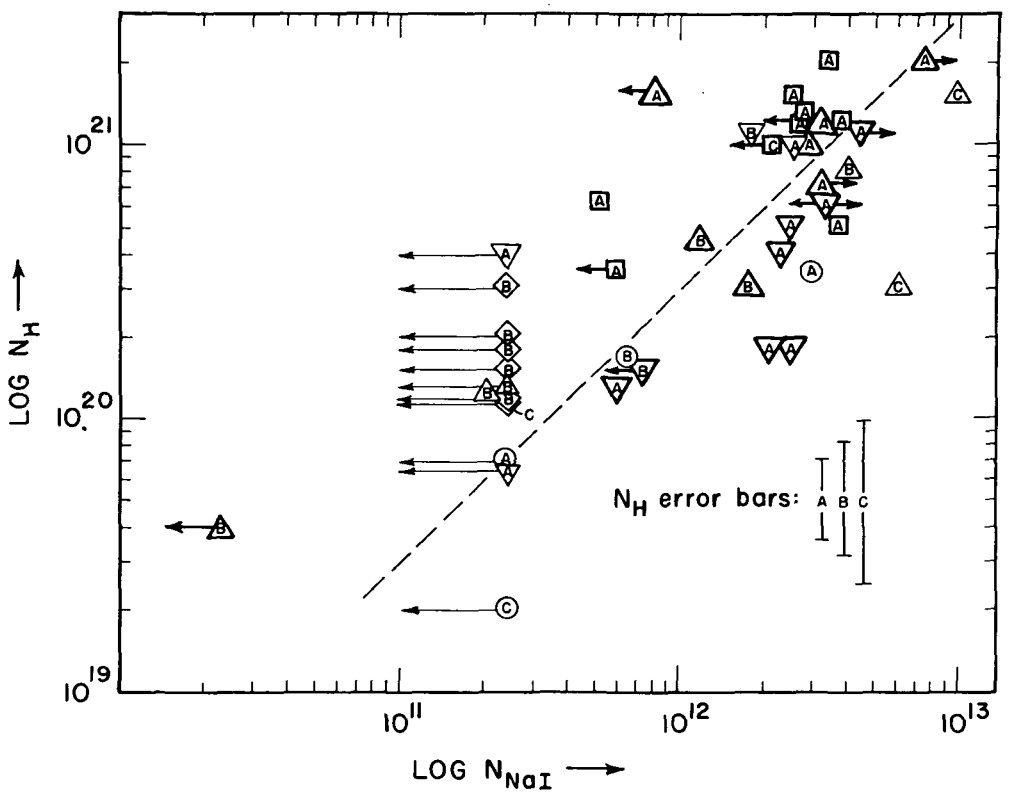

Figure 8a.—Correlation plots of the N_H measurements for those stars where we could obtain Na I and Ca II column densities (or their upper limits) by applying the doublet ratio method to equivalent width measurements or by integrating the D line optical depths over velocity in the high resolution observations of Hobbs (1969). The latter method of obtaining $N_{Na\ I}$ is considered more reliable than the former, and these better values are plotted with symbols having a bold border. The dashed lines correspond to our estimate for the average ratios of Na I and Ca II to H I of 3.5×10^{-9} and 2.5×10^{-9}, respectively.

n_H corresponds to 0.5 atoms cm^{-3}, which is a good representative value for the more trustworthy measures of Na I, Ca II and H I column densities. For electrons produced from ionizations of H I by X-rays or low energy cosmic rays, we expect to find

$$n_e \alpha n_H^{0.5} T^{0.35} \qquad (7)$$

if the ionization rate is constant everywhere (Habing 1969). Densities of 0.042 and 0.026 electrons cm^{-3} for the cold and

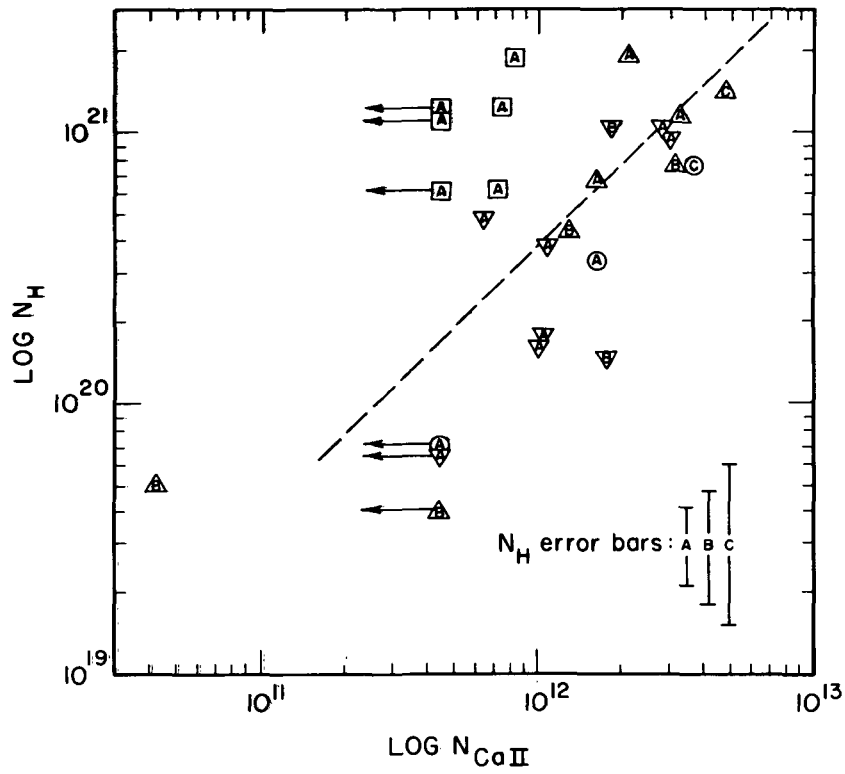

Figure 8b.—See Figure 8a caption.

hot portions, respectively, are consistent with equation (7) and the observed average of 0.03 electrons cm^{-3} for dispersion measures of pulsars at known distances (Davidson and Terzian 1969, Lang 1971). Our interpretation of the dispersion measure integral includes an extra rms fluctuation term (Lerche 1970) whose value corresponds to the expected variations of n_e between the two regions. Habing (1969) estimates representative values for Γ/α in the interstellar medium equal to $2.1(T/100)^{0.7}$ for Na I and $0.04(T/100)^{0.7}$ for Ca II. Substituting these values into equation (6) we find $\langle Na/H \rangle = 2.3 \times 10^{-7}$ and $\langle Ca/H \rangle = 6.8 \times 10^{-9}$ is consistent with both the model and our averages for the observed $\langle$ Na I/H I $\rangle$ and $\langle$ Ca II/H I $\rangle$ quoted earlier. These element abundance ratios are a factor of 7 and 230 below the cosmic abundance of 1.6×10^{-6} for both $\langle Na/H \rangle$ and $\langle Ca/H \rangle$ (Allen 1963). If we instead adopt a model for the interstellar medium closer to that suggested by Field, Goldsmith and Habing (1969) (3% of the volume with $n_H = 30$ atoms cm^{-3} and $T = 60°K$ surrounded by $n_H = 0.1$ atom cm^{-3} at $10^4°K$) and apply the same analysis as before, we obtain the even lower values of $\langle Na/H \rangle = 1.0 \times 10^{-7}$ and

$\langle Ca/H \rangle = 4.0 \times 10^{-9}$.

Figures 8a and 8b show the observed $N_{Na\ I}/N_H$ and $N_{Ca\ II}/N_H$ ratios are generally lower for the Scorpius stars (□) than for most of the others. This relative deficiency has been noted earlier for these stars by Buscombe and Kennedy (1968) in their comparisons of the interstellar lines with color excesses. We previously suggested (in § IVa) that large N_H values measured for the Scorpius region may result from a relatively dense gas complex near these particular stars. We can surmise from Figure 7b that much of this gas is probably rather cool since, as an exception to the rule, the $L\alpha$ N_H measurements are greater than the indications from 21-cm emission (i.e., $\tau_{21\text{-cm}} > 1$ and thus $T \gtrsim$ peak $T_b \approx 50°K$). If we combine equations (6) and (7) with the $T^{0.7}$ dependence for Γ/α, we would expect the extra gas near the Scorpius stars, which is probably cooler and denser than average, to exhibit larger $\langle$ Na I/H I $\rangle$ and $\langle$ Ca II/H I $\rangle$ ratios than usual—just the opposite to what is observed. It is possible, on the other hand, that the proximity of the stars to the gas may raise the ionizing radiation flux significantly above what is usually found in the galaxy.

c) Correlation of H I with Dust

A number of previous investigations have dealt with the relationship between interstellar hydrogen and interstellar dust. For a review of these observations see Kerr (1968). All these studies have utilized 21-cm emission or absorption data along with a number of different techniques to obtain line-of-sight extinction. However, our poor correlation of 21-cm and $L\alpha$ column densities exposes the weakness of the assumption that the 21-cm radio observations of the gas and the optical observations toward stars refer to the same regions of space. With the OAO $L\alpha$ absorption data and optical extinction data, one samples precisely the same regions of space so it is now possible to make a more reliable study of the H I to dust correlation.

Figure 9 shows the relationship between the OAO hydrogen column density and the E(B-V) color excess for all the stars included in Table 1. Lower case error symbols refer to B2 stars while capital letters refer to stars of spectral type earlier than B2. The subscript é on a symbol indicates an emission line star for which the computed E(B-V) color excess is probably affected by the emission.

In Figure 9 one can see a strong correlation between the hydrogen column density and color excess. The B2 stars do not lie significantly above the earlier type stars, which indicates that for B2 stars it is reasonable to assume that the stellar $L\alpha$ line is contained within the core of the interstellar line

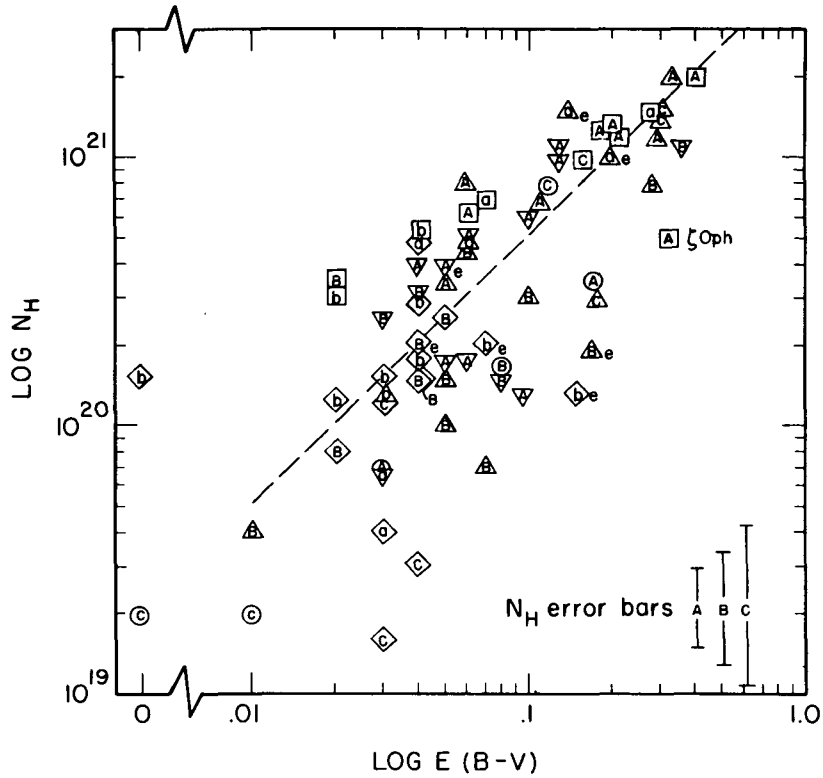

Figure 9.—A comparison of measured N_H versus B-V color excess for all of the stars observed. Symbols followed by an e are classified as emission line stars; we expect their E(B-V) values to be somewhat unreliable. Lower case error symbols identify the B2 stars. The dashed line represents our weighted average of 5×10^{21} atoms cm^{-2} mag^{-1} for the observed H I to E(B-V) ratios.

for most of the objects considered here. We found the situation to be quite different for stars of spectral type B2.5 or later. For these stars, it was apparent from the line strengths in unreddened objects that stellar $L\alpha$ was very strong. Because of these considerations we omitted all stars of spectral types later than B2 from this paper.

The points in Figure 9 show a fair amount of scatter. Some of this is definitely observational while some is definitely real. For example, several Be stars deviate significantly from the general correlation. In the figure the scatter is largest for stars with small color excesses. Much of this scatter can be understood as small errors ($0^m.02$) in the color excess determinations. In addition, the OAO column density measurements are less accurate for stars with small column densities due to the greater effect uncertainties in line blending

have on the L_α profiles.

The data plotted in Figure 9 can be used to estimate the mass density ratio of H I to dust in the interstellar medium. Previous estimates from the radio data are summarized by Kerr (1968). A mean of the numbers from various determinations (Kerr's Table 4) is $\langle \rho_{H\ I}/\rho_{dust} \rangle \approx 100$, although the determinations vary from a low of 8 to a high of 300. Using the OAO L_α data for stars other than Be stars and weighting each determination by the color excess we obtain,

$$\langle N_H/E(B-V) \rangle = 5 \times 10^{21} \text{ atoms cm}^{-2} \text{ mag}^{-1} \quad . \quad (8)$$

To relate H I and dust densities it is necessary to assume a grain model. The radio investigations mentioned above generally assumed a model consisting of a grain radius $A_g = 3 \times 10^{-5}$ cm, a grain density $\rho_g = 1$ gm cm^{-3}, and an extinction efficiency factor $Q = 2.0$. With this very simple model plus the assumption that the ratio of selective to total visual extinction $R_V = 3.0$, one can find from the relations given by Lilley (1955) and equation (8) that the OAO data imply $\langle \rho_{H\ I}/\rho_{dust} \rangle \approx 50$.

However, it is possible to obtain an improved estimate by using the best interstellar grain model presently available. The theoretical mixture of grains of graphite, silicon carbide and silicates of Gilra (1971) has been shown to reproduce reasonably well the basic observational data (including ultraviolet extinction) on interstellar grains. Gilra (1971) finds on the basis of his mixture of grains that a space density of 8×10^{-27} gm cm^{-3} is needed to produce 1 mag kpc^{-1} of extinction at the V filter. Again assuming $R_V = 3.0$ we find from equation (8) that this mixture implies $\langle \rho_{H\ I}/\rho_{dust} \rangle \approx 100$.

The general appearance of the distribution of points in Figure 9 suggests the existence of a relatively well-defined edge parallel to and above the dashed line which corresponds to the mean $N_H/E(B-V)$. On the other hand, there is a significant straggling of the points below the line. We could speculate that the upper edge (~2.5 times the number given in Equation 8) corresponds to an intrinsic total hydrogen to dust ratio, and that lower points in the diagram show evidence of varying degrees of depletion of atomic hydrogen by either molecule formation or ionization. One outstanding example of possible depletion is ζ Oph which is deficient of atomic hydrogen by about a factor of 3 from the average ratio we derived. The visual interstellar spectrum of ζ Oph is rich with molecular lines (Herbig 1968), and it is possible molecular hydrogen may also be abundant. McGee et al. (1963) observed a deficiency of 21-cm emission near ζ Oph which coincides with the Strömgren sphere for this O9.5 V star, but representative models for the size and density of the ionized re-

gion suggested by McGee et al. and Herbig imply the depletion of the observed N_H by ionization is negligible.

Carruthers (1970b) has observed a molecular hydrogen column density of 1.3×10^{20} molecules cm^{-2} in the direction of ξ Per. The fractional abundance by weight of molecular compared to atomic hydrogen implied by this number is about 0.13 if one uses the OAO hydrogen column density for ξ Per of 20×10^{20} atoms cm^{-2}. With such a low fractional abundance one might expect the $N_H/E(B-V)$ relation for ξ Per to be normal, and it is. An H_2 column density in the direction of ζ Oph of 5×10^{20} molecules cm^{-2} would explain the factor of 3 deficiency of H I. The implied difference in the H_2 abundance between these two stars might be explained by the fact that the far ultraviolet extinction in the direction of ζ Oph is much greater than for ξ Per (Bless and Savage 1972), and it is the far ultraviolet radiation field between 912 Å and 1108 Å that likely provides the destruction mechanism for the H_2 molecule (see Hollenbach et al. (1971) for a discussion on the formation and destruction of H_2).

V. CONCLUDING REMARKS

The primary data of our study are the hydrogen column densities toward the 69 stars listed in Table 1. The abstract summarizes a number of conclusions derived from a comparison of these column densities and other observables. We will not repeat these conclusions here but will indicate some additional projects that could be undertaken.

The comparison between 21-cm and L_α column densities discussed in § IVa would be more meaningful if one considered only the 21-cm observations with a small beam centered on each star and attempted to extract velocity components not appearing in the visual interstellar line data. For this project more star-centered radio observations are desirable.

In estimating the total sodium and calcium abundance ratios, it should soon become possible to reduce some of the uncertainties. The sky background ultraviolet flux used by Habing (1969) to estimate Γ can hopefully be replaced by OAO-2 broad-band photometry observations of this radiation field. Also, according to Hobbs (private communication), high resolution observations of the K line of Ca II should soon be available and will provide a more reliable Ca abundance estimate.

Column 19 of Table 1 contains data from Duke (1951), Stoeckly and Dressler (1964) and Wampler (1966) on the diffuse feature at 4430 Å. It should now be possible to investigate if this feature is more closely correlated with the interstellar gas or the interstellar dust. C. C. Wu (private communication) has undertaken an investigation of diffuse and semi-diffuse features in stars observed by the OAO. He has obtained

new observational data on the semi-diffuse features at 5780 Å and 5796 Å and will investigate the relationship between the central depths of 4430, 5780 and 5796 Å versus the L_α N_H, E(B-V) and E(2200 Å-V). In view of the work of Wu, we did not investigate the various correlations of diffuse features in this paper.

There remain a number of additional stars B2 or earlier for which L_α measurements can be made by OAO-2. We will try to observe these stars and fill some of the vacant areas in our sky coverage. Finally, as more high resolution prototype spectra become available, it should become possible to derive more accurate column densities for those OAO stars having large uncertainties. A rocket recently launched by the Kitt Peak National Observatory for the Princeton group obtained spectra for τ Sco (B0 V), κ Sco (B1.5 III) and λ Sco (B1.5 IV). Not only are these observations of excellent quality, but the actual column densities for the stars are relatively small so that reconstructions for small trial column densities will be more reliable.

Support for the preparation of this paper was provided by contracts NAS 5-1348 (for BDS) and NSr-31-001-901 (for EBJ) from the U. S. National Aeronautics and Space Administration. We wish to thank Dr. A. D. Code for making the OAO data available to us, and we are indebted to Drs. T. Houck, R. C. Bless, C. F. Lillie, A. Holm and M. Molnar for obtaining the observational material. Important contributions were made by C. C. Wu, who helped reduce the raw OAO data to derive useful L_α profiles, and J. Pritchard, who computed Na I column densities from the observations of Hobbs (1969). We are thankful to L. M. Hobbs for his helpful comments and advice about his high resolution measurements. Dr. G. R. Carruthers kindly provided us with an original tracing of his γ Ori spectrum. The Princeton rocket spectra were obtained on NASA flights 4.176UG, 4.226UG, and 4.271UG and were digitized by the microdensitometer at the Sacramento Peak Observatory. Finally, we wish to thank Mr. T. Matilsky for his help in deriving the intensity profiles of δ and π Sco and ζ Oph.

REFERENCES

Allen, C. W. 1963, Astrophysical Quantities, 2nd ed. (London: Athlone Press), p. 31.

Blaauw, A. 1963, Basic Astronomical Data, ed. K. Aa. Strand (Chicago: University of Chicago Press), p. 383.

Bless, R. C. and Savage, B. D. 1970, in Ultraviolet Stellar Spectra and Related Ground-Based Observations, I.A.U. Symp. No. 36, ed. L. Houziaux and H. E. Butler (Dordrecht: D. Reidel Publ. Co.), p. 28.

_____ 1972, preprint.

Bohlin, R. C. 1970, Ap. J. 162, 571.

Brandt, J. C., Stecher, T. P., Crawford, D. L. and Maran, S. P. 1971, Ap. J. 163, L99.

Buscombe, W. and Kennedy, P. M. 1968, M. N. R. A. S. 139, 417.

Carruthers, G. R. 1968, Ap. J. 151, 269.

_____ 1969, Ap. J. 156 L97.

_____ 1970a, Space Sci. Rev. 10, 459.

_____ 1970b, Ap. J. 161, L81.

Clark, B. G. 1965, Ap. J. 142, 1398.

Code, A. D. 1960, A. J. 65, 278.

Code, A. D., Houck, T. E., McNall, J. F., Bless, R. C. and Lillie, C. F. 1970, Ap. J. 161, 377.

Cousins, A. W. J. and Stoy, R. H. 1963, Bull. Roy. Obs. No. 64.

Davidson, K. and Terzian, Y. 1969, A. J. 74, 849.

Duke, D. 1951, Ap. J. 113, 100.

Dunham, T., Jr. 1941, Pub. A. A. S. 10, 50.

Field, G. B., Goldsmith, D. W. and Habing, H. J. 1969, Ap. J. 155, L149.

Gilra, D. P. 1971, Nature 229, 237.

Goldstein, S. J. and MacDonald, D. D. 1969, Ap. J. 157, 1101.

Gott, J. R., III and Ostriker, J. P. 1971, to appear in The Gum Nebula and Related Problems, ed. S. P. Maran, J. C. Brandt and T. P. Stecher, NASA.

Gum, C. S. 1955, Mem. R. A. S. 67, 155.

Habing, H. J. 1968, Bull. Ast. Inst. Netherlands 20, 120.

_____ 1969, Bull. Ast. Inst. Netherlands 20, 177.

Herbig, G. H. 1968, Z. Astrophysik 68, 243.

Hiltner, W. A., Garrison, R. F. and Schild, R. E. 1969, Ap. J. 157, 313.

Hjellming, R. M., Gordon, C. P. and Gordon, K. J. 1969, Astron. and Astrophys. 2, 202.

Hobbs, L. M. 1969, Ap. J. 157, 135.

_____ 1971, Ap. J. 166, 333.

Hollenbach, D. J., Werner, M. W., Salpeter, E. E. 1971, Ap. J. 163, 165.

Howard, W. E., Wentzel, D. G. and McGee, R. X. 1963, Ap. J. 138, 988.

Iriarte, B., Johnson, H. L., Mitchell, R. I. and Wisniewski, W. K. 1965, Sky and Telescope 20, 21.
Jenkins, E. B. 1970a, in Ultraviolet Stellar Spectra and Related Ground-Based Observations, I.A.U. Symp. No. 36, ed. L. Houziaux and H. E. Butler (Dordrecht: D. Reidel Publ. Co.), p. 281.
_____ 1970b, Presentation at Commission 44, I.A.U. 14th General Assembly (Brighton, England) August, 1970.
_____ 1971, Ap. J. 169, in press.
Jenkins, E. B. and Morton, D. C. 1967, Nature 215, 1257.
Jenkins, E. B., Morton, D. C. and Matilsky, T. A. 1969, Ap. J. 158, 473.
Johnson, H. L. 1963, Basic Astronomical Data, ed. K. Aa. Strand (Chicago: University of Chicago Press), p. 204.
Johnson, H. M. 1970, Ap. J. 160, 193.
_____ 1971, Ap. J. 164, 67.
Kerr, F. J. 1968, Nebulae and Interstellar Matter, ed. B. M. Middlehurst and L. H. Aller (Chicago: University of Chicago Press), p. 575.
Kerr, F. J. and Westerhout, G. 1965, in Galactic Structure, ed. A. Blaauw and M. Schmidt (Chicago: University of Chicago Press), p. 167.
Lang, K. R. 1971, Ap. J. 164, 249.
Lawrence, R. S. 1956, Ap. J. 123, 30.
Lerche, I. 1970, Astrophys. and Space Sci. 6, 287.
Lesh, J. R. 1968, Ap. J. Suppl. 17, 371.
Lilley, A. E. 1955, Ap. J. 121, 559.
Linblad, P. O. 1966, Bull. Ast. Inst. Netherlands Suppl. 1, 177.
McGee, R. X. and Milton, J. A. 1964, Australian J. Phys. 17, 128.
McGee, R. X., Milton, J. A. and Wolfe, W. 1966, Australian J. Phys., Astrophys. Suppl. No. 1, 3.
McGee, R. X. and Murray, J. D. 1961, Australian J. Phys. 14, 260.
McGee, R. X., Murray, J. D. and Milton, J. A. 1963, Australian J. Phys. 16, 136.
Menon, T. K. 1958, Ap. J. 127, 28.
Merrill, P. W., Sanford, R. F., Wilson, O. C. and Burwell, C. G. 1937, Ap. J. 86, 274.
Morton, D. C. 1967, Ap. J. 147, 1017.
Morton, D. C., Jenkins, E. B. and Brooks, N. H. 1969, Ap. J. 155, 875.
Muller, C. A. 1959, in Paris Symposium on Radio Astronomy, I.A.U. Symp. No. 9, ed. R. N. Bracewell (Stanford: Stanford University Press), p. 360.
Radhakrishnan, V., Murray, J. D. Lockhart, P. and Whittle, R. P. J. 1971, preprint.

Rodgers, A. W., Campbell, C. T., Whiteoak, J. B., Bailey, H. H. and Hunt, V. O. 1960, An Atlas of H-Alpha Emission in the Southern Milky Way (Canberra: Mount Stromlo Observatory).
Routly, P. M. and Spitzer, L., Jr. 1952, Ap. J. 115, 227.
Savage, B. D. and Code, A. D. 1970, in Ultraviolet Stellar Spectra and Related Ground-Based Observations, I.A.U. Symp. No. 36, ed. L. Houziaux and H. E. Butler (Dordrecht: D. Reidel Publ. Co.), p. 302.
Schmidt, M. 1957, Bull. Ast. Inst. Netherlands 13, 247.
Smith, A. M. 1969, Ap. J. 156, 93.
Spitzer, L., Jr. 1968, Diffuse Matter in Space (New York: Interscience), p. 67.
Spitzer, L., Jr., Epstein, I. and Hen, L. 1950, Ann. D' Ap. 13, 147.
Spitzer, L., Jr. and Zabriskie, F. R. 1959, Pub. A. S. P. 71, 412.
Stoeckly, R. and Dressler, K. 1964, Ap. J. 139, 240.
Strömgren, B. 1948, Ap. J. 108, 242.
Takakubo, K. 1967, Bull. Ast. Inst. Netherlands 19, 125.
Takakubo, K. and Van Woerden, H. 1966, Bull. Ast. Inst. Netherlands 18, 488.
Wampler, E. J. 1966, Ap. J. 144, 921.
Watanabe, K., Zelikoff, M. and Inn, E. C. Y. 1953, Absorption Coefficients of Several Atmospheric Gases, AFCRC Tech. Rep. No. 53-23.
Wiese, W. L., Smith, M. W. and Miles, B. M. 1969, Atomic Transition Probabilities, Vol. II (Washington: U. S. National Bureau of Standards).
Wisniewski, W. K. 1965, Sky and Telescope 30, 21.

Page intentionally left blank

PRELIMINARY RESULTS ON INTERSTELLAR REDDENING AS DEDUCED FROM FILTER PHOTOMETRY

Michel Laget*
National Aeronautics and Space Administration
Goddard Space Flight Center
Greenbelt, Maryland

ABSTRACT

Filter photometry has been used to derive the interstellar reddening law from stars through the study of a single spectral type, B0. The deficiency in the far ultraviolet flux of a supergiant relative to a main sequence star is compared with the difference in the flux distribution due to a change of one spectral class. Individual interstellar reddening curves show the general feature reported by Stecher (1969) and by Bless and Savage (1970). There is a large amount of scatter in the far ultraviolet which may be partially due to a real difference in interstellar extinction and partially due to observational inaccuracy. The mean ratio $E(m_\lambda-V)/E(B-V)$ computed from the color-color diagrams using a least squares fit to the reddening line shows an increasing probable error from long wavelength to short wavelength which cannot be explained by the expected mean instrumental error.

I. INTRODUCTION

The study of a single spectral type with the set of broad-band photometers on board the OAO-2 satellite is an appropriate means to observe the interstellar extinction from faint

---

*National Academy of Science Research Associate on leave from the Laboratoire d'Astronomie Spatiale, Les Trois Lucs 13, Marseille (12e), France.

stars which cannot be observed by the spectrum scanners. This type of observation provides additional data to recent results reported from relatively high resolution scans by Stecher (1969) and by Bless and Savage (1970) and allows us a statistical approach.

In this paper preliminary results are given about the interstellar reddening deduced from the study of twelve stars classified on the MK system as type B0. The visual magnitude ranges from 1.70 to 6.65; the maximum difference in B-V is 0.38. The choice of type B0 for this study is compatible with the following considerations: (i) a sufficient number of stars, including faint stars, was available to the satellite, (ii) the differential influence within the spectral type B0 of the strongest lines such as C IV and Si IV could be expected to be negligible in comparison to the FWHM of the band passes (about 250 Å), and (iii) problems of identifying correctly the effective wavelength are minimized. The effective wavelengths of the photometers are defined in terms of a uniform spectral intensity distribution.

II. THE OBSERVATIONAL DATA

The original signal for each star, in terms of number of counts, has been reduced in the way described by Code et al. (1970). In those cases in which the star was observed on more than one orbit, the mean value has been taken. Generally, the deviation was a few hundredths of a magnitude, but this remark does not refer to the filters ST4F1 (1550 Å) and ST4F3 (1430 Å) which have been corrected for a change in transmission with time. These corrections were made using information published by Holm (1972) and values derived from those stars observed several times in the course of several months. It appears that for filter ST4F3, in particular, the correction is large and uncertain. Filters ST4F5 (1680 Å) and ST4F4 (1330 Å) have not been used for the present work because of unreliable results which are suspected in ST4F5 and because ST4F4 covers the region of the L_α interstellar absorption line.

The ultraviolet extinction results are sensitive to the UBV characteristics of the star as well as to the spectral classification. In order to have a homogeneous set of stars we have used classifications by Lesh (1968), when available, or by Hiltner, Garrison and Schild (1969). Color excesses have been derived using the intrinsic colors of Johnson (1963). The data for all the stars used are summarized in Table 1, including the sources used. The observations are given in Table 2. Three stars are classified as B0.5 in the adopted sources although previously they were classified as B0. We shall assume that this difference has a negligible effect on the calculations presented in the next section.

Table 1. The Stars Observed

HD	Name	Sp	V	B-V	Ref	Remark
36512	υ Ori	B0 V	4.61	-0.28	L(A)	
36822	ϕ^1 Ori	B0.5 V	4.41	-0.17	L(A)	Spectral peculiarities noted by Lesh
37128	ε Ori	B0 Ia	1.70	-0.19	L(A)	
48434		B0 III	5.86	-0.02	L(A)	Monoceros. Spectral peculiarities noted by Lesh
122879		B0 Ia	6.41	+0.11	H	Centaurus
143275	δ Sco	B0.5 V	2.30	-0.11	H	
149038	μ Nor	B0 Ia	4.89	+0.08	H	
149438	τ Sco	B0 V	2.82	-0.25	H	
150898		B0.5 Ia	5.56	-0.08	H	Ara
202214		B0 V	5.64	+0.10	L(A)	Cepheus: Binary Δm_V=1
204172	69 Cyg	B0 Ib	5.94	-0.10	L(A)	Triple, Δm_V = 3
206773		B0 Vpe	6.93	+0.20		Cepheus
209339		B0 IV	6.65	+0.07	L(A)	Cepheus: Binary Δm_V=2

L: Lesh (1968). (A): Crawford. H: Hiltner et al. (1969).

Table 2. *The Observed Magnitudes* m_λ

HD	ST1F3 4250	ST1F1 3320	ST1F4 2980	ST2F2 2940	ST2F5 2390	ST2F1 2030	ST3F2 2460	ST3F1 1910	ST4F1 1550	ST4F3 1430
36512	-4.18	-3.29	-3.46	-3.69	-3.44	-3.26	-2.37	-1.25	-0.94	-0.93
36822	-4.28	-3.27	-3.36	-3.57	-3.11	-2.82	-2.11	-0.84	-0.38	(-0.36)
37128							(-4.91)	-3.31	-2.93	-2.99
48434	-2.69	-1.56	-1.54	-1.80	-1.00	-0.48	-0.06	(+1.10)	(+1.10)	(+1.13)
122870	-2.35	-0.94	-0.82	-1.04	+0.05	+0.45	+0.84	+2.49	+2.94	+3.1
143275							-3.92	-2.61	-2.25	-2.03
149038	-3.57	-2.42	-2.34	-2.57	-1.61	-0.92	-0.64	+0.88	+1.39	+1.46
149438							(-4.06)	-2.85	-2.54	-2.63
150898	-3.03	-2.03	-2.06	-2.35	-1.72	-1.24	-0.72	+0.74	+1.44	+1.43
202214	-2.86	-1.55	-1.41	-1.68	-0.49	-0.07	+0.38	+1.8	+2.15	+2.40
204172	-2.78	-1.71	-1.73	-1.97	-1.35	-0.88	(-0.23)	+0.90	+1.97	+2.05
209339	-1.88	-0.65	-0.57	-0.73	+0.20	+0.55	+1.09	+2.64	+3.15	+3.10

III. THE COLOR-COLOR DIAGRAMS

Diagrams of $(m_\lambda - V)$ vs. $(B-V)$ for representative effective wavelengths are shown in Figure 1. Mean reddening lines have

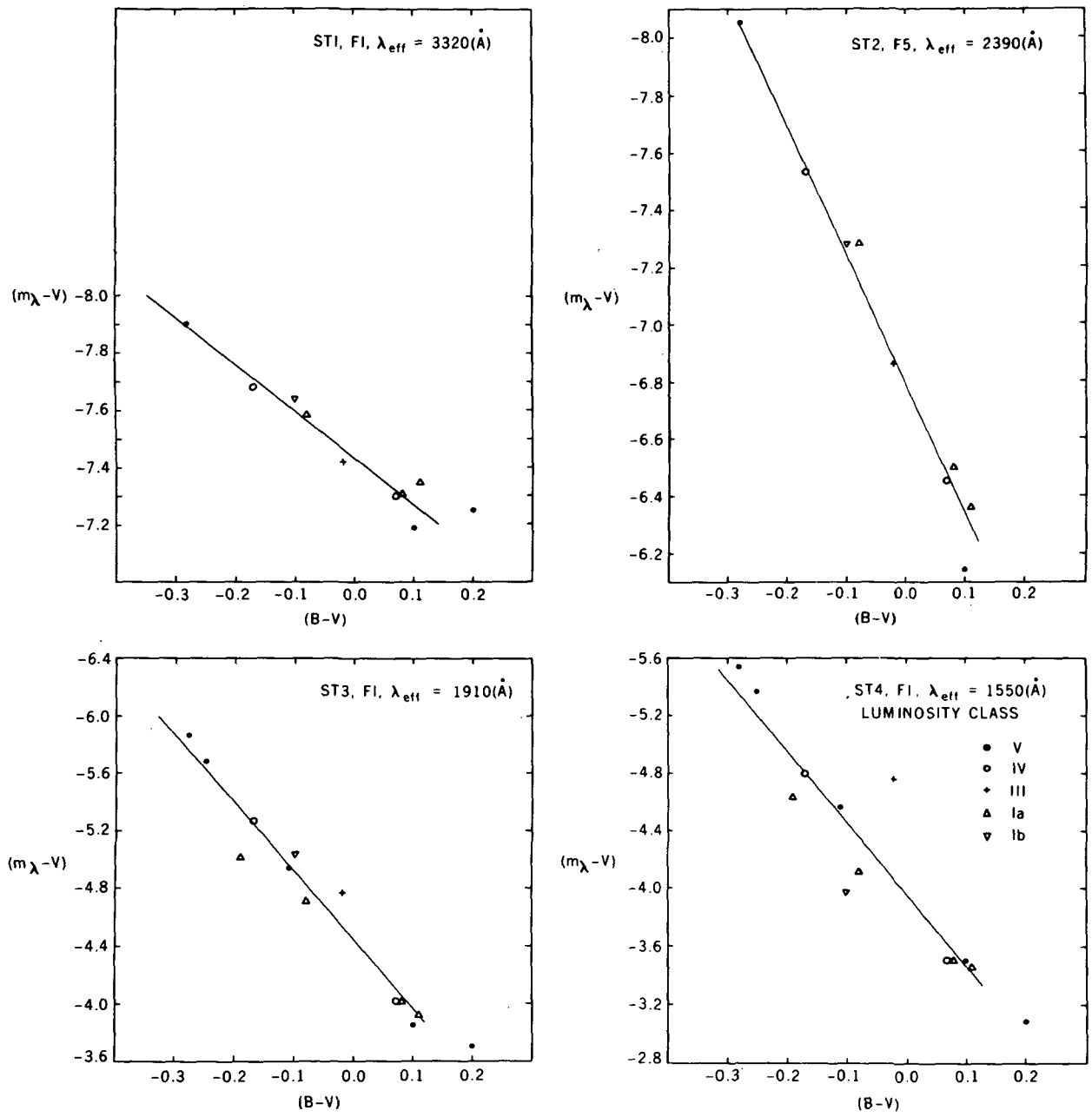

Figure 1.—Color-color diagrams for representative effective wavelengths. Note the increase of the scatter around the reddening line with decreasing wavelength.

been obtained by a least squares fit of a straight line to the observed points. The slopes of the reddening lines and their probable errors are listed in Table 3 together with the standard deviations. The scatter of the points is due to instrumental errors, possible errors in V and in (B-V), differences in the interstellar extinction and in the intrinsic properties of the stars themselves. The slope of the straight line represents a mean ratio $\Delta(m_\lambda - V)/\Delta(B-V)$ which can be used to estimate the ultraviolet extinction when the E(B-V) is known. The star HD 206773 (B0 Vpe) has been left out of the calculations.

Table 3. Statistical Properties of the Observed Reddening Lines

λ_{eff} (Å)	Stand. Dev.	$\frac{\Delta(m_\lambda - V)}{\Delta(B-V)}$	p.e.	λ^{-1} (μ^{-1})
4250	0.03	0.81	0.06	2.35
3320	0.05	1.63	0.08	3.01
2980	0.05	2.36	0.09	3.36
2940	0.06	2.41	0.10	3.40
2460	0.08	4.03	0.12	4.07
2390	0.09	4.62	0.15	4.18
2030	0.10	5.23	0.18	4.93
1910	0.14	4.71	0.21	5.24
1550	0.28	4.96	0.42	6.45
1430	0.30	5.29	0.44	6.99

The large standard deviations obtained for the filters with effective wavelengths shorter than 2000 Å may be due to intrinsic differences in the far ultraviolet spectra of the program stars. Bless and Savage have shown that for stars of the same spectral type but luminosity classes in the range II to V, the spectral distribution is closely the same. In order to investigate what differences may appear in the filter photometry, differences in magnitude between a supergiant and a

main sequence star (ε Ori, υ Ori) and between two main sequence stars (τ Sco, υ Ori) all of type B0 are shown in Figure 2. The differences are normalized to zero at the effective wavelength of the V pass band. The difference between types B0.5 V and B0 V is shown by the pair (λ Lep, ν Ori). Each of these stars has E(B-V) < 0.05, thus differential reddening is minimal.

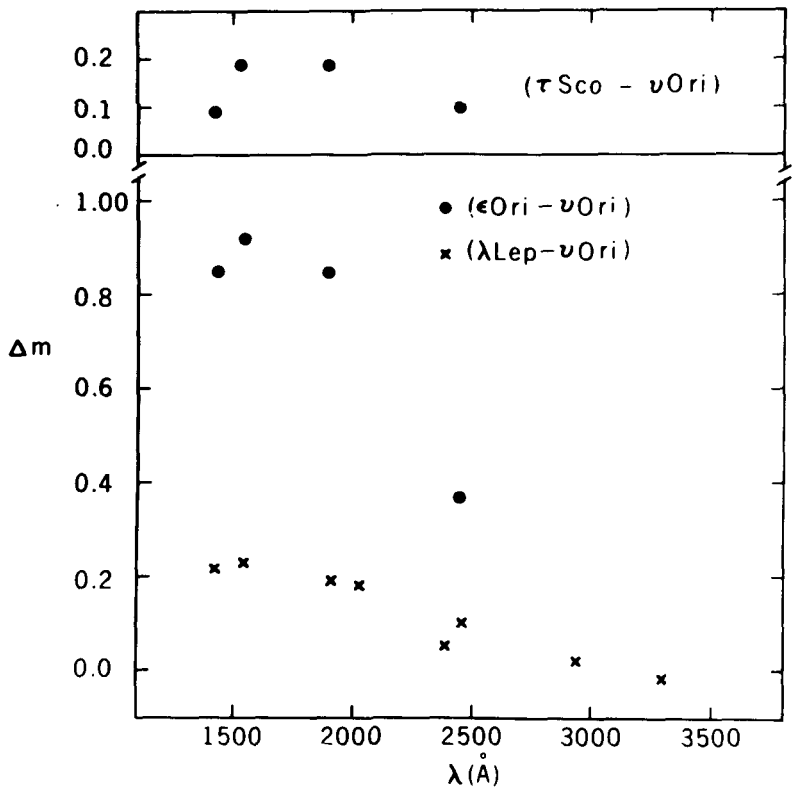

Figure 2.—Differences in magnitudes of the ultraviolet energy distribution of stars of similar spectral types relative to the visual magnitude.

The supergiant shows a large ultraviolet deficiency in comparison to a main sequence star. A similar deficiency was found by Carruthers (1969) at 1115 Å for ε Ori. Mihalas (1970) has commented upon this in terms of a decrease in the surface gravity and in effective temperature from main sequence to supergiant stars.

IV. THE WAVELENGTH DEPENDENCE OF THE INTERSTELLAR EXTINCTION

By comparing the spectral distribution of a reddened star with that of an unreddened star of the same spectral type and

luminosity class, one can deduce the wavelength dependence of the interstellar extinction in the different directions of the stars. This method assumes that stars of the same spectral type and luminosity class have identical flux distributions.

Figure 3 illustrates five reddening curves obtained by comparing four main sequence stars to the reference star υ Ori and one supergiant to ε Ori. The data are normalized to a difference in (B-V) = 1 mag for the pairs of stars considered and for ΔV = 0. The observed values of ϕ^1 Ori and δ Sco have been corrected from B0.5 to B0 using values given in Figure 2 for the pair (λ Lep, υ Ori). The shadowed area represents the probable error around the mean values computed in § III.

On the whole, the points show a maximum between 4.18 and 4.93 μ^{-1} and a minimum between 5.24 and 6.45 μ^{-1}. The profile of the maximum has been given by Stecher (1965,1969) and Bless and Savage (1970). The first explanations that the maximum is

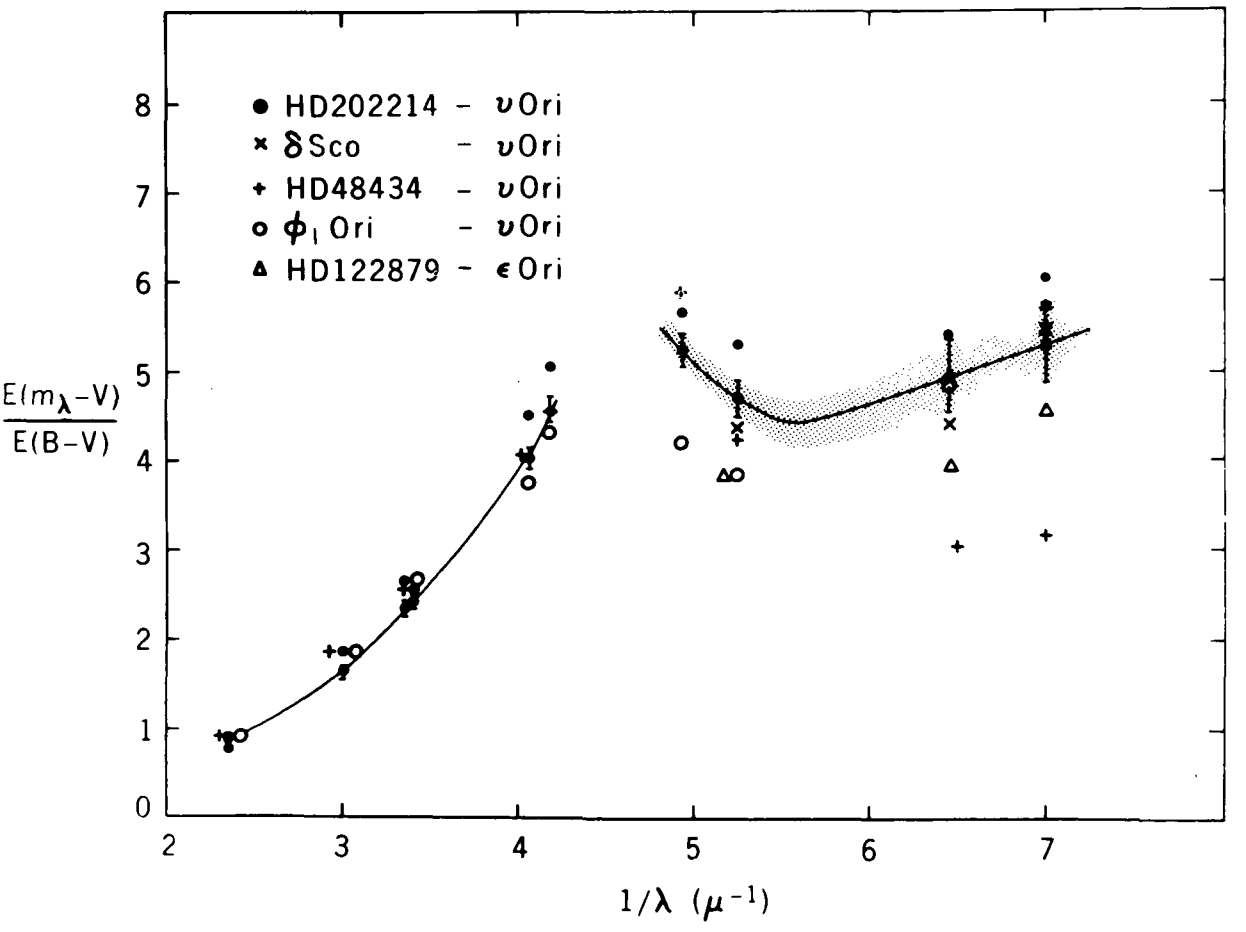

Figure 3.—Interstellar reddening found for HD 209339 compared with that for ζ Oph (Gilra 1971).

due to graphite particles were given by Stecher and Donn (1965) and by Wickramasinghe and Guillaume (1965).

The interstellar extinction law is known to vary in the visible and in the infrared (Johnson 1968). Figure 3 shows for representative pairs of stars that in the range 4.93 to 7 μ^{-1} the interstellar extinction seems to differ significantly from the average value. It is therefore of importance to find out whether or not this scatter is a real effect which can be attributed to an intrinsic property of the interstellar medium.

For such a purpose we must note first that a probable error of 0.1 mag in the difference between two stars is on the average magnified by a factor of 4 because $\langle \Delta(B-V) \rangle = 0.25$, and secondly, that points lying within 2 or 3 probable errors cannot be interpreted as basically deviant from the mean curve.

It follows that the case obtained for the star HD 48434 is significantly peculiar. However, it cannot be considered to be representative of a low interstellar extinction because of an uncertainty, difficult to evaluate, in the technical reduction of the far ultraviolet data.

The star HD 202214 is slightly above the mean curve but it cannot be considered to be different. This star is double with a companion 1 mag fainter than the primary component.

The stars ϕ^1 Ori and HD 122879 present an intermediate case. The uncertainties in the data in the far ultraviolet fall in the area corresponding to 2 or 3 p.e., while in the region 4.93 to 5.24 μ^{-1} a real deviation seems to be present, indicating that for these two cases the values of the interstellar extinction may be below the average.

The curve obtained for the star HD 209339, shown in Figure 4, has a peculiar profile which deserves additional comments. Indeed, the values obtained are within 2 p.e., indicating that this profile is not statistically different from the mean. But apparently there is no minimum in the range 4.93 to 7 μ^{-1}. The star HD 209339 is double with a companion 0.6 arc sec distant and 2 mag fainter. In addition, since this star is a standard B0 IV star in the Lesh classification system it is unlikely that the observed differences in the reddening curve are due to misclassification. It cannot be excluded that the wavelength dependence of the interstellar extinction in the direction of HD 209339 might be unusual, presenting some similarities with the results found for ζ Oph by Bless and Savage (1970).

V. DISCUSSION

In the case considered here, there are two ways in which to deduce the wavelength dependence of the interstellar reddening profiles:

1. Individual profiles deduced from the comparison of

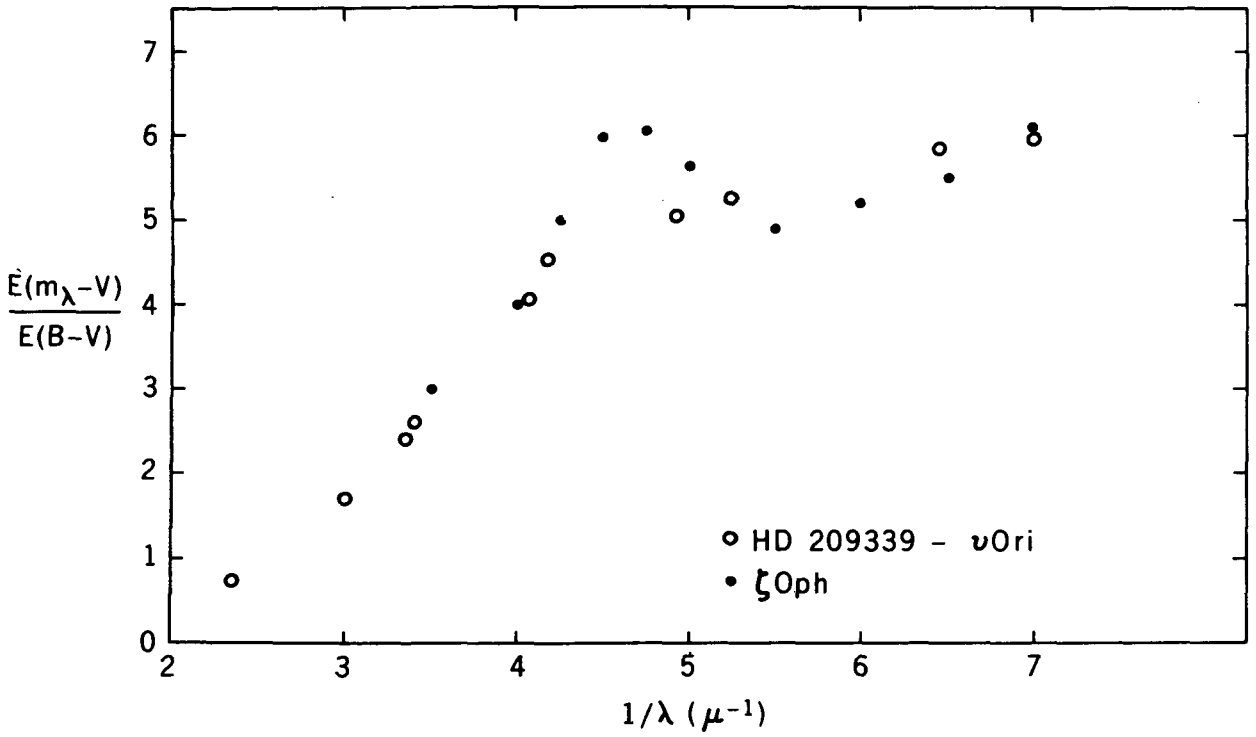

Figure 4.—The wavelength dependence of the interstellar reddening obtained from pairs of stars and from a statistical method.

pairs of stars. In this case each curve is sensitive to the accuracy of V, (B-V) and m_λ. The largest uncertainty is in Δm_λ between the two stars. The stars used generally have been observed at different epochs and it is difficult at present to give an upper limit to the expected accuracy at each time.

2. A statistical approach, considering all the stars as a whole, without any discrimination of luminosity class. The least squares fit to the straight line

$$m_\lambda - V = a(B-V) + b$$

is used at each wavelength. We can evaluate the error in m_λ from the mean error found by considering the results for several stars observed several times at different epochs.

We have pointed out in § IV that the first method gives peculiar results significantly different from the mean, and that among the sample of stars used it is difficult to evaluate whether or not these differences indicate real differences in the reddening law.

An attempt to understand the constant increase from long

wavelength to short wavelength of the standard deviation and of the probable error around the mean value found in case 2 can be made by estimating the statistical errors. We shall take the probable error of 0.42 computed for the 1550 Å filter as representative.

At this step we must briefly review the hypotheses used:

(1) All the stars have the same intrinsic spectral distribution.

(2) There is a linear relationship between $(m_\lambda - V)$ and $(B-V)$. The slope is the same for any luminosity class, and is characteristic of the interstellar medium.

(3) The method of least squares fit can be applied for twelve stars and the probable error of the derived slope is independent of intrinsic differences between main sequence stars and supergiants. This is confirmed by the fact that the probable errors computed separately in the sample case are respectively ±0.48 and ±0.33 for main sequence stars and supergiants.

Under these hypotheses, mean errors of ±0.1 mag in m_λ, ±0.04 on the correction added to allow for the variation of the sensitivity with time, and ±0.02 on V and (B-V) give an expected total probable mean instrumental error of ±0.11 mag in the derived mean slope.

It turns out that the instrumental error cannot explain the total probable error found. We conclude that a "natural" scatter of the data exists which can be attributed to a local change in the physical properties of the interstellar medium.

I am grateful to Prof. A. D. Code of the University of Wisconsin for the opportunity to make these observations with the OAO-2 as part of the Goddard Space Flight Center Guest Observer Program.

Also, I would like to thank Dr. A. B. Underhill, Dr. A. Boggess and Mr. L. Dunkelman for helping me in the completion of this work.

My thanks are extended to the National Academy of Science for the grant of a Research Associateship tenable at Goddard Space Flight Center.

REFERENCES

Bless, R. C. and Savage, B. D. 1970, I.A.U. Symp. No. 36, 28.
Carruthers, G. R. 1969, Ap. and Space Sci. 5, 387.
Code, A. D., Houck, T. E., McNall, J. F., Bless, R. C. and Lillie, C. F. 1970, Ap. J. 161, 377.
Gilra, D. P. 1971, Nature 229, 237.
Hiltner, W. A., Garrison, R. F. and Schild, R. E. 1969, Ap. J. 157, 313.

Holm, A. V. 1972, this volume.
Johnson, H. L. 1963, Basic Astronomical Data, ed. K. Aa. Strand (Chicago: University of Chicago Press), p. 204.
Lesh, J. R. 1968, Ap. J. Suppl. 17, 371.
Mihalas, D. 1970, Ap. and Space Sci. 8, 50.
Stecher, T. P. 1965, Ap. J. (Letters) 142, 1683.
Stecher, T. P. and Donn, B. 1965, Ap. J. (Letters) 142, 1681.
Stecher, T. P. 1969, Ap. J. (Letters) 157, L125.
Wickramasinghe, N. C. and Guillaume, C. 1965, Nature 207, 366.

COLLECTIVE EXCITATIONS AND DUST PARTICLES IN SPACE

D. P. Gilra
University of Wisconsin
Madison, Wisconsin

ABSTRACT

Due to collective processes small solid particles exhibit very strong resonances in absorption and scattering in the spectral regions in which ε_1, the real part of the dielectric constant, is negative. The precise positions depend on the particle shape, size and on the nature and amount of coatings it might have. A comprehensive discussion of these resonances is given in the Rayleigh approximation.

It is shown that the observed bands at 2200 Å and in the 10 μ region are most probably due to such collective excitations. Some other processes are also considered and are shown to be relatively inefficient and inadequate. The following specific conclusions are drawn: (a) the 2200 Å interstellar band is very likely due to graphite particles; (b) these graphite particles should be very small, approximately spherical, and should have no coating whatsoever; (c) the identification of circumstellar and interstellar silicates from the observations in the 10 μ region does not seem to be correct; (d) very valuable information about the shape of the circumstellar and interstellar dust particles can be obtained directly from observations; (e) narrow band polarization measurements in the spectral regions of these bands will be very helpful in determining the shape of the particles.

I. INTRODUCTION

Recent OAO-2 observations of the interstellar extinction curve have been discussed by Bless and Savage (1972; see also this volume). The observations show large intrinsic varia-

tions. Bless and Savage have concluded that a multi-component model of interstellar grains, such as I had proposed earlier (Gilra 1970, 1971), is needed to explain the observations.

The most significant feature in the entire extinction curve is the ultraviolet bump at about $\lambda^{-1} = 4.6\ \mu^{-1}$. The observations indicate that, in general, this feature is very strong, has a quite symmetrical profile, and is not "flat-topped". Also, the variations in the position of the extinction maximum are very small. In this paper our main concern is to identify the physical process and the substance which can give rise to such a feature at this wavelength (about 2170 Å).

It seems, as will be shown below, that the most plausible process which can satisfactorily explain this band is that of plasma oscillations. This process was introduced in astronomy by Unsöld (1964) to explain the diffuse interstellar band at 4430 Å. He also mentioned that the position of the resonance due to this process (plasma resonance) shifts to longer wavelengths as the size of the particles is increased, but he did not explain this effect. It was pointed out by van de Hulst (1964) that the strength and position of plasma resonances depend on the shape of the particles. Apart from the work of Unsöld (1964) and that of van de Hulst (1964) there is no discussion of this process in the astronomical literature. Similar resonances occurring in the infrared for some solids will be discussed. Observations also indicate a band in the 10 μ region (Woolf and Ney 1969, Hackwell et al. 1970).

It will be shown that the theoretical resonances occur due to "collective" processes. A comprehensive discussion of these resonances will be given in the small-size limit. In this limit they can be studied with the help of solutions of relatively simple problems in electrostatics. The following cases will be considered: homogeneous ellipsoids, coated ellipsoids, and ellipsoids with anisotropic optical properties. A very brief discussion of the effect of particle-size on the position of the resonances will be given. The physical processes which give rise to these resonances will be mentioned.

Next, the astronomical observations in the ultraviolet and infrared will be compared with the theoretical results. Some other physical processes will also be considered and the suggested identifications will be critically examined. Finally, some observationally verifiable predictions will be made.

II. THEORY

a) Small Homogeneous Ellipsoidal Particles

Let us discuss absorption and scattering by homogeneous ellipsoidal particles in the Rayleigh approximation. For a field applied along one of the main axes ($j = 1,2,3$) of the ellipsoid,

the polarizability α_j is a tensor and is written as (van de Hulst 1957, 1964)

$$\alpha_j = \frac{V}{4\pi} \frac{\varepsilon-\varepsilon_m}{L_j(\varepsilon-\varepsilon_m) + \varepsilon_m} \quad , \tag{1a}$$

where V is the volume of the particle, ε its dielectric constant, ε_m is the dielectric constant of the medium, the L_j depend on the ratios of the axes, and the values $4\pi L_j$ are known as the depolarization factors. The L_j satisfy the condition $0 \leq L_j \leq 1$, with the property $\sum_j L_j = 1$. If $m = n - ik$ is the complex refractive index, we have $\varepsilon \equiv m^2 = \varepsilon_1 - i\varepsilon_2 = n^2 - k^2 - i2nk$. If the particle is in free space, $\varepsilon_m = 1$, and equation (1a) reduces to

$$\alpha_j = \frac{V}{4\pi} \frac{\varepsilon-1}{L_j(\varepsilon-1) + 1} \tag{1b}$$

Equations (1a) and (1b) apply to the case of long elliptical cylinders also (van de Hulst 1957, p. 71).

The scattering cross-section, C^j_{sca}, and the absorption cross-section, C^j_{abs}, are given by

$$C^j_{sca} = \frac{8\pi}{3} \left(\frac{2\pi}{\lambda}\right)^4 |\alpha_j|^2 \quad , \tag{2}$$

and

$$C^j_{abs} = 4\pi\left(\frac{2\pi}{\lambda}\right) \mathrm{Re}(i\alpha_j) \quad , \tag{3}$$

where Re means "the real part of". Putting the value of α_j from (1a) in (2) and (3), we get

$$C^j_{sca} = \frac{8\pi^3}{3} \frac{V^2}{\lambda^4} \frac{(\varepsilon_1-\varepsilon_m)^2 + \varepsilon_2^2}{\{L_j\varepsilon_1+\varepsilon_m(1-L_j)\}^2 + (L_j\varepsilon_2)^2} \quad , \tag{4}$$

and

$$C^j_{abs} = \frac{2\pi}{\lambda} V \frac{\varepsilon_m\varepsilon_2}{\{L_j\varepsilon_1+\varepsilon_m(1-L_j)\}^2 + (L_j\varepsilon_2)^2} \quad . \tag{5}$$

Here we have assumed that ε_m is real; we shall also assume that its value does not change with wavelength.

From equations (4) and (5) we see that there is a resonance in the absorption and scattering cross-sections at the wave-

lengths where

$$L_j\varepsilon_1 + \varepsilon_m (1-L_j) = 0 \quad , \tag{6}$$

and $L_j\varepsilon_2 < 1$. This is because, as pointed out by van de Hulst (1964), the polarizability of the particles is very large as can be seen from equation (1a). As we see from equation (6) there is one resonance corresponding to each value of L_j. We therefore have three resonances for an ellipsoid, two for a spheroid and one for a sphere. These resonances occur where ε_1, the real part of the dielectric constant, is negative and are confined roughly within the maximum of ε_2, corresponding to $L_j = 0$, and the maximum of $(\varepsilon_1^2 + \varepsilon_2^2)^{-1}$, corresponding to $L_j = 1$. This is the case of a thin disc. The location of the particle in a medium of dielectric constant ε_m or in free space ($\varepsilon_m = 1$) does not affect the position of these boundaries. However, for intermediate values of L_j, the resonances in the case of free space are at

$$\varepsilon_1 = -\{(1/L_j) - 1\} \quad , \tag{7a}$$

and in the case of a medium at

$$\varepsilon_1 = -\varepsilon_m\{(1/L_j) - 1\} \quad . \tag{7b}$$

When discussing real solids we shall see that these conditions imply a shift in the position of the resonances to lower energies (or longer wavelengths) as the particles are placed in a medium of dielectric constant ε_m because of the way ε_1 varies with wavelength. As an example we take the case of a spherical particle. $L_1 = L_2 = L_3 = 1/3$, and in free space the resonance is at $\varepsilon_1 = -2$, whereas if the particle is in a medium of dielectric constant ε_m, the resonance occurs at $\varepsilon_1 = -2\varepsilon_m$, that is, at a higher negative value of ε_1.

We may remark in passing that C_{sca} has a minimum which occurs on the higher energy side of the resonance. The conditions from equation (4) are $\varepsilon_1 = \varepsilon_m$ and $\varepsilon_2 = 0$. These are the same conditions which give a minimum in the reflectivity, and the frequency at which these are satisfied in the infrared is known as the Christiansen frequency.

b) Size Dependence

As the size of spherical particles is increased the resonance shifts to longer wavelengths (Unsöld 1964). Similar results are obtained for spherical graphite particles (see, e.g., Gilra 1971). For very small sized graphite particles the extinction maximum is at about 2100 Å and as the mean size is increased the feature becomes broader and the maximum shifts

to longer wavelengths. We have to use the Mie theory to explain this (see, e.g., Doyle and Agarwal 1965, Ruppin and Englman 1968). A detailed discussion of size dependence will be given elsewhere (Gilra 1972). We just note that as the first departures from the Rayleigh approximation become apparent and we consider only the electric dipole term, the resonance occurs at a higher negative value of ε_1 given by

$$\varepsilon_1 = -2 - \frac{12}{5} x^2 \quad , \tag{8}$$

where $x = 2\pi a/\lambda$ and a is the radius. This result can be readily obtained from an equation given by van de Hulst (1964, p. 28), though he does not seem to have noticed this.

As the mean size becomes quite large the resonance becomes broad and shallow as can be seen in the extinction curves of SiC (Gilra 1971, Figure 2). The broad shallow feature shortward of about 1800 Å seen in that figure is due to such a resonance. Once again this resonance is to the high energy side of the maximum of ε_2.

c) Effect of Coatings

Let us consider an ellipsoid of dielectric constant ε_i having a coating in the shape of a confocal ellipsoid and a dielectric constant ε_o. Let this compound ellipsoid be placed in free space. Following Stepin (1965) and Bilboul (1969) we can derive an expression for the polarizability, α, for such an ellipsoid. For a field applied along one of the main axes the polarizability is given by

$$\alpha = \frac{V}{4\pi} \frac{(\varepsilon_o-1)\{L_i(\varepsilon_i-\varepsilon_o) + \varepsilon_o\} + \frac{V_i}{V}(\varepsilon_i-\varepsilon_o)\{L(1-\varepsilon_o)+\varepsilon_o)\}}{\{(\varepsilon_i-\varepsilon_o)L_i+\varepsilon_o\}\{1+L(\varepsilon_o-1)\} + \frac{V_i}{V} L(1-L)(\varepsilon_i-\varepsilon_o)(\varepsilon_o-1)}, \tag{9}$$

where V_i is the volume of the inner ellipsoid, V is the total volume, and $4\pi L_i$ and $4\pi L$ are the depolarization factors of the inner ellipsoid and the total ellipsoid respectively. For the sake of clarity we have suppressed the direction dependence. If $V_i/V = 0$, or $V_i/V = 1$, or $\varepsilon_i = \varepsilon_o$, or $\varepsilon_o = 1$, this equation reduces to equation (1b) for the case of homogeneous ellipsoids. If $\varepsilon_i = 1$, we get an expression for the polarizability of a hollow shell whose inner and outer surfaces are confocal ellipsoids.

In the degenerate cases, thin discs, spheres and thin needles, we have $L_i = L$. For coated spheres $L_i = L = 1/3$ and the result is identical to that obtained for the small size case from the rigorous solution (Güttler, 1952, van de Hulst 1957, p. 74). For a thin disc, or a highly flattened oblate spheroid, $L_i = L$ and there are two values of L, $L = 0$ and

L = 1. The results are quite interesting.
For L = 0,

$$\alpha = \frac{V}{4\pi}\{(1-\frac{V_i}{V})(\varepsilon_o-1) + \frac{V_i}{V}(\varepsilon_i-1)\}$$

or,
$$\alpha = \{\frac{V_o}{4\pi}(\varepsilon_o-1) + \frac{V_i}{4\pi}(\varepsilon_i-1)\} \quad , \tag{10}$$

and for L = 1,

$$\alpha = \frac{V}{4\pi}\{(1-\frac{V_i}{V})\frac{\varepsilon_o-1}{\varepsilon_o} + \frac{V_i}{V}\frac{\varepsilon_i-1}{\varepsilon_i}\}$$

or,
$$\alpha = \{\frac{V_o}{4\pi}\frac{\varepsilon_o-1}{\varepsilon_o} + \frac{V_i}{4\pi}\frac{\varepsilon_i-1}{\varepsilon_i}\} \quad , \tag{11}$$

where V_o is the volume of the shell and V_i is the volume of the inner ellipsoid. On comparing equations (10) and (11) with equation (1b) we note that the polarizability of such a compound disc (or, for limiting values of L) is equal to the sum of the polarizability of two separate thin discs having the volumes V_o and V_i, and with dielectric constants ε_o and ε_i respectively.

Scattering and absorption cross-sections in the Rayleigh approximation for compound ellipsoids can be calculated by using the value of polarizability from equation (9) in equations (2) and (3) respectively. The case of a compound thin disc is simple; we can use equations (10) and (11) in equations (2) and (3). For such a thin disc as in the case of polarizability, the absorption cross-section also is the sum of the absorption cross-sections of two separate thin discs having the volumes V_o and V_i, and dielectric constants ε_o and ε_i respectively. For other cases the final expression for C_{abs} and C_{sca} are somewhat complicated if both ε_i and ε_o are complex but they become relatively simple if ε_o is real. Before we write the expressions, let us compare the results for the case of a thin needle, or a highly elongated spheroid ($L = L_i$; $L = 0$ and $L = 1/2$), with those for a coated infinite circular cylinder in the small radius limit.

From the rigorous solution of Kerker and Matijević (1961) for perpendicular incidence, I have obtained the following dominant terms (up to x^2) in the approximation that the total radius is much smaller than the wavelength both outside and inside the cylinder. For the TE mode (E ⊥ symmetry axis) the

dominant term is

$$a_1 = \frac{i\pi x^2}{4}\left\{\frac{(\varepsilon_o-1)(\varepsilon_i+\varepsilon_o) + q^2(\varepsilon_i-\varepsilon_o)(1+\varepsilon_o)}{(\varepsilon_i+\varepsilon_o)(1+\varepsilon_o) + q^2(\varepsilon_i-\varepsilon_o)(\varepsilon_o-1)}\right\}$$
$$\equiv \frac{i\pi x^2}{4} A \text{ , say,} \qquad (12a)$$

and for the TM mode (E || symmetry axis) it is

$$b_o = \frac{i\pi x^2}{4}\{(1-q^2)(\varepsilon_o-1) + q^2(\varepsilon_i-1)\} \text{ ,}$$
$$\equiv \frac{i\pi x^2}{4} B, \text{ say,} \qquad (12b)$$

where $x = 2\pi r/\lambda$, r is the total radius, $q = r_i/r$, and r_i is the inner radius, and as before, ε_o and ε_i are dielectric constants of the shell and core respectively. These reduce in the appropriate limits to the case of a thin homogeneous infinite cylinder. C_{ext}, the extinction cross-section <u>per unit length</u> and C_{sca}, the scattering cross-section <u>per unit length</u> for the two cases are given by

TE mode:
$$C_{ext} = 2r \cdot \frac{2}{x} \mathrm{Re}(2a_1) \text{ ,}$$
$$C_{sca} = 2r \cdot \frac{2}{x} \cdot 2|a_1|^2 \text{ ;} \qquad (13)$$

TM mode:
$$C_{ext} = 2r \cdot \frac{2}{x} \mathrm{Re}(b_o) \text{ ,}$$
$$C_{sca} = 2r \cdot \frac{2}{x} |b_o|^2 \text{ .} \qquad (14)$$

Let us now compare the cross-sections for a thin infinite circular cylinder with those of a small highly elongated prolate spheroid. The TE mode corresponds to L = 1/2 and the TM mode to L = 0 for the highly elongated prolate spheroid. In terms of A and B, as defined in equations (12a) and (12b), the polarizabilities for a small highly elongated prolate spheroid are,

$$\text{for } L = 1/2, \quad \alpha = (V/4\pi)2A, \qquad (15)$$

$$\text{and for } L = 0, \quad \alpha = (V/4\pi)B, \qquad (16)$$

where we have made use of the fact that in this case $V_i/V = q^2$. If ℓ is the major axis and r the semi-minor axis of the whole spheroid, $V = 2/3\ \pi r^2 \ell$. The absorption and scattering cross-sections can now be calculated with the help of equations (3)

and (2) respectively. We note that for absorbing particles in this approximation $C_{ext} = C_{abs}$ and we can compare the two in a straightforward way.

So that a direct comparison is possible the cross-sections for the two cases, thin infinite circular cylinder and small highly elongated prolate spheroid, are presented in a tabular form. We note that for the former case the tabulated cross-sections are per unit length.

Thin Infinite Circular Cylinder	Small Highly Elongated Prolate Spheroid
TE mode:	L = 1/2:
$C_{ext} = \frac{2\pi}{\lambda} \cdot \pi r^2 \cdot 2 \cdot [\mathrm{Re}(iA)]$	$C_{abs} = \frac{2\pi}{\lambda} \cdot \frac{2}{3} \pi r^2 \ell \cdot 2 \cdot [\mathrm{Re}(iA)]$
$C_{sca} = \frac{\pi^2 r}{2} \cdot (2\pi r/\lambda)^3 \cdot [\lvert A \rvert^2]$	$C_{sca} = \frac{8}{27} \pi \ell^2 \cdot (2\pi r/\lambda)^4 \cdot [\lvert A \rvert^2]$
TM mode:	L = 0:
$C_{ext} = \frac{2\pi}{\lambda} \cdot \pi r^2 \cdot [\mathrm{Re}(iB)]$	$C_{abs} = \frac{2\pi}{\lambda} \cdot \frac{2}{3} \pi r^2 \ell \cdot [\mathrm{Re}(iB)]$
$C_{sca} = \frac{\pi^2 r}{4} \cdot (2\pi r/\lambda)^3 \cdot [\lvert B \rvert^2]$	$C_{sca} = \frac{2}{27} \pi \ell^2 \cdot (2\pi r/\lambda)^4 \cdot [\lvert B \rvert^2]$

C_{ext} and C_{abs} for the two cases are the same; the only difference is that in the corresponding volumes. For the scattering cross-sections the terms in the square brackets, and these are the more important terms, are the same because of the depolarization factor, but the other terms are different. For the infinite cylinder case we have a λ^{-3} dependence, whereas for the highly elongated prolate spheroid the wavelength dependence is λ^{-4}. (For all ellipsoids in general in this approximation the scattering cross-section has a λ^{-4} dependence.) The same is true for the corresponding homogeneous cases (cf., van de Hulst 1957, p. 316; Kerker 1969, p. 266).

We now write expressions for C_{abs} and C_{sca} for the compound ellipsoid on using equation (9) in equations (3) and (2) if ε_o is real.

$$C_{abs} = \frac{2\pi}{\lambda} V_i \frac{\varepsilon_o^2 \varepsilon_2}{(\varepsilon_1 T + \varepsilon_o U)^2 + (\varepsilon_2 T)^2} , \qquad (17)$$

and

$$C_{sca} = \frac{8\pi^3}{3} \frac{V^2}{\lambda^4} \frac{(\varepsilon_1 R + \varepsilon_o S)^2 + (\varepsilon_2 R)^2}{(\varepsilon_1 T + \varepsilon_o U)^2 \quad (\varepsilon_2 T)^2} , \qquad (18)$$

where we have substituted $(\varepsilon_1 - i\varepsilon_2)$ for ε_i, and

$$R = L_i\,(\varepsilon_o - 1) + \frac{V_i}{V}\{\varepsilon_o - L(\varepsilon_o - 1)\}\,,$$

$$S = (1 - L_i)(\varepsilon_o - 1) - \frac{V_i}{V}\{\varepsilon_o - L(\varepsilon_o - 1)\} = (\varepsilon_o - 1) - R\,,$$

$$T = L_i\{1 + L(\varepsilon_o - 1)\} + (\varepsilon_o - 1)\frac{V_i}{V}L(1 - L)\,,$$

and $$U = (1 - L_i)\{1 + L(\varepsilon_o - 1)\} - (\varepsilon_o - 1)\frac{V_i}{V}L(1 - L) = \{1 + L(\varepsilon_o - 1)\} - T.$$

We shall now make the further assumption that ε_o is independent of wavelength. Let us investigate the nature of the resonances. For the limiting cases $L = L_i$ and, $L = 0$ and $L = 1$ and the results can be easily obtained from equations (10) and (11). For C_{abs} the coatings do not have any effect on the position or the strength of the resonances but for C_{sca} the shell is also contributing and there is a slight change. For intermediate values of L, $0 < L < 1$, the resonances occur at a value of ε_1 given by

$$\varepsilon_1 = -\varepsilon_o\frac{U}{T} = -\varepsilon_o\left[-1 + \frac{L + L(\varepsilon_o - 1)}{L_i + L(\varepsilon_o - 1)\{L_i + \frac{V_i}{V}(1 - L)\}}\right]. \qquad (19)$$

It follows from equation (19) that if there is no coating the resonance occurs at $\varepsilon_1 = -(-1 + 1/L_i)$ as in the case of a homogeneous ellipsoid. It can be shown that as the relative amount of coating is increased (keeping V fixed and decreasing V_i) the resonance occurs at higher negative values of ε_1. Finally, if $V_i/V \to 0$, the resonance occurs at $\varepsilon_1 = -\varepsilon_o(-1 + 1/L_i)$, corresponding to the case of a homogeneous ellipsoid in a medium of dielectric constant ε_o. Thus whatever the amount of coating the resonance is always between $\varepsilon_1 = -(-1 + 1/L_i)$ and $\varepsilon_1 = -\varepsilon_o(-1 + 1/L_i)$. This result is similar to that for surface plasmons in the case of coated thin foils (Raether 1967) and is more general. (These results apply to the case of a coated thin infinite cylinder also.) As noted earlier, the boundaries of the resonances do not change because of coatings. We also note that the minimum in C_{sca} does not shift from $\varepsilon_1 = 1$ to $\varepsilon_1 = \varepsilon_m$ because the shell is also contributing to the scattering; the shift is actually to the lower energy side.

The result we shall be making use of in this paper is that even a slight coating makes a substantial change in the posi-

tion of the resonance.

Although the formula for polarizability, equation (9), is implicit in the work of Stepin (1965) and Bilboul (1969), most of the discussion in this section is believed to be new.

d) Small Ellipsoids with Anisotropic Optical Properties

Since graphite is a suggested interstellar particle and since its optical properties are highly anisotropic (that is, ε is a tensor), let us discuss the nature of these resonances for such particles in the small size limit. The polarizabilities can be calculated from the work of Jones (1945; see also van de Hulst 1957, p. 73). We consider an oblate spheroid whose axes coincide with the principal directions of the dielectric constant tensor. (The results can be extended to the more general cases.) If $\varepsilon_\perp$ and $\varepsilon_\parallel$ are the dielectric constants when $\vec{E}$, the electric vector of the incident radiation, is perpendicular and parallel to the symmetry axis respectively, and $4\pi L_\perp$ and $4\pi L_\parallel$ are the respective depolarization factors, the corresponding polarizabilities, $\alpha_\perp$ and $\alpha_\parallel$, are given by (Wickramasinghe 1967, Greenberg 1968)

$$\alpha_\perp = \frac{V}{4\pi} \frac{\varepsilon_\perp - 1}{L_\perp(\varepsilon_\perp - 1) + 1}$$

$$\alpha_\parallel = \frac{V}{4\pi} \frac{\varepsilon_\parallel - 1}{L_\parallel(\varepsilon_\parallel - 1) + 1} \qquad (20)$$

where V is the volume of the particle. These equations are similar to equation (1b). As before, we can calculate the scattering and absorption cross-sections from equations (2) and (3) for the two cases separately.

Let us write $\varepsilon_\perp = \varepsilon_{\perp,1} - i\varepsilon_{\perp,2}$ and $\varepsilon_\parallel = \varepsilon_{\parallel,1} - i\varepsilon_{\parallel,2}$. As in the case of a homogeneous oblate spheroid, there are two resonances, one for $\vec{E}$ perpendicular to the symmetry axis ($\vec{E}\perp c$) and the other for $\vec{E}$ parallel to the symmetry axis ($\vec{E}\parallel c$), assuming, of course, that both $\varepsilon_{\perp,1}$ and $\varepsilon_{\parallel,1}$ become negative in some energy ranges. There are several interesting aspects. Even for a spherical particle, which is one extreme case of an oblate spheroid, there are two resonances, one for $\vec{E}\perp c$ at $\varepsilon_{\perp,1} = -2$, and the other for $\vec{E}\parallel c$ at $\varepsilon_{\parallel,1} = -2$. As the particle becomes oblate the resonance for $\vec{E}\perp c$ shifts to higher negative values of $\varepsilon_{\perp,1}$ and for $\vec{E}\parallel c$ to lower negative values of $\varepsilon_{\parallel,1}$. Finally, for the limiting case of a thin disc (platelet or highly flattened oblate spheroid), the resonances are at the maximum of $\varepsilon_{\perp,2}$ and the maximum of $(\varepsilon_{\parallel,1}^2 + \varepsilon_{\parallel,2})^{-1}$ respectively.

e) Physical Processes

So far we have discussed the nature of these resonances in terms of ε, the dielectric constant. We noted that in spite of the possible changes in the shape, amount of coating, size and optical anisotropy, the resonances are confined within the maximum of ε_2 and the maximum of $(\varepsilon_1^2 + \varepsilon_2^2)^{-1}$. If all these parameters are specified the resonance occurs at a fixed negative value of ε_1, and hence for a given solid, at a fixed energy or wavelength. In other words, the excitations are quantized. The question now arises: what are the energy ranges in which ε_1 is negative for the solids of astrophysical interest?

Depending on the type of solid, ε_1 becomes negative, in general, in two energy ranges (Kittel 1966): one in the infrared due to lattice vibrations and the other in the ultraviolet. The behavior can be quite complicated and in each of these energy ranges there can be more than one such region. In the infrared the frequency corresponding to the maximum of ε_2 is called ω_T, the transverse optical phonon frequency, and the frequency at which $\varepsilon_1 \to 0$ and $\varepsilon_2 \to 0$ is called ω_L, the longitudinal optical phonon frequency. ω_T is less than ω_L. In the ultraviolet the frequency at which $\varepsilon_1 \to 0$ and $\varepsilon_2 \to 0$ is called ω_P, the plasma frequency. There is no frequency corresponding to ω_T, but there is a maximum in ε_2 due to the transitions of bound electrons on the lower energy side of ω_P.

We now very briefly discuss the physical processes involved in the excitation of the resonances we have been discussing in this paper. If infrared photons are incident on a diatomic crystal of ions $\pm e$, the positive and negative ions are displaced with opposite signs. Quantized vibrations that follow are designated as "material polaritons" (Englman and Ruppin 1968a,b; Ruppin and Englman 1968). In the ultraviolet the electrons take the place of negative ions. The electron gas starts moving as a whole with respect to the positive ion background. This is known as plasma oscillation and the quantum of this excitation is termed a plasmon (Kittel 1966). Both these processes can be characterized as collective excitations. Thus the resonances discussed earlier in this paper can be identified as occurring due to collective processes. Two qualifications should be made, however. The peak in ε_2 in the ultraviolet is, as noted earlier, due to the transitions of bound electrons. Therefore the resonances occurring at this energy for some shapes are <u>not</u> due to a collective process. In the case of gold and silver in the visual and near ultraviolet, for example, there is what is known as the free carrier plasma frequency, but there is no corresponding peak in ε_2 on the lower energy side of it. The discussion of the resonances has to be modified somewhat to take this fact into

consideration for such cases.

The discussion of the physical processes involved has been, of necessity, very simplified. For details reference should be made to papers cited in this section (see also, Kawabata and Kubo 1966, Steinmann 1968).

Let us now summarize all the theoretical discussion on these resonances. They are due to collective processes, with the exceptions noted above, and are confined within ω_T and ω_L in the infrared and within the maximum of ε_2 and ω_P in the ultraviolet. The precise position depends on the shape, size and amount of coating. We can invert this argument. From an observed feature, if it can be established that these processes are involved, we can determine, at least in principle, the shape and the size of the particles and also how much coating these particles have.

III. COMPARISON WITH OBSERVATIONS

a) The 2200 Å Band

As earlier calculations indicated there is an extinction band for small-sized spherical graphite particles at about 2200 Å. This has been attributed to transition of π electrons to the conduction band in the graphite crystal (Wickramasinghe 1967, Stecher 1969). This identification is incorrect because this band occurs where $\varepsilon_{\perp,1}$ is -2, and is therefore due to plasma oscillations in spherical graphite particles. The dielectric constant of graphite in the basal plane, $\varepsilon_\perp$, is given by Taft and Phillip (1965, and private communication) and is plotted in Figure 1 for energies between about 2.5 ev and 9.0 ev. The plasma frequency, ω_P, is at about 1800 Å (7.0 ev). The maximum in ε_2 is at about 2800 Å. For spherical particles the resonance is at $\varepsilon_1 = -2$ which is at 2205 Å. For an oblate spheroidal particle with the ratio of minor to major axis = 0.8 the resonance shifts to 2255 Å. Similarly, if we coat a spherical graphite particle of 50 Å radius with a shell of ice about 5 Å thick, the resonance shifts to 2255 Å.

In Figure 2 is plotted the absorption cross-sections using equations (20) for graphite particles for two extreme shapes, a sphere and a thin disc, normalized such that they are unity at the maximum. If $C^{\perp}_{abs}$ and $C^{\parallel}_{abs}$ are the absorption cross-sections on using $\varepsilon_\perp$ and $\varepsilon_\parallel$ respectively, the quantity plotted is $(2C^{\perp}_{abs} + C^{\parallel}_{abs})/3$, as is the case if the particles are randomly oriented. Values of $\varepsilon_\parallel$ for graphite were taken from Tosatti and Bassani (1970). There are no strong resonances in $C^{\parallel}_{abs}$.

The highest negative value of $\varepsilon^{\parallel}_1$ is -0.85 which occurs at 12.7 ev. In this approximation $C^{\parallel}_{abs}$ is greater than $C^{\perp}_{abs}$ between about 1300 and 850 Å, the exact wavelengths depending on

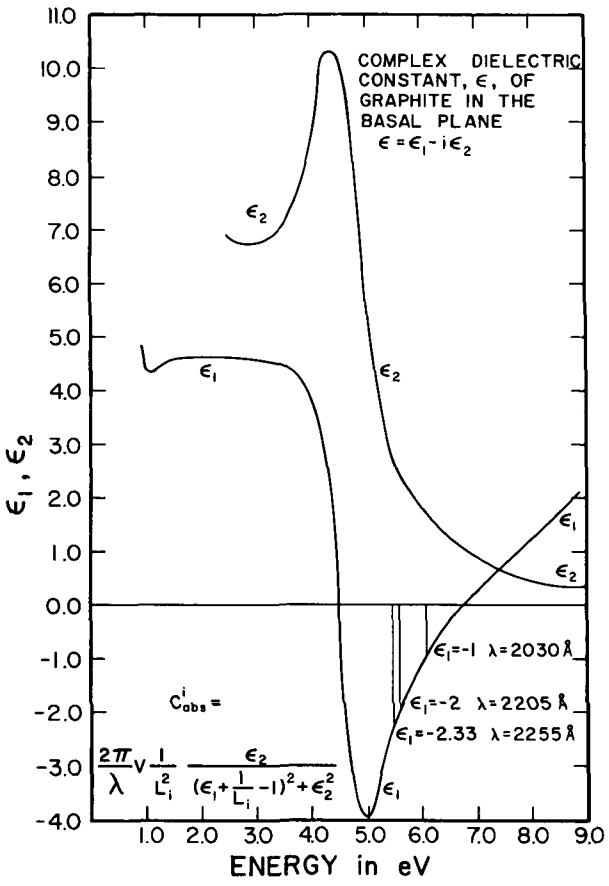

Figure 1.—The complex dielectric constant of graphite in the basal plane (see text for discussion).

the shape. The net effect is to increase somewhat the total C_{abs} in this wavelength range from what is obtained from $C^{\perp}_{abs}$. But at these wavelengths the Rayleigh approximation is not valid and we cannot say what the contribution is for larger sizes because the required theory is not available. It may be remarked that in $C^{\perp}_{abs}$ there is a much stronger resonance in the far ultraviolet than the one at 2070 Å. This resonance occurs at about 800 Å and is also due to the process of plasma oscillations.

The peak in the small size limit as calculated with equations (20) occurs at 2080 Å for spheres; however, $\epsilon_{\perp,1}$ is equal to -2 at 2205 Å. The shift to shorter wavelengths could occur for two reasons. From the formulas we see that the resonance occurs where ϵ_2 also satisfies the condition, $\epsilon_2 < 1$. It occurs at shorter wavelengths if this condition is not

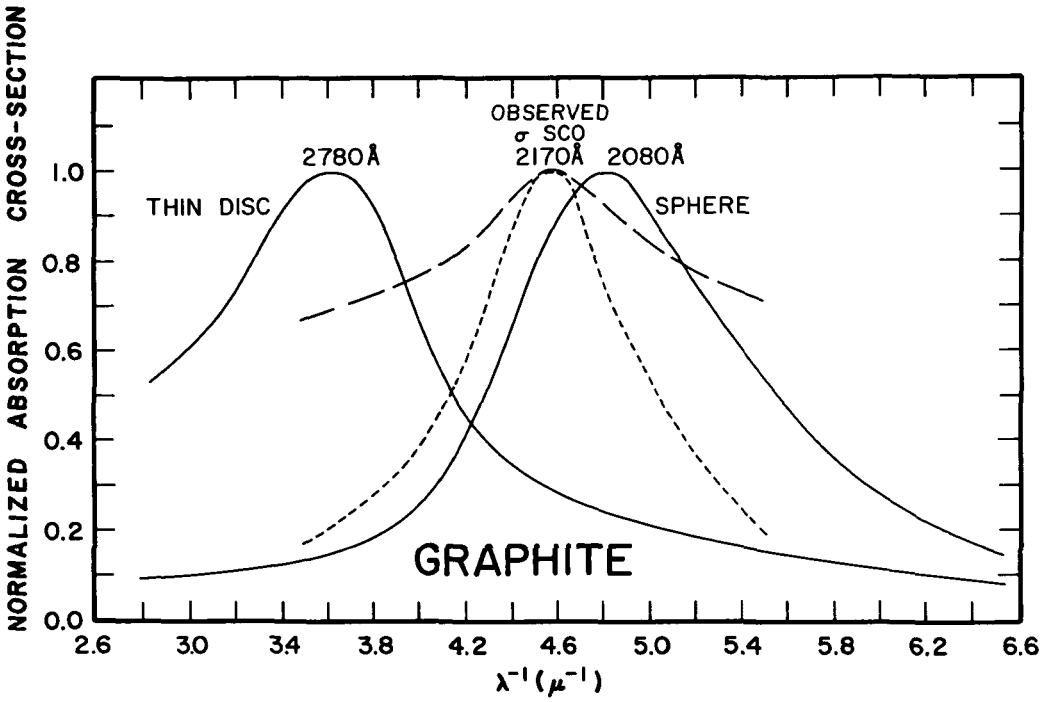

Figure 2.—Shape dependence of resonances in graphite. For comparison the observed extinction curve for σ Sco is also plotted using two different base lines (see text for discussion).

satisfied (see, Kawabata and Kubo 1966). The second factor is that C''_{abs} is also contributing and it is increasing towards shorter wavelengths, the net effect being to push the resonance to shorter wavelengths. The second factor is not important in this case, however.

Two other computational details should be noted about such resonances in general. If one does not anticipate where the resonances will be and does not compute cross-sections for a sufficient number of wavelengths, one is likely to get misleading results. Secondly, one should use the dielectric constant and not the refractive index to get physical and computational insight about these resonances.

The peak for spherical particles occurs at 2080 Å and as the oblateness increases it shifts to longer wavelengths. Finally, for thin discs it occurs at 2780 Å. Also plotted in Figure 2 is the observed interstellar extinction curve in the region 2860-1840 Å for σ Sco (Bless and Savage 1972) using two different base lines for its normalization. The broader one (large dashes) is obtained if the base line is parallel to the abscissa and starts at the furthest point observed in the

infrared. The narrower one (small dashes) is obtained if the base line is a smooth curve joining 2.6 μ^{-1} and 6.5 μ^{-1} in the extinction curve of σ Sco. The width of the observed feature depends critically on the choice of the base line. The peak in the observed curve is at 2170 Å and the feature is quite narrow.

It is obvious from Figure 2 that the observations put very stringent limits on the shape of the particles. We can definitely rule out graphite platelets (thin discs) as being responsible for the observed feature.

My calculations for spherical particles, using the Mie theory with $\varepsilon_\perp$, show that for a radius of 0.005 μ the peak is at 2070 Å, for 0.010 μ at 2100 Å, and for 0.020 μ at 2200 Å. If we now compare the theoretical curves taking all the factors into consideration with the observed curves, we can conclude that the suggested interstellar graphite particles should be fairly spherical, quite small (mean radius $\approx$ 0.015 μ) and have almost no coatings whatsoever. The minimum in the observed curves between about 1800-1500 Å is also consistent with the graphite hypothesis (Gilra 1971).

If we take the values of ε from Scouler (1969) for Mg_2Si, the calculations show a strong feature at about 2200 Å for spherical Mg_2Si particles due to plasma oscillations. The list could be made substantially bigger but it is not clear if the particles of other type will be formed anywhere.

As we have noted, the position and strength of the resonance depend critically on the precise values of $\varepsilon(\lambda)$. However, in the discussion so far we have tacitly assumed that we can use the bulk dielectric constants for particles in interstellar space. This may not be exactly true: for sizes $\lesssim$ 100 Å, ε depends on size due to quantum effects which tend to broaden the plasma resonance (Kawabata and Kubo 1966); we do not know what effect the temperature (the temperature of interstellar particles is ~20°K) has on ε; the interstellar particles may not be identical to bulk crystals in their crystalline structure. Surface "irregularities" also affect the nature of plasma resonances (Steinmann 1968). We still do not know how to calculate the extinction cross-section for particles with anisotropic optical properties if the size is arbitrary. The effects of these and perhaps some other related problems should be investigated.

Another suggestion to explain the 2200 Å band is that it is caused by an absorption edge. Huffman and Staap (1971) experimentally obtained the optical constants for one silicate, $(MgFe)SiO_3$, up to 12.4 ev. They suggested that the observed feature could be explained with a gaussian size distribution having a mean size 0.06 μ. In Figure 3 are plotted extinction (E), scattering (S) and absorption (A) cross-sections for spherical particles of this silicate for two mean radii,

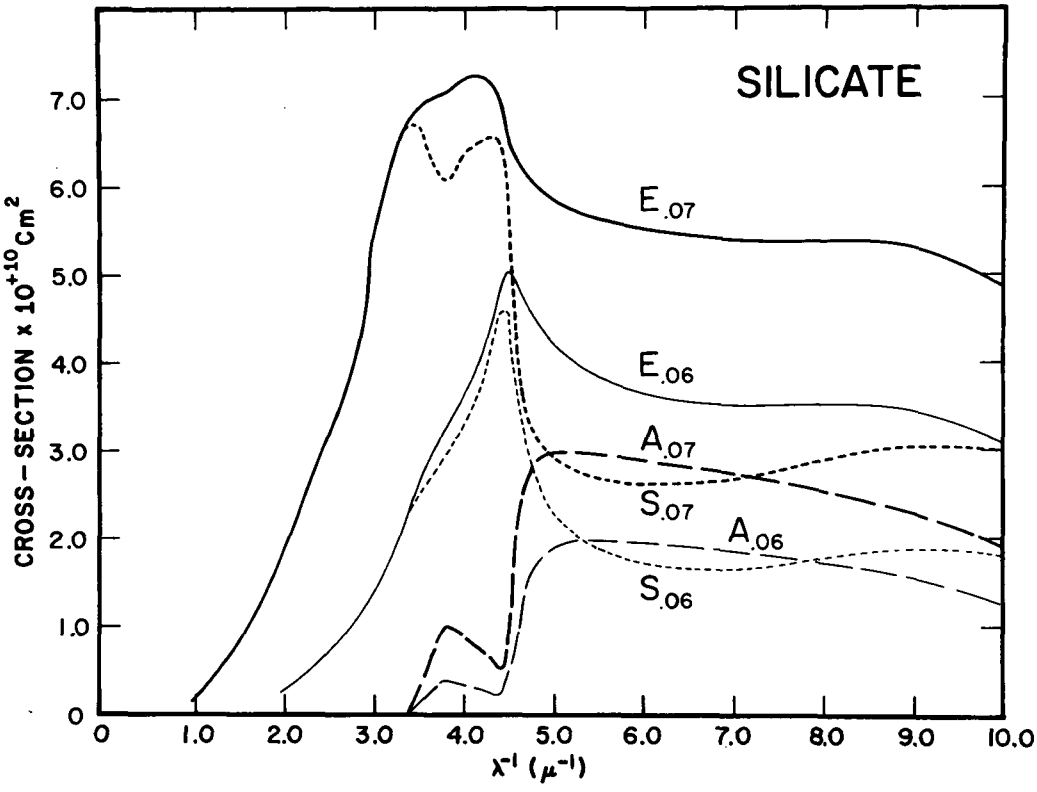

Figure 3.—Theoretical extinction (E), scattering (S) and absorption (A) cross-sections for (MgFe)SiO_3. The suffixes refer to the mean radii in microns (see text for discussion).

0.06 μ and 0.07 μ. The suffixes refer to the mean radii in microns. The curve $E_{.06}$ is the same which according to Huffman and Staap explains the observed feature.

At an absorption edge the imaginary part of the refractive index (or the imaginary part of the dielectric constant) increases rapidly. At this energy the absorption cross-section increases very rapidly and the scattering cross-section decreases very rapidly, as can be seen from the curves. For very small-sized particles the extinction is entirely due to absorption. The relative contribution from scattering increases as the mean size is increased. For a narrow size-range a "band" appears in the scattering cross-section due to the rapid decline on the high energy side (as already noted) and a rapid rise on the low energy side. With only a 15% increase in the mean size, the rapid rise on the low energy side occurs at much lower energies making the scattering "band" extremely broad. The resulting "band" in the extinction cross-

section is "flat-topped", asymmetric and extremely broad and bears no resemblance in shape, strength or position with the observed feature. Therefore it seems unlikely that such a well-defined observed feature can be caused by such a physical "process". Wickramasinghe and Nandy (1971b) have also noted some of these points independently.*

Another physical process could be considered. Some solids either due to an intrinsic property or due to an impurity or due to "physical damage" exhibit absorption bands in their bulk optical properties. For example, neutron irradiated quartz shows a band at about 2200 Å (Billington and Crawford, Jr. 1961). Let us investigate if such particles can explain the observed feature. (Dr. G. H. Herbig also mentioned this possibility during the discussion following my paper.) Van de Hulst (1957, p. 191) has already discussed such a theoretical problem. Let us refer to Figure 3. The feature in the absorption cross-section at 3.8 μ^{-1} is due to such a process. Only in the very small-size limit does it show up in the extinction cross-section. As the size increases the minimum in the scattering cross section makes it invisible. In fact, for the mean size 0.07 μ there is a minimum in the extinction cross-section at this wavelength, as already discussed by van de Hulst. It could still be argued, however, that only very small-sized quartz particles may be responsible for the observed feature. However, there is a stronger band in neutron irradiated quartz at 1650 Å which is not seen in the observed extinction curves. Also, since quartz has an absorption edge at somewhat higher energies (the scanner #1 on board the OAO has a quartz window and that is why no observations are possible with it shortward of about 1800 Å), the observed extinction curve should show a very rapid increase at higher energies. The observations of σ Sco and ρ Oph down to 1100 Å (Bless and Savage 1972) which show strong 2200 Å features belie this expectation. Thus it does not seem likely that such particles are responsible for the observed band.

Let us summarize the discussion on the identification of

---

* One remark should be made about my model of interstellar grains (Gilra 1971). In this model silicates are the chief contributor to the far ultraviolet rise. This conclusion was based on the assumption, which seemed most expedient at the time, that the optical constants are wavelength independent. As discussed here the optical constants are now available for one silicate. The calculations show that the suggested existence of silicates to explain the far ultraviolet rise may be somewhat uncertain now (see Bless and Savage (1972) for other possibilities).

the 2200 Å band. Three different physical processes were considered: plasma oscillations, absorption edges, and absorption bands in bulk crystals. It has been shown that the last two are relatively inefficient and inadequate. In these cases the behavior of scattering is almost opposite to that of absorption in the region of interest (Figure 3). As the size is increased beyond a certain critical value the extinction band becomes exceedingly broad and highly asymmetric in one case, and invisible in the other. On the other hand, the band due to plasma oscillations arises because there is almost identical structure in the bands in both scattering and absorption. Whatever changes we may make in the particle shape (Figure 2), size (Figures 1 and 2 in Gilra 1971) and coatings (as discussed earlier) the extinction band is always well defined and is very strong in the small-size limit. It can be concluded, therefore, that of all the suggestions made so far the process of plasma oscillations is the most plausible process to give rise to a feature of the type observed. It is correct, however, that quite stringent limits were placed on the geometrical and surface properties of the suggested interstellar graphite particles because the observed feature is quite narrow. Some theoretical problems were mentioned earlier and they should be investigated. It may be noted that the minimum in the observed curves between about 1800-1500 Å is also consistent with the graphite hypothesis (Gilra 1971).

b) The Bands in Infrared

It has been suggested (Friedemann 1969a,b; Gilman 1969) that particles of silicon carbide can form in the atmospheres of stars in which the carbon to oxygen ratio is ≥ 1. In the spectra of many of these stars the violet region is strongly depressed, the quasi-discontinuity setting in at about 4400 Å. It has been suggested (Stephenson and Ross 1970) that this phenomenon is "among the most outstanding of all opacity effects to be seen in stars of any spectral type." Silicon carbide has the fundamental absorption edge between 2.2 and 3.0 ev, the precise position depending on the polytype, impurities and temperature. Gilra and Code (1971, 1972) have suggested that circumstellar silicon carbide grains are responsible for the observed violet depression. Their theoretical results are in very good accord with the observations. The model of interstellar grains I have proposed (Gilra 1971) has silicon carbide as a major constituent. We are therefore interested in investigating the nature of resonances in small silicon carbide particles in the infrared so that the observations could confirm or disprove the suggested existence of such circumstellar and interstellar particles.

The fundamental absorption band in SiC is at 12.6 μ

(Spitzer et al. 1959a,b), that is, ω_T, the transverse optical phonon frequency, corresponds to this wavelength. ω_L, the longitudinal optical phonon frequency, corresponds to 10.3 μ. (The optical properties of cubic and hexagonal SiC are quite similar in this region and we shall consider only the cubic form.) My Mie calculations for spherical particles had shown (Gilra 1971) a weak band at ω_T but this was completely dwarfed by a very strong absorption feature at ~10.75 μ where $\varepsilon_1 = -2$. I had suggested that the feature will become broad if the particles are not exactly spherical. At that time I was not aware that experimental results existed (Pultz and Hertl 1966) which confirm this prediction. The theory has been discussed in several papers by Englman and Ruppin (Englman and Ruppin 1968a,b; Ruppin and Englman 1968).

Figure 4 shows the absorption cross-section for cubic SiC

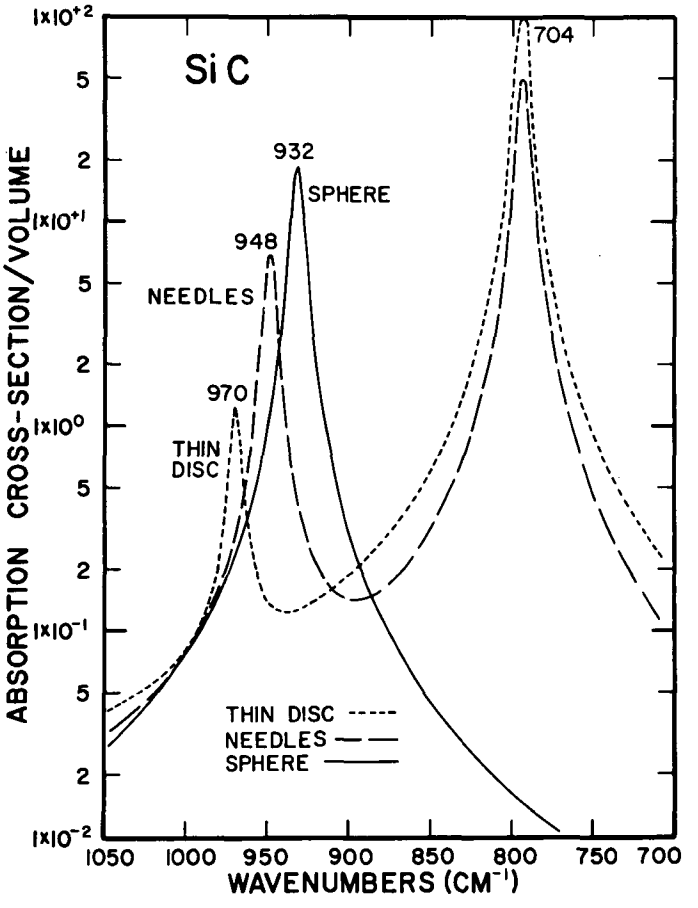

Figure 4.—Shape dependence of resonances in SiC in the 10-13 μ region (see text for discussion). 704 in the upper right corner should read 794.

particles of three shapes, thin disc, sphere and needles, using equation (5) with $\varepsilon_m = 1$. Random orientation has been assumed. For a thin disc the resonances are at 970 cm^{-1} (= 10.3 μ = ω_L) and at 794 cm^{-1} (= 12.6 μ = ω_T). As the oblateness decreases the resonances move towards each other and finally for the spherical case there is only one resonance at 932 cm^{-1} (= 10.73 μ; $\varepsilon_1 = -2$). As the particle becomes prolate, the resonances move away from each other and finally for the case of a needle they are at 794 cm^{-1} (= 12.6 μ = ω_T) and 948 cm^{-1} (= 10.55 μ; $\varepsilon_1 = -1$). If the particles are "highly irregular" there will be a broad feature between about 10.3 μ and 12.6 μ such as has been observed experimentally by Pultz and Hertl (1966). The results for needles are also in very good agreement with their experimental results for fibres.

We have no a priori way of determining the shape of the suggested circumstellar and interstellar silicon carbide particles. There should be a strong absorption band (or bands) between 10 μ and 13 μ in the interstellar extinction curves of the highly reddened stars. This feature should appear in emission in the stars which show strong violet opacity. However, in the latter case this predicted emission will be somewhat "filled in" by strong absorption in this wavelength region due to SiC_2 molecules (which give rise to the Merrill-Sanford bands in the late N-type carbon stars) and high spectroscopic resolution will be needed to separate the two effects (Gilra and Code 1972).

c) The 10 μ Band and Silicates

A broad emission feature centered at about 10 μ has been seen in the spectra of oxygen-rich late type variables (Woolf and Ney 1969). Perhaps a similar feature at 10 μ has been seen in absorption in the observations of the galactic center (Hackwell et al. 1970). These features have been attributed by the authors to circumstellar and interstellar silicates respectively. Since the dielectric constant for silicates is not yet available in this spectral region, let us investigate the theoretical basis for these identifications.

If n, the real part of the refractive index, is very close to one, and k, the imaginary part, is very much smaller than one, then equation (5) reduces to (van de Hulst 1957) with $\varepsilon_m = 1$

$$C_{abs} = (2\pi/\lambda)V \cdot 2k$$

and since the absorption coefficient $A = (4\pi k)/\lambda$, we get

$$C_{abs} = V \cdot A \ . \qquad (21)$$

Equation (21) gives the absorption cross-section in the Rayleigh-Gans approximation. This is the equation used by Woolf and Ney (1969) and Hackwell et al. (1970), following the work of Gaustad (1963), in identifying the silicates. Donn et al. (1970) have agreed with this assumption. But this is not correct because the conditions $n \simeq 1$ and $k << 1$ are not satisfied for silicates in this region. The structure in ε_1 and ε_2 should be somewhat similar to that for quartz (experimental absorptance results (Lyon 1963) show this very well) and that means very high values of ε_2 and ε_1 (both positive and negative for ε_1). The dielectric constant for quartz is given by Spitzer and Kleinman (1961) and theoretical calculations (Knacke 1968, for spherical particles, Martin 1971, for spherical and cylindrical particles, and my own for ellipsoidal particles) using equation (5) show no match at all with the values given by Gaustad (1963) using equation (21). (Most of the values in these spectral regions given by Gaustad (1963) are incorrect for other substances as well, for the same reasons.) There are strong resonances (as in the case of SiC) which depend on the shape of the particles. The same should be the case for silicates. For silicates Wickramasinghe and Nandy (1971a) have taken the value of k from Gaustad (1963) and assumed a wavelength independent value of n (= 1.66) throughout this spectral region. This assumption is also not correct. We thus conclude that the identification of circumstellar and interstellar silicates from observations in the 10 μ region is based on a wrong theoretical premise and inadequate experimental data and therefore seems to be premature.

There is one way, however, in which the experimental absorption coefficient can be compared directly with the observations, and that is if we assume that the distribution of shapes and sizes of the particles and their spatial arrangement are identical in the two cases. It is not clear if this is the case. The best way to resolve the controversy is to get experimental values of ε and to obtain observations at high spectroscopic resolution to see the structure within the broad feature. Then the theoretical curves using the values of ε obtained experimentally can be directly compared with the observations.

Some of the points in this section have been independently discussed by Martin (1971).

d) Polarization

From equation (5) we see that absorption, and therefore thermal emission, depend on the shape and orientation of particles. If the particles have any anisotropy, either in shape or in optical properties, and if they are suitably aligned, then the 2200 Å band and the bands in the infrared should be

polarized. There should be a polarity reversal at some wavelength in these spectral regions.

If the observed interstellar polarization in the visual is due to the same agent which is responsible for the 2200 Å band, then this band must be very strongly polarized, as Stecher and Donn (1965) have already pointed out for graphite. Recent balloon-borne wide band polarimetry of the reddened star ζ Oph by the University of Arizona astronomers (Coyne et al. 1971, and remarks at the 135th meeting of the American Astronomical Society) indicates that the polarization continues to decrease in the region 3000-2000 Å. If these observations are correct and if the observations of ζ Oph can be considered as representative of other stars as well, then we can conclude that the suggested interstellar graphite grains are not aligned and the polarization in the visual is not due to graphite grains.

If for the late-type variables the observed polarization in the visual is due to grains and the emission in the infrared is also due to the same grains and these grains are suitably aligned, then the emission feature(s) should be polarized with a polarity reversal at a fixed wavelength. However, very narrow band polarimetric observations will be required so that the polarizations with different polarity do not cancel each other. Dr. M. Dyck at the Kitt Peak National Observatory has started such an observational program.

In the model of interstellar grains I have proposed (Gilra 1971) SiC particles are responsible for the observed interstellar polarization in the visual. As discussed earlier SiC particles have resonances in the 10-13 μ regions. Therefore the suggested interstellar band(s) in the 10-13 μ region should be polarized with a polarity reversal in between.

It is obvious that narrow band polarization measurements in these spectral regions will give us important information about the shape, size and chemical composition of circumstellar and interstellar grains.

IV. FINAL REMARKS

Very strong resonances in absorption and scattering occur in the spectral regions in which ε_1, the real part of the dielectric constant, is negative. The precise positions depend on the particle shape and size and on the nature and amount of coating. The nature of these resonances was discussed with the help of solutions of relatively simple problems in electrostatics and the discussion given in this paper is essentially complete in the small-size limit. In this limit they are always confined within the maximum of ε_2 on the low energy side and the maximum of $(\varepsilon_1^2 + \varepsilon_2^2)^{-1}$ on the high energy side. As the size becomes comparable to the wavelength, new resonances

appear on the low energy side of the peak in ε_2 (see Ruppin and Englman 1968, Englman and Ruppin 1968b). These will be discussed elsewhere (Gilra 1972).

There are two distinct energy ranges in which these resonances occur. One is in the infrared in the region of strong lattice bands between ω_T and ω_L. The other is in the ultraviolet between the maximum of ε_2, which is due to the transitions of bound electrons, and ω_P. Broadly speaking, the process which gives rise to these resonances is that of collective excitations.

Taking all the factors into consideration and comparing the properties of these resonances with those of "bands" due to other processes, it can be concluded that these resonances are the strongest and, relatively speaking, the most permanent features in the whole domain of light scattering by small particles.

The discussion given in this paper can be applied to some problems in solid state physics, colloidal chemistry and astronomy. With these results it has been possible to explain (Gilra 1972) some experimental results in solid state physics and colloidal chemistry which have not yet been accounted for.

The conclusions concerning some astronomical problems are very interesting. It has been shown that the observed bands at 2200 Å and in the 10 μ region are most probably due to collective excitations. Graphite particles continue to be the best working hypothesis for the 2200 Å band, even though strict limits have been placed on their geometrical and surface properties because of the narrowness of the observed band. A very important result is that for the first time, at least in principle, it may be possible to determine the shape of the circumstellar and interstellar particles directly from observations. Narrow band polarization measurements in the regions of these bands will be very helpful in achieving this goal.

I am grateful to Dr. A. D. Code for his helpful advice and constant encouragement throughout the course of this work. Much of the work reported in this paper was conceived and a significant fraction of it was completed during the summer of 1970 while I was a Summer Research Student at the Kitt Peak National Observatory. I wish to take this opportunity to thank Dr. A. A. Hoag for his various acts of kindness during my stay in Tucson. I thank Dr. R. C. Bless and Dr. B. D. Savage for reading the first draft of this paper.

REFERENCES

Bilboul, R. R. 1969, Brit. J. Appl. Phys. (J. Phys. D), 2, 921.
Billington, D. S. and Crawford, Jr., J. H. 1961, Radiation Damage in Solids (Princeton: Princeton University Press).
Bless, R. C. and Savage, B. D. 1972, Ap. J. 171, 293.
Coyne, G. V., Gehrels, T. and Serkowski, K. 1971, Bull. Amer. Astr. Soc. 3, 390.
Donn, B., Krishna Swamy, K. S. and Hunter, C. 1970, Ap. J. 160, 353.
Doyle, W. T. and Agarwal, A. 1965, J. Opt. Soc. Amer. 55, 305.
Englman, R. and Ruppin, R. 1968a, J. Phys. C. 1, 614.
_____ 1968b, J. Phys. C. 1, 1515.
Friedemann, Chr. 1969a, Physica 41, 139.
_____ 1969b, Astron. Nach. 291, 177.
Gaustad, J. E. 1963, Ap. J. 138, 1050.
Gilman, R. C. 1969, Ap. J. (Letters) 155, L185.
Gilra, D. P. 1970, Bull. Amer. Astr. Soc. 2, 317.
_____ 1971, Nature 229, 237.
_____ 1972, in preparation.
Gilra, D. P. and Code, A. D. 1971, Bull. Amer. Astr. Soc. 3, 379.
_____ 1972, in preparation.
Greenberg, J. M. 1968, in Nebulae and Interstellar Matter, ed. B. M. Middlehurst and L. H. Aller (Chicago: University of Chicago Press), p. 221.
Güttler, A. 1952, Ann. Physik, 11, 65.
Hackwell, J. A., Gehrz, R. D. and Woolf, N. J. 1970, Nature 227, 822.
Huffman, D. R. and Staap, J. L. 1971, Nature Phys. Sc. 229, 45.
Jones, R. C. 1945, Phys. Rev. 68, 93 and 213.
Kawabata, A. and Kubo, R. 1966, J. Phys. Soc. Japan 21, 1765.
Kerker, M. 1969, The Scattering of Light and Other Electromagnetic Radiation (New York: Academic Press).
Kerker, M. and Matijević, E. 1961, J. Opt. Soc. Am. 51, 506.
Kittel, C. 1966, Introduction to Solid State Physics (New York: Wiley).
Knacke, R. F. 1968, Nature 217, 44.
Lyon, R. J. P. 1963, NASA Tech. Note TN D-1871.
Martin, P. G. 1971, Astrophys. Letters 7, 193.
Pultz, W. W. and Hertl, W. 1966, Spectrochim. Acta. 22, 573.
Raether, H. 1967, Surface Science 8, 233.
Ruppin, R. and Englman, R. 1968, J. Phys. C. 1, 630.
Scouler, W. J. 1969, Phys. Rev. 178, 1353.
Spitzer, W. G., Kleinman, D. A. and Walsh, D. 1959a, Phys. Rev. 113, 127.
Spitzer, W. G., Kleinman, D. A. and Frosch, C. J. 1959b, Phys. Rev. 113, 133.

Spitzer, W. G. and Kleinman, D. A. 1961, Phys. Rev. 121, 1324.
Stecher, T. P. 1969, Ap. J. (Letters), 157, L125.
Stecher, T. P. and Donn, B. 1965, Ap. J. 142, 1681.
Steinmann, W. 1968, Phys. Status. Solidi 28, 437.
Stephenson, C. B. and Ross, H. E. 1970, A. J. 75, 321.
Stepin, L. D. 1965, Soviet Physics - Technical Physics 10, 768.
Taft, E. A. and Philipp, H. R. 1965, Phys. Rev. 138, A197.
Tosatti, E. and Bassani, F. 1970, Il Nuovo Cimento 65B, 161.
Unsöld, A. 1964, Pub. Roy. Obs. Edinburgh 4, 35.
van de Hulst, H. C. 1957, Light Scattering by Small Particles (New York: Wiley).
_____ 1964, Pub. Roy. Obs. Edinburgh 4, 13.
Wickramasinghe, N. C. 1967, Interstellar Grains (London: Chapman and Hall).
Wickramasinghe, N. C. and Nandy, K. 1971a, Nature Phys. Sc. 229, 81.
_____ 1971b, Nature Phys. Sc. 230, 16.
Woolf, N. J. and Ney, E. P. 1969, Ap. J. (Letters), 155, L181.

Page intentionally left blank

THE CELESCOPE CATALOG OF ULTRAVIOLET OBSERVATIONS

Robert J. Davis
Smithsonian Astrophysical Observatory
Cambridge, Massachusetts

ABSTRACT

The Smithsonian Astrophysical Observatory is using data obtained from approximately 7500 ultraviolet television pictures to compile The Celescope Catalog of Ultraviolet Observations described in this paper. This catalog lists the magnitude as observed in each of Celescope's four ultraviolet color bands, the standard deviations of the observed ultraviolet magnitudes, positions, identifications, and ground-based magnitudes, colors, and spectral types for approximately 5000 stars.

A Preliminary Catalog of Celescope Ultraviolet Observations, containing data on about 500 stars, was distributed at the time this paper was presented.

I. INTRODUCTION

The Smithsonian Astrophysical Observatory operated an ultraviolet television photometer, called the Celescope experiment, in the second Orbiting Astronomical Observatory (OAO-2) of the National Aeronautics and Space Administration. During the 16 months that we operated Celescope (December 1968 through April 1970), we took 8784 television pictures, observing about 1000 star fields once and about 700 more than once. We are now compiling the results from 7407 of these pictures into The Catalog of Celescope Ultraviolet Observations. Of the remaining 1377 pictures, 272 were not received, and 1105 were of quality too poor for processing.

Included in this paper is a Preliminary Catalog of Celescope Ultraviolet Observations in the format in which we intend to publish the final catalog. We consider observational

material presented in this sample listing to be final. Since we are still reviewing the identifications and ground-based data, there may be a few changes in these quantities; however, the ultraviolet magnitudes will not change. We are finding that about 5 to 10% of our identifications as given in this preliminary catalog are incorrect. The probability of misidentification in the final catalog will be considerably lower. Incorrect identifications are most probable for the faintest stars.

This Preliminary Catalog supercedes a similar one that was given limited distribution in May 1971 with preliminary ultraviolet magnitudes. Comments are invited on the format in which the catalog is presented. These comments will be useful to us in improving The Catalog of Celescope Ultraviolet Observations, which will be available on magnetic tape early in 1972, and in printed form later in 1972.

This Preliminary Catalog of Celescope Ultraviolet Observations contains the reduced ultraviolet magnitudes measured by Celescope, accompanied by identifications, positions and auxiliary astrophysical information where known.

The columns of the listing are described in the following section. Bibliographical information concerning the references cited in this Preliminary Catalog is included. Complete bibliographic information concerning all references used in compiling the Celescope Identification Catalog, from which the auxiliary information was derived, can be found in CDL-100, available upon request from Project Celescope, Smithsonian Astrophysical Observatory.

A description of the Celescope experiment is available as Smithsonian Astrophysical Observatory Special Report No. 282. A description of the data-analysis techniques will become available early in 1972 as Smithsonian Astrophysical Observatory Special Report No. 310.

The data contained in the Preliminary Catalog of Celescope Ultraviolet Observations, and the individual observed magnitudes on which these data were based, are also available on magnetic tape. The tentative format for the magnetic tape is given following the "Explanation of Columns."

II. EXPLANATION OF COLUMNS

Column	Contents
CEL	Preliminary Celescope Catalog ID number
HD	Henry Draper Catalogue number (reference 922).
DM	Durchmusterung number: B BD, Bonner Durchmusterung (reference 898)

Column	Contents
DM (cont.)	C CD or CoD, Cordoba Durchmusterung (reference 899). P CPD, Cape Photographic Durchmusterung (reference 900).
R.A.(1950)DEC.	Right ascension and declination (1950.0). If 897 is listed among the references (SAO Star Catalog), the position is taken from that reference. If the DM number is given but reference 897 is not listed, the position is taken from the DM and precessed to 1950.0. If the star has not been identified with a known object, the position given has been determined directly from the Celescope measurements and has an accuracy of about 1 arcmin.
OBJ	If the object is nonstellar, one or more of the following letters will indicate the nature of the object: B Barred spiral galaxy. C Globular cluster. D Diffuse emission nebula. E Elliptical galaxy. G Galactic cluster. I Irregular galaxy. N Reflection nebula. O Object surrounded by or associated with nebulosity. P Planetary nebula. Q Quasi-stellar galaxy. R Radio source. S Spiral galaxy. X Peculiar galaxy. * Identification given in NONSTAR column.
V	The photoelectric V magnitude of the UBV system when available. Otherwise, in order of preference, m_v, m_{pv}, m_{pg}. To distinguish among these possibilities, the magnitude given may be followed by MV(m_v), PV(m_{pv}), or PG(m_{pg}). In compiling these data, if different sources agreed to within $0^m.10$, the arithmetic mean is given. If there was greater disagreement, an astronomer resolved the disagreement. If he could not resolve it, an asterisk (*) appears in the magnitude column following the truncated mean of the source magnitudes. If the star has a

Column	Contents
V (cont.)	V magnitude listed in the Naval Observatory Catalogue (reference A19), only data combined from that catalog were used for deriving the magnitude given here. Magnitudes given to one decimal place required consistency within $\pm 0^{m}.5$ in the source material and imply that no source listed the magnitude to more than one decimal place. Magnitudes given to two decimal places required consistency within $\pm 0^{m}.05$ from those sources reporting the magnitude to two decimal places and disregarded magnitudes given to only one place. We consider only the photoelectric magnitudes to have reasonable accuracy; the photographic and photovisual magnitudes come mostly from source catalogs having very low photometric accuracy.
B-V	The photoelectric B-V color of the UBV system, otherwise the magnitude m_{pg} if available. If m_{pg} is given, the magnitude is followed by PG. The same conventions with regard to accuracy and the use of reference A19 apply as for the V column.
U-B	The photoelectric U-B color of the UBV system, when available. Otherwise, in order of preference, U-V or $(U-B)_C$. To distinguish between these possibilities, the magnitude given may be followed by U-V or UBC. The same conventions for accuracy and use of A19 apply as in the V column.
PHOT	When additional information is available in regard to the photometric characteristics of the object, one or more of the following entries will indicate these characteristics: A Member of an OB association. B Visual binary. H High-velocity star. M Multiple star. P Polarization data available. S Standard on MK or UBV system. U Observed in the ultraviolet below 3000 Å wavelength. X X-ray source. Z X-ray source also observed in the ultraviolet.

Column	Contents
PHOT (cont.)	* Merged image; see remarks.
	numbers Variable Stars:
	1 RW Aurigae variable.
	2 Eclipsing variable.
	3 Early-type irregular variable (type Ia of Kukarkin and Parenago).
	4 Variable star of unspecified type.
	5 Beta Canis Majoris variable.
	6 Alpha Canum Venaticorum variable.
	7 Delta Scuti variable.
	8 W Ursae Majoris variable.
	9 Peculiar variable.
	10 Classical Cepheid variable.
	11 Flare star.
	12 Irregular variable other than type IA of Kukarkin and Parenago.
	13 Semiregular variable.
	14 RR Lyrae variable.
	15 Mira Ceti and long-period variables.
	16 Nova-like variable.
	17 Nova.
	18 R Coronae Borealis variable.
	19 Supernova.
	20 T Tauri variable.
	21 U Geminorum variable.
	22 RV Tauri variable.
	23 W Virginis variable.
	24 Z Camelopardalis variable.
SPECT	Spectrum and luminosity. If different sources agreed to within ±2 subclasses, the arithmetic mean was taken. If they disagreed by more than 2 subclasses, arbitrary subclass designations were assigned according to the average of the given subclasses: E (early), if 0-3 in average subclass; M (middle), if 4-6; and L (late) if 7-9. Intermediate spectral subclasses and luminosities have been truncated; i.e., a star of spectral type B0.5 II-III is listed as B0 II.
PEC	When additional information is available in regard to the spectral characteristics of the object, one or more of the following entries will indicate these characteristics:
	A Peculiar A-type star.
	B Spectroscopic binary.

Column	Contents
PEC (cont.)	C Composite spectrum. D Interstellar D lines of sodium. E Any type of emission. G Magnetic field. H Interstellar H and K lines of Calcium II. M Metallic-line star. N Nebulous lines. P Peculiar spectrum. R Measured axial rotation. S Sharp lines. W Broad lines. Y Shell spectrum. 4 Interstellar 4430 Å absorption band.
U1	U1 magnitude. The weighted mean of the Celescope observational results in the U1 color band (2100-3200 Å). Celescope magnitudes are based on spectral irradiance in MKS units: $U_n = -2.5 \log I$, where I is spectral irradiance from the observed star at the effective wavelength of the color band, in units of watts per square meter per meter of wavelength. The U1 magnitude is derived from the formula $$U1 = \frac{\Sigma[U1_i/(1 + w_i)]}{\Sigma[1/(1 + w_i)]},$$ where $U1_i$ is the ith observation of the U1 magnitude and w_i is its weighting factor assigned as follows: w=3 if the object could not be separated from a neighboring object by our standard computer program and was separated manually. w=3 if the object was within 15 arcmin of the line, through the center of the field, separating the two different optical filters that were rigidly mounted in front of each television camera. w=6 if the object was both manually split and near the filter split line. w=∞ if the object was within 5 arcmin of the filter split line, if the object was in a part of the picture having a bright background, or if the object

Column	Contents
U1 (cont.)	touched the edge of the picture. Observations with w=∞ are not included in this Catalog. w=0 otherwise.
SD1	The standard deviation of U1, based on the formula $$SD1 = \left[\frac{\Sigma[(U1_i - U1)^2/(1 + w_i)]}{\Sigma[1/(1 + w_i)]}\right]^{1/2}$$ If U1 is based on a single observation, the weighting factor is given rather than the standard deviation. Weighting factor is indicated by the letter W preceding the number and by the use of a single-digit number rather than a number printed to two decimal places.
U2	U2 magnitude. The weighted mean of the Celescope observational results in the U2 color band (1550-3200 Å). Derivation as for U1.
SD2	Standard deviation of U2, or weighting factor for a single observation of U2, computed as for SD1.
U3	U3 magnitude. The weighted mean of the Celescope observational results in the U3 color band (1350-2150 Å). Derivation as for U1.
SD3	Standard deviation of U3, or weighting factor for a single observation of U3, computed as for SD1.
U4	U4 magnitude. The weighted mean of the Celescope observational results in the U4 color band (1050-2150 Å). Derivation as for U1. Very few U4 magnitudes are given because of interference from the bright Lyman-alpha background of the geocorona.
SD4	Standard deviation of U4, or weighting factor for a single observation of U4, computed as for SD1.
CEL	Preliminary Celescope Catalog ID number.

Column	Contents
NONSTAR	Nonstellar objects, in the rare cases where they have been identified with Celescope images, have their catalog number preceded by one of the following identifiers: N NGC, New General Catalogue. I IC, Index Catalogue. 3C Third Cambridge Catalogue of Radio Sources.
R.A.(2000)DEC.	Right ascension and declination (2000.0). See entry for R.A.(1950)DEC.
REMARKS	Most commonly used for naming additional stars in a merged image. Also used to give names of bright stars and variable stars.
REFERENCES	The identification numbers of the references used in compiling the auxiliary information. References cited in the Preliminary Catalog of Celescope Ultraviolet Observations are identified in the listing that follows the catalog. References not cited in this catalog are identified in CDL-100.

III. TENTATIVE FORMAT FOR MAGNETIC-TAPE VERSION OF CELESCOPE CATALOG

The magnetic-tape version of The Catalog of Celescope Ultraviolet Observations will contain the same information as is printed in the catalog itself, in a format convenient for machine computation. In addition, the magnetic-tape version will list the individual observations for each star, and a small amount of information useful for record keeping.

The following tentative tape format is given here only for the purpose of eliciting comments from potential users; the final format may be considerably different. Each observational record will contain the following items:

Item No.	Contents
1	Celescope catalog number
2	RA (1950), seconds of time
3	Dec (1950), tenths of minutes of arc
4	RA (2000), seconds of time
5	Dec (2000), tenths of minutes of arc

Item No.	Contents
6	Durchmusterung identifier. One integer is created from the DM zone and number: DM item = (sign of zone) × [(|zone|) × (100000) + number].
7	Durchmusterung code: BD, CD or CPD
8	Nonstar code: 1 for nonstellar objects
9	NGC-IC-3C Designation
10	HD number
11-31	Peculiarity codes (print columns OBJ, PHOT, PEC)
32	M1 × 100
33	M2 × 100
34	M3 × 100
35	Magnitude code defining the type of magnitudes listed in M1, M2 and M3
36	Spectral type and subtype
37	Luminosity
38-57	References
58-59	Name or comment
60	U_1 average
61	Weight of U_1
62	Rms of U_1
63	U_2 average
64	Weight of U_2
65	Rms of U_2
66	U_3 average
67	Weight of U_3
68	Rms of U_3
69	U_4 average
70	Weight of U_4
71	Rms of U_4
72	Number of U_1 magnitudes
73	U_1^i
74	Identifier of U_1^i (tape-frame-contact-Object Number)
75	Weight of U_1^i
.	
.	
.	
L	Number of U_2 magnitudes
L+1	U_2^ℓ
L+2	Identifier of U_2^ℓ
L+3	Weight of U_2^ℓ
.	
.	
.	
M	Number of U_3 magnitudes
M+1	U_3^m

Item No.	Contents
M+2	Identifier of U_3^m
M+3	Weight of U_3^m
.	
.	
.	
N	Number of U_4 magnitudes
N+1	U_4^m
N+2	Identifier of U_4^m
N+3	Weight of U_4^m
.	
.	
.	
END	

REFERENCES

2. Hall, J. S. 1958, Pub. U. S. Naval Obs. 17, 275-342.
6. Roberts, M. S. 1962, Astr. J. 67, 79-85.
7. Buscombe, W. 1959, Mt. Stromlo Obs. Mimeo. No. 3, 10 pp.
8. _____ 1962, Mt. Stromlo Obs. Mimeo. No. 4, 15 pp.
12. Morgan, W. W., Code, A. D. and Whitford, A. E. 1955, Ap. J. Suppl. 2, 41-74.
16. Feast, M. W., Stoy, R. H., Thackeray, A. D. and Wesselink, A. J. 1961, Monthly Notices Roy. Astr. Soc. 122, 239-253.
158. Cousins, A. W. J. and Stoy, R. H. 1963, Bull. Roy. Obs. series E, no. 64, 103-248.
207. Fitch, W. S. 1959, Ap. J. 130, 1022-1023.
308. Velghe, A. G. 1957, Ap. J. 126, 302-317.
340. Smith, E. van P. 1956, Ap. J. 124, 43-60.
341. Merrill, P. W. and Burwell, C. G. 1943, Ap. J. 98, 153-184.
342. _____ 1933, Ap. J. 78, 87-140.
419. Rubin, V. C., Burley, J., Kiasatpoor, A., Klock, B., Pease, G., Rutscheidt, E. and Smith, C. 1962, Astr. J. 67, 491-531.
474. Walker, G. A. H. 1963, Monthly Notices Roy. Astr. Soc. 125, 141-167.
487. Evans, D. S., Menzies, A. and Stoy, R. H. 1959, Monthly Notices Roy. Astr. Soc. 119, 638-647.
488. Chubb, T. A. and Byram, E. T. 1963, Ap. J. 138, 617-630.
505. Evans, D. S., Menzies, A. and Stoy, R. H. 1957, Monthly Notices Roy. Astr. Soc. 117, 534-561.

508. De Vaucouleurs, A. 1957, Monthly Notices Roy. Astr. Soc. 117, 449-462.
620. Westerlund, B. 1959, Publ. Astr. Soc. Pac. 71, 156-161.
752. Kucewicz, B. 1963, Publ. Astr. Soc. Pac. 75, 192-193.
753. Bertaud, C. 1959, J. des Obs. 42, 45-73.
780. Wayman, P. A. 1962, Roy. Obs. Bull., series E, no. 50, 61-76.
781. Eggen, O. J. 1963, Astr. J. 68, 697-714.
783. Woods, M. L. 1955, Mem. Commonwealth Obs. 3, no. 2, 18 pp.
793. Hogg, A. R. 1958, Mt. Stromlo Obs. Mimeo No. 2, 7 pp.
835. Cousins, A. W. J. 1963, Monthly Notices Astr. Soc. South Africa 22, 58-62.
841. Lake, R. 1962, Monthly Notices Astr. Soc. South Africa 21, 56-61.
842. _____ 1963, Monthly Notices Astr. Soc. South Africa 22, 79-84.
884. Hoffleit, D. 1964, Catalogue of Bright Stars, 3rd ed., (New Haven: Yale University Obs.). Also available on tape and punched cards.
897. Staff of the Smithsonian Astrophysical Observatory 1966, Smithsonian Astrophysical Observatory Star Catalog: Positions and Proper Motions of 258,997 Stars for the Epoch and Equinox of 1950.0 (Washington, D. C.: Smithsonian Institution).
898. Argelander, F., Director, 1903. Bonner Durchmusterung des Nördlichen Himmels. A. Marcus und E. Weber's Verlag, Bonn.
899. Thome, J. M., Director, 1892-1914. Cordoba Durchmusterung. Results of the Natl. Argentine Obs., vols 16-21.
900. Gill, D. and Kapteyn, J. C. 1896-1897. The Cape Photographic Durchmusterung for the Equinox 1875. Ann. Cape Obs., vols. 3 and 4.
901. Code, A. D. 1966, University of Wisconsin, OAO Observing List, private communication, June.
921. Iriarte, B., Johnson, H. L, Mitchell, R. I. and Wisniewski, W. K. 1965, Sky and Tel. 30, 21-31.
922. Cannon, A. J. and Pickering, E. C. 1918-1936, Henry Draper Catalog, Harvard Ann., vols. 91-100.
969. Kukarkin, B. V. et al. 1970, Obschii Katalog Peremennykh Zvezd., Izd. Akad. Nauk SSSR, Moscow.
A 7. Wilson, R. E. 1953, Carnegie Inst. of Washington Publ. 601, 344 pp.
A19. Blanco, V. M., Demers, S., Douglass, G. G., and Fitzgerald, M. P. 1968, Publ. U. S. Naval Obs., second series, 21, 772 pp.

PRELIMINARY CATALOG OF CELESCOPE ULTRAVIOLET OBSERVATIONS. JULY 1971.

CEL	HD	DM	R.A. (1950) DEC.	OBJ	V	B-V	U-B	PHOT	SPECT	PEC.	U1	SD1	U2	SD2	U3
A 1P	67269	C-45 3741	8 3 35 -45 15.8		8.2 MV	8.2 PG		*	A				12.66	W0	
A 2P	67385	C-44 4032	8 4 7 -45 1.6		6.94MV				B5				9.36	.20	
A 3P	67460	C-45 3765	8 4 31 -45 15.0		8.70MV				A0				13.60	W0	
A 4P	67609	C-44 4054	8 5 4 -44 54.2		9.8 MV	9.1 PG			A0				13.21	W0	
A 5P	67760	C-44 4068	8 5 57 -45 .1		8.5 MV	7.4 PG			A0		12.66	.18	11.02	W0	
A 6P	67865	C-45 3799	8 6 26 -45 23.7		9.6 MV	9.0 PG			A0				13.24	W0	
A 7P	67890	C-44 4078	8 6 29 -44 54.7		8.9 MV	7.7 PG			B9		12.31	W0	10.89	W0	
A 8P		C-43 3977	8 6 34 -44 5.9		9.2 MV						14.27	W3	14.05	W3	
A 9P	67951	C-45 3807	8 6 48 -45 38.9		9.6 MV	8.4 PG			B8		12.77	W0	11.78	W0	
A10P	68007	C-45 3809	8 6 58 -46 6.8		9.1 MV	8.5 PG			B9		12.78	W0			
A11P	67982	C-44 4089	8 6 59 -45 .4		9.9 MV								12.73	W0	
A12P		C-44 4095	8 7 3 -44 34.4		8.1 MV								13.94	W0	
A13P	68006	C-44 4093	8 7 6 -44 17.2		9.2 MV	8.0 PG			B8		13.56	.09	13.43	W0	
A14P	68034	C-45 3811	8 7 7 -45 15.0		8.5 MV	9.5 PG			A0		12.92	W0	12.26	W0	
A15P	68217	C-43 3998	8 7 57 -43 58.5		5.20	-.20			B3		8.89	.19	7.88	.47	
A16P	68322	C-43 4002	8 8 22 -44 11.8		8.9 MV	7.5 PG			B8		12.05	.15	10.25	W0	10.68
A17P	68369	C-44 4116	8 8 33 -44 45.2			8.10PG							13.78	W0	
A18P	68417	C-44 4118	8 8 44 -44 27.6		10.5 MV	9.0 PG			B8		12.86	.00	12.13	.02	
A19P	68476	C-45 3849	8 8 57 -45 51.3		9.6 MV	8.1 PG			B9		12.32	W0	11.84	W0	
A20P	68539	C-43 4015	8 9 21 -44 10.1		9.6 MV	9.1 PG			A2				13.53	.15	
A21P	68554	C-45 3857	8 9 23 -45 42.1		9.0 MV	8.1 PG			B9		11.84	W0	11.40	W0	
A22P	68697	C-45 3872	8 9 58 -46 5.0		8.30MV				A0		10.68	W3	11.61	W3	
A23P	68695	C-43 4022	8 10 1 -43 55.3		10.2 MV	9.6 PG			A0				13.81	W0	
A24P	68718	C-43 4023	8 10 8 -44 5.2		9.1 MV	8.2 PG			A0		12.90	.28	11.69	.19	
A25P	68737	C-44 4148	8 10 12 -44 45.5		10.0 MV	9.2 PG			B9		12.57	.17	12.18	.14	
A26P	68717	C-43 4025	8 10 14 -43 36.6		9.6 MV	9.6 PG			B9				13.83	W0	
A27P	68786	C-45 3880	8 10 29 -45 14.1		10.2 MV				A0		14.12	W0	13.91	.03	
A28P	68825	C-45 3883	8 10 35 -45 42.1		9.4 MV	8.1 PG			B8		10.84	W3	11.39	W3	
A29P	68805	C-43 4034	8 10 38 -43 49.7		9.8 MV	9.1 PG			B8		12.91	W0	11.89	W0	
A30P	68893	C-45 3890	8 10 53 -45 17.5		10.5 MV	9.3 PG			B9		13.25	W0	13.56	W0	
A31P	68895	C-45 3892	8 10 56 -46 6.8		6.02	-.13		B	B3				8.69	W0	7.96
A32P	68921	C-45 3891	8 11 1 -45 25.5		9.8 MV	8.7 PG			A0		12.93	.15	13.76	.16	
A33P	68965	C-45 3894	8 11 8 -45 27.7		9.8 MV	8.7 PG			A0		12.97	W3			
A34P	68920	C-44 4163	8 11 8 -44 32.7		10.2 MV	8.7 PG			B9				13.56	.07	
A35P	68945	C-43 4044	8 11 9 -43 36.3		10.0 MV	9.4 PG			A2				13.88	W0	
A36P	69128	C-45 3902	8 12 0 -45 18.6		9.1 MV	9.2 PG			B8		12.09	.16	13.15	.13	
A37P	69109	C-46 3926	8 12 5 -46 28.7		10.2 MV	9.6 PG			A0		11.45	W3			10.21
A38P	69168	C-46 3931	8 12 11 -46 25.6		6.50MV				B3		10.33	W3	8.60	W0	7.88
A39P	69167	C-43 4061	8 12 16 -43 45.4		10.2 MV	9.3 PG			A0				12.81	W0	
A40P	69237	C-43 4069	8 12 21 -43 18.7		9.8 MV	9.8 PG			A0				13.28	W3	
A41P	69213	C-44 4192	8 12 26 -44 25.2		6.6 MV	6.4 PG		7	F0		11.57	.11	11.52	.03	
A42P	69302	C-45 3914	8 12 47 -45 40.9		5.80	-0.13		B	B3		9.06	.29	7.97	.03	7.36
A43P	69301	C-44 4202	8 12 49 -45 8.5		9.0 MV	9.0 PG			F5		13.95	W3			
A44P	69324	C-44 4203	8 12 54 -45 3.6		8.2 MV	7.9 PG			B8		10.69	.12	11.85	W3	11.10
A45P	69358	C-45 3917	8 13 4 -45 53.7		10.2 MV	9.2 PG			B3				12.24	W0	12.72
A46P	69344	C-43 4081	8 13 5 -43 47.0		10.5 MV	9.6 PG			A0				13.65	W0	
A47P	69356	C-43 4084	8 13 13 -43 20.6		9.6 MV	9.3 PG			B9				12.81	W3	
A48P	69404	C-46 3951	8 13 16 -46 19.9		6.43	-.15			B3V	EN	9.79	W0	8.37	.11	7.71
A49P	69360	C-43 4088	8 13 20 -44 1.7		9.9 MV								13.82	.12	
A50P	69448	C-43 4092	8 13 35 -43 21.9		9.0 MV	8.5 PG			A5				13.47	W3	
A51P	69513	C-44 4225	8 13 53 -45 4.0		9.4 MV	9.0 PG		*	A0		13.75	W3			12.89
A52P	69512	C-44 4222	8 13 54 -44 33.9		9.7 MV						12.83	W3			
A53P	69567	C-43 4104	8 14 3 -44 10.1		9.1 MV	8.5 PG			B8		12.36	W0	12.14	.05	11.68
A54P	69650	C-45 3942	8 14 17 -46 9.5		6.76MV				A2		12.27	.07	11.05	W0	13.12
A55P	69677	C-45 3943	8 14 18 -46 1.3		11.5 MV	10.1 PG			A0				13.56	W0	
A56P	69648	C-43 4113	8 14 23 -44 10.1		8.2 MV	7.8 PG			B2		11.75	.41	11.76	.15	11.12
A57P	69710	C-43 4120	8 14 39 -44 11.3		8.3 MV	9.4 PG			A0		12.06	W6	13.02	.07	
A58P	69822	C-45 3957	8 15 14 -45 51.4		10.0 MV	8.8 PG			B9		13.23	W0	12.73	.01	
A59P	69780	C-43 4125	8 15 14 -43 16.6		9.2 MV	8.8 PG			A3				13.94	W0	
A60P	69883	C-44 4254	8 15 32 -44 30.7		9.0 MV	8.2 PG			A0		12.78	W3	12.27	W3	11.73
A61P	69933	C-45 3962	8 15 33 -46 8.3		10.2 MV	9.4 PG			A0		13.07	W0	12.55	W0	
A62P	69931	C-44 4255	8 15 36 -45 .6		9.0 MV								14.76	W0	
A63P	69882	C-42 4090	8 15 36 -42 22.0		7.15	.3*	-.51		B2III		10.88	W0			
A64P	69952	C-46 4007	8 15 42 -46 44.2		7.8 MV	7.6 PG			A0		10.99	W0	10.58	.23	11.54
A65P	69953	C-46 4008	8 15 45 -46 51.4		10.0 MV	9.2 PG			B9		13.82	W0			
A66P	69930	C-43 4136	8 15 49 -43 27.7		9.1 MV	8.4 PG			B3		12.23	W0	12.05	W6	11.23
A67P	69932	C-45 3963	8 15 51 -45 30.7		9.7 MV				B9				13.12	.03	
A68P	69972	C-46 4010	8 15 52 -46 23.9		10.0 MV	9.3 PG			B9		13.72	W0	12.98	W0	
A69P	69951	C-41 3957	8 15 55 -41 33.1		10.2 MV			2	A0		12.90	W0	13.11	W0	
A70P	69989	C-43 4145	8 16 10 -43 23.3		9.8 MV	9.2 PG			B8				12.98	W6	
A71P	70024	C-41 3965	8 16 19 -41 57.1		8.9 MV	8.8 PG			B8		12.96	W0	12.59	W0	
A72P	70084	C-46 4025	8 16 27 -46 56.1		7.3 MV	7.1 PG			B5		10.64	.69	9.32	.08	9.18
A73P	70064	C-45 3972	8 16 36 -45 29.2		10.2 MV	9.6 PG		*	A0		13.34	.10	12.39	.04	13.28
A74P	70123	C-45 3981	8 16 38 -45 39.0		10.5 MV	9.9 PG			A0				13.64	.21	
A75P	70124	C-45 3982	8 16 40 -45 54.2		10.2 MV	9.3 PG			A2				13.87	W0	

PRELIMINARY CATALOG OF CELESCOPE ULTRAVIOLET OBSERVATIONS. JULY 1971.

SD3	U4	SD4	CEL	NONSTAR	R.A. (2000)	DEC.	-----REMARKS-----	----------REFERENCES----
			A 1P		8 5 10	-45 24.4	W/-45 3742	897 922
			A 2P		8 5 43	-45 10.2		897
			A 3P		8 6 6	-45 23.6		897
			A 4P		8 6 40	-45 2.9		922
			A 5P		8 7 33	-45 8.8		897
			A 6P		8 8 1	-45 32.5		922
			A 7P		8 8 5	-45 3.5		897
			A 8P		8 8 12	-44 14.7		899
			A 9P		8 8 23	-45 47.7		897
			A10P		8 8 32	-46 15.6		897
			A11P		8 8 35	-45 9.2		899
			A12P		8 8 40	-44 43.2		899
			A13P		8 8 44	-44 26.0		897
			A14P		8 8 43	-45 23.8		897
			A15P		8 9 36	-44 7.3		158 419 897 901 884
W0			A16P		8 10 0	-44 20.7		897
			A17P		8 10 10	-44 54.1		899
			A18P		8 10 22	-44 36.5		922
			A19P		8 10 32	-46 .2		897
			A20P		8 10 59	-44 19.0		922
			A21P		8 10 58	-45 51.0		897
	9.89	W0	A22P		8 11 33	-46 14.0		897
			A23P		8 11 40	-44 4.3		922
			A24P		8 11 47	-44 14.2		922
			A25P		8 11 49	-44 54.5		897
			A26P		8 11 54	-43 45.6		922
			A27P		8 12 5	-45 23.1		899
			A28P		8 12 11	-45 51.1		897
			A29P		8 12 17	-43 58.7		897
			A30P		8 12 29	-45 26.5		922
W0	8.61	W3	A31P		8 12 31	-46 15.8		897 901 884 419 841
			A32P		8 12 37	-45 34.5		922
			A33P		8 12 44	-45 36.7		922
			A34P		8 12 46	-44 41.7		899
			A35P		8 12 49	-43 45.3		897
			A36P		8 13 37	-45 27.7		897
W3			A37P		8 13 39	-46 37.8		922
.14			A38P		8 13 45	-46 34.7		897
			A39P		8 13 56	-43 54.5		922
			A40P		8 14 1	-43 27.8		897
			A41P		8 14 4	-44 34.3	AI VEL	207 969 897 922
.02			A42P		8 14 23	-45 50.0		897 901 419 884 A19
			A43P		8 14 26	-45 17.6		922
W3			A44P		8 14 31	-45 12.7		897
W0			A45P		8 14 40	-46 2.9		897
			A46P		8 14 45	-43 56.2		922
			A47P		8 14 53	-43 29.8		897
.30			A48P		8 14 51	-46 29.1		342 897 158 419
			A49P		8 14 59	-44 10.9		899
			A50P		8 15 15	-43 31.1		897
W3			A51P		8 15 30	-45 13.2	MERGED WITH 4228	922
			A52P		8 15 32	-44 43.1		899
W0			A53P		8 15 42	-44 19.3		897
W0			A54P		8 15 52	-46 18.7		897
			A55P		8 15 53	-46 10.5		897
W0			A56P		8 16 2	-44 19.3		897
			A57P		8 16 18	-44 20.6		897
			A58P		8 16 50	-46 .7		897
			A59P		8 16 55	-43 25.9		922
.29			A60P		8 17 11	-44 40.0		897
			A61P		8 17 8	-46 17.6		897
			A62P		8 17 14	-45 9.9		899
			A63P		8 17 19	-42 31.3		897 158 793
.03			A64P		8 17 16	-46 53.5		897
			A65P		8 17 19	-47 .7		897
.00			A66P		8 17 30	-43 37.0		897
			A67P		8 17 28	-45 40.0		899
			A68P		8 17 27	-46 33.2		897
			A69P		8 17 39	-41 42.4	AU PUP	969
			A70P		8 17 51	-43 32.6		897
			A71P		8 18 2	-42 6.5		897
			A72P		8 18 1	-47 5.5		897
.16			A73P		8 18 13	-45 38.6	W/-45 3978	897
.01			A74P		8 18 15	-45 48.4		899 922
			A75P		8 18 16	-46 3.6		897

A76P	70141	C-45	3983	8	16	55	-45	51.0	10.2	MV	9.6	PG				A0			13.68	W0		
A77P	70173	C-44	4278	8	16	59	-44	29.5	10.5	MV	9.6	PG				A0			14.39	W0		
A78P		C-40	4089	8	17	2	-40	53.4	8.7	MV	9.1	PG				A2			13.70	W0		
A79P	70198	C-44	4281	8	17	5	-44	25.2	10.5	MV	9.6	PG				A0			13.76	.27		
A80P	70172	C-41	3978	8	17	10	-41	43.1	10.3	MV	9.2	PG				A0			13.13	W0		
CEL	HD		DM	R.A. (1950)			DEC.	OBJ	V		B-V		U-B	PHOT	SPECT	PEC.	U1	SD1	U2	SD2	U3	
B 1P	70219	C-45	3991	8	17	14	-45	44.6	9.2	MV	9.2	PG			B8		13.15	.10	13.09	.15		
B 2P	70218	C-44	4282	8	17	15	-44	52.7	8.02	MV					A0		12.27	.04	11.41	.16	12.23	
B 3P	70217	C-41	3981	8	17	17	-41	49.4	9.5	MV	8.5	PG			B9		12.35	W0	12.09	W0		
B 4P	70250	C-43	4166	8	17	33	-43	49.1	9.0	MV	8.8	PG			A0						13.80	
B 5P	70307	C-41	3990	8	17	45	-41	51.0	8.9	MV	8.4	PG			B9		12.05	W0	11.80	W0		
B 6P	70308	C-42	3989	8	17	46	-42	13.7	9.3	MV	8.6	PG			A0		13.22	W0	13.05	W0		
B 7P	70368	C-46	4045	8	18	1	-46	16.9	8.53		.41				F2				14.15	W0		
B 8P	70366	C-41	3995	8	18	13	-41	38.4	9.7	MV	9.4	PG			A0				13.67	W0		
B 9P	70449	C-45	4014	8	18	31	-46	6.8	9.8	MV	9.0	PG			A0				13.12	W0		
B10P	70448	C-43	4187	8	18	37	-43	43.4			8.0	PG		2	B9						13.99	
B11P	70507	C-46	4064	8	18	48	-46	50.0	8.3	MV	7.8	PG			B9		10.95	W3	11.10	.30	11.42	
B12P	70506	C-43	4192	8	18	54	-44	5.7	7.08	MV					A0		10.28	.18	10.09	.18	9.33	
B13P	70505	C-41	4014	8	18	54	-41	16.1	9.5	MV	9.7	PG			B9				13.39	W0		
B14P	70531	C-40	4120	8	19	4	-40	54.7	7.5	MV	7.7	PG			A3		13.13	W0	12.75	W0		
B15P		C-46	4047	8	19	14	-46	17.2	10.0	MV									13.53	W0		
B16P	70615	C-45	4033	8	19	26	-45	52.3	9.8	MV	9.0	PG			A0		12.68	.04	12.65	.28		
B17P		C-42	4150	8	19	26	-42	15.1	9.4	MV	9.5	PG			B9		13.68	W3				
B18P	70643	C-46	4076	8	19	30	-46	50.4	9.0	MV	8.1	PG			B9		10.90	W3	12.11	W3	11.50	
B19P	70682	C-44	4325	8	19	46	-44	49.8	7.89	MV				*	A0		11.32	.07	9.83	.09	10.23	
B20P	70683	C-44	4326	8	19	47	-44	59.8	10.2	MV	9.6	PG			A0		13.26	.06	13.15	.11		
B21P	70700	C-44	4328	8	19	55	-44	22.7	10.0	MV	9.0	PG			A0		12.83	.08	12.41	.09	12.78	
B22P	70699	C-40	4140	8	19	55	-41	2.1	8.6	MV	8.3	PG			A0		12.67	W0	11.98	W0		
B23P	70715	C-42	4157	8	19	58	-42	40.5	8.03	MV					B9		12.78	W3	11.70	W3	11.87	
B24P	70716	C-43	4207	8	20	0	-44	4.0	9.2	MV	8.7	PG			A0		13.29	W3	13.02	.07		
B25P	70744	C-40	4147	8	20	14	-40	24.1	8.9	MV	8.9	PG			A0				13.00	W0	12.18	
B26P	70764	C-40	4151	8	20	22	-40	50.0	7.1	MV	7.5	PG			F5		12.65	W0	13.11	W0		
B27P	70850	C-45	4054	8	20	44	-45	38.3	8.8	MV	8.5	PG			B9		11.80	.05	11.17	.11	11.23	
B28P	70872	C-43	4223	8	20	55	-44	1.5	8.4	MV	7.5	PG			A0		12.49	.16	11.36	.05	11.87	
B29P	70873	C-44	4345	8	20	56	-44	34.5	9.6	MV	9.1	PG			F0				13.75	.57		
B30P	70892	C-44	4346	8	20	58	-44	42.2	7.3	MV	7.8	PG			F0		12.65	.32	12.31	.06		
B31P	70912	C-40	4173	8	21	9	-40	37.2	10.1	MV	9.4	PG			A0				12.57	W0		
B32P	70948	C-42	4178	8	21	14	-43	4.0	7.12	MV					B8		11.09	W0	10.39	W0	9.00	
B33P	70947	C-39	4274	8	21	21	-40	13.2	7.4	MV	7.3	PG			B8		10.85	W0	10.47	W0	9.37	
B34P	70976	C-42	4184	8	21	29	-42	49.5	8.6	MV	8.5	PG			A0				12.31	W0		
B35P		C-45	4072	8	21	32	-45	25.3	9.7	MV	9.8	PG					13.31	W3	13.65	W0		
B36P		C-44	4357	8	21	40	-44	48.2	7.78	MV					B5		11.13	.35	10.12	.15	9.97	
B37P	71017	C-40	4185	8	21	40	-41	13.2	9.9	MV	9.4	PG			A0				14.20	W0		
B38P	71019	C-42	4187	8	21	42	-42	38.7	8.26	MV					B8		11.73	W0	10.72	.00	10.83	
B39P	71042	C-45	4074	8	21	45	-45	35.5	10.0	MV	9.0	PG			A0		12.69	W3	12.95	.01		
B40P	71060	C-45	4075	8	21	50	-45	27.0	7.44	MV					A0		11.98	.04	12.31	.14		
B41P	71041	C-43	4234	8	21	50	-44	4.9	9.4	MV	8.8	PG			A0		13.19	W3	13.00	.04		
B42P	71059	C-43	4235	8	21	56	-43	34.4	10.0	MV	9.3	PG			B8				13.72	W0		
B43P	71123	C-42	4198	8	22	10	-42	23.5	8.4	MV	7.9	PG			B9		13.50	W0	12.41	.60	12.65	
B44P	71162	C-44	4372	8	22	23	-44	20.6	10.2	MV	9.3	PG			A5				14.15	W0		
B45P	71161	C-43	4244	8	22	30	-43	33.1	10.2	MV	9.6	PG			A0				13.94	W0		
B46P	71237	C-46	4128	8	22	41	-46	49.4	10.0	MV	9.4	PG			B9				12.73	W0	13.28	
B47P	71218	C-44	4381	8	22	43	-44	15.2	9.8	MV	9.3	PG			B9		11.15	W3	13.15	.09		
B48P	71216	C-40	4212	8	22	48	-40	35.0	7.1	MV	7.2	PG			B3		10.33	W0	9.44	.03	8.95	
B49P	71303	C-43	4258	8	23	7	-43	51.9	9.6	MV	9.1	PG			A2				14.23	W0		
B50P	71286	C-41	4098	8	23	8	-41	52.5	8.9	MV	8.6	PG			A3				13.81	W3		
B51P	71316	C-47	3919	8	23	12	-47	17.5	9.2	MV	9.0	PG			F0				14.13	W3		
B52P	71302	C-42	4219	8	23	13	-42	36.4	5.98		-.18			B	B3V	N	9.71	.12	8.63	.02	8.02	
B53P	71304	C-43	4259	8	23	15	-44	8.2	8.4	MV	8.2	PG			B0		12.46	W3	12.94	.01		
B54P	71336	C-42	4221	8	23	24	-43	12.1	8.0	MV	7.3	PG			B3		10.76	.18	10.68	W0		
B55P		C-44	4392	8	23	38	-44	59.9	9.0	MV	7.3	PG					11.94	.16	13.14	.18		
B56P	71384	C-42	4226	8	23	40	-42	30.0	9.8	MV	9.1	PG			A2				13.13	.16		
B57P	71383	C-40	4230	8	23	45	-40	48.3	8.4	MV	8.5	PG			A0		11.99	W3	12.61	W3		
B58P	71444	C-46	4152	8	23	54	-46	28.2	9.0	MV	8.2	PG			A0		12.55	.10	11.11	.11	11.47	
B59P	71441	C-41	4118	8	24	1	-41	46.6	10.3	MV	9.4	PG			A				13.69	W0		
B60P	71459	C-41	4119	8	24	7	-41	59.3	5.46		-.16			U	B3V		9.20	.05	8.14	.23	7.54	
B61P	71421	C-40	4235	8	24	7	-40	24.1	10.6	MV	9.4	PG			A2				13.42	W6		
B62P	71440	C-40	4236	8	24	8	-40	27.1	10.3	MV	10.3	PG			A0				13.47	W6		
B63P	71470	C-43	4276	8	24	17	-43	51.5	8.9	MV	7.8	PG			B8		11.97	.09	10.98	.01		
B64P	71490	C-42	4240	8	24	20	-43	8.3	10.9	MV	9.7	PG			B9				12.92	W3		
B65P	71508	C-42	4241	8	24	25	-42	41.9	10.0	MV	9.8	PG			B8		13.26	W0	12.89	.10		
B66P	71527	C-40	4245	8	24	30	-41	4.5	9.2	MV	8.6	PG			A0		13.68	W6				
B67P	71528	C-41	4127	8	24	31	-41	58.4	7.9	MV	7.6	PG			B3		11.65	.10	10.03	.00		
B68P	71545	C-42	4244	8	24	37	-42	27.7	10.5	MV	9.7	PG			A0				13.97	.12		
B69P	71544	C-40	4248	8	24	38	-41	1.3	8.02	MV					B9		11.69	W6			11.98	
B70P	71653	C-46	4171	8	24	51	-46	44.1	10.5	MV	9.6	PG			A0				13.35	W0		

			A76P		8 18 31 -46 .4		897	
			A77P		8 18 38 -44 38.9		922	
			A78P		8 18 47 -41 2.8		897	
			A79P		8 18 44 -44 34.6		899 922	
			A80P		8 18 54 -41 52.5		922	
SD3	U4	SD4	CEL	NONSTAR	R.A. (2000) DEC.	-----REMARKS-----	----------REFERENCES---	
			B 1P		8 18 51 -45 54.0		897	
.12			B 2P		8 18 53 -45 2.1		897	
			B 3P		8 19 1 -41 58.8		897	
W3			B 4P		8 19 13 -43 58.5		897	
			B 5P		8 19 29 -42 .4		897	
			B 6P		8 19 29 -42 23.1		922	
			B 7P		8 19 37 -46 26.4		897 A19	
			B 8P		8 19 57 -41 47.9		899 922	
			B 9P		8 20 7 -46 16.3		897	
WO			B10P		8 20 18 -43 52.9	AY VEL	969	
			B11P		8 20 23 -46 59.5		897	
WO			B12P		8 20 34 -44 15.2		897	
.15			B13P		8 20 39 -41 25.6		897	
			B14P		8 20 50 -41 4.2		897	
			B15P		8 20 50 -46 26.7		899	
			B16P		8 21 3 -46 1.8		897	
			B17P		8 21 9 -42 24.6		897	
.17			B18P		8 21 5 -46 59.9		897	
.04			B19P		8 21 25 -44 59.4	WITH C-44 4330	897	
			B20P		8 21 25 -45 9.4		897 922	
WO			B21P		8 21 35 -44 32.3		897 922	
			B22P		8 21 41 -41 11.7		897	
W3			B23P		8 21 41 -42 50.1		897	
			B24P		8 21 40 -44 13.6		922	
WO			B25P		8 22 1 -40 33.7		897	
			B26P		8 22 8 -40 59.6		922	
.02			B27P		8 22 21 -45 47.9		897	
WO			B28P		8 22 35 -44 11.1		897	
			B29P		8 22 35 -44 44.1		897 922	
			B30P		8 22 37 -44 51.8		922	
			B31P		8 22 55 -40 46.9		922	
WO			B32P		8 22 56 -43 13.7		897	
WO			B33P		8 23 8 -40 22.9		897	
			B34P		8 23 12 -42 59.2		897	
			B35P		8 23 10 -45 35.0		897	
.39			B36P		8 23 19 -44 57.9		897	
			B37P		8 23 25 -41 22.9		899 922	
WO			B38P		8 23 25 -42 48.4		897	
			B39P		8 23 23 -45 45.2		897	
			B40P		8 23 28 -45 36.7		897	
			B41P		8 23 30 -44 14.6		922	
			B42P		8 23 37 -43 44.1		897 922	
WO			B43P		8 23 54 -42 33.2		897	
			B44P		8 24 3 -44 30.3		922	
			B45P		8 24 12 -43 42.8		922	
WO			B46P		8 24 16 -46 59.1		897	
			B47P		8 24 23 -44 24.9		897 922	
WO			B48P		8 24 35 -40 44.7		897	
			B49P		8 24 48 -44 1.7		922	
			B50P		8 24 53 -42 2.3		897	
			B51P		8 24 46 -47 27.3		897	
WO			B52P		8 24 56 -42 46.2		158 419 897 884 901	
			B53P		8 24 56 -44 18.0		922	
			B54P		8 25 6 -43 21.9		897 922	
			B55P		8 25 17 -45 9.7		897	
			B56P		8 25 24 -42 39.8		897	
			B57P		8 25 31 -40 58.1		897	
.02	13.09	WO	B58P		8 25 30 -46 38.0		897	
			B59P		8 25 46 -41 56.4		897	
WO			B60P		8 25 52 -42 9.1		419 841 488 897 901 884 A19	
			B61P		8 25 54 -40 33.9		899 922	
			B62P		8 25 55 -40 36.9		899 922	
			B63P		8 25 58 -44 1.3		897 922	
			B64P		8 26 3 -43 18.1		922	
			B65P		8 26 8 -42 51.7		897	
			B66P		8 26 16 -41 14.3		922	
			B67P		8 26 16 -42 8.2		897	
			B68P		8 26 21 -42 37.6		922	
W6			B69P		8 26 24 -41 11.2		897	
			B70P		8 26 27 -46 54.0		897	

B71P	71609	C-42	4251	8	24	55	-43	14.6	7.7	MV	8.1	PG			B2	11.36	.20	11.64	.37	
B72P	71607	C-42	4250	8	24	56	-42	21.5	7.21	MV					A2	12.94	.16	11.84	.01	
B73P	71627	C-42	4253	8	24	57	-42	42.4	9.8	MV	9.3	PG			B8	12.69	W0	12.51	.09	12.77
B74P	71628	C-44	4413	8	25	1	-44	41.1	9.4	MV	8.4	PG			A0			11.69	W3	
B75P	71651	C-45	4137	8	25	2	-45	25.1	9.6	MV	9.1	PG			A0			13.52	W3	
B76P	71652	C-45	4140	8	25	6	-45	36.1	9.6	MV	9.1	PG			A0			12.98	.06	13.50
B77P	71694	C-47	3955	8	25	10	-47	16.4	9.6	MV	8.7	PG			B9	12.84	W0	12.32	W0	11.93
B78P	71693	C-43	4296	8	25	16	-43	41.8	9.6	MV	9.0	PG			B8			12.12	W0	
B79P	71743	C-46	4178	8	25	28	-46	20.6	10.0	MV	9.3	PG			B9			12.88	.16	
B80P	71719	C-44	4421	8	25	29	-44	25.1	10.5	MV	9.6	PG			A0	12.50	W6			

CEL	HD		DM	R.A. (1950)			DEC.	OBJ	V		B-V		U-B	PHOT	SPECT	PEC.	U1	SD1	U2	SD2	U3
C 1P	71742	C-41	4145	8	25	33	-41	33.6	8.3	MV	8.9	PG			A3				13.68	.03	
C 2P	71773	C-44	4425	8	25	40	-44	56.4	9.1	MV	8.6	PG			A0		14.55	W3	13.09	.31	
C 3P	71788	C-47	3963	8	25	41	-47	38.2	8.5	MV	8.2	PG			B9		11.92	W3			11.93
C 4P	71786	C-41	4149	8	25	46	-41	58.2	10.3	MV	9.4	PG			B9				12.79	.11	13.57
C 5P	71823	C-47	3967	8	25	53	-47	33.8	8.9	MV	8.4	PG			B5		11.60	W3			11.30
C 6P		C-42	4273	8	26	6	-42	48.4	10.3	MV	9.9	PG			A0				14.15	W0	
C 7P	71874	C-47	3973	8	26	12	-47	30.5	8.5	MV	8.2	PG			B9		11.55	W3			11.09
C 8P	71857	C-40	4277	8	26	14	-41	4.7	7.77	MV					A0		12.30	W0	11.31	W0	12.14
C 9P	71858	C-41	4162	8	26	15	-41	30.4	9.0	MV	10.2	PG			A0				13.51	.27	
C10P	71896	C-41	4166	8	26	26	-41	40.1	8.9	MV	9.0	PG			B9		13.23	.01	12.35	.13	12.84
C11P	71917	C-46	4198	8	26	27	-46	38.9	10.0	MV	9.3	PG			A2				13.95	W0	
C12P	71984	C-46	4205	8	26	48	-46	47.3	8.4	MV	7.9	PG			B9		11.99	.37	10.68	.14	11.17
C13P	71967	C-40	4285	8	26	50	-41	.4	7.70	MV					A0		12.68	W0	11.28	W0	12.01
C14P		C-45	4146	8	26	52	-45	58.0	10.	MV									14.07	W0	13.84
C15P	71998	C-41	4175	8	27	1	-41	22.0	8.6	MV	8.3	PG			B9				12.36	.10	12.85
C16P	72014	C-42	4290	8	27	7	-42	25.2	6.21		-.05		+1.14		B3V	EN	9.33	.27	9.64	1.30	7.57
C17P	72034	C-45	4167	8	27	9	-45	34.1	9.8	MV	9.2	PG			B9		13.12	W0	12.77	.00	
C18P	72067	C-43	4337	8	27	26	-43	59.6	5.94	MV	5.7	PG		U	B3V	E	10.22	.62	7.88	.12	
C19P	72089	C-45	4173	8	27	27	-45	23.4	7.7	MV	7.5	PG			B9		11.38	.10	10.52	.03	10.68
C20P	72108	C-47	4004	8	27	31	-47	45.4	5.32		-.15			B	B5	N			7.36	W0	11.11
C21P	72065	C-40	4297	8	27	31	-40	58.3	9.9	MV	9.1	PG			A0		13.42	W0	11.33	W0	12.14
C22P	72088	C-44	4459	8	27	32	-44	43.0	10.5	MV	8.9	PG			B9		12.97	.01	11.87	.22	11.70
C23P	72107	C-43	4338	8	27	34	-43	18.2	10.0	MV	9.4	PG			B8		13.78	W3	14.54	W3	
C24P	72128	C-45	4176	8	27	39	-45	17.8	9.20	MV	9.0	PG			A0		13.17	.15	12.24	.30	12.68
C25P	72140	C-46	4221	8	27	44	-46	43.3	10.2	MV	9.0	PG			B9		13.25	.15	12.70	W0	
C26P	72162	C-45	4177	8	27	46	-45	21.8	9.84	MV	9.6	PG			A0				13.43	W3	
C27P	72127	C-44	4462	8	27	46	-44	33.4	5.22					U8	B3V		8.35	.00	7.60	.18	5.36
C28P	72180	C-47	4012	8	27	50	-47	38.1	9.8	MV	9.0	PG			A0		13.05	W0	13.46	W0	
C29P	72139	C-41	4189	8	27	50	-41	21.4	8.00	MV					B9		13.02	.13	11.67	.15	12.34
C30P	72161	C-42	4305	8	27	53	-43	9.9	8.2	MV	7.9	PG			B9		11.11	W3	11.69	.19	
C31P	72179	C-43	4343	8	27	55	-43	55.9	8.6	MV	7.7	PG			B8		11.54	W3	10.66	.03	
C32P	72159	C-41	4193	8	27	58	-41	37.3	9.0	MV	9.1	PG			B9				12.54	.15	
C33P	72177	C-41	4194	8	28	5	-41	45.1	9.2	MV	9.9	PG		*	B9		12.07	.10	11.69	.16	11.13
C34P	72232	C-45	4183	8	28	8	-46	9.8	6.11						B8		9.68	.08	8.59	.18	7.77
C35P	72253	C-47	4023	8	28	9	-47	51.5	7.79	MV					B9				11.44	W3	
C36P	72230	C-44	4469	8	28	10	-44	34.5	9.0	MV	8.5	PG			A0		13.20	W0			
C37P	72250	C-41	4201	8	28	19	-41	28.2	9.9	MV	9.9	PG			B8				12.65	.22	12.68
C38P	72270	C-42	4315	8	28	23	-42	51.1	10.5	MV	9.4	PG			A2				13.88	W3	
C39P	72271	C-43	4350	8	28	25	-44	7.5	9.6	MV	9.1	PG			B8		12.84	W0	12.09	W0	
C40P	72319	C-42	4323	8	28	40	-42	28.6	9.1	MV	8.5	PG			A0		12.62	W0	12.19	W0	
C41P	72351	C-46	4244	8	28	48	-46	50.6	10.5	MV	9.3	PG			A0		14.21	W0			
C42P		C-45	4194	8	28	48	-46	8.6	9.7	MV	10.1	PG					12.82	W0	13.31	W0	
C43P	72350	C-44	4477	8	28	58	-44	34.1	6.49					B	B5IV		10.72	.20	9.69	.10	8.98
C44P	72387	C-45	4195	8	29	5	-45	42.3	10.2	MV	9.4	PG			A0				13.32	.01	
C45P	72402	C-44	4485	8	29	14	-44	26.7	9.6	MV	8.3	PG			A0		13.49	.17	12.80	.06	12.80
C46P	72401	C-41	4214	8	29	14	-42	1.4	9.3	MV	9.7	PG			B8				12.61	W0	
C47P	72439	C-41	4219	8	29	25	-41	53.8	9.3	MV	9.2	PG			A0				13.44	W0	
C48P	72453	C-44	4489	8	29	31	-44	19.7	9.8	MV	9.0	PG			B9		13.14	.07	12.24	.02	12.26
C49P	72485	C-47	4048	8	29	35	-47	41.8	6.4*		-.16				B4				8.67	W0	
C50P	72483	C-45	4207	8	29	43	-45	20.8	9.4	MV	9.1	PG		*	A0		12.75	.54	12.39	.04	12.19
C51P	72516	C-47	4050	8	29	50	-47	15.0	9.4	MV	8.4	PG			F5		13.47	W3			
C52P	72499	C-43	4368	8	29	51	-43	34.1	10.2	MV	9.4	PG			A0				14.37	W0	
C53P	72537	C-45	4215	8	29	57	-45	36.9	8.14	MV					B8		10.72	.05	9.60	.01	9.25
C54P	72515	C-43	4371	8	29	57	-44	14.8	8.8	MV	8.4	PG			B8		12.79	.22	12.50	.02	12.41
C55P	72535	C-41	4225	8	30	1	-41	51.8	7.7	MV	8.1	PG			B5		11.29	W0	10.88	W0	10.39
C56P	72555	C-46	4267	8	30	3	-47	4.2	6.81	MV					B3		8.08	W3	10.59	.63	8.25
C57P	72554	C-45	4219	8	30	6	-45	57.4	8.5	MV	8.1	PG			B0III		11.83	.19	12.28	.09	12.66
C58P	72576	C-43	4374	8	30	8	-43	39.1	8.4	MV	8.5	PG			B9		12.80	1.00	13.24	.38	13.58
C59P	72611	C-41	4232	8	30	30	-41	39.7	7.1	MV	7.4	PG			A0		11.17	W0	10.37	W0	10.99
C60P	72648	C-43	4382	8	30	36	-43	45.6	7.9	MV	7.5	PG			B3		12.22	.06	11.24	.35	10.83
C61P	72676	C-45	4227	8	30	41	-45	51.6	8.6	MV	8.4	PG			F5		14.05	W0	14.23	W0	
C62P	72675	C-45	4228	8	30	44	-45	36.9	8.6	MV	8.5	PG			A3		12.66	.05	12.94	.06	
C63P	72733	C-43	4390	8	30	59	-43	52.4	9.0	MV	8.2	PG			B9		12.82	W0	11.87	W0	12.25
C64P	72735	C-47	4065	8	31	0	-47	32.4	10.5	MV	9.1	PG			A0				14.76	W3	
C65P	72732	C-42	4365	8	31	0	-43	3.8	8.6	MV	8.3	PG			A0				12.67	W0	

			B71P	8 26 37	-43 24.5		897 922	
			B72P	8 26 40	-42 31.4		897	
W0			B73P	8 26 40	-42 52.3		897	
			B74P	8 26 41	-44 51.0		897 922	
			B75P	8 26 41	-45 35.0		897 922	
W0			B76P	8 26 44	-45 46.0		897	
W0			B77P	8 26 45	-47 26.3		897	
			B78P	8 26 58	-43 51.7		897 922	
			B79P	8 27 5	-46 30.5		897	
			B80P	8 27 9	-44 35.0		922	

SD3	U4	SD4	CEL	NOVSTAR	R.A. (2000)	DEC.	-----REMARKS-----	----------REFERENCES----------
			C 1P		8 27 19	-41 43.5		897
			C 2P		8 27 20	-45 6.3		897
.20			C 3P		8 27 15	-47 48.1		897
W0			C 4P		8 27 31	-42 8.1		922
W0			C 5P		8 27 27	-47 43.7		897
			C 6P		8 27 49	-42 58.3		922
W0			C 7P		8 27 47	-47 40.4		897
.18			C 8P		8 28 0	-41 14.6		897
			C 9P		8 28 1	-41 40.3		897
.31			C10P		8 28 11	-41 50.1		897
			C11P		8 28 3	-46 48.9		897
.19			C12P		8 28 24	-46 57.3		897
.37			C13P		8 28 37	-41 10.4		897
W0			C14P		8 28 30	-46 8.0		900
.30			C15P		8 28 47	-41 32.0		897
.02			C16P		8 28 51	-42 35.2		158 897 A19
			C17P		8 28 48	-45 44.1		897
			C18P		8 29 8	-44 9.6		488 752 897 901 884 419 922
.07			C19P		8 29 6	-45 33.4		897
W3			C20P		8 29 5	-47 55.4		897 901 884 158 419
.35			C21P		8 29 18	-41 8.3		897 922
.16	9.40	W6	C22P		8 29 12	-44 53.0		897 922
			C23P		8 29 17	-43 28.2		922
.00			C24P		8 29 18	-45 27.8		897
			C25P		8 29 20	-46 53.3		897
			C26P		8 29 25	-45 31.8		922
1.05			C27P		8 29 27	-44 43.4		901 884 419 897 488
			C28P		8 29 25	-47 48.1		897
.28			C29P		8 29 36	-41 31.4		897
			C30P		8 29 36	-43 19.9		897
			C31P		8 29 37	-44 5.9		897
			C32P		8 29 44	-41 47.3		897
.37			C33P		8 29 51	-41 55.2	INCL 72178	897
.02			C34P		8 29 46	-46 19.9		897 884 901
			C35P		8 29 43	-48 1.6		897
			C36P		8 29 51	-44 44.6		897
.40			C37P		8 30 5	-41 38.3		897
			C38P		8 30 7	-43 1.2		922
			C39P		8 30 7	-44 17.6		897
			C40P		8 30 24	-42 38.7		922
			C41P		8 30 24	-47 .7		922
			C42P		8 30 26	-46 18.7		897
.13	8.19	W0	C43P		8 30 39	-44 44.2		901 419 884 897
			C44P		8 30 44	-45 52.4		899 922
W3			C45P		8 30 55	-44 36.8		922
			C46P		8 30 59	-42 11.5		922
			C47P		8 31 11	-42 3.9		922
W3			C48P		8 31 12	-44 29.8		897
			C49P		8 31 10	-47 51.9		897 419 842 884 901
.07			C50P		8 31 22	-45 30.9	WITH -45 4213	897 922
			C51P		8 31 26	-47 25.2		897 922
			C52P		8 31 34	-43 44.3		922
.13			C53P		8 31 36	-45 47.1		897
W3			C54P		8 31 39	-44 25.0		897 922
W0			C55P		8 31 47	-42 2.0		897
.21			C56P		8 31 39	-47 14.4		897
W0			C57P		8 31 44	-46 7.6		12 897
W3	13.06	W0	C58P		8 31 51	-43 49.3		897 922
W0			C59P		8 32 16	-41 49.9		897
.10			C60P		8 32 19	-43 55.8		897 922
			C61P		8 32 20	-46 1.8		897 922
			C62P		8 32 23	-45 47.1		897
.05			C63P		8 32 41	-44 2.6		897 922
			C64P		8 32 35	-47 42.6		897
			C65P		8 32 44	-43 14.0		897

C66P	72731	C-41	4240	8	31	1	-41	42.5	8.9	MV	9.4	PG			B9			12.48	W0	
C67P	72751	C-45	4232	8	31	9	-45	28.0	9.1	MV	9.0	PG			A0	12.10	W0	12.07	.24	12.43
C68P	72772	C-43	4393	8	31	12	-43	14.2	8.3	MV	8.5	PG			F5			14.49	W0	
C69P	72773	C-44	4512	8	31	13	-45	10.4	9.2	MV	8.7	PG			A0	12.73	W0	12.72	.02	
C70P	72789	C-43	4396	8	31	15	-44	3.9	9.8	MV	9.3	PG			A0			13.52	W0	...
C71P	72800	C-47	4072	8	31	18	-47	26.0	6.61		.14				BLI	11.42	W3	11.11	W3	12.02
C72P	72798	C-45	4236	8	31	22	-45	34.9	6.45		-.14				B5III	10.20	.21	9.07	.03	8.34
C73P	72817	C-46	4296	8	31	28	-46	17.0	10.0	MV	9.0	PG			A0	12.65	.16	13.34	.02	
C74P		C-44	4518	8	31	28	-45	.8	9.52		.28				B3	13.03	W0	13.37	.06	
C75P		C-44	4520	8	31	30	-45	0.0	9.52		.28				B3			13.66	.06	
C76P	72836	C-42	4375	8	31	38	-42	54.4	9.4	MV	9.0	PG			B8			13.29	W0	
C77P	72874	C-42	4378	8	31	49	-42	36.2	9.8	MV	9.1	PG			A0			13.92	W3	
C78P	72875	C-42	4379	8	31	51	-42	50.4	9.8	MV	8.8	PG			A0			12.78	W0	13.56
C79P	72898	C-42	4380	8	31	53	-42	27.7	9.0	MV	8.2	PG			B9	13.07	W3	12.24	W3	12.53
C80P	72939	C-47	4087	8	31	57	-47	43.3	9.6	MV	8.9	PG			B5			11.79	W0	13.20

CEL	HD		DM	R.A. (1950)			DEC.	OBJ	V		B-V		U-B	PHOT	SPECT	PEC.	U1	SD1	U2	SD2	U3
D 1P	72918	C-43	4410	8	31	58	-43	16.6	9.6	MV	9.0	PG			B9				12.04	W0	13.15
D 2P	72919	C-44	4529	8	32	1	-44	46.4	8.2	MV	7.5	PG		*	B9		11.98	.17	11.45	1.31	11.31
D 3P	72959	C-44	4535	8	32	10	-45	13.6	10.2	MV	9.3	PG			A0		13.16	W0	13.30	.05	
D 4P	72997	C-44	4539	8	32	26	-44	22.3	7.6	MV	7.0	PG			B5		10.56	.20	9.52	.05	
D 5P	73010	C-45	4255	8	32	31	-45	27.8	7.50	MV					B8		11.02	.30	9.87	.03	9.93
D 6P	73009	C-44	4540	8	32	31	-44	37.8	9.8	MV	9.1	PG			B9		12.51	W0	11.93	.19	
D 7P	73042	C-43	4417	8	32	37	-43	50.4	8.8	MV	9.0	PG			B9				12.50	0.00	
D 8P	73061	C-46	4320	8	32	46	-46	51.0	9.8	MV	9.3	PG			A2				14.10	W3	
D 9P		C-43	4418	8	32	46	-44	.9	9.6	MV	9.2	PG			A				13.18	W0	
D10P	73059	C-44	4544	8	32	48	-44	20.0	9.6	MV	8.8	PG			B9		12.64	W3			
D11P	73055	C-40	4408	8	32	52	-41	3.7	8.6	MV	7.9	PG			B8						11.00
D12P	73076	C-44	4547	8	32	53	-44	15.9	8.7	MV	8.6	PG			B9		12.27	W0	11.81	1.16	
D13P	73090	C-44	4548	8	32	58	-44	21.3	8.2	MV	7.6	PG			B9		11.23	.41	10.48	1.06	
D14P	73125	C-45	4271	8	33	14	-45	18.2	10.0	MV	9.3	PG			A0		13.00	W0	12.81	.08	
D15P	73153	C-44	4555	8	33	26	-45	3.3	9.1	MV	8.4	PG			A0		12.57	W0	12.49	.03	
D16P		C-45	4267	8	33	27	-45	35.6	9.6	MV	9.4	PG			A		13.12	W3			
D17P	73186	C-43	4437	8	33	34	-44	7.4	9.8	MV	8.9	PG			B9		12.51	W0	11.98	.20	
D18P	73219	C-47	4114	8	33	39	-47	47.2	10.9	MV	9.6	PG			A2				12.97	W0	
D19P	73218	C-42	4418	8	33	43	-42	23.3	7.6	MV	7.7	PG			F5				13.53	W0	
D20P	73304	C-46	4344	8	34	13	-46	57.1	10.0	MV	8.7	PG			A3				14.66	.12	
D21P	73305	C-47	4119	8	34	15	-47	40.3	9.4	MV	8.5	PG			A0				11.34	W3	13.29
D22P	73303	C-43	4458	8	34	19	-44	13.3	9.1	MV	8.7	PG			B9		12.34	W0	11.71	.24	
D23P		C-46	4349	8	34	23	-46	19.6	7.46	MV					B5		10.56	.09	9.56	.03	8.82
D24P	73368	C-46	4354	8	34	28	-46	57.1	11.5	MV	9.6	PG			A3				14.41	.19	
D25P	73384	C-44	4584	8	34	40	-45	15.0	9.24	MV	8.5	PG			A0		12.98	W3			
D26P	73404	C-46	4360	8	34	42	-47	7.0	9.40		.07				A0				12.73	.07	
D27P	73421	C-47	4132	8	34	48	-47	25.0	9.19		.30				A2				14.19	W0	
D28P	73420	C-43	4467	8	34	54	-43	54.3	9.6	MV	8.3	PG			B3		12.20	W0	11.72	.04	
D29P	73461	C-47	4135	8	35	4	-47	19.5	7.36		.32				A5				12.36	W0	
D30P	73478	C-47	4136	8	35	7	-47	49.4	7.40	MV					B8		11.14	W0	10.01	W0	9.46
D31P	73477	C-45	4303	8	35	11	-46	8.9	8.2	MV	8.5	PG			G0				14.45	W3	
D32P		C-45	4304	8	35	15	-45	20.8	9.10		.19				B2III	4			12.17	.21	12.16
D33P	73589	C-46	4375	8	35	37	-47	1.4	8.84		.04				B8		12.33	.36	12.54	.28	11.79
D34P		C-45	4313	8	35	38	-45	56.7	10.53		.11				B3III	4			13.09	.27	
D35P	73568	C-44	4602	8	35	38	-45	1.9	8.33		.31				B1III				11.81	W0	
D36P	73567	C-41	4322	8	35	41	-42	10.8	8.6	MV	8.7	PG			B8		13.16	W0	11.82	W0	12.48
D37P	73634	C-42	4451	8	35	53	-42	48.8	4.13		.10		.12		A8I		10.79	W0	10.03	.04	12.15
D38P	73658	C-45	4322	8	36	0	-46	6.4	7.08	MV					B5		10.29	.05	9.82	.08	9.39
D39P	73738	C-44	4627	8	36	28	-45	9.7	8.5	MV	7.8	PG			B9		11.56	.28	10.88	.13	12.02
D40P	73774	C-43	4500	8	36	37	-44	7.3	9.6	MV	9.3	PG			B9				12.81	.35	
D41P	73813	C-46	4395	8	36	46	-46	36.0	7.58		-.02			*	B9		10.77	.02	9.68	.00	9.75
D42P		C-45	4398	8	36	50	-46	59.6	9.0	MV	9.5	PG					12.84	W0	12.92	W0	
D43P		C-45	4338	8	36	54	-45	45.1	8.2	MV	7.6	PG			B8		11.33	.04	10.87	.02	10.97
D44P	73811	C-42	4469	8	36	54	-42	16.2	8.4	MV	7.9	PG			B9		12.37	W0	11.57	W0	13.07
D45P	73830	C-45	4339	8	36	57	-45	37.3	8.2	MV	7.8	PG			A2				13.51	.27	
D46P	73847	C-46	4400	8	36	59	-46	36.3	8.20		-.04				B9						11.16
D47P	73903	C-45	4348	8	37	19	-46	3.0	8.96		.23			*	B4V		11.42	.24	10.74	.05	11.27
D48P				8	37	38	-46	15.4											14.56	W0	
D49P		C-46	4409	8	37	39	-46	20.2	9.8	MV	9.4	PG					12.79	.01	13.29	0.00	
D50P		C-45	4374	8	37	50	-46	7.0									12.99	.08	13.06	.01	
D51P	73986	C-42	4487	8	37	50	-42	18.5	8.34	MV					B9				11.45	W0	
D52P	74042	C-44	4659	8	38	6	-44	35.3	9.6	MV	8.4	PG		*	A0				12.31	.03	13.32
D53P	74069	C-44	4661	8	38	12	-44	57.5	9.8	MV	9.3	PG			A				13.22	W3	
D54P	74107	C-47	4194	8	38	29	-47	34.2	10.2	MV	9.4	PG			A0		13.43	W0			
D55P	74106	C-45	4380	8	38	29	-45	26.3	8.8	MV	8.3	PG			B9		13.01	.39	12.08	.16	12.63
D56P	74129	C-45	4389	8	38	40	-45	56.7	9.2	MV	9.0	PG			A		12.13	.04	12.23	.04	12.24
D57P		C-46	4432	8	38	57	-47	3.4	9.5	MV	10.1	PG		*			13.26	W0			
D58P	74180	C-46	4438	8	38	58	-46	28.2	3.90		.7*		.22	B	F2I		11.18	.13	12.01	.00	
D59P	74194	C-44	4683	8	39	5	-44	52.8	7.54		.23				BE		11.19	.18	10.90	.12	11.58
D60P	74209	C-44	4684	8	39	8	-44	34.2	9.6	MV	.90	PG			A0		13.70	W0	13.47	.02	

			C66P	8 32 47	-41 52.7		897		
.16			C67P	8 32 49	-45 38.2		922 897		
			C68P	8 32 56	-43 24.4		922		
			C69P	8 32 53	-45 20.6		897 922		
			C70P	8 32 57	-44 14.1		897 922		
W3			C71P	8 32 54	-47 36.2		158 897		
.56	9.64	W3	C72P	8 33 1	-45 45.1		897 158 419 A19		
			C73P	8 33 6	-46 27.2		897		
			C74P	8 33 8	-45 11.0		899 A19		
			C75P	8 33 10	-45 10.3		158		
			C76P	8 33 22	-43 4.7		897		
			C77P	8 33 34	-42 46.5		922		
W0			C78P	8 33 35	-43 .7		922		
.16			C79P	8 33 38	-42 38.0		897		
W0			C80P	8 33 32	-47 53.6		897		

SD3	U4	SD4	CEL	NONSTAR	R.A. (2000)	DEC.	-----REMARKS-----	----------REFERENCES--
W0			D 1P		8 33 42	-43 26.9		897
W3			D 2P		8 33 42	-44 56.7	MERGED CPD 2744	897
			D 3P		8 33 50	-45 23.9		897
	9.18	.16	D 4P		8 34 8	-44 32.6		897
.20			D 5P		8 34 11	-45 38.1		897
			D 6P		8 34 12	-44 48.1		897
			D 7P		8 34 20	-44 .7		897
			D 8P		8 34 23	-47 1.3		897
			D 9P		8 34 28	-44 11.2		897
	12.14	W3	D10P		8 34 30	-44 30.3		897
W0			D11P		8 34 39	-41 14.0		897
			D12P		8 34 35	-44 26.2		897
	10.64	.36	D13P		8 34 40	-44 31.6		897
			D14P		8 34 54	-45 28.6		897
			D15P		8 35 7	-45 13.7		922 897
			D16P		8 35 7	-45 46.0		897
			D17P		8 35 16	-44 17.8		897
			D18P		8 35 14	-47 57.6		922
			D19P		8 35 28	-42 33.7		922
			D20P		8 35 50	-47 7.5		897 922
W0			D21P		8 35 51	-47 50.7		897 922
			D22P		8 36 1	-44 23.7		897
.07			D23P		8 36 1	-46 30.0		897
			D24P		8 36 5	-47 7.5		922
			D25P		8 36 21	-45 25.4		897
			D26P		8 36 19	-47 17.4		158
			D27P		8 36 24	-47 35.4		158
			D28P		8 36 37	-44 4.7		897
			D29P		8 36 41	-47 30.0		897 158
W0			D30P		8 36 43	-47 59.9		897
			D31P		8 36 50	-46 19.4		897 922
.26			D32P		8 36 55	-45 31.3		16 474 897 158
.28			D33P		8 37 14	-47 11.9		158 897
			D34P		8 37 17	-46 7.2		900 16 474 158
			D35P		8 37 19	-45 12.4		16 897 158 A19
W0			D36P		8 37 27	-42 21.3		897
W0			D37P		8 37 38	-42 59.3		901 884 899 8 508 781 897 921 158 A19
.01	10.26	.35	D38P		8 37 39	-46 16.9		897
.13	13.27	W3	D39P		8 38 9	-45 20.2		897
			D40P		8 38 20	-44 17.8		897
.09	11.14	W0	D41P		8 38 24	-46 46.5	WITH 4400	897 158
			D42P		8 38 28	-47 10.2		897
.12	12.29	W0	D43P		8 38 34	-45 55.7		897
W0			D44P		8 38 40	-42 26.8		897
			D45P		8 38 37	-45 47.9		897
W3			D46P		8 38 37	-46 46.9		897 158
.10	12.07	W0	D47P		8 38 59	-46 13.6	W/-45 4351.4352	158 16 897
			D48P		8 39 17	-46 26.0		
			D49P		8 39 18	-46 30.8		897
			D50P		8 39 30	-46 17.6		899
			D51P		8 39 36	-42 29.1		897
W3			D52P		8 39 48	-44 45.9	W/-44 4662	897 922
			D53P		8 39 54	-45 8.1		922
			D54P		8 40 6	-47 44.8		897
.33			D55P		8 40 10	-45 36.9		897
.24			D56P		8 40 20	-46 7.4		899 922 897
			D57P		8 40 35	-47 14.1	DOUBLE STAR	897
			D58P		8 40 37	-46 38.9		921 783 793 899 620 897 884 901
.09	11.54	W3	D59P		8 40 47	-45 3.5		897 158
			D60P		8 40 51	-44 44.9		897

D61P		C-45	4394	8	39	10	-45	54.9	10.16	.21			B2V	EN	13.08	W0	13.06	.05		
D62P		C-45	4393	8	39	10	-45	19.6	9.3 MV	9.1 PG		*			12.18	.11	11.92	.10	12.18	
D63P		C-44	4691	8	39	31	-45	5.9	8.48	.40			B2I		12.74	W0	13.11	.21		
D64P	74272	C-46	4448	8	39	35	-47	8.3	4.76	.12	.12		A3II		10.63	W0	10.88	.51		
D65P		C-45	4401	8	39	35	-45	34.5	9.1 MV	8.7 PG			A		12.26	.40	12.04	.16	12.54	
D66P	74290	C-47	4217	8	39	38	-47	23.7	8.30MV				B8		11.93	W0	13.04	W0	12.09	
D67P	74319	C-44	4698	8	39	52	-44	48.7	6.63MV				B9		9.95	.08	9.32	.06	8.72	
D68P		C-45	4415	8	40	7	-45	22.3	9.0 MV	9.5 PG					14.52	W0	14.30	W0		
D69P	74371	C-44	4704	8	40	15	-45	13.8	5.24	.22	-.44	S	B5I		9.99	.00	9.71	.02	9.85	
D70P	74402	C-47	4239	8	40	18	-47	41.6	11.5 MV	9.0 PG			B9		12.88	W6				
D71P	74401	C-47	4241	8	40	22	-47	29.1	9.1 MV	9.1 PG			B8		11.34	W3	13.29	W3	11.85	
D72P	74386	C-47	4235	8	40	25	-47	36.0	9.4 MV	8.7 PG			F0		13.16	W3				
D73P		C-45	4425	8	40	38	-45	32.8	9.7 MV	9.2 PG			B		12.69	.04	12.78	.08	12.47	
D74P	74454	C-46	4474	8	40	42	-46	23.9	8.02MV				B9		11.61	.14	11.21	.05	12.01	
D75P	74496	C-47	4258	8	40	50	-47	20.4	7.4 MV	6.7 PG			A2		11.23	W3	12.71	W3		
D76P	74528	C-45	4435	8	41	2	-45	22.5	8.44	.16		*	B5V	N	12.16	.26	11.77	.19	11.75	
D77P	74558	C-46	4483	8	41	9	-46	37.7	6.94	.25			A5III		11.63	.14	12.18	.09		
D78P	74557	C-43	4571	8	41	13	-43	47.0	9.0 MV	8.5 PG			A3				13.58	W0		
D79P	74602	C-46	4486	8	41	25	-46	50.1	9.6 MV	8.6 PG			B9		12.94	.39	13.71	.69	11.70	
D80P	74620	C-47	4276	8	41	29	-47	30.4	9.4 MV	8.3 PG			B9						10.91	

CEL	HD	DM	R.A. (1950)			DEC.	OBJ	V	B-V	U-B	PHOT	SPECT	PEC.	U1	SD1	U2	SD2	U3
E 1P		C-46	4490	8	41	37	-46	16.0	10.01	.05			B2V		12.74	W0	12.96	.06	
E 2P	74650	C-47	4282	8	41	39	-47	37.5	7.49MV				B9						11.06
E 3P	74649	C-45	4449	8	41	44	-46	8.2	9.1 MV	8.7 PG			A0		12.18	.10	11.92	.17	12.01	
E 4P	74677	C-45	4455	8	41	55	-45	55.2	8.62	.22			B3III		12.02	.10	11.90	.21		
E 5P	74695	C-46	4496	8	41	57	-46	45.0	10.9 MV	9.3 PG			B9		11.96	.20	12.67	.28		
E 6P		C-45	4457	8	42	0	-45	21.8	9.0 MV	9.0 PG			B		12.25	.15	12.33	.14	11.83	
E 7P	74711	C-46	4504	8	42	8	-46	37.0	7.10	.08			B3		10.65	.24	10.49	.01	10.39	
E 8P		C-45	4463	8	42	17	-45	43.6	9.5 MV						11.44	W0	12.03	.13		
E 9P	74773	C-46	4512	8	42	30	-46	56.0	7.8 MV	6.9 PG			B5		10.38	W0	11.13	1.28	9.36	
E10P	74693	C-43	4581	8	42	53	-43	20.5	9.6 MV	9.0 PG			A2				13.90	W0		
E11P		C-45	4482	8	43	4	-45	48.0	10.0 MV				W8N	E	13.40	W0	13.73	W3		
E12P	74868	C-44	4771	8	43	6	-44	22.0	6.57	.57			G3IV		12.91	.10	13.58	.26		
E13P	74869	C-47	4312	8	43	16	-47	46.4	11.5 MV	9.6 PG			B9				13.09	.16		
E14P		P-45	2968	8	43	16	-46	.9							12.23	W3	13.18	W3		
E15P		C-44	4775	8	43	20	-44	23.9	9.9 MV	9.5 PG							14.09	.26		
E16P	74921	C-46	4531	8	43	22	-47	9.8	10.9 MV	9.6 PG			A				13.90	W3		
E17P		C-45	4494	8	43	23	-45	58.1	10.0 MV				B	E	11.75	W3	12.63	W3		
E18P	74937	C-46	4534	8	43	27	-47	1.1	8.5 MV	9.0 PG			A3				13.98	W3		
E19P	74920	C-45	4496	8	43	29	-45	51.3	7.53	.03			B3		10.41	.05	10.03	.21	9.15	
E20P	74936	C-45	4498	8	43	32	-45	43.4	8.26			*	B8		13.33	W0	13.32	.52		
E21P	74936	C-45	4501	8	43	38	-45	46.6	8.26	.22			B8		11.82	.21	12.31	.03		
E22P	74952	C-45	4502	8	43	39	-45	43.9	7.90	.21		*	A3		11.58	.03	11.55	.01	12.49	
E23P	74968	C-46	4537	8	43	43	-46	30.2	9.8 MV	8.5 PG			B9				12.66	W0		
E24P		C-45	4509	8	43	58	-45	34.8	9.9 MV						12.37	.05	13.08	.05		
E25P	75028	C-47	4329	8	44	2	-47	44.8	8.5 MV	7.9 PG			A0		13.22	W0	11.79	.17	12.10	
E26P	75009	C-43	4611	8	44	3	-44	3.9	7.0 MV	6.6 PG			B9		10.98	.12	10.57	.26	9.57	
E27P	75061	C-43	4617	8	44	10	-43	15.9	9.8 MV	9.0 PG			A0				14.01	W0		
E28P	75064	C-47	4332	8	44	16	-47	23.6	9.6 MV	8.6 PG			B9				12.64	.09		
E29P	75062	C-43	4615	8	44	18	-43	34.1	8.0 MV	7.4 PG			B9		11.94	.03	11.04	W0	11.42	
E30P	75063	C-45	4517	8	44	20	-45	51.5	3.90	.00	-.02		A0III		9.53	.36	9.11	.35	8.75	
E31P	75103	C-46	4557	8	44	30	-47	12.7	8.4 MV	7.8 PG			F2				13.62	W0		
E32P		C-46	4560	8	44	37	-46	23.0	9.7 MV	9.5 PG							12.53	W3	13.23	
E33P	75129	C-47	4337	8	44	40	-47	22.0	6.78MV				B8		12.20	.25	11.14	.02	12.04	
E34P		C-44	4805	8	44	42	-44	43.1	9.5 MV	9.5 PG							13.67	.06		
E35P	75149	C-45	4526	8	44	48	-45	43.7	5.47	.23			B3I		10.45	W0	10.04	.13	9.90	
E36P	75128	C-46	4564	8	44	49	-46	28.5	9.6 MV	9.0 PG			A0				12.32	W3		
E37P	75148	C-43	4624	8	44	53	-43	47.1	9.0 MV	7.9 PG			A2		13.04	W0	12.93	.12		
E38P	75212	C-48	4097	8	45	6	-48	34.9	8.5 MV	8.1 PG			A0		12.16	W0	11.20	W0		
E39P		C-45	4534	8	45	9	-46	16.0	9.5 MV	9.4 PG					13.64	.15	12.50	.29	12.19	
E40P	75243	C-47	4348	8	45	13	-47	37.3	9.6 MV	8.7 PG			A0		12.54	W0	11.36	W3		
E41P	75211	C-43	4635	8	45	16	-43	53.4	7.50	.41	-.65		B5		11.74	.24	11.52	.07	11.54	
E42P	75241	C-44	4818	8	45	22	-44	53.4	6.59	-.12			B5III		9.61	.31	9.81	.04	8.56	
E43P		C-47	4341	8	45	24	-48	16.5	9.1 MV								13.19	W0		
E44P		C-47	4339	8	45	37	-47	51.9	8.6 MV								13.80	W0		
E45P	75276	C-45	4541	8	45	37	-45	58.2	5.75	.5*	.3*	S	F2I				13.19	W3		
E46P	75293	C-47	4358	8	45	39	-47	40.0	9.4 MV	9.1 PG			B9		13.34	W0	12.04	.57	11.91	
E47P	75275	C-43	4643	8	45	39	-43	52.9	9.1 MV	8.6 PG			B3		11.70	.13	11.02	.04	11.15	
E48P	75309	C-45	4547	8	45	47	-46	16.0	7.84	.02			B2		10.74	.30	10.33	.24	10.25	
E49P	75310	C-46	4587	8	45	49	-46	29.3	10.2 MV	8.7 PG			A0				12.34	.22	13.10	
E50P	75349	C-46	4590	8	45	57	-47	1.3	9.2 MV	8.9 PG			B9		13.06	W0	12.15	.39	12.03	
E51P	75348	C-43	4649	8	46	3	-44	2.9	8.7 MV	9.0 PG			A3				14.24	.12		
E52P		C-47	4364	8	46	17	-47	30.6	9.6 MV	9.5 PG							12.90	.17		
E53P	75398	C-43	4658	8	46	24	-43	45.0	9.4 MV	8.4 PG			A0		12.34	W0	12.35	.15		
E54P	75465	C-46	4605	8	46	40	-46	43.5	9.00	.22			B3V	EN			12.87	.24	13.12	
E55P		C-45	4571	8	46	49	-45	47.5	9.5 MV								13.46	W0		

SD3	U4	SD4	CEL	NONSTAR	R.A. (2000) DEC.	-----REMARKS-----	----------REFERENCES----
			D61P		8 40 50 -46 5.6		341 900 899 308 A 7 158
.38	12.45	W0	D62P		8 40 51 -45 30.3	W/-45 4392	897
			D63P		8 41 13 -45 16.6		16 897 A 7 158
			D64P		8 41 13 -47 19.0		158 897 781 901 884 921
.23	12.67	W0	D65P		8 41 16 -45 45.2		897
W0			D66P		8 41 15 -47 34.4		897
.00	8.96	W3	D67P		8 41 34 -44 59.4		897
			D68P		8 41 48 -45 33.0		897
.15	9.90	W0	D69P		8 41 57 -45 24.5		884 901 897 620 158 419 793 7
			D70P		8 41 55 -47 52.3		897
W0			D71P		8 41 59 -47 39.9		897
			D72P		8 42 2 -47 46.8		922
W3			D73P		8 42 19 -45 43.6		897
.35			D74P		8 42 22 -46 34.7		897
			D75P		8 42 28 -47 31.2		897
.24			D76P		8 42 44 -45 33.3	W/-45 4441	16 897 158
			D77P		8 42 48 -46 48.5		897 505 158
			D78P		8 42 57 -43 57.8		897
W6			D79P		8 43 4 -47 .9		897
W0			D80P		8 43 7 -47 41.2		897
			E 1P		8 43 17 -46 26.8		158 900 16
.09			E 2P		8 43 16 -47 48.3		897
.18			E 3P		8 43 24 -46 19.0		897 922
			E 4P		8 43 36 -46 6.0		158 16 897
			E 5P		8 43 36 -46 55.8		897
W0	12.44	W0	E 6P		8 43 42 -45 32.6		897
.04			E 7P		8 43 47 -46 47.8		158 897
			E 8P		8 43 58 -45 54.5		897 899
.06			E 9P		8 44 9 -47 6.9		897
			E10P		8 44 38 -43 31.4		922
			E11P		8 44 45 -45 58.9		899 308 6
			E12P		8 44 50 -44 32.9		158 487 A19
			E13P		8 44 53 -47 57.3		899 922
			E14P		8 44 57 -46 11.8		897
			E15P		8 45 4 -44 34.8		897
			E16P		8 45 1 -47 20.7		897
			E17P		8 45 4 -46 9.0		899 308
			E18P		8 45 6 -47 12.0		897
.18			E19P		8 45 10 -46 2.2		158 897
			E20P		8 45 13 -45 54.3	INCLUDES 74952	897
			E21P		8 45 19 -45 57.5		158 897
.46			E22P		8 45 20 -45 54.8	INCL 4498,4501	897 158
			E23P		8 45 23 -46 41.1		897
			E24P		8 45 40 -45 45.8		897
W3			E25P		8 45 40 -47 55.8		897
.00			E26P		8 45 47 -44 14.9		897
			E27P		8 45 56 -43 26.9		922
			E28P		8 45 54 -47 34.6		897
.24			E29P		8 46 3 -43 45.1		897
.28			E30P		8 46 1 -46 2.5		921 158 783 781 897 901 884
			E31P		8 46 9 -47 23.7		897
W3			E32P		8 46 17 -46 34.0		897
W0			E33P		8 46 19 -47 33.0		897
			E34P		8 46 25 -44 54.1		897
.13			E35P		8 46 30 -45 54.7		620 897 901 884 158
			E36P		8 46 29 -46 39.5		922
			E37P		8 46 38 -43 58.1		897
			E38P		8 46 42 -48 45.9		897
W6			E39P		8 46 50 -46 27.0		897
			E40P		8 46 51 -47 48.3		922
.19			E41P		8 47 1 -44 4.4		158 897 A19
.05			E42P		8 47 5 -45 4.4		158 897
			E43P		8 47 1 -48 27.5		899
			E44P		8 47 15 -48 2.9		899
			E45P		8 47 18 -46 9.2		7 158 793 835 884 901 620 897
.16			E46P		8 47 17 -47 51.0		897
.31			E47P		8 47 24 -44 3.9		897
.05			E48P		8 47 28 -46 27.0		897 158
.13			E49P		8 47 29 -46 40.4		897
.49			E50P		8 47 36 -47 12.4		897
			E51P		8 47 48 -44 14.0		897
			E52P		8 47 56 -47 41.7		897
			E53P		8 48 9 -43 56.1		922
.03			E54P		8 48 20 -46 54.6		16 897 158 A19
			E55P		8 48 31 -45 58.6		899

E56P	75478	C-47	4377	8	46	50	-47	21.1	8.9 MV	8.1 PG			F0				13.68	.07		
E57P	75534	C-47	4381	8	47	6	-47	34.6	8.0 MV	8.1 PG			B5	12.16	W0		11.73	W0	12.24	
E58P		C-46	4615	8	47	10	-47	6.2	9.4 MV	9.1 PG				13.22	W0		12.38	W3		
E59P	75549	C-43	4668	8	47	17	-43	34.5	7.32	-.13			B3V	10.31	.10		9.63	.09	9.04	
E60P	75587	C-45	4581	8	47	24	-45	27.0	8.8 MV	8.7 PG			F0				13.17	.13		
E61P	75610	C-47	4388	8	47	29	-47	29.3	10.0 MV	9.3 PG			A0				13.49	W0		
E62P		C-45	4583	8	47	32	-45	57.4	9.2 MV								13.68	W0		
E63P	75608	C-42	4676	8	47	34	-43	11.0	7.55MV				B8	11.02	W0		10.25	.14	9.44	
E64P	75631	C-42	4677	8	47	38	-42	49.1	9.2 MV	8.2 PG			A2	12.46	W0		11.43	W0	11.42	
E65P	75658	C-47	4393	8	47	45	-47	18.1	8.10	.21			B3	11.92	W0		10.97	.03	11.15	
E66P		C-45	4592	8	47	50	-46	12.5	9.8 MV					13.31	W0		13.15	W0		
E67P	75657	C-42	4684	8	47	52	-42	38.2	7.59MV				B8	10.32	W0		9.34	.19	8.93	
E68P	75710	C-44	4861	8	48	4	-45	7.3	5.02			*	A2	10.60	.05		9.97	.04	9.97	
E69P	75744	C-47	4411	8	48	16	-47	26.6	10.2 MV	9.1 PG			B8	12.88	W0		11.96	W3		
E70P	75726	C-43	4680	8	48	18	-43	20.7	10.2 MV	9.6 PG			A0				13.27	W0		
E71P		C-45	4606	8	48	30	-45	20.1	8.92	.38		:	B0V	13.30	W0		13.54	.11	13.61	
E72P	75760	C-44	4873	8	48	33	-45	12.4	9.19MV	9.4 PG			A2				14.45	W3		
E73P	75823	C-48	4146	8	48	40	-48	30.3	8.9 MV	9.0 PG			F8				13.94	W0		
E74P	75820	C-45	4613	8	48	44	-46	3.6	9.8 MV	8.7 PG			A0	12.96	.16		11.86	.11	12.33	
E75P	75822	C-47	4421	8	48	46	-47	36.3	9.6 MV	8.6 PG			B8	11.83	W0		11.23	W0	11.53	
E76P	75821	C-46	4661	8	48	52	-46	20.5	5.09	-.22			O9II	8.51	.00		6.58	W3	6.95	
E77P		C-45	4615	8	48	53	-45	21.9	9.1	.40			B2V	EN			13.72	W0	13.36	
E78P	75819	C-42	4708	8	48	57	-43	0.0	10.2 MV	9.1 PG			A2				13.32	W0		
E79P	75851	C-42	4711	8	49	3	-42	51.4	10.2 MV	9.5 PG			A0				14.62	W3		
E80P	75873	C-45	4625	8	49	6	-46	7.3	9.1 MV	9.1 PG			A2	13.57	W0		13.62	W3		

CEL	HD		DM	R.A. (1950)			DEC.	OBJ	V	B-V	U-B	PHOT	SPECT	PEC.	U1	SD1	U2	SD2	U3
F 1P	75860	C-43	4691	8	49	6	-43	33.8	7.6	.73		SP	B1I		12.26	W3	13.85	W3	
F 2P	75872	C-43	4693	8	49	13	-44	13.9	9.8 MV	9.4 PG			B9				12.93	.13	13.05
F 3P	75887	C-47	4432	8	49	21	-47	40.9	9.8 MV	9.0 PG			A0				12.86	W0	
F 4P	75927	C-43	4700	8	49	29	-44	13.3	9.6 MV	8.9 PG			B9		13.80	W3	12.89	.13	13.67
F 5P		C-45	4635	8	49	33	-45	29.3	8.97	.40			B0III		13.63	.16	13.64	.29	13.82
F 6P	75955	C-45	4641	8	49	42	-45	26.1	7.8 MV	7.9 PG			A0		12.60	.09	11.82	.33	12.30
F 7P	75968	C-46	4683	8	49	51	-46	25.3	8.4 MV	7.9 PG			B8		12.11	.27	11.06	.10	10.91
F 8P	75991	C-47	4441	8	49	53	-47	23.0	10.0 MV	8.7 PG		*	B3		11.81	W0	11.38	W0	11.42
F 9P	75966	C-43	4707	8	49	53	-43	51.5	9.2 MV	8.4 PG			A0		14.49	W3	13.17	.03	
F10P	76005	C-48	4169	8	49	58	-48	33.9	9.08	.21			B8		12.20	W6	13.18	W3	
F11P	76004	C-43	4711	8	50	4	-43	57.7	6.68MV				B3		9.13	.13	9.23	.03	7.93
F12P		C-47	4429	8	50	5	-47	42.2	8.4 MV								14.29	W0	
F13P	76031	C-43	4716	8	50	18	-43	49.2	9.1 MV	9.4 PG			B3		14.60	W0			13.85
F14P	76060	C-45	4653	8	50	20	-46	6.0	8.2 MV	7.6 PG			B8		11.68	.19	10.42	.18	10.67
F15P	76074	C-43	4718	8	50	34	-43	58.4	9.4 MV	8.7 PG			A0		14.23	W0	12.86	.19	
F16P		C-48	4183	8	50	50	-49	3.0	9.5 MV								12.40	W3	12.60
F17P	76137	C-46	4703	8	50	56	-46	49.3	10.2 MV	9.3 PG			A0		13.46	W0	13.38	W0	
F18P		C-47	4459	8	50	59	-47	23.0	9.66	.22			B5V				13.28	W0	
F19P	76161	C-47	4460	8	51	0	-48	10.2	6.0*	-.16			B6V	N			8.80	W3	7.99
F20P	76183	C-43	4727	8	51	6	-44	5.8	8.41MV				A0		13.53	W3	13.24	.19	
F21P	76186	C-46	4707	8	51	7	-47	12.2	6.79MV				B9		11.01	.04	10.51	.05	
F22P		C-46	4755	8	51	14	-47	2.1	9.2 MV								13.93	W0	
F23P	76184	C-44	4920	8	51	17	-45	12.8	9.34MV	9.4 PG			A0		13.46	.01	12.94	.08	13.32
F24P	76211	C-44	4923	8	51	19	-45	11.0	9.0 MV	8.5 PG			A0		13.59	W0	13.50	.11	
F25P		C-46	4716	8	51	22	-47	2.9	9.2 MV								13.86	W0	
F26P	76256	C-43	4732	8	51	35	-43	33.8	9.4 MV	8.2 PG			B9		12.41	.08	11.90	.05	12.73
F27P	76268	C-43	4735	8	51	36	-44	8.6	7.53MV				A0		12.86	.11	12.04	.08	13.49
F28P		C-43	4739	8	51	47	-44	11.3	9.0 MV	8.8 PG							13.54	W3	
F29P	76307	C-47	4472	8	51	48	-47	19.7	9.8 MV	8.8 PG			B9		11.27	.05	12.27	.33	
F30P	76306	C-44	4931	8	51	48	-45	6.2	9.6 MV	9.0 PG			B9		12.63	.11	12.04	.05	12.65
F31P	76282	C-43	4740	8	51	49	-43	20.5	8.2 MV	7.5 PG			A0		12.44	.12	11.77	.02	12.70
F32P	76325	C-48	4208	8	51	56	-48	52.8	8.9 MV	8.9 PG			A2		13.75	W0	11.76	W3	12.41
F33P		C-45	4679	8	52	0	-46	18.5	10.5 MV	8.9 PG			A2				14.02	W0	
F34P	76342	C-48	4213	8	52	1	-48	34.5	9.4 MV	9.3 PG			A0				12.89	W3	13.63
F35P		C-49	3929	8	52	7	-49	26.4	8.5 MV								13.58	W0	
F36P	76360	C-47	4480	8	52	10	-47	19.8	5.32	.27	1.58	B	A4	AM	10.49	.23	11.23	.15	
F37P	76358	C-44	4933	8	52	10	-45	11.2	7.74MV	8.4 PG			K0				14.35	.22	
F38P	76341	C-42	4762	8	52	11	-42	17.7	7.21MV				B2		11.20	W0	10.62	.06	
F39P	76359	C-46	4732	8	52	16	-46	59.6	9.2 MV	8.5 PG			A0		12.22	.07	12.58	.14	
F40P	76425	C-48	4222	8	52	31	-48	56.2	9.0 MV	8.7 PG			A0				12.13	W3	
F41P		C-45	4685	8	52	32	-45	58.8	9.5 MV						12.80	W0	13.62	W0	
F42P	76424	C-46	4735	8	52	34	-46	18.2	9.8 MV	9.6 PG			A0		12.70	.33	12.66	.16	
F43P		C-48	4221	8	52	35	-48	42.5	9.3 MV								13.87	W3	
F44P		C-48	4225	8	52	40	-48	40.5	9.8 MV								12.84	W3	
F45P	76439	C-44	4939	8	52	40	-45	15.8	8.1 MV	7.7 PG			B9		11.50	.09	10.70	.33	11.09
F46P		C-43	4757	8	52	51	-44	14.3	9.5 MV	9.4 PG							13.56	.10	
F47P	76516	C-43	4762	8	53	15	-43	38.4	8.3 MV	8.0 PG			A0		13.07	.13	12.16	.05	13.42
F48P	76536	C-47	4504	8	53	18	-47	24.0	9.0 MV	8.8 PG			W C		13.74	W6	12.03	W6	
F49P	76534	C-42	4780	8	53	21	-43	16.5	7.9 MV	7.5 PG			B3		11.93	.34	11.27	.06	12.32
F50P	76556	C-47	4505	8	53	26	-47	24.9	8.20	.41			B3		12.91	W6			12.32

| | | |

F51P	76567	C-45	4694	8	53	26	-46	10.1	7.8 MV	7.5 PG			A0		11.60	.23	11.84	.15		
F52P	76566	C-44	4951	8	53	34	-44	51.0	6.25	-.17		B	B3V		9.61	.02	8.91	.80	7.89	
F53P	76565	C-43	4764	8	53	36	-43	36.5	8.5 MV	7.8 PG			A0		13.24	.04	12.22	.11		
F54P	76588	C-45	4698	8	53	40	-45	29.2	9.1 MV	8.7 PG			A0				14.06	.01		
F55P	76589	C-46	4758	8	53	41	-46	41.9	8.2 MV	8.2 PG			B9		11.17	W6	12.16	W3		
F56P		C-43	4770	8	54	4	-44	13.3	9.0 MV								13.76	W0		
F57P	76649	C-45	4707	8	54	7	-46	9.0	8.0 MV	8.1 PG			B8		12.07	.14	13.14	.09		
F58P	76693	C-46	4769	8	54	18	-47	17.3	10.0 MV	9.6 PG			A0				13.24	W3	14.29	
F59P	76745	C-48	4249	8	54	29	-48	56.6	9.1 MV	8.4 PG			A0				11.96	W0		
F60P	76725	C-44	4963	8	54	30	-45	12.3	8.8 MV	8.6 PG			B9		11.91	W0	11.73	.03		
F61P	76744	C-45	4710	8	54	35	-46	8.4	8.5 MV	8.2 PG			A0		12.47	.10	13.51	.10		
F62P	76777	C-47	4531	8	54	47	-47	44.4	9.1 MV	9.0 PG			A0				13.05	W0		
F63P	76776	C-43	4782	8	54	49	-43	43.7	9.2 MV	8.8 PG			A5				13.78	W0		
F64P	76764	C-42	4802	8	54	50	-43	.5	9.6 MV	9.4 PG			B8		12.60	W0	12.47	W0		
F65P	76775	C-41	4656	8	54	57	-42	4.0	9.0 MV	8.9 PG			A2				13.54	W0		
F66P	76803	C-47	4532	8	55	1	-47	40.1	8.9 MV	8.4 PG			A0				13.41	W0		
F67P	76802	C-41	4657	8	55	7	-41	57.7	8.3 MV	8.6 PG			F0				13.68	W0		
F68P	76852	C-48	4265	8	55	14	-48	52.4	10.5 MV	9.6 PG			B				12.79	W3		
F69P	76838	C-42	4808	8	55	19	-43	3.8	7.31	+0.00		*	B3V		10.26	W0	9.57	.01		
F70P	76874	C-48	4267	8	55	21	-48	55.7	10.5 MV	9.6 PG			A5				13.36	W3		
F71P	76915	C-47	4543	8	55	40	-48	.7	8.9 MV	8.8 PG			A0				12.62	W0	13.52	
F72P	76898	C-43	4794	8	55	41	-44	4.3	7.39	-.15			B4V	N	10.78	.17	9.48	.23	9.52	
F73P	76940	C-43	4797	8	55	55	-43	21.1	9.1 MV	8.6 PG			A0		12.70	W3	13.42	W3		
F74P	76954	C-42	4822	8	56	3	-42	19.8	8.2 MV	7.7 PG			B9		11.15	W0	10.53	W0		
F75P	76967	C-42	4824	8	56	5	-42	57.6	9.6 MV	9.2 PG			B8		12.06	W0	11.86	W0		
F76P		C-47	4551	8	56	12	-47	33.0	9.0 MV				O7				14.37	W0		
F77P	76998	C-44	4991	8	56	14	-44	40.5	9.8 MV	9.0 PG			A0		12.50	W0	12.59	.08		
F78P		C-43	4813	8	56	40	-43	34.2	9.2 MV								13.79	W0		
F79P	77115	C-46	4808	8	56	58	-46	33.9	9.6 MV	9.0 PG			A0				12.41	.23		
F80P	77114	C-43	4819	8	57	9	-43	25.7	9.2 MV	8.7 PG			A0				12.96	W0		

CEL	HD	DM	R.A. (1950)	DEC.	OBJ	V	B-V	U-B	PHOT	SPECT	PEC.	U1	SD1	U2	SD2	U3
G 1P	77140	C-46	4810	8 57 11	-47	2.5	5.17	.26	.17	B	FOIII	A	11.47	W0	10.39	.28	13.39
G 2P	77112	C-42	4846	8 57 16	-43	13.7	9.2 MV	9.1 PG			A0				12.70	W0	
G 3P	77166	C-42	4853	8 57 32	-42	24.4	9.8 MV	8.9 PG			B9				12.62	W3	12.23
G 4P	77167	C-42	4855	8 57 33	-43	9.6	10.0 MV	9.0 PG		*	B9				13.01	W0	12.12
G 5P		C-46	4822	8 57 43	-46	50.4	9.1 MV								12.80	W0	
G 6P		C-43	4816	8 57 44	-44	.1	9.3 MV								15.01	W0	
G 7P		C-44	5012	8 57 57	-44	50.7	9.7 MV	9.7 PG					14.16	W3			
G 8P		C-47	4571	8 58	4	-47	57.4	7.7 MV							13.82	W0	
G 9P	77320	C-42	4875	8 58 33	-42	58.6	6.08	-.18			B2V	CEN	9.37	W3	8.61	W3	8.08
G10P	77400	C-46	4826	8 58 35	-47	2.3	9.2 MV	8.7 PG			A0				12.69	W0	
G11P	77343	C-43	4839	8 58 38	-43	43.2	9.0 MV	8.7 PG			A2				14.17	.02	
G12P	77384	C-46	4823	8 58 39	-46	31.1	8.9 MV	8.5 PG			A5				12.39	.03	13.70
G13P		C-45	4773	8 58 44	-45	31.9	9.4 MV								14.32	W0	
G14P	77383	C-42	4881	8 58 51	-43	8.7	10.2 MV	9.4 PG			A0				13.28	W3	
G15P	77420	C-43	4848	8 58 58	-43	39.6	9.0 MV	8.3 PG			A3				14.23	.04	
G16P	77433	C-45	4772	8 59 1	-45	41.9	8.3 MV	8.6 PG			A3				12.74	.30	
G17P	77453	C-45	4774	8 59 9	-45	26.1	8.3 MV	8.2 PG			A3				13.10	.13	
G18P	77511	C-46	4836	8 59 22	-47	2.6	7.7 MV	7.5 PG			F0				12.48	W0	
G19P	77651	C-45	4788	9 0 23	-46	15.6	9.1 MV	9.0 PG			A0				13.24	.21	
G20P	77650	C-42	4905	9 0 32	-42	18.3	10.0 MV	9.4 PG			A				13.19	W3	13.70
G21P	77669	C-43	4873	9 0 38	-43	46.3	8.5 MV	7.7 PG			B9		12.74	.07	11.36	W0	12.15
G22P	77684	C-42	4906	9 0 45	-42	30.5	7.23MV				A0		11.96	W0	11.28	W0	11.71
G23P		C-45	4797	9 0 52	-45	27.8	9.3 MV								14.64	W0	
G24P	77741	C-45	4798	9 0 58	-45	58.5	9.5 MV				A0				13.34	.34	
G25P	77740	C-44	5064	9 0 59	-44	26.7	8.5 MV	8.3 PG			A0		13.57	.17	12.21	W0	
G26P	77739	C-43	4877	9 1 1	-44	2.8	8.4 MV	7.7 PG			A0		12.15	.17	11.15	W3	11.49
G27P	77769	C-46	4861	9 1 5	-46	45.9	9.6 MV	9.1 PG			B8				13.01	W0	
G28P	77754	C-42	4913	9 1 7	-42	41.1	9.6 MV	8.3 PG			A0		13.65	W0	12.62	W0	13.60
G29P		C-45	4794	9 1 8	-46	11.9	9.4 MV								14.22	W0	
G30P	77812	C-44	5072	9 1 18	-45	11.1	9.39MV	8.7 PG			A0				13.20	W0	
G31P	77850	C-44	5073	9 1 31	-44	42.3	10.5 MV	9.4 PG			A2				14.96	W0	
G32P	77849	C-43	4885	9 1 34	-43	51.0	9.4 MV	8.8 PG			A0				12.80	.03	
G33P	78080	C-42	4941	9 2 55	-43	4.0	9.0 MV	9.4 PG			A0				13.26	W0	
G34P	78116	C-45	4840	9 3 18	-45	40.5	8.2 MV	8.0 PG			A0				12.29	W3	
G35P	78265	C-44	5115	9 3 52	-44	57.6	8.5 MV	8.1 PG			A0				13.25	W0	
G36P	78616	C-44	5150	9 5 54	-44	25.8	6.78	-.02	-.75UBC		B2		10.84	W0			

		F51P	8	55	9	-46	21.6	897
.02		F52P	8	55	19	-45	2.5	158 897 419 901 884
		F53P	8	55	23	-43	48.0	897
		F54P	8	55	24	-45	40.7	899 922
		F55P	8	55	23	-46	53.4	897
		F56P	8	55	50	-44	24.8	899
		F57P	8	55	50	-46	20.5	897
W3		F58P	8	55	59	-47	28.8	922
		F59P	8	56	7	-49	8.1	922
		F60P	8	56	14	-45	23.8	897
		F61P	8	56	18	-46	19.9	897
		F62P	8	56	27	-47	55.9	897 922
		F63P	8	56	36	-43	55.2	899 922
		F64P	8	56	38	-43	12.0	897
		F65P	8	56	47	-42	15.5	897
		F66P	8	56	41	-47	51.6	897
		F67P	8	56	57	-42	9.3	922
		F68P	8	56	52	-49	4.0	922
		F69P	8	57	7	-43	15.4 WITH 4806	897 158 A19
		F70P	8	56	59	-49	7.3	922
W0		F71P	8	57	20	-48	12.3	897
W3		F72P	8	57	28	-44	15.9	158 419 897 A19
		F73P	8	57	43	-43	32.7	897 922
		F74P	8	57	52	-42	31.4	897
		F75P	8	57	53	-43	9.2	897
		F76P	8	57	53	-47	44.6	A 7
		F77P	8	58	0	-44	52.1	897
		F78P	8	58	28	-43	45.8	899
		F79P	8	58	41	-46	45.5	897
		F80P	8	58	57	-43	37.4	897

SD3	U4	SD4	CEL	NONSTAR	R.A. (2000)	DEC.	-----REMARKS-----	----------REFERENCES--
W0			G 1P		8 58 53	-47 14.2		158 505 897 780 781 884 901 753
			G 2P		8 59 4	-43 25.4		899 922
W0			G 3P		8 59 22	-42 36.1		897
W6			G 4P		8 59 21	-43 21.3	WITH -42 4864	897
			G 5P		8 59 25	-47 2.1		899
			G 6P		8 59 31	-44 11.8		899
			G 7P		8 59 43	-45 2.4		897
			G 8P		8 59 44	-48 9.1		899
W3			G 9P		9 0 22	-43 10.3		752 897 901 884 158
			G10P		9 0 17	-47 14.0		922
			G11P		9 0 26	-43 54.9		897
W0			G12P		9 0 22	-46 42.8		897
			G13P		9 0 29	-45 43.6		899
			G14P		9 0 40	-43 20.4		922
			G15P		9 0 46	-43 51.4		897
			G16P		9 0 46	-45 53.7		897
			G17P		9 0 54	-45 37.9		897
			G18P		9 1 4	-47 14.4		922
			G19P		9 2 7	-46 27.4		897 922
W3			G20P		9 2 22	-42 30.1		922
W0			G21P		9 2 26	-43 58.1		897
.36			G22P		9 2 35	-42 42.3		897
			G23P		9 2 37	-45 39.6		899
			G24P		9 2 43	-46 10.4		899
			G25P		9 2 46	-44 38.6		897
W0			G26P		9 2 49	-44 14.7		897
			G27P		9 2 48	-46 57.8		897
W0			G28P		9 2 57	-42 53.0		922
			G29P		9 2 52	-46 23.8		899
			G30P		9 3 4	-45 23.0		922
			G31P		9 3 18	-44 54.2		899 922
			G32P		9 3 22	-44 2.9		922
			G33P		9 4 45	-43 16.0		897
			G34P		9 5 4	-45 52.5		922
			G35P		9 5 39	-45 9.6		897
			G36P		9 7 42	-44 37.9		897 419 158 A19

Page intentionally left blank

ABSOLUTE ULTRAVIOLET SPECTROPHOTOMETRY OF ALPHA CANIS MAJORIS, GAMMA ORIONIS, KAPPA ORIONIS AND ALPHA LEONIS

Dennis C. Evans
National Aeronautics and Space Administration
Goddard Space Flight Center
Greenbelt, Maryland

ABSTRACT

Spectral observations of the stars Alpha Canis Majoris, Gamma Orionis, Kappa Orionis and Alpha Leonis have been obtained in the range 1150-4000 Å, using rocket borne spectrometers. The payloads have a 13-inch diameter telescope, a rotatable concave diffraction grating, and three pulse counting photomultiplier photometers. The laboratory standards used as photometric references derive their primary calibration directly or indirectly from the National Bureau of Standards. An error range of up to ±10 percent is attributed to these laboratory standards, ±8 percent to the calibration procedure, and ±10 percent is assigned as an accidental error range. The overall RMS precision error range is about ±15 percent. The observations are systematically lower than those of Carruthers (1968) at 1270 Å, of Smith (1967) at 1376 Å, and of Campbell (1970) at 2150 and 2550 Å. The data are also about 15 percent lower than the ground-based photometry reported by Schild, Peterson and Oke (1971). Comparison with the provisional calibration of the OAO-2 long wavelength scanner shows good agreement longward of 2200 Å. From 2200 to 1800 Å the OAO-2 calibration infers flux values systematically higher than the present observations, by amounts up to 30 percent. The OAO-2 short wavelength scanner calibration agrees with the α Leo observations, but disagrees for κ Ori and γ Ori.

I. THE OBSERVATIONS

Three Aerobee sounding rockets with ultraviolet spectrometer payloads have been launched from White Sands Missile Range. The payloads were each intended to measure the ultraviolet fluxes of four stars. The range of spectral observation was from 1150 to 4000 Angstroms.

The first rocket (NASA 4.251) was launched 14 March 1969. Good data was obtained from the observation of α Leo, but that payload was destroyed during re-entry. A second flight (NASA 4.252) was made on 13 December 1969. No observations were completed; however, the payload was recovered in excellent condition. Post-flight recalibration showed the sensitivity of the instrument to be within 5 percent of the pre-flight values. The third flight (NASA 13.041) was made 31 October 1971. Recalibration of the spectrometer showed no change in the instrumental sensitivity from pre-flight to post-flight. The observational data available are summarized in Table 1. For flight 13.041 the observing sequence was in

Table 1. Rocket Observations

Rocket Flight	Star	Sp.	V	Number of Scans
4.251	α Leo	B7 V	1.36	2
13.041	α CMa	A1 V	-1.47	1
	γ Ori	B2 III	1.64	6
	κ Ori	B0.5 Ia	2.04	2
	α Leo	B7 V	1.36	3

the order listed in the table. Repeated scans of γ Ori were made as the rocket changed altitude from 140 to 204 kilometers. Each complete spectral scan required 20 seconds. No spectral variations due to residual atmospheric absorption were detected. Thus, no corrections for atmospheric absorption have been applied to any of the data.

II. THE PAYLOAD

The payload telescope optics possess a Dall-Kirkham figure with a focal ratio of f/9.7, a clear aperture of 32.8 cm, and a central obscuration of 15.5 cm. The image of the telescope

defines the limiting resolution since there is no entrance slit. The entrance slot is about 10 × 15 arc minutes. Behind this slot, the light beam diverges until it strikes a 600 line per millimeter concave diffraction grating of 40.07 cm radius. The dispersed light, approximately collimated, is focussed onto three pulse counting photomultiplier photometers by means of a spherical mirror mounted on the back of the primary mirror support structure. Instantaneous resolution of 10 Å is fixed by the slit placed in front of each photomultiplier. The exit slits, fixed in the spectrometer focal plane, are separated by 750 Å. The grating moves at a constant rate over a spectral interval of 1500 Å and the wavelength values during successive scans alternately increase and decrease. Three EMR photomultipliers were used in each payload. The short wavelength one had a lithium fluoride window with a cesium telluride cathode; the medium wavelength, a sapphire window and a bialkali cathode; and the long wavelength, a 9741 glass window and a bialkali cathode. The photomultipliers were operated in a pulse counting mode with low level discrimination. The digital output of each was converted to analog rate signals for telemetry to several ground stations. The ground station magnetic tapes were reconverted into digital format and the digital tapes made available for post-flight analysis.

III. THE CALIBRATION REFERENCES

Each payload was calibrated by placing it in a vacuum chamber where its response to ultraviolet light could be directly compared with that of several laboratory reference photomultipliers. The light source was the exit slit of a one-third meter monochromater placed at the focal point of a Dall-Kirkham collimator. Two photomultipliers, one coated with sodium salicylate, were mounted on an X-Y scanning device which enabled the entire collimated beam to be surveyed. Two laboratory reference photomultipliers were located at fixed positions in the collimated beam, between the X-Y scanner and the flight payload. The scanner monitors were used to determine the relative distribution of light in the beam incident on the payload. The average incident flux was found by comparison of the scanner data with the flux values determined at the fixed monitor locations. Data were discarded when the uniformity of the incident beam varied more than ±10 percent from its average value.

Prior to the successful conclusion of flight 13.041, the laboratory reference photomultipliers were calibrated at Goddard Space Flight Center, using standards traceable to the National Bureau of Standards. Each of four reference photomultipliers were calibrated at 2537 Å using four Eppley ther-

mopiles. The photomultipliers were also calibrated at 1216 Å using an open window nitric oxide ion chamber. The ion chamber results indicated the same quantum efficiency for sodium salicylate at 1216 and 2537 Å, within about ±5 percent. However, the ion chamber measurements could not be used to determine absolute sensitivity of the reference photomultipliers because the cathode surfaces could not be uniformly or fully illuminated. Thus, the pre-flight absolute calibrations were based on the 2537 Å comparison with the thermopiles and the assumption that sodium salicylate has a uniform quantum efficiency as a function of wavelength.

Following flight 13.041, four EMR photodiodes calibrated by the National Bureau of Standards have become available for comparison with the laboratory reference photomultipliers. The diodes have magnesium fluoride windows and rubidium telluride cathodes. Direct comparison of the laboratory references and the diodes in the spectral region 2000-2385 Å indicates agreement to within ±5 percent of the original thermopile calibration and the assumption about sodium salicylate. The present flux values derived for the stars are dependent on the assumption of uniform quantum efficiency for sodium salicylate below 2000 Å. A preliminary recalibration of the laboratory reference photomultipliers shortward of 2000 Å indicates that the uniform quantum efficiency assumption for sodium salicylate is correct, but this conclusion is based on data from a series of low light level measurements of low precision. Post-flight recalibration is continuing.

The use of sodium salicylate as a relative reference cannot be extended longward of 3400 Å. In the spectral range 2600-4000 Å, the relative response of the 13.041 flight payload was determined directly by using the payload to observe the output of three tungsten iodide coiled filament irradiance standard lamps, calibrated by the National Bureau of Standards. In the overlapping range 2600-3400 Å, the spectral responses derived by both techniques were the same within ±5 percent.

The final sensitivity values determined for the 4.251 payload were based on the laboratory reference, calibrated at 2537 Å and extended longward and shortward of that wavelength using sodium salicylate. The final sensitivity values for the 13.041 payload were determined in the same manner, checked in an absolute sense by comparison with diodes calibrated by the National Bureau of Standards in the range 1164-2385 Å, and extended longward to 4000 Å by comparison with tungsten irradiance lamps also calibrated by the National Bureau of Standards.

IV. THE CALIBRATION TRANSFER PROCEDURE

The basic problem encountered in the transfer of the calibration from the laboratory reference to the payload is one of dynamic range. The reference photomultipliers must be illuminated intensely enough to provide a strong signal without overloading the payload photomultipliers. This problem was solved by using the "dynamic" technique described below.

The exit slit of the monochromater used as the light source has a dispersion scale of 26.5 Å per millimeter. The image of this slit in the focal plane of the payload is dispersed an additional 53 Å per millimeter by the payload grating. Thus, a monochromater output having a real spectral purity of 26.5 Å could have an apparent bandwidth equivalent to 79.5 Å in the payload focal plane if the monochromater dispersion and the payload dispersion directions were the same, or only 26.5 Å if the dispersion directions were opposed. With a two millimeter exit slit width on the monochromater (the maximum possible), the real spectral width is 53 Å while the maximum apparent width is 159 Å in the payload focal plane. Because the laboratory reference photomultiplier responds to the entire output of the monochromater and the payload responds to only 10 apparent Angstroms at a time, the intensity ratio between the reference and the payload photomultipliers can be increased by up to a factor of 16. At each calibration wavelength four payload spectrometer scans were recorded on magnetic tape. Data were also recorded from the two photomultipliers on the X-Y scanner, which were kept in a "standard" location and from the two reference photomultipliers. Data points were recorded every 0.081 seconds, corresponding to 6.55 Å intervals at the payload scan rate of 81 Å per second. For the widest slits, 24 non-zero data points were recorded during each of the four spectral scans. By integrating the response of the payload to this well-defined spectral band and comparing it to the signals from the laboratory standard photomultipliers, the calibration was derived. The flight instrument was calibrated at 25 Å intervals over the entire spectral range from 1150-3400 Å. During the course of the calibration, the monochromater exit slits were always kept small enough that the incident spectral purity was small compared to the variations in spectral response of the payload.

The repeatability of the raw data was within ±10 percent using this calibration procedure. Corrections for non-uniformity of the collimated beam based on X-Y scans of the beam at periodic intervals improved the repeatability to about ±5 percent. Based on the stated accuracy of the thermopiles, the repeatability limits, and a comparison of the pre- and post-flight calibrations limit the accuracy of the final results to

no better than ±10 percent.

Additional errors were introduced because of pointing uncertainties coupled with the somewhat non-uniform response of each payload photomultiplier across the field of view. There were also errors associated with the ground recording of the telemetered flight data. These two sources contribute about ±5 to ±10 percent to the estimate of overall error. Finally, an estimate must be made of remaining systematic errors. A "best guess" is ±10 percent. The RMS average of all of the sources of error is ±15 percent. Some of the factors are slightly wavelength dependent but their variation does not significantly affect the overall error estimates.

V. THE DATA

The spectra obtained on the rocket flights are presented in Table 2 and Figure 1. The data are divided into three spectral ranges (vertical lines in Figure 1) corresponding approximately to the range of most reliable data from each photometer. The dividing points are 2350 and 2800 Å. The 2350 Å wavelength is where energy from the second order spectrum begins to contaminate data from the short wavelength detector. The 2800 Å point allows for 600 Å of overlapping between the medium and long wavelength detector. The division into these sections has significance only for interpretation of the 13.041 spectra.

The spectrum of α Leo obtained in flight 4.251 is plotted directly, based on the thermopile absolute calibration at 2537 Å and on the assumption that sodium salicylate has constant quantum efficiency. For this flight, calibrated data are available from only the short and medium wavelength detectors. The independent calibrations of the short and medium wavelength detectors agree within 5 percent and the data are adjusted to the average value in the overlapping region surrounding 2350 Å.

For flight 13.041, an absolute calibration exists only for the short wavelength detector. The relative spectral calibrations for the medium and long wavelength detectors are reliable, but their absolute level is suspect due to amplifier instabilities. The short wavelength calibration can be extrapolated to the longer wavelength flight data by normalizing the medium wavelength relative data to the short wavelength absolute values, and then normalizing the long wavelength relative data to the adjusted medium wavelength values. If this is done, the resultant RMS error range is about ±20 percent in the long wavelength region. The resulting values in the 3300-3500 Å region are about 15 percent lower than the fluxes in that same range reported by Schild, Peterson and Oke (1971). A much smaller error range, about ±10 percent, could be attri-

Table 2. Preliminary Stellar Spectra

(photon cm^{-2} sec^{-1} $Angstrom^{-1}$)

Wavelength (Angstroms)	α CMa (1)	γ Ori (1)	κ Ori (1)	α Leo (1)	α Leo (2)
1200	70	700	400	110	70
1300	197	850	580	190	160
1400	540	910	660	255	240
1500	780	900	660	290	280
1600	1100	880	540	300	290
1700	1400	860	540	305	300
1800	1630	870	590	320	335
1900	1720	820	550	305	335
2000	1800	760	580	305	325
2100	1950	820	560	325	320
2200	1850	800	560	330	320
2300	1730	820	610	300	305
2400	1670	760	620	280	290
2500	1700	770	620	300	315
2600	1820	780	640	285	330
2700	2000	770	600	300	330
2800	2180	800	600	305	320
2900	2530	850	590	345	340
3000	2670	820	620	370	---
3100	2500	750	550	355	---
3200	2720	720	540	380	---
3300	2700	650	480	360	---
3400	2450	570	450	310	---
3500	2430	580	420	330	---
3600	2700	550	390	320	---
3700	2450	510	380	365	---
3800	3850	540	380	470	---
3900	4900	540	375	490	---
4000	4700	520	335	620	---

(1) Data from Rocket 13.041
(2) Data from Rocket 4.251

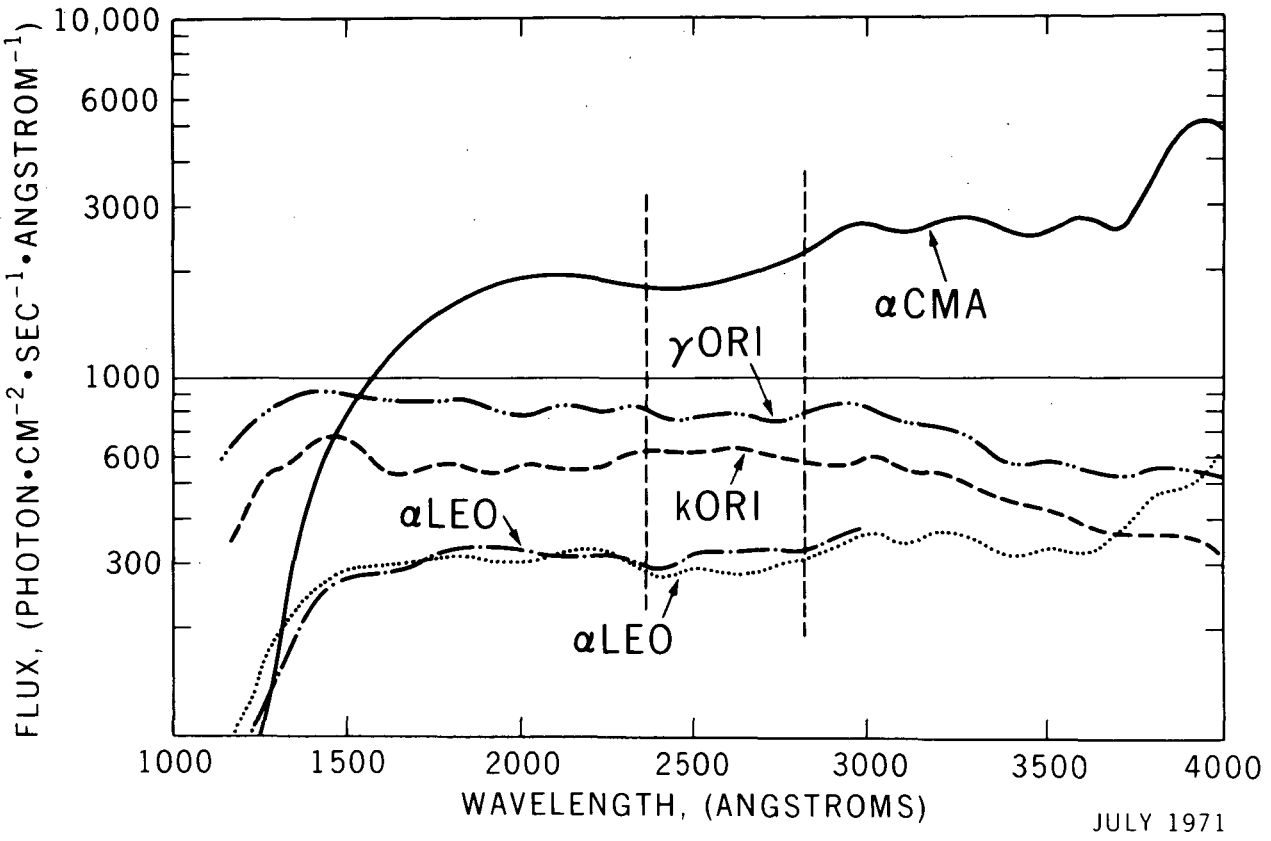

Figure 1.—Preliminary stellar spectra. The observation of α Leo from flight 4.251 ends at 3000 Å. All other spectra are from flight 13.041. The short wavelength region is based on the present absolute calibration; the long, normalized to the observations of Schild, Peterson, and Oke (1971); and the medium has been adjusted (see text).

buted to the long wavelength values by normalizing directly to Schild, Peterson and Oke's ground-based observations. For the data presented in Table 2 and Figure 1, this normalization in the region 3300-3500 Å has been carried out. No further adjustment of data has been made in the long wavelength region. In the medium spectral region, a linear adjustment has been applied to the data in order to match it simultaneously to the long wavelength data at 2800 Å and to the short wavelength data at 2350 Å.

The spectra of α Leo from the two different flights are not averaged. They indicate the repeatability of the whole payload calibration procedure. There is no significant difference between the two observations longward of 1400 Å. Shortward of 1400 Å the 13.041 observation is more reliable because

a more detailed calibration was made in that region, and because post-flight recalibration showed no change from the pre-flight sensitivity. All four spectra presented as the results of the 13.041 flight have been treated identically and then averaged.

VI. COMPARISON WITH OTHER OBSERVATIONS

Broad bandpass observations of the four target stars, as reported by five other groups of observers, are presented in Table 3.

The observations reported by Carruthers (1968) are almost a factor of 2 greater in value than the fluxes determined during these rocket observations. The ratios between the three stars are the same, within ±10 percent.

Chubb and Byram (1963) report a flux for α Leo that is about 50 percent lower than the present observation. They observed none of the other stars discussed here.

The fluxes for α Leo and γ Ori reported by Smith (1967) have very large absolute error flags, which overlap the present data. The ratio of his fluxes for the two stars matches that from the 4.251 and 13.041 data within the present rocket error limits.

The values of flux levels determined by Yamashita (1968) are normalized to Smith's observations of α Leo, but they have a much larger scatter. Nevertheless, the spectral shape indicated by Yamashita agrees with the results of the scanner observations.

Campbell (1970) has made observations of α Leo using an absolutely calibrated set of broad band photometers. At 2150 Å, Campbell's observational error limits and the error limits for the 4.251 observations overlap. The 13.041 data are separated from Campbell's by the sum of our stated error limits, i.e., the error 'flags' just touch.

An observation of α CMa with an instrument nearly identical to the ones used for this calibration series has been reported by Stecher (1970). His data are presented here in graphical form in Figure 2. Stecher's payload was calibrated in the same facilities as were 4.251 and 13.041; however, a different technique of calibration and a different reference chain traceable to the NBS were used. Compared with the 13.041 observation, his reported flux levels are slightly lower (about 20 percent) at 1650 and 1750 Å and significantly lower (up to 30 percent) at 2850 to 3150 Å.

Earlier observations by Stecher (1969) and Stecher and Milligan (1962) longward of 1700 Å infer similar spectral shapes, but the error limits on those data are larger than on Stecher's more recent observation of α CMa.

The four stars observed during rocket flight 13.041 have

Table 3. Other Ultraviolet Observations of the Target Stars

Star	Wavelength (Angstroms)	Wavelength Limits	Flux Value (photon $cm^{-2}sec^{-1}Å^{-1}$)	Absolute Error* (%)	Reference
α CMa	1270	1230-1350	275	±20	1
"	1314	1290-1350	>205	NS	2
γ Ori	1270	1230-1350	1118	±20	1
"	1290	1230-1350	396	±30	3
"	1314	1290-1350	>218	NS	2
"	1376	1280-1570	1143	±50	4
"	1415	1350-1480	648	±15	3
κ Ori	1270	1230-1350	645	±20	1
"	1290	1230-1350	201	±45	3
"	1314	1290-1350	>264	NS	2
"	1415	1350-1480	292	±20	1
α Leo	1290	1230-1350	181	±45	3
"	1314	1290-1350	123	NS	2
"	1376	1280-1570	304	±50	4
"	1415	1350-1480	313	±20	3
"	2150	1875-2525	342	±15	5
"	2550	2300-2900	407	±15	5

* Reported by the author or not stated (NS).

References: 1. Carruthers (1968). 2. Chubb and Byram (1963).
3. Yamashita (1968). 4. Smith (1967).
5. Campbell (1970).

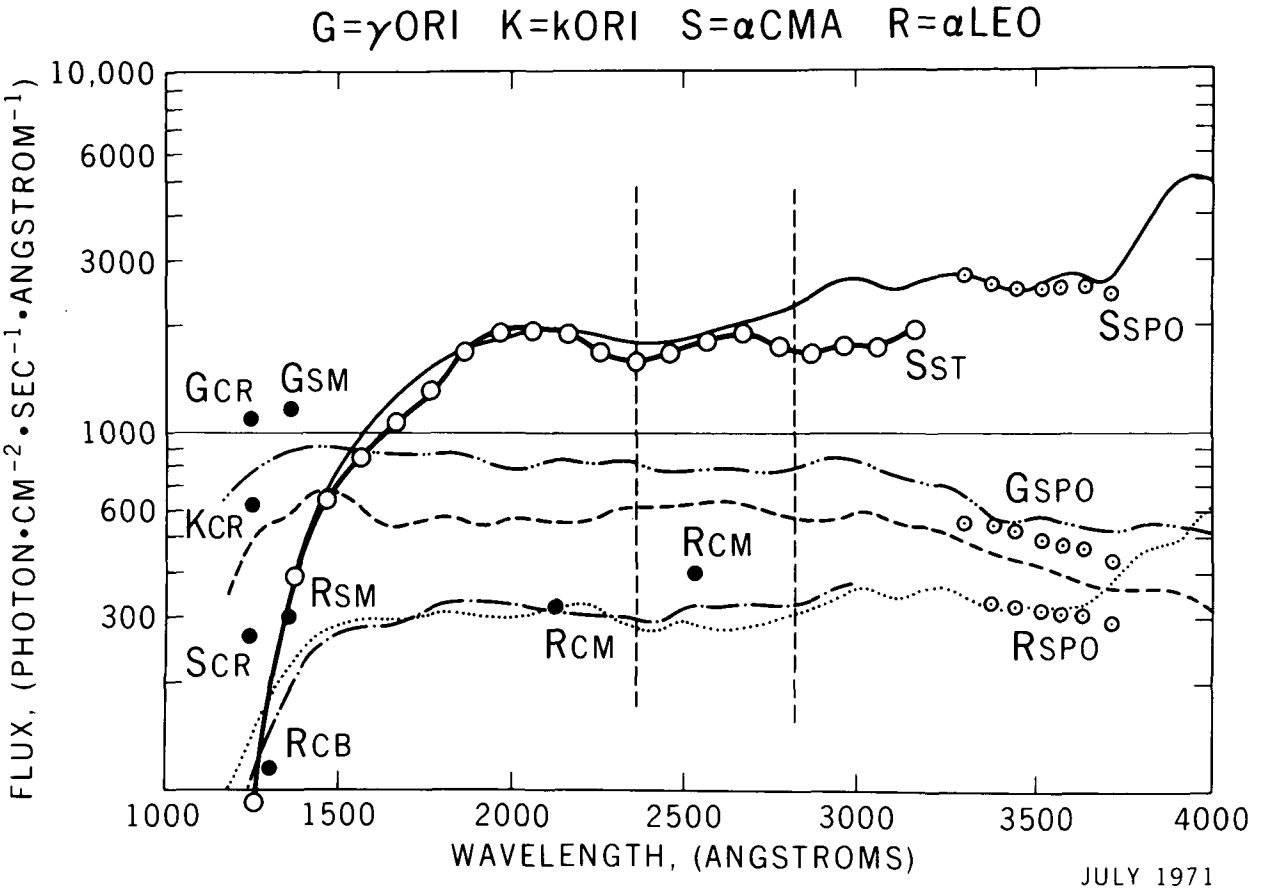

Figure 2.—Other observations. Comparison of the present observations with other reported flux values. CR = Carruthers (1968); CB = Chubb and Byram (1963); SM = Smith (1967); SPO = Schild, Peterson and Oke (1970); ST = Stecher (1970). See Figure 1 for identification of the present spectra.

also been observed using the Wisconsin Experiment Package aboard OAO-2, but at different times. The relative flux ratios derived from the OAO-2 filter photometers at 1300, 1400, 1500 and 1600 Å agree within error limits with the ratios derived from the rocket data. At 1900 and 2500 Å, the fluxes measured by the OAO-2 photometers have very wide error limits because of very high count rates. The longer wavelength OAO-2 photometers were saturated and produced no data on these bright stars.

The relative shapes of the spectra determined by the OAO-2 long wavelength scanner agree with the 4.251 and the 13.041 observations within about ±5 percent longward of 2200 Å. Shortward of 2200 Å, the OAO values increase, becoming 30 per-

cent higher than the rocket data at 1800 Å, which is the short wavelength limit of the OAO-2 scanner. This comparison is based on observational data supplied by B. Savage (personal communication) to Anne B. Underhill (1972).

Comparison with OAO-2 scans of α Leo using the short wavelength scanner indicates agreement to within ±15 percent of the provisional calibration of the short wavelength scanner determined by A. Code (personal communication). In the case of γ Ori and κ Ori, the rocket data is about 10 to 30 percent lower than that determined by the provisional OAO-2 calibration, the larger discrepancies occurring at shorter wavelength. The flux ratios between stellar spectra obtained using the short wavelength scanner data are not in as good agreement with the rocket data as are the ratios derived from the OAO-2 photometer data.

In the spectral range longward of 3000 Angstroms, stellar spectra are measurable from the ground. From about 3000 to 3300 Å large corrections must be made to the observations because of extinction of radiation by the earth's atmosphere, and large uncertainties exist in ground-based observations. Longward of 3300 Å, accurate photometric observations of stars can be made. For comparison to the present observations, the absolute spectral energy distribution of α Lyrae determined by Oke and Schild (1970) is used. Spectra of three of the four stars observed by the rocket (α CMa, γ Ori and α Leo) have been published by Schild, Peterson and Oke (1971), photometrically referenced to the 1970 α Lyrae observation. Thirteen color photometric observations of all four stars have been reported by Mitchell and Johnson (1969). The ratio between the spectra of α CMa and α Leo can also be determined from the work of Aller, Faulkner and Norton (1966). The errors in the relative flux ratios between stars using ground-based data are equal to or superior to the rocket ratios.

The data from these rocket observations and the other comparison observations are presented graphically in Figure 2. Only the best ultraviolet observations from Table 3 have been included in that figure. Also, only the ground-based observations of Schild, Peterson and Oke (1971) are included in the figure.

VII. DISCUSSION OF PRESENT DATA

After all calibration procedures have been completed and final flux values have been derived, there are still some suspected problem areas.

First, based entirely on the rocket data itself, is the "tie" with ground-based observations. From 3300 to 3500 Å a dip can be observed in the spectra presented in Figure 1. This dip, or the corresponding hump at about 3500 Å, is sus-

pect, because it is in this region that sodium salicylate becomes transparent. Also in this spectral region the primary laboratory reference is switched from the sodium salicylate to tungsten-iodide irradiance standards calibrated by the National Bureau of Standards. There is a definite shift in sensitivity of the payload in this spectral region indicated by both calibration references. A judicious smoothing of the calibration curve could eliminate the 3400 Å dip and also remove the 15 percent discrepancy that develops when the short wavelength absolute calibration is extrapolated to meet the ground-based data. The present laboratory calibration data do not justify making this correction, but a systematic error may exist. This spectral region will be investigated intensively during the calibration of the next flight payload.

Second is the existence of some disagreement in the comparison data available in the short wavelength range. Preliminary data available from the University of Wisconsin calibration rocket (Bless, personal communication) indicates agreement with the present data from 2000 to 2800 Å (2800 Å is the long wavelength limit of the Wisconsin rocket data). Shortward of 2000 Å the Wisconsin values for the spectrum of α Leo indicate a smooth tie with Carruthers' values (1968). The present rocket data is therefore about 30 to 50 percent low, relative to the Wisconsin observations. This is a very disconcerting disagreement, because it is larger than the combined error flags of the two observations. A thorough reinvestigation of the 13.041 calibration procedures did not reveal any sources of systematic error that could account for the discrepancies. A weakness in the calibration below 2000 Å is its reliance on the assumption that the quantum efficiency of sodium salicylate is wavelength independent. It is now possible to use calibrated photodiodes as standards in this spectral region, and the uncertainties due to sodium salicylate will be avoided on future flights.

REFERENCES

Aller, L. H., Faulkner, D. J. and Norton, R. H. 1966, Ap. J. 144, 1073-1100.
Campbell, J. W. 1970, Ap. and Space Sci. 9, 128-145.
Carruthers, G. R. 1968, Ap. J. 151, 269-284.
Chubb, T. A. and Byram, E. T. 1963, Ap. J. 138, 617-630.
Hoffleit, D. 1964, Catalogue of Bright Stars (New Haven: Yale University Press).
Mitchell, R. I. and Johnson, H. L. 1969, Comm. Lunar and Plan. Lab. Vol. 8, No. 132, Part 1 (Tucson: Univ. of Arizona).
Oke, J. B. and Schild, R. E. 1970, Ap. J. 161, 1015-1023.
Schild, R., Peterson, D. M. and Oke, J. B. 1971, Ap. J. 166,

95-108.
Smith, A. M. 1967, Ap. J. 147, 158-171.
Stecher, T. P. 1970, Ap. J. 159. 543-550.
_____ 1969, Astr. J. 74, 98-102.
Stecher, T. P. and Milligan, J. E. 1962, Ap. J. 136, 1-13.
Underhill, A. B. 1972, this volume.
Yamashita, K. 1968, Ap. and Space Sci. 2, 4-22.

ABSOLUTE CALIBRATION OF ULTRAVIOLET FILTER PHOTOMETRY

R. C. Bless, T. Fairchild and A. D. Code
University of Wisconsin
Madison, Wisconsin

The original spectrophotometric calibration of the Wisconsin telescopes on OAO-2 suffered from at least two important deficiencies: light sources available at that time radiated rather feebly in the far ultraviolet; and because of the requirements of spacecraft testing, the final laboratory calibration had to be performed 18 months before launch, although a limited field calibration in the 2000-4000 Å region was performed somewhat later.

When it became apparent that the OAO photometric system was stable and capable of considerable precision, we thought it important to attempt a new absolute ultraviolet calibration, both for OAO-2 and the then soon-to-be-launched OAO-B. Thus began the collaborative effort between the Wisconsin and Goddard groups (Evans 1972). Our intention was to fly small, simple telescopes in an Aerobee sounding rocket and measure the ultraviolet flux in several wavelength bands from a few bright, early-type stars which had also been observed by OAO. Such a rocket payload could undergo pre- and post-flight calibrations within a few weeks of the flight, as well as field calibrations a few days before and after the flight. Furthermore, a new source of ultraviolet radiation had become available to us, namely the synchrotron radiation from high energy electrons circulating in a storage ring. This facility, operated by the University of Wisconsin, consists of a synchrotron which accelerates electrons to about 50 mev, injects them into a storage ring in which, after further acceleration to about 240 mev, they can circulate for times of several hours at this energy. Thus the source is stable in time. In addition, the spectral energy distribution of the radiation approximates that of a B5 type star, i.e. the energy distribution of the stars we wish to calibrate; scattered light problems, which have plagued ultraviolet calibrations in the past, are thereby minimized. Finally, the absolute intensity of the beam can be

determined apart from any thermal sources so that the storage ring provides a calibration source completely independent of any previous absolute radiation standards. Such an absolute calibration is realized because it is possible to measure the synchrotron radiation from only one or two circulating electrons. Thus, by starting with about 50 electrons and measuring the step-wise decrease in intensity of the radiation each time an electron is ejected from the beam, one can determine the number of electrons producing a given signal. A simple extrapolation then gives the number of electrons (typically 300-500) used in the calibration, and thus the absolute intensity of that radiation.

The rocket payload consisted of seven telescopes, aligned to a common optical axis, each operating independently of the others with its own amplifier and power supply. Four of these were of a type we have flown before (see Bless et al. 1968), namely, two-inch suprasil quartz refractors with EMI 6256B photomultipliers as detectors, and three were four-inch aperture reflecting telescopes with EMR 541-type detectors at their focus. In each of the two-inch telescopes, transmission bands were shaped by two essentially identical three-layer aluminum-dielectric interference filters; the second filter significantly decreases the transmission in the wings. The 1550 Å band in one of the four-inch instruments was shaped by a single interference filter, whereas none were used in the remaining two reflectors, the long wavelength transmission edge being set by the photomultiplier response, the short wavelength edge by a CaF window. Peak photometer sensitivities were at about 2900 Å, 2400 Å, 2100 Å, 1900 Å (the two-inch instruments), 1550 Å and two at 1370 Å; bandwidths (FWHM) were about 250 Å. The field of view of each instrument was determined to be flat (to ~1%) over a 1° diameter circle; the total field was only slightly larger than this. An amplifier twenty times more sensitive than the primary amplifiers measured the background sky radiation, which was very small at all wavelengths.

The essential features of the calibration procedure can be divided into three parts. First, the shape of the bandpass of each photometer was determined by measuring the transmissions of the individual optical components and also by measuring the response of the photometer as a whole. For these relative measurements, a hydrogen lamp and ultraviolet monochromator provided the source radiation and sodium salicylate-coated photomultipliers served as the standard detectors. (Possible variations in the quantum efficiency of sodium salicylate are minimized here since constancy is assumed over only a few hundred angstroms for each instrument.) In calibrating the photometer as a whole, the objective was illuminated point-by-point by a nearly-collimated radiation bundle. Typically, six

points were measured at 25 Å intervals over the whole wavelength region of interest, and about 40 points were measured at two or three wavelengths.

Secondly, each photometer was placed in the essentially-collimated synchrotron radiation bundle maintained at a constant intensity level, and the output signal (using the flight electronics) determined from about 100 points on the objective. The sensitivity variations over the objective were small, about ±10%.

Finally, two or three points on the objective were illuminated by synchrotron radiation at several different intensity levels covering the dynamic range of the photometers. The output signals were placed on an absolute basis by the electron counting technique described earlier.

This laboratory calibration was made several weeks before, and repeated a few weeks after, the flight. To monitor photometer response in the interval between these calibrations, a field calibration unit was constructed. The two-inch photometers were illuminated with uncollimated light having a bandpass defined by double interference filters essentially identical to those in the flight photometers. Reproducibility was assured by tight, positive mechanical coupling between the flight photometers and the calibration unit and by monitoring the source intensity. The calibration was carried out in air. The four-inch instruments were calibrated using parallel radiation from a four-inch collimator which could be sealed to the flight photometers and the whole system evacuated. The photometer responses were compared to those of two "standard" photometers which were constructed and calibrated in a manner similar to that of the flight instruments. Calibrations were made with this instrument a few weeks and a few days before the flight, one day after the flight, and finally a few weeks after the flight. The four-inch photometer responses varied by ±9% during this interval whereas that of the two-inch instruments varied by ±5%.

The payload was flown on March 1, 1971 on an Aerobee 170 rocket and reached an altitude of 134 miles. All systems performed well and the three program stars, α Vir, η UMa and α Leo were observed as planned, viz., each object was observed at two to four mean altitudes for totals of from 40 to 80 seconds. This enabled an evaluation to be made of the extinction by the residual atmosphere of the earth, as well as that by rocket outgassing. These effects were not detectable except at the shortest wavelengths, where they required a correction of a few percent to the signals observed at or near peak altitude.

The results for η UMa are typical and are given in Figure 1 by the filled circles; open circles are the absolute measures of Schild *et al.* (1971). The observation at 1900 Å

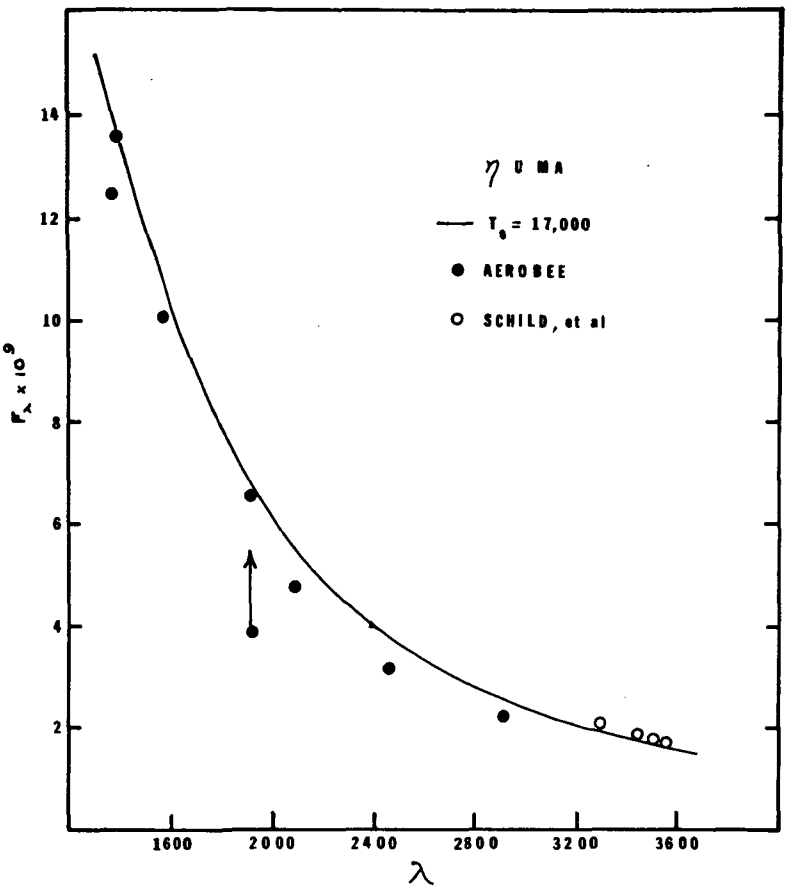

Figure 1.—Preliminary absolute ultraviolet fluxes from η UMa (filled circles), ground-based observations (open circles), compared with a hydrogen line blanketed model atmosphere with T_e = 17000°K, fitted at the V magnitude.

falls below the general run of points for all three stars by the same factor; multiplying the observed flux in this band by 1.7 "corrects" this measurement. At this time we don't know what happened here; the pre- and post-flight laboratory and field calibrations are in good agreement for this photometer. In addition, the interpretations of the measurements at the three shortest wavelengths are somewhat ambiguous because these bandpasses include strong stellar absorption lines. The values plotted in Figure 1 may change by 10-15% when these ambiguities are resolved.

The solid line represents a hydrogen line blanketed model atmosphere with an effective temperature of 17000°K, calculated by Klinglesmith. This temperature is about the average of

that derived by Schild et al. (1971) and by Kodaira (1970) for this star. The model was fit only to the V magnitude of η UMa and represents the ultraviolet as well as the visual observations reasonably well. The points in the 2000-3000 Å region fall below the model atmosphere by about $0^m.15$-$0^m.20$. Line blanketing of this order was derived by Underhill (1972) for η UMa and probably explains most of the observed difference between our observations and the model in this spectral region. That line blanketing is affecting our measurements in the 2000-3000 Å region is also suggested by our results for α Vir and α Leo; in the former, the observations fall only slightly below an appropriate model, while in the latter, they fall farther below a model than do those of η UMa, just as Underhill's measurements of blanketing suggest they should.

These results indicate that model atmospheres, suitably corrected for blanketing, can be used to represent ultraviolet energy distributions, at least until the final observational results are available.

We gratefully acknowledge the invaluable contributions of Mr. Don Michalski and Mr. Jack Stanton to this program, as well as the expert assistance of the Sounding Rocket Branch of Goddard Space Flight Center.

REFERENCES

Bless, R. C., Code, A. D., Houck, T. E., McNall, J. F. and Taylor, D. J. 1968, Ap. J. 153, 557.

Evans, D. 1972, this volume.

Klinglesmith, D. A. 1971, Hydrogen Line Blanketed Model Stellar Atmospheres, NASA SP-3065.

Kodaira, K. 1970, Ap. J. 159, 931.

Schild, R., Peterson, D. M. and Oke, J. B. 1971, Ap. J. 166, 95.

Underhill, A. B. 1972, this volume.

Page intentionally left blank

THE NEAR ULTRAVIOLET SPECTRUM OF B AND A TYPE MAIN SEQUENCE STARS

Anne B. Underhill
National Aeronautics and Space Administration
Goddard Space Flight Center
Greenbelt, Maryland

ABSTRACT

Scans of λ Lep, η UMa, ζ Dra, ε Dor, α Leo, φ Dra, ν Dra, β Aur, α Pic and δ Dor have been obtained with scanner No. 1 of OAO-2 over the range 1800-3600 Å on the OAO guest observer program. These scans have been reduced to tracings of F_λ in the 20 Å pass band vs. wavelength using a wavelength conversion scale and a relative spectral sensitivity function kindly communicated by B. D. Savage. The general trend of the relative flux plots compares well with the continua predicted by simple model atmospheres. The line blocking per 100 Å in the region 2000-3000 Å relative to theoretical continuous spectra is tabulated. At type B6 and later the blanketing is due chiefly to the many lines of Fe II and Cr II. In the stars of types B0.5 to B3, the lines from the third spectra of the metals contribute a blanketing similar to that predicted by Elst for a B1 star. The significant line blocking that can occur in early type atmospheres, particularly in stars with extended atmospheres, throughout the range $4.0<\lambda^{-1}<5.5\mu^{-1}$, raises doubts whether the hump in the interstellar extinction curve found in this region by Stecher and by Bless and Savage is solely due to the interstellar medium. The severe line blanketing which occurs in the range 2000-3000 Å for stars of types B6 and later will make the interpretation of broad and narrow band photometry in this range difficult.

The results of a study of spectrum scans requested by the author as an OAO-2 guest observer while she was at the

Utrecht University, Netherlands are reported. The purpose was to obtain OAO observations of a few of the stars that will be observed with the Utrecht scanning spectrometer (experiment S59) which will be on the ESRO astronomical satellite TD1 which is to be launched early in 1972. The satellite will be launched in a circular near polar synchronous orbit and in the course of six months the scanning spectrometer should observe the whole sky. When a sufficiently bright star enters the field of view of the telescope, a scanning mechanism is triggered so that three bands of 100 Å centered at 2085, 2520 and 2800 Å, respectively, are scanned in steps of 1 Å. The resolution is about 1.4 Å per step. By obtaining OAO scans of a few objects which should frequently appear in the field of view of S59, it is hoped to be able to relate the Utrecht results, which will cover only limited spectral regions, to the extensive body of OAO data.

Reliable spectral scans of 10 main sequence B and A stars were kindly made available by the Wisconsin Principle Investigator, Dr. A. D. Code. The scans extend from about 1800 Å to about 3700 Å. The raw data were converted from grating step and number of counts per 20 Å pass band using conversion formulas kindly communicated by B. D. Savage. The wavelength scale is not precise because to establish an accurate zero point one must recognize at what grating step the blended Mg II resonance lines occur. This is not always possible. An uncertainty of one grating step means an uncertainty in wavelength of about 20 Å. The conversion formulas of Savage are strictly valid only for wavelengths longer than 2200 Å. The short wavelength formula was extrapolated shortward in order to obtain a wavelength scale to the end of the data range. The same extrapolated nominal wavelength scale has been used for all the stars using an estimated position for the Mg II resonance lines as zero point.

The stars observed are listed in Table 1 together with their color excesses and some further information. Unless otherwise noted, the spectral types, V magnitudes and B-V colors have been taken from the Bright Star Catalogue (Hoffleit 1964). The intrinsic colors of Johnson (1963) were adopted.

The relative flux distributions over the range 1800-3400 Å for a 20 Å pass band are shown in Figures 1 and 2. (The flux distribution for α Pic is not shown; it is similar to that of δ Dor.) In Figures 1 and 2 each observed flux distribution (solid line) is compared with the relative continuous spectrum from an LTE, hydrogen-line blanketed model atmosphere (Klinglesmith 1971). The composition of the models is X = 2/3, Y = 1/3; log g is 4.0. Appropriate effective temperatures are adopted for each type. The predicted

Table 1. The Stars Observed

HR No.	Name	Sp. Type	V	B-V	E(B-V)	Remark
1756	λ Lep	B0.5 IV	4.28	-0.28	0.00	
2015	δ Dor	A6 IV	4.34	+0.22	+0.05	
2064	ε Dor	B5	5.10	-0.15	-0.01	1.
2088	β Aur	A2 V	1.90	+0.03	+0.03	2.
2550	α Pic	A5 V	3.26	+0.21	+0.06	
3982	α Leo	B7 V	1.36	-0.11	+0.01	3.
5191	η UMa	B3 V	1.86	-0.20	0.00	4.
6396	ζ Dra	B6 III	3.20	-0.15	-0.01	
6554	ν Dra	Am	4.86	+0.25	+0.08	5.
6555			4.84	+0.28	+0.11	
6920	φ Dra	A0p(Si)	4.18	-0.00	0.00	6.

1. According to Hiltner, Garrison and Schild (1969) the MK spectral type is B6 V.
2. This star is a double-lined spectroscopic binary and it appears in the catalogue of rotational velocities of Bernacca and Perinotto (1970).
3. Blanco, Demers, Douglass and Fitzgerald (1968) list V = 1.33 and B-V = -0.12; this star is in Bernacca and Perinotto (1970).
4. Blanco, Demers, Douglass and Fitzgerald (1968) list V from 1.85 to 1.96 and B-V from -0.170 to -0.20; this star is in Bernacca and Perinotto (1970).
5. Both stars are observed together; HR 6555 is a spectroscopic binary; these stars are in Bernacca and Perinotto (1971) who list types A6 V and A4m respectively.
6. This star is a spectroscopic binary listed in Bernacca and Perinotto (1971); Cowley, Cowley, Jaschek and Jaschek give V = 4.22 and B-V = -0.10. It is also a magnetic star.

continuous spectra from these admittedly simple models are used as convenient reference flux distributions with which to compare the observed flux distributions. None of the stars are reddened by a significant amount. Little weight should be placed on the apparent intensity distribution at $\lambda < 2000$ Å because at these wavelengths the sensitivity of the equipment is low, with the result that the observed number of counts has been multiplied by a number of the order of 5 or 6. In fact, comparison with the results of Evans (1971) indicates that the adopted sensitivity function is too low at $\lambda < 2000$ Å.

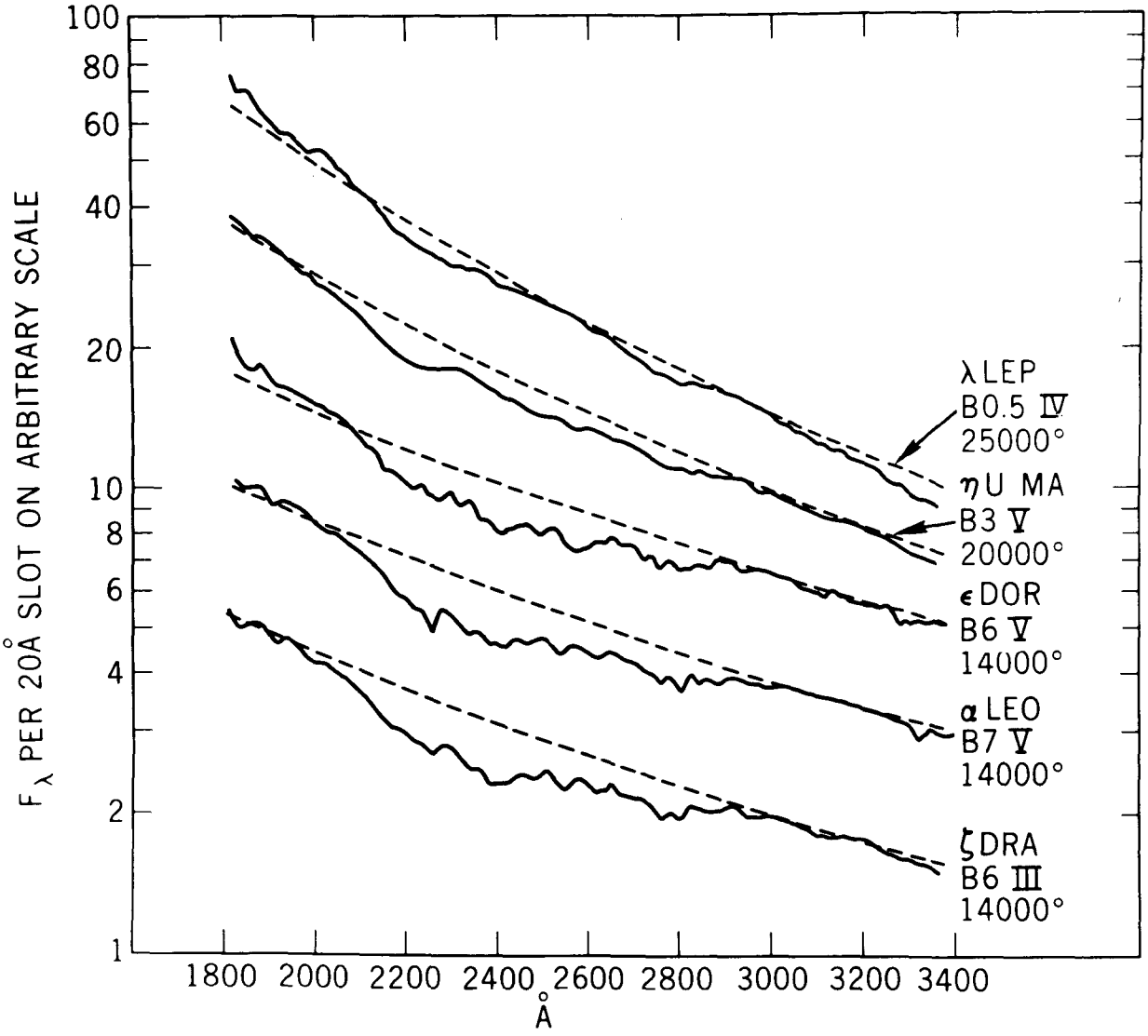

Figure 1.—Relative flux distributions in a 20 Å bandpass for B stars relative to continua predicted from hydrogen line blanketed model stellar atmospheres having log g = 4.0 and the indicated value of effective temperature.

At spectral type B0.5 IV, there is very little line blanketing. However, by type B3 V (η UMa) the blanketing is quite significant. The spectrum from about 2000-2900 Å is depressed from what is predicted when the effects of all lines except those due to hydrogen are ignored. At types B6 and B7 the blanketing is conspicuous. The luminosity class III star ζ Dra seems to have slightly stronger blanketing

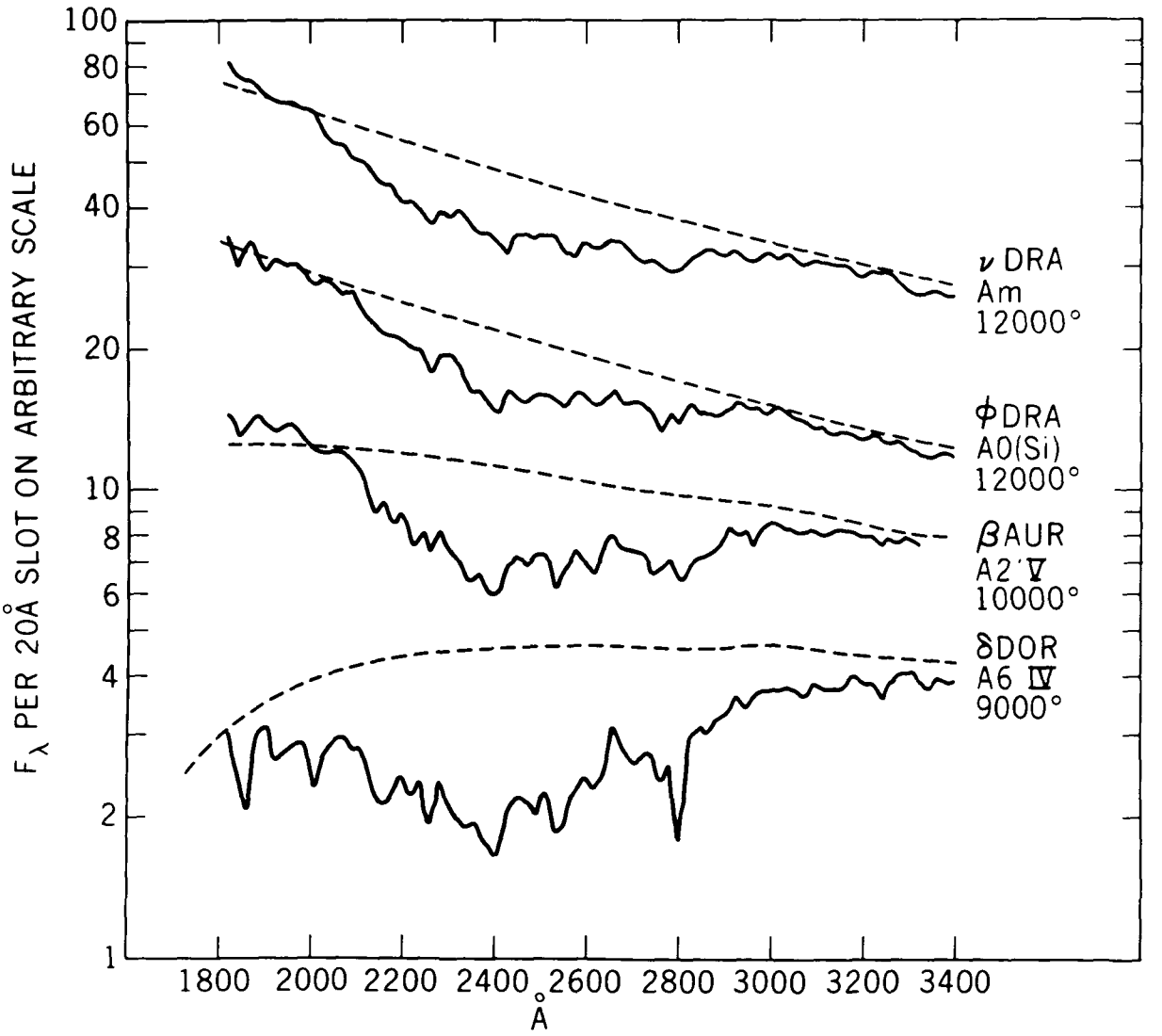

Figure 2.—Relative flux distributions in a 20 Å bandpass for A stars relative to continua predicted from hydrogen line blanketed model stellar atmospheres having log g = 4.0 and the indicated value of effective temperature.

than do the class V stars. One may suspect that the Mg II resonance lines near 2800 Å would be resolved at 10 Å resolution. Scans of some A type main sequence stars are shown in Figure 2 compared with cooler model atmospheres of the same grid. The line blanketing increases rapidly with advancing spectral type and the Mg II lines become prominent by type A5 or A6. The scan for ν Dra records the spectrum of all stars of this composite system. The line blanketing at wavelengths

shortward of 2200 Å seems to be stronger for this Am spectrum than it is for normal A stars.

The A type stars are probably quite nearby. Their apparent color excesses must reflect a systematic effect in Johnson's intrinsic colors for types A2 and A5. The reasonable fit of the theoretical continua to the observed spectral distributions at wavelengths between 3000-3700 Å indicates that the sensitivity function communicated by Savage is acceptable.

An attempt was made to identify some of the more prominent dips, but it is impossible to make detailed line assignments because this part of the spectrum is full of lines. A resolution of the order 1 Å rather than 20 Å will be required to make progress with identifications. A measure of the density of lines from the more abundant metals (Ti, Cr, Mn, Fe, Co and Ni) has been obtained by counting all the lines of the second and third spectra of these elements per 100 Å range between 1700-3000 Å. The results are shown in Figure 3. There are very many lines from the second spectra of the metals, in particular from Fe II and Cr II. The density of

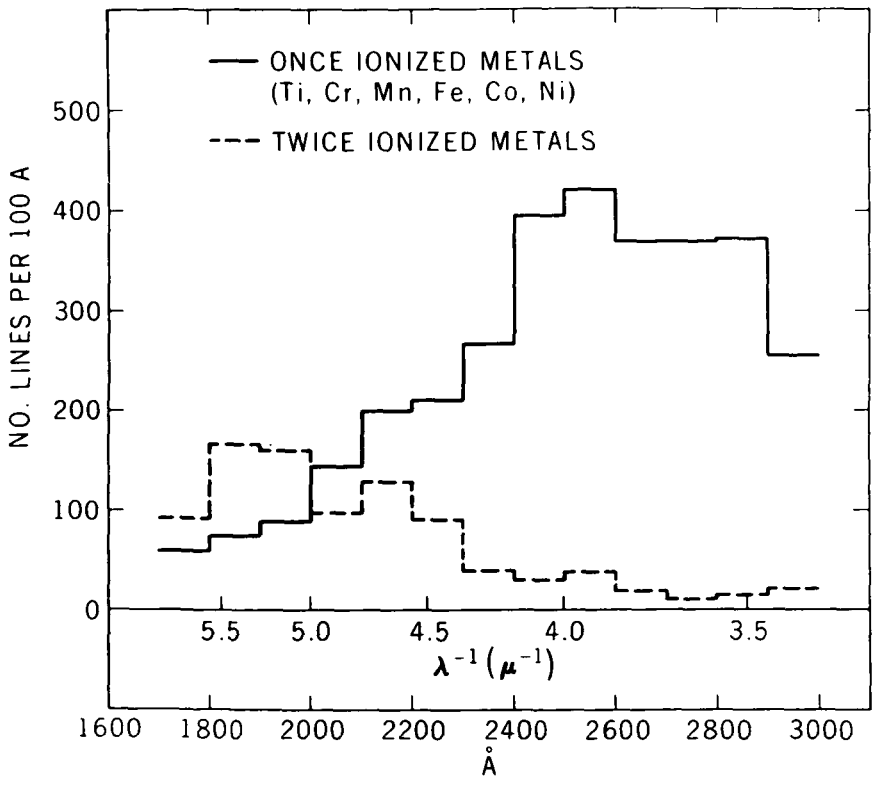

Figure 3.—The relative density of spectral lines per 100 Å of the second and third spectra of the metals.

lines from the second spectra of the metals is particularly large from 2300-2900 Å. The lines of the third spectra of the metals fall mostly in the range 1900-2300 Å; they peak between 1800-2200 Å. Reference to Figures 1 and 2 shows that line blanketing at types B0.5 and B3 is concentrated most strongly near 2200 Å; at types B6 and later, the blanketing is strongest over the range 2300-2900 Å. It is at least as strong as that found in the 3400-4400 Å region of F type spectra (see Melbourne 1960).

The line blocking per 100 Å relative to the adopted nominal continua has been measured and is tabulated in Table 2 as $\Delta m = 2.5 \log (F_\lambda/F_C)$ averaged over a 100 Å range. It is shown in Figure 4. The line blocking for λ Leporis is rather similar to that predicted by Elst (1969) using a model atmosphere of nominal type B1.5 V. The line blocking increases

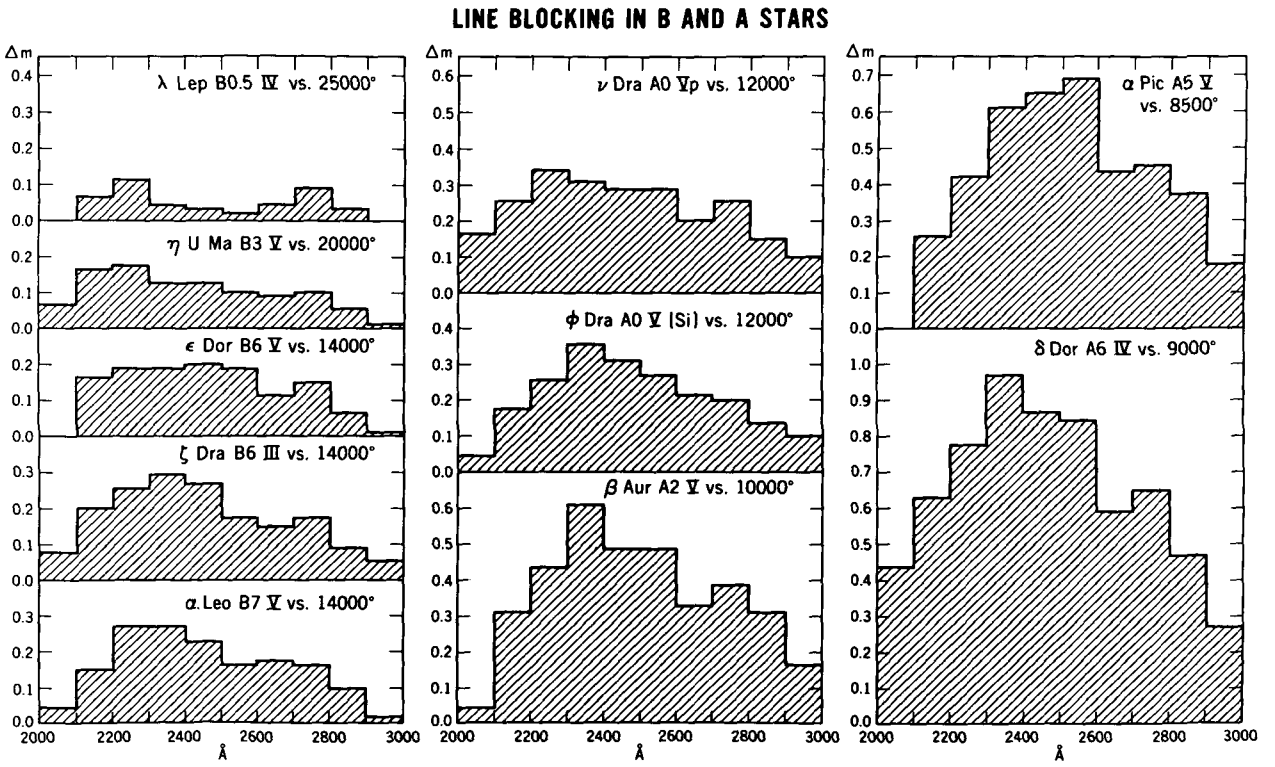

Figure 4.—The line blocking in B and A main sequence stars per 100 Å relative to theoretical continuous spectra. The ordinate, Δm, is the flux per 100 Å of the star relative to the continuous spectrum expressed in magnitude units. The amount of line blocking shortward of 2100 Å is uncertain owing to uncertainties in the adopted sensitivity function at λ < 2100 Å.

Table 2. The Line Blanketing Relative to a Grid of Reference Models Expressed in Magnitudes

Star Sp.Type T_{eff}	λ Lep B0.5 IV 25000	η UMa B3 V 20000	ε Dor B6 V 14000	α Leo B7 V 14000	ζ Dra B6 III 12000	ν Dra Am 12000	φ Dra A0p(Si) 12000	β Aur A2 V 10000	α Pic A5 V 8500	δ Dor A6 IV 9000
20-21	--	0.07	0.00	0.04	0.08	0.16	0.04	0.04	--	0.44
21-22	0.07	0.16	0.16	0.15	0.20	0.26	0.18	0.31	0.26	0.63
22-23	0.11	0.18	0.19	0.27	0.26	0.34	0.26	0.44	0.42	0.78
23-24	0.04	0.13	0.19	0.27	0.30	0.31	0.36	0.61	0.61	0.97
24-25	0.03	0.13	0.20	0.23	0.27	0.28	0.31	0.48	0.65	0.87
25-26	0.02	0.10	0.19	0.16	0.18	0.28	0.27	0.48	0.69	0.84
26-27	0.04	0.09	0.11	0.18	0.15	0.20	0.22	0.33	0.44	0.59
27-28	0.09	0.10	0.15	0.16	0.18	0.26	0.20	0.39	0.45	0.65
28-29	0.03	0.06	0.07	0.10	0.09	0.15	0.14	0.31	0.37	0.47
29-30	0.00	0.01	0.01	0.02	0.06	0.10	0.10	0.16	0.18	0.27

rapidly with advancing spectral type. By type A6 V nearly 1 mag per 100 Å is being removed from the spectrum in the neighborhood of 2300 Å. This is probably chiefly due to the numerous very strong lines of Fe II and Cr II.

The considerable line blocking that occurs in spectral types B6 and later between 2100-2900 Å means that study of this region by broad or narrow band photometry will not result in an accurate approximation to the shape of the continuous spectrum. Because the line blocking is not entirely negligible even at type B0.5, the derivation of the shape of the interstellar reddening curve by comparing spectra of two stars of not precisely the same spectral type is fraught with danger. The principal lines which are causing the line blocking are from low-lying configurations and are of such a spectroscopic character that one may expect them to be enhanced in strength in a star with a somewhat extended atmosphere. It is well known that the lines of the ionized metals are enhanced in the spectra of giants and supergiants. That large numbers of these lines fall in the neighborhood of 2200 Å makes it particularly difficult to establish what part of the apparent blocking of radiation here in a reddened star relative to an unreddened star, is due to the stellar atmosphere and what part is truly due to interstellar reddening.

Stecher (1969) and Bless and Savage (1970) have suggested that there is a hump in the interstellar reddening curve throughout the range $4.0<\lambda^{-1}<5.5\mu^{-1}$. However, to be certain of the reality of this feature, one would have to demonstrate that there is significantly less than 0.1 mag difference in the line blocking for the two stars being compared. In all published cases, the measured difference in the spectrum profiles between the reddened and the unreddened star in the neighborhood of 2200 Å has been magnified by a factor of the order of 5 owing to the normalization procedure adopted.

The significant line blocking shown by the 20 Å resolution scans of B and A stars is a fascinating indication of how rich in lines the spectra of B and A stars will be in the 2000-3000 Å region when viewed at high resolution. The predicted line strength for types near B1 V of Guillaume, van Rensbergen and Underhill (1965), Guillaume (1966), and Elst (1969) and for type A0 by Maran, Kurucz, Strom and Strom (1968), inadequate as they are, give an indication of what is to be expected. The Bp and Ap stars when examined at adequate resolution in the 2000-3000 Å range should reveal many spectral peculiarities because of the great density of spectroscopically significant lines. It may be possible to set up a finely divided spectral classification system for late B and early A stars when spectra of moderate resolution in the 2000-3000 Å region are available. In this way some present anomalies may be resolved.

This survey of the near ultraviolet spectra of B and A stars was made possible by the generosity of the NASA OAO-2 Guest Observer Program. Particular thanks is due to Dr. B. D. Savage of the University of Wisconsin for communicating the scanner data and the wavelength and sensitivity conversion factors in a most convenient form.

REFERENCES

Bernacca, P. L. and Perinotto, M. 1970, A Catalogue of Stellar Rotational Velocities, Parts I and II, Contrib. Osserv. Astrofisico, Padova in Asiago, No. 239.

_____ 1971, ibid, Part III, No. 249.

Blanco, V. M., Demers, S., Douglass, G. G. and Fitzgerald, M. P. 1968, Pub. U. S. Naval Obs., Vol. XXI.

Cowley, A., Cowley, C., Jaschek, M. and Jaschek, C. 1969, Astr. J. 74, 375.

Elst, E. W. 1969, Bull. Astron. Inst. Netherlands 19, 90.

Guillaume, C. 1966, Bull. Astron. Inst. Netherlands 18, 175.

Guillaume, C., van Rensbergen, W. and Underhill, A. B. 1965, Bull. Astron. Inst. Netherlands 18, 106.

Hiltner, W. A., Garrison, R. F. and Schild, R. E. 1969, Ap. J. 157, 313.

Hoffleit, D. 1964, Yale Catalogue of Bright Stars (New Haven: Yale University Observatory).

Johnson, H. L. 1963 in Basic Astronomical Data (Chicago: University of Chicago Press), p. 214.

Klinglesmith, D. A. 1971, Hydrogen Line Blanketed Model Stellar Atmospheres, NASA SP-3065; additional models were computed at our request.

Maran, S. P., Kurucz, R. L., Strom, K. M. and Strom, S. E. 1968, Ap. J. 153, 147.

Melbourne, W. G. 1960, Ap. J. 132, 101.

THEORETICAL EFFECT OF VARIOUS BROADENING PARAMETERS ON ULTRAVIOLET LINE PROFILES

Eric Peytremann
Smithsonian Astrophysical Observatory
Cambridge, Massachusetts

ABSTRACT

We study the relative importance of various damping parameters in ultraviolet lines under conditions of normal stellar atmospheres ($10{,}000°K \leq T_{eff} \leq 30{,}000°K$, $\log g = 4$). It is found that the damping by electron collisions is always much smaller than either the radiative or the classical damping, except for lines that arise from high-excitation levels and do not therefore develop strong damping wings. A damping constant equal to 10 times the classical value is always much too large when compared to the more realistic (electron + radiative) damping.

I. INTRODUCTION

The spectra of O and B stars show a large number of metallic lines in the ultraviolet region of the spectrum — that is, between the Lyman limit and approximately 2000 Å. We refer the reader to the results presented at the IAU Symposium 36 (Houziaux and Butler, 1970). Some of these lines are so strong that they can be observed with a resolution as low as 10 Å (Code and Bless, 1970). These strong lines can be heavily saturated and hence develop important damping wings. So one must pay some attention to the damping parameters that one is going to use in line-profile calculations. In addition to the ordinary spectral analysis of each individual line, calculation of the wings of these strong lines must be carried out carefully because (a) they may account for a nonnegligible fraction of the total blanketing effect, and (b) they may block out a substantial amount of energy from the spectral

ranges (narrow or broad) to which they belong. Point (a) concerns the structure of atmospheric models, and (b) relates to the effects of these lines on such observable quantities as low-resolution spectroscopy, or narrow-to-broad-band photometry. Earlier attempts to calculate blanketed models with ultraviolet lines have included a damping constant equal to 10 times its classical value (see Adams and Morton, 1968; Hickok and Morton, 1968; Bradley and Morton, 1969; Wayne van Citters and Morton, 1970). The reason is perhaps that their value represents empirically rather well the damping in solar-type atmospheres. But under solar conditions, the broadening by collisions with neutral particles is a predominant damping mechanism, whereas in the hotter atmospheres studied here, it is not. In this paper, we compare various damping parameters and from them calculate a number of line profiles. The range of temperatures considered is such that damping by collisions with neutral hydrogen can be neglected — that is, the temperatures are representative of model atmospheres with effective temperature T_{eff} larger than 10,000°K. The upper limit of the temperature range has been taken equal to T_{eff} = 30,000°K because in hotter atmospheres, the effects of non-LTE are expected to be very large (Mihalas and Auer, 1970).

II. DAMPING PARAMETERS

For metallic lines, which are the only ones considered in this study, we shall consider two damping mechanisms:

1. Natural, or radiative, damping γ_R, which, for a line with upper level u and lower level ℓ, is given by

$$\gamma_R = \sum_{E_i<E_\ell} A_{\ell i} + \sum_{E_j<E_u} A_{uj} \quad . \qquad (1)$$

Here, the $A_{\ell i}$'s are the transition probabilities from level ℓ to level i, and A_{uj}, from level u to level j, measured in sec^{-1}. The summations are carried over all levels i lower than level ℓ, and all levels j lower than u. The line-opacity profile is Lorentzian, with damping constant γ_R.

2. Broadening by electron collisions. According to Sahal-Bréchot (1969a,b) and to Chapelle and Sahal-Bréchot (1970), the impact approximation is valid for electron collisions under the conditions of normal stellar atmospheres. Hence, the line-opacity profile is Lorentzian, with a damping parameter γ_e (sec^{-1}), where γ_e is proportional to the number density of the perturbers, that is to the electron density N_e (cm^{-3}).

Because both these broadening mechanisms give rise to Lorentzian profiles, the resulting profile is Lorentzian, with damping γ equal to

$$\gamma = \gamma_R + \gamma_e \quad (\text{sec}^{-1}) \ . \tag{2}$$

The damping due to collisions with protons or He^+ ions is much less than the electron damping (Sahal-Bréchot and Segré, 1970). As we shall see, the electron damping itself plays a minor role in all cases where damping wings are strong. Hence, we neglect the damping due to collisions with H^+ and He^+ ions. We shall also compare the radiative and electron damping to the classical damping γ_C,

$$\gamma_C = 0.221 \times 10^{16}/\lambda^2 \quad (\text{sec}^{-1}) \ , \tag{3}$$

where λ is the wavelength of the line in angstroms. A number of model atmospheres with ultraviolet line blanketing have been computed with 10 times γ_C, the value of Morton and his coworkers cited earlier. Because the classical value for damping is easy to compute, it would be useful to derive an empirical value of the damping constant as a multiple of γ_C, for the following reasons. First, the computation of line-blanketing effects involves lengthy calculations (hundreds or thousands of lines); it is desirable to keep the number within reasonable limits. Second, for many of these lines, the data for γ_R and γ_e are simply unavailable. If, however, the radiative damping γ_R and the electron damping γ_e are available for the very strong lines, we can make the following predictions. If γ_R is predominant, the damping mechanism does not give any information on the properties of the atmosphere, because γ_R is essentially an intrinsic atomic parameter. On the other hand, if γ_e is predominant, the damping part of the line profiles would give us information on the state of the gas, mainly the electron density and only slightly, the temperature. This information would then play the role of a gravity indicator.

To carry out these various comparisons, we selected those multiplets for which the necessary data were available. These data, together with some other basic line data, are displayed in Table 1. For each multiplet, we indicate the name of the ion in the first column, followed by the abundance by number log ε (with log $\varepsilon(H) = 12$), the ionization potential χ(in ev), the wavelengths λ(Å), and the oscillator strengths log gf of each multiplet's lines. Next, we give the excitation potentials (in ev) of the lower (χ_ℓ) and upper (χ_u) levels. Finally, the last three columns contain the electron damping $C_e = 10^6\ \gamma_e/N_e$ at T = 20,000°K, the radiative damping γ_R, and

Table 1. $C_e = (\gamma_e/N_e \times 10^6)_{T = 20{,}000°K}$

Ion	log ε	χ(ev)	λ(Å)	log gf	χ_ℓ	χ_u	C_e	γ_R × 10^{-8}	γ_c
C II	8.50	24.38	1334.53	-0.28	0	9.29	0.3	5.9	12.5
			1335.66	-0.97					
			1335.71	-0.02					
C IV	8.50	64.48	1548.20	-0.42	0	8.01	0.5	2.6	9.3
			1550.77	-0.72					
N II	8.00	29.59	1083.98	-0.77	0	11.43	0.3	5.8	18.9
			1084.57	-0.42					
			1084.57	-0.90					
			1085.50	-2.07					
			1085.54	-0.90					
			1087.70	-0.15					
Si II	7.50	16.34	1260.42	0.38	0	9.83	2.7	30.0	14.0
			1264.73	0.63					
			1265.02	-0.32					
			1304.37	-0.44	0	9.50	0.5	10.6	13.0
			1309.27	-0.74					
			1526.72	-0.59	0	8.12	2.0	11.1	9.5
			1533.45	-0.28					
			1808.00	-1.89	0	6.86	0.5	0.1	6.8
			1816.92	-1.63					
			1817.45	-2.60					
			2500.93	-0.67	9.83	14.79	93.6	31.1	3.6
			2501.97	-0.51					
			2502.00	-1.82					
			2904.28	-0.29	9.83	14.10	35.9	32.2	2.6
			2905.69	-0.14					
			2905.70	-1.44					

Table 1, continued

Ion	log ε	χ(ev)	λ(Å)	log gf	χ_ℓ	χ_u	C_e	$\gamma_R \times 10^{-8}$	$\gamma_c \times 10^{-8}$
Si III	7.50	33.46	993.52	-0.93	6.54	19.01	1.3	23.6	22.4
			994.79	-0.45					
			997.39	-0.23					
			1108.37	-0.05	6.54	17.72	0.9	29.1	18.1
			1109.94	-0.18					
			1109.97	0.32					
			1113.17	-1.35					
			1113.20	-0.18					
			1113.23	0.57					
			1206.51	0.23	0	10.27	1.1	23.6	15.3
			1294.54	-0.15	6.55	16.13	1.8	22.3	13.2
			1296.73	-0.25					
			1298.89	-0.37					
			1298.96	0.32					
			1301.15	-0.25					
			1303.32	-0.15					
			1206.53	0.73	10.27	20.55	2.2	74.5	15.2
			2541.82	-0.81	10.27	15.15	1.1	26.2	3.4
Si IV	7.50	45.13	1066.63	0.97	19.88	31.50	4.0	65.5	19.5
			1122.49	0.22	8.84	19.88	1.0	35.6	17.6
			1128.33	-0.48					
			1128.34	0.48					
			1393.76	0.03	0	8.89	1.0	9.2	11.4
			1402.77	-0.27					
			1533.22	0.25	30.99	39.07	44.0	23.9	9.4
			1796.16	-0.82	30.99	37.89	17.0	13.5	6.9
			1790.17	-1.77					
			1797.50	-1.08					

the classical damping γ_C. The two latter are in units 10^{-8} sec^{-1}, and γ_C has been calculated according to equation (3).

The values of the electron damping have been taken from Sahal-Bréchot and Segré (1970). It should be noted that the temperature dependence of γ_e is weak. In most cases of interest, γ_e varies like $T^{-0.25}$. Also, the damping γ_e is the same for all lines of a given multiplet (Chapelle and Sahal-Bréchot, 1970).

The radiative damping γ_R has been calculated according to equation (1) by searching through the tables of atomic-transition probabilities by Wiese, Smith and Miles (1969) and by Wiese, Smith and Glennon (1966). The log gf values have also been taken from these tables. No critical discussion of the contents of these tables has been attempted. It could be that lifetimes of some levels are missing, which would lead to radiative-damping constants that are too small. (This may be the case of multiplet Si II at λ = 1808 Å.) We give only one value of γ_R for each multiplet because the variations of γ_R within a given multiplet are at most $\pm 0.1 \times 10^8$ (sec^{-1}).

Before we discuss these various damping parameters, we describe Figure 1. It shows the damping log γ_e and log γ_R for each multiplet of Table 1 (in units sec^{-1}). The open circles indicate the electron damping, and the crosses the radiative damping. Each multiplet is labeled by its wavelength. The γ_e is for an electron density $N_e = 10^{14}$ (cm^{-3}) and a temperature T = 20,000°K. This density corresponds to rather high values of the optical depth ($\tau_{5000} \simeq 1$) in atmospheres with a gravity log g = 4 and $T_{eff} > 10{,}000$°K. In shallower layers, where the lines are more likely to be formed, the electron damping would be lower. And in atmospheres with lower gravities, it would be still lower. Thus, the values of γ_e in Figure 1 must be considered as upper limits in most cases of astrophysical interest. Also shown in Figure 1 is the classical damping γ_C, together with 10 times γ_C, as a function of wavelength.

From Table 1 and Figure 1, we can easily draw the following conclusions:

1. The electron damping is nearly always lower than the radiative damping, even with the rather high value of $N_e = 10^{14}$(cm^{-3}). The only lines for which the electron damping is important are those arising between very highly excited levels. Hence, these lines are not strong, and damping does not play an important role.

2. For most lines whose lower level is not too highly excited (and which may therefore be very strong), the radiative damping is between 1/3 and 3 times the classical damping. One exception is the already mentioned multiplet of Si II at

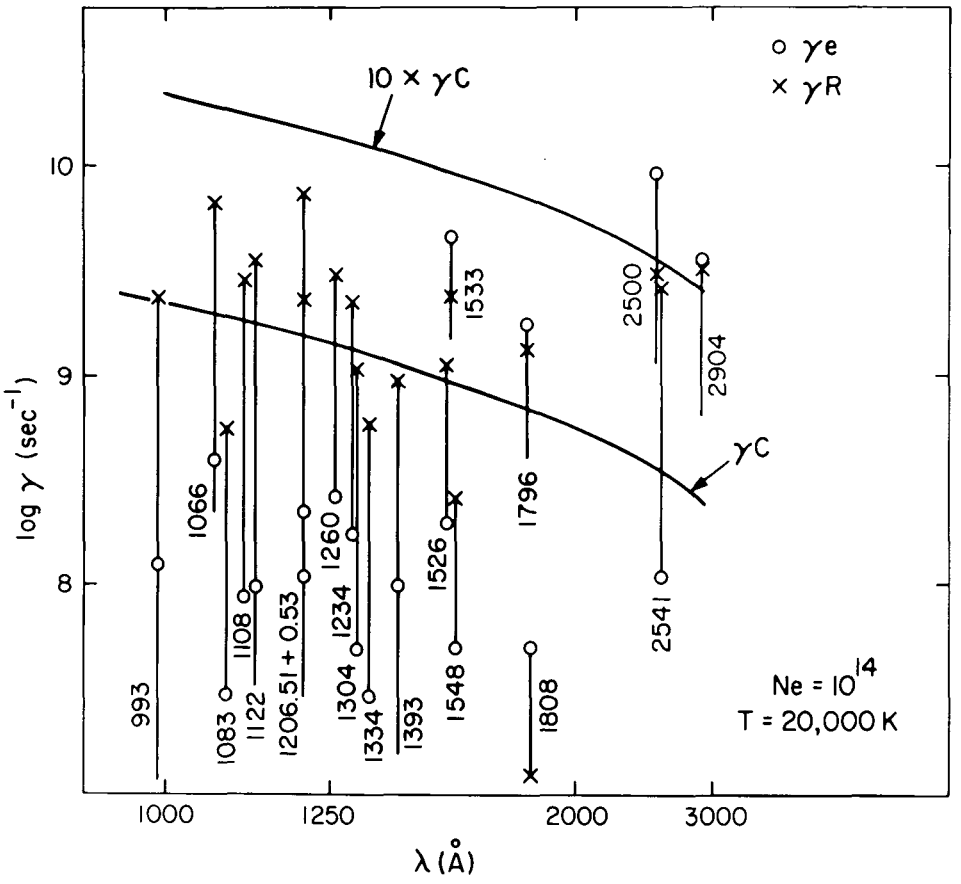

Figure 1.—Damping log γ of a number of ultraviolet multiplets. Crosses indicate radiative damping. Open circles indicate electron damping. The data of each multiplet are labeled with its wavelength. Solid lines show classical and 10 times classical damping.

λ = 1808 Å.

3. For all lines that qualify to develop strong damping wings, the value $\gamma = 10\ \gamma_C$ is much too large, by a factor 3 at least, with respect to either γ_R or $\gamma = \gamma_R + \gamma_e$.

4. The radiative damping being predominant, we do not expect any gravity effect on the line profiles via the damping mechanism. This answers the question that we raised previously.

III. ULTRAVIOLET LINE PROFILES AND EQUIVALENT WIDTHS

In this section, we consider how our various damping parameters influence the profiles and equivalent widths of strong lines. These lines are supposed to be formed in stellar

atmospheres with effective temperatures T_{eff} ranging from 10,000 to 30,000°K and with a surface gravity log g = 4. However, because we want to study the relative effects of the damping parameters with respect to each other, we do not worry too much about the degree of realism of our computations (i.e., abundances, microturbulence, etc.). So we simply indicate how the calculations have been performed, without any critical discussion of matters not directly related to the damping problem.

To calculate our line profiles, we used the program ATLAS (Kurucz, 1969), modified to calculate metallic-line profiles and equivalent widths (Peytremann, 1970). The basic assumptions are those of classical model atmospheres: plane-parallel and in hydrostatic and radiative equilibrium. Occupation numbers are given by the Saha-Boltzmann relations. The source function is calculated according to the Milne-Eddington relation, with scattering by free electrons. (Rayleigh scattering is negligible at these high temperatures.) The line opacities are treated in pure absorption. With these assumptions, it is clear that the line cores are incorrect, but they are rather narrow as compared to the strong damping wings. As stated previously, we are currently interested in these damping wings, and it is precisely these that contribute mostly to the equivalent widths of strong lines, as we shall see later.

The line-opacity profiles are given by Voigt functions calculated according to Baschek, Holweger, and Traving (1966). At each frequency, we sum up the continuous opacities and the opacities of all the relevant lines (blends). In our case, we take into account all lines of a given multiplet. Also, for clarity, we do not include the opacities of nearby hydrogen lines. The equivalent widths have been computed according to Baschek et al. (1966) with the following exception. Most of the lines studied here are so broad that the residual fluxes

$$r_\lambda = F(\lambda)/F_c(\lambda) \qquad (4)$$

are calculated with respect to the continuum $F_c(\lambda)$ and not, as usual, to the continuum at the line-center wavelength ($F(\lambda)$ is the flux in the line, and $F_c(\lambda)$ is the continuum flux). However, since the computation of the flux at each frequency point is time consuming, we calculate only three continuum points for each multiplet and obtain the $F_c(\lambda)$ values by parabolic interpolation. This completes our description of the computational method.

The actual data entering the computations are (a) the model atmospheres and (b) the line data. (a) The models are hydrogen line-blanketed models calculated with the unmodified pro-

gram ATLAS (Kurucz, 1969). The ratio of helium to hydrogen by number is equal to 1/9. At our temperature ($10{,}000 \geq T_{eff} \geq 30{,}000°K$), metals are unimportant as electron donors. The gravity has been taken as log g = 4. As we shall see, the effect of the electron density (and hence of the gravity) is so weak that no attempt has been made to calculate line profiles at lower gravities, where the contribution of the electron broadening would be still weaker. Finally, the ad hoc microturbulence parameter that enters the Voigt function has been set equal to 5 km sec^{-1}. The strong lines studied here depend very little on the microturbulence velocity, because their damping wings are far broader than the Doppler core, and some calculations with velocities equal to 0 and 10 km sec^{-1} have indeed confirmed this. (b) The line data are contained in Table 1. The actual values of the abundances and of the partition functions are those contained in our version of the program ATLAS (Peytremann, 1970).

IV. RESULTS AND DISCUSSION

We did not calculate the profiles of all the lines listed in Table 1, at each temperature. In Figures 2 to 9, we display typical results. At the present time, we cannot compare our results to observations, because, for one reason, the instrumental profiles must be known in order to fold them into the theoretical profiles. Moreover, the definition of observed residual fluxes or equivalent widths depends on an accurate definition of the continuum. This is difficult, and perhaps impossible, if the observed spectral feature is blended with a large number of adjacent lines; this indeed is what is observed on ultraviolet spectral scans (Houziaux and Butler, 1970).

Figures 2 and 3 show the profiles of the multiplets λ1083 (N II), and λ1206.51 (Si III). The ordinates are the residual fluxes r_λ defined by (4), and the abscissas give the wavelength in angstroms. The profiles shown here are for models with $T_{eff} = 20{,}000°K$. The various profiles are labeled with γ_e for electron damping, $\gamma_R + \gamma_e$ for electron plus radiative damping, and γ_C for classical damping (Figure 3 only). Also shown are the profiles with 10 times the classical damping. Figure 3 also shows the pure Doppler profile ($\gamma = 0$). It is seen that 10 γ_C gives lines much too broad, as compared to the more realistic $\gamma = \gamma_R + \gamma_e$ case; γ_e alone gives too weak profiles, but its effect is important if we compare it to the zero-damping case ($\gamma = 0$, Figure 3). Figure 2, which displays a six-component multiplet, shows a striking difference between the cases γ_e and $(\gamma_e + \gamma_R)$ and the case 10 γ_C. Whereas the former profiles are resolved into four components, the

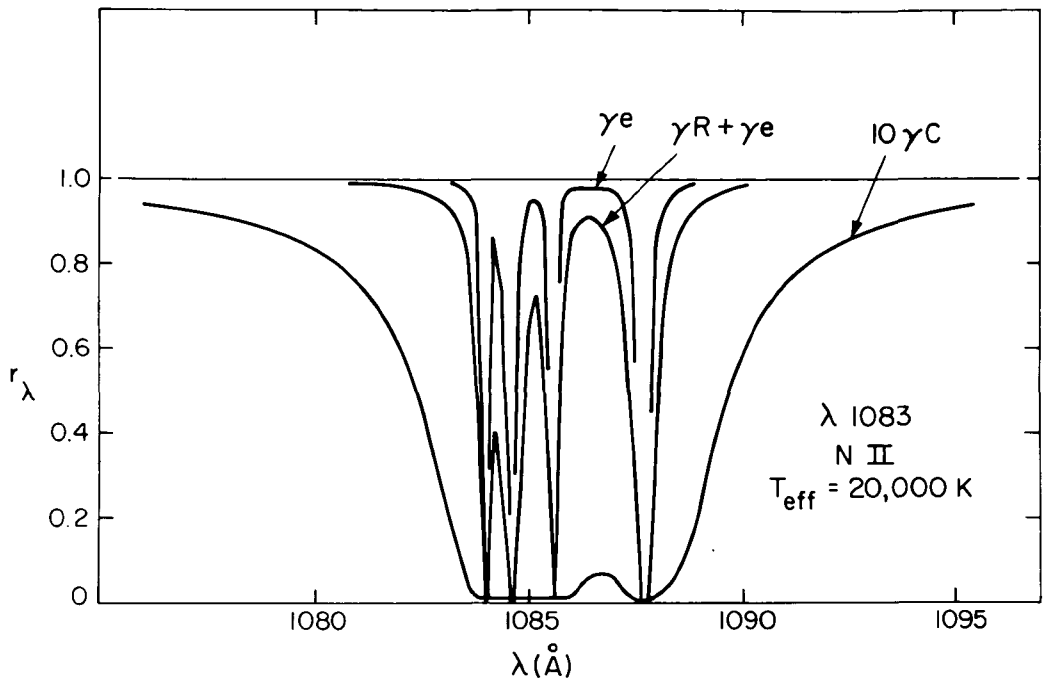

Figure 2.—Profiles of the multiplet of N II at λ = 1083 Å, for a model with T_{eff} = 20,000°K. γ_e, $\gamma_R + \gamma_e$, and 10 γ_C label profiles calculated with electron, electron plus radiative, and 10 times classical damping, respectively.

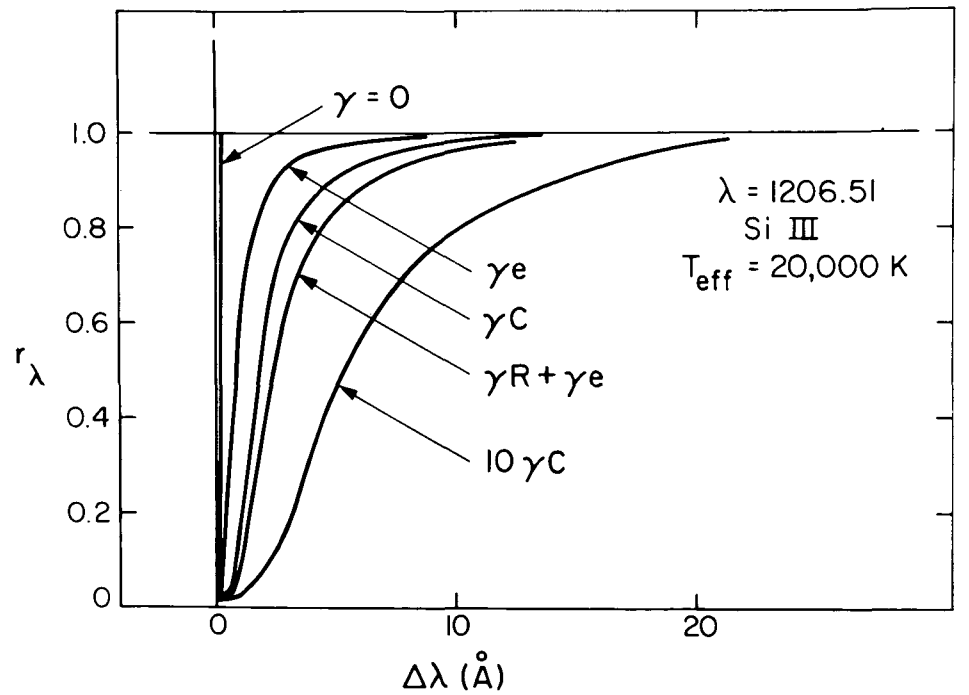

Figure 3.—Same as Figure 2, for a Si III line at 1206.51 Å.

latter does not show any significant resolution of the multiplet's components. To check this, one would need instrumental resolutions on the order of 0.5 Å at $\lambda \simeq 1100$ Å, provided that the multiplet is not blended with other lines.

Figures 4 to 9 show the equivalent widths log W as a function of the effective temperature log T_{eff} of the models. The equivalent widths are in angstroms and are defined as usual by

$$W = \int_0^\infty (1 - r_\lambda) d\lambda \quad , \tag{5}$$

where r_λ has been defined by (4). The various curves are labeled with the same damping parameters given in Figures 2 and 3 and defined in Section 2. Each figure shows the results for a multiplet defined by its wavelength. Also shown are the ion and the number of components of each multiplet (for details, see Table 1). The multiplets of our sample all develop strong damping wings (compare with the pure Doppler case, $\gamma = 0$). Some of them (λ1083, Figure 4; λ1108, Figure 5; λ1206, Figure 6; λ1334, Figure 8) show these strong damping wings over large effective temperature ranges. We reach the same conclusions as in §II and from the analysis of Figures 2 and 3. We note that although the electron damping has little effect, its relative contribution to the total damping $\gamma_R + \gamma_e$ is larger at $T_{eff} = 10{,}000°K$ than at higher temperatures (see, for example, Figures 5 and 6) because in the layers at which the wings of these lines are formed, the electron densities are higher at $T_{eff} = 10{,}000°K$, than at higher temperatures. An indirect consequence is that if any non-LTE effects exist in these regions of line-wing formation, they would be enhanced at higher temperatures.

We now summarize. As stated before, the conditions considered here are those that prevail in atmospheres hotter than, say, 10,000°K, that is, where collision broadening by neutral particles is negligible.

First a damping constant of 10 times the classical value is much too large, by comparison with the more realistic case of electron-plus-radiative damping. This is not necessarily true for lines whose lower level is highly excited, but these lines are not expected to form strong damping wings anyway.

Second, for the strong lines we are dealing with, the effect of electron damping is generally much smaller than that of radiative damping. So we do not expect observable gravity effects due to the broadening mechanisms.

Third, in most cases studied here, the electron-plus-radiative damping gives more or less the same results as the classical damping. Compared to many other sources of errors, these differences are not dramatic. For calculations that

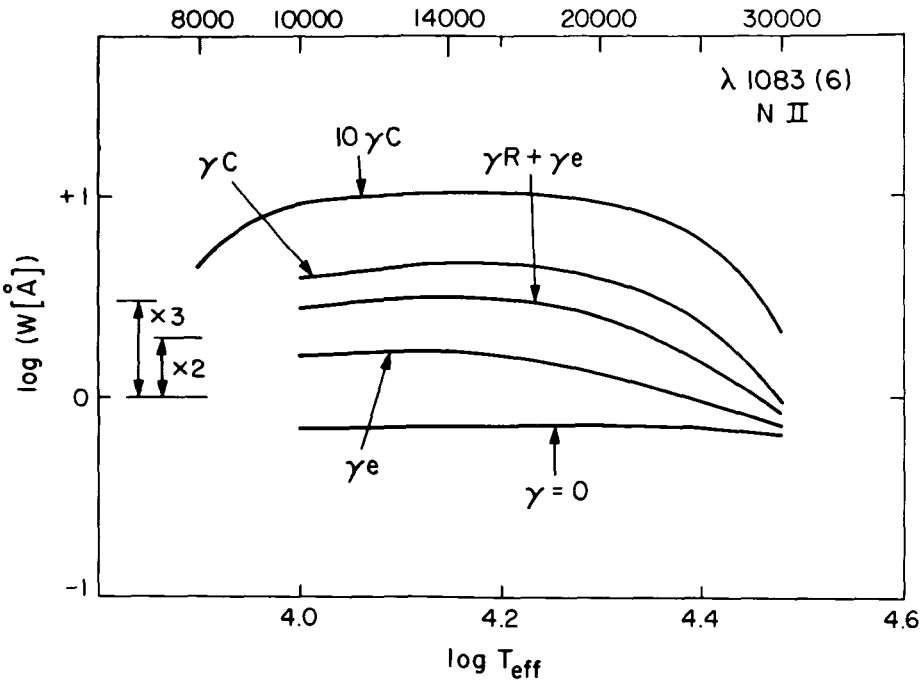

Figure 4.—Equivalent widths log W as a function of effective temperature T_{eff}. W is in angstroms. Multiplet of N II at 1083 Å. The curves are labeled with the damping parameters defined in the text.

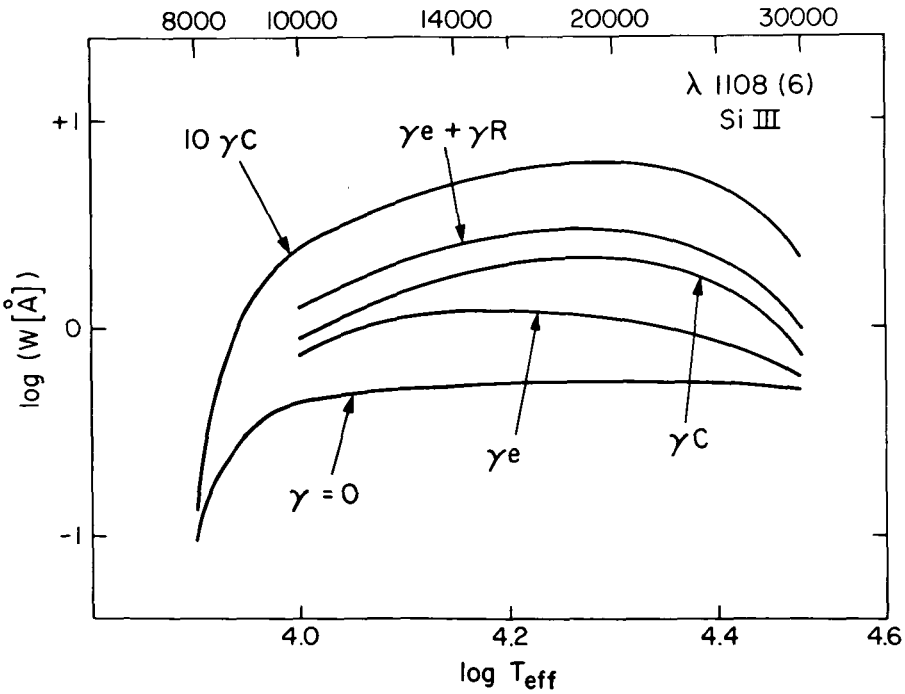

Figure 5.—Same as Figure 4. Multiplet of Si III at 1108 Å.

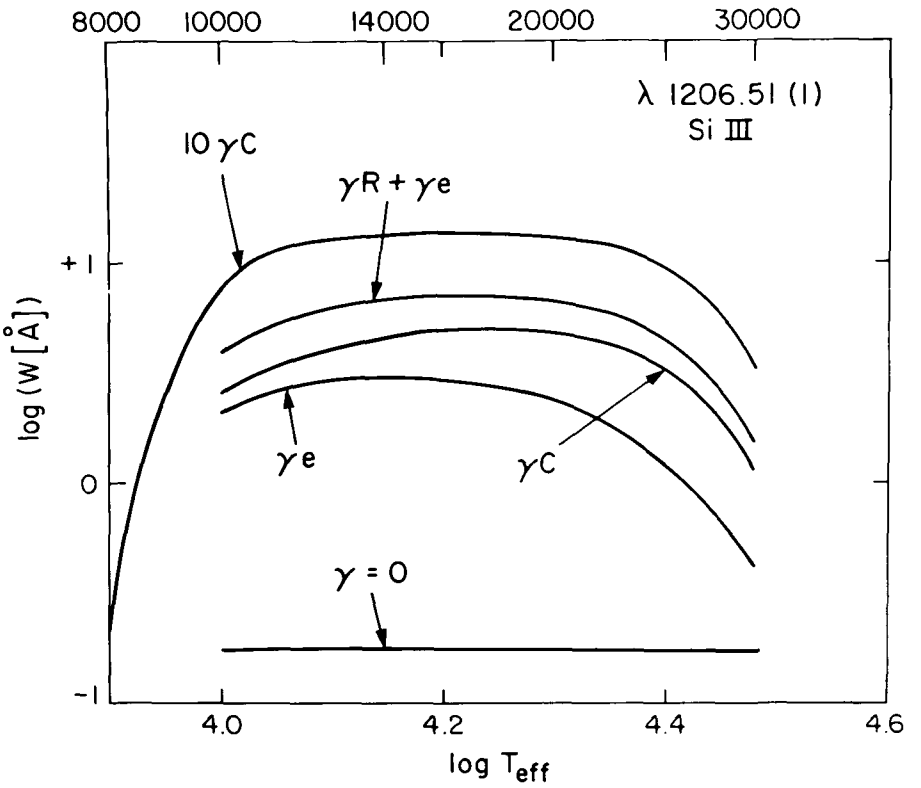

Figure 6.—Same as Figure 4. Multiplet of Si III at 1206.51 Å.

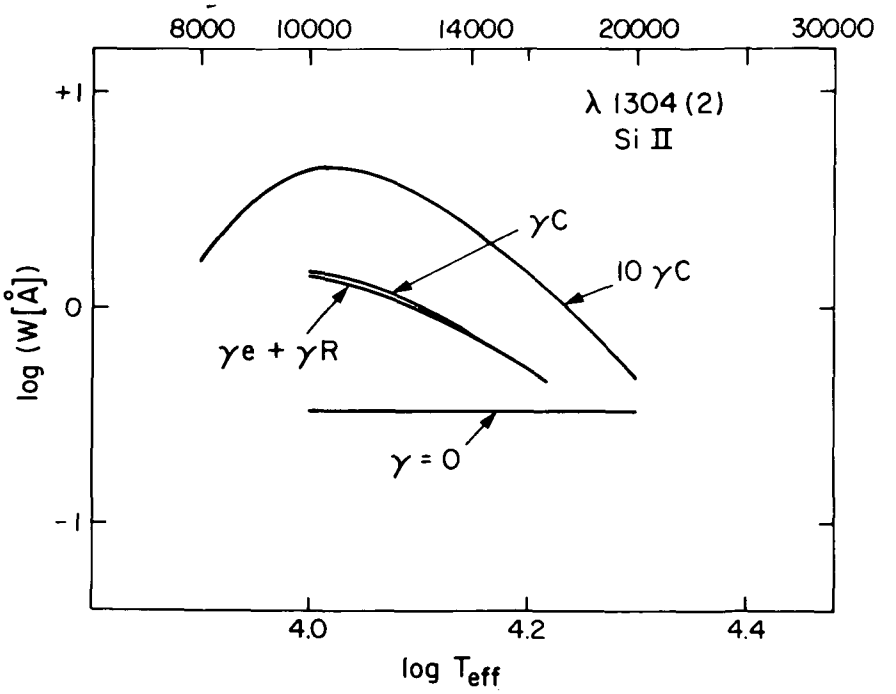

Figure 7.—Same as Figure 4. Multiplet of Si II at 1304 Å.

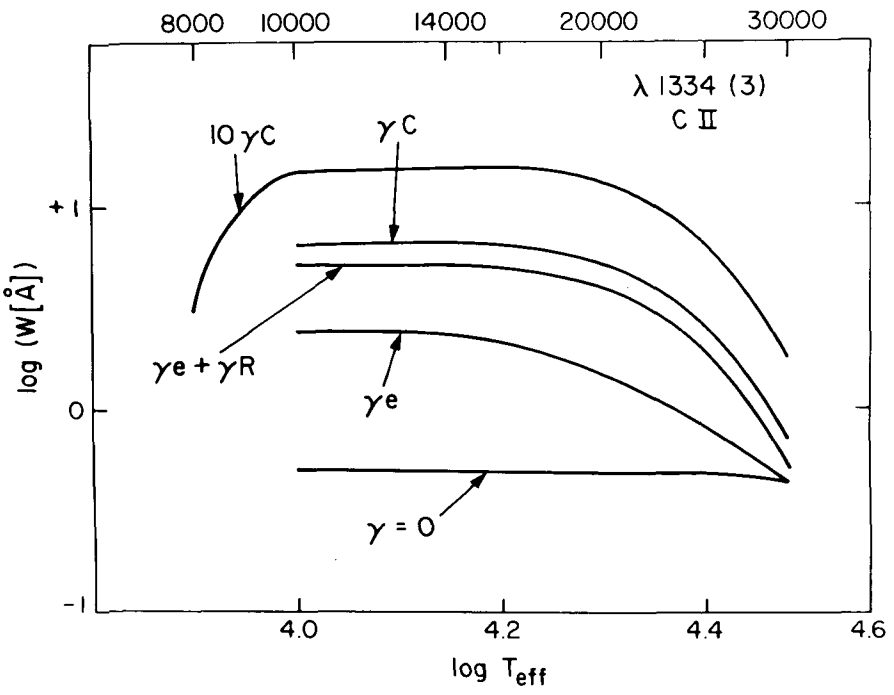

Figure 8.—Same as Figure 4. Multiplet of C II at 1334 Å.

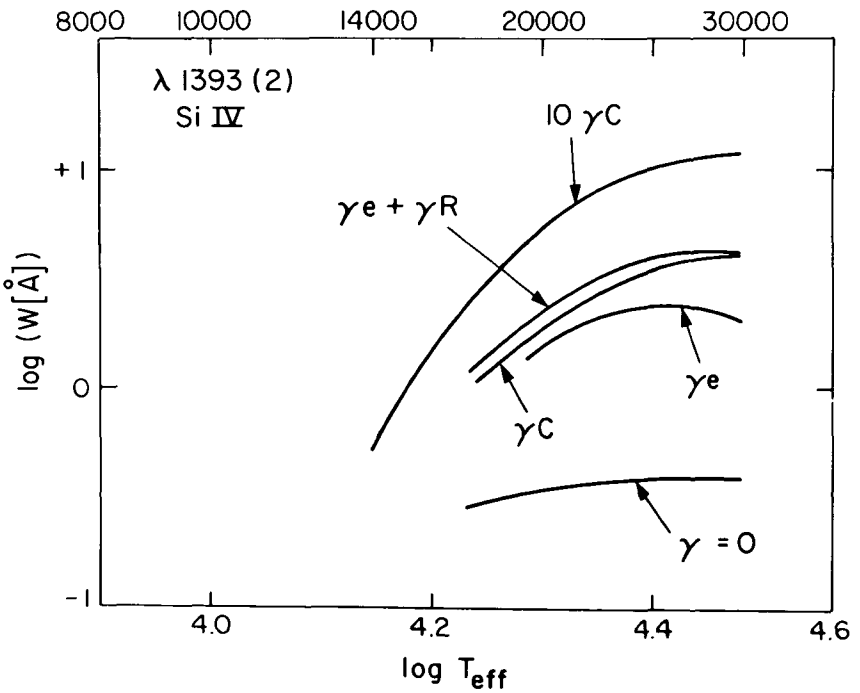

Figure 9.—Same as Figure 4. Multiplet of Si IV at 1393 Å.

involve hundreds or thousands of lines (blanketed model atmospheres) or that concern lines with unavailable damping data, we would therefore suggest, as a rule of thumb, to use the classical damping constant rather than that 10 times greater.

This work has been done while the author held an ESRO-NASA International Fellowship. The research was supported in part by contract NAS 5-1535 from the National Aeronautics and Space Administration.

REFERENCES

Adams, T. F. and Morton, D. C. 1968, Ap. J. 152, 195.
Baschek, B., Holweger, H. and Traving, G. 1966, Abhandl. Hamb. Sternw. VIII. no. 1.
Bradley, P. T. and Morton, D. C. 1969, Ap. J. 156, 687.
Code, A. D. and Bless, R. C. 1970, in Ultraviolet Stellar Spectra and Related Ground-Based Observations (Dordrecht: D. Reidel Publ. Co.) p. 173.
Chapelle, J. and Sahal-Bréchot, S. 1970, Astr. and Ap. 6, 415.
Hickok, F. R. and Morton, D. C. 1968, Ap. J. 152, 203.
Houziaux, L. and Butler, H. E., eds. 1970, in Ultraviolet Stellar Spectra and Related Ground-Based Observations (Dordrecht: D. Reidel Publ. Co.).
Kurucz, R. L. 1969, in Theory and Observation of Normal Stellar Atmospheres, ed. O. Gingerich (Cambridge: M. I. T. Press), p. 375.
Mihalas, D. and Auer, L. H. 1970, Ap. J. 160, 1161.
Peytremann, E. 1970, Thesis, Université de Genève.
Sahal-Bréchot, S. 1969a, Astr. and Ap. 1, 91.
_____ 1969b, Astr. and Ap. 2, 322.
Sahal-Bréchot, S. and Segré, E. 1970, to be published in Highlights for Astronomy.
Wayne van Citters, G. and Morton, D. C. 1970, Ap. J. 161, 695.
Wiese, W. L., Smith, M. W. and Glennon, B. M. 1966, NSRDS-NBS, 4.
Wiese, W. L., Smith, M. W. and Miles, B. M. 1969, NSRDS-NBS, 22.

Page intentionally left blank

AN UNUSUAL ABSORPTION FEATURE IN THE FAR ULTRAVIOLET SPECTRUM OF EARLY-TYPE SUPERGIANTS

A. B. Underhill, D. S. Leckrone and D. K. West
National Aeronautics and Space Administration
Goddard Space Flight Center
Greenbelt, Maryland

ABSTRACT

The OAO-2 satellite has been used to obtain far ultraviolet scans of six early-type supergiants. The data reveal the presence of a distinct, broad absorption feature centered near 1720 Å. This feature is unique in that it remains essentially constant in strength, breadth and central position over the spectral type range B0 I to A2 I. The feature also appears in the spectrum of the B-type shell star ζ Tauri, with a strength comparable to that observed for the supergiants. It appears weakly, or not at all, in the B and A main sequence spectra we have examined. The presence of the feature in spectra of supergiants and a shell star supports the hypothesis that it is an extended envelope phenomenon. We discuss in detail the hypothesis that the feature is due to a fortuitous blend of intrinsically strong lines arising primarily from the ground configurations of abundant metallic ions. An alternative possibility, that the feature results from the superposition of a "diffuse" band of undetermined origin upon the metallic line spectrum of the supergiants cannot be ruled out on the basis of the present data. Its remarkable constancy with spectral type may make the feature a useful indicator of early-type supergiants and shell stars in future programs involving narrow-band ultraviolet photometric observations of faint stars.

Apparent ultraviolet flux distributions for six early-type supergiants are plotted in Figure 1. Similar distributions for five main sequence stars and for the shell star ζ Tauri are given in Figure 2. Spectral types and luminosity classes are from the survey of Hiltner et al. (1969) or from Hoffleit (1964). All of the data were obtained with spectrometer 2 of OAO-2 (Code et al. 1970). The effective resolution of the instrument is 12 Å (B. D. Savage, private communication 1971); consecutive data points are obtained at increments of about 10 Å.

The spacecraft boresight tracker (BST) was used for the spectral scans of all six supergiants. It is thus reasonable to assume that the wavelength scale and zero point determined for one scan applies equally well to all. This is of particular importance in the case of the scan of α Cygni, for which a scale and zero point could not be determined unambiguously from identified spectral features. The validity of the adopted wavelength zero point for α Cygni was confirmed by BST scans of β Cephei, B2 III (not illustrated here), taken within eight orbits of the α Cygni observations.

We have used line identifications and observed wavelengths given by Morton et al. (1968) for ε Orionis to establish a mean relation between wavelength and grating orientation over the range 1170-1550 Å. A relation was established over the range 1486-1718 Å by use of prominent emission features identified in OAO-2 spectrometer 2 scans of the WN5 star HD 50896 now being studied by Lindsey F. Smith (private communication 1971). Here we utilized only subordinate lines, which, by analogy with subordinate lines observed in the visual, are unlikely to be red-shifted significantly from their laboratory wavelengths. The two relations were joined in their region of overlap and the resulting function was extrapolated smoothly from 1718 Å to about 1800 Å.

Numbered vertical lines in Figures 1 and 2 indicate twenty wavelengths near which prominent absorption features appear in one or more of the spectrum scans. Possible major contributors to these features are listed in Table 1. The multiplet numbers are from the Ultraviolet Multiplet Tables (Moore 1950, 1962, 1965). No attempt has been made to list the many lines of the second and third spectra of the metals which fall in the regions of interest. Such lines are probably present but better resolution than that available is required to show them.

The feature at position 3 in Figure 1 has been cross-hatched to facilitate identification. It appears as a well defined, pointed dip with a central flux which is about 0.80 of the flux in adjacent regions outside the feature. The apparent total width of the feature lies in the range 20-40 Å. We estimate the central wavelength to be 1720 Å. We believe it unlikely

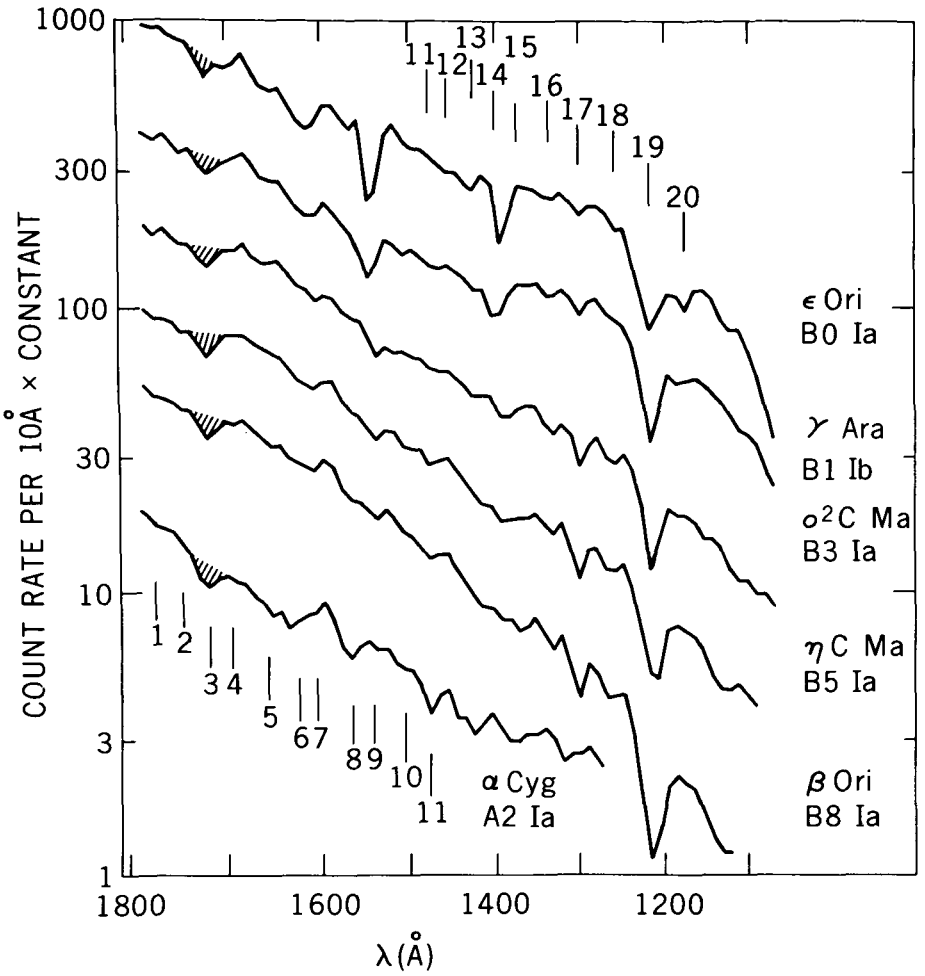

Figure 1.—Spectrum scans of six early-type supergiants. Count rates in a 10 Å band are multiplied by an arbitrary constant and plotted logarithmically vs. wavelength. Twenty positions near which prominent features occur are indicated (see Table 1). The cross-hatched feature near 1720 Å is discussed in the text.

that this estimate could be in error by more than ±7 Å; most of this uncertainty is systematic owing to our inability to specify increments less than one grating step. The constancy of the zero point is determined by the positional stability of the BST (about ±0.8 Å). The 1720 Å value derived here is in close agreement with the central wavelength of the feature, 1718 Å ± 4 Å, estimated by Code (private communication 1971) on the basis of an extended investigation of the dispersion curve for spectrometer 2.

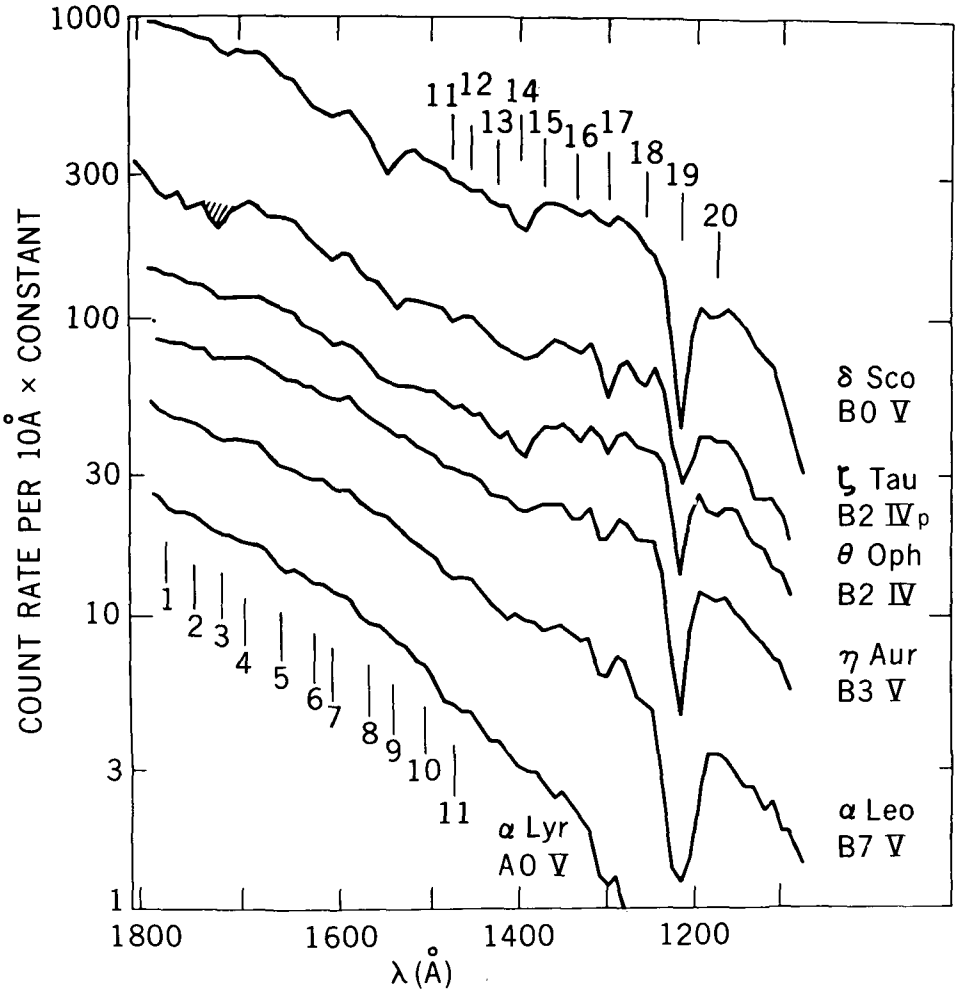

Figure 2.—Spectrum scans of five early-type main sequence stars and a shell star, ζ Tauri. Count rates in a 10 Å band are multiplied by an arbitrary constant and plotted logarithmically vs. wavelength. Twenty positions near which prominent features occur are indicated (see Table 1). The cross-hatched feature near 1720 Å in the scan of ζ Tauri is discussed in the text.

At 12 Å resolution one cannot distinguish between a simple broad absorption feature and a pattern of sharp features spread more or less symmetrically over the apparent line width. In accepting either possibility one must be prepared to explain the unique constancy of the feature in strength, breadth and central position over the spectral type range B0 I to A2 I. That the feature is indeed unique in this respect, within the

Table 1.

Possible Contributors to the Prominent Absorption Feature

Position	Position Wavelength (Å)	Possible Contributors	Multiplet	Wavelength (Å)
1	1773	S I	13	1782
		P I	1	1775-1788
		Ni II	3	1774
		* Sr II	4	1770,1778
		Al II	5	1764-1768
		Ni III	14,21,27,29	1761-1790
		C II	10	1760,1761
		* Zr III	2,3,11,12	1759-1783
2	1747	* Zr III	2,12	1754,1759
		N III	19	1748-1752
		N I	9	1743-1745
		Ni II	4,5	1742-1755
		Ni III	15,21	1741-1752
		Cr IV	13,14	1739-1750
3	1720	Mn II	13	1734-1738
		Cr IV	14	1731
		Si IV	10	1722-1727
		C II	14.02	1720-1722
		Al II	6	1719-1725
		N IV	7	1719
		Cr III	34	1712,1720
		Fe II	37,38,39	1710-1725
		Ni II	4	1710
		S I	10	1706,1707
		Si II	10,10.01	1705-1711
		Ni III	15,16,25,28,30,31	1702-1739
4	1697	S I	10	1706,1707
		Ni II	4,5	1703
		Cr III	34,71	1700
		Ni III	16,25,30	1688-1708
		Fe II	38,39,40,41	1686-1708
		P I	6	1686
		Ne II	7	1682,1688
5	1659	Si IV	27	1673
		P I	2	1672,1675
		Al II	2	1671
		A III	6	1670-1676

Table 1 (continued)

Position	Position Wavelength (Å)	Possible Contributors	Multiplet	Wavelength (Å)
5	1659	S I	11	1667
		C I	2	1656-1658
		Ni III	17	1650
		Fe II	40,41,42	1644-1671
		Ca II	1,5	1644-1652
6	1626	He II	12	1640
		Si IV	28	1635
		Ni III	17	1632
		Al II	9	1626
		Fe II	8,42,43,68	1622-1640
		* Zr III	29	1621-1638
		* Sr II	5	1620
7	1613	* Sr II	5	1613
		* Zr III	29	1612
		Fe II	8,43	1608-1618
		* Sc III	1	1598-1610
8	1568	Ca III	4	1563
		Si II	10.02,11	1562-1564
		A II	14	1560,1575
		C I	3	1560-1561
		Fe II	44,45,46	1559-1588
9	1542	Ca II	6	1554,1555
		Fe II	45	1550
		C IV	1	1548,1551
		Al II	10	1540
		* Ga II	5	1535
		P II	1	1533-1544
		Si II	2	1533
		Si IV	24	1533
		* Sr II	6	1531,1538
10	1508	Si II	11.01	1509-1512
		* Ga II	5	1505,1515
		P III	6	1502-1505
		Ni II	6,7	1500,1511
		Ti III	3	1499
		N I	4	1493,1495

Table 1 (continued)

Position	Position Wavelength (Å)	Possible Contributors	Multiplet	Wavelength (Å)
11	1478	* Sr II	7	1483,1489
		S I	3,4	1474-1487
		Si II	12,12.01, 12.02,15.04	1474-1485
		Ni II	6	1468
		Ti IV	3	1467,1469
12	1457	Ni II	7	1455
		Ti III	5	1455
		Ti IV	3	1452
		S I	12	1448
13	1426	Si II	13,13.01	1434-1439
		Ca II	7	1433-1434
		C I	65	1432-1433
		Si III	9	1417
		* Ga II	2	1414
		S I	5,6	1413-1437
		Fe II	47	1413-1425
		N I	10	1412
14	1399	Si II	13.02,13.03,14	1404-1410
		Si IV	1	1394,1403
		Cl I	1	1390-1397
		S I	6,7	1386-1413
		Mn II	14	1386
		Cr III	35	1384-1400
15	1372	S I	7	1382
		P III	7	1380-1382
		Mn II	14	1378-1383
		Ni II	8,9	1370-1381
		Si IV	19	1366-1369
		Cl I	1,2	1364-1380
		Mn III	8	1361-1372
		Cr III	35,36	1357-1384
16	1334	Ca II	2	1342
		Cl I	2	1336-1352
		P III	1	1335-1345
		C I	4	1329-1330
		Ti III	4	1328
		C II	1,11	1324-1336

Table 1 (concluded)

Position	Position Wavelength (Å)	Possible Contributors	Multiplet	Wavelength (Å)
16	1334	S I	8	1324,1327
		N I	11,12	1319-1328
17	1298	N I	13	1311
		Si II	3,13.04	1304-1310
		P II	2	1302-1311
		O I	2	1302-1306
		S I	9	1296-1306
		Si III	4,10	1295-1303
		Mn II	6	1291,1292
		Ti III	1,2	1286-1299
		Mn III	9	1284-1292
		Cr III	12,28,37	1280-1316
18	1256	Fe II	9	1261-1267
		C I	9	1261-1262
		S II	1	1251-1260
		Si II	4,8,13.05	1247-1265
		C III	9	1247
		Cr III	5,6,13,20	1245-1273
		N I	5	1243
19	1214	Mn III	3,5,6	1220-1229
		H I	1	1216
		He II	13	1215
		Fe II	70,71,72	1213-1221
		Si IV	16	1211
		Si III	2	1207
		N I	1	1200-1201
		Cr III	7,14,15	1197-1230
		S III	1	1190-1202
		Si II	5,8.01,8.02	1190-1229
		Mn II	3,15	1189-1201
		C I	10,11,12,13,14	1189-1194
20	1172	N III	20	1183-1185
		Mn III	4,7	1180-1193
		C III	4	1175-1176
		* Ga II	6	1168-1187
		N I	6,7	1164-1168
		Mn II	4	1162-1164

*We include lines of some elements of low abundance on the possibility that they may be particularly strengthened in absorption by non-LTE excitation conditions.

range of wavelengths covered by spectrometer 2, becomes evident when one carefully compares the spectra illustrated in Figures 1 and 2 point by point. We have attempted to document in a rough way the constancy with spectral type of the feature. In Table 2 the ratio of the count rate, corrected for dark current, at 1720 Å to that near the apparent edge of the feature at 1740 Å is listed for each supergiant and for ζ Tauri. We have also included data for the B0.5 I star κ Orionis, which is not illustrated in Figure 1. The adopted criterion of line strength is susceptible to various sources of uncertainty and should not be taken too literally. However, it does indicate that the relative flux at the center of the feature lies within ±0.03 of 0.80, i.e. that it is constant to within the uncertainty of the data, for all the stars except α Cygni. The statistical uncertainty in the data for α Cygni is larger than for any of the other stars considered. The greater than average value of the central depth of the 1720 Å feature in α Cygni may not be real.

Table 2.

Relative Central Flux of the 1720 Å Feature	
Star	$\frac{\text{Count Rate at 1720 Å}}{\text{Count Rate at 1740 Å}}$
ε Ori	0.78
κ Ori	0.77
γ Ara	0.82
ζ Tau	0.82
o^2CMa	0.83
η CMa	0.81
β Ori	0.79
α Cyg	0.73

No feature of comparable strength occurs near 1720 Å in the scans of main sequence stars shown in Figure 2. Broad, shallow undulations do occur in the vicinity of 1720 Å, especially at the earlier spectral types. However, these are not so

constant in appearance or position as the feature observed at 1720 Å in supergiants (see also Figures 1 and 2 of Code and Bless 1970). The present data demonstrate once again how much stronger, in general, absorption lines are in supergiant spectra than in main sequence spectra. However, it is not obvious that the weak absorption features near 1720 Å in the main sequence spectra are also responsible for the feature observed at 1720 Å in the supergiant spectra. We note for example that the central minimum of the shallow feature near position 3 in the spectrum of the B0 V star δ Scorpii lies closer to 1710 Å than to 1720 Å, while the central minimum near position 3 in the spectrum of the B0 Ia star ε Orionis lies squarely at 1720 Å. Similarly, the central minimum near position 3 in the η Aur (B3 V) spectrum lies closer to 1730 Å than to 1720 Å.

It is noteworthy that an absorption feature does occur at 1720 Å in the spectrum of ζ Tauri (Figure 2) with a strength and breadth comparable to that observed in the supergiant spectra. It is well known that the shell spectrum of ζ Tauri at visual wavelengths resembles to some degree the spectrum of a B8 supergiant, although particle densities in the shell are probably lower than those prevailing in the extended supergiant atmosphere (see the discussion by Underhill 1966). This resemblance also applies to the ultraviolet spectrum of ζ Tauri as may be confirmed by comparing the ζ Tauri spectrum with that plotted for β Orionis in Figure 1. The appearance of the 1720 Å feature in supergiant spectra and in the spectrum of a B-type shell star argues strongly for the hypothesis that the 1720 Å feature is an extended envelope phenomenon, that it is formed at low particle densities in dilute radiation fields.

An alternative hypothesis, which cannot be entirely excluded on the basis of our data, is that the feature is of interstellar origin and is comparable to the diffuse interstellar bands observed at visual wavelengths. The most highly reddened star illustrated here is δ Scorpii, $E(B-V) = 0.18$. If the feature were correlated in a simple way with interstellar extinction, it should appear in great strength in the spectrum of this star. That this is not the case casts doubt on the hypothesis of interstellar origin.

With the low resolution data at hand we can only speculate about the species from which the 1720 Å feature arises. One possibility, which we currently favor, is that the feature is the product of a fortuitous blend of lines of the sort listed for position 3 in Table 1. For example, it is possible that the N IV and Si IV lines dominate the feature near B0. As one proceeds toward later spectral types the intrinsically strong lines arising from the ground configurations of Ni II and Ni III become dominant. The Ni III spectrum seems especially likely for stars such as ζ Tau, γ Ara, o^2 CMa and η CMa whose spectra also contain prominent absorption features near 1750 Å

and 1770 Å where other strong Ni III lines occur. At the late B and early A spectral types Ni II, Fe II, Al II, etc. may dominate. However, this explanation is not without difficulties. If Fe II plays a major role near 1720 Å, it should also produce a major feature near 1670 Å. This is apparently not the case for the stars observed here. Similar considerations apply to the lines of Al II, Cr III, Cr IV, S I and Si II which fall in the neighborhood of 1720 Å.

Smit (1969) has measured equivalent widths of blue-violet and red lines of C II, Si II and Fe II in ground-based spectra of β Orionis. We note the weakness of Si II 3862, 3856 and 3853 Å in his spectra. These lines should be much stronger than the lines near 1711 Å arising from the same level. The blue lines of Fe II at 4549 Å and 4233 Å are quite weak in β Orionis. It is unlikely that the Fe II lines in the range 1710-1725 Å would be significantly stronger. Finally all of the C II lines listed by Smit are very weak, including those at 6578 and 6583 Å. It is improbable that the subordinate C II lines of ultraviolet multiplet 14.02 could be present in strength.

Of all the species listed for position 3 in Table 1, the only one likely to be of great importance in a late B-type spectrum is Ni II, with possible contributions also from Ni III and Mn II. It is difficult to understand how these ions alone could preserve the observed symmetry of the feature. The dominant multiplet (16) of Ni III contains, for the most part, lines lying shortward of 1720 Å. The dominant line of Ni II in this region falls at 1710 Å. Only the Mn II lines fall longward of 1720 Å and they lie rather close to the red edge of the feature.

This discussion may be summarized by noting that a certain degree of implausibility must be attached to an hypothesis requiring that a feature which remains so constant in general appearance, strength and central wavelength over a wide range of spectral types should be composed of blended lines which individually are variable over that spectral type range. Not only must a sufficient number of lines from various ionization states be present but also the lines must each be capable of growing to great strength in an extended low density envelope. Moreover, such lines must maintain rigidly defined relative strengths, i.e. the strongest of the lines must lie closest to 1720 Å at all spectral types. It is possible that strong lines may exist within the interval 1700-1740 Å which have not been observed in laboratory spectra. Alternatively the 1720 Å feature may arise from a "diffuse band" of undetermined origin superposed upon the metallic line spectrum of the supergiants. We know of no autoionization lines which fall near this wavelength. We hope to investigate these alternatives in two ways: (1) by a detailed theoretical spectrum synthesis of the region

around 1720 Å and (2) by exploration of the region at higher resolution on future spacecraft missions or with rocket-borne spectrographs.

The great strength of the 1720 Å feature in supergiant and shell star spectra and its constancy over such a wide spectral type range makes it an ideal one-dimensional indicator of stars with extended atmospheres. For example, the ratio of the flux in the bandpass 1700-1740 Å to that in a nearby bandpass outside this range should serve to discriminate between early-type stars possessing extended envelopes and normal main sequence stars in narrow band ultraviolet photometric surveys. A second criterion would have to be found to discriminate between shell stars and supergiants.

We wish to express our appreciation to A. D. Code for generously granting us time as guest observers with the OAO-2 Wisconsin spectrum scanner. We thank T. E. Houck, M. Molnar and A. Holm of the University of Wisconsin and S. R. Heap of the Goddard Space Flight Center for their help in obtaining the observations.

REFERENCES

Code, A. D. and Bless, R. C. 1970, in Ultraviolet Stellar Spectra and Related Ground-Based Observations, eds. L. Houziaux and H. E. Butler (Dordrecht: Reidel Publishing Co.), p. 173.

Code, A. D., Houck, T. E., McNall, J. F., Bless, R. C. and Lillie, C. F. 1970, Ap. J. 161, 377.

Hiltner, W. A., Garrison, R. F. and Schild, R. E. 1969, Ap. J. 157, 313.

Hoffleit, D. 1964, Catalogue of Bright Stars (New Haven: Yale University Observatory).

Moore, C. E. 1950, An Ultraviolet Multiplet Table (N.B.S. Circ. 488, sections 1 and 2).

_____ 1962, An Ultraviolet Multiplet Table (N.B.S. Circ. 488, sections 3, 4 and 5).

_____ 1965, National Standard Reference Data Series (N.B.S. 3, sections 1, 2 and 3).

Morton, D. C., Jenkins, E. B., Bohlin, R. C. 1968, Ap. J. 154, 661.

Smit, A. B. M. 1969, Bull. Astr. Inst. Netherlands 20, 274.

Underhill, A. B. 1966, The Early Type Stars (Dordrecht: Reidel Publishing Co.), p. 234.

ENERGY DISTRIBUTIONS AND SPECTRA OF ORION B STARS

Rudolph E. Schild and Frederic Chaffee
Smithsonian Astrophysical Observatory
Cambridge, Massachusetts

ABSTRACT

New MK spectral types and energy distributions are presented for B stars in Orion for which far ultraviolet flux excesses have recently been discovered. Significant differences between HD spectral energy distributions show the Orion late B stars to have smaller Balmer discontinuities than do field stars of the same spectral types. For the late B stars, these effects cause the 1500 Å fluxes to be under-estimated by approximately 0.5 mag. No comparable systematic effects were found for the early B stars.

Recent studies of ultraviolet fluxes of the Orion B stars by Weber, Henry and Carruthers (1970) and by Celescope appear to have shown that some stars are upwards of 1 magnitude too bright in the 1500 Å region. It is important to realize that these inferences are based largely on spectral classifications and UBV photometry, which are combined to infer the temperature and reddening. Because modern MK spectral types are unavailable for many Orion stars, and frequent reference is made to the HD catalogue, we first investigate the possible errors in the classifications.

New spectrograms for classification were obtained with a small grating spectrograph at the Cassegrain focus of the new Mt. Hopkins 60" Tillinghas reflector. The disperson was 85 Å/mm, and all spectra were widened to 1 mm. Stars observed include the Orion objects identified by Celescope as too bright in the far ultraviolet by at least one magnitude, and the B stars in the stellar ring surrounding ε Orionis.

The new spectral types are shown in Figure 1, where the HD spectral types are shown in comparison. It is evident from

Figure 1 that large systematic differences are present for the late B stars in Orion. Available UBV photometry confirms the correctness of the new MK types.

We conclude that substantial errors affect the HD spectral types of the Orion B stars, and that many are hotter and more reddened than had previously been determined.

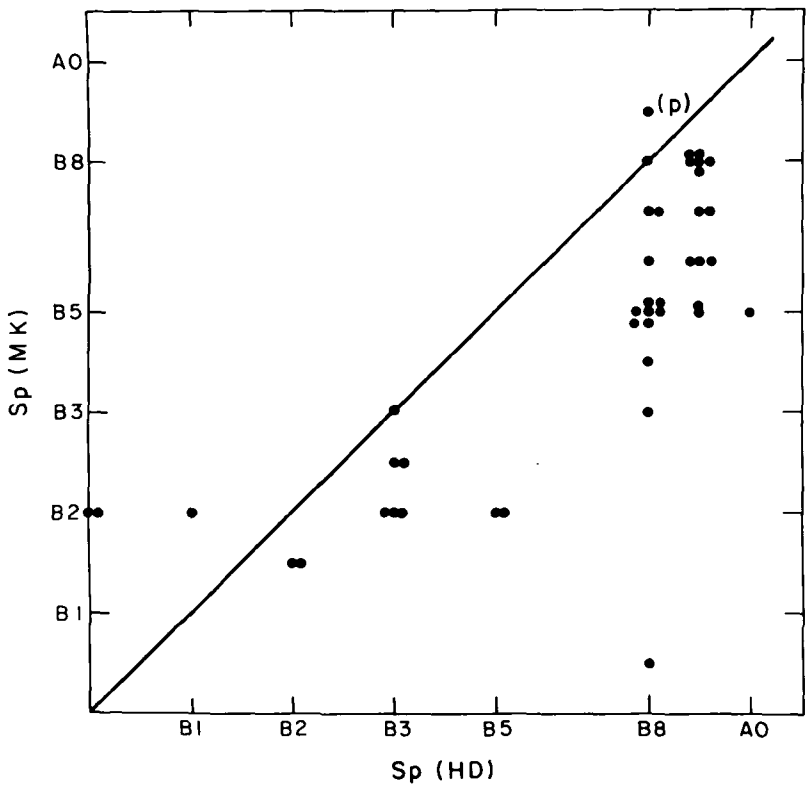

Figure 1.

To investigate the possibility that stars found too bright in the far ultraviolet may have energy distributions inconsistent with their absorption line spectra, we have measured the energy distributions for all of the stars in the Celescope list, except for θ Ori. We used the Mt. Hopkins 60" telescope and a scanner constructed by Dr. Latham. The scanner has a McPherson monochromator with a pre-programmable grating drive, punched card output, and a refrigerated ITT FW 130 photomultiplier. Nightly extinction coefficients were computed, and the agreement between scans of the same star on different nights was better than $0^{m}.015$ at all wavelengths.

In Figure 2 we show the comparison between the observed energy distribution of HD 36936 and an Atlas model for T_{eff} =

16000°K, log g = 4.0. The models incorporate the far ultraviolet silicon opacities and hydrogen line blanketing. Similar comparisons for the 18 stars observed permit effective temperatures to be estimated, primarily from the size of the Balmer discontinuity.

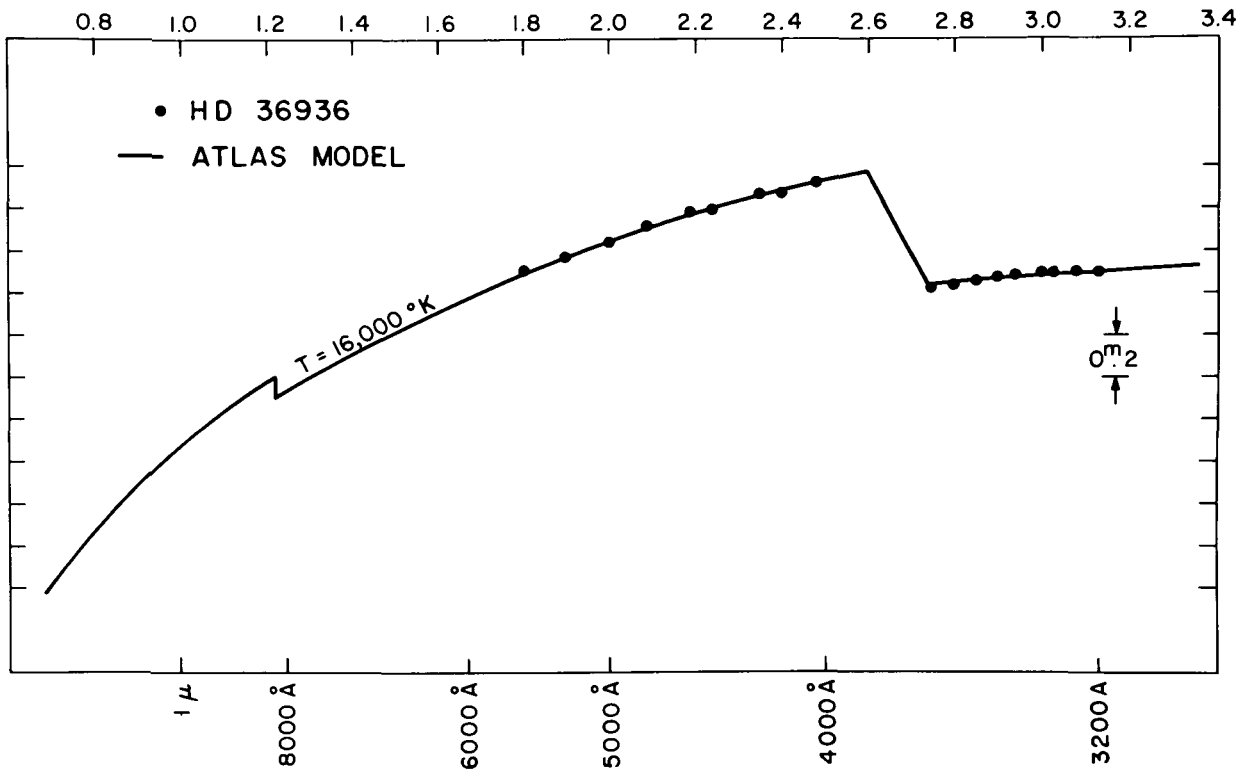

Figure 2.

The effective temperature-spectral type relation found for the Orion stars is shown in Figure 3, in comparison with the mean relation found from similar data for field stars. While scatter may appear to be relatively large for the early B stars because of the steepness of the spectral type-effective temperature relation, systematic effects appear to be present for the late B stars. In particular, at given late B spectral type, an Orion star is likely to have a higher effective temperature than a field star.

A similar effect has been found by Garrison in his comparison of MK spectral types with UBV photometry of the Scorpio Centaurus stars, which probably are of similar age to the Orion objects. The effect is illustrated in Figure 4, which compares MK spectral types of Orion and Scorpio Centaurus

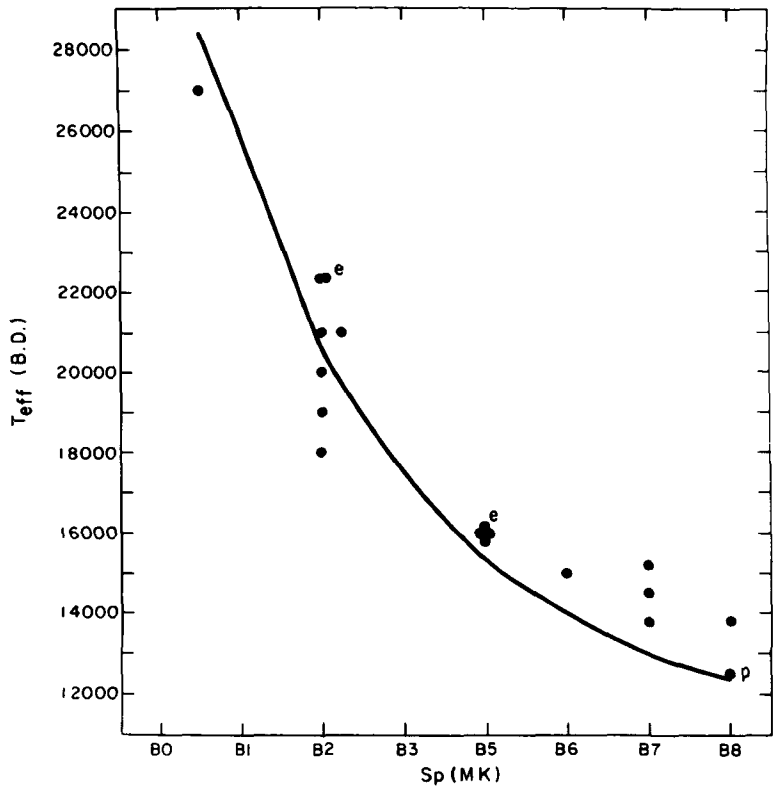

Figure 3.

stars with spectral types inferred from the Q method using UBV photometry. Stars identified as peculiar by Garrison are found to depart most strongly from the regression line, but it appears that many more stars show the effect to some extent. The effect appears to be limited to stars having MK spectral type B5 or later.

Results to this point suggest that reddening will have been underestimated by the procedure adopted in the past, where temperature has been estimated from HD or MK spectral type and reddening from UBV photometry. The two effects tend to cancel one another.

We may attempt to estimate the net effect on the 1500 Å fluxes by the following procedure. We note first that the reddening law appropriate to the Orion Belt stars appears to be $E_{1500-V}/E_{B-V} = 6.0$. An integration of the 1500 Å fluxes from Atlas models gives $\Delta(1500-V)/\Delta(B-V) = 12\pm1$ over the relevant range of effective temperature. Thus we find for a typical star having an HD spectral type of B8 and an intrinsic color of (B-V) = -0.16, corresponding to B5, that the 1500 Å

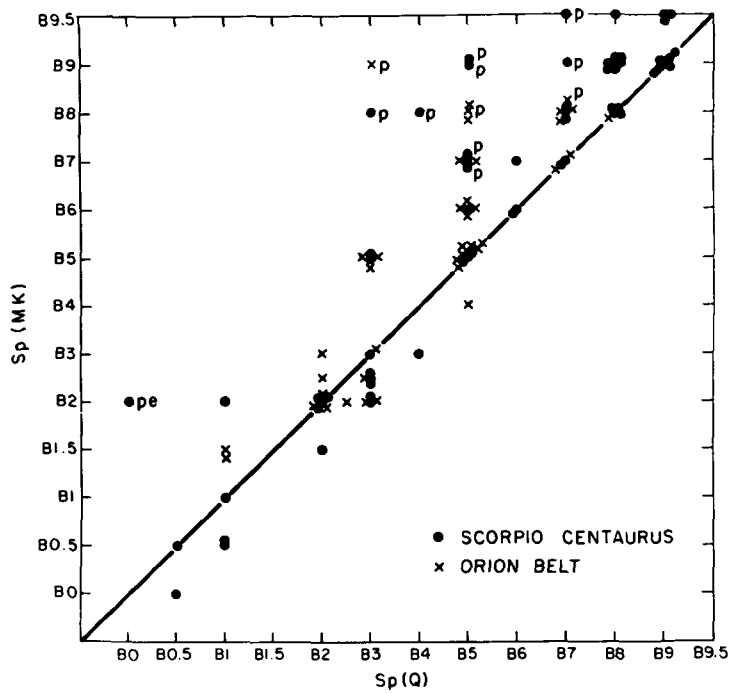

Figure 4.

flux will have been underestimated by nearly 0.5 magnitudes. This is only about half the amount found in the Celescope photometry.

Page intentionally left blank

PHOTOMETRY OF LATE TYPE STARS

Lowell R. Doherty
University of Wisconsin
Madison, Wisconsin

I. INTRODUCTION

OAO-2 was launched December 7, 1968 carrying optical ultraviolet instrumentation of SAO and the University of Wisconsin. A description of the Wisconsin Experiment Package has been published elsewhere (Code et al. 1970). Here we present broad-band filter photometry for 57 bright stars of spectral type A2 and later observed between February 1969 and October 1970. Four filter bands are discussed with peak instrument response at 3320, 2980, 2460 and 1910 Å. The data include nearly all usable filter observations of G, K and M types. Sampling is nearly complete for A and F giants and supergiants, with the exception of Cepheid variables, which are not included here. Only a few representatives of the A and F main sequence were selected.

The basic results presented here are relative digital counting rates obtained with a field-stop aperture of 10 minutes of arc. Characteristics of the four filter-photometer combinations and errors are discussed in § II. Because the aperture is large, and the contrast between stars of different spectral type is dramatically increased in the ultraviolet, some observations require substantial correction if they are to represent the visually brightest star in the field. Possible corrections of $0^{m}.01$ or more due to identified secondary stars must be considered for one-third of the pointings. These corrections and the effects of interstellar reddening are discussed in § III. The adjusted counts are then used (§ IV) to construct color-color diagrams and are compared to the recent SAO grid of model atmospheres.

II. PHOTOMETRY

Each of the four 8-inch stellar telescopes aboard OAO-2 has a filter wheel with three interference filters, a Sr^{90} calibration source and a dark position. Thus there are 12 filter-photometer combinations labelled, e.g. S1F1 (Stellar 1, Filter

1). All filters are used in the first order. In his study of planetary albedoes derived from OAO data, Caldwell (1970) found systematic differences between filters which he attributed to pin hole defects in S2F1 (2030 Å) and S2F5 (2390 Å). Proximity to the calibration source appears to affect S3F5 (1680 Å). S2F2 (2940 Å) is erratic for as yet unknown reasons. We have chosen not to include data from these filters here. Of the remaining ultraviolet bands, Stellar 4 (1200-1700 Å) provides very little data for this spectral range and will not be included. The four bands used here are S1F1 (3320 Å), S1F4 (2980 Å), S3F1 (1910 Å) and S3F2 (2460 Å). They appear to be quite stable. Stellar 3 is particularly well suited to photometry of late type stars because its Ascop 541F photomultiplier is insensitive longward of 3500 Å. Stellar 1 employs an EMI 6256, whose response extends well into the red. S1F1 includes a UG11 filter to reduce this response, while S1F4 does not.

One "observation" typically consists of a sequence of measurements with all filters and various integration times. The minimum set of data or data output frame provides 24 individual measurements. These consist of, for each photometer, 6 successive integrations over the same time interval at one filter wheel position. These times need not be and usually were not the same for all photometers. Integration times used were 1/8, 1, 8 and 64 seconds. A spacecraft counter truncates the data before storage and eventual transmission to the ground. One count in the output equals 64 photomultiplier events. Hereafter, any reference to a specific number of counts means OAO (reduced) counts.

Errors in the photometry arise principally in variations in instrument sensitivity and dark noise. CAL (radioactive source) readings show variations in sensitivity of one or two percent over several orbits and larger variations up to about ten percent over months of operation. Long-term changes presumably depend on the spacecraft environment. To account for such changes the data are reduced according to the scheme:

$$R = \left(\frac{\text{STAR-DARK}}{\text{CAL-DARK}}\right)_i T_i - \left(\frac{\text{SKY-DARK}}{\text{CAL-DARK}}\right)_k T_k \ . \qquad (1)$$

$T = T(t)$ corrects for the decay of the source. Small CAL-DARK differences from one orbit to the next may also be environmental or may simply reflect differences in positions of the filter wheels. It was discovered early in OAO operation that rapid, extreme changes in DARK occur near the South Atlantic Anomaly in the earth's radiation belts. We now know that no part of the orbit is free of contamination. Later observations have avoided the region of the Anomaly entirely and include more DARK readings. Nevertheless, our information about how DARK

varies with time is poor. The spacecraft typically moves through a quarter of the earth's circumference during an observational sequence that may include DARK at only one or two positions. Variations in STAR within one frame and between frames serve as a guide, but both changes in DARK and sensitivity may be involved.

At present it does not appear feasible to program the full data reduction. Here each frame has been treated individually and suspicious data discarded according to our judgment. In any sequence with low, reproducible DARK Stellar 1 counts are repeatable to the photon noise limit of one percent or better. Different orbits reproduce less well. For three observations of η Cas (3.4 G0 V) made over some ten orbits, the spread in the data is less than one percent. However, the spread is two percent for three observations of η Dra (2.7 G8 III) made over ten orbits, and this increases to four percent if we include a fourth observation of η Dra made several hundred orbits earlier. Good Stellar 3 frames have the same high internal consistency as Stellar 1 for all but the faintest ultraviolet objects. For later spectral types with low counting rates, the ambiguity due to integer counts can be important. Data has also been extracted from some sequences with variable DARK or minimal information. This is possible where information from neighboring orbits helps to estimate the degree of contamination. Often a SKY sequence identical to the stellar observation follows in the next orbit and a constant DARK difference can be applied to all frames.

The first term in equation (1) is probably determined to ±2 percent for all Stellar 1 observations, for A, F and G stars at 2460 Å, and for A and F stars at 1910 Å. Exceptions to this general rule will be mentioned later. Net SKY counts at galactic mid-latitudes mimic a 10th magnitude F star. Thus the second term in equation (1) becomes important for the fainter G stars and for all K and M stars. Again with exceptions, the error in R for K and M stars at 2460 Å is probably within ±10 percent.

Table 1 contains the basic data. Where possible, UBV are taken from Iriarte *et al.* (1965). Other principal sources are Cousins and Stoy (1963) and the Naval Observatory catalog (Blanco *et al.* 1968). C_λ has the same value for all entries in a single column. Its purpose is to make equal entries correspond approximately to equal flux per unit wavelength at the nominal wavelengths. This correspondence is approximate for two reasons. First, the calibration is based on model atmospheres of early type stars rather than laboratory sources. Conventional laboratory sources are subject to large systematic errors in the ultraviolet. Using synchrotron radiation from a storage ring, as described elsewhere in this volume by Bless and Fairchild, should eventually provide much more accurate calibration of the OAO photometry. Until this is possible, however, it has proved useful at SAL to adopt an absolute cali-

Table 1. Observations

HD	Name	Spectral Type	V	U-V	B-V	2.5 Log $R_\lambda + C_\lambda$ 3320	2980	2460	1910	Remarks
1522	ι Cet	K2 III	3.55	2.39	1.22	-0.10	-1.13	-3.61		
1581	ζ Tuc	G2 V	4.22	0.59	0.58	1.34	0.87	-0.46	-1.84	
2151	β Hyi	G1 IV	2.79	0.72	0.62			0.56	-1.08	
3712	α Cas	K0 II-III	2.22	2.30	1.17	1.35	0.35	-2.20		S
4614	η Cas	G0 V	3.43	0.62	0.58	2.12	1.63			
6178	σ Scl	A2 V	5.50	0.21	0.08	0.44	0.37	0.29	0.71	S
6860	β And	M0 III	2.04	3.53	1.57	0.14	-0.83	-3.59		S
8538	δ Cas	A5 V	2.69	0.28	0.13	3.03	2.96	2.78	3.17	
9053	γ Phe	K5 II	3.40	3.40	1.56	-1.10	-1.91	-3.27	-4.14	S
11443	α Tri	F6 IV	3.44	0.57	0.49	2.16	1.81	0.69	-0.77	
11937	χ Eri	Gv IV	3.70	1.31	0.85	0.96	0.28	-1.75	>-4.29	
12929	α Ari	K2 III	2.00	2.27	1.15	1.60	0.57	-2.44	-4.13	
13161	β Tri	A5 III	3.00	0.30	0.16	2.74	2.70	2.07	2.32	
13174	14 Ari	F2 III	4.99	0.34	0.34	0.62	0.32	-0.46	-0.69	S
29129	α Tau	K5 III	0.86	3.50	1.55	1.26	0.18	-2.77	-4.41	S
31964	ε Aur	F0 Ia	3.00	0.86	0.54	1.64	1.09	-0.38	-0.96	S,0.20
36079	β Lep	G5 III	2.81	1.31	0.82	1.93	1.27	-0.72	-2.59	
38393	γ Lep	F6 V	3.60	0.44	0.48	2.14	1.76	0.65	-0.42	
39801	α Ori	M2 Ib	0.69	3.92	1.86	0.99	0.21	-1.50	<-3.33	1.64
48329	ε Gem	G8 Ib	2.98	2.87	1.40	-0.01	-0.84	-3.06		S,1.03
56986	δ Gem	F0 IV	3.52	0.40	0.34	2.14	1.93	1.12	1.20	
68457	56 Cam	A7 V	6.45	0.31	0.20	-0.76	-0.90	-1.24	-1.14	
72905	π^1 UMa	G0 V	5.63		0.61	-0.24	-0.74	-2.21	-3.55	
76644	ι UMa	A7 V	3.15	0.27	0.19	2.76	2.67	2.37	2.47	
82210	24 UMa	G4 IV	4.56	1.11	0.77	0.37	-0.27	-2.09	-3.77	
82328	θ UMa	F6 IV	3.20	0.52	0.46	2.45	2.10	1.05	0.16	
84441	ε Leo	G0 II	2.98	1.27	0.81	1.78	1.08	-0.77	-2.44	0.70

106591	δ UMa	A3	V	3.33	0.15	0.08	2.60	2.60			
108903	γ Cru	M3	II	1.66	3.37	1.61	0.77	0.95?	-0.74	-0.52	S
124897	α Boo	K2	III	-0.06	2.52	1.24	3.39	2.17	-0.76	-0.81	
128620	α Cen	G2	V	-0.01		0.68			2.89	1.03	S
128898	α Cir	F0	V	3.18	0.34	0.24	2.57	2.46	2.17	2.09	
129078	α Aps	K5	III	3.82	3.11	1.44	-1.46:		-4.78		S
139063	υ Lib	K5	III	3.58	2.97	1.38	-0.80	-1.88	-4.50		S
147675	γ Aps	K0	IV	3.88	1.53	0.91			-2.28	-3.90	
148387	η Dra	G8	III	2.74	1.61	0.91	1.66	0.87	-1.46	-3.34	S
148856	β Her	G8	III	2.77	1.63	0.94	1.63	0.90	-1.11		
150680	ζ Her	G0	IV	2.81	0.86	0.66	2.47	1.93	0.27	-1.54	
150997	η Her	G7	III-IV	3.50	1.53	0.92	1.05	0.28	-1.93	-4.16	
159181	β Dra	G2	II	2.78	1.63	1.00	1.59	0.93	-0.80	-2.32	0.85
163506	89 Her	F2	Ia	5.44	0.65	0.34	-0.59	-0.99	-2.86		S,0.25
163588	ξ Dra	K2	III	3.75	2.40	1.18	-0.33	-1.33	-4.44		
164058	γ Dra	K5	III	2.23	3.39	1.51	0.06	-1.02	-4.82		
165341	70 Oph	K0	V	4.05	1.35	0.84	0.68	-0.05	-2.49		S
170153	χ Dra	F7	V	3.57	0.44	0.48	2.16	1.84	0.60	0.10	
180711	δ Dra	G9	III	3.07	1.78	1.00	1.14	0.24	-2.33		
185395	θ Cyg	F4	V	4.49	0.34	0.37	1.33	1.04	0.22	-0.31	S
197345	α Cyg	A2	Ia	1.25	-0.15	0.09			4.03	4.38	
197989	ε Cyg	K0	III	2.46	1.91	1.03	1.56	0.82	-2.04	-3.89	
200905	ξ Cyg	K5	Ib	3.70	3.45	1.65	-1.66	-1.86	-3.85	-4.48	
202109	ζ Cyg	G8	II	3.19	1.76	1.00	1.07	0.41	-2.58		
207260	ν Cep	A2	Ia	4.29	0.64	0.51	0.86	0.48		-3.06	S,0.05
210459	π Peg	F5	II	4.27	0.66	0.48	1.00	0.62	-0.42	-1.10	0.37
210745	ζ Cep	K1	Ib	3.36	3.27	1.55	-0.88	-1.67	-4.60	-4.91	S,1.18
217906	β Peg	M2	II-III	2.42	3.62	1.67			-4.28		S
222107	λ And	G8	III-IV	3.75	1.74	1.01			-2.22		
222404	γ Cep	K1	IV	3.21	1.98	1.03	0.73	-0.26	-2.92	-5.64	

bration for preliminary interpretation of the data. A. D. Code (private communication) derived values of C_λ by comparing filter observations of unreddened early B stars with models by D. C. Morton. These values are listed in Table 2 and have been incorporated in the SAL data reduction program, DROOP. The second reason that entries in Table 1 do not represent the actual flux at the nominal filter wavelengths is that no correction for changes in effective wavelength with different spectral type have been included.

Table 2. Absolute Calibration Constants

λ	1910	2460	2980	3320	U	V
C_λ	4.11	2.04	0.31	0.00	-6.09	-6.14

Remarks are of two kinds: the letter S means that secondary field stars may be important, and the named star is therefore also listed in Table 3. A number in the remark column is the intrinsic B-V value (Johnson 1966) for the spectral type of the named star. Intrinsic colors are included only for stars with excesses greater than about $0^m.1$.

III. CORRECTIONS FOR FIELD STARS AND REDDENING

The photometers are equipped with both 2 and 10 minute of arc stops, but the smaller aperture has been used sparingly. This policy is aimed to minimize the chance that a malfunction would leave the smaller stop permanently in position. Even slightly poorer pointing stabilization would make that photometer useless. All of the observations reported here used the 10 minute stop. Uncertainties in spacecraft pointing, alignment of the optical axes of the stellar telescopes, and image size make it impossible to identify all secondary stars exactly. Moreover, spectral type and reddening for the fainter secondary stars are not accurately known. Secondary stars listed in Table 3 are those ADS and DM stars which may contribute one percent or more of the total flux. To select these stars we have supposed that the center of the field aperture may be displaced up to 2 minutes. Thus stars within a radius of 7 minutes were examined, but not all of these can necessarily be seen at the same time. For most faint stars, visual magnitudes and spectral types taken from the SAO Catalog (1966) were used to compute fluxes without correction for reddening. As will be shown in § IV, ultraviolet fluxes correlate well with B-V. Tabulated spectral types were converted to colors according to Johnson

(1966). Where no spectral type is available, we have used the earliest type consistent with available visual and ultraviolet data. We assume, however, that types earlier than A are unnecessary because they are strongly reddened in this visual magnitude range.

Table 3 lists the corrections, in magnitudes, to be applied to the corresponding fluxes in Table 1. In some cases the corrections are quite large. We have included these because very little data would otherwise be available for the latest spectral types. Some stars in Table 3 require individual comment:

γ Phe: the computed secondary flux at 1910 Å is approximately that observed.

ε Gem: correction assumes only one 7 minute star in the field with 1910 Å flux equal to the detection limit (approximately type A).

γ Cru: Cousins and Stoy (1963) give B-V = 0.16 for the secondary, which seems red for A2. Fluxes were computed for an unreddened star of this color and a reddened star with B-V = 0.08. The resulting 2460 Å primary fluxes differ by a factor of two. The tabulated correction refers to the mean. For 1910 Å the correction based on an unreddened secondary is tabulated. This gives an approximate upper limit to the γ Cru flux since the reddened secondary leaves no net flux.

α Cen: α^2 photometry from Gliese (1969).

α Aps: the 6 minute secondary is probably not in the field; if the 5 minute secondary is F, it can account for the total observed flux at 2460 Å.

Interstellar extinction in the ultraviolet is complex. Bless and Savage (1972) have discussed the OAO reddening data in detail. Here we will use a mean reddening curve. For the color ratios $E(\lambda-V)/E(B-V)$, we adopt the values 1.8 (3320 Å), 2.15 (2980 Å), 3.0 (2460 Å) and 5.0 (1910 Å).

IV. DISCUSSION

The narrow band photometry of Mitchell and Johnson (1969) includes a band labelled "33" whose peak response, at 3370 Å, nearly coincides with S1F1. We will define "3320" as an arbitrary magnitude whose value is the negative of the entry in Table 1. Figure 1 plots 3320-33 against B-V. Vertical bars show the uncertainty due to secondary stars near the edge of the field. The very discrepant point at B-V = 1.65 is ξ Cyg. Although the original data look perfectly good, Figure 1 and subsequent comparisons suggest that 3320 for this star is wrong. The scatter in Figure 1 does not depend strongly on color. However, the points fill a band about $0^m.2$ wide, which is greater than internal errors lead us to expect (§ II). We will see below (Figures 2 and 3) that $\pm 0^m.02$ is a realistic estimate of 3320 error for all but a few stars. Thus most of the scatter

Table 3. Corrections for Secondary Stars

Pri	Sec	Separation (arc min)	m_v	Spectral Type	Δm 3320	2980	2460	1910	Remarks
α Cas	+55 138	1	8.8	K0	.01	.01	:02		
σ Scl	-32 406	5	8.8	F8	.045	.03	.01		max
β And	+34 199	6	8.6	F5	.08	.145	.91		max
γ Phe	-43 451	1	8.5	F0	.295	.555	1.33		1910≃obs
14 Ari	+25 354	2	8.6	F2	.05	.05	.05	.03	
α Tau	+16 628	7	9.3	?	.01	.03	.30		1910≃obs
	+16 630	2	9.5	?					
ε Aur	+43 1168	3	9.0	K?	.025	.05	.12	.81	max
	+43 1170	6	8.6	A0					
γ Lep	BS 1982	2	6.4	G5	.06	.045	.03	.02	min
	-22 1217	6	8.0	A0	.08	.08	.11	.46	max
ε Gem	+25 1407	2	9.0	K2	.015	.015	.01		min
	+25 1400	7	9.5	?	.055	.085	.32		max
	+25 1403	7	9.5	?					
	+25 1404	7	9.4	?					
γ Cru	BS 4764	2	6.41	A2	.365	.275	2.35	1.85	1910=obs?
α^1 Cen	α^2 Cen	9"	1.33	K0			.07	.06	B-V = 0.88
α Aps	-78 890	6	9.0	A?					2460>>obs
	-78 891	5	9.4pg	?	.25				2460 ≅ obs
υ Lib	-27 10459	7	9.9	?	.05	.12	.31		max
	-27 10468	7	9.8	?					
η Dra	ADS	5"	8	K1	.01	.01			
89 Her	+26 3118	5	9.2	F2	.09	.10	.26		max
70 Oph	ADS	4"	6.0	K5	.065	.05	.02		
θ Cyg	BS 7465	5	6.5	G9 III	.055	.065	.04	.08	max
	R Cyg	4	6.5	S4					
	+49 3065	4	9.0	A5					
ν Cep	+60 2290	5	8.4	G0	.035	.03		.06	max
ζ Cep	+57 2472	6	9.3	B(11.4pg)					assume negl.
β Peg	ADS	4	9.4	?			.96		max

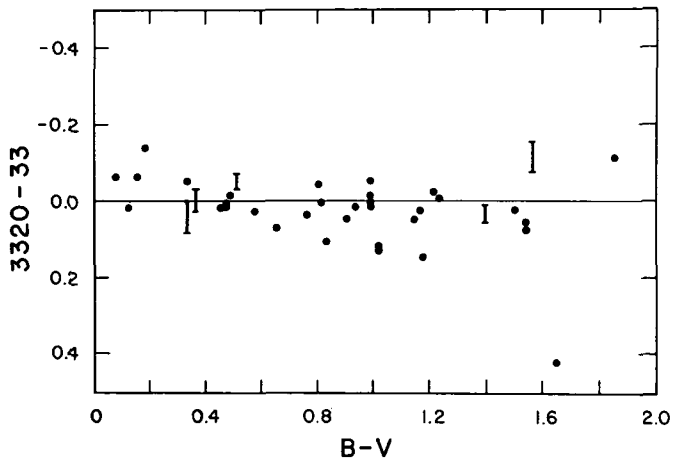

Figure 1.—OAO 3320 filter magnitudes minus Mitchell and Johnson 33 band. Zero point arbitrary.

in Figure 1 must be attributed to the ground-based photometry.

In the several color-color diagrams below, five luminosity classes are distinguished by different graph symbols. Secondary corrections have been applied according to Table 3. Stars with intrinsic B-V given under Remarks in Table 1 have been adjusted according to the mean reddening ratios of § III and are plotted at their unreddened positions. All colors except B-V have been plotted on an absolute scale. For colors that involve V or U, this required zero-point shifts C_V and C_U in addition to the C_λ already described. C_V is defined by the equation

$$\delta m = 3320\text{-}V\text{-}C_V \quad ,$$

where δm gives the ratio of the flux per unit wavelength at 3320 Å to the flux at 5500 Å. C_V and C_U, which is similarly defined, are given in Table 2. Figure 2 plots 3320-U against B-V. Main sequence and subgiant stars between θ UMa (F6 IV, B-V = 0.46) and γ Cep (K1 IV, B-V = 1.03) show a remarkably tight color correlation. If we allow errors up to $0^m.02$ in both colors all of these points can be placed on the curve shown, which for discussion purposes we have extrapolated to M0. Yellow and red giants together define a roughly parallel sequence. The four stars well below this sequence are probably misplaced. The giant is α Aps, for which 3320 is uncertain due to the radiation belt. ξ Cyg is discrepant in the same sense as in Figure 1, and by about the same amount. The remaining supergiants are γ Phe and γ Cru, both very red, deep southern objects whose V magnitudes may be systematically different from the bulk

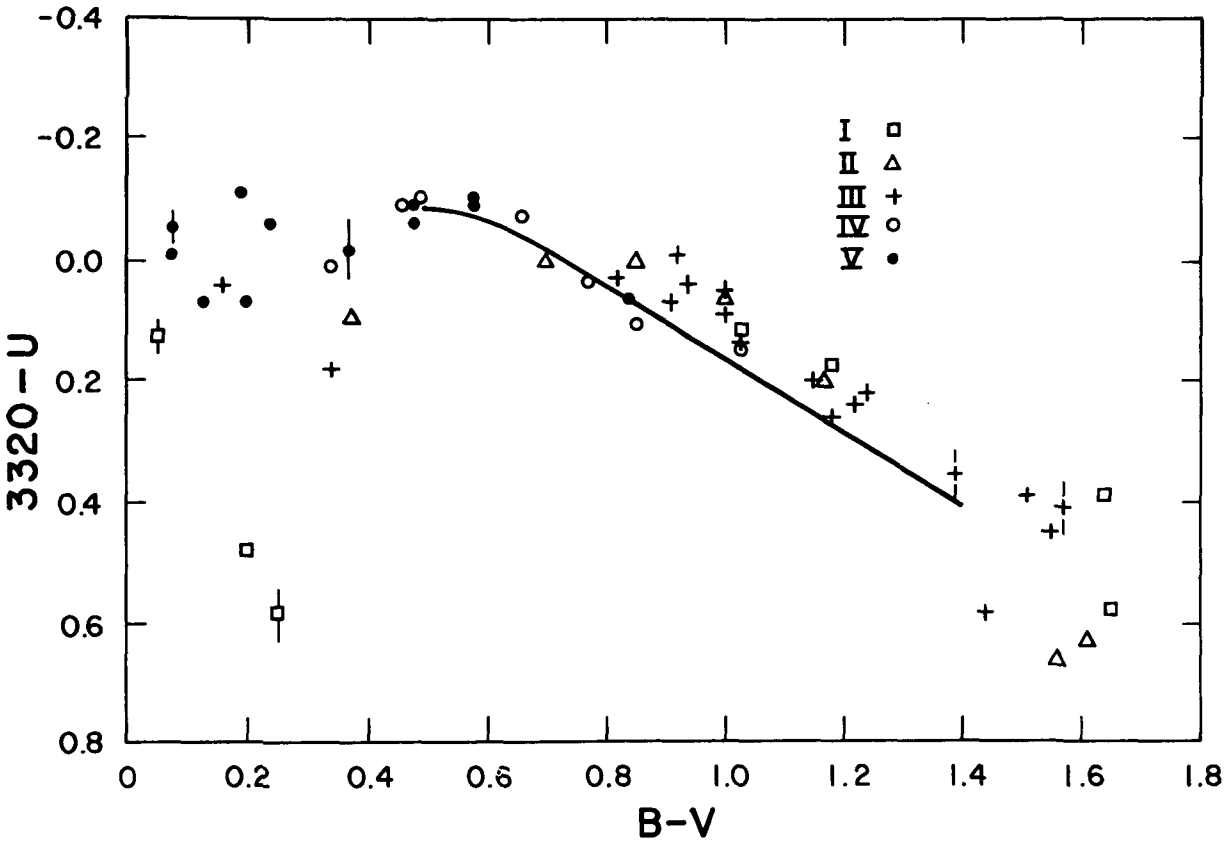

Figure 2.—3320-U vs. B-V with colors corrected for secondary stars and reddening. Ordinate zero point corresponding to equal flux per unit wavelength. The line shows extrapolated dwarf sequence.

of stars here.

Figure 3 makes use of two OAO magnitudes, 2980 and 3320. Their differences should be independent of all but very rapid changes in photometer characteristics (except filter deterioration). Again, class IV and V stars show excellent correlation with B-V. This is not surprising for the earlier spectral types, where the relation involves essentially the slopes of the Balmer and Paschen continua, i.e. the relation is not a strong function of temperature and gravity. It is worth mention for the cooler stars in which the source function is more sensitive to temperature and in which line opacity plays a greater part. Notice the clear separation of a class I sequence but almost no discrimination between II and III. According to Figure 1, ξ Cyg should be lowered about $0^{m}.4$ from its position in the upper right corner of Figure 3. Stars with

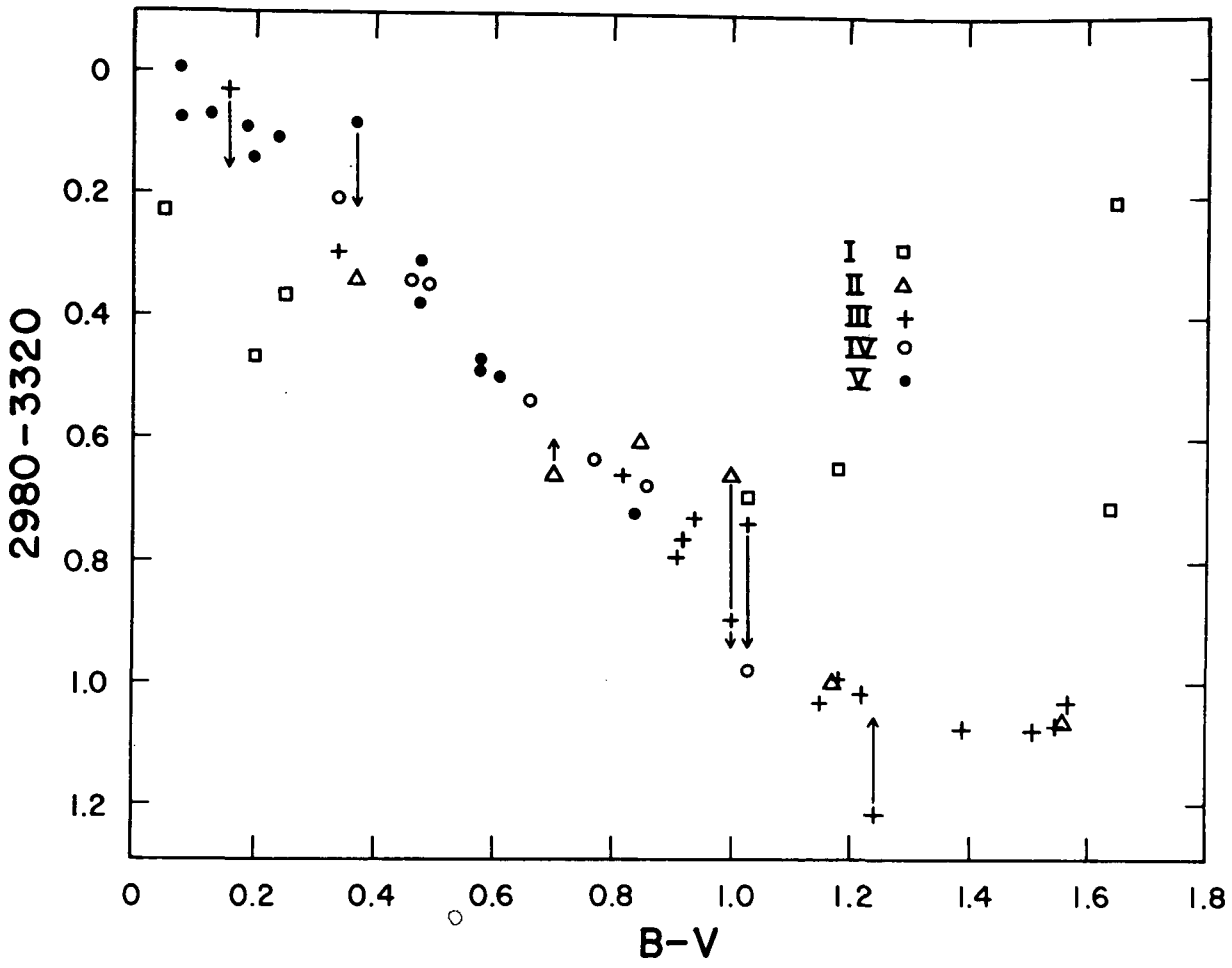

Figure 3.—2980-3320 vs. B-V with corrected colors and ordinate zero shift as in Figure 2. Arrows indicate possible corrections due to photometric errors, as discussed in text.

arrows probably have ξ Cyg type errors. Ignore the arrows for the moment.

Two features of Figure 3 persist over the broader color base 2460-V, which is plotted in Figure 4. The main sequence is well defined, especially at F and G. The class I separation is present but not as clear cut. Reddening errors could obscure a smoother relation among these supergiants if one exists, since ε Aur, ε Gem and ζ Cep have apparent excesses greater than $0^m.3$ in B-V and 1^m in 2460-V. The lower part of Figure 4 resembles a fan with its apex an F star. At least some of this spreading is luminosity-dependent. Identify the position of a point in the fan by the slope of the line joining the point to the apex.

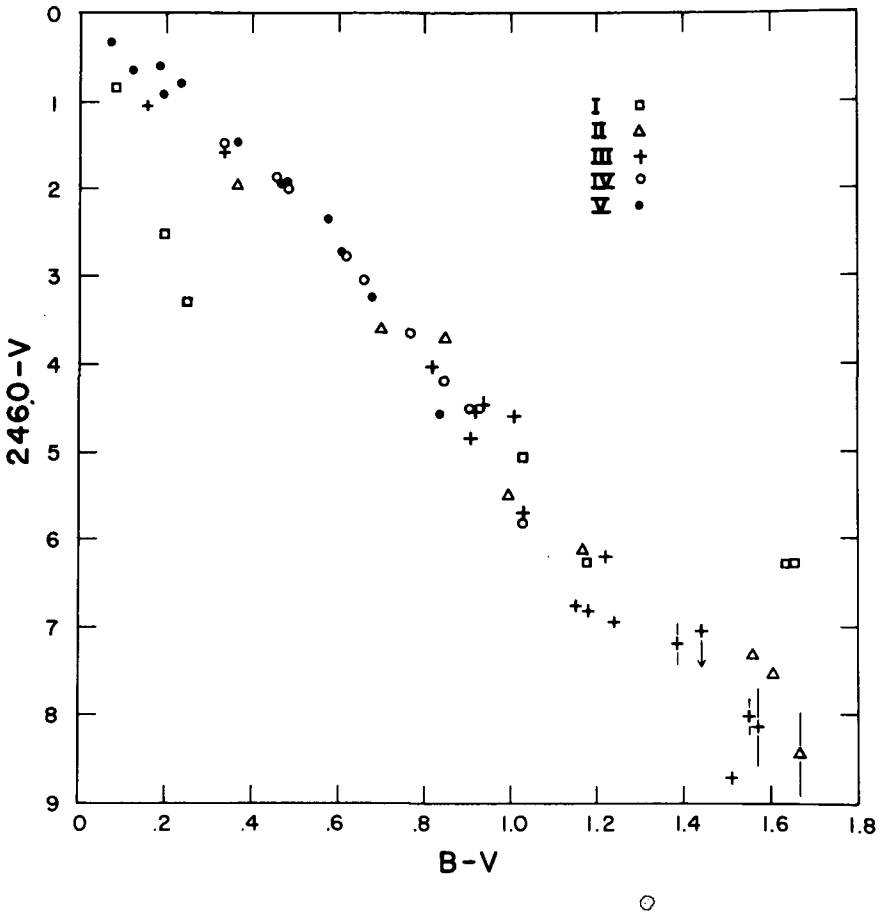

Figure 4.—2460-V vs. B-V with corrected colors and ordinate zero shift as in Figure 2.

Take the position of the apex arbitrarily as 2460-V = 2.1 and B-V = 0.54. Figure 5 compares this slope with M_V determined from the width of the Ca II K emission (Wilson and Bappu 1957). Only stars with B-V > 0.8 are included. One-third of these do not have K-line luminosities. Class I stars are plotted according to their observed colors. Depending on the exact slope of the reddening line, these stars can go up or down. Note that M_V = -5.7 for β Dra, +1.2 for ζ Cyg and -1.2 for ι Cet, in disagreement with their spectroscopic classes. Luminosity effects and scatter for II-V stars in Figure 4 are much reduced if the abscissa is instead 2980-3320, as in Figure 6. In fact, the evidence for a single sequence is strong enough to justify correcting 2980-3320 for stars that appear most discrepant. β Tri, θ Cyg, ζ Cyg, ε Cyg and α Boo are marked with underbars. If we shift these stars horizontally to fit a smooth curve

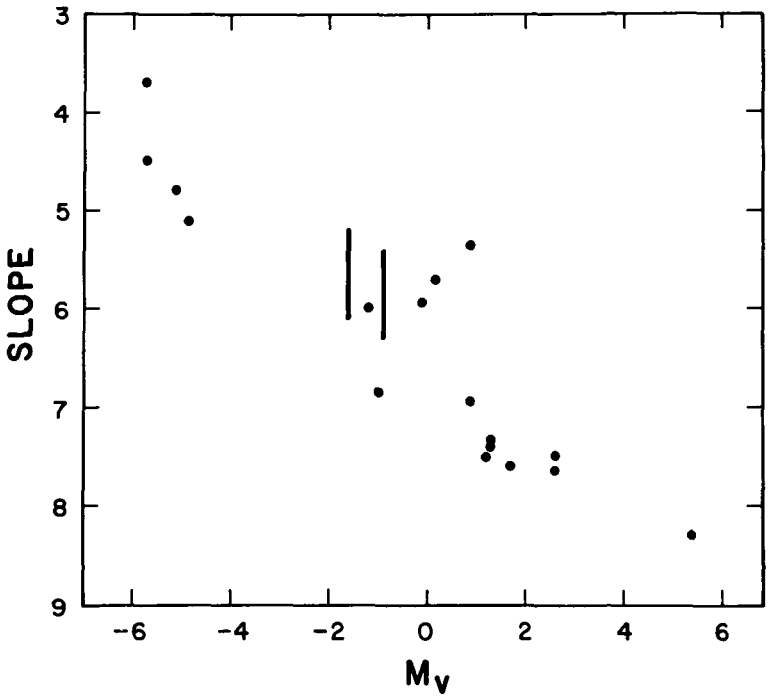

Figure 5.—SLOPE vs. Wilson and Bappu absolute magnitude. SLOPE identifies the positions of stars in Figure 4 for which B-V > 0.8.

through the remaining points, we then shift these stars vertically in Figure 3 as shown by the arrows. The result in every case improves the correlation of ultraviolet with visual color for II-V stars taken as a group.

For α Cyg there is no measurement of 2980-3320. In Figure 6 this star has been placed arbitrarily at 0.6.

Figure 7 shows 1910-V. Most of the stars with B-V > 0.9 register only a few net 1910 counts at the longest integration time. With uncertainties in DARK up to about 4 counts, errors of $\pm 0^m.5$ are likely. α Boo (B-V = 1.24) has a high count and its position should be well determined. It appears brighter than the other giants, which is not true for other wavelengths. Unfortunately, only one observation is available.

Figures 8-10 compare the OAO data for selected stars with model atmospheres from the extensive grid of models computed at the Smithsonian Astrophysical Observatory (Carbon and Gingerich 1969). These models include convective transport and statistical treatment of metal line blanketing. Models without convection and blanketing are also given. Only blanketed models are used in this comparison. The light lines represent the continuum flux, while the heavy lines are the continuum flux multiplied

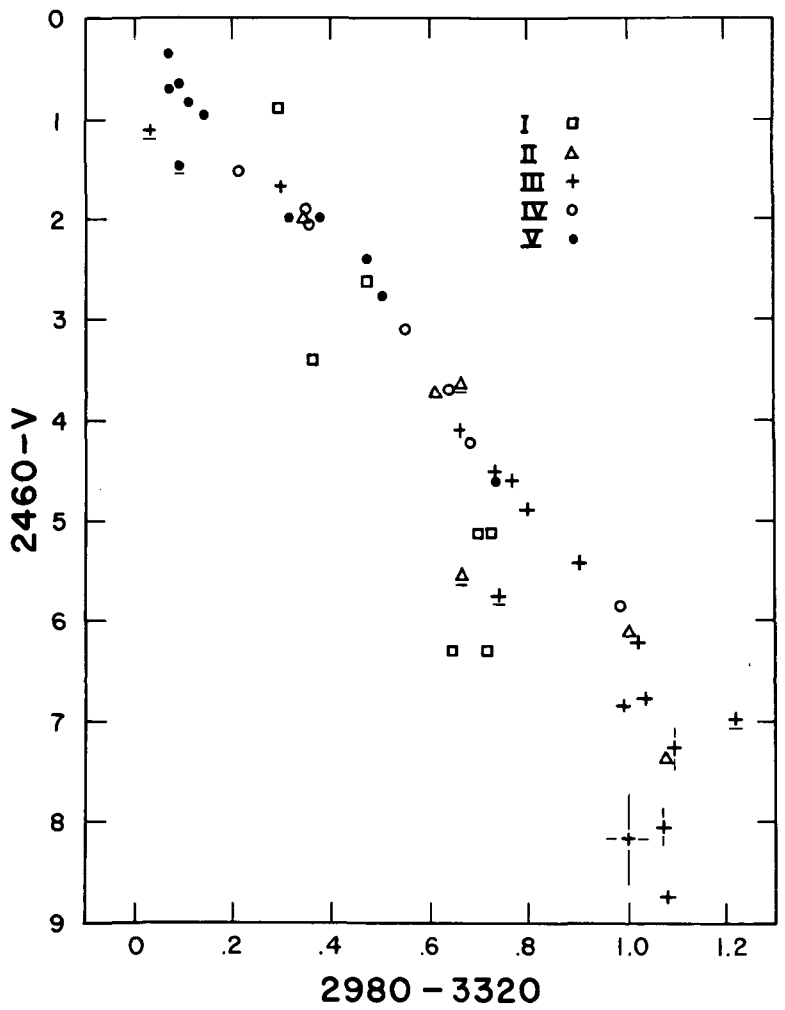

Figure 6.—2460-V vs. 2980-3320 with corrected, absolute colors. Underbars indicate observations with probable photometric errors in 2980-3320, as discussed in text.

by (1-η), where η is the tabulated blanketing coefficient. Filled circles are narrow-band observations of Mitchell and Johnson (1969) that have been calibrated against Oke and Schild's (1970) Vega measurements. Mitchell and Johnson's bands 52 and 80 were used to determine the effective temperatures of the models to the nearest 50°K. The observed and theoretical fluxes are normalized at 5180 Å.

The OAO data are plotted for two absolute calibration schemes. Open circles are based on the model atmosphere which Schild et al. (1971) fit to Vega. Crosses show the observations based on Code's calibration (Table 2). In both cases the

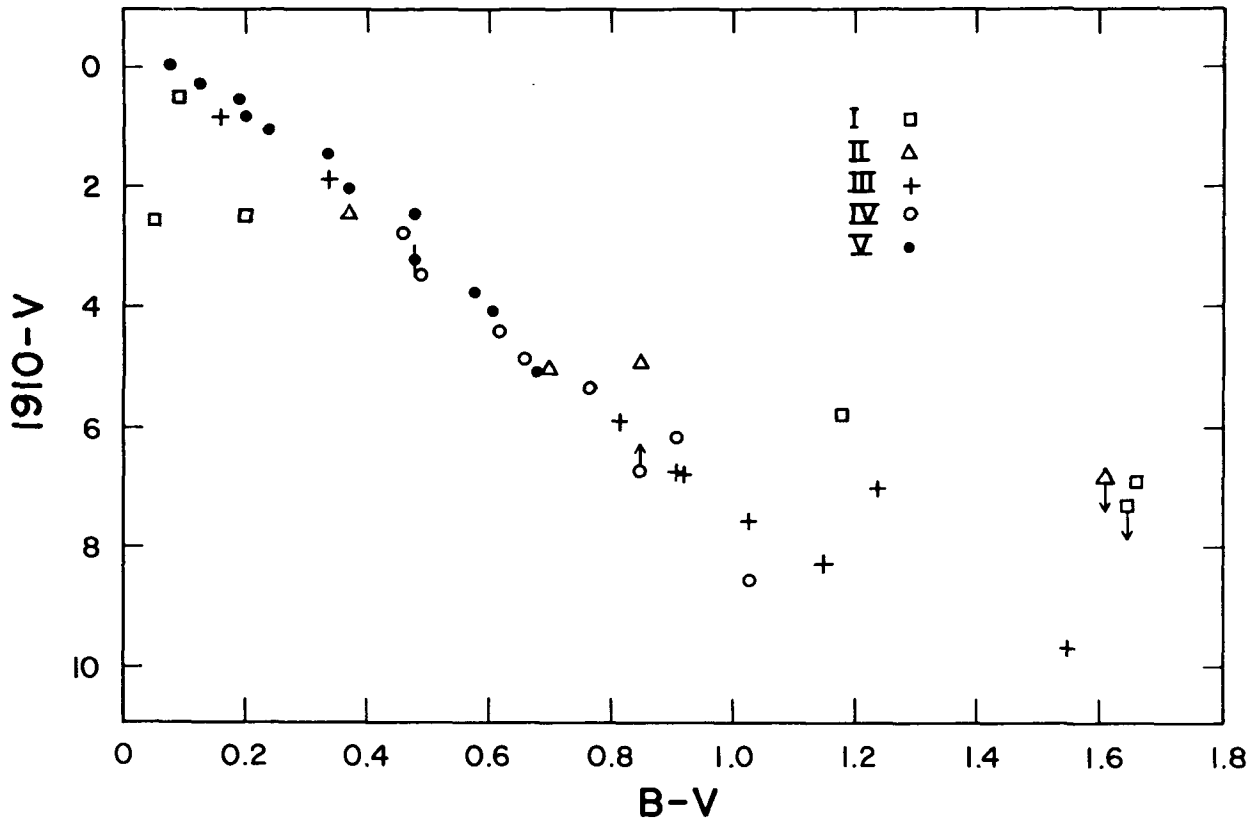

Figure 7.—1910-V vs. B-V with corrected colors and ordinate zero shift.

observed fluxes are plotted at the nominal filter wavelengths, but the fluxes have first been multiplied by the factor

$$\frac{F^{*}_{\lambda_0} \int F^{c}_{\lambda} S_{\lambda} d\lambda}{F^{c}_{\lambda_0} \int F^{*}_{\lambda} S_{\lambda} d\lambda} .$$

Here F_λ is a model flux and S_λ is the photometer response. λ_0 is the nominal filter wavelength. The superscripts * and c refer, respectively, to the models employed in Figures 8-10 and to the calibrating model (or mean model). Below 7000°K the corrections to 1910 and 2460 become substantial. The greatest correction used here is a reduction of $1^{m}.70$ in the observed flux of α Ari at 1910 Å.

The agreement between theory and observation is quite good

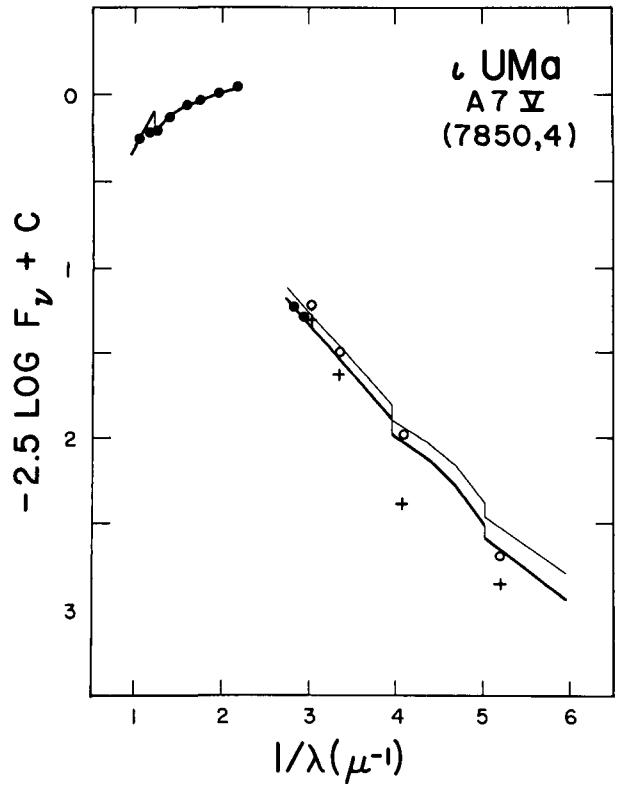

Figure 8.—Comparison of ι UMa observations with SAO blanketed model atmosphere. Filled circles, Mitchell and Johnson narrow-band data; open circles, OAO calibrated with Vega model; crosses, OAO calibrated with B star models; light line, model continuum; heavy line, model net flux.

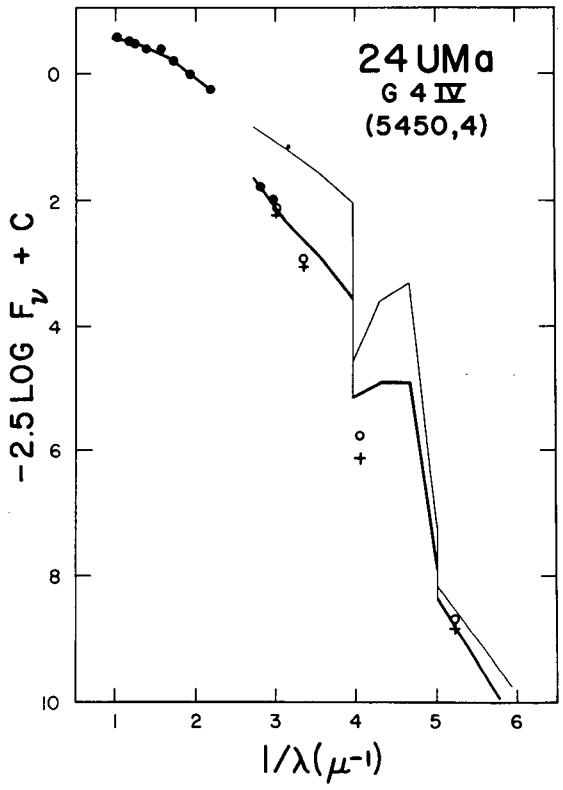

Figure 9.—Comparison of 24 UMa observations with SAO blanketed model, as in Figure 8.

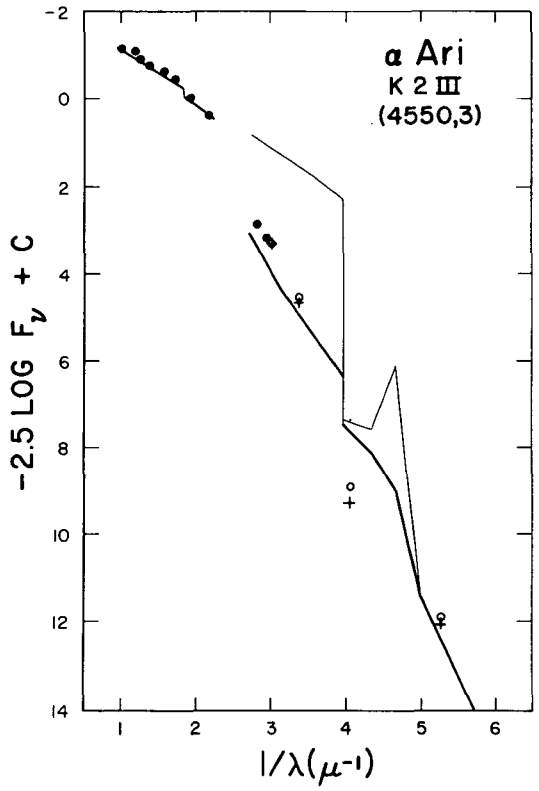

Figure 10.—Comparison of α Ari observations with SAO blanketed model, as in Figure 8.

over the entire range of wavelengths with the exception of 2460 Å. For ι UMa (7850°K), all points calibrated with the Vega model agree very well. This is not surprising, since both are ATLAS models and differences between models and stars could be nearly the same at A0 and A7. However, 2460 based on early B stars is a half magnitude fainter than the model for ι UMa and, by implication, for A0 stars also. This discrepancy increases with later spectral type. A deficiency in the neighborhood of 2500 Å is, of course, a long-standing problem in the interpretation of the solar spectrum. The origin of the required additional opacity is not known. If the B stars are also deficient at 2460 then the 2460 crosses in Figures 8-10 must be lowered even further.

I thank Dr. J. Caldwell for making his data on late-type stars available to me and Dr. R. Bottemiller for his computations of filter effective wavelengths. This research was supported by NASA NAS 5-1348 contract.

REFERENCES

Blanco, V. M., Demers, S., Douglass, G. G. and Fitzgerald, M. P. 1968, Publ. U. S. Naval Obs. (Washington: U. S. Gov't Printing Office), Vol. 21.
Bless, R. C. and Savage, B. D. 1972, Ap. J., in press.
Caldwell, J. J. 1970, Ph. D. Dissertation, University of Wisconsin.
Carbon, D. and Gingerich, O. 1969, in Proc. 3rd Harvard-Smithsonian Conference on Stellar Atmospheres, ed. O. Gingerich (Cambridge: M. I. T. Press).
Code, A. D., Houck, T. E., McNall, J. F., Bless, R. C. and Lillie, C. F. 1970, Ap. J. 161, 377.
Cousins, A. W. J. and Stoy, R. H. 1963, Roy. Obs. Bull. No.64.
Gliese, W. 1969, Veröff Astr. Inst. Heidelberg No. 22
Iriarte, B., Johnson, H. L., Mitchell, R. I. and Wisniewski, W. K. 1965, Sky and Telescope 30, 21.
Johnson, H. L. 1966, Ann. Rev. Astr. and Ap. 4, 193.
Mitchell, R. I. and Johnson, H. L. 1969, Comm. Lunar and Plan. Lab. (University of Arizona), No. 132.
Oke, J. B. and Schild, R. E. 1970, Ap. J. 161, 1015.
Schild, R. E., Peterson, D. M. and Oke, J. B. 1971, Ap. J. 166, 95.
Smithsonian Astrophysical Observatory Star Catalog, 1966 (Washington: Smithsonian Institution).
Wilson, O. C. and Bappu, M. K. V. 1957, Ap. J. 125, 661.

HD 50896 AND THE COMPOSITION OF WOLF-RAYET ATMOSPHERES

Lindsey F. Smith*
National Aeronautics and Space Administration
Goddard Space Flight Center
Greenbelt, Maryland

ABSTRACT

Measurements of the Pickering lines of He II in the spectrum of HD 50896 suggest that the upper limit to the H/He ratio is 0.05 by numbers. Spectral scans from OAO-2 show strong lines, nitrogen being observed most strongly as N IV, but also as N III and N V. Carbon and oxygen are observed dominantly in the triply ionized states. Thus, the degree of ionization of C, N and O are comparable. No indication of extensive selective excitation effects is observed. It is concluded that the differences between the WN and WC stars cannot be explained by selective excitation or ionization effects in the WN stars.

I. INTRODUCTION

Wolf-Rayet spectra are dominated by broad strong emission lines of helium, carbon, nitrogen and oxygen. The spectra are divided into two sequences, the WN spectra, dominated by helium and nitrogen, with little or no evidence of carbon, and the WC spectra dominated by helium, carbon and oxygen with little or no evidence of nitrogen. Ever since the first identification of the lines (Perrin 1920, Beals 1930, Payne 1933) and classification of the spectra (Beals 1938), it has been wondered whether the lack of conspicuous hydrogen lines indicates a real deficiency of hydrogen in the atmospheres and whether there is a difference in the carbon and nitrogen abundance between the

---

*Present address: Institut d'Astrophysique
B-4200 Cointe-Ougrée, Liège, Belgium

stars in the two sequences.

Many WR stars are binaries and the presence of the spectrum of the companion greatly complicates analysis of the WR spectrum. HD 50896 is a WR star which does not have a conspicuously composite spectrum and is the only such star bright enough to be observed by OAO-2. The present paper presents ground-based and OAO observations that are relevant to the problem of determining the atmospheric abundances in this star. It is demonstrated that if the atmosphere is optically thin in the Balmer lines, the H/He ratio is no greater than 0.05 by number, and that the relative excitation and ionization of carbon, nitrogen and oxygen are comparable.

II. THE H/He RATIO

Figure 1 shows a graph of the flux in the Pickering lines of He II as a function of n, the principal quantum number of the upper level. The data are taken from Kuhi and Smith (1971) and are derived from spectrograms at 16 Å/mm obtained with the Coudé spectrograph of the 120-inch telescope of Lick Observatory. Conversion to fluxes is made by the use of the continuum fluxes measured by Kuhi (1966, 1968) with an improved estimate of the reddening correction (Smith and Kuhi 1970).

The hydrogen Balmer lines are nearly equal in wavelength and oscillator strength to every second Pickering line. Thus, if hydrogen emission contributes to the spectrum, we would expect that Pickering lines with even values of 'n' would be relatively stronger than lines with odd values of 'n'. Clearly, in Figure 1 this is not the case. The relationship between log (Flux) and 'n' is extremely smooth; hydrogen would appear to make no contribution to the spectrum whatsoever.

In order to place a quantitative upper limit to the amount of hydrogen that may be present, it is necessary to know something about the conditions under which the lines are formed. If the lines are optically thin, the line strengths are dependent only on the numbers of electrons in the upper levels and on the transition probabilities. Due to the similarity of the He II and H I ions the transition probabilities and the Boltzmann factors for the relative populations of the levels are nearly equal. The 'n' values considered here are large enough that the b_n will not differ radically from 1. Hence, the number ratio of H^+ to He^{++} equals the ratio of the flux of the contribution of hydrogen and helium to the Pickering lines. The full equations are given by Castor and Van Blerkom (1970) who find that, for level 14, the ratio of the transition probabilities is 0.94; a 6 percent correction is unimportant in the present context. The assumption that the ratio of the b_n is equal to 1 will not introduce an error greater than 10 percent.

The important requirement for application of this method to

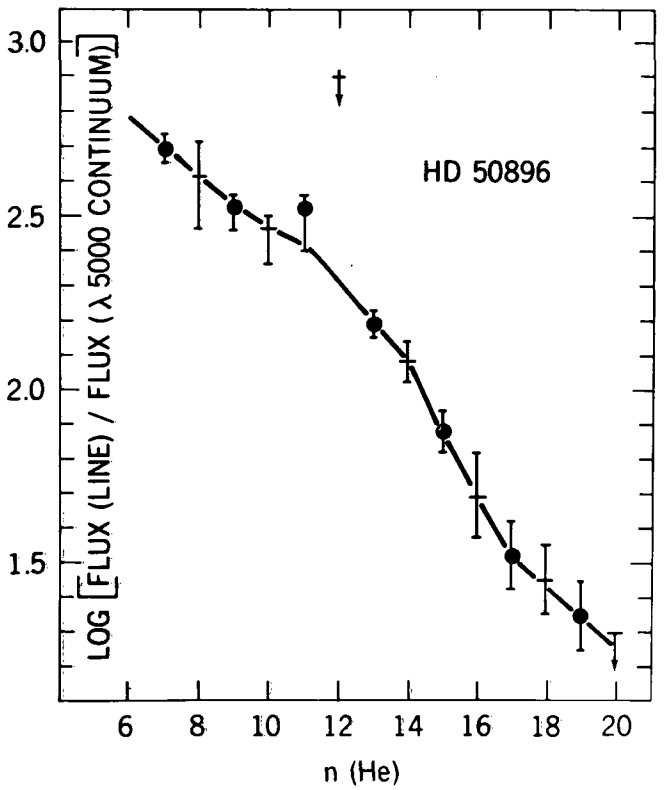

Figure 1.—The logarithm of the observed flux in the Pickering lines, in units of the continuum flux at 5000 Å, plotted as a function of the principal quantum number, n, of the upper level of the transition. Hydrogen Balmer lines coincide with lines with even values of n; these are plotted as crosses. Error bars include possible errors due to the presence of unresolved blends with nitrogen. The line from n = 12 is 4100 Å and is blended with strong lines of N III and Si IV.

the determination of the abundance ratio is that both the hydrogen and the helium lines be optically thin. Castor and Van Blerkom's (1970) analysis of the spectrum of HD 192163 (WN6) indicates that the lines in the Pickering series of He II of that star are optically thin for n > 10. The diagram for the fluxes of the Pickering lines in the spectrum of HD 192163 is very similar to that in Figure 1 for HD 50896. The change of slope between n = 10 and n = 13 appears to correspond to the change from optically thick to optically thin lines, in agreement with Castor and Van Blerkom's analysis. Observation of the Pickering decrements in a large number of WR spectra further supports the assertion that the He II lines with n > 10

are optically thin (see Smith 1971). The hydrogen lines have been seen neither in emission nor in absorption at $n \geq 7$. Assuming their absence is due to a real deficiency of hydrogen, then the hydrogen lines are optically thin and we may place an upper limit of 5 percent on the contribution of hydrogen to the emission, and thus an upper limit of 0.05 to the number ratio of H^+/He^{++}.

To obtain the total H/He ratio, the possible presence of other ionization states needs to be considered. The He I lines appear only weakly in absorption and moderately in emission in the spectrum of this star (cf Smith 1955); thus, while there may be a small amount of He^+, neutral H and He can probably be neglected. Thus, the upper limit of the total H/He ratio is also 0.05.

To place this result in perspective, it should be noted that it is an extreme case. Hydrogen emission is found to contribute to the Pickering series in some WN spectra, with relative fluxes that indicate H^+/He^{++} ratios as high as 2.3 (Smith 1971). It should also be noted that this is not a new observation. Many investigators have noted, qualitatively, the smoothness or bumpiness of the Pickering series. However, the higher resolution spectrograms now available allow much more accurate measurements of the equivalent widths of the lines and continuum flux measurements, while the theoretical studies of Castor and Van Blerkom allow equivalent width measurements of optically thin lines to be converted to a quantitative value of the H/He ratio.

III. THE CNO ABUNDANCES

One can, in theory, use the same procedure to obtain number ratios of some ions of carbon, nitrogen and oxygen to helium. In practice, however, this requires observation of lines from high values of 'n' in the CNO spectra; these lines are weak. The spectra are dominated by lines from lower levels of the ions, and a theory for the relative strengths of these lines is not available at this time.

A further complication arises from the fact that C, N and O can each exist in many ionization states, the relative populations of which are certainly variable through the atmosphere and are not known. Some of the ions do not have strong lines in the visual region of the spectrum; thus their presence or absence cannot be unequivocally determined from ground-based observations. At this point observations from OAO become pertinent. Within the range 1000-6000 Å all ions have some strong lines, and we may, therefore, make firm statements regarding the presence and relative strengths of lines from all ions.

Figures 2 and 3 show OAO spectra of HD 50896 obtained by Bless. Figure 2 is a sum of seven scans, Figure 3 is a sum of

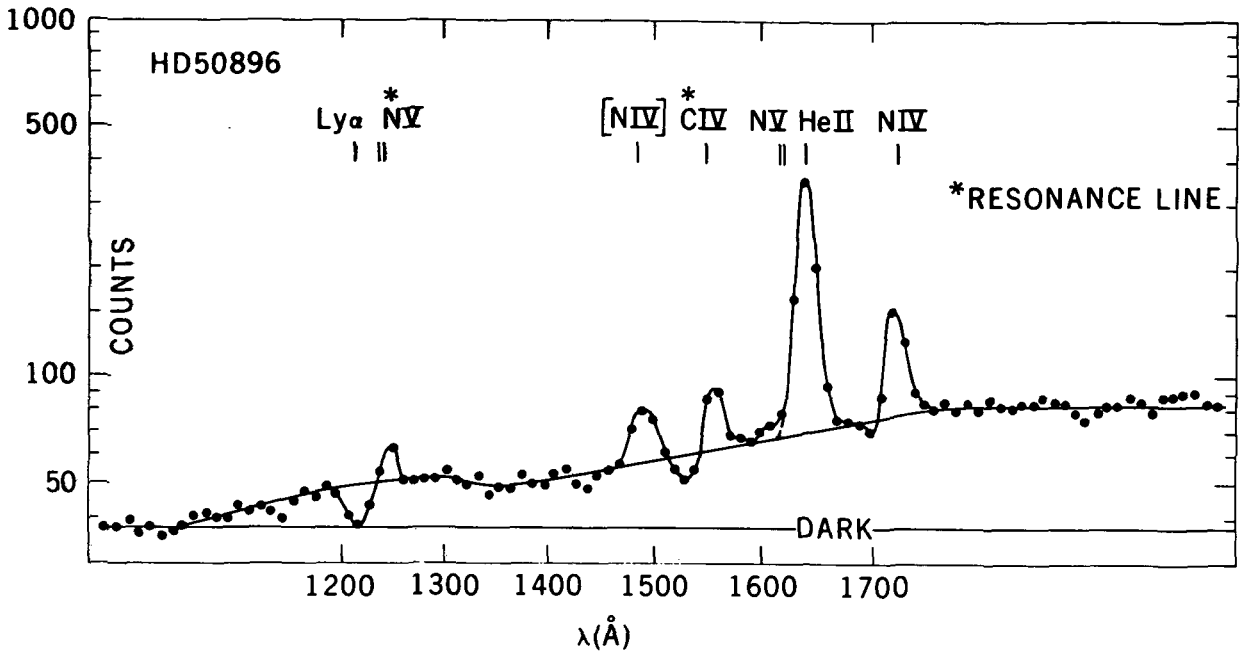

Figure 2.—Sum of counts from seven OAO scans of the wavelength region 1000-2000 Å. The most probable identification of the strong features are shown.

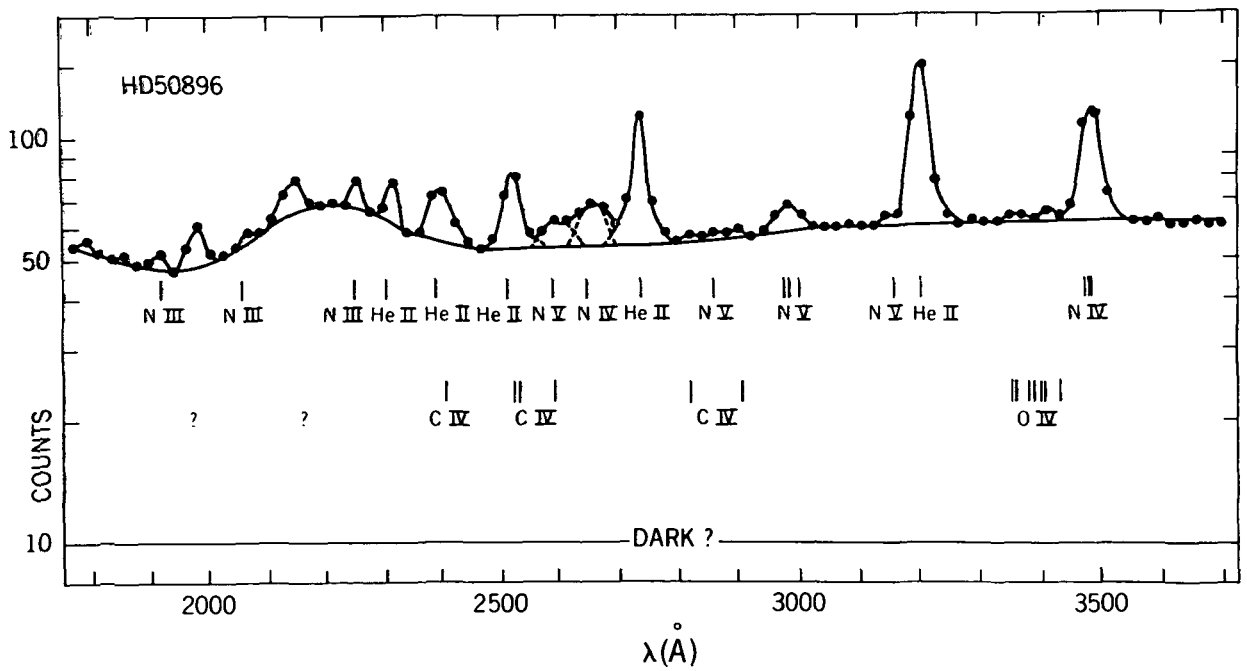

Figure 3.—Sum of counts from two OAO scans of the wavelength region 2000-4000 Å. Background is assumed to be 5 counts for each scan.

two. Background counts in Figure 1 are estimated from the region shortward of 1000 Å where the detectors are insensitive. In Figure 2 the background is taken to be 10 counts, representing 5 counts per scan, in accordance with the estimate given by Savage (private communication). No correction has been made for the sensitivity functions of the receivers, since these are poorly known at the present time. The continua that have been drawn are, however, of the same shape as the preliminary sensitivity functions.

Several points in these figures are of obvious interest.

(1) C IV lines are clearly present. It should be recalled in this context that C IV 5806 Å is a strong line in most WN spectra. Clearly the spectrum of C IV is quite well developed, and 5806 Å is not an isolated line.

(2) O IV is observed at 3400 Å. That wavelength is accessible from the ground. However, because of the presence of ozone absorption in ground-based spectra, OAO spectra provide as accurate a measurement of this line as is obtained from higher dispersion ground-based spectrograms.

(3) The forbidden line, N IV] 1488 Å is clearly present. This is the analogue of C III] 1909 Å observed in the spectrum of γ^2 Vel by Stecher (1968).

Measurement of equivalent widths of all features in the spectrum, together with tentative identifications, are given in Table 1. The equivalent widths are obtained by numerical integration of the observed counts over the line. It should be noted that the results for the lines 3480 and 3203 Å differ by nearly a factor of 2 from the values, 94 and 100 Å, respectively, obtained by Kuhi and Smith from ground-based spectrograms. It seems most likely that this is due to an underestimate of the background count level at these wavelengths. However, it does not seem possible that the background counts are much higher than 10 at the shortest wavelengths, and the reason for the discrepancy remains uncertain. Fortunately, we are mostly interested in the presence or absence of lines, and a factor of two will not invalidate any of the qualitative conclusions to be drawn from these data.

Table 2 contains line strengths from Table 1 and from Kuhi and Smith (1971) arranged in groups of iso-electronic ions. When a line is not observed, an upper limit has usually been estimated. Very strong lines of O III occur at 3759, 3774 and 3791 Å but these lines are not observed in HD 50896. An upper limit of 3 Å is estimated for their equivalent widths.

From the similarity of iso-electronic ions we expect, a priori, that relative line strengths of corresponding transitions will be similar. It is easily seen that this is the case and, further, that the lines which are observed are, in general, those that are observed to be the strongest in the laboratory spectra. The strengths of C IV lines appear to be comparable

Table 1. Equivalent Widths of Lines in the Ultraviolet Spectrum of HD 50896

Identification*		E.W.(Å)	Identification	E.W.(Å)
§ H I 1215	a	22.9	He II 2520	
§ N V 1240	a		C IV 2524	26
§ N V 1240		15.7	C IV 2530	
N IV 1486		34.8	N V 2591	10
§ C IV 1549	a	9.0	C IV 2595	
C IV 1549		19.6	N IV 2646	18
N V 1618		3.6	He II 2740	48
He II 1640		183.0	C IV 2819?	1
N IV 1718	a	2.0	N V 2859	1
N IV 1718		39.7	C IV 2906	1
N III 1805		2	N V 2974	
N V 1860		1	N V 2981	8
N III 1921		2	N V 2998	
? 1980		9	N V 3160	3.5
N III 2064		1.5	He II 3203	61
? 2150		7.5	† O IV 3400	4.5
N III 2248		3.5	† N IV 3480	46
He II 2300		6.5		
He II 2390		18		
C IV 2405				

* 'a' indicates an absorption line
† blend of two multiplets
§ resonance line

Table 2. Equivalent Widths in the Spectrum of HD 50896

Lab Int (N)	C II	N III		O IV		Transition
10	Resonance	1751.7		1338.6		
9	lines	1747.8	<2Å	1343.0	<3Å	$2p^2\ ^2P - 2p^3\ ^2D^o$
6	λ1335.7	1751.2		1343.5		
	λ1334.5					
8	not	1184.5		923	-	$2p^2\ ^2P - 2p^3\ ^2P^o$
7	observed	1183.0	?			
10		1885.2	<2Å	1068	-	$3d\ ^2D - 4f\ ^2F^o$
10		2064.0		1164.3		
10		2063.5	1.5Å	1164.5	-	$3d\ ^2F^o - 4f\ ^2G$
6		2068.2				
10		4097.3	≤30Å	3063.5	<1Å	$3s\ ^2S - 3p\ ^2P^o$
9		4103.4	(HeII, ?SiIV)	3071.7		
10		4640.6		3411.8		
9		4634.2	7Å	3403.6		$3p\ ^2P^o - 3d\ ^2D$
7		4641.9		3413.7		
7		4510.9		3381.3		
6		:	3Å	:	4Å	$3s'\ ^4P^o - 3p'\ ^4D$
4		4534.6		3409.8		
10		4379.1	5Å			$4f\ ^2F^o - 5g\ ^2G$

?( ) Possibly blended with

Table 2, continued

Lab Int (N)	C III		N IV		O V		Transition		
2	1909	?(NIII) <2Å	1486.5	35Å	1218.4	?(Lyα)	$2s^2$	^1S - 2p	$^3P^O$
20	2296.9	?(HeII) <3Å	1718.6	40Å	1371.3	<6Å	2p	$^1P^O$- $2p^2$	^1D
15	4647.4	?(NIII) <4Å	3478.7	91Å	2781.0	?(HeII) <2Å	3s	^3S - 3p	$^3P^O$
14	4650.2		3483.0		2787.0				
13	4651.4		3484.9		2789.9				
10	4067.9	?(NIV) <12Å	2645.6	18Å	1643.7	?(HeII)	4f	$^3F^O$- 5g	^3G
11	4068.9		2646.2						
12	4070.3		2647.0						
8	5695.9	<1Å	4057.8	23Å	3144.7	?(NV) <3Å	3p	$^1P^O$- 3d	^1D

?( ) Possibly blended with

Table 2, concluded

Lab Int (N)	C IV		N V		O VI		Transition		
20 19	1548.2 1550.8	20Å	1238.8 1242.8	>16Å	1031.9 1037.6	-	2s	^2S - 2p	$^2P^O$
12 10	5801.5 5812.1	28Å	4603.3 4619.1	34Å	3811.4 3834.2	?(HeII) <<1Å	3s	^2S - 3p	$^2P^O$
9 12	2524.2 2530.0	?(HeII)	1616.3 1619.7	?(HeII) ~4Å			4d 4f	^2D - 5f $^2F^O$ - 5g	$^2F^O$ ^2G
6 8 10	4647.0 4668.3	?(HeII)	2974.5 2980.8 2981.3	8Å			5d 5f 5g	^2D - 6f $^2F^O$ - 6g ^2G - 6h	$^2F^O$ ^2G $^2H^O$
9	7726.2	§yes	4944.6	6Å			6h	$^2H^O$ - 7i	^2I
6	2906.3	1.5Å	1860	1Å			5g	^2G - 7h	$^2H^O$
6	2404.4 2405.1	?(HeII)	1548 1549.3	?(CIV)			4p	$^2P^O$ - 5d	^2D

§ Kuhi (private communication) confirms the presence of this line from scanner observations

?( ) Possibly blended with

in all cases to those of the corresponding lines in N V. The single band of O IV that is observed corresponds to two of the strongest bands in the spectrum of N III. The great strength listed for N III 4100 Å is a high upper limit owing to unresolved blending with He II 4100 Å and possibly with Si IV 4088 Å and 4116 Å.

In general, it is confirmed that when an ion is present in the spectrum of a WR star, the spectrum of that ion is well developed; selective excitation processes are relatively unimportant.

Table 3 gives the ionization potentials of each of the ions, and indicates, qualitatively, by the number of slashes, the relative strength of the spectrum of the ion in the spectrum of HD 50896. Nitrogen is observed most strongly as N IV, but N V is also strong and N III is present. Carbon appears strongly as C IV; C III is not observed, but many of the lines are blended. Smith (1955) has seen C III 5696 Å weakly in this spectrum; it certainly is not present on our spectrograms.

Table 3. Summary - Relative Equivalent Widths / Ionization Potential /

	C	N	O
II	24.3	29.6	35.1
III	?47.9?	//47.4//	54.9
IV	///64.5///	////77.4////	/77.4/
V	392	///97.9///	113.8
VI	490	552	138.1
VII	-	668	739
Cosmic Abundance	45	13	100

Oxygen occurs weakly as O IV, while Smith has seen O V. Clearly the ions of O and C that are observed are those with ionization potentials closest to that of N IV, the strongest nitrogen ion. This is certainly what one would, a priori, expect, and it demonstrates that there are no peculiar ionization conditions in the atmosphere of this star. The failure to observe strong lines of carbon and oxygen in the visual spectra of WN

stars is repeated in the ultraviolet region longward of 1200 Å, and no evidence is found for these atoms being present in ionization states that do not contribute strongly to the visual spectrum.

IV. CONCLUSIONS

It has been demonstrated that hydrogen may be essentially absent from the spectrum of HD 50896. This implies that all of the hydrogen-rich envelope has been removed at some time after a pure helium core has been created.

All the observed emission features of C, N and O arise from similar levels of excitation and ionization and can be produced under conditions approximating thermodynamic equilibrium. Of course, the differences between WC and WN spectra may be due to peculiar conditions in the WC atmospheres. However, it should be emphasized that since the atmosphere of HD 50896 contains no hydrogen, it has obviously been processed by thermonuclear reactions, and there is no reason to expect that the relative abundances of C, N and O should have their primordial value. The obvious conclusion is that nitrogen is grossly overabundant with respect to C and O in WN atmospheres, and that C and O are overabundant with respect to N in WC atmospheres. It is to be hoped that a theory adequate to predict line strengths of some of the observed transitions will soon be forthcoming so that the ratios of C, N and O may be placed on as quantitative a basis as the H/He ratios now are.

REFERENCES

Beals, C. S. 1930, Pub. Dom. Ap. Obs. Victoria 4, 288.
_____ *1938, Trans. I. A. U.* 6, 248.
Castor, J. I. and Van Blerkom, D. 1970, Ap. J. 161, 485.
Kuhi, L. V. 1966, Ap. J. 143, 753.
_____ *1968, Wolf-Rayet Stars, ed. K. G. Gebbie and R. N. Thomas (N.B.S. Special Pub. 307), pp. 110, 112.*
Kuhi, L. V. and Smith, L. F. 1971, in preparation.
Payne, C. H. 1933, Z. Astrophys. 7, 1.
Perrin, C. D. 1920, Mon. Not. Roy. Astr. Soc. 81, 142.
Smith, H. J. 1955, Southern Wolf-Rayet Stars (Dissertation, Harvard University).
Smith, L. F. 1971, Proc. I. A. U. Symp. 49. In press.
Smith, L. F. and Kuhi, L. V. 1970, Ap. J. 162, 535.
Stecher, T. P. 1968, Wolf-Rayet Stars, ed. K. G. Gebbie and R. N. Thomas (N.B.S. Special Pub. 307), p. 70.

OAO-2 OBSERVATIONS OF C III] 1909 Å LINE IN GAMMA^2 VELORUM

Donald K. West
National Aeronautics and Space Administration
Goddard Space Flight Center
Greenbelt, Maryland

ABSTRACT

The C III] 1909 Å emission line in Gamma^2 Velorum was observed over a period of 24 hours in an attempt to find short period time variability. Analysis of this data found no periods in the range of 0.5 to 200 minutes, and placed an upper limit of 3% on the amplitude of the stellar pulsations. Improved spectral resolution data for this line was obtained by offsetting the OAO-2 pointing in steps of 15 seconds of arc. The line profile derived by combining this offset data with the slit function shows a definite asymmetry. Although the improved resolution gives results which are barely sufficient for comparison with the prediction from model envelopes, some information concerning the abundance of carbon and the physical conditions of the envelope can be gained.

I. INTRODUCTION

Gamma^2 Velorum is a binary with a period of 78.5 days, containing a Wolf-Rayet star WC8 and an O9 star. The ultraviolet spectrum has been observed from a rocket and by the OAO-2 in regions from 1100 to 4000 Å. Figure 1 shows an OAO spectrum at 10 Å resolution. This scan was made with a spacecraft offset of 13 arc min in order to shift 1909 Å into spectrometer 2 (Code et al. 1970). The offset introduces an uncertainty in the wavelength scale between 1600 and 2000 Å of about ±10 Å.

One of the strongest lines in the spectrum has been identified from rocket spectra by Stecher (1970) as an intercombination line of C III] $2s^2\,{}^1S$-$2s2p\,{}^3P$ at 1909 Å. The strength of

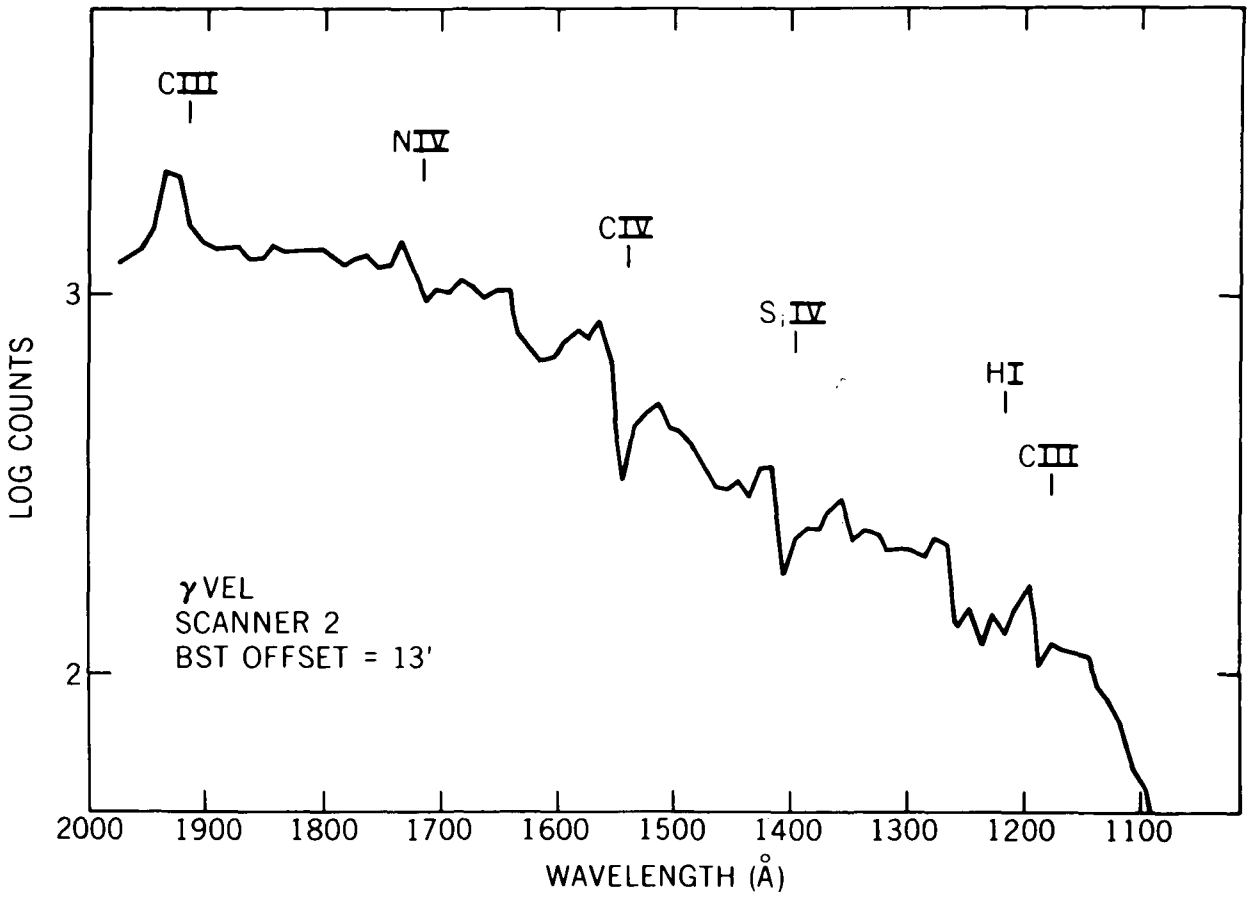

Figure 1.—OAO-2 spectral scan of γ^2 Velorum. Counts are raw data with 10 Å slit. Six prominent features have been identified.

this emission feature is most surprising because its transition probability is one million times smaller than a C III line of equal strength at 2297 Å, not shown in this figure.

The extent of excitation in this line has been investigated by Stecher and West (1968 and 1971) with the intent to determine if the population ratio was large enough to produce laser action. Model envelopes assumed spherically symmetric distribution of radially ejected mass and velocity. Equivalent widths resulting from these models were compared with the observed value of 15 Å for 1909 Å. A detailed profile fit was not possible because the rocket profile, although defined by about 40 points, was subject to instrumental rise and decay times. The OAO scans did not have this problem but the number of data points defining the core of the line was never more than 3.

The models were able to match the observations without requiring laser action, but it was necessary to increase the normal abundance of carbon by factors of 10 to 30. Additional and more detailed observations with higher resolution were required to answer questions of laser action, abundance anomalies, and model envelope choices.

Further observations of γ^2 Velorum were made as part of the Goddard guest observer program with the intent to search for periodic light variation in the line which might be associated with laser discharges in the envelope or with pulsational instabilities in the star. In addition, more closely spaced data points in the core of 1909 Å could be used with a knowledge of the instrumental slit function to deconvolve the profile to better than 10 Å resolution.

II. PERIODIC VARIABILITY

The amplitude of the line was monitored by offsetting the spacecraft optical axis by 13 arc min, which shifted 1909 Å into the far ultraviolet spectrometer. The slit of the spectrometer was then stepped in real time until a maximum output signal was observed near the peak of the line. Stellar photometer 1 was used as a background monitor. All data were taken under the best pointing stability obtainable with OAO, i.e. with the boresight startracker control. Readouts of the line and background were taken at 8 second time-intervals throughout the 20 minutes of spacecraft darkness for every orbit throughout 24 hours. Except for those orbits in which the South Atlantic Anomaly background saturated the detectors, all data were of high quality.

The data were analyzed for periodic amplitude variations in the range 0.5 to 200 minutes by T. M. Kelsall of Goddard, who supplied the computer programs and the interpretation of the output. The search was limited to only those amplitude changes which were outside of the noise band, because power spectrum analysis programs for periods hidden in noise require continuous data with equally spaced sample times.

The results of the analysis showed very strong periodic variations in the line and in the background, with a period of 100 minutes. Of course, this is the orbital period of OAO. Variability in the background was due to the anomaly and the small variation in the line was probably caused by thermal cooling distortions during the 20 minutes of night. No other periods were found.

III. LINE PROFILE

Figure 2 illustrates how a highly resolved profile $P(\lambda)$ is smeared by the slit function $S(\lambda)$ to produce the degraded ob-

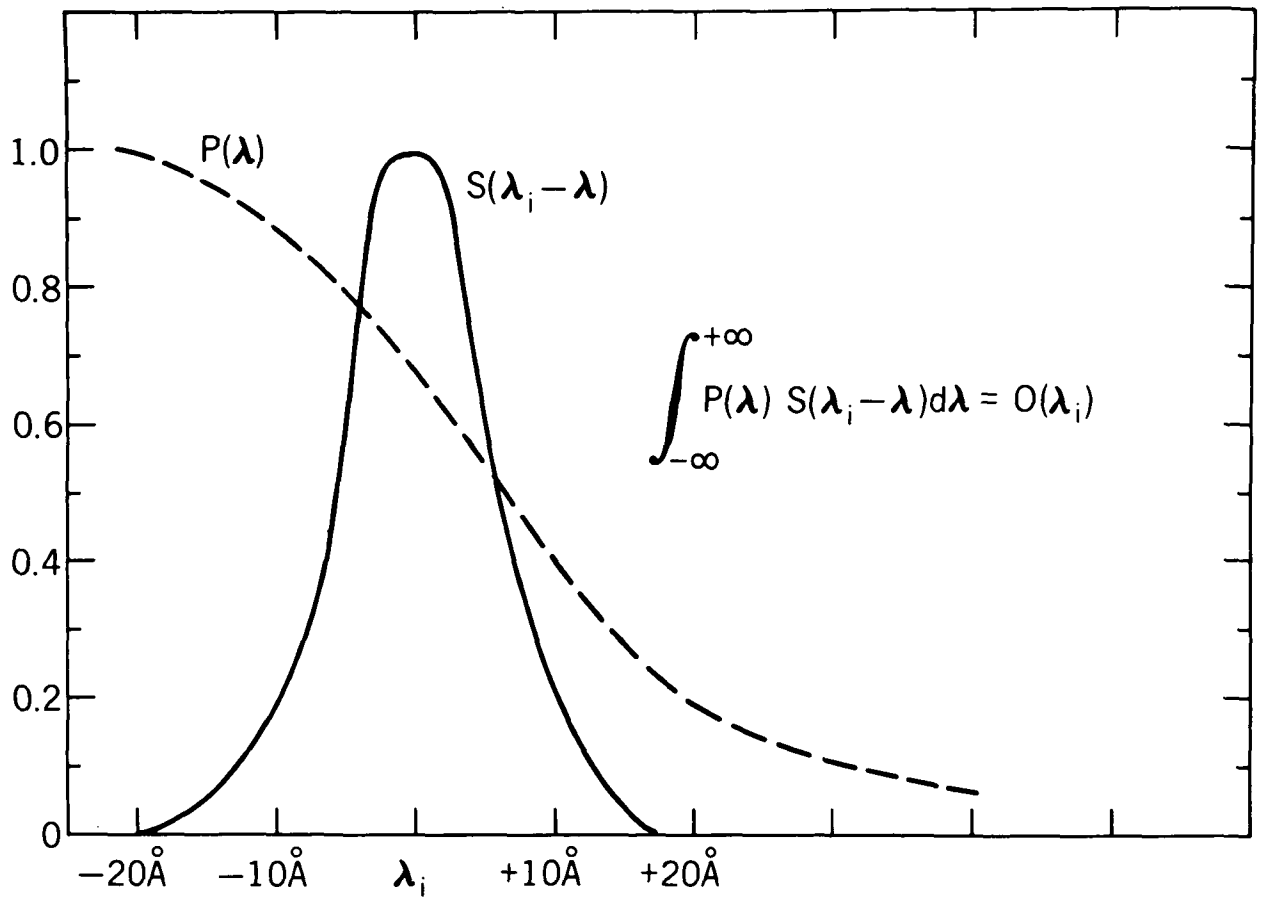

Figure 2.—The relative response of the instrumental slit function as a function of wavelength.

served profile O(λ). The slit function was provided by B. D. Savage of Wisconsin. The shape is nearly Gaussian with a half-width at half-maximum of 6 Å. The slit function is known with an accuracy no better than 10 percent and it is thus not suited for an analytic inverse Laplace transform solution for S(λ). This accuracy, however, is good enough to use the slit function to degrade an assumed or theoretically determined profile and then compare the result with the observed profile.

Line-profile data spaced at about 2.5 Å intervals were obtained by offsetting the spacecraft pointing in small increments of 15 arc sec. The spacecraft was stabilized at each position while about 30 readouts of the line and the background were taken over a period of 6 minutes. All data were taken in spacecraft darkness, in low background, and under boresight startracker control. A total of 12 data points on the line

were obtained over a 5 hour period. This data produced the observed profile O(λ) shown on the left side of Figure 3. The long wavelength side of the line is closely Gaussian in shape but the short wavelength side appears to be depressed in a manner suggestive of an absorption component. No systematic effects in the observing procedures which might produce this kind of asymmetry at 1909 Å were uncovered.

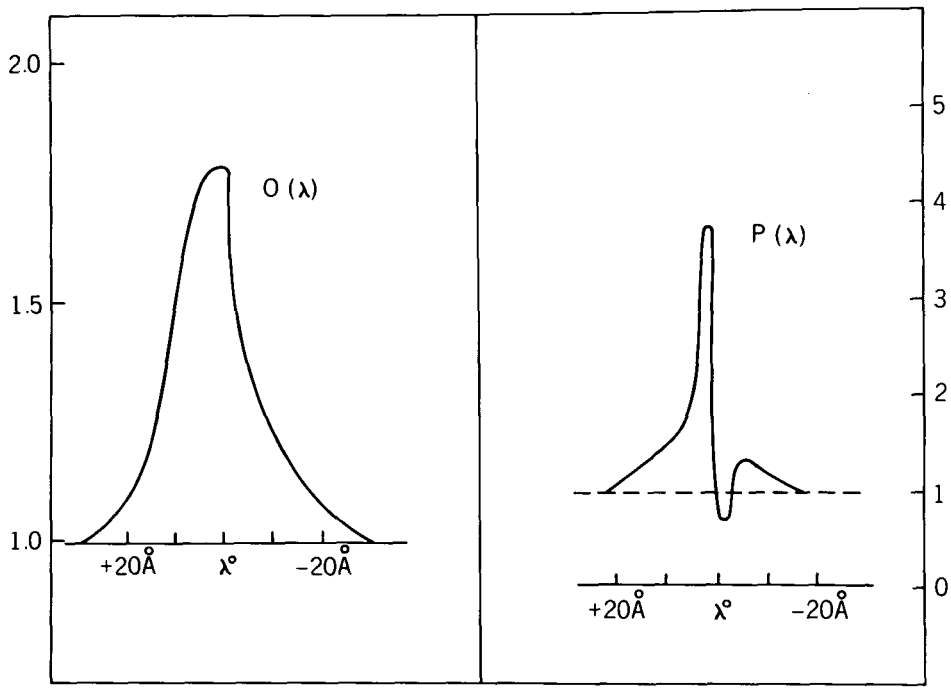

Figure 3.—The observed profile at 1909 Å, O(λ), and the iterative solution profile, P(λ).

The next step was to find a profile which when smeared by the slit function produced the observed profile. An iterative correction method was used in which the integration over the slit function, placed at λ_i, was carried out for an assumed starting profile of Gaussian shape. The result was compared with the observed $O(\lambda_i)$ and a correction was applied to the starting profile. This was done for 50 wavelengths spaced 1 Å apart.

The process was repeated until the difference between the observed profile and the iterated one converged to a small value. Several starting profile shapes were tried, but all converged to about the same shape with the difference between

the observed profile and the final iterated profile being about 10 percent. At this point the solution began slowly to diverge with the emission peak growing higher and the absorption component growing deeper. A typical example of a best-fit profile is shown on the right side of Figure 3. Considering the uncertainties involved in this analysis and the uncertain uniqueness of the solution, the uncertainty on the depth of the absorption and the height of the emission is about 20%. One can be fairly certain, however, that the long wavelength side of the profile must be steeper than the short wavelength side in order to fit the observations.

IV. DISCUSSION

The results of the line variability analysis show no periods in the range of 0.5 to 200 minutes. If periodic amplitude variations exist, they are small, with amplitudes less than ±3%.

An alternative to increased carbon abundance may be found in models with non-spherically symmetric envelopes. The presence of the O star companion could, by the influence of its gravitational field and ultraviolet radiation, perturb non-uniformly the velocity field and the ionization of C III in envelopes of the WR star. Such an effect should be an observable function of phase. The phase of γ^2 Vel was determined from the zero point given by Ganesh and Bappu (1967) and the 78.5 day period. At the time of these observations the phase was found to be 0.90 which places the WR star almost completely behind the O star. In the simple picture of an expanding envelope atoms producing the short wavelength side of the line are located in the hemisphere of the envelope which is facing the observer. At the time of the observation this hemisphere was also facing the O star and could have experienced an increase in the ionization of C III to C IV due to the radiation field of the O star. This would decrease the number of C III atoms producing the short wavelength side of the line and produce the observed asymmetry. Although γ^2 Vel shows some light variability in the visible, it is not known to be an eclipsing variable.

Observations by OAO-2 at different phases could determine if there is a 78.5 variability in the ultraviolet. More detailed geometric models including gravitation and radiative effects of the companion star are needed before we can completely answer important questions of abnormal abundances in γ^2 Vel and other WR stars.

I wish to express my appreciation to A. D. Code for the generous grant of guest observer time on OAO-2. I thank T. E. Houck, M. Molnar and A. Holm for their help in obtaining the observations. I am most grateful to T. M. Kelsall of Goddard for his valuable help in the analysis of time dependent data. I am also very appreciative of T. P. Stecher for his initial

suggestions for the observations. Finally, one must acknowledge the tireless work of the OAO ground crews and project staff at Goddard without whom observations of this type would not be possible.

REFERENCES

Code, A. D., Houck, T. E., McNall, J. F., Bless, R. C. and Lillie, C. F. 1970, Ap. J. 161, 377.
Ganesh, K. S. and Bappu, M. K. V. 1967, Kodaikanal Observatory Bulletins, Series A, No. 183.
Stecher, T. P. 1970, Ap. J. 159, 543.
Stecher, T. P. and West, D. K. 1968, Wolf-Rayet Stars, eds. K. B. Gebbie and R. N. Thomas, N.B.S. Special Publ. 307, p. 221.
_____ 1971, Ap. J. (Letters), in preparation.

Page intentionally left blank

METAL LINE BLANKETING AND OPACITY IN THE ULTRAVIOLET OF ALPHA^2 CANUM VENATICORUM

Michael R. Molnar
University of Colorado
Boulder, Colorado

ABSTRACT

Ultraviolet photometry by OAO-2 was made of α^2 CVn covering the entire $5^d.5$ period of this magnetic Ap variable. The light curves ranging from 1330 Å to 3320 Å indicate the dominant role of rare-earth line-blanketing in redistributing flux. In a broad depression of the continuum covering 2300-2600 Å, scanner observations possibly identify strong lines of Eu III as major contributors to this feature. At maximum intensity of the rare-earth lines, the ultraviolet continuum shortward of 2900 Å is greatly diminished while the longer wavelength regions into the visual become brighter. Thus, the light variations in α^2 CVn are due to the variable strong line-blanketing by the abundant rare-earth elements.

In addition, there is evidence that the hydrogen line opacity is variable and the photoionization edge of Si I at 1680 Å is identified. These ultraviolet observations suggest the importance of metal line-blanketing and opacity in the redistribution of flux in Ap variables.

I. INTRODUCTION

α^2 Canum Venaticorum is one of the brightest ($2^m.9$) and most studied members of the anomalous group of Ap stars whose spectra are characterized by strong and profuse metal lines. This star is well-known for its periodic ($5^d.47$) spectral variations

of line intensities and radial velocities of overabundant rare-earths and iron-peak elements as well as other metals. In addition, there are with the same period a strongly variable magnetic field (-1000 to +2000 gauss) and small variations in light and colors.

Many models have been proposed for α^2 CVn and the most successful at present are the oblique-rotator models advanced by Deutsch (1958), Böhm-Vitense (1966), Kodaira and Unno (1969), Pyper (1969) and Cohen (1970). These models describe the observed periodic phenomena as due to the rotation of the star. A magnetic dipole field inclined to the axis of rotation and concentrations or "patches" of metals on the surface will rotate with the star causing the observed periodic changes. The mapping of these surface metal concentrations for α^2 CVn has been extensively carried out by Pyper (1969) and with her model most of the observed spectral changes can be understood.

These models were made, however, to describe the magnetic and spectral variations neglecting for the most part, or failing to explain, the perplexing problem of the light and color variations. The UBV photometry of Pyper (1969) and scanner observations of Cohen (1970) both show α^2 CVn being reddest and brightest at rare-earth maximum at phase E = 0.0, while it is bluest and faintest at rare-earth minimum at E = 0.5. Such light and color variations cannot be easily explained as the result of a change in temperature. The fact that the equivalent width ratio, Dy II/Dy III, remains constant over the period (Pyper, 1969) gives further support that a temperature change is not the cause of the light and color variations. Cohen (1970) shows that differential line-blanketing (in the visual), as well, cannot explain the changes in light and color.

In this investigation the nature of the light and color variations will be examined using extensive far ultraviolet data from the Wisconsin Experiment Package on board the Orbiting Astronomical Observatory, OAO-2. The design and operation of the spacecraft and experiments are described by Code, Houck, McNall, Bless and Lillie (1970).

II. PHOTOMETRY OBSERVATIONS

The OAO photometry data presented here was obtained by observing α^2 CVn every orbit of 100 minutes for six consecutive days completely covering the $5^d.47$ period. A standard photometry sequence was used which consists of dark readings at the start and conclusion of the filter and calibration source readings. This serves as a check for any changing background radiation from the South Atlantic Anomaly (SAA); however, during this observing run, the SAA never coincided with the spacecraft nighttime when the observations were made. This gave

continuously high-quality data uninterrupted by the SAA throughout the six days of observing.

Table 1 gives the pertinent information concerning the photometry. Only the highest unsaturated gains were used; these are listed along with the number of times each orbit the measurement was made. In addition, the digital counts, minus sky and dark backgrounds and prescaled by 1/64, are given for phase E = 0.0. The relative statistical fluctuations indicate the good quality of these data.

Table 1. OAO Photometry Statistics for α^2 CVn

Filter Wavelength (Å)	Gain (Exposure) (sec)	Observations /Orbit	Signal Counts minus Background × 1/64 Phase E = 0.0	Statistical Fluctuation (±%)
3317	1/8	2	631.3	0.41
2985	1/8	2	533.1	0.44
2945	1/8	2	258.9	0.63
2462	1	1	1403.	0.39
2386	1/8	2	113.5	0.95
1913	8	2	2797.	0.19
1554	8	1	471.5	0.66
1430	8	1	190.5	1.05
1332	8	1	40.5	2.26

Also in this table are the effective wavelengths of the filters for a uniformly flat energy distribution. Note that not all of the available filters were used. The 4250 Å filter was ruinously saturated even at the lowest gain; the 2050 Å filter has severe "pinholes" and the 1680 Å filter has apparently developed opaque patches. The data from these filters were discarded after verifying that they could not be used.

One final note concerning these observations is that the companion, α^1 CVn, was always included in the 10 arc-minute diaphragm because these stars are separated by only 20 arc-seconds; however, its MK type is F0 V and m_V = 5.60. A faint late-type star such as this relative to α^2 CVn is overwhelmed in the far ultraviolet so that, for all intents and purposes, it contributes nothing to the signal.

III. FAR ULTRAVIOLET LIGHT CURVES

The far ultraviolet curves are given in Figure 1 which shows the data for each filter relative to phase E = 0.0 in units of 10%. The phase, E, is calculated from the elements of Farnsworth (1932)

J.D.(Eu II maximum) = J.D. 2419869.720 + 5.46939E.

The most striking feature about these light curves is that the two curves near 2960 Å remain relatively flat while the 3317 Å curve varies nearly in antiphase with the curves around 2300 Å. If we compare the variations of the light curves in the 2300 Å region with the spectral line variations, we find that these curves match remarkably well the curves of the rare-earths in that minimum light occurs at maximum intensity of the rare-earth elements. Upon examining the spectra of the singly and doubly ionized rare-earths, we find that their lines, which are exceedingly numerous, fall heavily between 2000-2900 Å (Dieke, Crosswhite and Dunn 1961). Thus, the filters in this region see strong line-blanketing which is the greatest at maximum intensity of the rare-earths at phase E = 0.0. The evidence strongly suggests so far that the 3317 Å curve is reflecting the redistribution of flux from rare-earth blanketing around 2300 Å; however, the 3317 Å curve peaks at E = 0.1, not at rare-earth maximum at E = 0.0. As we will see later, the 3317 Å light curve is due to another effect.

The three lowest wavelength light curves, 1554, 1430 and 1332 Å, are different than those around 2300 Å. They all have a very strong minimum at E = 0.1 and a second smaller minimum at E = 0.5; however, this feature is not very evident at 1554 Å. Although we can correlate the 2300 Å region light curves with the rare-earths, we encounter great difficulty with these curves. The strong minimum at E = 0.1 cannot be correlated with spectral variations of any metal lines. The secondary minimum, however, does occur at the maximum intensity of the iron-peak elements. In order to discuss the light curves further, the scanner data must be examined.

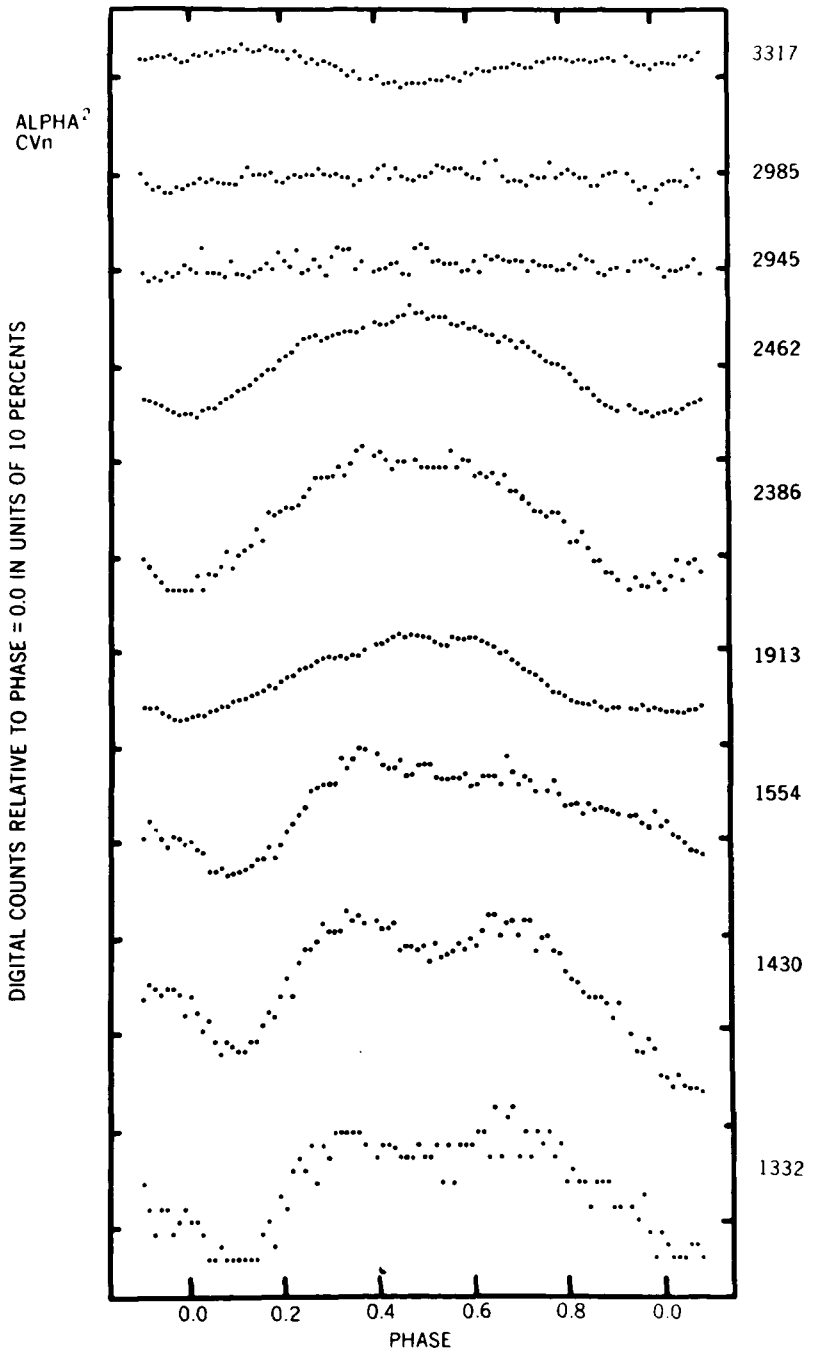

Figure 1.—Far ultraviolet light curves of α^2 CVn in digital counts relative to phase E = 0.0 in units of 10%.

IV. SCANNER OBSERVATIONS

Spectrometer #1 covers the wavelength interval ~1900~3700 Å in 20 Å steps. When these observations were made, the sensitivity had degraded to where the digital output was non-usable even for a star as bright as α^2 CVn. The analog signal can be used, however, so the analog output from six scans at phases near E ~ 0.1 and ~0.5 was averaged and smoothed. These two mean scans are shown in Figure 2 relative to η UMa.

These scans were made with the intention of identifying any large features due to strong line-blanketing by the rare-earths or the iron-peak elements (Underhill 1972). It appears that at E = 0.1, near rare-earth maximum, many features appear stronger; and the strongest feature corresponds, perhaps fortuitously, to the strongest lines of Eu III which is the most overabundant of the rare-earths (Cohen 1970). Although these scans indicate strong blanketing, the higher resolution of OAO-C or SAS-D will be needed to identify some of the numerous lines contributing to the extensive blanketing in this region.

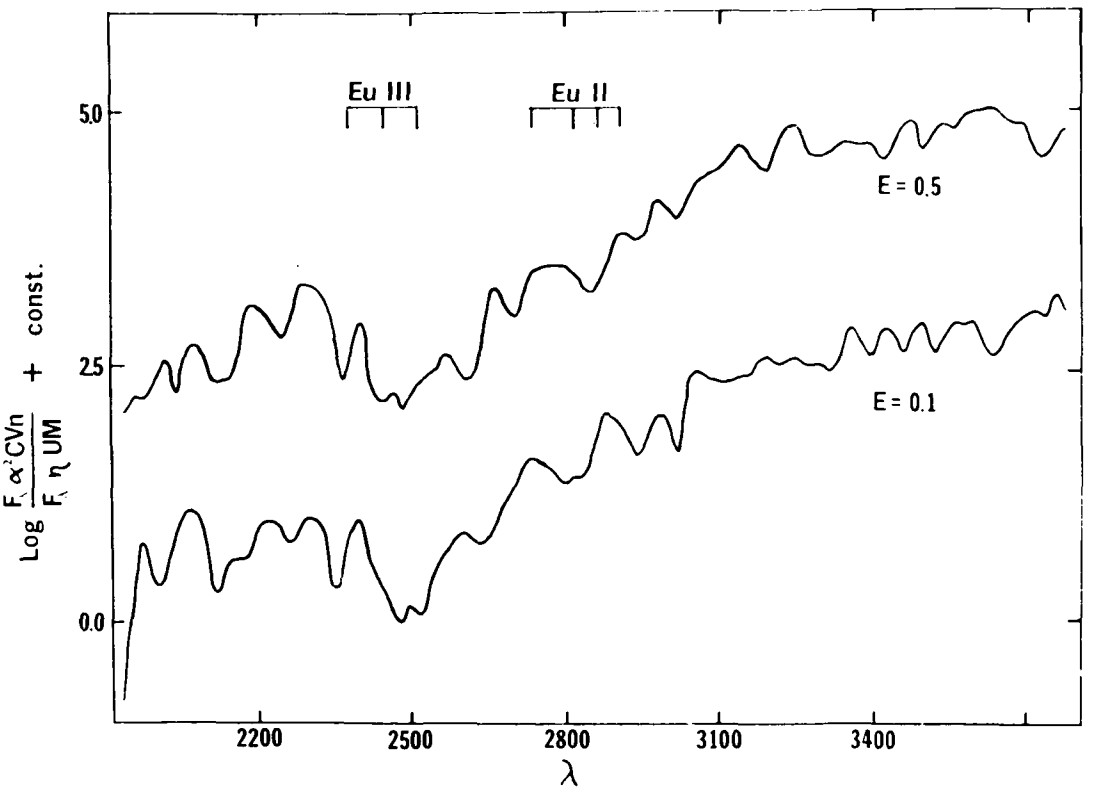

Figure 2.—Mean of six analog scans relative to η UMa for Spectrometer No. 1 at phases E ≈ 0.1, ~0.5.

Spectrometer #2 scans from ~1100~1800 Å in 10 Å steps and Figure 3 shows relative to η UMa two scans averaged together. The dashed line indicates the continuum derived from a scan made with the spacecraft offset from α^2 CVn which shifted the effective wavelength (Code, et al. 1970). No strong spectral variations with phase were noticed in spectrometer #2, so only one mean scan is illustrated.

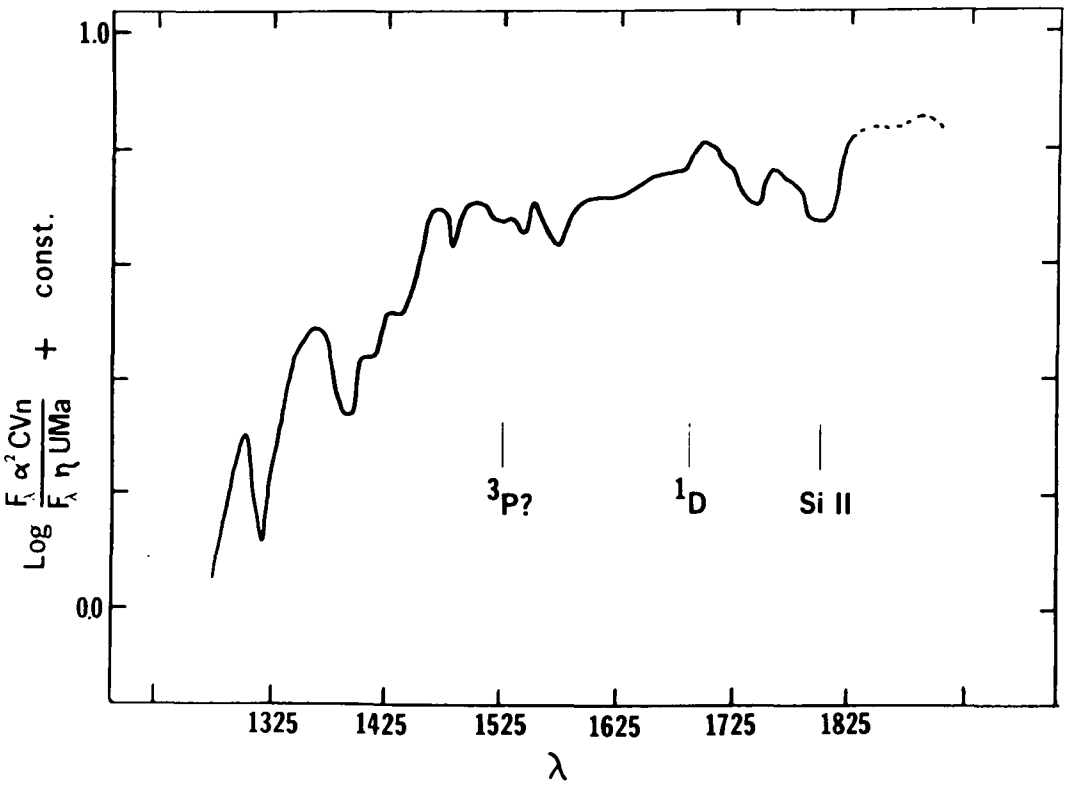

Figure 3.—Mean of two digital scans relative to η UMa for Spectrometer No. 2. Broken line is derived from an offset scan.

The most striking feature is an ionization edge corresponding to the ^1D level of Si I which lies 0.04 volts above the ground level at 1680 Å. Strong silicon edges would be expected in α^2 CVn since silicon is about 50× overabundant (Cohen 1970). It is disappointing, though interesting, not to find the ground level ^3P edge at 1520 Å; however, there may be several reasons why it is not seen. First, if there is a discontinuity, there are lines of Si II and other metals which will mask or "wash out" the edge. Second, Praderie (1969) has shown that as the silicon abundance is increased, the 1680 Å edge grows while the 1520 Å edge is diminished due to a satu-

ration effect of the silicon opacity. We can then expect for α^2 CVn that the 1680 Å edge will be much larger than the 1520 Å edge which might even be too small to be detected. The last important effect to consider is that the continuum opacity in this region is heavily dominated by the confluence of the Lyman lines and notably the broad wing of Lyman-α to such a degree that any additional opacity due to silicon is insignificant (Klinglesmith 1971). This indicates that the edges would be diminished due to the Lyman-α opacity and the 1520 Å edge would be affected more than the upper 1680 Å edge. It is plausible that some combination of these three effects will explain the absence of the 1520 Å edge.

V. DISCUSSION

With these far ultraviolet light curves and scans we can begin to understand the visual light curves. Recently, Wolff and Wolff (1971) have correctly proposed that the photometric variability results from a redistribution of flux, which is caused by variable absorption below 3000 Å. In this work we find that at phase E = 0.0 the rare-earths are at maximum intensity and the line-blanketing around 2300 Å is the strongest. The flux from this region is redistributed into the visual region making the star appear brighter notably in the V filter (Pyper 1969). The V filter photometry shows, in fact, a curve that is exactly in antiphase with the 2300 Å region. The reason that the star is reddest at this phase can be better understood if we first discuss the farthest ultraviolet light curves.

It is noted above that the three lowest wavelength curves are different than the 2300 Å light curves. They have a strong minimum at E = 0.1 which does not correlate with any metal line variations. The secondary minimum at E = 0.5 is much weaker and cannot be attributed to an increasing silicon opacity since the Si II lines are maximum at E = 0.4 (Pyper 1969) rather than E = 0.5. This minimum may be due to the numerous lines of the iron-peak elements in this region which in general reach maximum intensity at E = 0.5. Line-blocking may also explain the minor differences in the 1554 Å light curve from the lower light curves.

Since no metals apparently cause the strong minimum at E = 0.1, we propose that these three light curves are due primarily to variations in the wings of Lyman-α which is the most important opacity source in this region for late B and A type stars. If we are truly seeing variations in the large wing, it might be expected that the amplitude in the 1332 Å curve would be larger than at 1554 Å which is less affected being farther out in the wing. In examining the relative depth of the minima of the curves, a 3% increase in the minimum for the 1332 Å curve is noted with a probable error of 1%.

We further note that the U and B filters, as well as the 3317 Å filter, lie on or near the confluence of the Balmer lines. The ground level for the Balmer lines is the upper level, n = 2, for Lyman-α and we might expect coupling of any Lyman-α variations with the Balmer lines. The U, B (Pyper 1969) and 3317 Å light curves closely resemble the reflection or inverse of the lowest light curves except for the secondary minimum at E = 0.5 which is probably due to lines of the iron-peak elements. These lowest curves are at minimum at E = 0.1 while the light curves in the Balmer confluence are then at maximum which strongly suggests that this is a variation in the strength of the hydrogen lines where the Balmer confluence is in antiphase with Lyman-α. If the amplitudes of the U and B light curves are any indication of the size of the Balmer line variations, they must be on the order of a few per cent or less.

The V light curve is less influenced, if at all, by the confluence of Balmer lines and, as we noted above, it reflects the redistribution of flux from the rare-earth line-blanketing. On the other hand, the U and B light curves are strongly influenced by the Balmer lines and are much less influenced by the redistribution of flux. Thus, the star appears redder, as well as brighter, at E = 0.0 due to a flux redistribution and not a changing temperature. Figure 4 shows the far ultraviolet continuum for 14 CVn, an unreddened B9 V star, and α^2 CVn at two phases which illustrates the severely suppressed continuum of this anomalous star. If energy is to be conserved, the flux removed by blanketing must be redistributed longward which will distort the slope of the Paschen continuum. Scanner observations of the Paschen continuum by Cohen (1970) show, in fact, that the amplitude in the light variation increases proportionately away from the Balmer discontinuity. In the infrared α^2 CVn might have very large light amplitudes. However, we point out that temperatures derived from the continuum slope are adversely affected by the flux redistribution.

VI. SUMMARY

We have seen strong evidence that the light and color variations in α^2 CVn are due to the effects of variable line-blanketing by the rare-earths which is consistent with the oblique-rotator models. Furthermore, the ultraviolet and visual continua are severely distorted by line-blanketing and the redistribution of flux, so that colors will indicate erroneous temperatures.

We have also seen evidence that there may be variations in the hydrogen lines. In addition, it appears that the influence of the hydrogen lines is important in affecting the light curves. On the other hand, the Si I opacity has apparently no

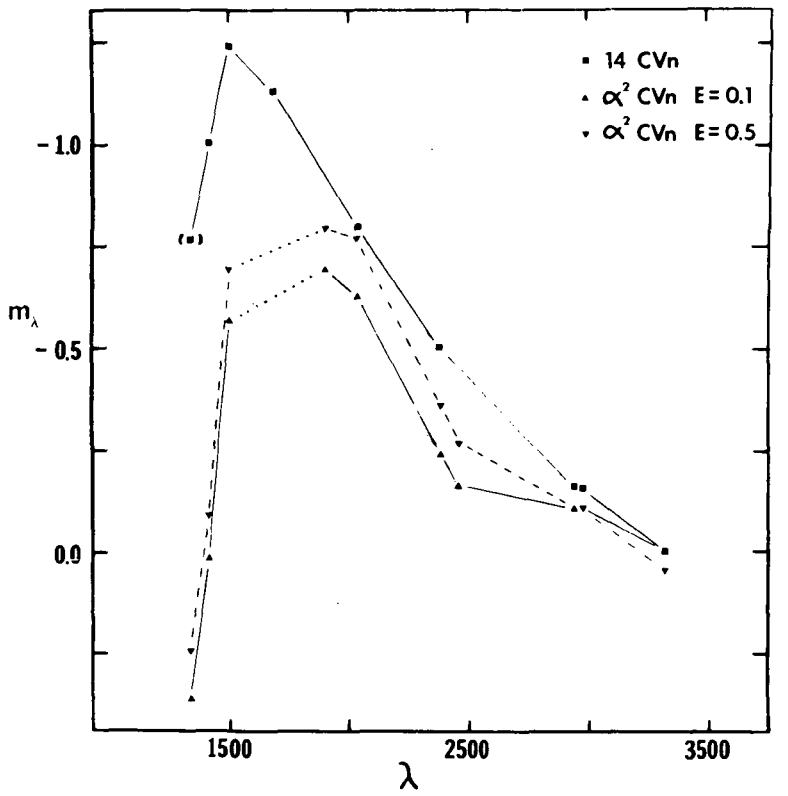

Figure 4.—Far ultraviolet continua of 14 CVn, B9 V and α² CVn at phases E = 0.1, ~0.5.

effect on the curves, although an ionization edge is found.

Based upon these observations, we can predict that the other Ap variables will probably also have variable line-blanketing. The lines of Cr, Fe and Sr are also effective (Underhill 1972) and variations in these should cause light and color changes.

The author wishes to express his gratitude to Professors A. D. Code, R. C. Bless and T. E. Houck and the personnel of the Space Astronomy Laboratory of the University of Wisconsin for the opportunity to work with OAO. And special thanks is given to Dr. A. V. Holm who assisted in taking these data.

REFERENCES

Böhm-Vitense, E. 1966, Zs. F. Ap. 64, 326.
Code, A. D., Houck, T. E., McNall, J. F., Bless, R. C. and Lillie, C. F. 1970, Ap. J. 161, 377.
Cohen, J. G. 1970, Ap. J. 159, 473.
Deutsch, A. J. 1958, Hbd. d. Phys. 53, 689.
Dieke, G. H., Crosswhite, H. M. and Dunn, B. 1961, J. Opt. Soc. Amer. 51, 820.
Farnsworth, G. 1932, Ap. J. 76, 313.
Klinglesmith, D. A. 1971, private communication.
Kodaira, K. and Unno, W. 1969, Ap. J. 157, 769.
Praderie, F. 1969, Proc. Third Harvard-Smithsonian Conference on Stellar Atmospheres, ed. O. Gingerich (Cambridge: M. I. T. Press), p. 215.
Pyper, D. M. 1969, Ap. J. Suppl. 18, 347.
Underhill, A. B. 1972, this volume.
Wolff, S. C. and Wolff, R. J. 1971, A. J. 76, 422.

Page intentionally left blank

COMPARISON OF CELESCOPE MAGNITUDES WITH MODEL ATMOSPHERE FLUXES FOR A, F AND G SUPERGIANTS

Sidney B. Parsons
Warner and Swasey Observatory
Case Western Reserve University
East Cleveland, Ohio

This report concerns preliminary results from a comparison between theory and observation in the ultraviolet for fairly cool stars of high luminosity. During a two week visit to the Smithsonian Astrophysical Observatory, I searched the composite observation file of Project Celescope for all stars of luminosity classes I and II between spectral classes A and G. Fourteen such stars were found, all brighter than V = 6.0; most were observed with the U_2 filter (λ_{eff} ~2400 Å for an F0 star) and a few with U_1 (2600 Å) and/or U_3 (~1750 Å).

Figure 1 shows a color-color diagram for those stars measured with the U_2 Celescope filter: U_2 - V is plotted against B-V. For comparison, we show theoretical colors calculated by Dr. Eric Peytremann from the SAO conference grid of model atmospheres. Computed B-V has been transformed to the observational system above 7000° by the relation* given by Matthews and Sandage (1963) and below 7000° by the relation* I published (1970). The computed U_2 - V index has been shifted down by 3.6 mag; this figure is simply the conversion of visual magnitudes to a scale of -2.5 times the log of the

---

* Unnormalized colors must be used in these relations, so that the normalized computed

$$B\text{-}V = -2.5 \log \frac{\int F_\lambda S_B(\lambda)\, d\lambda}{\int F_\lambda S_V(\lambda)\, d\lambda} \cdot \frac{\int S_V(\lambda)\, d\lambda}{\int S_B(\lambda)\, d\lambda}$$

first must be shifted by about -0.18 (this is a compromise between Peytremann's value of -0.16 and my value of -0.21).

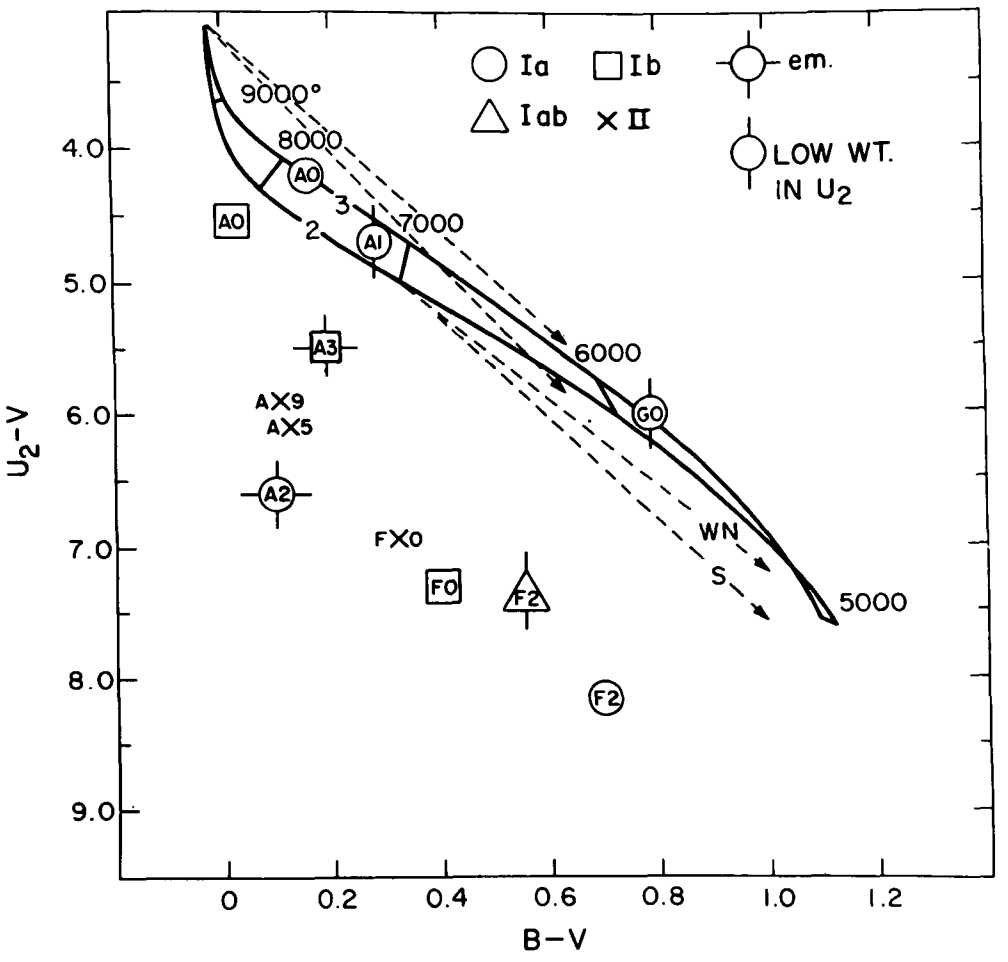

Figure 1.

flux in watts/m^2/m, so we assume here that the calibration of the ultraviolet magnitudes on this scale is essentially correct. The curves are for two surface gravities, log g = 2 and 3, and the dashed lines show the reddening trajectories according to Stecher's observations (1965) and Wickramasinghe and Nandy's model (1968) (parameter x = 0.23) of the ultraviolet interstellar extinction. Since reddening and temperature changes behave in similar ways, separation of these two parameters requires knowledge of the spectral class.

We see that most stars are deficient in ultraviolet flux, relative to the models, by 1.5 to 2 mag. The simplest explanation is that not enough line blocking has been included in the model atmospheres. The quantity 1 minus the blocking coefficient needs to be decreased by a factor of about 5, how-

ever; at 8000° we need to change the 8% assumed blocking coefficient to about 80%, and at 6000° to change the 58% blocking to about 90%. The high microturbulence, ~10 km/sec, deduced for supergiant stars will help to account for such heavy line absorption. On the other hand, the low-resolution ultraviolet spectrum from Gemini XI of Canopus (F0 Ib or II), as analyzed by Kondo, Henize, and Kotila (1970) did not indicate such excessive absorption. The line absorption around 2500 Å appears to be around 50%, similar to Underhill's result (elsewhere in these procedings) for the A6 star δ Doradus. The apparent continuum which Kondo et al . drew for the spectrum did agree reasonably with my model-atmosphere fluxes. If the absolute calibration of the Celescope magnitudes is revised upward, I would be happier than I am with 90% or more line absorption.

Analysis of those stars with U_1 and/or U_3 observations also indicates deficient fluxes, generally about 2 to 3 mag. There is no evidence for strong chromospheric emission except for two G0 stars that may be several magnitudes brighter in U_3 than the models predict, although the identifications for these stars are not certain. Of course G0 is where the Wilson-Bappu effect begins, and more definite and more detailed observations are eagerly awaited. Further analysis of these Celescope data will include the calculation of ultraviolet fluxes from model atmospheres computed by myself and by Eric Peytremann; these differ somewhat from the Smithsonian models.

I am indebted to the Smithsonian Astrophysical Observatory and its staff for making available the data for this study.

REFERENCES

Kondo, Y., Henize, K. G. and Kotila, C. L. 1970, Ap. J. 159, 927.
Matthews, T. A. and Sandage, A. R. 1963, Ap. J. 138, 30.
Parsons, S. B. 1970 Ap. J. 159, 951.
Stecher, T. P. 1965, Ap. J. 142, 1683.
Wickramasinghe, N. C. and Nandy, K. 1968, Nature 219, 1347.

Page intentionally left blank

Mg II 2800 Å EMISSION IN LATE TYPE STARS

Lowell R. Doherty
University of Wisconsin
Madison, Wisconsin

I. INTRODUCTION

Emission in Ca II H and K and the occurrence of He I 10830 Å and 5876 Å absorption in stars of spectral type G and later have been, until recently, the most compelling evidence for the existence of chromospheres in stars other than the sun. Ultraviolet observations of late-type stars are now beginning to extend the list of spectral features which have a direct bearing on our understanding of stellar chromospheres. Strong emission in the 2795, 2803 Å doublet of Mg II has been seen in the rocket spectrum of Arcturus with 7 Å resolution (Kondo 1972) and in OAO-2 scans of Arcturus and a number of other bright K and M stars at 25 Å resolution (Doherty 1971). Rottman et al. (1971) have detected Lyman alpha emission in Arcturus.

The largest body of data on ultraviolet spectra of late-type stars now available is the series of scans made with the long wavelength Spectrometer 1 on board OAO-2. Some features of selected scans from this series and estimates of Mg II emission fluxes were reported earlier (Doherty 1971). Since that time, the effects of sky background, scattered light and variable instrumental sensitivity have become better understood. Additional stars define more clearly the transition from Mg II 2800 Å absorption to emission with advancing spectral type, and additional scans of α Sco provide a better estimate of Mg II emission strength for this supergiant. For these reasons it is appropriate to re-examine the OAO results on Mg II emission here.

II. APPEARANCE OF THE SCANS

Characteristics of Spectrometer 1 and OAO-2 operation have been described by Code et al. (1970). The spectrometer is stepped at intervals of 20 Å and has an exit slot 20 Å wide.

Comparison of OAO-2 planetary scans with the solar spectrum indicates that the actual resolution is closer to 25 Å (B. D. Savage, private communication).

Figure 1 shows averaged scans of three of the brightest K and M stars observed, α Boo (K2 III), α Tau (K5 III) and α Ori (M2 Iab). The dashed lines represent approximately the fluxes that would be observed if these stars radiated as black bodies at the temperatures (θ) indicated. For all of these stars the flux decreases rapidly toward shorter wavelengths and reaches the level of the sky background by about 2300 Å. The radiation temperature, however, is fairly constant over a broad region of the spectrum of each star. Emission at 2800 Å

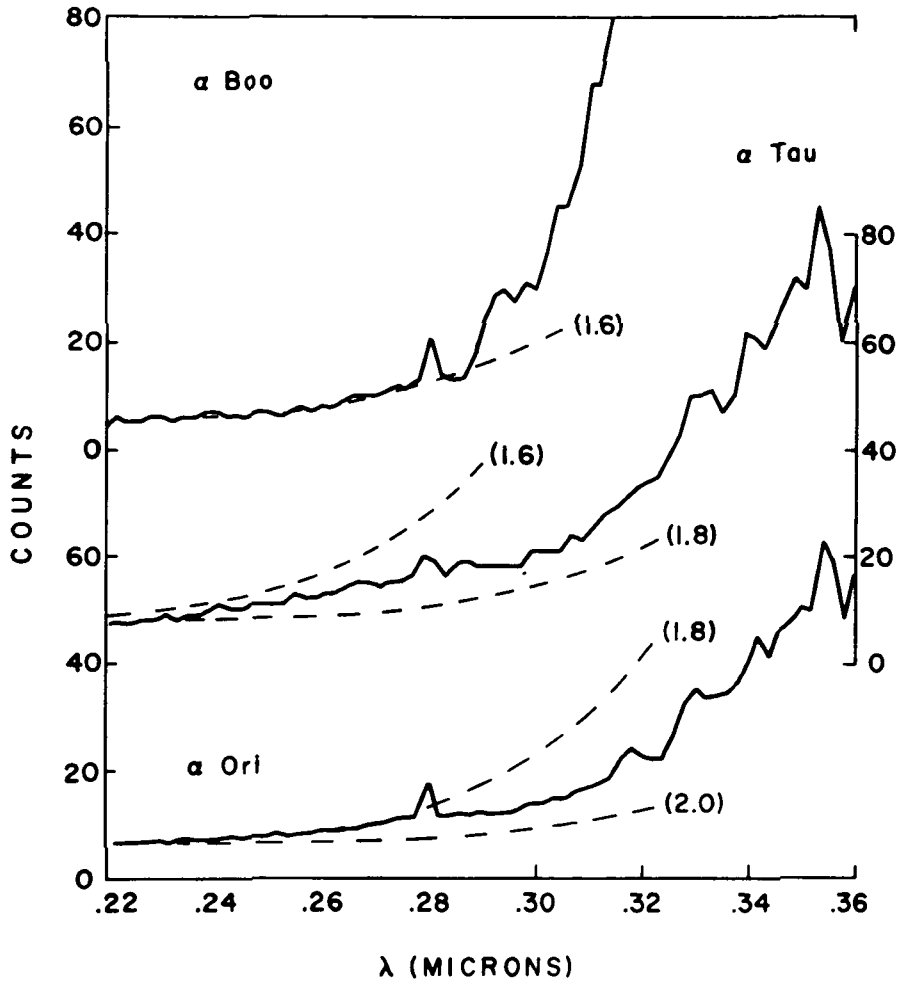

Figure 1.—Averaged OAO scans of α Boo (K2 III), α Tau (K5 III) and α Ori (M2 Iab). The dashed lines show black body fluxes for the temperatures (θ) indicated.

is a prominent feature of all of these scans. The peak near 3180 Å in α Ori is due to emission in a number of Fe II lines (Weymann 1962). No other emission features have been identified in these scans.

Figure 2 shows segments of scans of stars chosen to illustrate the transition from net absorption to emission at 2800 Å. Luminosity classes I, II and III are grouped separately. No wavelengths are indicated in Figure 2. Differences in wavelength registration up to 20 Å between scans are possible due to spacecraft pointing variations, and the scan segments have been plotted so that, numbering from the left, 2800 Å falls between channels 5 and 6. Each segment of 11 channels thus covers 220 Å centered on the Mg II doublet. The approximate level of the sky background is indicated by the short horizontal line next below each scan segment, except for α Sco, where the contribution of the B companion cannot be determined accurately. Pointing variations and therefore wavelength differences are usually quite small for scans made in the same orbit or in closely following orbits, where the same star-tracker configuration is employed. Thus two or more scans can often be averaged, and where this has been done, the number averaged for each segment in Figure 2 is given in parentheses. In the case of β Her and η Dra, both G8 III, the full scans were enough alike to warrant combining the segments for the two stars.

We look first at the qualitative differences in the scans. In β Her and η Dra, the 2800 Å region has three strong absorption features and strongly resembles the solar spectrum seen with the same resolution [see Doherty (1971) or the OAO scan of Mars in Wallace, Caldwell and Savage (1972)]. The flux drops steeply from 2900 Å to the 2852 Å line of Mg I, then falls even lower in the (unresolved) Mg II doublet. A third absorption feature near 2740 Å is due principally to Fe II. With advancing spectral type, the Mg II feature fills in, and is clearly in emission by K2. For class I supergiants, emission appears to dominate by late G. Although β Dra is an MK standard for class II, Kron (1958) lists this star as G2 Ib. The width of Ca II K (Wilson and Bappu 1957) and OAO-2 ultraviolet filter photometry (Doherty 1972) agree with the higher luminosity. Thus I have put β Dra in the class I sequence, where the absence of any Mg II line fits this sequence well. The appearance of Mg II in class II stars more nearly resembles that in class III than in I, and, as far as can be judged from the small number of stars, the transition from absorption to emission takes place at somewhat earlier spectral type than in class III.

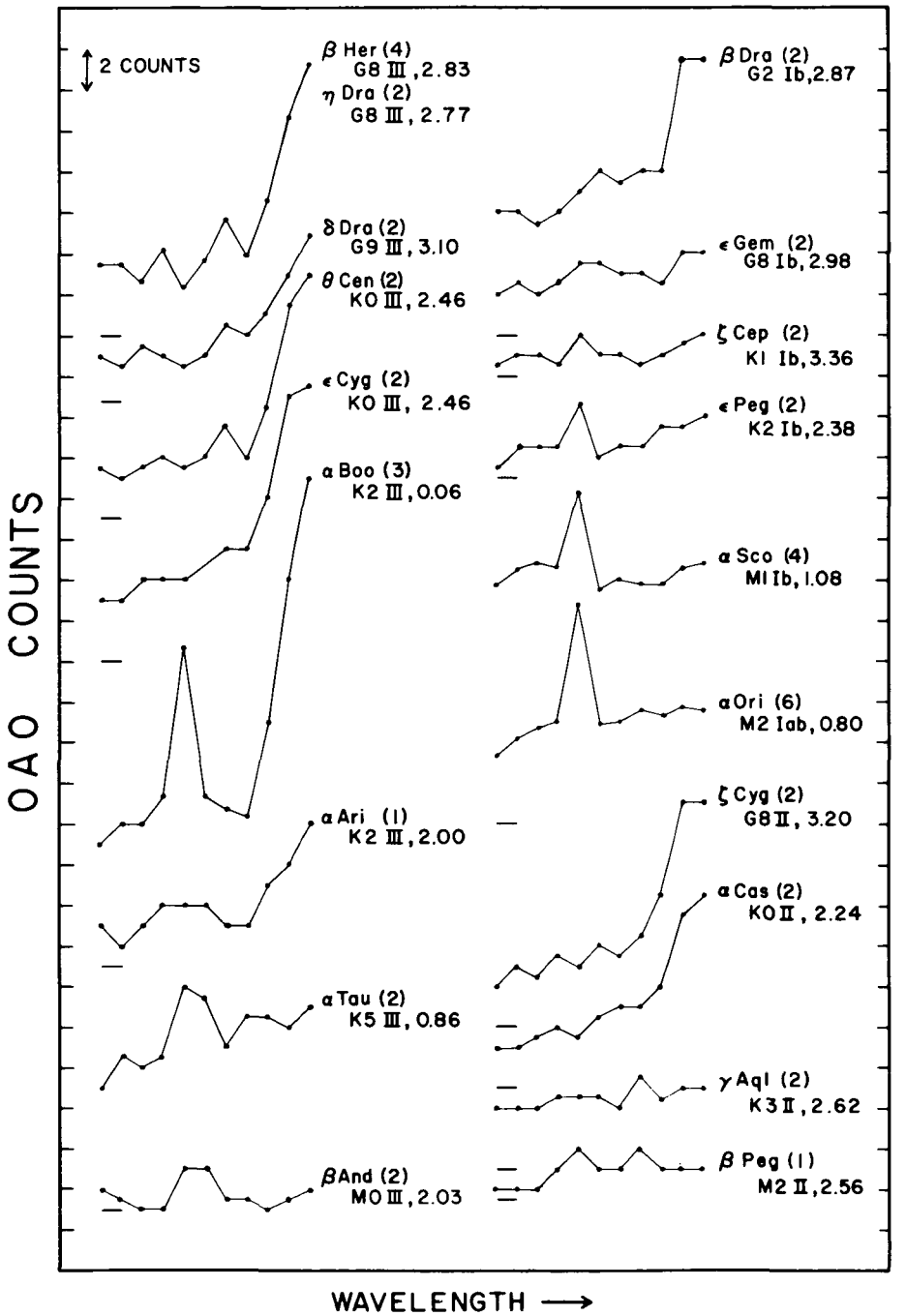

Figure 2.—Averaged OAO scan segments for the region of the Mg II doublet. Each segment covers 220 Å of the spectrum. Numbering from the left, 2800 Å falls between channel 5 and 6. The horizontal line next below each scan shows the level of the sky background. Spectral type, visual magnitude, and number of scans averaged (in parentheses) are given for each star.

III. Mg II EMISSION FLUXES

It is difficult to measure the Mg II emission flux accurately. The strength of the underlying absorption feature is not known but must be significant for many of these stars. No separate measurement of the background of sky plus dark counts is made, and this background must be estimated from the counts at the short wavelength end of the scan, where the contribution from the star is normally negligible. Unfortunately, not all scans cover the full range of the spectrometer. Variation in dark counts during a scan due to the earth's radiation belt can also introduce errors in the estimated background. Only the best scans were selected for Figure 2, and the background indicated for each segment is probably good to one count. Another difficulty in determining Mg II fluxes is the variation in wavelength registration. For some stars, notably α Ori, all the emission appears to fall within a single channel. Mg II H and K are separated by only 7 Å, and if we suppose the widths of the stellar emission cores have the same relation to the width of Ca II K as we observe in the sun, then we can expect one channel to contain all the Mg II emission if this channel is centered between the H and K components. For α Tau and β And, however, the emission is divided equally between two channels. The best interpretation of the α Tau and β And scans would appear to be that these scans are shifted in wavelength by about one-half channel relative to α Ori, rather than that extremely broad Mg II emission cores exist in some stars. Other lines in the scans of α Tau have profiles consistent with a wavelength shift of this amount.

Table 1 gives estimated maximum values for the number of Mg II emission counts in the stars of Figure 2. These values are based on the following assumptions: 1) the underlying absorption profile has the same shape and equivalent width as in the sun, 2) 2800 Å falls either at the center or at the edge of the spectrometer slit, and 3) H and K have equal fluxes, with widths much less than 25 Å. For α Sco the underlying absorption line is taken to be that of a B5 star. For stars with 2800 Å flux greater than the nearby apparent continuum we can determine minimum emission counts, and these are given in Table 1 for eight stars.

Spectrometer 1 sensitivity varied by ±30 percent over intervals of a few days, but no variation is detectable within single scans. To adjust the counts for any star to a standard sensitivity, multiply the counts by the factor f listed in Table 1. This correction factor is determined from a comparison of the 3370 Å narrow-band filter magnitudes of Johnson, Mitchell and Latham (1967) with the scan amplitude in this region after subtraction of the background. The 3370 Å magni-

Table 1

HR	Name	Mg II OAO Counts Max	Min	f	IW (Ca II K)
168	α Cas	2		1.1	
337	β And	4	3	1.4	0.56
617	α Ari	2		1.0	0.48
1231	γ Eri	2		>1.0	
1457	α Tau	10	5	0.7	1.29
2061	α Ori	8	6	0.7	2.23
2473	ε Gem	3	1.5	0.9	0.40
5288	θ Cen	1		1.5	
5340	α Boo	12	8	1.0	2.96
5563	β UMi	1		1.0	0.44
6132	η Dra	1		1.1	0.36
6134	α Sco	6	4		1.85
6148	β Her	1		1.3	0.28
6536	β Dra	4		1.4	1.32
7310	δ Dra	1		1.0	
7525	γ Aql	2		1.0	0.30
7949	ε Cyg	3		0.9	0.43
8115	ζ Cyg	2		0.9	0.15
8308	ε Peg	3	2	1.0	0.86
8465	ζ Cep	1.5	0.5	>1.0	0.24
8775	β Peg	2			0.46

tude of θ Cen was estimated. For faint stars with few 3370 Å counts above sky and for the composite α Sco spectrum, a limiting value of f or no value is tabulated. For the remaining stars, f is known to within about ±10 percent. α Boo is arbitrarily taken as the standard (f = 1). A preliminary calibration of the absolute response of the spectrometer at 2800 Å based on scans of solar-type stars yields the value 4.6×10^{-11} ergs cm^{-2} sec^{-1} per adjusted OAO count.

IV. COMPARISON OF Mg II AND Ca II EMISSION

To what extent the regions that form the Ca II and Mg II H and K lines in stars resemble the solar chromosphere is still largely conjecture. Athay and Skumanich (1968a) have investigated the formation of Ca II emission in a sequence of idealized stellar chromospheres. There is no similar treatment for Mg II. It is known that Mg II and Ca II brightness variations are directly correlated on the solar disk (Fredga 1969). The

eight stars in Table 1 for which maximum and minimum counts are available provide the opportunity to compare Mg and Ca fluxes for a variety of stars that are all quite different from the sun and have a wide range of T_{eff} and gravity. As a measure of total Ca II emission flux at the earth we will take the quantity IW, where I is a measure of the peak flux in the K line and W is the width (km/sec) measured by Wilson and Bappu (1957). Their eye estimates of emission intensity relative to the nearby continuum have been calibrated by Liller (1968). Call this relative intensity I' and define I by the equation

$$I = I'F$$

where F is the continuum flux. To the accuracy required here we may compute F from

$$m = -2.5 \log F$$

where m is the apparent magnitude of the star in the 4000 Å filter of Johnson, Mitchell and Latham (1967). IW can be evaluated for most of the stars in Table 1.

Adjusted Mg II counts are plotted against IW in Figure 3, with the maximum and minimum Mg II values connected by verti-

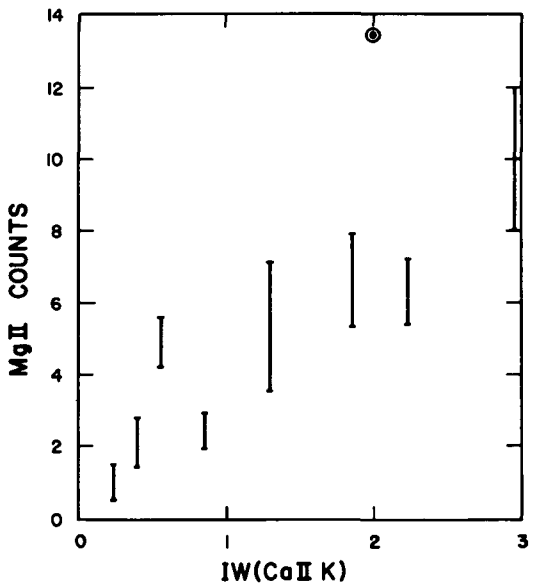

Figure 3.—Mg II 2800 Å emission flux (OAO counts) vs. IW, an approximate measure of Ca II K emission flux. The Mg II counts have been adjusted to a common spectrometer sensitivity (except α Sco), and for α Ori and α Sco the counts have been corrected for differential reddening.

cal bars. Counts for α Ori and α Sco have been increased by 0.3 mag to correct for differential interstellar reddening between 3933 Å and 2800 Å. With the exception of β And the stars in Figure 3 have the same ratios of line strengths within the uncertainties of observation. Unfortunately the uncertainties are rather large. If the underlying absorption features in these stars are actually much weaker than in the sun, then the lower limits in Figure 3 are closer to the true Mg II emission counts. These lower limits determine a single value of Mg II/IW to somewhat better accuracy. In this case Mg II /IW ~ 2.8. The remaining stars in Table 1 for which Ca II K data are available are at least consistent with this value.

Some stellar Ca II K profiles have been observed to change with time (Liller 1968), but there is no evidence for peak intensity differences greater than a few percent. No variations have been detected in the OAO Mg II data. The assumption that each of the two channels showing emission in β And and α Tau measures one component may be wrong. If the resolution is in fact greater than 20 Å and the emission cores in these stars are wide enough, then the number of counts in Table 1 can be too large. How much error this introduces depends on the details of the instrumental and stellar line profiles, which we do not know. It is difficult to reduce the emission by more than about 30 percent by this means alone. However, if the background at 3370 Å in β And is 2 counts lower than the 5 counts assumed in getting the tabulated spectrometer sensitivity, then Mg II for β And could be reduced in total by a factor of 2.

The solar symbol in Figure 3 shows the position the sun would have with V = 0. Solar Mg II counts are estimated from the profiles shown in Athay and Skumanich (1968b) and refer to a moderate level of solar activity. IW is calculated for the quiet sun (Smith 1960). On the basis of Sheeley's (1967) results we may expect IW to increase no more than a factor of 1.4 at solar maximum, so that the sun apparently lies somewhat above the run of stellar points. Considering that the emission line data for the sun and stars depend on different types of measurement, however, we cannot rule out the possibility that all of the stars in Figure 3, including the sun, have nearly the same value of the ratio Mg II/IW.

This research was supported by NASA NAS 5-1348.

REFERENCES

Athay, R. G. and Skumanich, A. 1968a, Ap. J. 152, 141.
_____ 1968b, Solar Phys. 3, 181.
Code, A. D., Houck, T. E., McNall, J. F., Bless, R. C. and Lillie, C. F. 1970, Ap. J. 161, 377.

Doherty, L. R. 1971, Phil. Trans. Roy. Soc. A270, 189.
_____ 1972, this volume.
Fredga, K. 1969, Solar Phys. 9, 358.
Johnson, H. L., Mitchell, R. I. and Latham, A. S. 1967, Comm. Lunar and Planetary Lab., No. 92.
Kondo, Y. 1972, Ap. J. 171, 605.
Kron, G. E. 1958, Pub. A. S. P. 70, 561.
Liller, W. 1968, Ap. J. 151, 589.
Rottman, G. J., Moos, H. W., Barry, J. R. and Henry, R. C. 1971, Ap. J. 165, 661.
Sheeley, N. R. 1967, Ap. J. 147, 1106.
Smith, E. van P. 1960, Ap. J. 132, 202.
Wallace, L., Caldwell, J. J. and Savage, B. D. 1972, Ap. J., in press.
Weymann, R. 1962, Ap. J. 136, 844.
Wilson, O. C. and Bappu, M. K. V. 1957, Ap. J. 125, 661.

Page intentionally left blank

ULTRAVIOLET OBSERVATIONS OF BETA CANIS MAJORIS AND BETA CEPHEI

D. Fischel and W. M. Sparks
National Aeronautics and Space Administration
Goddard Space Flight Center
Greenbelt, Maryland

The star Beta Canis Majoris is a second magnitude B1 II with a radial velocity variation of 6-12 km/sec in a 6^h02^m period. The star Beta Cephei is a $3^m.3$ B2 III with a radial velocity variation of 18-46 km/sec in a 4^h34^m period. Observations of β CMa were taken by OAO-2 on March 12, 1971 with Scanner 2. A typical scan is shown in Figure 1. One can see the H I, Si IV and C IV resonance lines. All parts of the spectrum (lines and continuum) show the 6^h02^m variation.

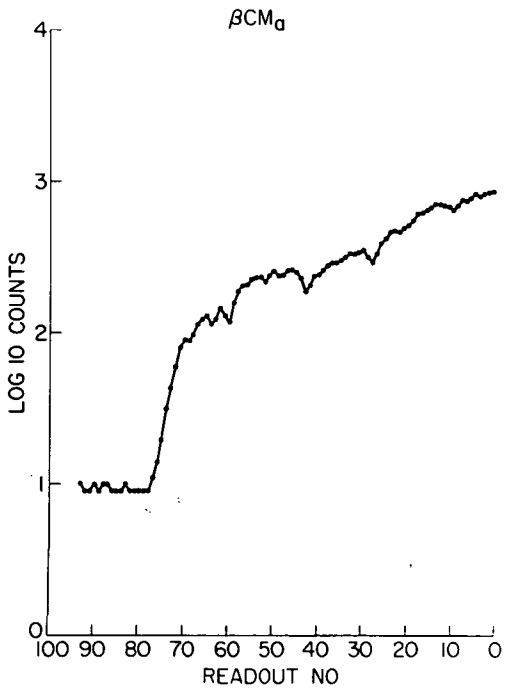

Figure 1.—Log_{10} of the counts versus grating position of Scanner 2 for β CMa on March 12, 1971.

Similar observations of β Cep were taken on April 5, 1971 which are shown in Figure 2. The Si IV and C IV lines are both present and strong. Additional scans were obtained on April 19, 1971, one of which is shown in Figure 3. It is very obvious that the C IV line has disappeared. Because of this unusual effect, more data was obtained on the 6, 7, 8, 9, 11, 13, 15, 17, 18, 19 and 20 of June 1971. A total of 64 scans of β Cep, covering 400 cycles of the 4^h34^m pulsation over 76 days were obtained.

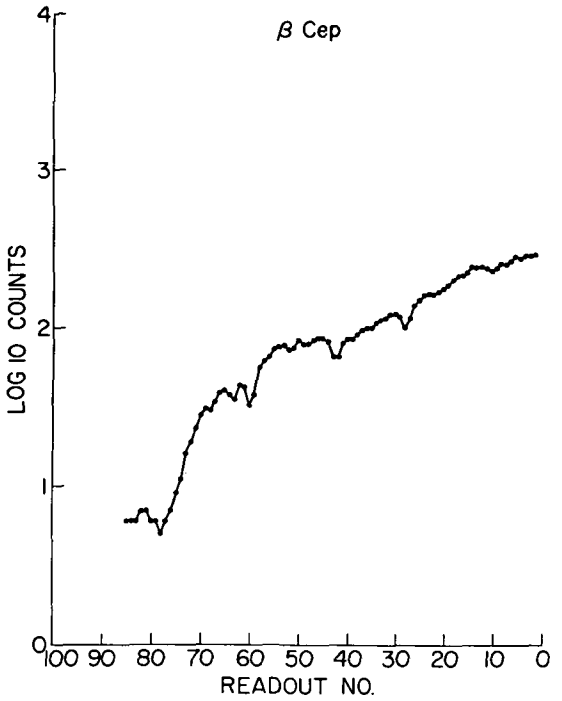

Figure 2.—Same as Figure 1 for β Cep on April 5, 1971.

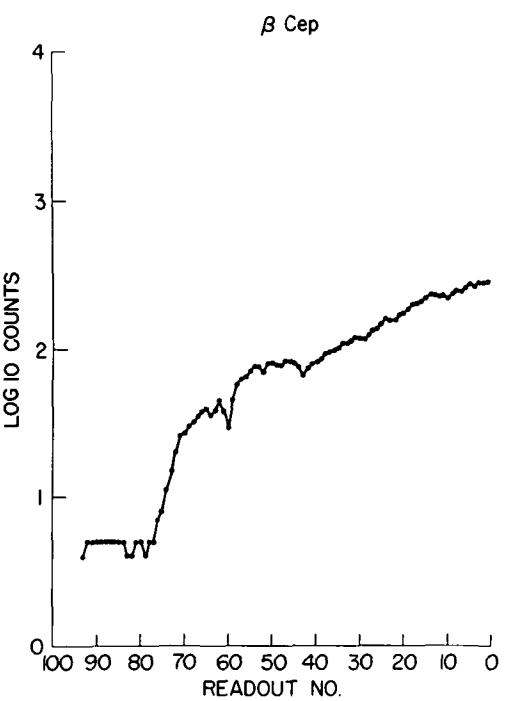

Figure 3.—Same as Figure 2 on April 19, 1971.

The bottom of Figure 4 shows the light curve at 1570 Å, the continuum near the C IV line at 1550 Å. The phase is over the 4^h34^m pulsation. The upper curve is at 1550 Å, which is approximately the center of the C IV line. The lower points on this curve occur when the line is very strong and the upper when it is weak. The earliest data are shown, for convenience, with special symbols. (Julian Day 47 is April 6, 1971, day 61 is April 19, day 109 is June 6, etc.) Looking at the X's which represent data taken on June 8 and 9, we see the short period variation is the same as the continuum.

Figure 5 shows the "equivalent width" in counts for the C IV line using data at 1540, 1550 and 1500 Å with the continuum being drawn between 1530 and 1570 Å. The variation at 1530 Å is the same as that at 1570 Å. The phase is over a

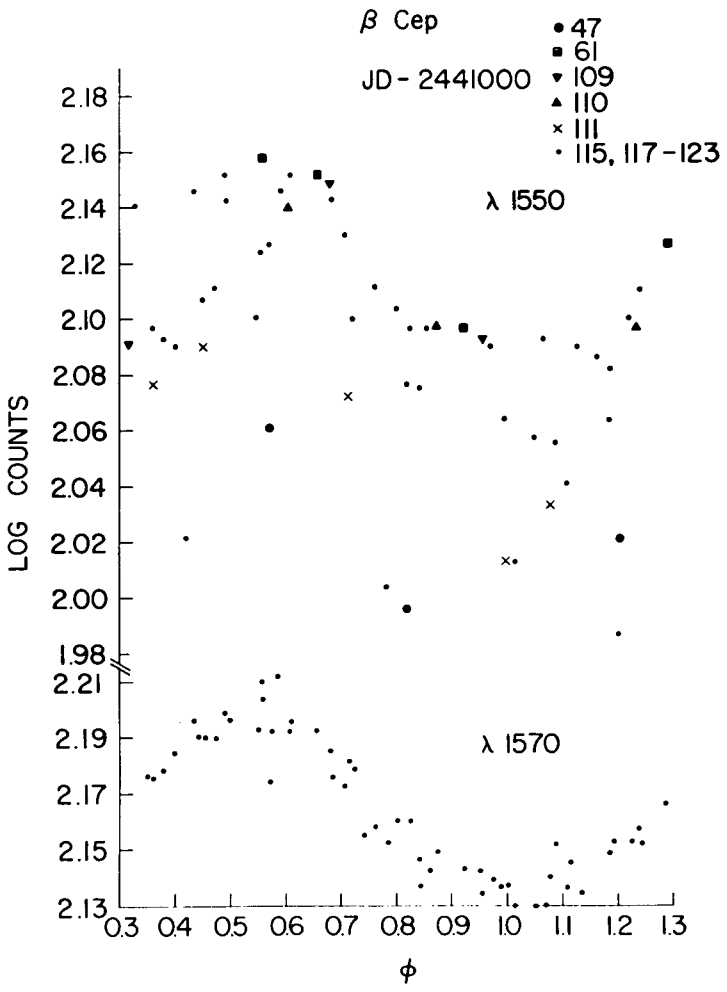

Figure 4.—Log₁₀ of the counts versus phase of 4^h34^m period of β Cep. The lower curve is at 1570 Å, the upper curve at 1550 Å. See text.

period of 6 days. The estimated uncertainty is less than ± 1/4 day. The 4^h34^m variation has not been removed from the equivalent widths because of the difficulty in estimating the amplitude of the short period variation. There is no six day variation in the continuum.

The C IV line is very luminosity sensitive whereas Si IV is not (Sparks and Fischel, 1971 NASA SP-3060 and Code, Utrecht Meeting).

We can only hypothesize three possible mechanisms giving rise to such an effect: a beat phenomenon, shock waves or tidal distortions. If it is a beat phenomenon, the other pulsation has a period of 4^h34^m and no such variations are known.

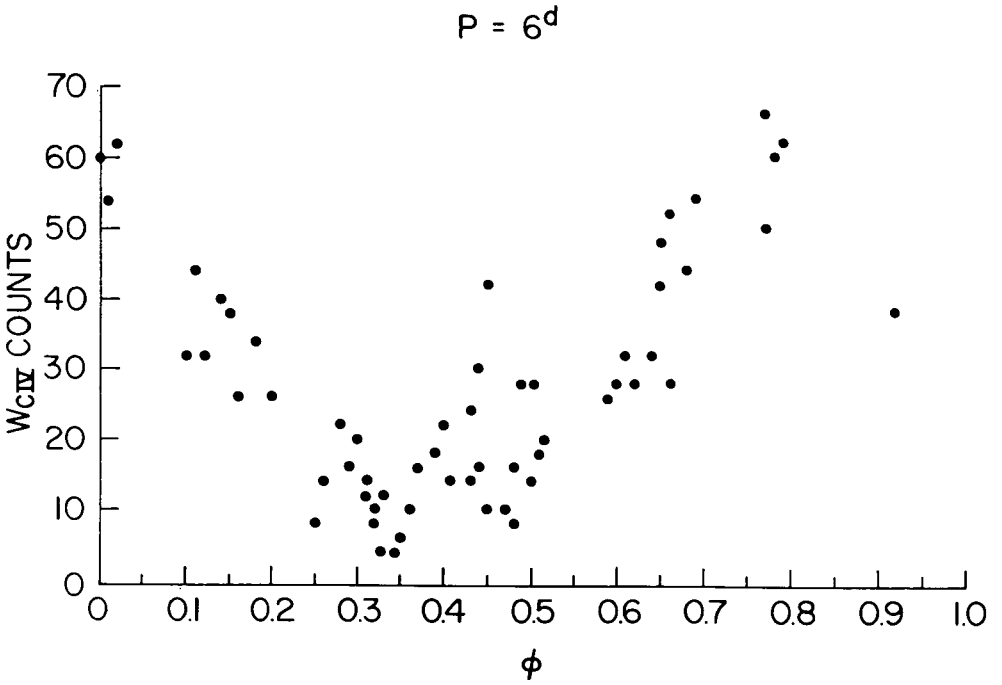

Figure 5.—The "equivalent width" of the C IV line 1550 Å versus phase over 6^d period.

It is difficult to understand how a shock wave would affect only C IV and not have any thermal effects on the continuum or Si IV.

A tidal effect is possible. Fitch (1969) has presented evidence that β Cep is a single line spectroscopic variable with a period of approximately $10^d.9$, and an eccentricity of approximately 0.5. The mass function and $\underline{a}\sin\underline{i}$ that he obtained are very low. However, the mean radial velocity due to binary motion of about 3 km/sec makes the analysis difficult.

If the effect is due to tidal distortion, the period of revolution could be 12 days if the inclination is sufficiently small to keep one tidal bulge out of sight and large enough to keep the secondary from eclipsing the primary.

In any event, future analyses of β Cephei will have to account for the periodic variation of the C IV resonance line.

The authors gratefully acknowledge the University of Wisconsin for the opportunity to obtain this data and to Drs. M. R. Molnar and A. V. Holm for their advice and assistance.

REFERENCES

Fitch, W. S. 1969, Ap. J. 158, 269.

SPECTROPHOTOMETRY OF BETA LYRAE

Theodore E. Houck
University of Wisconsin
Madison, Wisconsin

Two hundred and fourteen scans over the wavelength region 1100 Å to 1800 Å with 10 Å resolution were obtained for the eclipsing binary Beta Lyrae between JD 2440889.5 and JD 2440904.5. The scans were made regularly at 100 minute intervals corresponding to 0.0054 intervals of the binary's cycle and extend from phase -0.245 to +0.912. Exposure times were 8 seconds per 10 Å step. Correcting for the 1/64 prescaler, the count rate was typically of the order of 16,000 counts per exposure at 1800 Å decreasing to about 300 counts per exposure in the vicinity of Lyman alpha, both measures above a typical background count of 300 counts per exposure. Except at primary and secondary minima (where the star was too faint), the OAO spacecraft was kept under Boresight Tracker control to reduce wavelength shifts in the objective grating spectrometer due to errors in pointing to less than 1 Å and all scans were made in the same direction, 1800 Å to 1100 Å, to reduce effects of backlash in the grating drive, the scanner being reset to the long wavelength end while the star was being occulted by the earth. All scans were made while the spacecraft was in the earth's shadow and the extinction of the star by the earth's atmosphere could be observed during the reverse resetting scan.

While computer reduction of the resulting 18,000 measurements is still in progress, some preliminary results can be indicated. Figure 1 shows the average of four successive scans near primary minimum compared with four scans at phase 0.25 and similarly Figure 2 compares a four scan average near secondary minimum with the average scan at phase 0.25. In all cases the scans have been corrected for a possible variable background count by using the dark readings of Stellar Photometer No. 2 to monitor the effects of the radiation belt, and a preliminary calibration of the spectrometer has been applied to reduce the raw data to a relative energy per unit wavelength. It should be emphasized that because of the preliminary nature of the calibration for the spectrometer, the resulting curves may be in error, particularly at the short wavelength end, but since the same calibration reduction was made to all data pre-

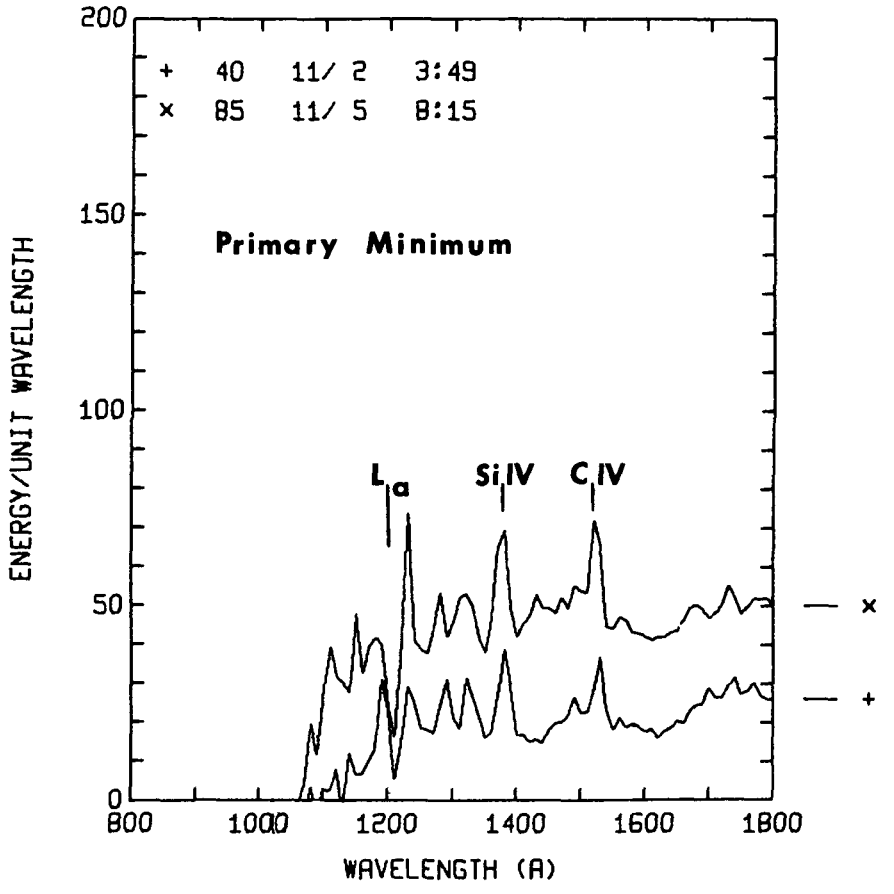

Figure 1.

sented here, a relative comparison of the scans remains valid. The data in the upper left corners of Figures 1 and 2 are simply a running number identifying the first scan of the four scan average and the GMT month, day, hour and minute of the average scan or the center point of the 0.021 phase interval covered by the four scans.

Several points are illustrated by Figures 1 and 2.

1. The intensity at primary minimum is almost exactly one-half that at maximum, i.e., over the wavelength region covered, the primary eclipse is less deep than in the visual or longer ultraviolet wavelengths. This trend is also shown in simultaneous filter photometry light curves of the following paper (Kondo, McCluskey and Houck 1972).

2. Except for the 1100-1200 Å region, the depth of the primary eclipse appears remarkably independent of wavelength. It should be remembered that for the 1100-1200 Å region the signal is less than the background noise and a small error in

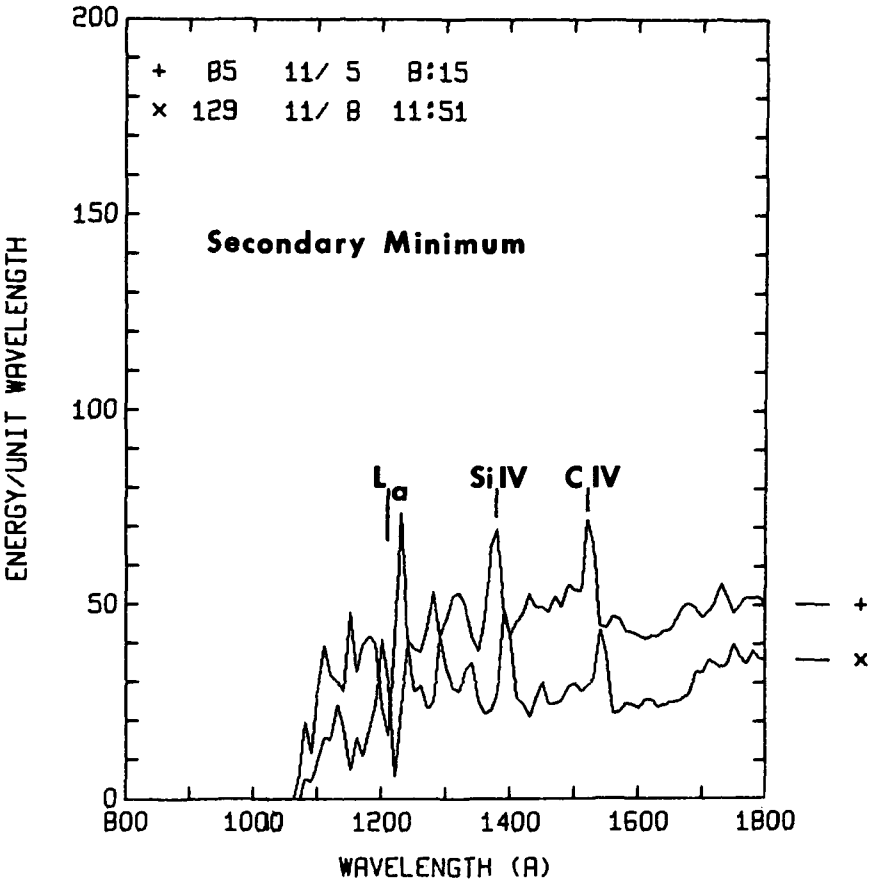

Figure 2.

the latter will more seriously affect the reduced curve.

3. The energy distribution at secondary minimum is similar to that at primary and again about half that of maximum and similarly independent of wavelength; thus, the secondary eclipse cannot be a geometric eclipse of a star of later spectral type than the primary whose energy distribution approximates that of a normal star.

4. While identification of spectral lines at a 10 Å resolution is difficult, the two most prominent emission lines, other than the features near Lyman α, match well both in position and intensity with Si IV and C IV emission observed in the Wolf-Rayet star γ Vel, and if so would seem to imply an exciting source of rather high temperature.

5. As can be seen in Figures 1 and 2, the emission lines, other than the features near Lyman α, do not show appreciable variation with phase and must therefore arise from a region which is largely unaffected by the geometrical eclipse.

The primary variation in the scans is the feature near the interstellar Lyman α. This is shown in more detail in Figure 3 which shows a sample of four scan averages from 1100-1400 Å, with the phase indicated in degrees. The interstellar Lyman α absorption line is indicated, and on either side there appear to be emission features which vary with phase from 0° to 180° and are relatively constant from 180° to 360°. It should be remembered that with the 10 Å resolution, the line profiles are essentially instrumental, and do not represent the true profiles of the star. With the low resolution of the spectrometer one cannot rule out the possibility that the features of interest arise from variable spectral lines adjacent to Lyman α, but it is exceedingly tempting to interpret them as arising from an interplay between the interstellar Lyman α absorption line and a broad emission Lyman α line in β Lyrae which is Doppler shifted by the varying geometry of the system.

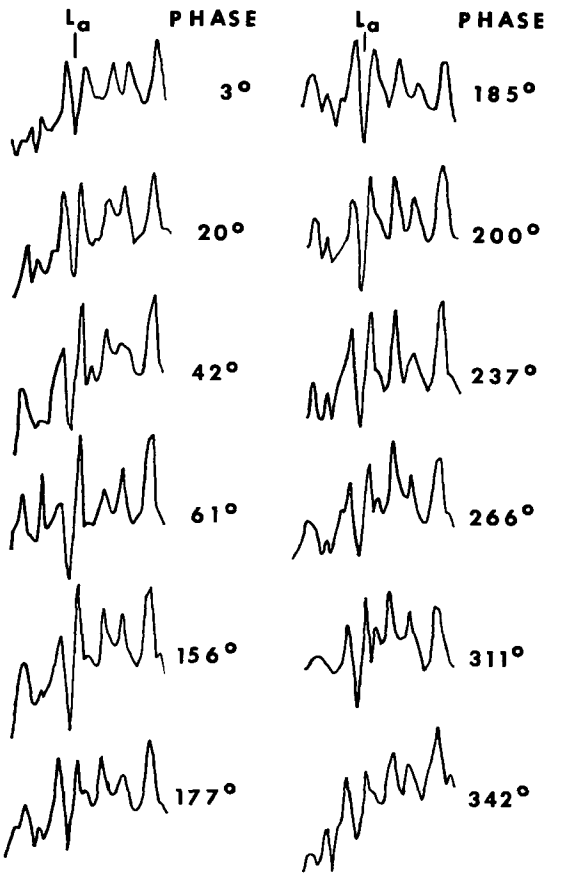

Figure 3.

Suppose the assumed Lyman α emission has a comparable width because of Doppler broadening to the interstellar line, then a portion of the emission line will lie in the wings of the interstellar line where the absorption is less than unity and can be detected by the low resolution spectrometer. If the radial velocity of the emission matches that of the interstellar absorption, equal intensities would be observed on either side of the center wavelength. If the emission line as a whole is now Doppler shifted in either direction, a corresponding increase in intensity will be observed on the appropriate side of the center wavelength even if the resolution of the spectrometer is low compared to the Doppler wavelength shift. In short, the interstellar line acts as a discriminator converting the frequency modulated Lyman α emission into an amplitude modulated signal of the low resolution spectrometer. Ideally if the instrumental profile is known with sufficient accuracy, and the interstellar absorption profile is also known with comparable accuracy, radial velocity effects can then be measured where the wavelength shift is considerably smaller than the wavelength resolution of the detecting spectrometer. The alternative interpretation that the emission feature on the longward side of Lyman α results from a variation in strengths of other lines such as N V, 1240 Å, is far less attractive. It would require a very asymmetric spatial or temporal variation not shared by any other line in the spectrum of β Lyrae.

Since the scans in the vicinity of Lyman α show primarily emission features and the location of the continuum is uncertain, Figure 4 shows a plot of L/S vs. phase of β Lyrae, where L equals the height of the longward emission feature above the bottom of the interstellar Lyman α core and S is the height of the shortward feature. By choosing the interstellar Lyman α core as a reference, a direct quantitative interpretation is difficult, but the figure does show that the variation is well correlated with the phase of the binary system. The dots and crosses in the figure separate the overlap in the observations beyond a single cycle of the binary system. The figures at the top indicate the orientation of the system where the primary is defined as the object producing the spectral lines in the visual used to determine the radial velocity curve of the system as a spectroscopic binary.

One might end with the speculation that if the variation in features observed is correctly interpreted as resulting from Doppler shifted Lyman α, Figure 4 would seem to imply that either there is a strong local influx of hydrogen on the "backside" of the secondary with velocities of the order of several hundred km/sec which is obscured between phase 180°-360° by the secondary, or that the shortward shifted Lyman α emission is selectively absorbed within the cloud surrounding the binary system.

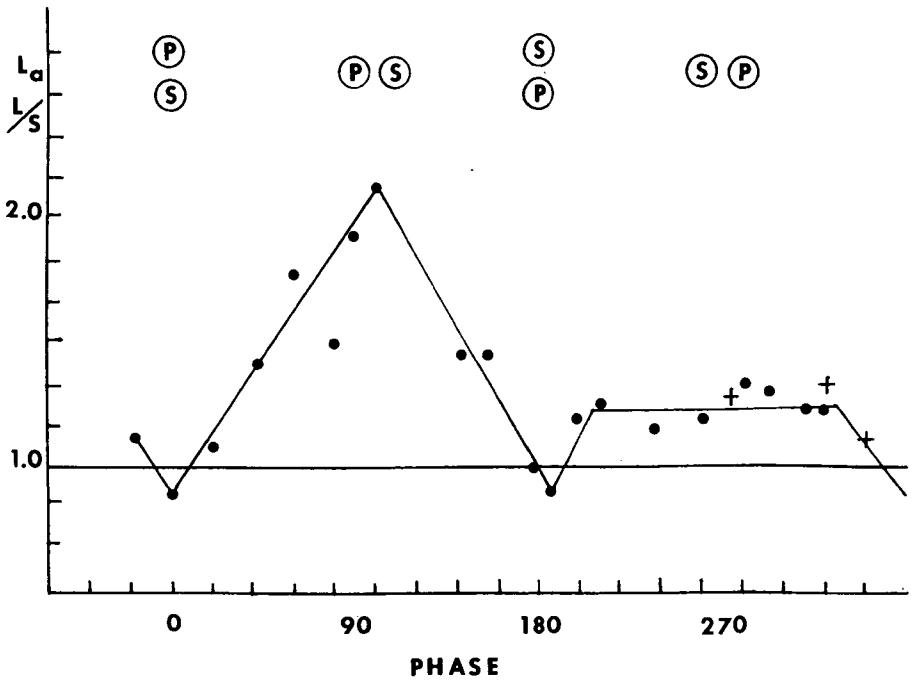

Figure 4.

The author is highly indebted to Mr. T. Jones for the computer programs involved in generating Figures 1-3, and to NASA and Grumman personnel for the existence and operation of the spacecraft.

REFERENCES

Kondo, McCluskey and Houck 1972, this volume.

OAO-2 OBSERVATIONS OF BETA LYRAE

AND A PROVISIONAL INTERPRETATION

Yoji Kondo
National Aeronautics and Space Administration
Manned Spacecraft Center
Houston, Texas

George E. McCluskey, Jr.
Lehigh University
Bethlehem, Pennsylvania

Theodore E. Houck
University of Wisconsin
Madison, Wisconsin

ABSTRACT

Six-color ultraviolet photoelectric observations of Beta Lyrae obtained with OAO-2 are presented. These observations, made at 1380, 1500, 1920, 2460, 2980 and 3330 Å, represent the first truly continual coverage of the light changes of Beta Lyrae during one orbital revolution and were obtained in November 1970. The photometric data are supplemented by spectral scans in the wavelength intervals 3800-1800 Å and 2000-1050 Å; the latter interval was scanned at 10 Å resolution once during every OAO-2 orbit, i.e., about 100 minutes. Anomalous features, such as asymmetries and short and long term variations, are present in the light curves. A tentative discussion of solutions of the light curves is given. The problems of combining the photometric and spectroscopic information to arrive at a model of the system are also discussed.

I. INTRODUCTION

This paper reports on ultraviolet photoelectric observations of Beta Lyrae obtained with OAO-2. This eclipsing

binary system has been studied extensively both observationally and theoretically during much of this century. The properties of the system have been reviewed by Struve (1958) and Huang (1963) among others. Because of the wide spread interest in this binary system, and also in view of the desirability of concerted continual effort to observe the entire orbital period of the system, an internationally coordinated campaign to observe Beta Lyrae was conducted in 1958-59 and again this year.

II. OBSERVATIONS

The six-color ultraviolet light curves to be discussed in this paper represent the first continual coverage of a single cycle of Beta Lyrae and were obtained in November 1970. During this period, 10 Å resolution spectral scans from 1800-1100 Å were made once during each OAO-2 orbit; the period of revolution of OAO-2 is about 100 minutes, with simultaneous filter photometry measurements at each step of the scan. On alternate orbits the filters used were 2980 Å, 2460 Å, 1500 Å and 3300 Å, 1920 Å, 1380 Å. The filters have a typical half width of 200 Å. One observing sequence consists of about eighty 8-second filter exposures plus a spectrometer scan. Only about 10% of the available observations were utilized in this discussion. In addition, the spectral energy distribution of the system was observed at various phase angles in the wavelength interval 3800-1800 Å with a resolution of about 20 Å; and from 2000-1100 Å at a resolution of about 10 Å.

The light curves shown in Figure 1 were drawn through the observed points, and the flux has been arbitrarily chosen to be unity at maxima. The estimated error of observation was typically less than 0.01 magnitude.

The coverage of the light curves begins at about phase angle -90° and continues for a little more than one orbital period. A number of interesting anomalies are present. Short term variations with a time scale on the order of 5-20 hours and amplitudes of $0^m.01$ to $0^m.05$ occur in all wavelengths. Several of these, particularly the features at phases of about 5°, 220° and 300° occur in several, if not all, of the wavelengths. The maxima also show prominent short term variations. A long term, i.e., on the order of an orbital period or so, variation is prominent at 1380 Å and 1500 Å. The light level decreased by nearly 20% at 1380 Å in about 13 days and decreased by about 9% at 1500 Å between phases 90° and 270°. The 3330 Å light curve shows an increase in brightness of about 5% between phases -90° and 90°. The light curve at 1920 Å has eclipses which are much shallower than those in the other wavelengths. The eclipses are asymmetric in all wavelengths as are the

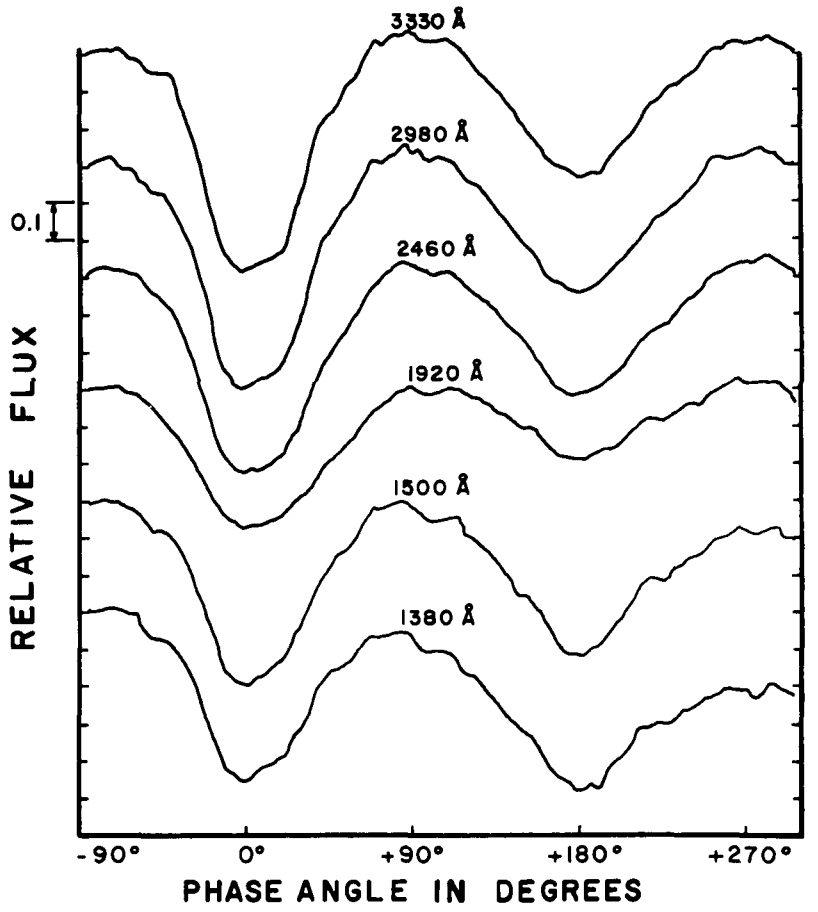

Figure 1.

maxima. Another anomaly is the fact that the depth of the secondary eclipse becomes deeper at 2460 Å, 1500 Å and 1380 Å than it is at 3330 Å, 2980 Å and 1920 Å. It should be emphasized that there is excellent reason to believe that the performance of the OAO-2 provides a high degree of confidence in the reality of the observed anomalies.

III. ANALYSIS AND INTERPRETATION

a) Light elements

An attempt was made to determine the epoch of the mid-primary eclipse from the OAO-2 observations, but difficulty was encountered due to the asymmetry of shape of the eclipse, and the fact that additional observations made with OAO-2 over a two year period are too scattered in time to aid in deter-

mining the time of minimum. Consequently, for this preliminary analysis, previously published light elements by Wood and Forbes (1963), which appeared to give a reasonable time of minimum light, were used. The phase zero computed from the above elements is JD2440892.66132 and P = $12^{d}.932724$. In order to determine whether or not this time of minimum might be in error, the minimum was arbitrarily shifted by ±3° and ±6°. This generally increased the asymmetry of the primary eclipse and did not improve the situation. The coordinated international campaign on Beta Lyr being conducted this year under coordination by Dr. Batten at the Dominion Astrophysical Observatory is expected to produce an improved ephemeris for this system.

b) Rectification

Rectification was carried out following the technique developed by Merrill (1970). The coefficients are listed in Table 1. The coefficients were determined through 4θ. Sine terms were not negligible. The rectification yielded maximum light which was reasonably constant. However, the eclipses still showed pronounced asymmetries both for the primary and secondary minima. For comparison, ground-based observations in visual light by Wood and Walker (1960) were incorporated into this work. The rectified visual observations also exhibited asymmetries in the eclipses.

c) Discussion

The form of the light curves suggested that the egress of the primary eclipse was anomalous. It was felt, therefore, that taking an average of both branches was unadvisable. Solutions were made separately for the ingress and the egress. Solutions were indeterminate for the 1380 Å, 1500 Å and 1920 Å light curves: this point will be amplified later on. No satisfactory solutions were found for the egress at any wavelength. The resulting solution from the ingress is presented in Table 2. The fit of the solution with the rectified light curve is reasonable. However, the light curve solution is difficult to reconcile with the spectroscopic observations. The spectroscopic observations show only one component of the binary, which we shall herein call the primary component, although variable emission features have been associated with the secondary component by some investigators. The difficulty is that according to the solution, the secondary component contributes some 60-70% to the total light of the system. Normally, a secondary component that contributes this much light to the system should be easily detected on a spectrogram. The spectroscopic observations show that the primary

Table 1. Fourier Coefficients for Rectification

	1380 Å	1500 Å	1920 Å	2460 Å	2980 Å	3330 Å	5500 Å
A_0	+0.8560	+0.8730	+0.8810	+0.8330	+0.8440	+0.8340	+0.8650
A_1	+0.0061	-0.0092	-0.0596	-0.0304	-0.0242	-0.0180	-0.0311
A_2	-0.1480	-0.1090	-0.1185	-0.1650	-0.1700	-0.1620	-0.1370
A_3	-0.0265	-0.0191	-0.0122	-0.0144	-0.0136	-0.0095	+0.0015
A_4	-0.0160	+0.0070	-0.0015	-0.0010	-0.0000	-0.0200	-0.0030
B_1	-0.0139	-0.0130	-0.0231	-0.0164	-0.0007	-0.0012	-0.0036
B_2	-0.0220	-0.0300	-0.0375	-0.0476	-0.0349	-0.0340	-0.0155
B_3	-0.0079	-0.0069	-0.0181	-0.0138	-0.0066	-0.0011	-0.0022
B_4	+0.0011	-0.0081	-0.0018	-0.0064	-0.0056	-0.0051	+0.0001
C_0	+0.0334	+0.0334	+0.0334	+0.0334	+0.0334	+0.0334	+0.0334
C_1	-0.0061	+0.0092	+0.0596	+0.0304	+0.0242	+0.0180	+0.0311
C_2	+0.0111	+0.0111	+0.0111	+0.0111	+0.0111	+0.0111	+0.0111

Table 2. Orbital Solutions

(Solution for the Ingress: Primary Eclipse is an Occultation)

Geometric Quantities		Photometric Quantities	
		α_o^{oc}=1.00	α_o^{tr}=1.07
k = 0.4		1 - l_o^{oc}	1 - l_o^{tr}
r_g = 0.475	5500 Å	0.300	0.136
r_s = 0.190	3330 Å	0.390	0.105
i = 76°.82	2980 Å	0.356	0.105
θ_e = 40°	2460 Å	0.318	0.155
p_o = -1.30	1920 Å	0.095	0.040
	1500 Å	0.298	0.269(?)
	1380 Å	0.162(?)	0.250(?)

component is the one behind its companion at the time of the primary eclipse. Also, spectroscopic observations give a mass function (Struve, 1958) of about 8.5 solar masses. Table 3 shows the masses of the components for different mass ratios assuming that the light curve solution gave the correct orbital inclination. As seen in the table, unless both components are more massive than about $40M_\odot$, the secondary component, which is spectroscopically undetected, is the more massive of

Table 3. Mass Ratio and Individual Masses

M_1/M_2	M_1 (⊙)	M_2 (⊙)
0.10	1.1	11.1
0.20	2.6	13.2
0.30	4.7	15.5
0.40	7.2	18.0
0.50	10.4	20.7
0.70	18.6	26.6
1.00	36.8	36.8

the two. OAO-2 observations of the spectral energy distribution of Beta Lyrae show an energy distribution similar to that of Eta UMa, which is a B3 V star (Houck, 1971).

If this ultraviolet spectral energy distribution represents basically the temperature of the primary component, and not hot circum-binary gas, this star should ordinarily have a mass of about $8M_{\odot}$ or greater. However, in a rapid mass exchange phase (Kippenhahn, 1969; Refsdal and Weigert, 1969; Harmanec, 1970a,b) the evolved star that is losing mass becomes very overluminous for its mass. The absolute visual magnitude for such a star could be as high as -4 to -6, although its mass may have become as small as one to two solar masses or less.

If we accept the light curve solution, the mass function may be written as:

$$\frac{M_2^{\,3}}{(M_1 + M_2)^2} = 9.2M_{\odot}$$

If we impose a restricting condition that neither of the components shall exceed its own critical Roche limiting surface, this places an upper limit on the mass ratio. This upper limit is about 0.4 according to the table of dimensions of Roche limiting lobes prepared by Plavec and Kratochvil (1964). Assuming that the relative radius of the larger star, i.e., the more massive secondary, is about 0.5, the Roche lobe will be unable to contain this star if the mass ratio is greater than 0.4. If we impose the condition that the less massive primary component fills its Roche limiting surface, the mass ratio must be about 0.1. With a mass ratio of 0.1, the mass of the primary star is about $1.1M_{\odot}$ and the mass of the secondary is about $11.1M_{\odot}$. Absolute dimensions have been computed for this model and are listed in Table 4.

This interpretation means that the primary component is a star near the end of the phase of fast mass exchange and may well be in a very luminous pre-white dwarf stage. In the mass exchange phase, the less luminous of the two becomes more massive. If we accept this model, the secondary component will have to be a very unusual star that is large enough to occult the primary component, contributing a substantial amount of light to the total light of the system, yet producing no detectible spectral features except possibly some unusual emission lines. (This difficulty may be partially overcome by stipulating that the total light of the system consists of three contributing sources, i.e. the primary component, the secondary component, and the light from the emitting [and reflecting] hot gas cloud that surrounds the system as a whole. If we assume the preceding, then we will have to abandon the solutions from the light curves since the unknown extent of the contribution from circum-binary gas cloud makes

Table 4. Absolute Dimensions of Beta Lyrae

M_1/M_2	a (10^6km)	R_p (10^6km)	R_s (10^6km)
0.10	37.17	17.66	7.06
0.20	40.55	19.26	7.70
0.30	43.93	20.87	8.35
0.40	47.31	22.47	8.99
0.50	50.69	24.07	9.63
0.70	57.44	27.28	10.91
1.00	67.58	32.10	12.84

the solution indeterminate.) It is at this point appropriate to comment that no calculation has been carried out to estimate the dimensions and temperature for the star gaining the mass during the mass exchange. Consequently, we do not know if the secondary spectrum should be visible. Hall (1971) has suggested that the secondary component is disk-shaped and has not yet reached a post mass-exchange equilibrium state. Such a secondary component, if it has a low surface temperature, could account for the observations, but no quantitative work has been done and the details are yet to be worked out.

Huang (1963) has suggested that the secondary component is imbedded in a disk of gas which is opaque and thus explains the invisibility of the secondary component. However, the formation and maintenance of such a disk, particularly at a temperature low enough so that it does not produce spectral features which are not observed, seems as difficult to explain as the problem of the secondary component itself.

One might assume the presence of a collapsing neutron star inside a relatively low temperature gaseous shell which may be either spherical or disk-like. This model has the advantage of being able to contain a massive secondary component without heating the surrounding mass. Also, since the collapsing neutron star does not require large dimensions, the gaseous shell may assume a smaller diameter which reduces the heating problem due to the primary component. However, here too, the initial acquisition of the gaseous shell must be explained.

Perhaps, in this case, a hot gas flowing in from the primary component has had the time to cool off. The principal problem in this model is avoiding the disruption of the binary in a supernova explosion, which is, according to the currently accepted theories of stellar evolution, required for formation of a collapsing neutron star. Exact physical conditions of a supernova explosion are not well understood: however, work by McCluskey and Kondo (1971) shows that if only a small fraction (several percent) of the mass is lost from the exploding star, the system may remain bound. The orbit, if originally circular, would acquire a small eccentricity (a few hundredths). A similar model was recently suggested for ε Aurigae by Cameron (1971).

An attempt to find a solution was made assuming that the primary eclipse is a transit. However, no satisfactory solution was found to fit the rectified light curves.

The change in light levels for the maxima at 1380 Å and, to a lesser extent, at 1500 Å may be attributable to a contribution of light from the emitting gas cloud which is variable. The shallowness of the eclipses at 1920 Å may be explained in terms of the influence of the strong emission feature adjacent to it, if we assume that the emission originates primarily from the circum-binary hot gas cloud. The asymmetry of the eclipse might also be accounted for by assuming the existence of an additional hot gas cloud at or near the Lagrangian triangular point preceding the primary component in the sense of its orbital revolution. Such an effect will raise the level for the egress in the primary eclipse and the ingress in the secondary eclipse, which is what the light curves appear to show. This interpretation may be partially justified on the ground that it is the ingress in the primary eclipse that renders a shape relation more amenable to solution. The apparent increase in the relative depths of the secondary eclipse as compared with the depth of the primary eclipse, at 1380 Å and 1500 Å, must also be explained. Here one might assume that the side of the secondary (or the circum-secondary gas cloud) that faces the primary component is heated by the latter in such a way that the effect is more pronounced in the shorter wavelengths. Or, one might assume an anomalous reflection effect which is more enhanced at shorter wavelengths. However, we do not know of a specific physical process that will produce such an effect.

Our interpretation admittedly is, to an uncomfortable extent, qualitative. Photoelectric and spectroscopic observations are hard to reconcile with each other. Perhaps, when techniques are developed to investigate, more quantitatively, the qualitative models, the choice of the model may be narrowed down. Also, infrared observations might provide data that will enable us to discriminate among various models.

REFERENCES

Cameron, A. G. W. 1971, Nature 229, 178.
Code, A. D., Houck, T. E., McNall, J. F., Bless, R. C. and Lillie, C. F. 1970, Ap. J. 161, 377.
Hall, D. S. 1971, personal communication.
Harmanec, P. 1970a, Bull. Astron. Inst. Czech. 21, 113.
———— 1970b, ibid. 21, 316.
Houck, T. E. 1971, unpublished observations.
Huang, S. S. 1963, Ap. J. 138, 342.
Kippenhahn, R. 1969, Astron. Astrophys. 3, 83.
McCluskey, G. E. and Kondo, Y. 1971, Astrophys. Sp. Sci. 10, 464.
Merrill, J. E. 1970, Vistas in Astronomy (New York: Pergamon Press), 12, 43.
Plavec, M. and Kratochvil, P. 1964, Bull. Astron. Inst. Czech. 15, 165.
Refsdal, S. and Weigert, A. 1969, Astron. Astrophys. 1, 167.
Struve, O. 1958, Bull. Astron. Soc. Pacif. 70, 5.
Wood, D. B. and Walker, M. F. 1960, Ap. J. 131, 363.
Wood, D. B. and Forbes, J. E. 1963, A. J. 68, 257.

BALMER CONTINUOUS EMISSION AND POLARIZATION IN BE STARS

George V. Coyne, S. J.
University of Arizona
Tucson, Arizona*

ABSTRACT

Observations by OAO-2 of two Be stars, Gamma Cassiopeiae and 60 Cygni, are analyzed to show that unpolarized radiation produced by Balmer continuous emission in the extended atmospheres of Be stars is probably a significant factor in explaining the polarization observed shortwards of the Balmer discontinuity. The ratio of the energy flux (normalized at 2200 Å) of Be stars to normal B stars with the same amount of reddening varies from about 1.4 at 3600 Å to 1.05 at 2500 Å. This is interpreted as due to Balmer continuous emission in the Be stars. For γ Cas the polarizations at 3300 and 3600 Å are respectively 0.6 and 0.7 of the values one expects from interstellar polarization. Neutral polarization produced by Thomson scattering and thence modified both by hydrogen absorption and Balmer continuous emission in the extended atmospheres of Be stars is adduced to explain the observed wavelength dependence of the polarization.

I. INTRODUCTION

For some time it has been clear from both the variability of the polarization in Be stars (Coyne and Kruszewski 1969, Serkowski 1970) and from the wavelength dependence of the polarization (Coyne and Kruszewski 1969, Coyne 1971a) that at least some of the observed polarization is produced in the

---

* Present address: Vatican Observatory, Castel Gandolfo, Rome

extended atmospheres or shells about these stars. The observed polarization differs from that of the interstellar medium in both the blue and red spectral regions: there is a steeper drop in the polarization for the Be stars between 5200 Å and 3300 Å; there is a minimum at about 6600 Å and an increase into the red (see Fig. 4). In the past we have attributed the polarization to scattering from free electrons and subsequent absorption in a hydrogen plasma. A careful analysis, however, shows that the hydrogen absorption is not adequate by itself to explain the wavelength dependence of the polarization. Balmer continuous emission, revealed in the OAO data, must also be an agent.

II. OBSERVATIONS

Spectrophotometric scans with the long-wavelength Wisconsin spectrometer (Code et al. 1970) were obtained for two Be stars, Gamma Cassiopeiae ($\overline{B0}$ $\overline{IV}$e) and 60 Cygni (B1 Ve) and these results plus scans for two normal stars, Upsilon Orionis (B0 V) and Alpha Crucis (B1 IV), were supplied to me as a Guest Investigator. These data consist of digital counts made at about every 20 Å. A zero point for the wavelengths was determined by identifying the Mg I feature at 2800 Å. This was easily done on all of the scans. The wavelength scale, supplied by the Wisconsin group, was determined by a comparison of the OAO planet data with a smoothed version of the high resolution NRL solar spectrum.

It has already been established that the wavelength dependence of the flux measured with the Wisconsin spectrometers for unreddened B type stars of the same spectral class and of any luminosity class except supergiants is the same (Bless and Savage 1970, Bless and Savage 1972). The reddening for the stars with which we are concerned is small (not greater than +0.08); the color excess, E(B-V), for γ Cas minus that for υ Ori is +0.03, and the color excess for 60 Cyg minus that for α Cru is +0.06. We have, therefore, directly compared the digital output for these respective pairs of stars.

In Fig. 1 the relative fluxes (the ratio of the digital counts for the Be stars to the normal B stars) are plotted versus wavelength. The flux ratios are normalized at 2200 Å. The scans of γ Cas were made on two different orbits; both the flux ratio (with respect to υ Ori) from the individual scans and the mean flux ratio are plotted at the bottom of Fig. 1; at the top the flux ratio for 60 Cyg (with respect to α Cru) is plotted. The flux ratios are the largest (about 1.4) at the Balmer limit and decrease towards shorter wavelengths. This is the kind of wavelength dependence that one would expect from Balmer continuous emission.

There appears to be a difference in the flux from γ Cas as

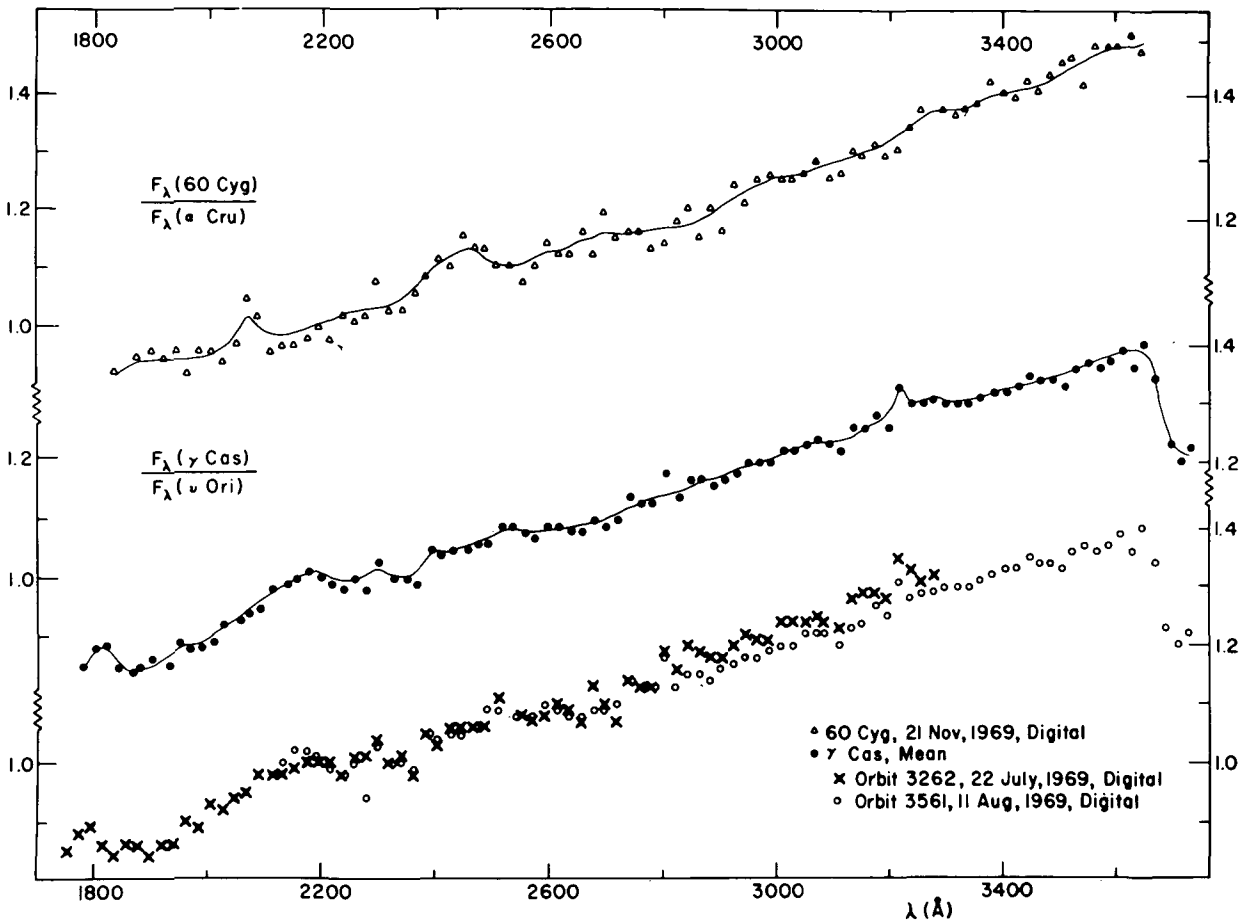

Figure 1.—The ratios of the energy flux in the two Be stars, γ Cas and 60 Cyg, to that in the two respective normal stars, υ Ori and α Cru, are plotted as a function of wavelength. The ratios are normalized at 2200 Å. Both the individual observations for two different orbits and the mean curve for γ Cas are plotted. The energy flux in the Be stars exceeds that in the normal B stars, the excess being the greatest at the Balmer limit (3647 Å) and decreasing to shorter wavelengths. This is interpreted as being due to Balmer continuous emission in the Be stars.

compared to that from 60 Cyg. In Fig. 2 we present a check of the response of the system to the two respective comparison stars, υ Ori (B0 V) and α Cru (B1 IV) by plotting the respective counts for each star at the same wavelength. The spectral energy distribution and the response of the system are the same for the two comparison stars.

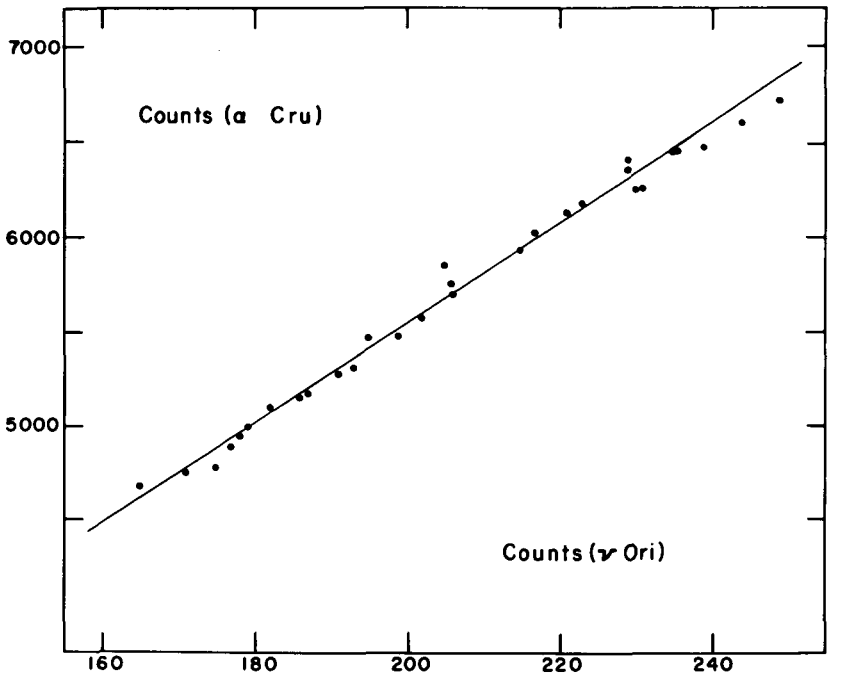

Figure 2.—The digital counts for the two comparison stars, υ Ori and α Cru, at each wavelength are compared. The difference in the reddening, E(B-V), for these two stars is only $0^m.02$. The relative spectral energy distributions are the same in the region of the spectrum covered.

In Fig. 3 we show the relative flux of the two Be stars as a function of the wavelength (normalized at 3000 Å). We see that the flux from γ Cas is relatively less at longer wavelengths. Apparently the spectral gradient of the Balmer continuous emission varies among the Be stars.

III. DISCUSSION

At the University of Arizona we have detailed polarization measurements on several Be stars (Coyne 1971b), especially on γ Cas, and these shall now be discussed in terms of the Balmer continuous emission indicated by the OAO data.

Fig. 4 shows the mean polarization of γ Cas contrasted with the mean polarization for the interstellar medium (Coyne and Gehrels 1967). The polarization of γ Cas varies with time with an amplitude of about 0.5% (Coyne 1971b). Here are plotted the mean of all the observations at each filter. The inverse effective wavelengths for our seven filters and the location of the Balmer and Paschen limits are indicated on the

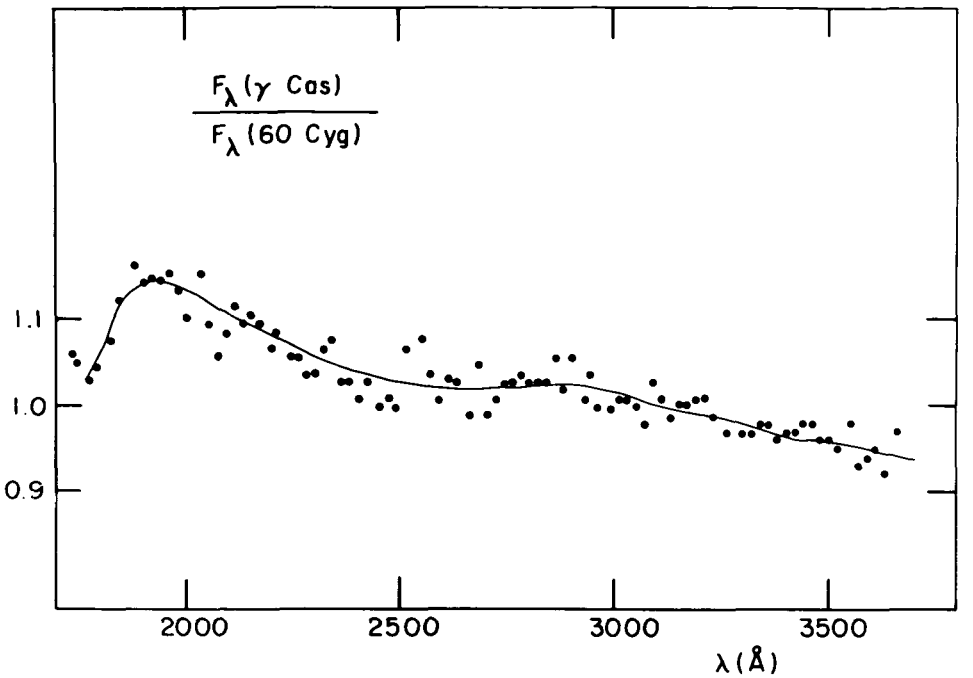

Figure 3.—The ratio of the energy flux, normalized at 3000 Å, in γ Cas to that in 60 Cyg as a function of wavelength. Since from Fig. 2 the spectral energy distribution is the same for the two comparison stars, we may interpret this curve as due to real differences in the energy distribution from these stars.

abscissa scale. The interstellar curve is normalized to the curve for γ Cas at the B filter. The typical wavelength dependence of the polarization in Be stars (see description in § I) is shown by γ Cas.

The location of the filters is important for a discussion of both hydrogen absorption and Balmer continuous emission in Be stars. In Fig. 5 we have plotted the detailed spectral response of the various filter-phototube combinations (right hand ordinate scale) and the hydrogen absorption coefficient for an electron temperature, T_e = 10,000°K and an electron density, $N_e = 10^{12} cm^{-3}$ (left hand ordinate scale). The response of the various filters has been determined by ourselves, but the manufacturer's mean curve is used for the phototube response. The response curves are determined for white light (which approximates the flux for B stars) through 1.3 airmasses of atmospheric extinction. [The color system is described in detail by Coyne and Gehrels (1967.] The hydrogen absorption coefficient, which is a function of the inverse cube of the frequency between successive discontinuities, var-

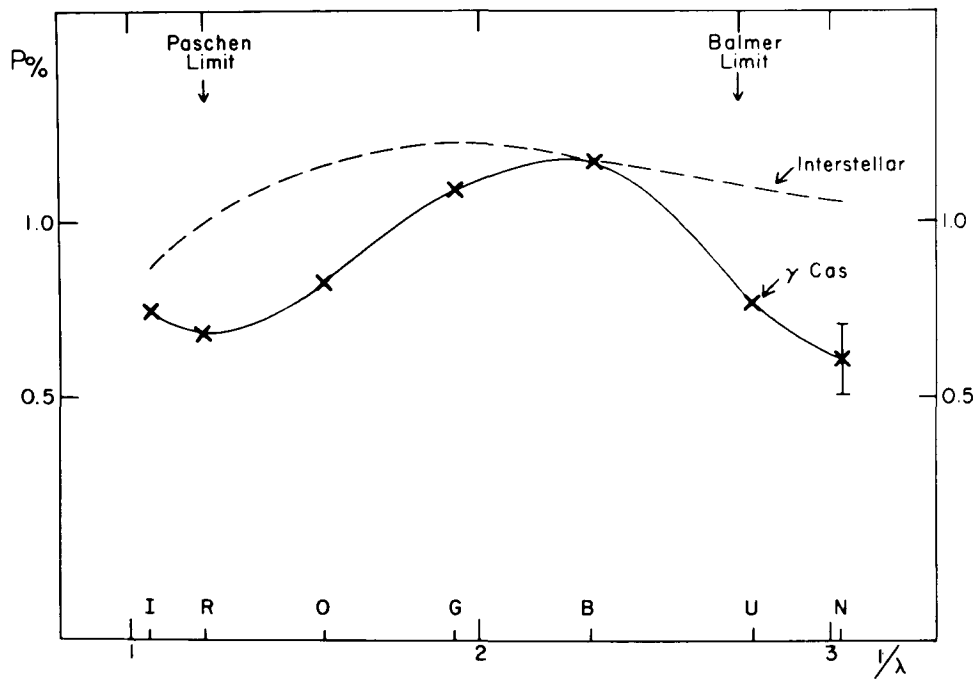

Figure 4.—The mean polarization for γ Cas and that for the interstellar medium are plotted versus inverse wavelength. The interstellar curve is adjusted to the curve for γ Cas at the B filter. The inverse effective wavelengths of the various filters and the location of the Balmer and Paschen limits are indicated on the abscissa scale.

ies significantly over the wavelength band of the respective filter-phototube response curves, especially over the U, N and R filters. In our past discussion of the polarization in Be stars (Coyne and Kruszewski 1969) this has not been considered quantitatively. In order to make some quantitative comparison between the intrinsic polarization and hydrogen absorption, we do the following. For each response curve an effective hydrogen absorption coefficient is determined by evaluating from Fig. 5 the integral $1/2 \int S_{\bar{\nu}}\, a_{\bar{\nu}}\, d\bar{\nu}$ over the wavelength band of the respective filter-phototube response curves, where $S_{\bar{\nu}}$ is the filter-phototube response, $a_{\bar{\nu}}$ the hydrogen absorption coefficient and $\bar{\nu} = 1/\lambda$ is the wavenumber. As a measure of the wavelength dependence of the intrinsic polarization in γ Cas the ratio P(γ Cas)/P(interst.) is determined for each of our filters.

In Fig. 6 we plot the ratio of the polarization of γ Cas to that of the interstellar medium as a function of the effective hydrogen absorption coefficient, defined in the previous para-

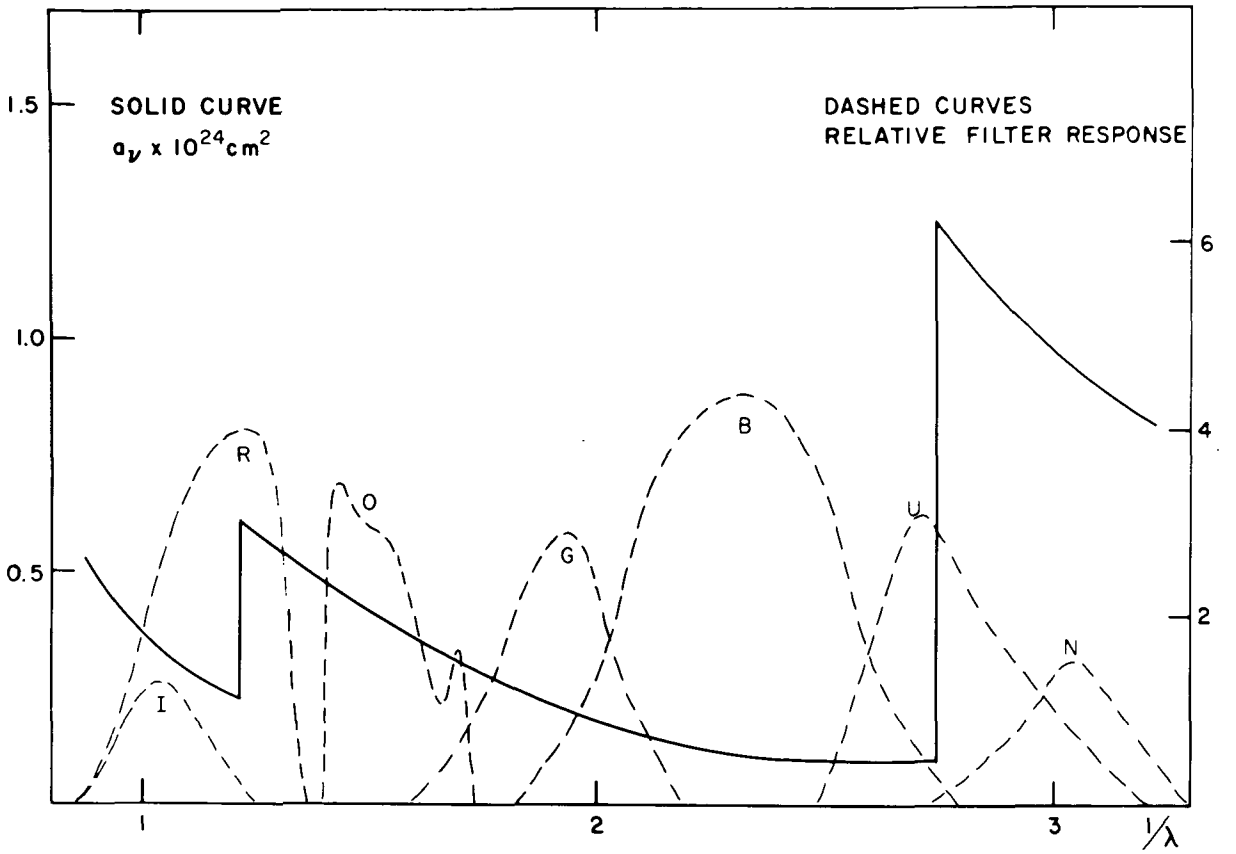

Figure 5.—The solid curve (left hand ordinate scale) gives the absorption coefficient as a function of inverse wavelength for hydrogen gas at an electron temperature of 10000°K and an electron density of $10^{12} cm^{-3}$. The dashed curves (right hand ordinate scale) give for the various filter-phototube combinations the relative distribution of radiant energy received from B stars through 1.5 air-masses of atmospheric extinction.

graph. There is, in general, a correlation of the hydrogen absorption and the polarization, but it is precisely the filters at the Balmer and Paschen discontinuities which do not fit this correlation well. If we accept the hypothesis that it is only hydrogen absorption which causes the wavelength dependence of the polarization, then we should observe even less polarization in the N, U and R filters than that actually observed. There will, of course, be a gradient in the electron temperature and electron density with the height of the absorbing and scattering layers above the photosphere and therefore, a similar gradient in the hydrogen absorption coefficient.

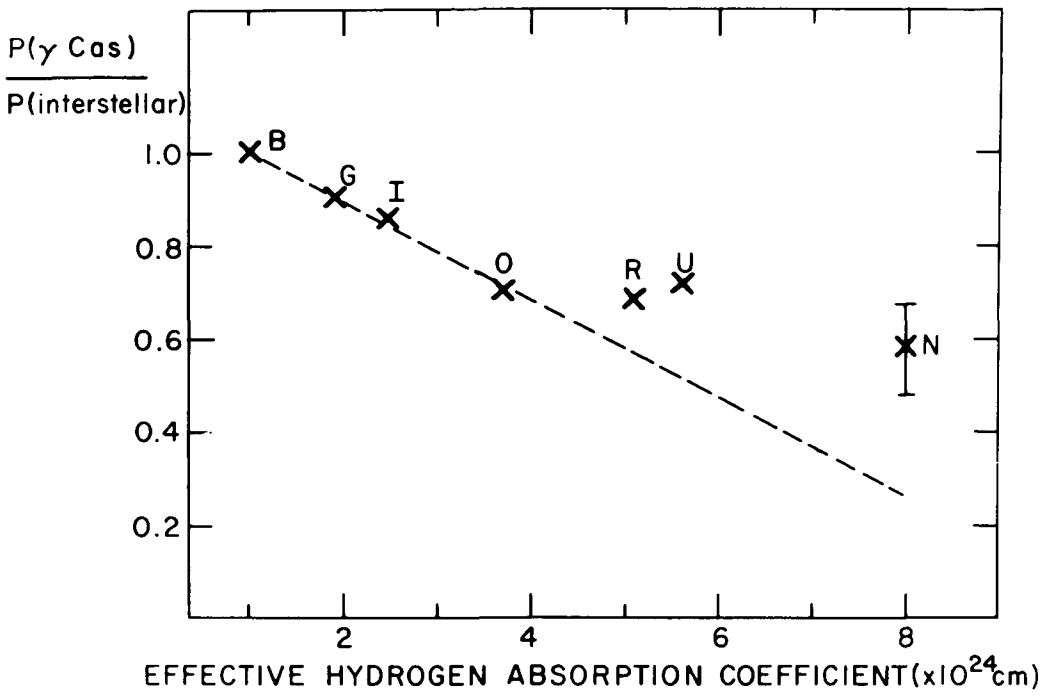

Figure 6.—The ratio of the mean polarization in γ Cas to that in the interstellar medium is plotted for each filter as a function of the effective hydrogen absorption coefficient defined as $1/2 \int S_{\bar{\nu}}\, a_{\bar{\nu}}\, d\bar{\nu}$ *(see Fig. 5 and text). The polarizations at the R, U and N filters, which lie at or near the Paschen or Balmer limits, do not fit as well as do the polarizations for the other filters.*

Assuming also that the absorption and scattering will vary differently with height for different spectral regions, we cannot expect that there will be a strict correlation between the polarization and the effective hydrogen absorption coefficient, determined for one specific temperature for all filters. Nevertheless, it seems fortuitous that only those filters which lie at or near the Balmer and Paschen discontinuities require a hydrogen gas at a lower temperature and electron density.

Since the OAO data shows that there is Balmer continuous emission in Be stars, this must also be considered as a possible agent in suppressing the polarization in the U and N filters. Unpolarized Balmer continuous emission would decrease the polarization in the U and N filters while not affecting the other filters. Paschen continuous emission might be present, of course, and this would affect the polarization especially in the R and I filters. It appears, therefore, that

the intrinsic polarization in Be stars is due to three mechanisms: (1) scattering of light from electrons in a flattened disk or ring of partly ionized hydrogen; (2) self-absorption in the hydrogen gas before and after scattering; (3) unpolarized radiation from Balmer and, perhaps, Paschen continuous emission.

The physical model is the following. There is a flattened disk with a thickness at least several times smaller than the star's radius in order to have the asymmetry required to produce the observed intrinsic polarization. This disk consists of a partly ionized hydrogen gas with a mean electron temperature of about 10,000°K and a mean electron density of about $10^{12}cm^{-3}$. A path length of at least 20 $R_\odot$ (about 3 stellar radii) is required in order to have enough scattering to produce the observed polarization. This path length is equivalent to unit optical thickness for Thomson scattering under the stated electron temperature and density conditions. Within this disk extending at least 2 or 3 stellar radii from the star there is, of course, a gradient of the electron temperature and density. The current polarimetric data are not sufficient to specify with precision at which levels in the disk each of the three mechanisms enumerated in the previous paragraph plays a major role. It would seem, however, that the major part of the scattering and the production of neutrally polarized radiation takes place in the inner parts of the disk where the electron density is higher and that the Balmer continuous emission, producing unpolarized radiation, is concentrated to the outer regions of the disk where the electron density is lower.

This model is not inconsistent with what is otherwise known about the extended atmospheres of Be stars. From emission line intensities in Be stars it is estimated that the radius of the emitting region is about 10 stellar radii with an electron density of $10^{13}cm^{-3}$ (Burbidge and Burbidge 1956). From the rotational broadening of the absorption lines, it is deduced that the main body of the gas lies 2 or 3 stellar radii from the star. The region extending out to about 10 stellar radii beyond this main concentration of gas would presumably be the region in which the major part of the Balmer continuous emission occurs. As unpolarized radiation it would suppress the polarization (observed in our N and U filters) produced by Thomson scattering in the inner parts of the disk. This polarized radiation would have also been modified by absorption in the hydrogen gas.

I wish to thank Dr. A. Code and his colleagues at the University of Wisconsin, especially Dr. Blair Savage, for transmitting to me the OAO data and for discussions concerning this data.

REFERENCES

Bless, R. C. and Savage, B. D. 1970, Ultraviolet Stellar Spectra and Ground-Based Observations, I.A.U. Symposium No. 36, ed. L. Houziaux and H. E. Butler (Dordrecht: D. Reidel Publ. Co.).
Bless, R. C. and Savage, B. D. 1972, this volume.
Burbidge, E. M. and Burbidge, G. R. 1956, in Vistas in Astronomy, ed. A. Beer (London and New York: Pergamon Press).
Code, A. D., Houck, T. E., McNall, J. F., Bless, R. C. and Lillie, C. F. 1970, Ap. J. 161, 377.
Coyne, G. V. 1971a, Ricerche Astronomiche 8, 201.
_____ 1971b, Astron. J. 76, to be published.
Coyne, G. V. and Gehrels, T. 1967, Astron. J. 72, 887.
Coyne, G. V. and Kruszewski, A. 1969, Astron. J. 74, 528.
Serkowski, K. 1970, Ap. J. 160, 1083.

PRELIMINARY RESULTS OF ULTRAVIOLET PHOTOMETRY OF SHELL STARS

Robert L. Bottemiller
University of Wisconsin
Madison, Wisconsin

ABSTRACT

Photometry of 40 B stars acquired by the OAO-2 has been examined for systematic differences between the 25 standard stars and 15 program objects. The latter include shell and Be stars and a few objects with at least a modest infrared excess. Although individual deviations did occur, no definite distinction between the program and comparison stars was found. A possible, but very weak, tendency for the program objects to lie somewhat below the standards in color-color plots is discussed, especially with reference to errors of misclassification and variability of the ultraviolet reddening law.

I. INTRODUCTION

Be stars, and the shell star sub-species, are differentiated from normal B-type stars in the visual region by line phenomena. Conversely, line emission and rotational effects, if they are significant, do not serve to separate these objects from the conventional early-type stars in color-color plots generated from UBV data.

However, modifications of the continuous flux distribution do occur in the ultraviolet for some objects. A previous paper in this volume by Coyne showed the emission in the Balmer continuum observed for γ Cas. OAO spectral scans of several other objects have displayed signs of similar behavior. Ground-based observations by Boone (1970) have also shown the tendency of Be stars to fill in the Balmer jump, occasionally to the

point of exhibiting a higher continuum level shortward of the Balmer limit. Other influences on the ultraviolet continuum of unproven importance are rotation (Collins and Harrington 1966) and the conversion of ultraviolet radiation into the infrared region by grains (Huang 1969).

With a considerable body of observational material available from the OAO, it is now possible to examine not only many normal early-type stars but also a number of Be and shell stars in the ultraviolet. The available OAO photometry provides a larger sample of shell star data than does the scanner material and also can be corrected for interstellar reddening in a straightforward manner.

The following paragraphs present the results of a comparison between normal, early-type and a sample of Be and shell stars in the form of reddening-corrected color-color plots based on OAO photometry. Errors in classification and in the application of the ultraviolet reddening curve are discussed in relation to these plots.

II. DATA REDUCTION

Ultraviolet magnitudes in five bandpasses were derived for 15 program and 25 standard stars. MK spectral types, V magnitudes and (B-V) indices were obtained from Lesh (1968) or Hiltner, Garrison and Schild (1969) with the exception of four standard and two program stars. For each object an unreddened $(B-V)_o$ value was assigned according to spectral type by means of Johnson's (1958) calibration.

A comparison of 12 program star spectral types determined spectroscopically with those found by the Q-method showed good agreement. With a single exception, the agreement was within one and a half spectral sub-types, or within about 0.03 units in (B-V). The one maverick, σ Cyg, is generally listed as B9 Iab but appears on a $(U-B)_o$-$(B-V)_o$ plot as slightly earlier than B5.

The magnitudes derived from data taken through the various OAO filters are denoted by the approximate effective wavelength for a specific filter; thus, the index $(m_{3320}-V)$ is written as (3320-V). With an estimate of E(B-V) in hand, the associated excess in $(\lambda-V)$ was computed using the mean $E(\lambda-V)/E(B-V)$ relation of Bless and Savage presented elsewhere in this volume. The interstellar reddening relation is highly non-linear in this wavelength region, besides being variable in direction. This difficulty together with uncertainties in $(B-V)_o$ and, hence, E(B-V) comprise the largest source of error in the computations.

The program stars were chosen on the following basis of decreasing desirability: i) shell stars, ii) Be stars, preferably with some indication of an infrared excess, and iii) ordi-

nary B stars with a known infrared excess. When the candidates were narrowed to those non-variable objects with satisfactory photometry, 15 stars remained. However, the OAO observing list has not been completely exhausted of interesting objects in this category, especially those with scans but little photometry and objects earlier than B1.

Table 1a lists the program stars, their MK types, V, B-V and indicates if the object has a noticeable infrared excess (with a reference) or a shell spectrum. Also tabulated are the ultraviolet magnitudes which form the basis for the reddening-corrected plots of $(\lambda-V)_o$ versus $(B-V)_o$.

The 25 standard stars (see Table 1b) span the spectral region from B0 to B9. Four of the latest types not classified by either Lesh or Hiltner, Garrison and Schild were assigned MK types from the Bright Star Catalog. The average E(B-V) for this sample is 0.05, with six objects having an excess greater than 0.10. The mean excess for 14 of the program stars, neglecting P Cygni's large excess, is 0.08. Including P Cygni raises the average excess to 0.12.

III. RESULTS

Color differences corrected for reddening, $(\lambda-V)_o$, were computed for all the program and comparison stars and plotted against $(B-V)_o$ for each of five ultraviolet filters. The results are all rather similar so graphs for only three bandpasses are presented in Figures 1a, b and c.

As one would expect, the normal B stars (filled circles) form well-defined sequences in these plots. A slight downturn at B9 in some filters may be due in part to minor misclassification and in part to observational inaccuracy. In any event, more standards of type B5 and later are desirable to solidify the definition of the sequence in this region.

A straight-line relation of the form $(\lambda-V)_o = m(B-V)_o + b$ was hand-fit to the data in a very approximate manner. The coefficients of slope, m, and intercept, b, are listed in Table 2 for all five filters.

The inverse relationship between slope and wavelength found in Table 2 naturally reflects the more rapid increase of flux in the near-to-far ultraviolet for stars in this spectral (temperature) range.

The small figure in the lower left corner of the first 3 plots represents the corrections to be made to the position of any given data point if it were assigned an incorrect $(B-V)_o$ or extinction ratio. If an object were misclassified so as to yield a $(B-V)_o$ too large or small by 0.02 units, its corrected horizontal displacement would be just that amount. In addition, a slight vertical correction would be necessary due to

Table 1a. Program Stars

Name/HD	MK	V	B-V	IR Excess?	Shell?	Ultraviolet Magnitudes 3320	2990	2390	2040	1680
P Cyg	B1 p	4.78	+0.41	Yes (1,2)	Yes	-1.76	-1.73	-1.05	-0.78	----
60 Cyg	B1 Vn	5.41	-0.20	---	No	-2.22	-2.61	-3.31	-3.65	-4.20
ω Ori	B2 IIIe$_1$	4.58	-0.11	Small (1)	No	-2.91	-3.23	-3.76	-3.88	-4.20
μ Cen	B2 IV-Ve$_3$	3.26	-0.16	---	No	-4.02	-4.40	-5.15	-5.53	-6.01
υ Cyg	B2 Ve$_{1+}$	4.28	-0.08	---	No	-2.96	-3.26	-3.78	-4.08	-4.47
ξ Cas	B2.5 V	4.81	-0.11	Small (1)	No	-2.30	-2.57	-3.00	-3.33	-3.85
ε Cas	B3 Vp	3.37	-0.16	No (1)	Yes	-3.78	-4.13	-4.62	-4.93	-5.24
217050	B4 IIIpe$_1$	5.42	-0.09	---	Yes	-1.44	-1.73	-2.11	-2.56	-2.95
ζ Tau	B4 IIIp	2.95	-0.19	---	Yes	-4.32	-4.67	-5.33	-5.42	-5.88
48 Lib	B5 IIIp	4.87	-0.10	Yes (2)	Yes	-2.16	-2.43	-2.74	-3.06	-3.55
ο And	B6 p	3.62	-0.09	---	Yes	-3.30	-3.55	-3.93	-4.27	-4.63
κ Dra	B6 IIIp	3.82	-0.11	Yes (1,2)	Yes	-3.25	-3.52	-4.02	-4.23	-4.44
23 Tau	B6 IV	4.18	-0.06	Small (1)	No	-2.67	-2.90	-3.35	-3.58	-3.89
η Tau	B7 III	2.87	-0.09	Small (1)	No	-3.84	-4.04	-4.48	-4.72	-5.15
σ Cyg	B9 Iab	4.23	+0.13	Small (1)	No	-2.21	-2.20	-1.92	-2.22	-2.50

[1]Johnson (1967), [2]Geisel (1970)

Table 1b. Standard Stars

Name/HD	MK	V	B-V	Ultraviolet Magnitudes 3320	2990	2390	2040	1680
69 Cyg	B0 Ib	5.94	-0.10	-1.67	-1.99	-2.50	-2.66	-3.17
τ Sco	B0 V	2.82	-0.25	-4.99	-5.35	-6.18	-6.69	-7.31
υ Ori	B0 V	4.61	-0.28	-3.25	-3.74	-4.53	-5.03	-5.44
δ Sco	B0.5 IV	2.30	-0.11	---	---	---	---	-7.08
ϕ^1 Ori	B0.5 IV-V	4.41	-0.17	-3.23	-3.62	-4.23	-4.58	-4.98
23 Ori	B1 Vn	4.99	-0.15	-2.59	-2.95	-3.47	-3.83	-4.23
ω^1 Sco	B1 V	3.96	-0.04	-3.40	-3.69	-3.99	-4.33	-5.01
148703	B2 III	4.22	-0.17	-3.24	-3.62	-4.24	-4.55	---
φ Cen	B2 IV	3.82	-0.22	-3.76	-4.15	-4.90	-5.26	-5.76
ρ Sco	B2 IV-V	3.88	-0.20	-3.71	-4.11	-4.69	-5.02	-5.63
υ^1 Cen	B2 IV-V	3.86	-0.21	-3.63	-4.03	-4.82	-5.20	-5.70
22 Sco	B2 V	4.78	-0.12	-2.58	-2.94	-3.50	-3.81	-4.42
χ Cen	B2 V	4.35	-0.20	-3.14	-3.52	-4.24	-4.60	-5.13
129116	B3 V	3.99	-0.18	-3.41	-3.78	-4.4	-4.71	-5.19
125823	B3 V	4.41	-0.19	-3.06	-3.44	-4.07	-4.36	-4.89
λ Cru	B4 Vn	4.62	-0.16	-2.59	-2.94	-3.51	-3.82	-4.43
ϕ^2 Lup	B4 V	4.53	-0.16	-2.81	-3.14	---	-4.03	-4.40
137432	B4 Vp	5.42	-0.15	-1.80	-2.08	-2.63	-3.13	-3.47
ν And	B5 V	4.57	-0.16	-2.65	-2.98	-3.48	-3.76	-4.09
143699	B6 IV	4.88	-0.15	-2.35	-2.62	-3.09	-3.39	-3.80
144661	B7 IIIp	6.32	-0.06	-0.58	-0.81	-1.24	-1.39	-1.42
α Scl	B8 III	4.30	-0.16	-2.68	-2.94	-3.38	-3.76	-3.96
20 Tau	B8 III	3.87	-0.07	-3.00	-3.22	-3.47	-3.77	-3.96
41 Eri	B8.5 V	3.55	-0.11	-3.20	-3.43	-3.86	-4.27	-4.13
4622	B9 V	5.56	-0.06	-0.72	-0.85	-1.20	-1.61	-1.97
14 CVn	B9 V	5.15	-0.08	-1.31	-1.48	-1.78	-2.07	-2.29

the new E(B-V) and, hence, E(λ-V). The net effect is represented by the nearly horizontal dashed line.

If, on the other hand, the $(B-V)_o$ were precise but the ratio E(λ-V)/E(B-V) were incorrect by ±20% then the resultant correction, for E(B-V) = 0.20, is shown by the short vertical dashed line. The worst combined effect of the two influences is demonstrated by the solid arrows with the uncertainty in $(B-V)_o$ being the dominant factor.

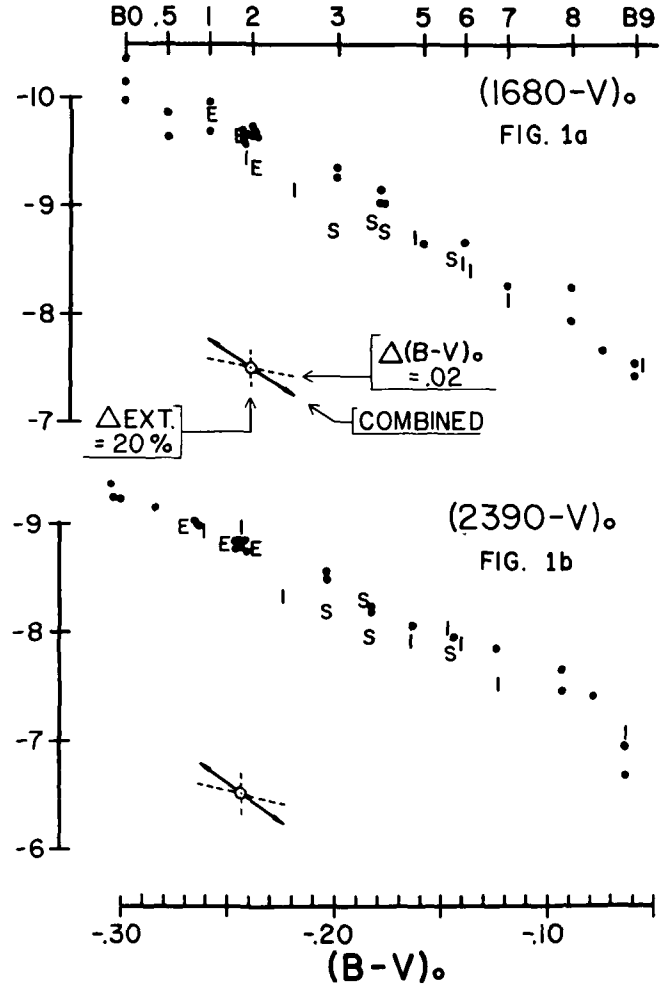

Figure 1a and 1b.—Color-color plots for the 25 standard stars and 15 program objects. Filled circles represent the standards; the letter "E", Be stars with no known shell or infrared excess; "S", shell stars with no known infrared excess; "I", any object with some degree of excess infrared flux. The graphs are of the color index $(\lambda-V)_o$ versus $(B-V)_o$, where, in (a), λ is the 1680 filter, in (b) it is the 2390 filter, and in (c), the 3320 filter.

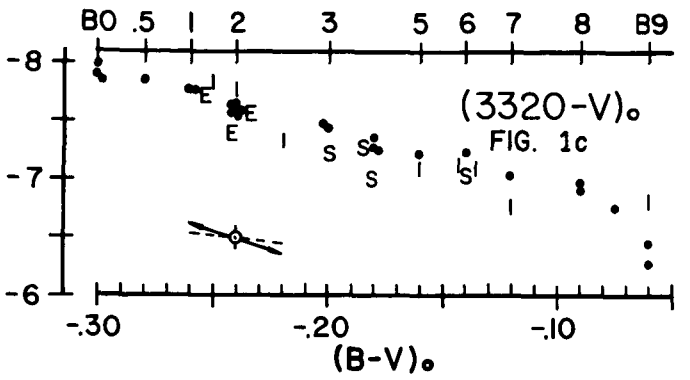

Figure 1c.

In order to graphically separate the potential effects of an infrared excess from a more conventional shell phenomenon and both of these from an even less complicated Be object, the program stars are plotted in a hierarchy of three symbols. If an object has an infrared excess to any noticeable degree it is plotted with an "I," regardless of any other characteristic. This scheme includes three shell stars at B1 (P Cyg), B5 (48 Lib) and B6 (κ Dra). The four remaining shell stars, either with a known lack or an unknown amount of infrared excess, are denoted with an "S." Emission objects with no known infrared excess are represented by an "E."

An examination of the figures reveals no significant difference between the program and comparison objects. Pushing "eyeball analysis" near its limits, one might conclude that there is a weak tendency for the program objects to lie below

Table 2

Coefficients for Approximate Linear Fit $(\lambda-V)_o = m(B-V)_o + b$		
λ	Slope, m	Intercept, b
1680	12.2	-6.77
2040	9.79	-6.86
2390	9.17	-6.58
2990	6.34	-6.50
3320	5.37	-6.36

the standard stars a couple of tenths in $(\lambda-V)_o$. However, if real, this is certainly not correlated with infrared excess since the three shell stars with a significant excess, mentioned above, are not leaders in this tendency. In fact, ε Cas is among the more deviant stars but Johnson's (1967) data show no unexpected infrared flux.

It is quite possible that a combination of observational error and "natural scatter," both in the stars and the reddening law, is at work here, with the apparent downward trend being an accidental bias due to the small sample size.

A slight, systematic underestimation of the reddening would produce a similar result. It is not impossible that an additional source of reddening is present in Be stars; witness, for example, the evidence for intrinsic polarization found by Coyne and Kruszewski(1969) and Serkowski (1970), which may be partly due to the presence of grains, and the fact that some Be stars do indeed exhibit an infrared excess. But, again, no correlation was found here between any ultraviolet deficiency and large infrared excesses.

Another possibility with a similar outcome would be slightly too-early classification. An object so categorized would be shifted to the left in Figures 1a, b and c, and, thus, would lie somewhat below the standard stars. However, the intercomparison of spectroscopic and Q-method spectral types mentioned earlier showed no such trend.

Figure 2 displays data from two ultraviolet filters in a slightly different manner. Here the spectral type-$(B-V)_o$ relationship does not fix the horizontal location of an object, although it retains an influence via the reddening-correction procedure. But, since there are fairly well-defined relationships between $(B-V)_o$ and the $(\lambda-V)_o$ color differences, there is naturally also a clearly defined sequence of stars in this figure distinguished by spectral type. The arrow in the lower left corner indicates the corrections to be made if the extinction ratio $E(\lambda-V)/E(B-V)$ is in error by ±20%.

The tick marks at the top of the figure indicate the spread of standard stars with the same classification. The only two discrepancies here are a B8 standard shifting into the B7 region and a B8.5 object moving to B8 but this may be the result of their not being classified on a scheme completely consistent with the earlier objects. The program stars' positions generally agree with the MK intervals defined by the standard stars. Although four objects show up at about one sub-type later and one appears slightly earlier, this is only a minor inconsistency and does not indicate any systematic misclassification of shell stars.

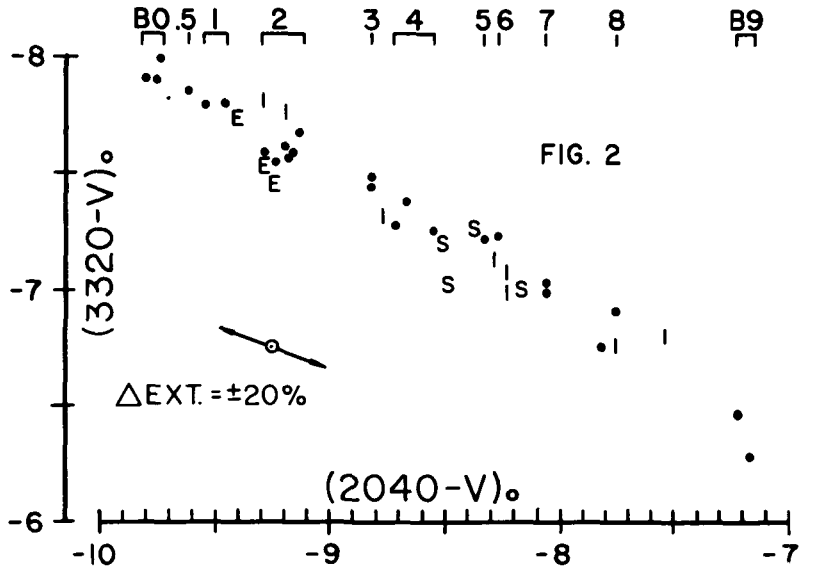

Figure 2.—A plot of the color differences $(3320-V)_o$ versus $(2040-V)_o$ with the ordering by spectral type indicated at the top. The arrows in the lower left area of the graph display the data point trajectories for a ±20 percent error in the interstellar extinction.

IV. SUMMARY

Examination of OAO photometry in the form of various color-color plots for some 40 B-type stars shows, not surprisingly, a smooth sequence of objects well-ordered by spectral type. Of specific interest was the behavior, in these plots, of a sub-set of 15 shell stars, Be stars and objects with some degree of infrared excess. No systematic difference was found that could be pointed to with confidence. A very slight tendency for the program objects to be dimmer in the ultraviolet filters is most likely due to either a modest underestimate of the reddening involved or an accidental bias caused by the small sample size.

The number of standard stars could usefully be increased and extended to earlier spectral types but the current file of shell stars with satisfactory photometry is nearly exhausted. Some scanner data does exist for an additional few shell stars. Another comparison that could be made in this same vein is one between the normal B stars and those with very high rotational velocities.

REFERENCES

Boone, J. C. 1970, Ph. D. thesis, University of Wisconsin.
Collins, G. W. and Harrington, J. P. 1966, Ap. J. 146, 152.
Coyne, G. V. and Kruszewski, A. 1969, A. J. 74, 528.
Geisel, S. L. 1970, Ap. J. (Letters), 161, L105.
Hiltner, W. A., Garrison, R. F. and Schild, R. E. 1969, Ap. J. 157, 313.
Huang, S.-S. 1969, Ap. J. 157, 835.
Johnson, H. L. 1958, Lowell Obs. Bull., No. 90, 4, 37.
_____ 1967, Ap. J. (Letters), 150, L39.
Lesh, J. R. 1968, Ap. J. Suppl. 17, 371.
Serkowski, K. 1970. Ap. J. 160, 1083.

ULTRAVIOLET OBSERVATIONS OF WEAK-HELIUM STARS

P. L. Bernacca*
National Aeronautics and Space Administration
Goddard Space Flight Center
Greenbelt, Maryland

Michael R. Molnar
Laboratory for Atmospheric and Space Physics
Boulder, Colorado

ABSTRACT

Ultraviolet filter photometry with the Wisconsin experiment package aboard OAO-2 has been carried out for the weak-helium stars 3 Cen A, 3 Sco, HD 144334, HD 21699, HD 144844, α Scl, HR 8535, HR 8770 and HD 144661. The flux distribution is compared with that of B3 to B8 main sequence and giant stars in terms of color-color diagrams.

When allowance is made for line blocking shortward of 2800 Å due to lines of P II, Ga II, Si II, Si III, Ti II and Sr II we find that most of the weak-helium stars have normal fluxes in good agreement with their ground-based colors. It is difficult to consider HR 8535, HR 8770 and HD 144661 as having a normal flux distribution and the suggestion is made they may be brighter than normal at 3320 Å.

The star α Scl is a light and spectrum variable. The strengthening of Ti II and Sr II lines around 2400 Å appears to redistribute flux longward of the Balmer discontinuity. The flux distribution indicates an effective temperature about 1500°K higher than previously determined which would increase the apparent helium underabundance.

*ESRO Fellow 1971 on leave from Asiago Observatory, Italy

I. INTRODUCTION

Reporting observations in the unknown ultraviolet region for a number of the little understood weak-helium stars of Population I is per se of interest. We explore how the ultraviolet photometry may clarify whether or not these stars have normal fluxes. Most of these stars are given a late B spectral type and sometimes a luminosity class III [Garrison (1967), Bernacca (1968), Jaschek, Jaschek and Arnal (1969), Molnar (1971), Ciatti and Bernacca (1971), and Schild and Chaffee (1971)], although their colors imply a spectral type as early as B3 to B5. The stars selected for this investigation and the data reduction procedure are described in the next two sections. In § IV the results are discussed in terms of the color indices m_λ(1920 Å) - m_λ(3320 Å), m_λ(2460 Å) - m_λ(3320 Å) and m_λ(4250 Å) - m_λ(3320 Å) by comparing the weak-helium stars with a sample of main sequence and giant stars of spectral type B3 to B8.5. The conclusions in § V show how line blocking may play an important role in these stars and that a few cases of abnormal flux distribution may exist.

II. PROGRAM STARS AND OBSERVATIONS

The stars considered in this investigation are listed in Table 1 where the meaning of the columns is evident. The star 3 Cen A was reported by Bidelman (1960) as having strong phosphorous lines. Later it was found that most of the apparent helium abundance (~ 0.01 by number) is due to He^3 [Jugaku and Sargent (1963), Hardorp (1967)]. Bertiau (1958) has given the type B5 III and A. de Vaucouleurs (1957) B5 IV for 3 Cen A. Alpha Scl has been described as helium deficient and classified as nearly B4 V by Jugaku and Sargent (1961); HR 8535 and HR 8770 have recently been found by Molnar (1971) and the peculiarity of the other stars has been noted by Garrison (1967). The La Plata Catalogue of stars classified on the MK system (Jaschek, Conde, De Sierra 1964) contains estimates of spectral type for 3 Sco (B7 IV, B8 IV), HD 144334 (B8 V, B9 III), HD 14461 (B7 IV, B7 V) and HD 144844 (B9 V).

A number of main sequence and giant stars are listed in Table 2 and have been selected as comparison stars. It should be recalled that 20 Tau was considered to be "weak-helium" by Searle and Sargent (1964). Because it is a rather anomalous star, we will not consider it further. In addition, 41 Eri is a double-lined spectroscopic binary where both components are Mn-stars according to Searle and Sargent (1967). The (B-V) color excess in Table 2 is based on the photometric classification S_Q and the standard colors given by Johnson (1966).

Table 1. Weak-Helium Stars

Star	V	B-V	U-B	S_Q	Sp. Type	Region	Remarks
3 Cen A	4.31	-0.13	-0.59	B4	B5 Vp	Sco-Cen Assn	1
α Scl	4.30	-0.14	-0.52	B5	B8 III	Field	2
3 Sco	5.86	-0.06	-0.58	B3	B8 p	Sco-Cen Assn	3,7
HR 8535	6.16	-0.12	-0.56	B5	B8 IIIp	Field	4
HR 8770	(6.39)	-0.08	-0.56	B4	B9 III	Field	4
HD 21699	5.48	-0.10	-0.58	B4	B8 III	α Per cl.	5,6
HD 144334	5.92	-0.08	-0.56	B4	B8 p	Sco-Cen Assn	3,8
HD 144661	6.32	-0.06	-0.52	B5	B7 III(p?)	Sco-Cen Assn	3
HD 144844	5.88	+0.02	-0.32	B7	B9 IV(p?)	Sco-Cen Assn	3,6,9

Remarks:

1. Spectral type by Slettebak (1963); visual binary; the secondary is B9 V ($\Delta m = 1.6$).
2. Spectral type quoted in Jugaku and Sargent (1961); ADS 16474 ($\Delta m = 3.2$).
3. Garrison (1967).
4. Molnar (1971); Hg II λ3984 strong in HR 8535.
5. Peculiarity noted by Garrison (1967); spectral type by Roman and Morgan (1950).
6. Reported as suspected variable in Hoffleit (1964).
7. Photometry from Garrison (1967).
8. Possible spectrum variable (Norris 1971).
9. SB2 ($\Delta m \approx 1.6$); the secondary is ~A0 (Norris 1971).

Table 2. Comparison Stars

Star	S_Q	Sp. Type	E(B-V)*
35 Ari	B3	B3 V	0.07
HD 142990	B3	B3 V	0.11
ι Her	B3	B3 V	0.02
HD 68324		B3 V	(0.00)
114 Tau	B2.5	B3 V	0.04
ρ Aur	B4	B5 V	0.03
115 Tau	B5	B5 V	0.05
HD 67341		B5 Vn	(0.00)
16 Pup	B5	B5 V	0.01
HD 93194	B4	B5 V	0.04
19 Tau	B6	B6 V	0.02
HD 21362	B6	B6 V	0.10
17 Tau	B7	B6 III	0.01
16 Tau	B7.5	B7 IV	0.05
η Tau	B7.5	B7 III	0.01
20 Tau	B7	B7 III	0.04
τ^5 Eri	B7.5	B8 V	0.01
ι Lep	B7.5	B8 V	0.00
18 Tau	B7.5	B8 V	0.02
27 Tau	B7.5	B8 III	0.02
41 Eri	B8	B8.4 V	0.00

*The color excess is based on the photometric spectral type S_Q except when in parentheses.

The photometry in Tables 1 and 2 has been taken from Blanco, Demers, Douglass and Fitzgerald (1968) or from Garrison (1967).

The Wisconsin Experiment Package (WEP) flown in the OAO-2 has been described by Code, Houck, McNall, Bless and Lillie (1970). The first column of Table 3 lists the photometers and the filters used in this investigation. Columns 2 and 3 present the effective wavelengths for constant energy and the bandpass at half maximum sensitivity. Our observations range roughly from 1750-4700 Å. Following Code (1971) the net count rates from each filter have been normalized to filter S1F1 (3320 Å) and relative fluxes have been derived as a function of wavelength using the correction factors Δ listed in the fourth column of Table 3.

Table 3. WEP Filter Characteristics

Photometer + Filter	λ_{eff}(Å)	$\delta\lambda$(Å)	Δ
S3F1	1913	260	43.70
S2F5	2386	330	2.890
S3F2	2462	380	6.540
S2F2	2945	440	1.102
S1F4	2985	420	1.330
S1F1	3317	540	1.000
S1F3	4252	840	0.208

III. REDDENING CORRECTION AND OBSERVATIONAL DATA

When estimating the reddening correction, two sources of uncertainty are encountered. In Table 4 we have derived E(B-V) for the weak-helium stars by matching the standard colors (Johnson 1966) with the photometric classification S_Q (case a) and with the spectral types of Table 1 (case b). If one considers case (a) to give the true color excess, one has assumed *a priori* that the flux measured in U, B and V is normal. However, using case (b) causes more difficulties. The stars HR 8535, HR 8770, HD 21699 and α Scl must then be assumed to be unreddened and the remaining Sco-Cen stars become the least reddened stars in that region (*c.f.* Garrison 1967). The mean color excess for the α Per Cluster is 0.08 mag (Mitchell 1960), which agrees with the value derived from the S_Q for HD 21699. We have adopted case (a) for all stars.

Table 4. Color excess of the weak-helium stars derived on the basis of S_Q, case (a), and spectral type, case (b)

Star	E(B-V) a	b
3 Cen A	0.05	0.02
α Scl	0.02	-0.04
3 Sco	0.14	+0.04
HR 8535	0.04	-0.02
HR 8770	0.10	-0.02
HD 21699	0.08	0.00
HD 144334	0.10	+0.02
HD 144661	0.10	+0.06
HD 144844	0.14	+0.08

A second source of uncertainty is the shape of the reddening curve in the ultraviolet. Since Stecher's relation (shown in Figure 1 by a broken line) for the Perseus region (Stecher 1969) was derived, it has been found (Bless and Savage 1970, 1972) that the ultraviolet reddening curve can change drastically for different areas of the sky. Therefore, we have decided not to treat the data below 1920 Å where the variations are the greatest. For the region above 1920 Å we have adopted the 'mean' curve of Bless and Savage (1971) (shown in Figure 1 by the solid line). The difference between the two curves at 1920 Å will bear on the interpretation of the results. In Figure 1 both curves are normalized to E(B-V) = 1. The observed data are presented in Table 5. Under each wavelength, the observed flux, its standard deviation, the flux corrected for reddening and the corresponding standard deviation are entered in order. Errors are generous estimates computed on the basis of the fluctuation in the count rates only. They could be reduced by a factor of about $\sqrt{6}$ quite safely. Entries following the star names give the number of observations.

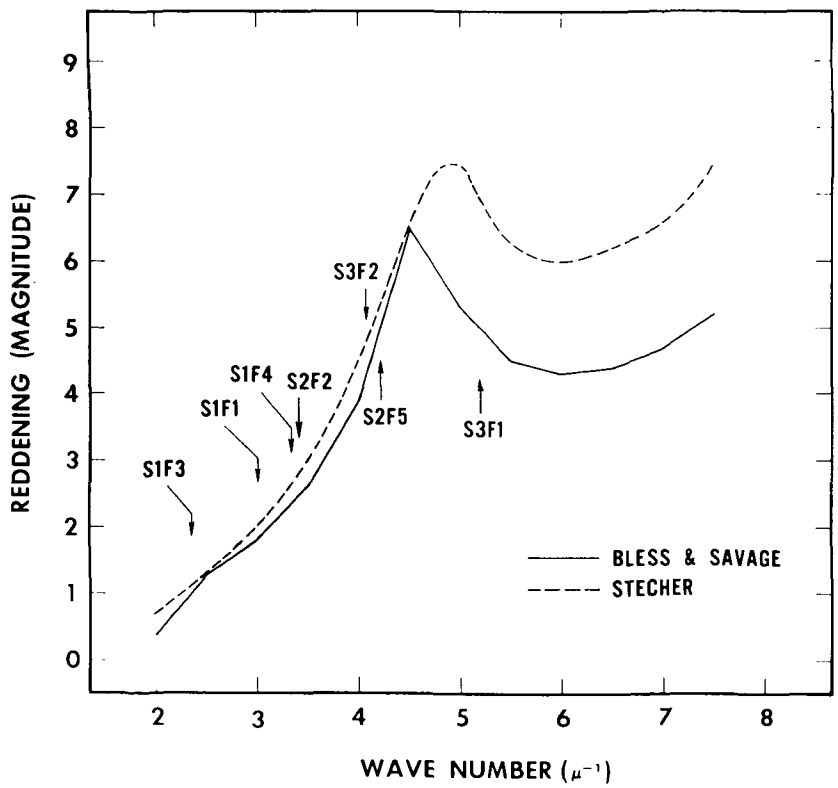

Figure 1.—Stecher's (1969) reddening curve (dashed line) and Bless and Savage's (1972) "mean" reddening curve (solid line) as a function of wavelength. Both curves are normalized to E(B-V) = 1. The arrows point out the effective wavelength of the various photometers.

Table 5. Observed and unreddened relative fluxes as a function of wavelength for the peculiar and comparison stars.

Star	No.of obs.	Effective wavelength (Å)						
		1913	2386	2462	2945	2985	3317	4252
3 Cen A	6	3.43	2.19	1.95	1.29	1.36	1.00	0.75
		0.02	0.01	0.01	0.00	0.00	0.00	0.00
		3.96	2.54	2.18	1.33	1.40	1.00	0.73
		0.02	0.01	0.01	0.00	0.00	0.00	0.00
Alpha Scl	2	3.17	1.98	1.88	1.24	1.27	1.00	0.86
		0.03	0.01	0.01	0.01	0.01	0.00	0.00
		3.36	2.10	1.96	1.26	1.28	1.00	0.85
		0.03	0.02	0.01	0.01	0.01	0.00	0.00
Alpha Scl	4	3.07	1.82	1.70	1.25	1.25	1.00	1.08
		0.02	0.01	0.01	0.01	0.00	0.00	0.00
		3.26	1.93	1.78	1.27	1.27	1.00	1.07
		0.02	0.01	0.01	0.01	0.00	0.00	0.00
3 Sco	1	2.38	1.63	1.48	1.18	1.27	1.00	0.84
		0.10	0.05	0.03	0.03	0.03	0.00	0.01
		3.57	2.46	2.04	1.29	1.37	1.00	0.76
		0.14	0.07	0.05	0.03	0.03	0.00	0.01
HR 8535	2	2.63	1.88	1.66	1.25	1.26	1.00	0.88
		0.08	0.04	0.03	0.02	0.02	0.00	0.01
		2.95	2.11	1.82	1.28	1.28	1.00	0.86
		0.09	0.05	0.03	0.03	0.02	0.00	0.01
HR 8770	2	2.13	1.45	1.38	1.13	1.20	1.00	0.84
		0.10	0.05	0.03	0.03	0.03	0.00	0.01
		2.85	1.96	1.73	1.20	1.26	1.00	0.79
		0.13	0.07	0.04	0.03	0.03	0.00	0.01
HD 21699	2	2.64	1.87	1.76	1.25	1.28	1.00	0.85
		0.05	0.03	0.02	0.02	0.01	0.00	0.01
		3.33	2.37	2.11	1.31	1.34	1.00	0.80
		0.07	0.03	0.03	0.02	0.02	0.00	0.01
HD 144334	2	2.70	1.86	1.64	1.24	1.30	1.00	0.88
		0.08	0.04	0.03	0.02	0.02	0.00	0.01
		3.60	2.50	2.06	1.31	1.37	1.00	0.82
		0.10	0.05	0.04	0.02	0.02	0.00	0.01

Table 5 (continued)

Star	No. of obs.	Effective wavelength (Å)						
		1913	2386	2462	2945	2985	3317	4252
HD 144661	2	2.26		1.37		1.25	1.00	0.87
		0.09		0.03		0.03	0.00	0.01
		3.02		1.72		1.31	1.00	0.81
		0.12		0.04		0.03	0.00	0.01
HD 144844	2	2.15	1.54	1.35	1.12	1.21	1.00	1.18
		0.09	0.04	0.03	0.03	0.03	0.00	0.02
		3.23	2.33	1.86	1.22	1.31	1.00	1.07
		0.13	0.07	0.04	0.03	0.03	0.00	0.02
35 Ari	2	3.85	2.12	1.99	1.34	1.33	1.00	0.76
		0.04	0.02	0.01	0.01	0.01	0.00	0.00
		4.71	2.61	2.34	1.39	1.38	1.00	0.73
		0.05	0.02	0.02	0.01	0.01	0.00	0.00
HD 142990	1	3.17	1.73	1.72	1.27	1.28	1.00	0.78
		0.08	0.03	0.03	0.02	0.02	0.00	0.01
		4.36	2.39	2.21	1.36	1.36	1.00	0.72
		0.11	0.05	0.03	0.02	0.02	0.00	0.01
Iota Her	1	4.30	2.50	2.17	1.40	1.41	1.00	0.63
		0.04	0.02	0.01	0.01	0.01	0.00	0.00
		4.55	2.65	2.27	1.42	1.43	1.00	0.62
		0.04	0.02	0.01	0.01	0.01	0.00	0.00
HD 68324	1	4.45		2.55		1.51	1.00	0.56
		0.07		0.03		0.01	0.00	0.00
		4.45		2.55		1.51	1.00	0.56
		0.07		0.03		0.01	0.00	0.00
114 Tau	1	4.23	2.21	2.10	1.42	1.39	1.00	0.68
		0.06	0.02	0.02	0.01	0.01	0.00	0.00
		4.75	2.49	2.29	1.45	1.42	1.00	0.66
		0.07	0.03	0.02	0.01	0.01	0.00	0.00
Rho Aur	3	3.92	2.19	2.04	1.34	1.34	1.00	0.85
		0.04	0.02	0.02	0.01	0.01	0.00	0.00
		4.28	2.39	2.19	1.37	1.36	1.00	0.83
		0.05	0.02	0.02	0.01	0.01	0.00	0.00

Table 5 (continued)

Star	No.of obs.	Effective wavelength (Å)						
		1913	2386	2462	2945	2985	3317	4252
115 Tau	2	3.50	1.94	1.84	1.34	1.29	1.00	0.89
		0.06	0.03	0.02	0.02	0.01	0.00	0.01
		4.05	2.25	2.06	1.39	1.33	1.00	0.86
		0.07	0.03	0.02	0.02	0.01	0.00	0.01
HD 67341	1	2.88		1.92		1.34	1.00	0.79
		0.13		0.05		0.03	0.00	0.01
		2.88		1.92		1.34	1.00	0.79
		0.13		0.05		0.03	0.00	0.01
16 Pup	1	4.03	2.17	2.08	1.28	1.36	1.00	0.84
		0.05	0.02	0.02	0.01	0.01	0.00	0.00
		4.15	2.23	2.13	1.29	1.37	1.00	0.84
		0.05	0.02	0.02	0.01	0.01	0.00	0.00
HD 93194	1	3.99	2.21	2.11	1.37	1.34	1.00	0.82
		0.06	0.03	0.02	0.02	0.01	0.00	0.01
		4.48	2.49	2.31	1.40	1.37	1.00	0.80
		0.07	0.03	0.02	0.02	0.01	0.00	0.01
19 Tau	1	2.55		1.59		1.28	1.00	0.95
		0.04		0.02		0.01	0.00	0.01
		2.70		1.66		1.29	1.00	0.93
		0.05		0.02		0.01	0.00	0.01
HD 21362	2	2.48	1.77	1.57	1.18	1.27	1.00	1.02
		0.07	0.03	0.02	0.02	0.02	0.00	0.01
		3.32	2.38	1.97	1.25	1.35	1.00	0.95
		0.09	0.04	0.03	0.02	0.02	0.00	0.01
17 Tau	1	2.62		1.58		1.37	1.00	0.89
		0.03		0.01		0.01	0.00	0.00
		2.70		1.62		1.38	1.00	0.89
		0.03		0.01		0.01	0.00	0.00
16 Tau	1	2.26		1.39		1.20	1.00	1.13
		0.09		0.03		0.03	0.00	0.02
		2.62		1.55		1.23	1.00	1.09
		0.10		0.04		0.03	0.00	0.02

Table 5 (concluded)

Star	No. of obs.	Effective wavelength (Å)						
		1913	2386	2462	2945	2985	3317	4252
Eta Tau	4	2.19		1.40		1.22	1.00	0.84
		0.01		0.00		0.00	0.00	0.00
		2.25		1.43		1.22	1.00	0.84
		0.01		0.00		0.00	0.00	0.00
20 Tau	1	2.11		1.32		1.26	1.00	0.97
		0.03		0.01		0.01	0.00	0.01
		2.37		1.44		1.29	1.00	0.94
		0.04		0.01		0.01	0.00	0.00
Tau 5 Eri	1	2.71		1.68		1.26	1.00	1.05
		0.05		0.02		0.01	0.00	0.01
		2.79		1.72		1.27	1.00	1.05
		0.05		0.02		0.01	0.00	0.01
Iota Lep	1	2.79		1.73		1.29	1.00	1.03
		0.05		0.02		0.01	0.00	0.01
		2.79		1.73		1.29	1.00	1.03
		0.05		0.02		0.01	0.00	0.01
18 Tau	1	2.32		1.47		1.24	1.00	1.10
		0.10		0.04		0.03	0.00	0.02
		2.46		1.54		1.25	1.00	1.09
		0.10		0.04		0.03	0.00	0.02
27 Tau	1	2.37		1.35		1.21	1.00	0.97
		0.03		0.01		0.01	0.00	0.00
		2.51		1.41		1.22	1.00	0.96
		0.03		0.01		0.01	0.00	0.00
41 Eri	3	2.59		1.59		1.26	1.00	0.99
		0.02		0.01		0.00	0.00	0.00
		2.59		1.59		1.26	1.00	0.99
		0.02		0.01		0.00	0.00	0.00

IV. RESULTS AND DISCUSSION

The data of Table 5 are presented as color-color diagrams in Figures 2 and 3. The horizontal bars in Figure 3 indicate the shift of the weak-helium line stars if Stecher's reddening curve had been adopted. The shift of the comparison stars would not be larger than 0.1 mag except for HD 142990 (B3 V) and HD 21362 (B6 V). The dashed line joins different observations of α Sculptoris.

The color indices m_λ(1920 Å) - m_λ(3320 Å) and m_λ(2460 Å) - m_λ(3320 Å) are essentially temperature dependent. The color m_λ(4250 Å) - m_λ(3320 Å) is related to the Balmer discontinuity which for B type stars is related to the effective temperature. Thus, by using the color-color diagrams we can perform an interesting comparison between inferences about temperature from different parts of the spectrum.

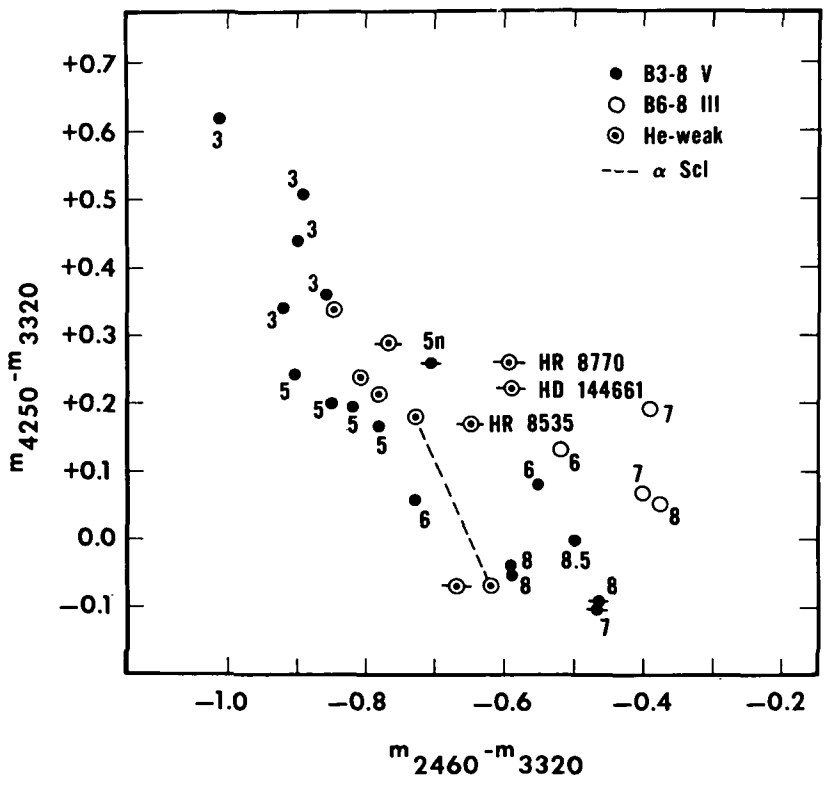

Figure 2.—Plot of the color index m_λ(4250) - m_λ(3320) vs. m_λ(2460) - m_λ(3320). The symbols are explained in the inset. The number near a dot indicates the spectral class. The dashed line joins observations of α Scl at two epochs (see Figure 6).

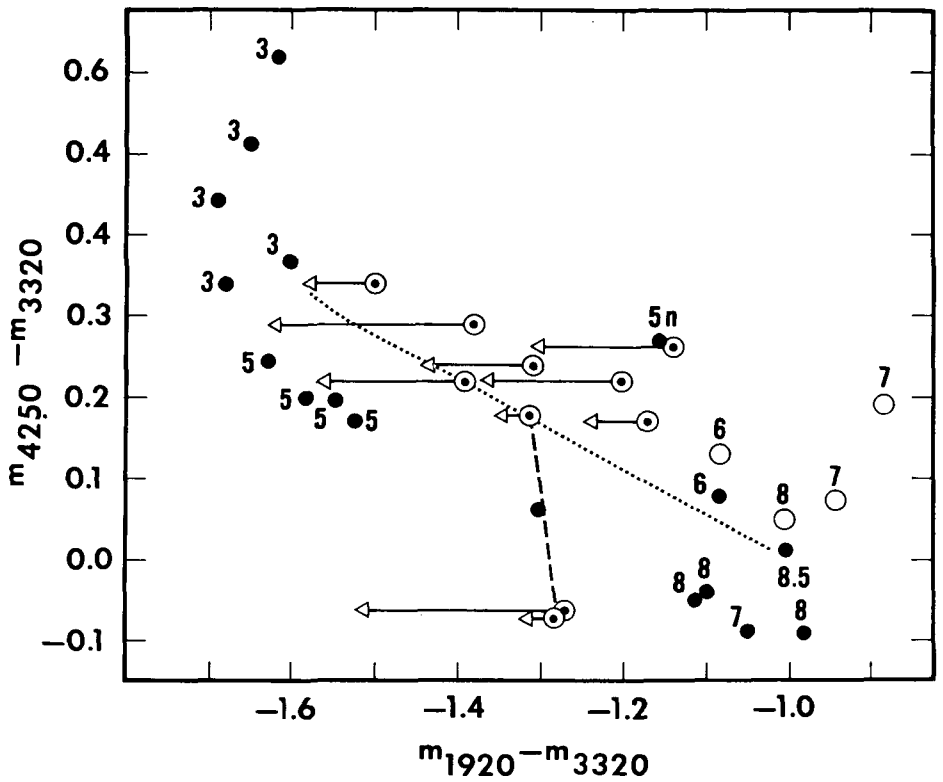

Figure 3.—The Balmer discontinuity is plotted against $m_\lambda(1920) - m_\lambda(3320)$. Symbols are the same as in Figure 2. The arrows indicate the position of the weak-helium stars according to Stecher's reddening curve. The broken curve is assumed as the upper edge of the main sequence band.

Identification of the weak-helium stars may be achieved by reference to Table 6. On both diagrams dwarf stars form a scattered sequence. A distinction between B3, B5 and B8 stars is clearly evident and enables us to infer a photometric classification from the ultraviolet spectrum. The spread in $m_\lambda(4250\ \text{Å}) - m_\lambda(3320\ \text{Å})$ is of the order of 0.1 mag. The giants, as a group, have a smaller Balmer discontinuity than their main sequence counterparts and are fainter at 2460 Å. Underhill (1972) has shown clear evidence of line blocking around 2400 Å for stars later than B5 due mainly to the second spectrum of the metals. The effect is certainly enhanced in the spectra of the giant stars and accounts for their location in Figure 3.

In Figures 4 and 5 we have schematically represented the distribution in wavelength of the multiplets of most of the elements known to be strong in the weak-helium stars. The

Table 6. Color indices of the weak-helium stars corrected by means of the Bless and Savage reddening curve

Star	m(4250)-m(3320)	m(2460)-m(3320)	m(1920)-m(3320)
3 Cen A	0.343	-0.847	-1.495
α Scl	0.179*	-0.733*	-1.315*
3 Sco	0.294	-0.774	-1.380
HR 8535	0.166	-0.650	-1.174
HR 8770	0.261	-0.596	-1.136
HD 21699	0.242	-0.810	-1.305
HD 144334	0.216	-0.784	-1.392
HD 144661	0.225	-0.591	-1.200
HD 144844	-0.074**	-0.671	-1.272

*on January 23, 1971
**not corrected for duplicity

dashed curves show the sensitivity curves of photometers S3F1 (1920 Å) and S3F2 (2460 Å) as a function of wavelength.

a) The Weak-Helium Stars at 2460 Å

In Figure 6 the flux of α Scl at two epochs is compared with the flux from a hydrogen line-blanketed model atmosphere (Klinglesmith 1971). We can infer an effective temperature of at least 16000°K which may be compared with 14600 ± 200°K determined by Norris (1971). It can be shown that Norris' measurements of the continuous energy fit a hydrogen line-blanketed model of about 14000°K so that the difference of about 1500°K appears to be real.

The appearance of the depression in the continuum at 2400 Å on July 10, 1970 may be attributed to strengthening of Ti II and Sr II lines (see Figure 5) which have been observed to be strong in the ground-based spectrum of this star. Alpha Scl has been reported as a possible spectrum variable by Jugaku and Sargent (1961). The flux removed from the 2400 Å region is redistributed longward of the Balmer discontinuity. The black dot at 4250 Å in Figure 6 can be fitted to a model atmosphere of 14000°K in better agreement with Norris' estimate.

The stars 3 Cen A, 3 Sco, HD 144334 and HD 21699 are the hottest weak-helium stars. Their location in Figure 2 in the range B3-B5 agrees well with the photometric temperature classification (Table 1). We note, in addition, that 3 Sco and HD 144334 have strong Si II and Si III lines (Norris 1971) and

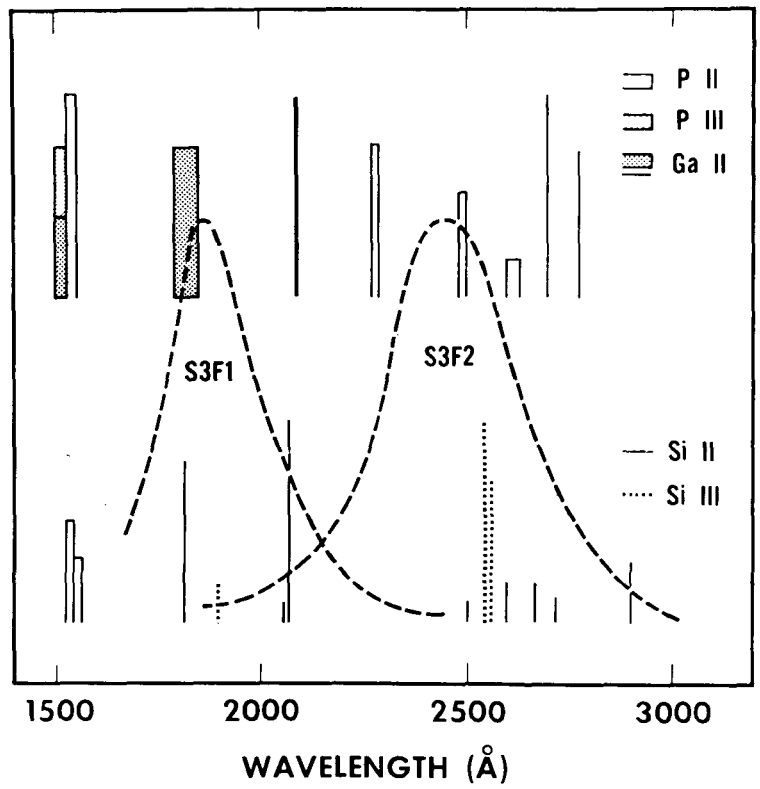

Figure 4.—The distribution in wavelength of the lines of the elements with spectra strong in the weak-helium stars is shown behind the sensitivity curves of photometers S3F1 (1920 Å) and S3F2 (2460 Å). Ordinates are in arbitrary units.

phosphorous is overabundant in 3 Cen A (e.g. Hardorp 1967). Figure 4 shows that the filter S3F2 is affected by line blocking due to the above elements. This effect supports further the conclusion that the stars considered have normal fluxes at 2460 Å.

The stars HR 8770, HD 144661 and possibly HR 8535 seem to be peculiar. They are either considerably fainter at 2460 Å than expected according to their ground-based colors or if they have types B7 to B9 III they have an excess of radiation at 2460 Å.

We have two good spectrograms of HR 8770 and one each for HR 8535 and HD 144661 at a dispersion of 40 Å/mm. They have been obtained using the GSFC 36-inch telescope, employing a blue sensitive Carnegie Image Tube and a IIa-O emulsion behind a BG-12 filter. The spectra of both HR 8535 and HD 144661 are similar in H, Mg, Si II and He I line strengths. The ratio Mg II λ4481/He I λ4471 would indicate B8. However, the ratio He I λ4026/Ca II-K excludes B8 or a later type. The line

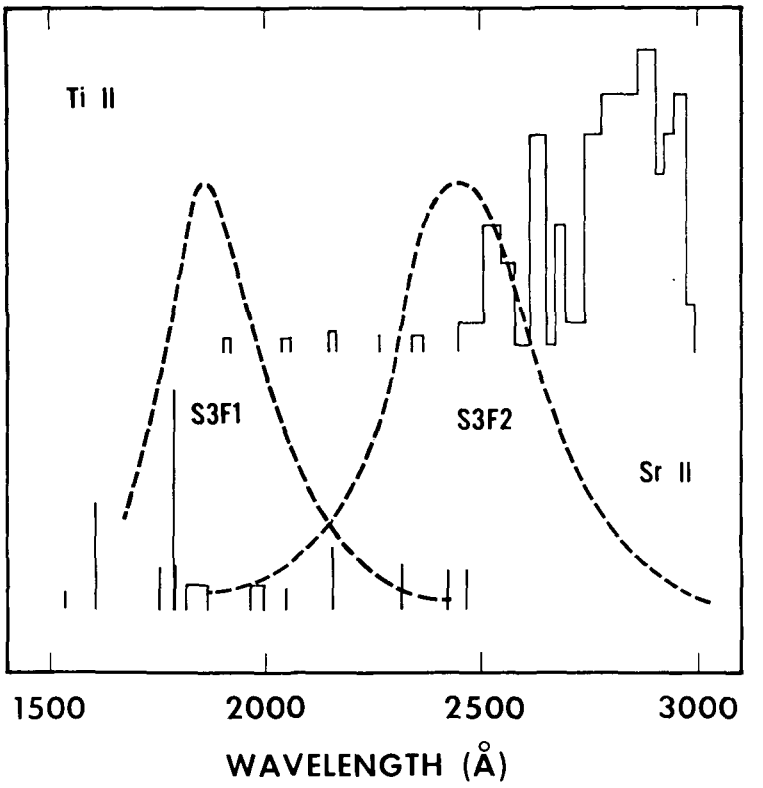

Figure 5.—The meaning is the same as in Figure 4.

Hg II λ3984 in HR 8535 observed by Molnar (1971) is not obviously present on our spectrograms. This star may be a spectrum variable.

The star HR 8770 has fainter helium lines and stronger Si II λ4128-30 than the above two stars. The Balmer lines are somewhat sharper and Si II λ4200 may be present on one of the spectrograms. The ratio λ4026/K excludes type B9. The faintness of the K-line and Mg II λ4481 in all three stars places some doubt on considering them as giants around B7-8. We cannot exclude that HR 8770 may be related to the silicon stars. Norris (1971) suspects the presence of P II lines in the spectrum of HD 144661. Hence line blocking around 2400 Å due to silicon and phosphorous cannot be discounted for explaining the flux deficiency of HR 8770 and HD 144661. The evidence, however, is not as clear as for the hottest weak-helium stars discussed above. We do not have data on B5 III and B6 III stars with which to support the inference that HR 8770 and HD 144661 are giants of earlier type than B7 in analogy with the location of the late B-type giants on the diagram. We may suggest as an alternative hypothesis that these two stars are brighter at 3320 Å than normal.

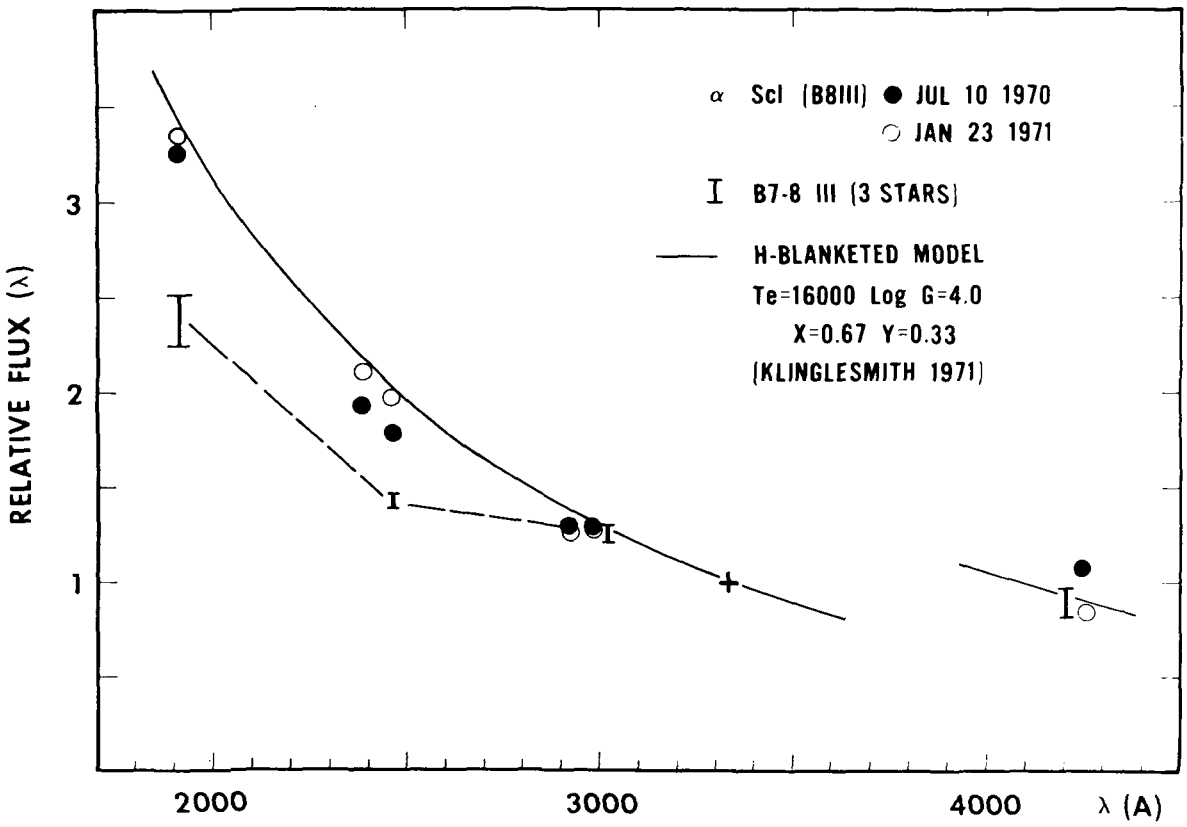

Figure 6.—The observations of α Scl at two epochs are compared with the flux of a hydrogen line blanketed model atmosphere (Klinglesmith 1971). The observations of three stars of the same spectral type as α Scl are shown by the vertical bars. The flux is normalized to 3320 Å.

We conclude the discussion of Figure 2 by noting that HD 144844 is on the lower edge of the main sequence band. One would expect to find a strong deficiency at 2460 Å because of blanketing due to P II, Ga II, Si II and Fe II lines which have been observed in the ground-based spectrum by Norris (1971). We may argue as follows: first, the E(B-V) is rather large (see Table 4) so that the correction for reddening may be over-estimated. Second, HD 144844 is a double-lined spectroscopic binary. According to Norris (1971) the secondary is three times fainter and of spectral type A0 or slightly earlier. If we assume T_e = 12000°K for the secondary, Klinglesmith's models give $F_\lambda(4250)/F_\lambda(3320) = 1.35$. The ratio of 1.07 observed for the mixed components (Table 5) requires a ratio of 1.0 for the primary if we assume the secondary to be three times fainter in S1F1. Thus, m_λ(4250 Å) - m_λ(3320 Å) ≃ 0.0

might be a more correct color index for the brighter star alone. Third, we wonder whether we have observed HD 144844 in a phase similar to that of α Scl on July 10, 1970. Its location in Figure 2 agrees with that of α Scl when the star has an increased Balmer discontinuity.

In summary, when allowance is made for the uncertainties due to a qualitative accounting for line blocking around 2400 Å, the following picture emerges:

a. Most of the program weak-helium stars appear to have normal fluxes corresponding to the range of the hot stars.
b. The temperature determination and hence, helium abundance derived from ground-based observations may be affected by large uncertainties. In α Scl the apparent helium underabundance is probably larger than previously reported.
c. It is difficult to interpret HR 8770, HD 144661 and perhaps HR 8535 as having a normal flux distribution on the basis of the present knowledge of their spectra.

b) The Weak-Helium Stars at 1920 Å

The weak-helium stars are fainter at 1920 Å than main sequence stars of the same color in Figure 3. If we assume 0.1 mag as the natural width of the main sequence band in m_λ(4250 Å) - m_λ(3320 Å), we see that α Scl and HD 144334 are on the upper edge as defined by the broken line, thus not necessarily peculiar. Moreover, we have seen that the continuum of α Scl fits nicely to a model atmosphere. For HD 144334 we may advocate line blocking around 2000 Å from Si II and Si III (see Figure 4). By reference to Figure 4, the position of 3 Cen A may be attributed to the overabundance of gallium (c.f. Hardorp 1967).

The discrepancy could also be removed for 3 Sco if we consider both line blocking by Si II and Si III and the possibility of having underestimated the reddening. Finally, we can shift HD 21699 to within the main sequence band since Stecher's curve is likely to represent more correctly the reddening law for the Perseus region than does the law we have adopted.

The position of HD 144844 is still embarrassing. If, for consistency, we admit that line blocking due to P II, Ga II, Si II and Fe II plays a role in filter S3F1, we should conclude that this star is brighter at 1920 Å for its color (B7) and much brighter for its spectrum (B9) than expected. We feel, however, that the evidence is not strong enough to suggest an excess of radiation.

The stars HR 8535 and HR 8770 are "peculiar" in Figure 3 even when their position corrected according to Stecher's reddening curve is considered. We note that HD 144661 and

HD 144844 are relatively close in the Sco-Cen association, so that it is reasonable to assume they undergo the same reddening law. The fact that the Bless and Savage curve seems more reliable for HD 144844 supports the conclusion that HR 8535, HR 8770 and HD 144661 may form a separate group from the other weak-helium stars. They have comparable color indices and are fainter by about 0.4 mag at 1920 Å than their colors would predict. The possible presence of P II in the spectrum of HD 144661 cannot account for line blocking in filter S3F1 (Figure 4); it is not ascertained whether Si II lines may play a role in HR 8770, although the effect is expected to be stronger than at 2460 Å (Figure 4).

New spectrograms and the ultraviolet photometry show that all three stars are definitely earlier than B8. If their position on the diagram is to be explained by giantism in analogy with the B6-8 III stars, their type is possibly about B6 III. Contrary to this hypothesis we note, however, that Norris (1971) has determined log g = 3.95 for HD 144661, a value typical of dwarf stars, and that HR 8535 has a similar spectrum to that of HD 144661.

V. SUMMARY AND CONCLUSIONS

We should emphasize that the conclusions that we can draw from the previous sections are certainly biased by the qualitative character of the analysis and by selection effects in the choice of the comparison stars.

Do the program weak-helium stars have normal fluxes? We feel the answer is affirmative for 3 Cen A, 3 Sco, HD 144334, HD 21699, α Scl and possibly HD 144844, after allowance is made for line blocking shortward of 2800 Å due to the abnormal strength of lines from the heavier elements. The existence of blanketing is likely to distort the continuum longward of the Balmer discontinuity, as in the case of α Scl, placing an uncertainty on the temperature and helium abundance derived from ground-based observations. The effective temperature and helium underabundance of α Scl are probably higher by a significant factor than previously reported.

Norris (1971) has found that a number of weak-helium stars on the (θ_e, log g)-plane are beyond the helium-ionization convective boundary which is thought to constitute the limit for the Ap stars (Searle and Sargent 1967). If line blocking in the ultraviolet redistributes energy longward of the Balmer discontinuity as in α Scl, the hottest weak-helium stars could be given a higher temperature, which would support Norris' discussion about the mechanism of the Ap phenomenon.

It is difficult to interpret HR 8535, HR 8770 and HD 144661 as having a normal flux distribution. New spectrograms and the ultraviolet photometry exclude that they are later than B7 and

of luminosity higher than V. However, they are fainter at 1920 Å and 2460 Å than the UBV photometry and the color index m_λ(4250 Å) - m_λ(3320 Å) would predict by about 0.4 mag and 0.2 mag respectively. Only as a suggestion we have mentioned the possibility that they are brighter at 3320 Å than normal, which would account for the smaller Balmer discontinuity and the apparent faintness shortward of 2800 Å. For HR 8770 line blocking by Si II lines cannot be excluded.

We have discussed the important role of metal line blocking only. We might add that metal continuous opacity sources are negligible in the weak-helium stars. These stars have temperatures of B3 to B5 stars and the important continuous opacity sources such as Si I will be completely ionized. The uncertainty in the reddening correction for each star places a restriction on any finer analysis of the observational material presented in this investigation.

One of us (P. L. Bernacca) wishes to thank the European Space Research Organization for granting a post-doctoral fellowship and Dr. A. B. Underhill, Dr. A. Boggess III and Dr. D. A. Klinglesmith, whose interest made it possible for him to come to the Goddard Space Flight Center. He wishes also to thank Prof. L. Rosino, Prof. L. Gratton and Prof. K. Wurm who encouraged him to obtain an opportunity of working on OAO data.

We are indebted to Prof. A. D. Code for making available the necessary information, to Dr. R. C. Bless and Dr. B. D. Savage for providing the 'mean' reddening curve and to Dr. A. V. Holm who helped us to obtain the data.

M. R. Molnar wishes to thank the Space Astronomy Laboratory of the University of Wisconsin for the opportunity of working with OAO-2

Finally, we thank Dr. D. S. Leckrone for helpful discussions.

REFERENCES

Bernacca, P. L. 1968, Contr. Oss. Astr. Asiago, No. 202.
Bertiau, F. C. 1958, Ap. J. 128, 533.
Bidelman, P. W. 1960, Publ. A. S. P. 72, 24.
Blanco, W. M., Demers, S., Douglass, G. G. and Fitzgerald, M. P. 1968, Publ. U. S. Naval Obs., II Series, Vol. XXI.
Bless, R. C. and Savage, B. D. 1970, I. A. U. Symp. No. 36, p. 28.
_____ 1971, private communication.
_____ 1972, this volume.
Ciatti, F. and Bernacca, P. L. 1971, Astr. and Ap. 11, 425.
Code, A. D., Houck, T. E., McNall, J. F., Bless, R. C. and Lillie, C. F. 1970, Ap. J. 161, 377.
Code, A. D. 1971, private communication.

Garrison, R. F. 1967, Ap. J. 147, 1003.
Hardorp, J. 1967, The Magnetic and Related Stars, ed. R. C. Cameron (Baltimore: Mono Book Co.), p. 445.
Hoffleit, D. 1964, Catalogue of Bright Stars (3rd ed.; New Haven: Yale University Observatory).
Jaschek, M., Jaschek, C. and Arnal, M. 1969, Publ. A. S. P. 81, 650.
Jaschek, C., Conde, M. and DeSierra, A. C. 1964, Catalogue of Stellar Spectra Classified in the Morgan-Keenan System, La Plata.
Johnson, H. L. 1966, Ann. Rev. of Astr. and Ap. 4, 193.
Jugaku, J. and Sargent, W. L. W. 1961, Publ. A. S. P. 73, 249.
_____ 1963, Ap. J. 138, 90.
Klinglesmith, D. A. 1971, NASA SP-3065.
Mitchell, R. 1960, Ap. J. 132, 68.
Molnar, M. R. 1971, Ph. D. Thesis, University of Wisconsin.
Norris, J. 1971, Ap. J. Suppl. 23, 213.
Roman, N. G. and Morgan, W. W. 1950, Ap. J. 111, 426.
Schild, R. E. and Chaffee, F. 1971, Ap. J. (in press).
Searle, L. and Sargent, W. L. W. 1964, Ap. J. 139, 793.
_____ 1967, The Magnetic and Related Stars, ed. R. D. Cameron (Baltimore: Mono Book Co.), p. 219.
Slettebak, A. 1963, Ap. J. 138, 118.
Stecher, T. P. 1969, Ap. J. (Letters) 157, L125.
Underhill, A. B. 1972, this volume.
Vaucouleurs, de, A. 1957, M. N. R. A. S. 117, 449.

ULTRAVIOLET PHOTOMETRY OF NOVA SERPENTIS 1970

Arthur D. Code
University of Wisconsin
Madison, Wisconsin

I. INTRODUCTION

The appearance of the bright nova, Nova Serpentis 1970, provided the first opportunity to obtain spectrophotometric observations of a nova in the vacuum ultraviolet. OAO-2 carried out systematic measurements from shortly after outburst on through the first sixty days of nova activity. This data consists of filter photometry and spectral scans utilizing the Wisconsin instrumentation described by Code et al. (1970). It is the purpose of this paper to describe general characteristics of the light and spectral variations in the ultraviolet exhibited by this set of data.

II. OBSERVATIONS

Nova Serpentis 1970 was discovered on February 13, 1970 by M. Honda (Hirose 1970). The first attempt to observe the object by the OAO occurred on February 17 with negative results. Dr. C. M. Anderson obtained a photograph position of Nova Serpentis with the 36-inch Pine Bluff reflector on the night of February 18. On the basis of this revised position, OAO-2 obtained the first measurements of a nova in the ultraviolet on February 18.5008, 1970 (JD 2440636.008). Reliable photometry was obtained for all filter bandpasses longward of 1500 Å. A spectral scan with the long wavelength spectrometer provided data with a resolution of approximately 20 Å longward of 2500 Å. The spectrum displayed absorption lines similar to those characteristic of an early F star, although the energy gradient was steeper, suggesting significant interstellar extinction. Throughout the following two months of observations the radiation shortward of 3000 Å gradually increased in intensity while the spectral scans were characterized by a com-

plex development of emission line features. Thus while the visual light curve declined 2.5 magnitudes the flux at 2460 Å, for example, increased by approximately 2.5 magnitudes.

Figure 1 shows three representative spectral scans obtained with Spectrometer 1 on February 20, March 9 and April 4, 1970. At the spectral resolution of 20 Å, the emission features first made their appearance about six days after discovery. Most of the features have not as yet been identified and are probably blends of several strong lines. Two of the features have been tentatively attributed to Fe II emission while the strong line at 2800 Å is the Mg II resonance doublet. During the period covered by these spectra, the visual magnitude decreased by about 2.5 magnitudes. It is apparent from examination of the spectra presented that the flux at the long wavelength limit of the scan is decreasing while both the underlying continuum and the broad emission features shortward of 3200 Å continued to brighten. In the final spectra on April 4, the Mg II emission line at 2800 Å dominates the spectrum.

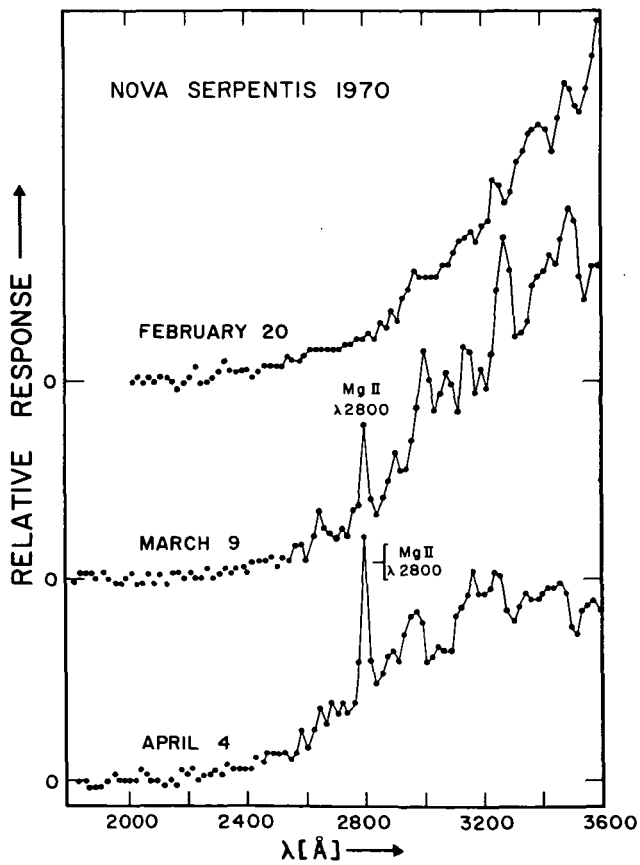

Figure 1.

Figure 2a shows the visual light curve during the period of observation based on the data from Borra and Anderson (1970). Figure 2b shows the variation in the continuum adjacent to the 2800 Å emission while in Figure 2c the emission line intensity is plotted. The simplest interpretation of the Mg II resonance line strength is that through the first 50 days we are observing an optically thick shell. On the basis of a constant velocity of expansion of the order of 800 km/sec the observed intensity variation is consistent with a radial expansion accompanied by a decrease in shell temperature from 10000°K to 8000°K. We may estimate the total number of resonance Mg II ions if we assume that the optical depth becomes unity about 50 days after outburst, corresponding to the time when the intensity begins to decrease. The total mass of Mg II under these assumptions is quite small, of the order of 10^{22} grams.

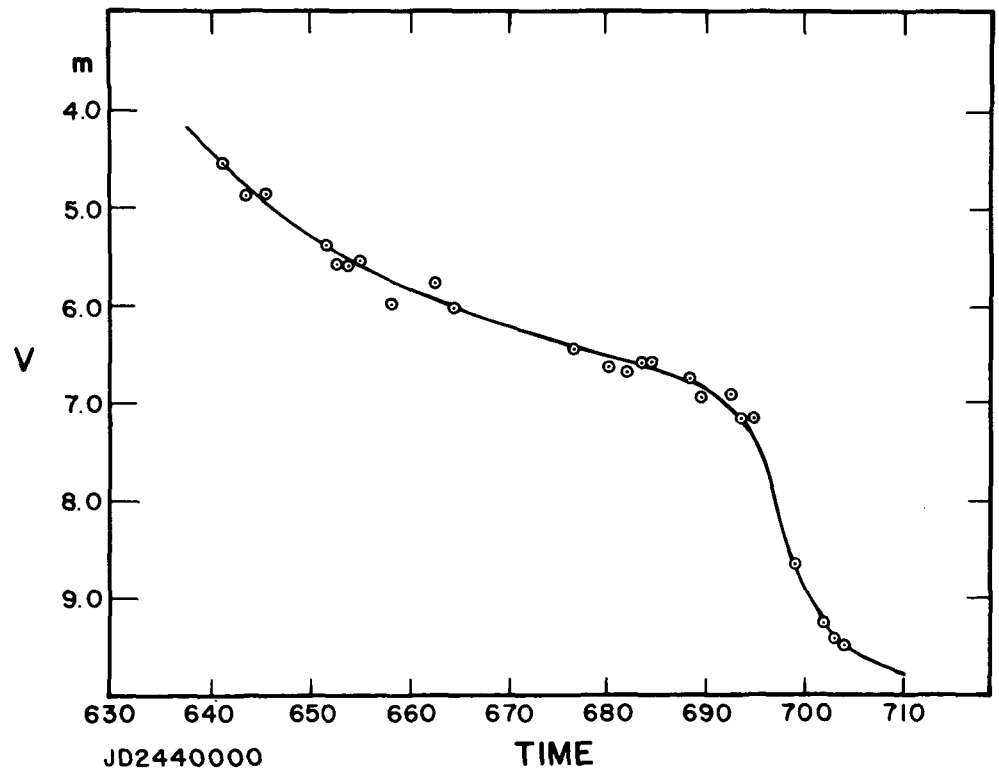

Figure 2a.

The broad band filter photometry exhibits the same property displayed by the spectral scans. The longest wavelength bandpass at 4250 Å yields a light curve similar to the visual curve. The light curve at about 3000 Å increases about 2.5

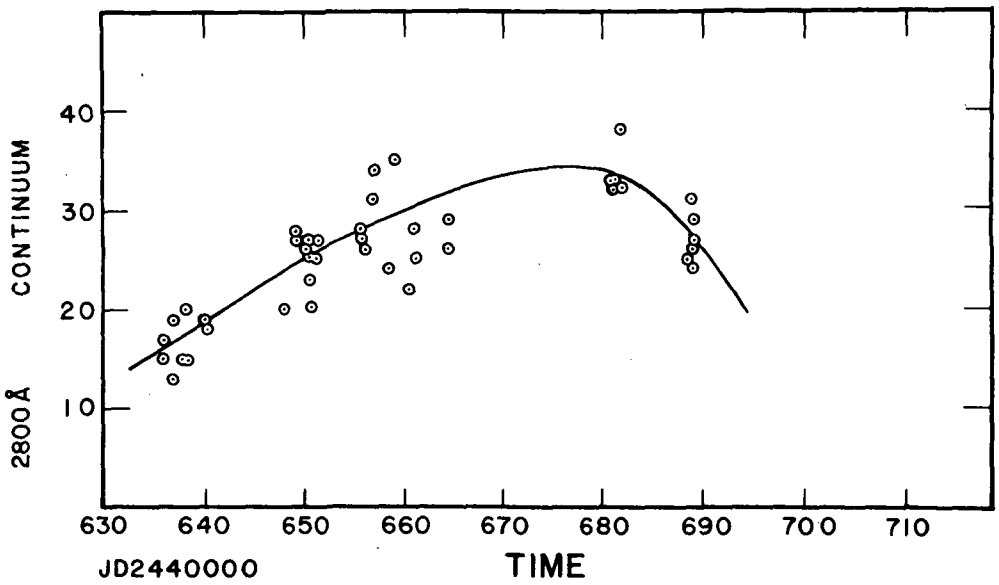

Figure 2b.

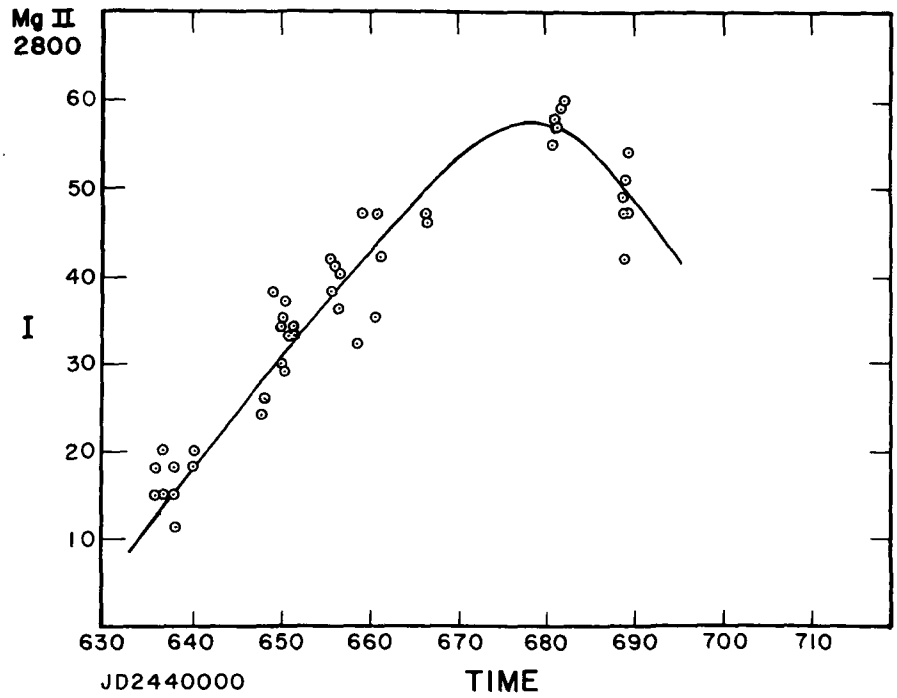

Figure 2c.

magnitudes during the first 25 days and then starts a slow decline throughout the remainder of the observing period. At 2460 Å and 1550 Å the intensity continued to increase during the entire period of observations. The B-V colors of Nova Serpentis, the existence of a very strong diffuse 4430 Å band, and the ultraviolet spectral distribution indicate a B-V color excess of the order of 1 magnitude or a visual extinction A_V ~ 3.0 magnitudes. Figure 3 shows the ultraviolet energy distribution derived from filter photometry measurements, assuming the average extinction given by Bless and Savage (1972) for A_V = 3.0 magnitudes.

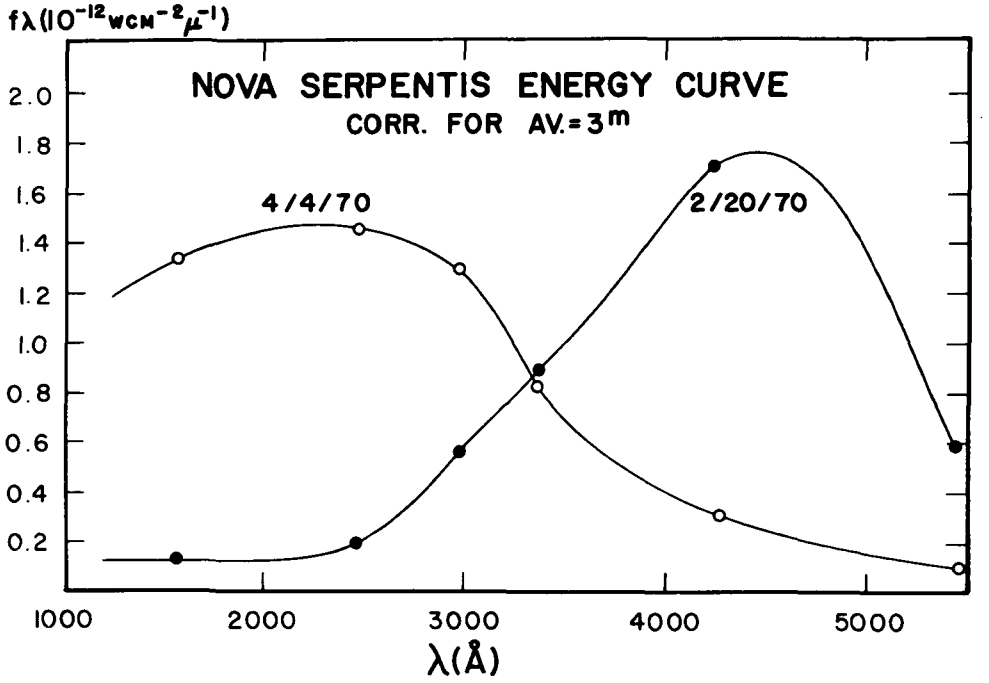

Figure 3.

The ultraviolet energy distribution defined by the filter photometry yields approximately constant total flux between 1000 and 6000 Å during the first 60 days, the decrease in light in the visual being due to a shift of the energy curve towards the ultraviolet as the system evolves. These results suggest a model in which the bolometric luminosity remains relatively constant but the conversion of far ultraviolet photons to longer wavelengths undergoes a secular change as the density of the shell decreases. The system is thus somewhat analogous to the rapid evolution of a planetary nebula.

If the visual extinction suggested by the ultraviolet energy curve and the B-V measurements arises from a nearby dust cloud, the energy absorbed by the grains is more than sufficient to account for the infrared emission commencing 50 days after outburst (Geisel, Kleinman and Low 1970). The infrared radiation at 10 μ reached a maximum about 100 days after outburst at which time it was characterized by a black body temperature of the order of 900°K. Whether or not the ultraviolet radiation absorbed by the grains would raise the temperature to 900°K depends upon the albedo and infrared radiation properties of the grains. Another important input to the grain temperature is the mass motion of the expanding shell. Virtually all hydrogen atoms would be stopped by an optically thick dust cloud. Estimates of the grain heating by atom-grain collisions yield temperatures and infrared emission similar to the observed radiation.

REFERENCES

Bless, R. C. and Savage, B. D. 1972, this volume.
Borra, E. F. and Anderson, P. H. 1970, P.A.S.P. 82, 1070.
Code, A. D., Houck, T. E., McNall, J. F., Bless, R. C. and Lillie, C. F. 1970, Ap. J. 161, 377.
Geisel, S. L., Kleinman, D. E. and Low, F. J. 1970, Ap. J. (Letters) 161, L101.
Hirose, H. 1970, I.A.U. Circ. No. 2212.

ULTRAVIOLET PHOTOMETRY OF GLOBULAR CLUSTERS

G. A. Welch
Wesleyan University
Middletown, Connecticut

A. D. Code
University of Wisconsin
Madison, Wisconsin

ABSTRACT

Filter photometry measurements of the integrated light from several globular clusters between 1500 and 4000 Å are discussed. The techniques and problems associated with carrying out photometry of faint extended sources with the OAO-2 instrumentation are described first. The energy distribution for globular clusters determined from these data are corrected for interstellar extinction on the basis of B-V color excesses and a mean ultraviolet extinction curve. The results are compared with synthetic cluster calculations. The ultraviolet energy distribution is primarily determined by the number of stars at the blue end of the horizontal branch. For the bluer globular clusters the number of blue horizontal branch stars required is greater than that usually inferred from ground-based observations.

I. INTRODUCTION

The University of Wisconsin experiment on OAO-2 was designed initially to conduct observations of early-type stars in the ultraviolet. For the brighter early-type stars photometric accuracies of the order of $0^{m}.01$ have been obtained. The observation of faint, extended late-type objects, however, is compromised by the instrumental design; nevertheless, with care it has been possible to obtain a substantial body of data on globular clusters and external galaxies. The conversion of raw data, gathered by the stellar photometers, into reliable measurements of the spectral energy distribution of faint

sources involves an intricate series of considerations. Some are problems common to all observations which push the satellite to its limiting sensitivity, while others arise only when extended sources are viewed. Additional problems are encountered with red objects where the bulk of the radiation is longward of the nominal filter bandpass. General information on the satellite operating procedure is given by Code et al. (1970), while some of the problems associated with photometry of later type stars are discussed by Doherty (1972). Although some of the following discussion overlaps with these papers, it is felt that a fairly complete treatment will give a better feeling for the reliability of the results presented here and in the separate discussion of extragalactic objects (Code, Welch and Page 1972).

The University of Wisconsin package contains four 8-inch telescopes (stellar photometers) which are provided with separate photomultipliers and associated electronics. The optical path of each stellar photometer is intercepted by a filter wheel having five positions. Three of these positions are occupied by interference filters while the others hold a dark mask and a Cerenkov calibration source. The filters are all used in their first order so that transmission by higher orders occurs at wavelengths too short to be transmitted or detected. The filter composition and photomultiplier types are given by Code et al. (1970). The filters are identified either by their position in the filter wheel (e.g., S3F1 ≡ stellar photometer three, filter one) or by their constant energy wavelength (S3F1 ≡ 1910 Å). At low signal levels the photometer pulse counting mode is the most accurate. After pulse amplification and shaping the photomultiplier pulses are fed to a precounter which scales by 64. The exposure time generator gates the output of the prescaler to the pulse count registers. Each digital count stored in the spacecraft memory and transmitted to the ground, therefore, corresponds to 64 photoelectron events and a single measurement to the number of digital counts accumulated in one exposure time. The counts referred to throughout this paper will be these scaled-down counts for a single exposure time. In the following section we shall discuss photometric problems arising from the nature of this instrumentation and in the next section the related observing difficulties will be discussed.

II. INSTRUMENTAL CONSIDERATIONS

There are three principal sources of problems introduced by the photometric instrumentation: 1) transmission leaks in the interference filters, 2) fluorescence of the filter material produced by incident particles or photons, and 3) the finite bandpasses of the filter-photomultiplier combinations. These

effects are now considered separately.

1) The transmission of an ideal multilayer interference filter longward of the first order bandpass should be determined by the total thickness of the aluminum layers. For the filters employed in the OAO photometers, this transmission should be about 10^{-4}. Typical measured transmissions are about a factor of two greater than this theoretical value. Examination of the filters reveals microscopic pinholes which developed shortly after filter fabrication. After the first few weeks the filters stabilize and remain constant with time. In an investigation of the consistency of the stellar photometers, Caldwell (1971) found evidence of serious pinhole defects in S2F3 (2390 Å) and S2F1 (2030 Å). The red leaks in these two filters make measurements of late-type objects unreliable and the data on globular clusters and galaxies from these filters have been discarded. For the remaining filters an estimate has been made of the maximum likely effect of microscopic pinholes from the results of tests run by T. Fairchild and described by Doherty (1972). The results are described in (3) below.

2) The photomultipliers may generate spurious events as a result of fluorescence or Cerenkov radiation in the filter substrate or the photomultiplier window due to incident particles or photons. The effect of the terrestrial radiation belts are discussed in a later section. The presence of the Sr^{90} in the calibration sources, however, introduces a measurable background count, which depends upon the filter position. The background count relative to the dark slide position has been measured several times with the spacecraft sunshade closed. The effect is insignificant for stellar photometers 1 and 2. The maximum effect for stellar 3 is approximately 6 counts on the 64 second exposure time, Gain E4, and for stellar 4 approximately 10 counts. This filter bias is constant and the statistical fluctuations correspond to less than 1/3 of a count. This effect, therefore, does not degrade the measurements of faint objects. The Sr^{90} Beta particles do, however, cause fluorescences in the CaF_2 substrate of S3F5 (1680 Å), S4F1 (1550 Å) and S4F3 (1430 Å). Of these, the stellar 4 filters are unaffected because fluorescence occurs at wavelengths to which the photocathode (CsI) is not sensitive. In the 1680 Å filter, however, about 34 counts are introduced by fluorescence. Although the random statistical fluctuation should be $\sqrt{64n}/64$ or about 3/4 of a count, we do not feel confident about reducing data corresponding to a few counts in the presence of this fluorescence and have decided not to use the data from this filter.

3) The relation between heterochromatic photometry and monochromatic magnitudes for finite bandwidths depends upon the spectral energy distribution of the source. It is most

convenient to compare data for such sources at fixed wavelengths; thus we can discuss the question in terms of a flux correction which must be applied to the measurements (cf. Code 1962) at these (constant energy) wavelengths.

Corrections relative to the S1F1 (3320 Å) measurements have been calculated for spectral energy distributions representing the following types of diffuse objects (Code, Welch and Page 1972): spiral galaxies, ellipticals with turnups below 2200 Å, ellipticals whose energy distribution below 3000 Å drops with wavelength in the manner given by $\log (F_\lambda/F_{3330}) = \lambda/1020 + \text{const.}$

These energy distributions are based on examination of the most reliable observations of galaxies presently available, and adequately represent the globular clusters as well. The prelaunch filter-phototube response functions have been used; there is no indication of significant changes since launch. The influence of possible red leaks, including pinholes, has been estimated by performing the calculations twice with different red tails added to the response functions. In one case the functions were extrapolated smoothly to zero in the red. The other case consisted of using a flat tail having a transmission of 0.1 percent of the filter maximum out to red cutoff of the photocathode. This value is based on Fairchild's test of the transmission at 4037 Å and 5210 Å of a filter made in the evaporator at the same time as the flight filter S3F2 (2460 Å). The test was run in January 1971 after scrubbing the filter with a piece of paper to produce excessive degradation. Since the filter had not been carefully handled at the Space Astronomy Laboratory, it was assumed to have suffered greater deterioration than any of the spacecraft filters.

The results are as follows. For objects having a fairly flat energy distribution (spiral and irregular galaxies and all globular clusters reduced to date excepting M80 and 47 Tuc) the corrections for both assumed red leaks is in the range of 1-3 percent for all filters except S4F1 (1550 Å) and S1F4 (2980 Å). For the former the correction in both cases is about 9 percent while addition of the 0.1 percent red leak raises the S1F4 correction from 2 to 8 percent. These corrections are less than the uncertainties introduced by other factors (for example, the filter calibrations and counting statistics) and have not been applied.

In the case of objects having energy distributions similar to elliptical galaxies the breadth of the bandpasses can produce larger corrections. However, their magnitude depends very little on the shape of the red tails as long as they transmit at about the 0.1 percent level. If the intensity falls exponentially below 3000 Å the corrections are never greater than about 8 percent because the slope of the spectrum does not change by much throughout the ultraviolet. However,

if a sharp turnup is present the corrections for filters below S1F1 rise to between 20 and 30 percent, and their sense is to lower the observed intensities relative to 3330 Å. Thus if an ultraviolet excess exists we are underestimating it. We do not feel such corrections are justified at present. The data for ellipticals below 2460 Å is inconclusive (Code, Welch and Page 1972) and turnups of this nature have not been found in globular clusters (based on exclusion of 1680 Å filter data).

We now discuss questions arising from the way in which data is collected.

Each precounter continuously receives and stores incoming phototube events, running through its 64-event cycle regardless of whether or not an integration is in progress. As the result of a single command the number of times the precounter is currently cycling within the specified integration time is stored in spacecraft memory (one cycle is referred to as one "count"). Approximately eight seconds after the first integration ends the process is repeated, and the observation is complete after six such integrations have been separately stored. The integration time and/or filter may then be changed for another observation.

The electronic process which terminates an integration can also cause a single count to be stored in memory, depending on whether or not the last (32-place) binary bin in the precounter is on or off at that instant. Since this happens on the average half of the time, the result is that a single observation (six integrations) will on the average be too large by three counts. The number used to represent the observation is almost always the mean of the six integrations and will thus be too large by 0.5 count on the average. A bias of -0.5 count is used in the averaging process to correct for this. At the count levels encountered in practice the measured mean of the six integrations is always biased by 0.5 counts.

The first integration begins at a random point in the precounter cycle, and the rate of incoming events is usually large enough to randomize the precounter within the 8-second delay between successive integrations. The mean of six integrations should therefore be an accurate representation of the incoming event rate, and its statistical uncertainty is expected to be given by the square root of the <u>total</u> number of photomultiplier events recorded. Because on stellar photometers 3 and 4 this amounts to 6000-12000 events per E4 observation even for a faint elliptical galaxy, even a mean difference of a single net count ($\cong$ 384 events per observation) becomes statistically meaningful in principle. Other sources of error (e.g. background variation, miscollimation) unfortunately raise this to probably somewhere between 1 and 2 net (E4) counts.

Estimations of the size of statistical uncertainties for representative early- and late-type galaxy observations are

shown in Table 1. These refer to the intensity expressed on the OAO relative system which is described later. The statistics for ellipticals below 2460 Å are too poor at this time to enable meaningful uncertainties to be estimated. Statistical uncertainties in the globular cluster data are adequately represented by the results for the spirals.

Table 1. Percent Statistical Uncertainties for Representative Galaxy Types

Object	Wavelength Region (Å)			
	>2460	2460	1910	1550
Spirals-Irregulars (Globular Clusters)	<2	2	2	11
Ellipticals	$\lesssim$4	13	?	?

III. OBSERVATIONAL DIFFICULTIES

Observational difficulties are of two types: those caused by the nature of the satellite and instrument package, and those due to the environment. Little can be done in general about the former since the satellite is not available for physical modification after launch. Difficulties of the latter kind can sometimes be minimized by well planned observing sequences.

1) Spatial smearing. A large field of view introduces no complication a priori into the photometry of point sources of radiation beyond the increase in background radiation. However, most galaxies and globular star clusters observed by the satellite are almost completely contained within the 10'-diameter field of view of the stellar photometers (M31 and M33 are important exceptions). For objects—globular clusters, early-type galaxies—whose content is to some degree homogeneously distributed the spectral energy distribution should be somewhat (but not completely) independent of the size of the region sampled. The situation is clearly more complicated for spiral galaxies, especially at ultraviolet wavelengths where young stars in the spiral arms will be very bright. Appropriate caution should therefore be used when attempting to interpret observations of extended sources.

2) Aperture centering. The spacecraft can point its pitch axis to a selected sky position to within about ±1' and maintain this pointing to within a few seconds of arc. The optical

axis of each stellar photometer is collimated to the satellite axis. Momentary perturbations in the pointing may be introduced during an observation sequence when a startracker is reassigned to a different reference star or is taken into or out of the feedback system which maintains stability (cf. Code et al. 1970). The importance of this phenomenon has been investigated by a detailed search of command sequence records for correlations between tracker reassignments during observations and fluctuations in the count rates. No evidence for such correlations has been found.

The fields of view (spatial response) of the stellar photometers relative to the pitch axis has been mapped at a number of times since launch by selecting a bright star and slewing the satellite in steps along the yaw and pitch axes. The optical axes are found to drift slowly with time as a result of thermal stresses. This can amount to miscollimation of up to about 3' and seems to occur on time scales of several hundred orbits. The data on stars does not seem to be affected by such shifts. However, there are indications that objects having dimensions on the order of or greater than 10' may be affected. In general the worst cases are expected to be spiral galaxies because the contribution of the outer regions rises rapidly at short wavelengths. The results of a comparison of different observations of a dozen spirals are presented in Table 2.

Table 2. Percent Collimation Errors in Data for Spiral Galaxies

Apparent Size	ST1 Data	ST3 Data	Examples
$< 10'$	~10	~10	M51, 101, 81
$\gtrsim 10$	~20	~50	NGC 4449, 1068 4736

The numbers are expressed as percentages of the net signals averaged over all filters of a given photometer. Most observed globular clusters have diameters in the range 8'-20', and therefore some miscollimation effects might be expected in this data as well. However, the consistency of counts between different photometers is good enough to make unlikely an effect of more than about 20 percent.

3) Contamination by foreground stars. Measurements of sky background for faint objects have been carried out in areas free of stars to the limit of the Becvar atlas ($m_{pg} \sim 8$). Unfortunately, stars as faint as 13th magnitude, depending on spectral type, may seriously affect the results if present

either in the sky field or that of the object itself. This problem is being investigated in two ways.

Given three items of information—the net E4 counts received from a diffuse source, the net counts expected from stars of various spectral types and magnitudes, and the number per square degree of stars with a given type brighter than some limiting apparent magnitude—one can estimate the probability that within the diaphragm (10' diameter) there is a star whose brightness is a certain fraction of that of the source. This has been done for typical elliptical and spiral galaxies and for globular clusters by using the data given by Allen (1955) and OAO observations kindly provided by Dr. L. R. Doherty. The results are as follows. There appears to be a chance of 10-20 percent, depending on galactic latitude, that within the diaphragm is a star at least 10 percent as bright at 2460 Å and 1910 Å as the average late-type spiral or globular cluster. Such stars would be of type O, B or A with $m_{pg} \lesssim 12$. The chances that the star would be equal in brightness are roughly an order of magnitude less. When observing early-type (E, S0, Sa) galaxies on the other hand, the chances of contamination by a star of equal brightness at 2460 Å are roughly 12 percent. This would occur for F stars as faint as $m_{pg} \sim 12$ ($m_{pg} \sim 13$ for earlier types).

It thus appears that, excepting faint red objects, only a small fraction of the data may be seriously contaminated by foreground stars. Nevertheless, both sky and object fields are being scrutinized on the prints of the Palomar Sky Survey to isolate cases of suspected contamination. Special attention will be given to early-type galaxies. Rough corrections may be attempted on the basis of colors and magnitudes estimated from the prints.

4) Background variation. A complete observing sequence for a faint source requires usually about 30 minutes and is carried out while the satellite is in the earth's shadow (34 min per orbit maximum). During this time the satellite passes through a constantly changing flux of charged particles, which over the South Atlantic Ocean is large enough to completely swamp the detectors. Care is exercised to observe as far from this region as possible, but it is nevertheless common for dark current readings taken during the observations to vary by 10-20 percent. For the short wavelength photometers (ST3, ST4) this variation usually amounts to a somewhat larger percentage of the net signal and sometimes even surpasses it. For this reason dark current readings on all photometers are recorded immediately prior to and after the observations, and an intermediate reading on at least one photometer is taken as well. This allows interpolation of dark readings accurate to ±1 count at longest integration time. Since the particle background even at the same positions over the earth is constantly changing,

this technique must be used both for object and nearby sky readings, usually taken on successive orbits.

In planning observations we have attempted to carry out all observations in the dark and well away from the South Atlantic Radiation Anomaly. Carefully selected sky regions have been observed under as closely similar conditions as for the object so that many of the problems described in the preceding paragraphs are minimized by a direct subtraction of sky readings from object plus sky measurements.

IV. CALIBRATION OF THE OAO FILTER PHOTOMETRY

The net counts have been converted to flux on the basis of a preliminary calibration which defines the current OAO photometric system used for all data reduction. This system expresses the flux per unit wavelength interval at the corresponding constant energy wavelengths relative to the flux measured through S1F1 (3330 Å). This filter was chosen as the standard for several reasons. The bandpass is well defined, does not present any red leak problems nor require any significant corrections for band width. The signal levels are always high enough that measurement errors are small compared with all filter measurements shortward of S1F1. The 3330 Å region can be tied to ground-based measurements with little extrapolation and is free of any ambiguities due to the Balmer discontinuity.

The absolute calibration of this standard OAO photometric system in terms of ergs cm^{-2} sec^{-2} $Å^{-1}$ is still in progress. The results obtained by Bless, Fairchild and Code (1972) are in good agreement with the relative fluxes of this photometric system. It also agrees with earlier although less accurate calibrations by Carruthers (1969), Stuart (1969), Sudbury (1971) and Campbell (1970). Evans (1972), however, has reported measurements which diverge from this calibration shortward of 2000 Å, the differences becoming about a factor of two below 1500 Å, with his calibration implying the lower flux. These differences have not yet been reconciled.

The preliminary calibration relative to S1F1 has been derived by fitting photometry of several little reddened B1 V and B3 V stars with the line blanketed model atmospheres of Morton and collaborators (cf. Hickok and Morton 1968). The stars were corrected for reddening using the color excesses and the mean ultraviolet extinction curve (Bless and Savage 1972). Studies so far indicate that such stars are indeed similar to the appropriate models down to about 1500 Å and that the errors in the calibrations should not exceed 15 percent. The calibration determined in this manner yields fluxes for late-type stars in reasonable agreement with the solar spectrum. Figure 1 shows a comparison of the smoothed energy dis-

tribution for the star β Hyi (G2 IV) determined from OAO filter photometry with the solar spectrum. Also indicated on this plot is the flux of a B3 V model atmosphere and the measured flux for η Her (G7 III-IV). The spectrum of η Her is similar to that of early-type galaxies and the redder globular clusters in the photographic region.

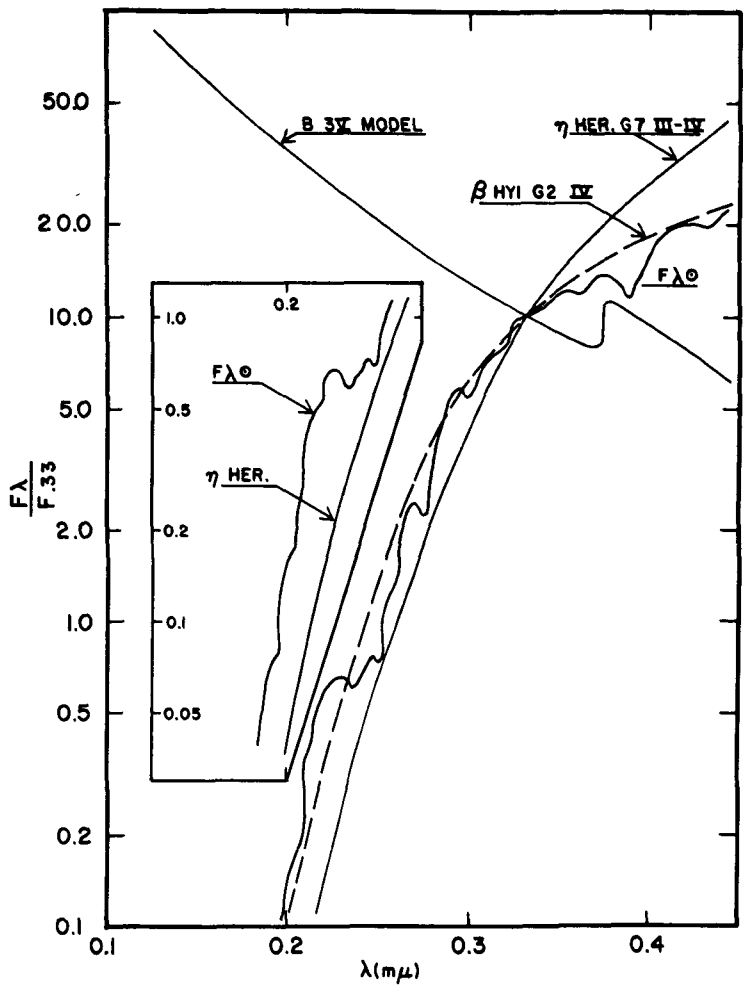

Figure 1.

The standard OAO photometric system is defined in the following manner. The flux F through a filter of constant-energy wavelength λ_0 relative to S1F1 is expressed as

$$\log F_{\lambda_0} = \log\left[\frac{*\text{-d}}{\text{cal-d}} - \frac{\text{sky-d}}{\text{cal-d}}\right]_{\lambda_0} - \log\left[\frac{*\text{-d}}{\text{cal-d}} - \frac{\text{sky-d}}{\text{cal-d}}\right]_{3330} + \log\Delta_{\lambda_0}.$$

The calibration is expressed operationally by Δ for each filter. The quantity *-d denotes the counts for the object plus sky corrected for dark counts. To allow for any gradual secular changes in sensitivity, data from each photometer is divided by a mean (over approximately 100 orbits) of the calibration source reading. These means appear to be accurate to about ±3 percent.

V. OBSERVATIONS OF GLOBULAR CLUSTERS

The measurements of the integrated radiation of 6 globular clusters which have been obtained and processed by the techniques described in the preceding sections are discussed here. In general the globular clusters are sufficiently bright that collimation errors introduce the largest uncertainty. In the results discussed in this section it is unlikely that the errors in the absolute fluxes exceed 30 percent even for the shortest wavelengths. In the case of ω Cen and 47 Tuc the angular diameter is significantly greater than the 10' diaphragm size and some variation (approximately 25 percent) in the energy distribution was found for different diaphragm positions. The results discussed here are in general, however, the integrated light of the entire globular cluster.

Table 3 presents preliminary data on several globular clusters. The first column gives the identification of the object and the (B-V) color excesses adopted to correct for interstellar reddening. Subsequent column headings list the constant energy wavelengths for the filter combinations employed. For each filter the measured flux per unit wavelength interval relative to 3320 Å is recorded. Below the measured flux is the flux corrected for interstellar reddening on the basis of the mean extinction curve given by Bless and Savage (1972) and the (B-V) color excess. The results given in Table 3 are the mean values of several observations for each system. The color excesses for M80 and M4 are based on a secant law. The others are approximate values based upon color-magnitude diagrams.

The fluxes corrected for interstellar reddening are illustrated in Figure 2. The most striking feature of Figure 2 is the large decrease in the ultraviolet integrated flux of 47 Tuc relative to the other systems. 47 Tuc is regarded as an extreme among globular cluster types. It is characterized by a very sparsely populated horizontal branch in contrast to ω Cen, for example, with a very heavily populated horizontal branch. The giant branch in 47 Tuc is less steep than the other clusters illustrated, being about 0.4 magnitudes fainter at $(B-V)_0 = 1.4$. This is taken to represent a metal rich globular cluster. We would expect the difference in the ultraviolet energy distribution of these globular clusters to represent the differences in the number of blue horizontal branch members. M80 is the only other cluster showing a similar

Table 3. Preliminary Data on Globular Clusters

Object E(B-V)	λ_0 = 4250	3320	2980	2460	1920	1550
	F_{λ_0}/F_{3320}					
NGC 104						
47 Tuc	2.76	1.00	0.58	0.16	0.06	0.04
0.12	2.50	1.00	0.62	0.21	0.08	0.06
NGC 5139						
ω Cen	2.03	1.00	0.91	0.70	0.34	1.01
0.18	1.75	1.00	0.98	1.00	1.00	1.45
NGC 6093						
M80	3.40	1.00	0.52	0.16	0.05	0.14
(0.18)	2.92	1.00	0.57	0.24	0.09	0.17
NGC 6121						
M4	3.10	1.00	0.63	0.31	0.29	0.81
(0.22)	2.60	1.00	0.70	0.51	0.54	1.29
NGC 6205						
M13	5.00	1.00	0.79	0.80	0.80	1.11
0.06	4.75	1.00	0.81	0.91	0.95	1.26
NGC 6656						
M22	3.70	1.00	0.71	0.30	0.29	0.76
0.39	2.70	1.00	0.86	0.71	0.91	1.72

ultraviolet deficiency; however, published information on M80 is sparse. In the next section we compare the observed fluxes with energy distributions synthesized from simple representative models.

VI. SYNTHETIC GLOBULAR CLUSTERS

In order to facilitate the discussion of composite systems a flexible computer program called GLOB has been compiled. The program is capable of accepting up to 200 classes of unique objects, determining the spectral distribution of each class, and summing the contributions of each class to the integrated flux at designated wavelengths. Four separate arrays referred to as giant branch, horizontal branch, main sequence, and special are available. A single data input specifies the array, the number of stars, the V magnitude, and the B-V color. Fifty such data points can be read into a sin-

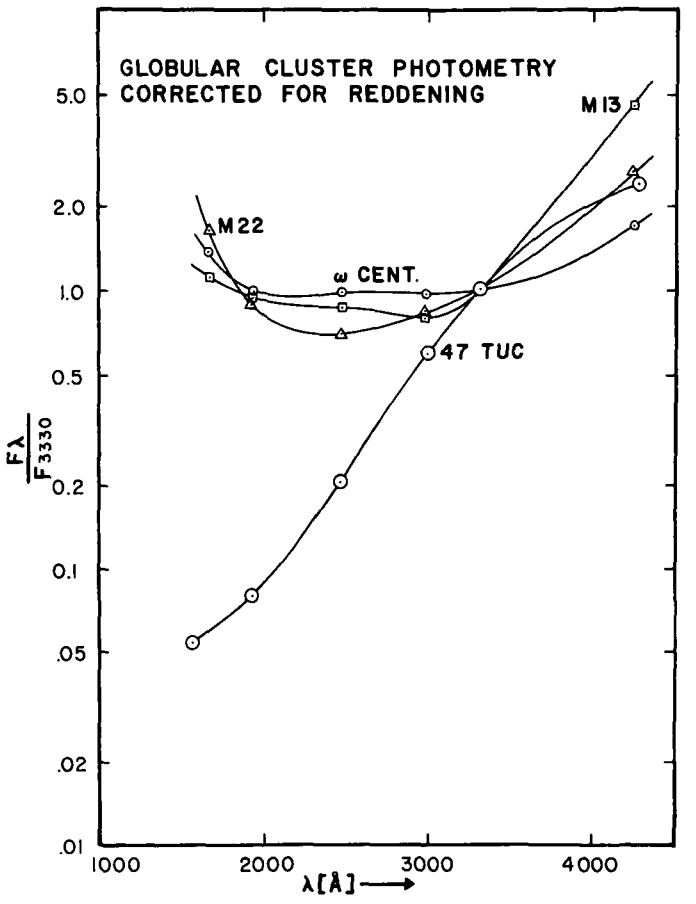

Figure 2.

gle array. For given array and B-V color the flux at any particular wavelength is determined by interpolation between energy distributions stored in the program. The interpolation is based upon a polynomial representation of the stellar flux for a given B-V. The polynomial itself provides a good representation of the observed flux for little reddened population I stars observed by OAO. The use of this polynomial for interpolation between specified energy distributions, however, makes it possible to carry out the investigations for theoretical model atmospheres or population II objects. The program plots color-magnitude arrays at designated wavelengths for the composite system and a plot of the integrated energy distribution.

Figure 3 shows the color-magnitude arrays for one of our sample populations. The first plot for the magnitude at 5460 Å vs. B-V represents the input data. The diameter of each point is proportional to the logarithm of the number of stars

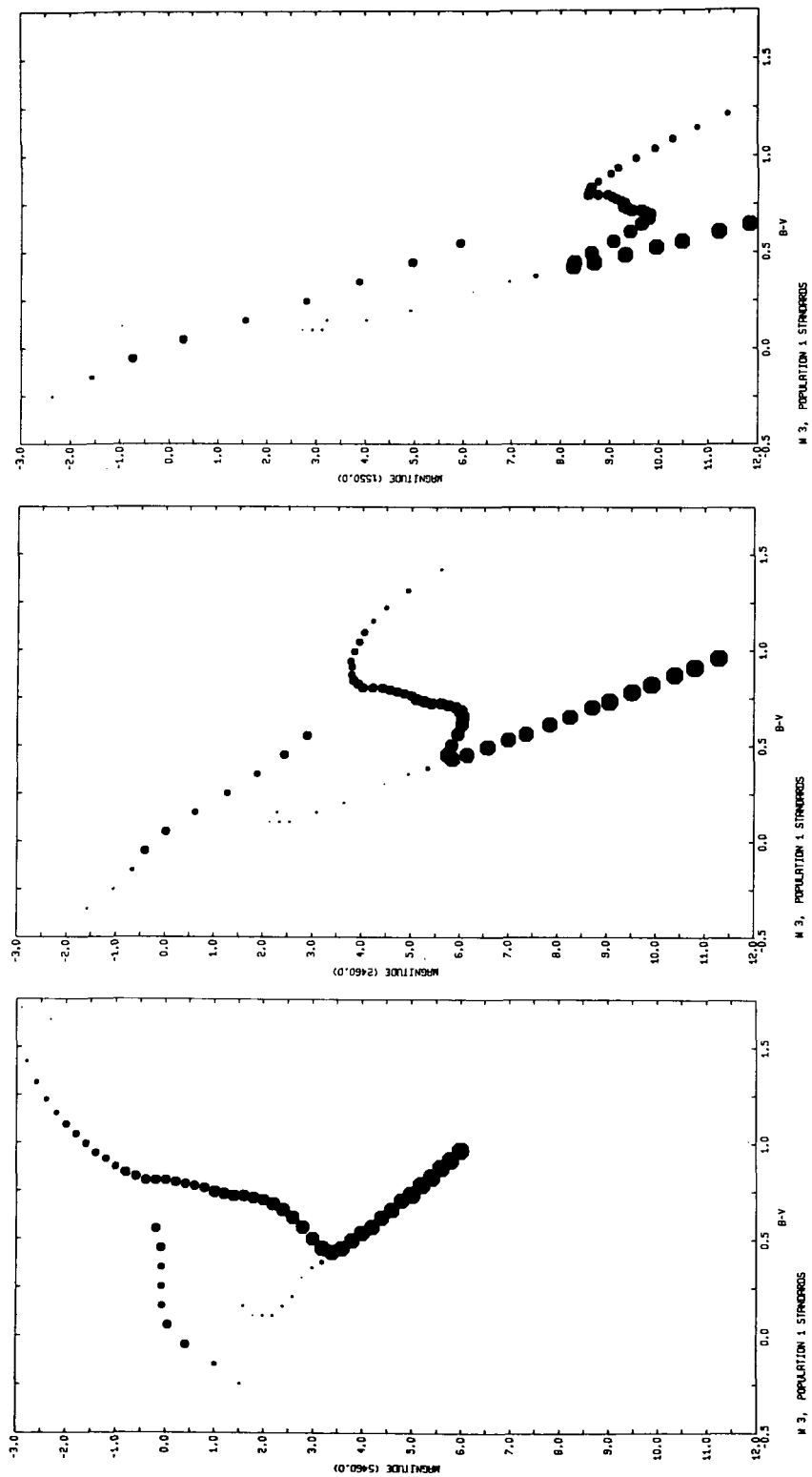
MAGNITUDE (1550.0)
MAGNITUDE (2460.0)
MAGNITUDE (5460.0)
B-V
M 3, POPULATION 1 STANDARDS

Figure 3.

at that point. The distribution of stars on this plot is based on the luminosity function for M3 tabulated by Sandage (1957). The next two plots show the color-magnitude diagrams for this composite system at 2460 Å and 1550 Å respectively. These figures graphically illustrate the dominance of the blue horizontal branch in the ultraviolet. At 5460 Å the bluest horizontal branch stars contribute about one percent of the light of the brightest giants or about as much light as six main sequence stars at the turnoff point. At 1550 Å, however, one blue star contributes as much radiation as 2×10^4 main sequence stars or 10^6 red giants.

These arrays are calculated on the assumption that the energy distributions of the stars are the same as found for normal population I stars. This assumption may not be too unreasonable for a cluster such as 47 Tuc. Figure 4 compares the observed flux for 47 Tuc, represented by the continuous line with calculated fluxes at the filter wavelengths. The flux is expressed relative to 5460 Å in unit wavelength intervals and the computed points are indicated by crosses. The synthetic cluster was similar to Figure 3 except that the population of the horizontal branch has been reduced by a factor

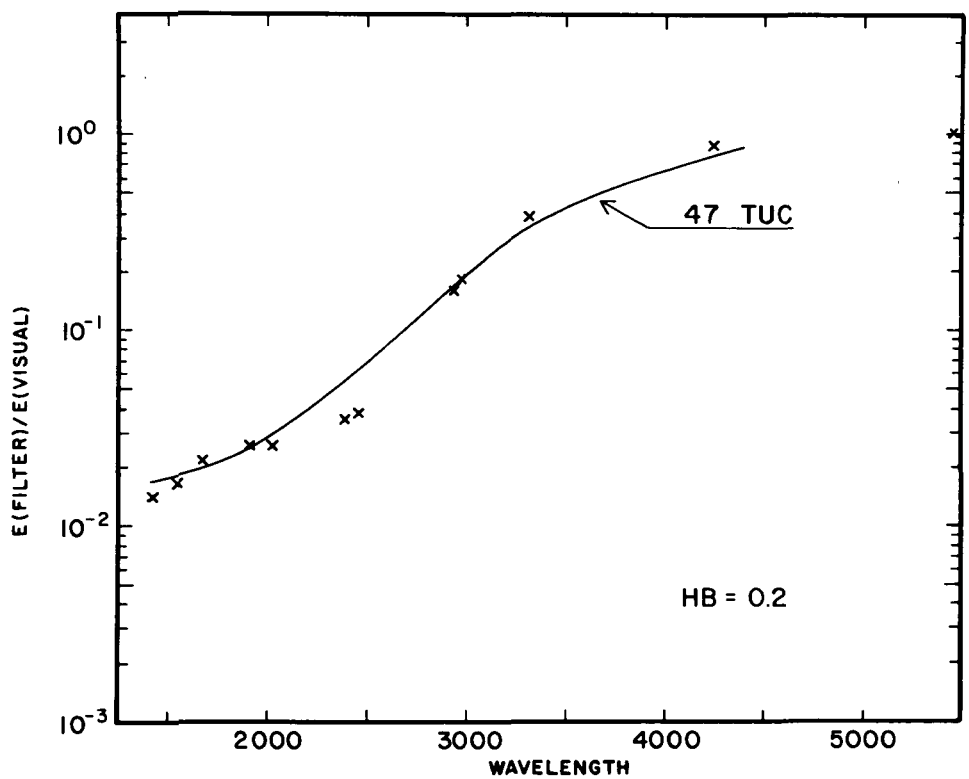

Figure 4.

of five. The giant branch was modified to represent the slope of the observed color-magnitude diagram for 47 Tuc; however, the results are insensitive to variations in the giant branch. The agreement between the observed and computed fluxes is quite satisfactory. The largest deviations occur at about 2500 Å where A stars make the largest contribution. A small decrease in line blanketing that would accompany a decrease in metal abundance would remove this small discrepancy.

Current observational information on the ultraviolet energy distribution of weak line or population II stars is very fragmentary. Some estimate of the effect of chemical composition on the stellar fluxes can be made by appeal to model stellar atmospheres. Figure 5 shows the difference in the color-magnitude diagrams at 2460 Å, where the effect is largest, based on model atmosphere fluxes. The grid of model atmospheres is

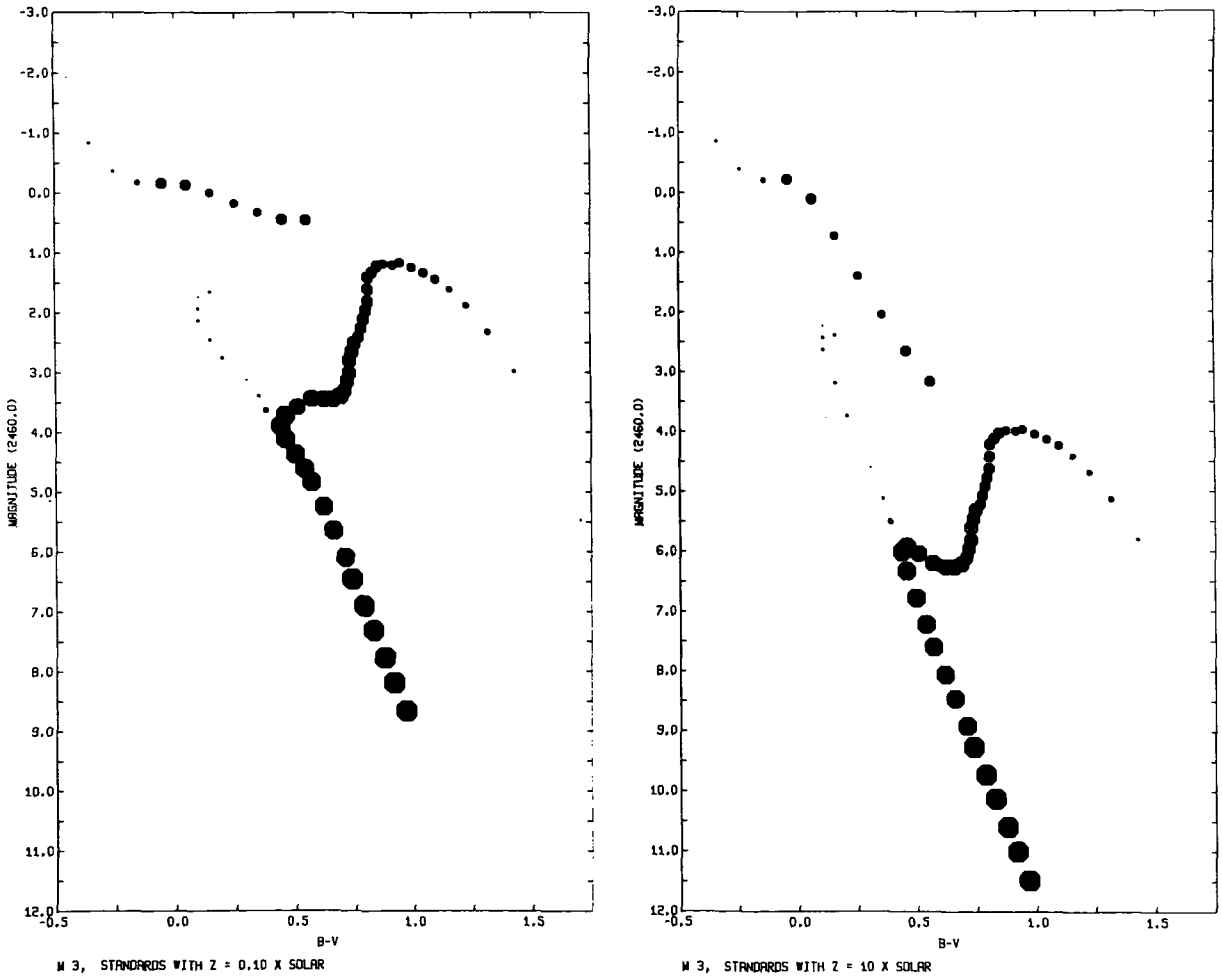

Figure 5.

based upon calculations with the Smithsonian ATLAS program (Gingerich 1969) and include statistical line blanketing as well as continuous opacity and hydrogen line blanketing. The first figure shows the result for 0.10, the solar abundance, while the second diagram is for 10 times solar abundance. The most important modification for our purpose is the increase in flux produced in the A stars and early F stars as the metal abundance is decreased. Computations of the composite energy curves show an increase in flux for low metal abundances of approximately 1.5 magnitudes at 2460 Å but little change longward of 3500 Å or shortward of 2000 Å. This is shown in Figure 6 where the composite flux for 10 times solar abundance is indicated by the crosses and for 0.1 times solar abundance by the circled points.

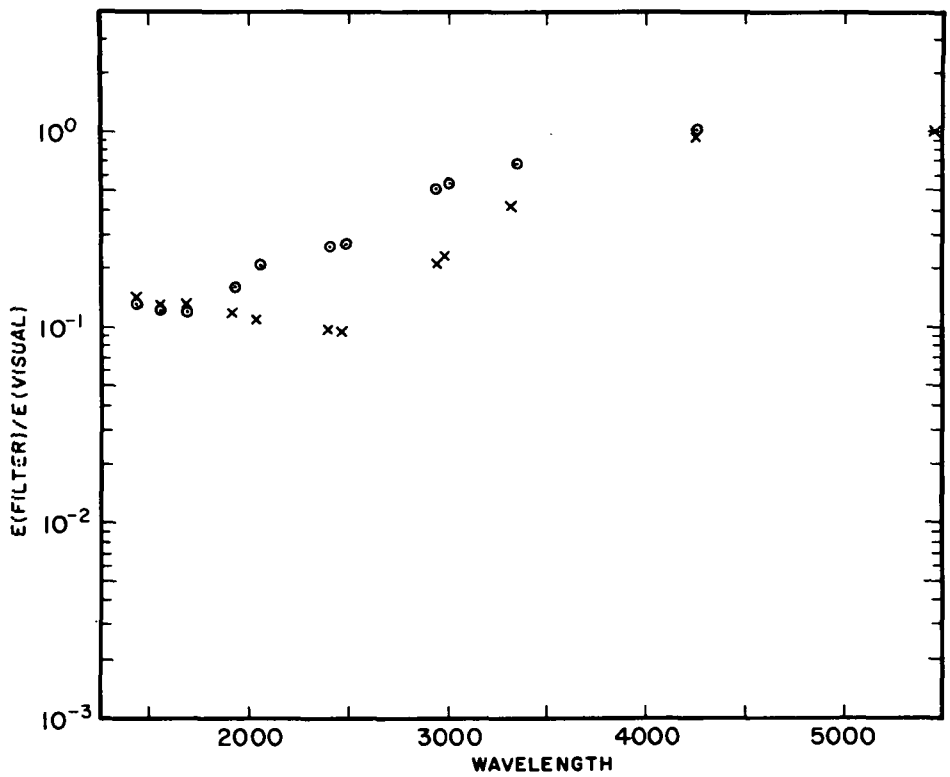

Figure 6.

We have attempted to fit the observed energy curves of globular clusters such as ω Cen and M3 with the standard luminosity function and allowances for low metal abundance with little success. What is required to achieve a fit is the increase in the number of stars at the blue end of the horizontal branch.

The computations were based upon the observed number of blue horizontal branch stars. The completeness factor at the ultraviolet tip of the horizontal branch has been discussed by Minkowski and Osterbrock (1959) and by Hills (1971). It is likely that only a small fraction of the ultraviolet stars in a cluster are catalogued. We may indeed take the measured flux at 1550 Å as a measurement of the number of ultraviolet stars. Preliminary analysis suggests an increase of the order of 10× for these bluest stars.

REFERENCES

Bless, R. C., Fairchild, T. and Code, A. D. 1972, this volume.
Bless, R. C. and Savage, B. D. 1972, this volume.
Caldwell, J. J. 1971, Ph. D. Dissertation, University of Wisconsin.
Campbell, J. W. 1970, Astrophys. Space Sci. 9, 128.
Carruthers, G. R. 1969, Ap. J. (Letters) 157, L113.
Code, A. D. 1962, Stellar Atmospheres, ed. J. L. Greenstein (Chicago: The University of Chicago Press).
Code, A. D., Houck, T. E., McNall, J. F., Bless, R. C. and Lillie, C. F. 1970, Ap. J. 161, 377.
Code, A. D. Welch, G. A. and Page, T. L. 1972, this volume.
Doherty, L. R. 1972, this volume.
Evans, D. 1972, this volume.
Gingerich, O. 1969, Theory and Observation of Normal Stellar Atmospheres (Cambridge: M. I. T. Press).
Hickok, F. R. and Morton, D. C, 1968, Ap. J. 152, 203.
Hills, J. G. 1971, Astron. & Astrophys. 12, 1.
Minkowski, R. and Osterbrock, D. 1959, Ap. J. 129, 583.
Morton, D. C., for model atmospheres used in calibration.
Sandage, A. R. 1957, Ap. J. 125, 422.
Stuart, F. E. 1969, Ap. J. 157, 1255.
Sudbury, G. C. 1971, M. N. R. A. S. 153, 241.

PRELIMINARY RESULTS OF OAO ULTRAVIOLET PHOTOELECTRIC PHOTOMETRY OF GALAXIES

A. D. Code
University of Wisconsin
Madison, Wisconsin

G. A. Welch
Wesleyan University
Middletown, Connecticut

T. L. Page
Naval Research Laboratory
Washington, D. C.

ABSTRACT

General results are presented based on nearly completed reductions of data for approximately 35 galaxies of all Hubble types having $m_{pg} \lesssim 11$. In general the visual and ultraviolet energy distributions are well correlated. The energy distribution in late-type galaxies appears to turn up sharply in the region around 2000 Å, and this is tentatively interpreted as due to the presence of early-type stars whose energy distribution is modified by interstellar dust within these objects. Similar turnups may be present in several elliptical galaxies but the evidence at this time is not definitive.

I. INTRODUCTION

Intended chiefly to make ultraviolet measurements of stars within our galaxy, the University of Wisconsin experiment on board OAO-2 has also collected a large amount of valuable data on extragalactic objects. During the first three years of operation more than seventy galaxies of all Hubble types have been observed, and reductions are largely complete for about half. A limiting magnitude of $m_{pg} \approx 11$ has been found for obtaining statistically significant data through filters having constant-energy wavelengths from 1910 Å longward, for late

spirals, and from 2460 Å for ellipticals.

Detailed discussion of spacecraft operation has been given by Code et al. (1970). The many problems involved in observation of and reduction of data for faint extended sources are discussed by Welch and Code (1972), and in the following section we shall briefly summarize the most important features affecting galaxy photometry. In § III a general discussion is given of the results so far obtained and specific examples are presented for illustration.

II. SUMMARY OF ERRORS AND UNCERTAINTIES

Although there are many considerations in the photometry of galaxies, four seem to be of prime importance in dealing with this body of OAO data.

1. Unreliable filters. Two of the twelve medium-band filters [S2F1 (2040 Å) and S2F5 (2390 Å)] are now known to possess significant red leaks for late-type objects. Another [S3F5 (1680 Å)] because of its substrate is seriously contaminated by radiation from the nearby Cerenkov calibration source. Two other filters [S4F3 (1430 Å) and S4F4 (1330 Å)] include the strong and variable Lyman alpha emission in the earth's geocorona, although the effect on S4F3 is minimal. Data from these filters has therefore not been used.

2. Counting statistics. The background rates on all four photometers are large enough so that the statistical uncertainties are accurately given by the square root of the number of incoming events. For late-type spirals these uncertainties increase toward short wavelengths and are on the average less than or equal to about 10 percent depending on wavelength. Because ellipticals become very faint at short wavelengths, the uncertainties rise rapidly to about 13 percent at 2460 Å and are poorly determined below 2000 Å.

3. Miscollimation. Because of thermal gradients, the optical axes of the four photometers show slight temporal shifts with respect to each other. The photometers therefore often view slightly different parts of sources whose size is comparable to the 10' field of view. For such galaxies these miscollimation errors can amount to 50 percent of the net signal at shortest wavelengths. Smaller objects are very little affected — errors of roughly 10 percent seem normal at all wavelengths.

4. Foreground stars. There appears to be roughly a ten percent chance of accidentally including a significantly bright foreground star while observing a galaxy or nearby sky. We do not believe such contamination will alter the conclusions of this paper. However, each field is being carefully searched on prints of the Palomar Sky Survey to isolate possible cases before data for individual objects is released.

III. RESULTS

a) Late-type galaxies

Important conclusions may be drawn regarding the ultraviolet energy distribution in galaxies by comparing their ultraviolet colors with the B-V values tabulated by de Vaucouleurs and de Vaucouleurs (1964). For two filter combinations the corresponding two-color diagrams are shown in Figures 1 and 2. Data for thirty-six galaxies are plotted in Figure 1, while due to the faintness of the early types below 2400 Å, only thirty-three appear in Figure 2. Different observations of the same object are connected by vertical bars and results for two Seyfert galaxies, NGC 1068 and NGC 4051, are indicated in

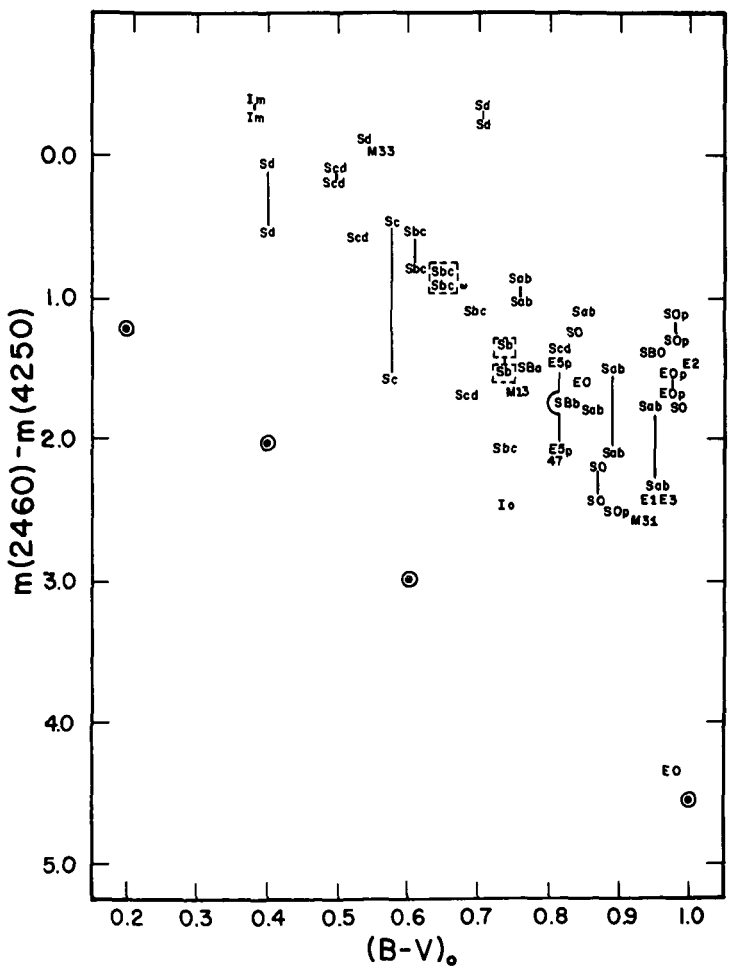

Figure 1.

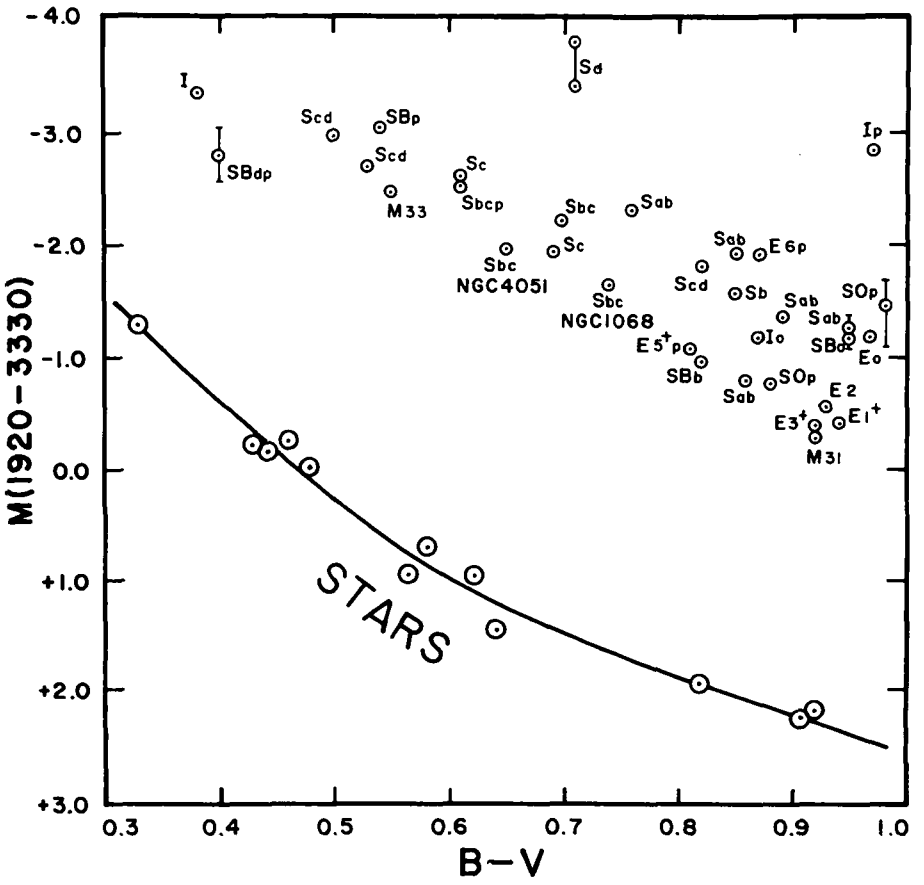

Figure 2.

the figures (in Figure 1 as dotted boxes). For comparison we have included the globular cluster ω Centauri (whose HR diagram displays a very richly populated blue horizontal branch), M13 (showing a less well populated blue horizontal branch), and 47 Tuc (whose horizontal branch is almost devoid of blue stars). Also shown is the line occupied by main sequence stars having small or zero color excess.

Several conclusions can be drawn from these figures:

1. Simple and composite systems are separated qualitatively in the same manner as when U-B values are used for the ordinate, and probably for the same reason: observations at shorter wavelengths are more greatly influenced by the hottest stars present in a galaxy or cluster. As expected the separation increases with the difference in wavelengths sampled by the ordinate.

2. There is a fairly good correlation between both a galaxy's visual color index and morphological type and its ultraviolet energy distribution. The sense of these correla-

tions might be predicted on the basis of ground-based information alone. Galaxies which are the bluest in the visual region tend to remain the bluest at shorter wavelengths.

3. Early-type galaxies, especially the ellipticals and SO's, are in general very close to the limit of detection below 2500 Å. However, the continuity with which the morphological classes are distributed in Figure 2 suggests (but does not prove) that the data on early types at 1910 Å has value at least for statistical purposes. Thus the elliptical galaxies which have spectra and colors in the photograph equivalent to a late G or K star display a color equivalent of early F in the 2000 Å region.

4. The two Seyfert galaxies in no way stand out as peculiar in our observations. This should perhaps be expected. The photometer diaphragm includes virtually the whole galaxy in each case and the bright young stars in the spiral arms will make an important, perhaps overwhelming, contribution to the integrated signal. The same comments apply to M87.

The ultraviolet filter photometry may be placed on an absolute energy basis using the calibration described by Welch and Code (1972). Two observations of the Magellanic irregular, NGC 4449, are shown in Figure 3, where the flux per unit wavelength interval is plotted relative to the flux at 3330 Å. This galaxy has the bluest integrated color index of any we have observed. For objects this blue all filters yield reliable data. The ultraviolet energy output is relatively large and the two sets of measurements are in excellent agreement. The smooth curve through the data has been fitted by eye.

The upturn in the energy distribution of NGC 4449 below 2000 Å is a feature found, to some degree, in the vast majority of galaxies later than Sa for which reductions are complete. It may be described quantitatively by attempting to fit the data points with semi-empirical energy distributions for stars of various B-V values. These distributions have been obtained by a computer program which extrapolates or interpolates the ultraviolet fluxes of stars having both good OAO data and normal visual colors (cf. Welch and Code 1972).

In the region 2400 Å $\lesssim \lambda \lesssim$ 4250 Å the best fit is found for a model having B-V $\approx$ -0.05. However, at shorter wavelengths a reasonable match is obtained only for B-V $\approx$ -0.45, a more negative color index than those of the hottest stars known in our galaxy. Consequently the question arises whether the observations in this region really represent only thermal emission from the brightest stars or whether an additional process makes a contribution.

In Figure 4 are shown data for two spiral galaxies, M101 (Sc, B-V = 0.50) and M94 (Sb, B-V = 0.76). These results are typical for objects of these morphological classes, and they

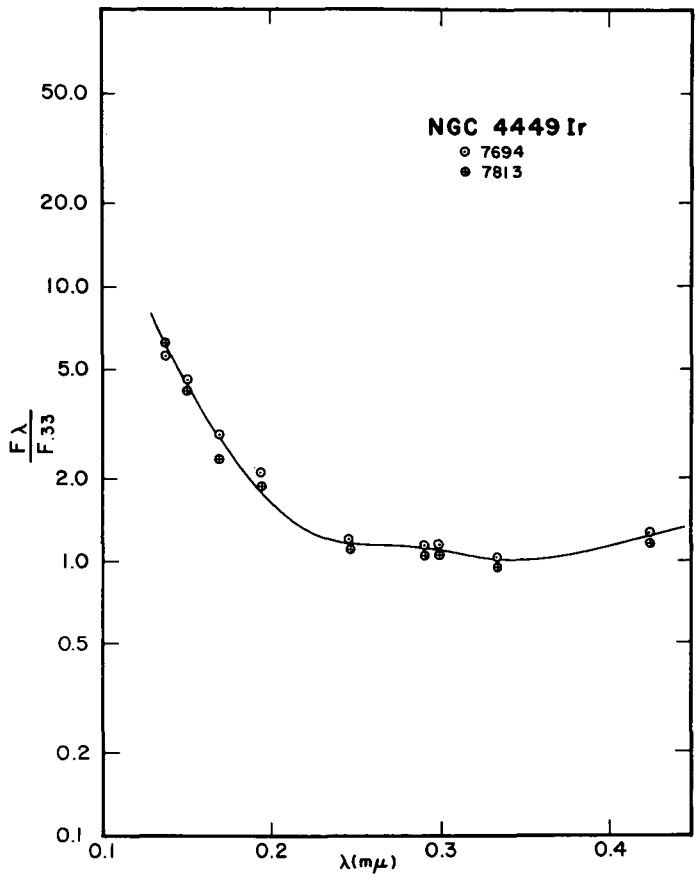

Figure 3.

illustrate beautifully the general correlations between B-V, morphological class and ultraviolet brightness shown in the two-color plots. The upturn below 2400 Å is not as extreme in spirals as in NGC 4449 but is nevertheless quite pronounced in most cases. The best fit to the data for these two galaxies below about 2000 Å is obtained for a model star having B-V ≈ -0.4.

It is important to recognize that these measurements, in general, refer to the integrated light of the entire galaxy. It is reasonable to suppose that the spiral arms make an increasingly greater contribution to the total flux as the measurements are extended shortward. There are only two spirals near enough to permit even rough spatial mapping of the energy distribution with the OAO-2 instrumentation. M31 and M33 have been mapped in detail with the 10' field of view and in less detail with a 2' diaphragm. We present here a part of the results of this mapping.

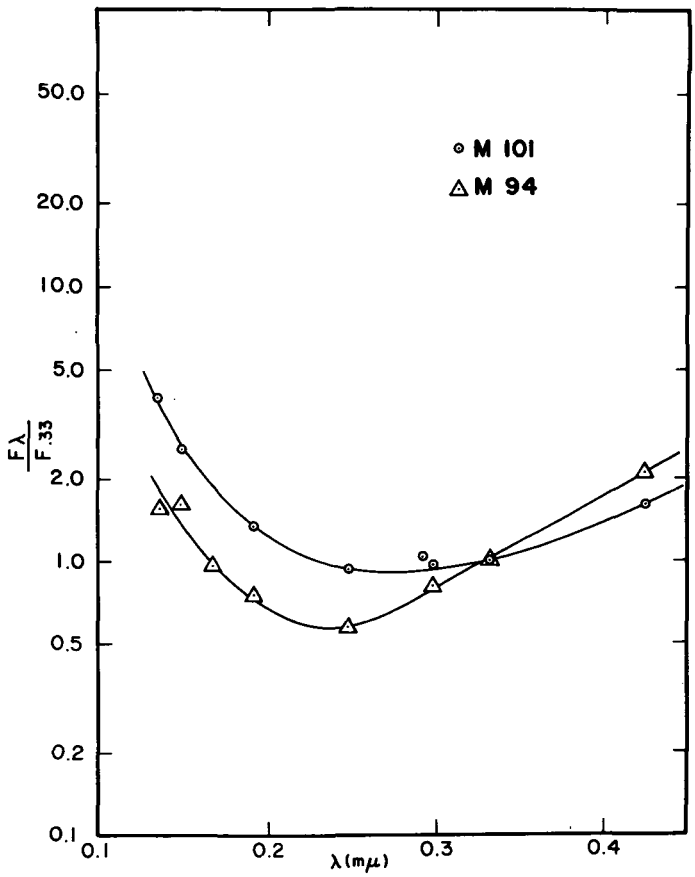

Figure 4.

Two observations of different areas of M31 are shown in Figure 5. Data for the "nucleus" actually refer to the entire central bulge out to a distance of 5' (1000 pc). We should point out the difference between these data and the preliminary observations presented in a previous paper (Code 1968). The latter were based upon a pre-launch calibration of the photometric system which has since been empirically revised (cf. Welch and Code 1972) and also suffered from collimation errors. The nucleus now appears much fainter below 2600 Å and begins to brighten slightly only around 2000 Å instead of at 2700 Å as previously indicated. However, as shown in Figures 1 and 2, the nucleus remains much bluer below 3000 Å than a star having the same visual color index. It has been suggested by Tinsley (1972) that enough young blue main sequence stars may be present in the inner disk to account for this fact (although not the observed gradient). An earlier study by Hills (1971), based on the 1969 data, invoked the presence

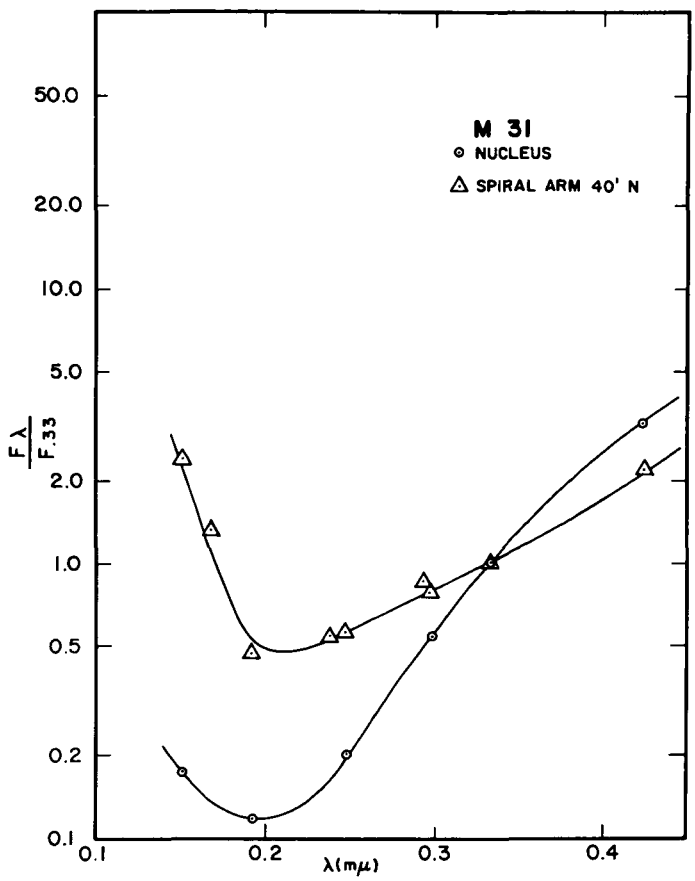

Figure 5.

of hot highly evolved stars and should perhaps be revised on the basis of this new data.

It is no surprise to find that the arms of a spiral are bluer than its center in ultraviolet wavelengths. The one energy distribution shown in Figure 5 seems to be typical of those found in areas of the galaxy well away from the nucleus. The steepness of the upturn is remarkable, however, because it is steeper even than that of an infinitely hot black body (for which $F_\lambda \propto \lambda^{-4}$). Again it appears that radiative processes other than simple thermal emission are becoming important at short wavelengths.

Figure 6 is a reproduction of M31 from a Curtis Schmidt blue plate together with results at two wavelengths of a point-by-point scan through the center along the major axis. In this orientation the scan passed through the bright super-association (40' south of the nucleus) which appears to the left in the figure. Within 10' of the nucleus the step inter-

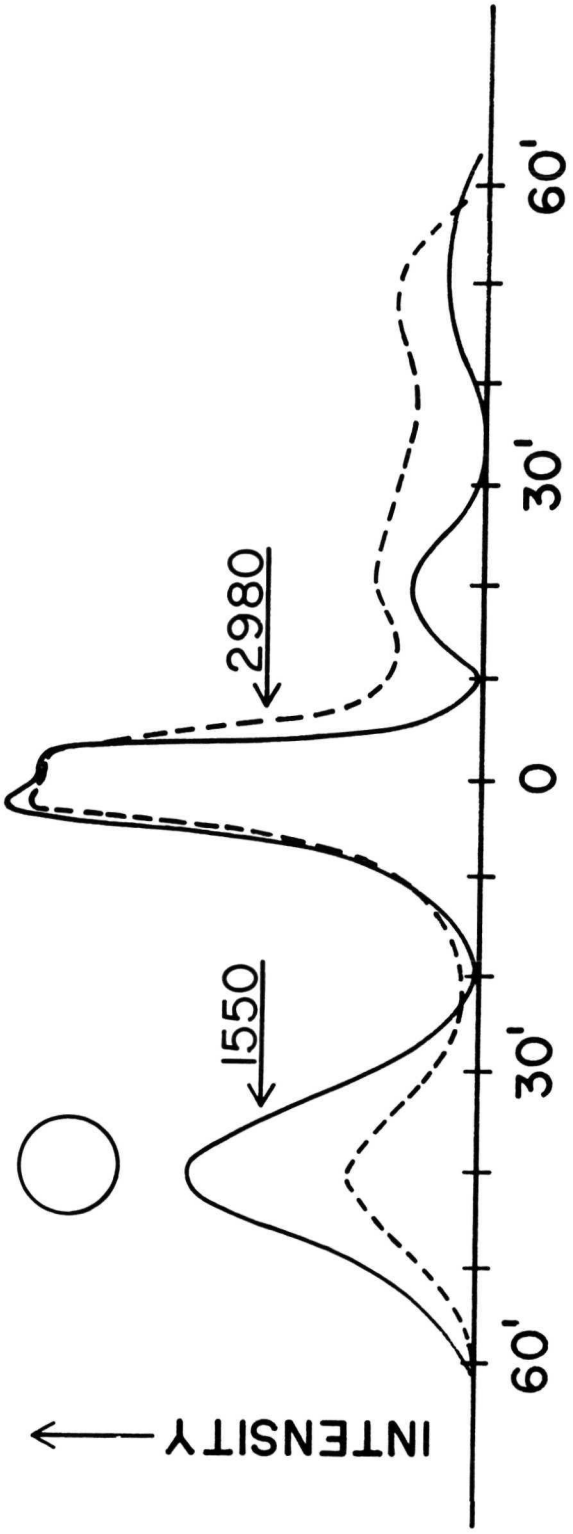

Figure 6.

val between integrations was 2'.5; beyond this point it was increased to 10'. Smooth lines have been drawn through the data and the scans are normalized at r = 0. The intensity at this point corresponds to ~300 net counts at 2980 Å and ~13 net counts at 1550 Å, both in the 64 second integration time.

All references to net counts have the following meaning. The net count represents the difference in digital readings, during one integration time, between the object plus sky and the corresponding sky reading. A single measurement, however, corresponds to six separate integration times, thus for example 13 net counts represents the average of six readings and a total of approximately 78 counts. Furthermore each count corresponds to 64 photoelectrons. Thus 13 net counts represents a total of 5000 photoelectric events and is statistically determined in this example to 3 percent.

At 2980 Å the distribution of intensity is quite similar to what one might expect by examining the direct photograph of the galaxy. At 1550 Å, however, the contribution from bright blue giants to the signal becomes much greater and the intensity distribution should more closely reflect the distribution of these objects. The relative brightness of the superassociation has greatly increased and on the opposite side of the nucleus the spiral arms have become more distinct. On this basis it would appear likely that the spiral arm regions would contribute most of the integrated flux at short wavelengths for the more distant spiral galaxies which completely fill the field of view.

Mapping has also been undertaken of the other nearby spiral M33. A direct photograph of M33 in the blue is reproduced in Figure 7. The superimposed 10'-diameter circles enclose regions whose energy distributions appear in Figure 8 as solid lines. As M33 is a late-type spiral with a widespread population of young blue stars and H II regions, each area contains many such stars. These will be strong contributors to both energy distributions at short wavelengths.

The energy distribution resulting from the difference in raw net counts between the two regions is shown in Figure 8 as a broken curve. To some degree this curve should be free from the direct contribution of young blue stars. Since, in fact, there may be greater numbers of such stars near the nucleus, it is understandable that the curve above 2000 Å should be fairly flat. However, the sharp upturn at shorter wavelengths cannot be explained by invoking the presence of even the hottest stars. In fact, if the number of net counts in the outer region is increased in order to remove the sharp upturn, a negative intensity is found at longer wavelengths.

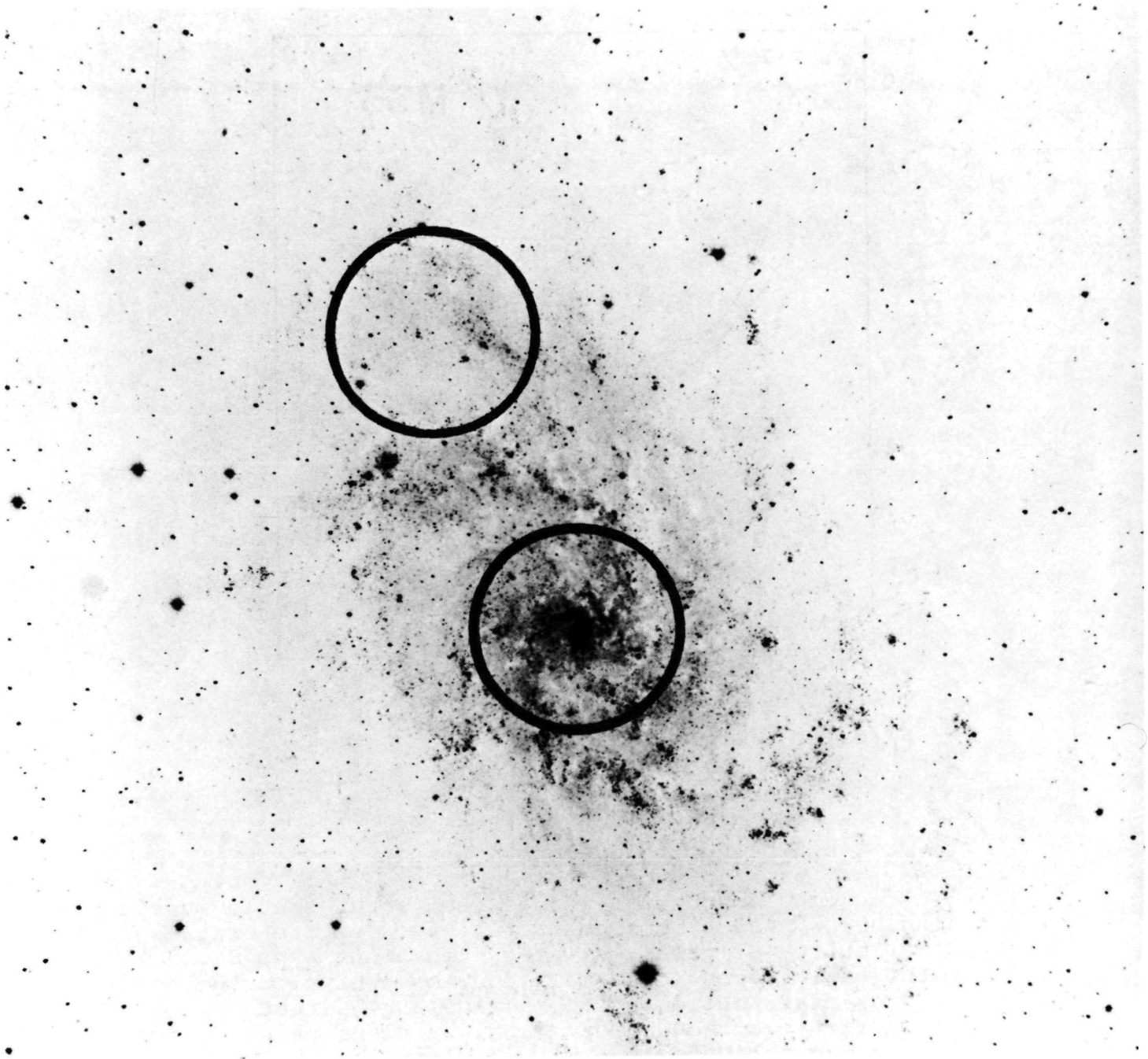

Figure 7.

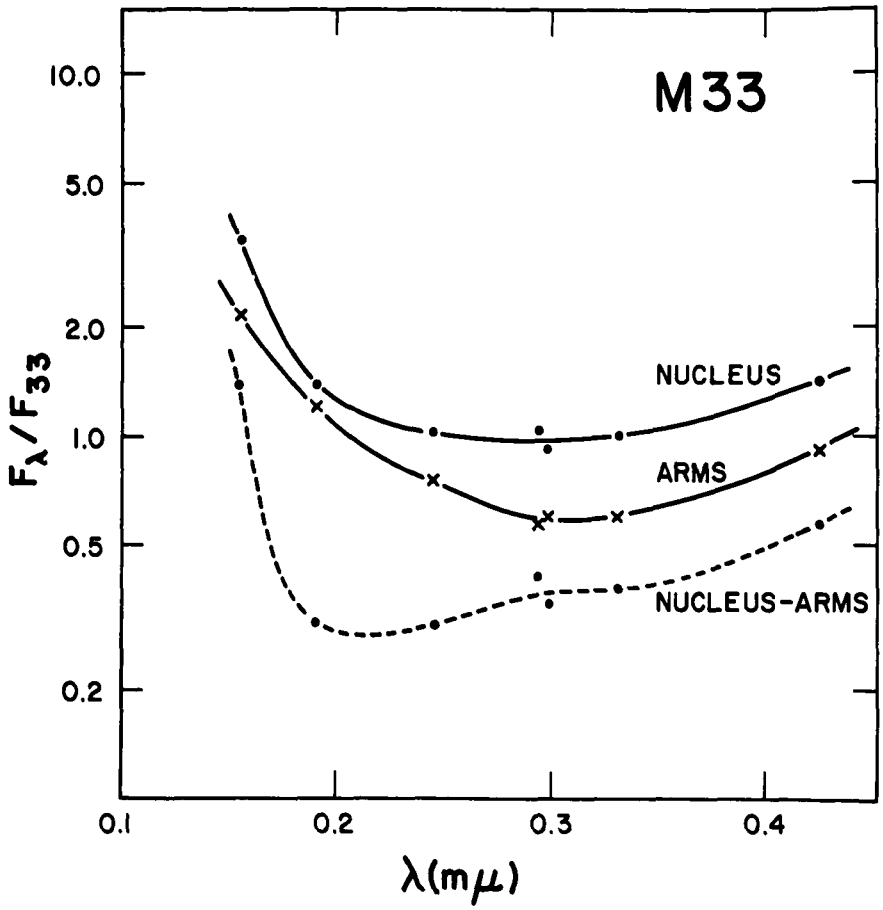

Figure 8.

b) The Short Wavelength Upturn

In the preceding discussion it has been shown that a marked brightening below 2000 Å is a characteristic feature of the energy distribution of galaxies later than about type Sa. Even for the early types (e.g. M81) and the central bulge of M31 the energy distribution at short wavelengths tends to show this characteristic although more weakly. Although early-type stars certainly contribute at these wavelengths, the steep rise exhibited in several systems cannot be understood in terms of stellar radiation alone. It is worth emphasizing that the conclusion that the energy distribution at short wavelengths cannot be synthesized from stellar radiation is independent of the absolute calibration of the OAO photometry since the same calibration was used to determine the stellar energy distribution.

We suggest that scattering of starlight by interstellar dust is a plausible way of producing a steep turnup in this spectral region. This could explain both why the turnup is much stronger in the spiral arms of M31 than its nucleus (great amounts of dust often appear in the arms of early spirals) and also why partial removal of the spiral arm contribution at the center of M33 enhances the turnup (dust in this galaxy appears present in much greater quantity near the center).

From their investigation of the diffuse galactic background in a number of Kapteyn's selected areas, Witt and Lillie (1972) have derived a mean wavelength dependence for the scattering and absorption efficiency of the interstellar grains. Their Figure 3 illustrates how the albedo of these particles rises rapidly from around 0.2 at 2000 Å to 0.9 at 1500 Å.

A relatively high albedo shortward of 2000 Å has also been suggested from observations of reflection nebulae (Code 1971). Furthermore, several theoretical investigations of the nature of the 2200 Å peak in the interstellar extinction curve attribute this feature to an absorption process (cf. Gilra 1972). The albedo is higher both longward and shortward of this feature.

In Figure 9 we show how the energy distribution of an early B-type star model atmosphere will be modified by passing through a circumstellar cloud of such material. The radiation transfer equations were solved for a scattering and absorbing efficiency similar to that given by Witt and Lillie although the albedos were taken from earlier calculations by Gilra (1971). Where the albedo is high most of the radiation escapes, however; because of the sharp peak in absorbing efficiency of the grains at about 2200 Å, a large fraction of the input energy at this wavelength is lost, to reappear in the infrared. Below ~2000 Å both scattering and absorption efficiencies change rapidly with wavelength such that at 1500 Å much less energy is absorbed.

The way in which light emitted from a star is modified by dust depends critically upon the geometry of the situation, and it is clear that one averages the effects of many such geometries when observing an entire galaxy. Furthermore, there is evidence that even within our own galaxy the particles in different regions show different optical properties (Bless and Savage 1972). We therefore do not feel justified in attempting to match specific observations with detailed calculations.

Some additional support for this interpretation comes from examining the correlation between the ultraviolet color indices and the tilt of the galaxy's fundamental plane to the line of sight. There is a tendency for those galaxies viewed edge-on

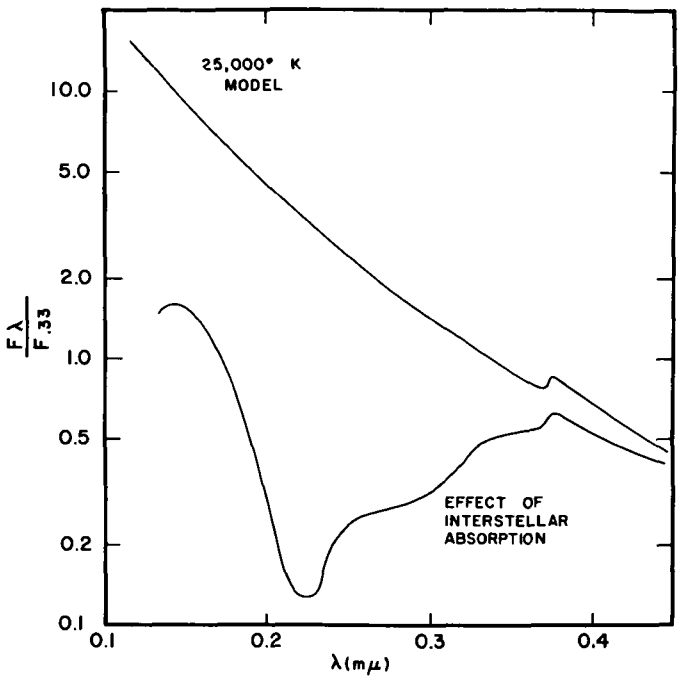

Figure 9.

to be bluer in the ultraviolet than similar type galaxies viewed face-on. This result is consistent with a relatively high albedo and fairly strong diffuse galactic light. The correlation is not a strong one due to the small amount of data available, and will require more extensive discussion in future investigations.

c) Elliptical Galaxies

Considerable effort has gone into obtaining the best possible data for early-type galaxies because of two facts. 1) They are commonly considered as being of a more homogeneous stellar content than spirals and it was hoped this would facilitate the interpretation of the ultraviolet energy distribution. 2) Knowledge of the shape of the spectrum at short wavelengths is necessary for estimation of the K-correction for very distant giant ellipticals.

Because of the small energy output of even the brightest early-type galaxies below 2000 Å we are unable to reach a definite conclusion at this time as to the shape of the spectral energy distribution at wavelengths shorter than those included by the 2460 Å filter (cf. Welch and Code 1972). Nevertheless, if we accept the 1910 Å filter data at face

value, the results obtained are often as shown in Figure 10. (An argument for the statistical reliability of the 1910 Å data has already been made from Figure 2.) The mean of two observations of M102 (NGC 5866) are plotted. At 2460 Å using the 64-sec (E4) integration time, these observations yielded means of 4 and 5 net counts out of a total of 50, while at 1910 Å the mean net counts were 2 and 0 out of a total of 31. As pointed out by Welch and Code (1972) each net E4 count is the result of a total of 384 incident events recorded by the precounter during the observation. The observation of M89 yielded means of 3 net counts out of 43 total and 2 net counts (28 total) through these respective filters. We stress that until reductions are completed, firm conclusions should not be drawn from these data.

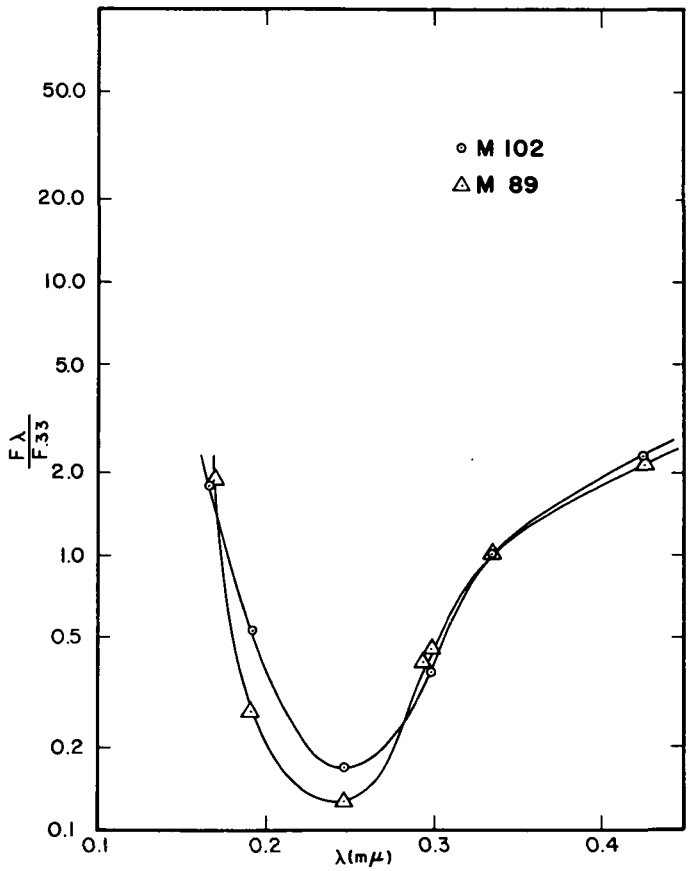

Figure 10.

The short wavelength turnups indicated by these data are very similar to those in spirals, and if real could imply the presence of significant amounts of interstellar dust in many elliptical galaxies. This would have important consequences

for our ideas of the stellar composition of these objects, because there would actually be more radiation being generated below 2000 Å than shown by the uncorrected observations. Furthermore, the K-corrections for ellipticals with $Z \gtrsim 1$ depend upon the energy distribution in this region. Although there are cases (NGC 205, NGC 1052) where hot stars and interstellar material are believed to exist, as well as evidence for interstellar gas, it remains to be seen whether an ultraviolet brightening could be accounted for in general without having significant consequences for ground-based observations.

IV. SUMMARY

Some general properties of the integrated ultraviolet energy distributions in galaxies have been discussed. The results are based on nearly complete reduction of approximately 35 galaxies of all types brighter than $m_{pg} \approx 11$.

The energy distribution of late-type spirals and probably also Magellanic irregulars appears to turn up sharply around 2000 Å. This can be interpreted qualitatively in terms of the scattering properties of interstellar dust.

Elliptical galaxies are brighter at 2460 Å than single stars of the same B-V. We cannot at this time state definitely whether or not this brightening continues or increases at shorter wavelengths although such is suggested by the data in several cases. It is hoped that careful analysis of present and future observations of early-type galaxies will resolve this very important question.

REFERENCES

Allen, C. W. 1955, Astrophysical Quantities (London: Athlone Press).

Bless, R. C. and Savage, B. D. 1972, this volume.

Code, A. D. 1968, P. A. S. P. 81, 475.

_____ 1972, this volume.

Code, A. D., Houck, T. E., McNall, J. F., Bless, R. C. and Lillie, C. F. 1970, Ap. J. 161, 377.

Gilra, D. P. 1971, Nature 229, 237.

_____ 1972, this volume.

Hills, J. G. 1971, Astron. & Astrophys. 12, 1.

Tifft, W. G. 1963, A. J. 78, 302.

Tinsley, B. M. 1972, this volume.

Vaucouleurs, G. de and Vaucouleurs, A. de 1964, Reference Catalogue of Bright Galaxies (Austin: University of Texas Press).

Welch, G. A. and Code, A. D. 1972, this volume.

Witt, A. N. and Lillie, C. F. 1972, this volume.

POSSIBILITY THAT THE FAR ULTRAVIOLET EXCESS IN M31 IS DUE TO MAIN SEQUENCE STARS

Beatrice M. Tinsley
The University of Texas
Dallas, Texas

ABSTRACT

The far ultraviolet excess in the central region of M31, observed by OAO-2, could be due to young main sequence stars. More than enough such stars are present in the model for the M31 inner disk population derived by Tinsley and Spinrad (1971) to match line- and color-indices at longer wavelengths. If the far ultraviolet radiation of typical galaxies arises from young stars, the theoretical ultraviolet background is enhanced greatly by evolutionary effects. For evolution at the rate of Tinsley and Spinrad's model for M31, or of Arnett's (1971) "linear" model for our galaxy, the enhancement is a factor 2.5 to 14, depending on the Hubble constant and the spectrum at wavelengths below 1700 Å.

I. INTRODUCTION

Hills (1971) has suggested that the far ultraviolet excess in the central region of M31, observed by OAO-2 (Code, 1969), is due to hot, highly evolved stars such as are found in globular clusters. Here, hot, young, main sequence stars are suggested as an alternative stellar source, on the basis of a model by Tinsley and Spinrad (1971) for the inner disk population of M31.

Scanner and filter studies of line strengths (Spinrad et al., 1971) indicate that the stars in M31 in the region covered by the OAO-2 "nuclear" measurement (1800 pc diameter) have predominantly Population I abundances. This fact argues in favor of the present suggestion rather than Hills'. How-

ever, since the model used here is based on detailed line strengths in a region only 200 pc south of the M31 nucleus, and since the angular resolution of the OAO-2 observations is insufficient to show if the ultraviolet excess is confined to much closer to the nucleus, the present suggestion is merely tentative.

II. THEORETICAL AND OBSERVED FLUX AT 1700 Å

The population model considered, called model D1, is an evolutionary model containing stars formed continuously at a rate depending on stellar mass according to

$$dN/dm \propto m^{-2.5} \quad . \tag{1}$$

Equation (1) holds for stars more massive than 0.14 solar masses, which are the only stars of interest here; further details are given by Tinsley and Spinrad (1971). The stellar birthrate is also proportional to the mass of gas, which changes roughly exponentially with time; over the past two billion years the function is closely represented by

$$m_g(\tau) = m_g(0)\ e^{\tau/T} \quad , \tag{2}$$

where τ = time ago, and $T = 2.28 \times 10^9$ year. This birthrate gives a synthetic galaxy at age 12×10^9 years (τ=0) which has narrow-band line indices closely matching those observed (Spinrad et al., 1971) in the inner disk of M31, and broad-band colors close to those observed (Spinrad et al., 1971; Sandage et al., 1969) from 0.36 to 3.4 micron.

The ultraviolet luminosity of the model at age 12×10^9 years, for comparison with M31, can be obtained at wavelength 1700 Å using the stellar data presented by Code (1970) and kindly made available to the author. These data show that the stellar flux at 1700 Å, corrected for interstellar extinction, is given approximately by

$$M(1700-V) = -0.82 + 11.2(B-V), \quad -0.3<B-V<+0.5 \ . \tag{3}$$

It will be assumed here that this relation holds also for redder stars; these contribute negligibly at 1700 Å so that the assumption is of no importance.

The resulting ultraviolet flux for model D1 at 12×10^9 years is related to that at the effective wavelength of the U filter band (3600 Å) by

$$F_{1700} / F_U = 0.34 \ , \quad \text{model D1,} \tag{4}$$

where the U, V magnitudes have been reduced to absolute units using the calibration given by Johnson (1966).

The observed ratio for the inner 1800 pc-diameter region of M31, obtained by interpolation between filter photometer measurements (Code, 1970), is

$$F_{1700} / F_{3600} = 0.09, \quad \text{observed M31.} \qquad (5)$$

The latter ratio can be corrected approximately for extinction in the local galaxy by adopting, for M31, E(B-V) = 0.11, E(U-V) = 0.2, and from Figure 7 of Code (1969), E(1700-V)~4.5 E(B-V). Hence,

$$(F_{1700} / F_{3600})_c \sim 0.12, \quad \text{observed M31.} \qquad (6)$$

Extinction within M31 may require further correction upwards in the observed ratio.

No attempt will be made here to follow Hills in synthesizing a detailed spectrum from below the Lyman limit to 5000 Å, because of the large and uncertain effects of interstellar extinction on the spectral shape.

III. DISCUSSION

Model D1 is about three times as bright in the far ultraviolet, relative to 3600 Å, as the observed region of M31, according to equations (4) and (6). Because of the considerable uncertainties in the interstellar extinction (local and in M31), and in the preliminary observations available here, the factor 3 discrepancy is not serious. Of chief interest is the fact that at least enough far ultraviolet light to account for the observed excess can arise from young main sequence stars, present in proportions already suggested by a study of line and color indices at longer wavelengths.

IV. IMPLICATIONS FOR THE BACKGROUND RADIATION

If the far ultraviolet excess in M31 and other galaxies arises from young stars, the theoretical ultraviolet background radiation will be increased by evolutionary effects, because of the greater number of such stars in the past. This effect will be illustrated here by finding the effect on the theoretical background intensity at 1700 Å of galactic evolution at the rate of model D1 for the M31 inner disk, and at the rate of the "linear" model of Arnett (1971) for our galaxy. The latter may be more representative of the "average" galaxy contributing to the background.

Since the stars contributing most of the far ultraviolet light have lifetimes much less than the time-scale of evolu-

tion of a galaxy, it can be assumed that the ultraviolet luminosity of a galaxy is proportional to the stellar birthrate, which in both models considered is proportional to the mass of gas. This is given by equation (2), with $T = 2.28 \times 10^9$ year for model D1, and $T = 3 \times 10^9$ year for Arnett's model.

It is a standard result that for cosmological models with zero cosmological constant (Λ), the background intensity at 1700 Å is given by

$$I_{1700} = \frac{n_o c}{4\pi H_o} \int_0^{z_{max}} \frac{L_\lambda(\lambda,\tau)\, dz}{(1+z)^4 (1+2q_o z)^{1/2}} \text{ ergs sec}^{-1}\text{cm}^{-2}\text{ster}^{-1}\text{Å}^{-1} \quad (7)$$

where z is the redshift; λ is the wavelength of emission, $\lambda = 1700$ Å$/(1+z)$; $L_\lambda(\lambda,\tau)$ is the luminosity of a galaxy at wavelength λ and past time τ, in units ergs $\text{sec}^{-1}\text{Å}^{-1}$; H_o is the Hubble constant, in sec^{-1}; n_o is the local number density of galaxies, in cm^{-3}; q_o is the cosmological deceleration parameter.

The available preliminary OAO-2 observations do not establish the spectral index below 1700 Å accurately, so two extreme alternatives will be considered here, with the true spectrum probably lying between them:

$$L_\lambda(\lambda,\tau) = L_\lambda(1700,\tau) e^{b(1700 - \lambda)/1700}, \quad 912\text{Å} \leq \lambda \leq 1700\text{Å} \quad (8)$$

where b = 3 or zero. Also it will be assumed that

$$L_\lambda(\lambda,\tau) = 0, \quad \lambda < 912 \text{ Å} . \quad (9)$$

Therefore the upper limit to the integral in (7) is $z_{max} = 1700/912 - 1 = 0.863$. Assumption (9) means that the lowest possible limit to the contribution to the background from greater redshifts is used.

The integral will depend to some extent on q_o, but not critically since z_{max} is not large. The mathematically simplest case, $q_o = 0$, will be used; this behaves very similarly to the cosmological model with Oort density ($\sigma_o = q_o = 0.015$). In this case,

$$\tau = t_o\left(1 - \frac{1}{1+z}\right), \qquad t_o = H_o^{-1}, \quad (10)$$

where t_o is the age of the universe. Introducing equations (8) to (10), with (2) for the time-dependence of $L_\lambda(\lambda,\tau)$, into (7), gives

$$I_{1700} = \frac{n_o c L_{1700}}{4\pi H_o} \int_0^{0.464 t_o} (1-\tau/t_o)^2 e^{(a+b)\tau/t_o} \, d\tau/t_o \, , \quad (11)$$

where $L_{1700} \equiv L_\lambda(1700,0)$, and $a = t_o/T$. The value of a depends on H_o and the evolutionary model, as shown in Table 1. Also tabulated are the values of $\tau(z_{max}) = 0.464\ t_o$. The values of H_o chosen for illustration are 50 km $sec^{-1}Mpc^{-1}$, as one of the lowest values commonly used, and 80 km $sec^{-1}Mpc^{-1}$, as the largest value consistent with model D1, which requires $t_o \geq 12\times10^9$ year. The factor before the integral in equation (11) is independent of H_o if the same distance scale is used in determining n_o ($\propto$ distance^{-3}) and L_{1700} ($\propto$ distance^2).

Table 1. Parameters for calculation of the background intensity

H_o (km sec^{-1} Mpc^{-1})	80	50
a in model D1	5.30	8.56
a in Arnett's model	4.1	6.5
$\tau(z_{max})$ (10^9 years)	5.6	9.1

The results of analytical integration of equation (11) are given in Table 2, for the illustrative values of b and H_o and the two evolutionary models. Evolutionary effects are found to enhance the theoretical far ultraviolet background due to stars by a factor 2.5 to 13.6. Similar values would be obtained with other values of q_o in cosmological models with $\Lambda = 0$, and the larger values in long-lived models with $\Lambda > 0$. Uncertainties in the spectrum below 1700 Å and in the Hubble constant are more important. The two evolutionary models give similar results, which lends some weight to the effects found here since the rate of evolution in Arnett's model was derived from considerations entirely independent of those used in deriving model D1. Also, the relative theoretical intensity of the background with and without evolutionary effects is not affected by the discrepancy between D1 and the observed far ultraviolet luminosity of M31, noted in §III.

Table 2. Normalized background intensity at 1700 Å, $\left(\frac{4\pi H_o}{n_o c L_{1700}}\right) I_{1700}$

Spectral parameter	b=3		b=0	
H_o (km sec^{-1} Mpc^{-1})	80	50	80	50
No evolution	0.53	0.53	0.28	0.28
Model D1	2.37	7.26	0.97	2.58
Arnett's model	1.62	3.03	0.70	1.36

If the hypothesis of this paper is correct, that the far ultraviolet excess observed in M31 and other galaxies is due to young main sequence stars, evolutionary enhancement of the theoretical ultraviolet background will place severe constraints on possible cosmological models, since Code (1970) has shown that even without such enhancement some models are ruled out by this test. These constraints will be evaluated when further observational data on the ultraviolet background intensity are available.

I am very grateful to Dr. A. D. Code for making some graphical data from OAO-2 available to me prior to its publication, after his presentation at the Texas Symposium on Relativistic Astrophysics in Austin, Texas, December 1970.

This work was partially supported by NSF Grant GP-30455X and by a Grant-in-Aid from Sigma Delta Epsilon.

REFERENCES

Arnett, W. D. 1971, Ap. J. 166, 153.
Code, A. D. 1969, P. A. S. P. 81, 475.
Code, A. D. 1970, oral presentation at the Fifth Texas Symposium on Relativistic Astrophysics, Austin, Texas.
Hills, J. A. 1971, Astron. Astrophys. 12, 1.
Johnson, H. L. 1966, A. Rev. Astr. Astrophys. 4, 193.
Sandage, A. R., Becklin, E. and Neugebauer, G. 1969, Ap. J. 157. 55.
Spinrad, H., Gunn, J. E., Taylor, B. J., McClure, R. D. and Young, J. W. 1971, Ap. J. 164, 11.
Tinsley, B. M. and Spinrad, H. 1971, Astrophys. Space Sci., in press.

Page intentionally left blank

THE EXTRAGALACTIC COMPONENT OF THE ULTRAVIOLET SKY BRIGHTNESS

Charles F. Lillie
The University of Colorado
Boulder, Colorado

ABSTRACT

The surface brightness of the night sky has been measured at 12 wavelengths in the 1250-4300 Å spectral region with the stellar photometers on OAO-2. From observations at high galactic latitudes it is possible to set upper limits on the brightness of the extragalactic sky background at several wavelengths. In the wavelength range 1420-1680 Å the extragalactic background is not greater than 1.2×10^{-8} ergs $cm^{-2}s^{-1}ster^{-1}Å^{-1}$. Observations of nearby galaxies with OAO-2 are used to predict the background due to extragalactic nebulae. It is shown that instruments which are an order of magnitude more sensitive would be required to detect the extragalactic component of the light of the night sky.

I. INTRODUCTION

In principle, measurements of the surface brightness of the extragalactic sky should provide a sensitive test for cosmological models of the universe and provide information on the density and temperature of the intergalactic gas.

In practice, however, the extragalactic light is only a minor component of the light of the night sky (LONS) when compared with the contribution of scattered light, airglow, zodiacal light, integrated starlight and diffuse galactic light (Roach and Smith 1968). Thus present observations only provide upper limits to the brightness of the "cosmic light." It is apparent that observations from above the atmosphere are necessary to reduce the contribution of the other sources of

the LONS.

Observations from vehicles in earth orbit avoid the contributions of atmospheric scattering and airglow which contribute about a third of the LONS. When it becomes possible to send vehicles beyond the orbit of Saturn, the contribution from the zodiacal light can also be avoided and the extragalactic light should become a measurable quantity.

Kurt and Sunyaev (1970) have suggested that the contribution from the zodiacal light can also be minimized by observing in the 1000-2000 Å spectral region where the solar flux is down by 2 or 3 orders of magnitude from the visible. In addition, nearly all the starlight in this spectral region is from early-type stars which are not numerous near the galactic pole and can easily be avoided with an instrument having a small field of view.

Since the stellar photometers in the Wisconsin Experiment Package on OAO-2 meet these criteria, we felt it would be useful to present the limits to the surface brightness of the extragalactic sky which can be set with this experiment. In addition, we use the results of OAO observations of nearby galaxies to predict the contribution to the LONS from extragalactic nebulae.

II. OBSERVATIONS

The instrumentation and operation of the Wisconsin Experiment Package (WEP) on OAO-2 have been discussed in detail by Code et al. (1970). Observing techniques and data analysis for sky background measurements are discussed by Lillie (1972) and Witt and Lillie (1972). Briefly, the surface brightness of the night sky can be measured with the four stellar photometers of the WEP. These photometers have 12 medium band filters covering the 1000-4000 Å spectral region. With a 10 arcminute field of view, the sky background can be detected in a 64-second integration time using the digital data output. The precision of this digital readout is one count (which represents 64 photoelectric events).

The sky background data which we present was obtained by observing regions of the sky near the galactic poles in which there were no stars brighter than 10th magnitude.

The galaxy data was obtained by the observation of bright, nearby galaxies which could be detected with WEP.

III. RESULTS

a) Upper Limits to the Extragalactic Background

In Table 1 we present the upper limits to the extragalactic sky brightness determined from OAO data compared with those

Table 1. Upper Limits to the Surface Brightness of the Extragalactic Sky.

Author	Wavelength λ	Brightness F_λ (1)	Brightness F_ν (2)
Roach and Smith (1968)	5300 Å	6.6×10^{-9}	6.2×10^{-20}
Roach (1971) (3)	5300	2.4	2.2
DeVaucouleurs (1949) (4)	4300	1.2	0.8
Lillie (1968)	4100	2.4	1.5
Hayakawa et al. (1969)	1415	17.0	1.1
Kurt and Sunyaev (1970)	1283	1.8	0.1
Kurt and Sunyaev (1970)	1115	17.0	0.7
Present Study	2460	0.74	0.15
Present Study	2030	2.2	0.30
Present Study	1910	4.9	0.60
Present Study	1550	12.0×10^{-9}	0.95×10^{-20}

(1) ergs/cm^2-sec-Å-ster
(2) ergs/cm^2-sec-ster-Hz
(3) a tentative measurement
(4) calculated from galaxy counts

from previous observations. The OAO data is for four wavelengths at which no residual signal could be found after correcting for instrumental effects (dark current, substrate scintillation) and removing the contribution from zodiacal light (Lillie 1972). It was thus assumed that no extragalactic signal greater than one count could be present. Data from the other filters is not presented because of known red leaks and uncertainties in removing the contributions of integrated starlight and zodiacal light. The absolute flux equivalence of one count was found with an interim calibration for the WEP photometers which should be accurate to ±20%.

It is important to note that two of the values in Table 1

are not upper limits. De Vaucouleurs (1949) has calculated the surface brightness of the extragalactic sky to be expected on the basis of galaxy counts and Roach (1971) has extended the analysis of his sky background data (Roach and Smith 1968) to arrive at a tentative measurement of the extragalactic light.

b) The Background from Extragalactic Nebulae

In order to predict the ultraviolet background due to extragalactic nebulae, we have constructed a composite galactic spectrum using OAO observations of nearby galaxies. The data used in this study are shown in Figure 1. The curve for an Sa galaxy is a linear extrapolation from the Sb and Sc data. A more complete description of the ultraviolet energy distribu-

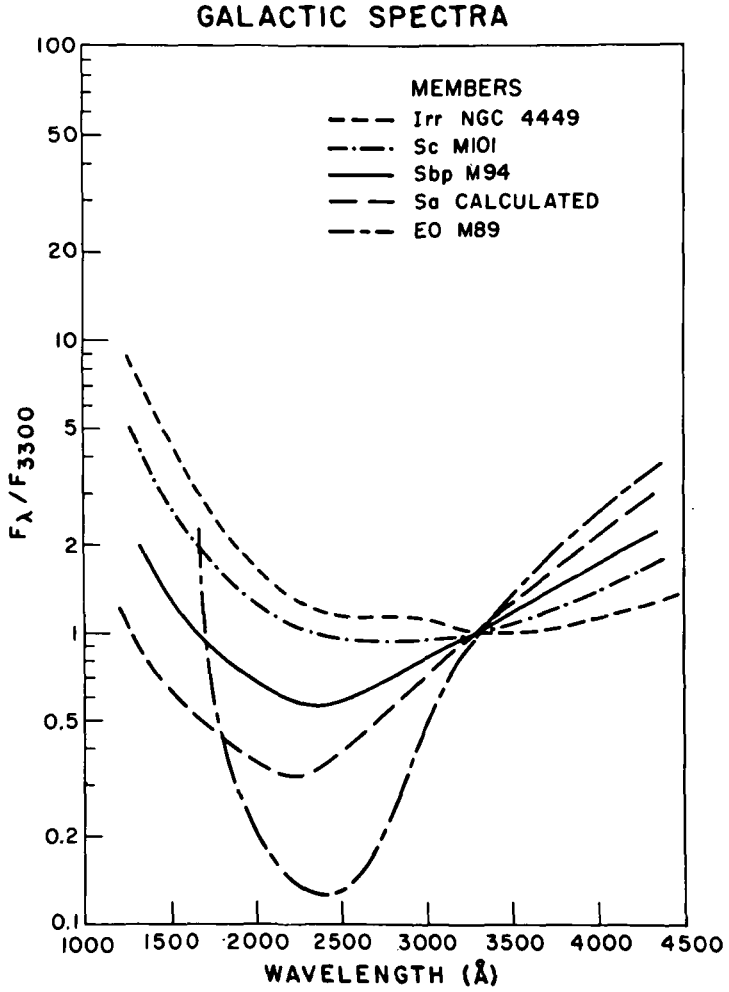

Figure 1.—Galactic spectra for a range of morphological types in the 1000-4500 Å spectral region.

tion of galaxies has been presented by Code, Welch and Page (1972). The upturn in the EO galaxy spectrum is based on a very small signal and may not be real. The other spectral features repeat well from one galaxy to another.

The calculations follow a similar computation by Kurt and Sunyaev (1967) and are summarized in Table 2.

The composite spectrum which we derive is essentially that of an Sb galaxy with an enhancement below 2000 Å due to SO and elliptical galaxies. The effects of evolution and the Hubble red shift are not considered in these calculations, so the spectrum is that of a static, Newtonian universe.

In Figure 2 we show the composite spectrum, normalized to the galaxy counts of De Vaucouleurs, along with the observed upper limits to the surface brightness of the extragalactic sky from Table 2. We show the case in which there is no upturn in the spectrum of elliptical galaxies below 2000 Å. We also show the extragalactic background predicted by Kurt and Sunyaev (1970) for the hot, diffuse, intergalactic gas which, presumably, would be present if the universe is closed by luminous matter.

The effect of the red shift on our composite spectrum can be estimated with the calculations of McVittie and Wyatt (1959). They computed the flux density for a Milne universe in which recessional (but not gravitational) effects are considered and compared with that from a Newtonian universe. The effect of recession is to enhance the infrared and deplete the ultraviolet spectral region. In Figure 2 the composite spectrum for a Milne universe normalized to 4300 Å would be a factor of 1.3 brighter than that for a Newtonian universe at 5300 Å and a factor of 3.7 fainter at 1380 Å.

IV. CONCLUSIONS

The purpose of this study was to examine the upper limits to the surface brightness of the extragalactic sky which can be set with observations from the Wisconsin Experiment on OAO-2 and to estimate the background which would be expected from extragalactic nebulae on the basis of OAO observations of nearby galaxies.

From the results, shown in Figure 2, we can draw several conclusions:

1. The instrumental sensitivity of the OAO photometers would have to be increased by about an order of magnitude in the 1000-2000 Å spectral region to detect the extragalactic component of the "light of the night sky."

2. The background due to extragalactic nebulae is of the same order of magnitude as the radiation from the intergalactic gas predicted by Kurt and Sunyaev (1967) and not, as they

Table 2. Composite Galactic Spectrum for a Newtonian Universe

Type of Galaxy	E	SO	Sa	Sb	Sc	Sd	Sm	Irr	Composite
%	22	18	12	15	19	8	3	3	100
Mpg	-14	-16	-18	-19	-17	-16	-16	-15	-19
Effective %	0.9	5.2	18.8	60	12	2.2	0.7	0.3	100

Observed Galaxy		M 89	Calc	M 94	M 101	NGC 4449	
	λ 4250	2.19	2.80	2.05	1.61	1.21	2.14
f_λ/f_{3330}	3330	1.00	1.00	1.00	1.00	1.00	1.00
	2980	0.47	0.68	0.57	0.95	1.10	0.65
	2460	0.13	0.37	0.56	0.95	1.12	0.56
	2380	0.13	0.35	0.65	0.96	1.16	0.61
	2040	0.19	0.34	0.74	1.21	1.53	0.71
	1680	1.60	0.50	0.97	1.89	2.80	1.07 (0.89)
	1500	20.3	0.64	1.30	2.62	4.30	2.57 (1.32)
	1380	200	0.86	1.71	3.95	8.80	14.16 (1.84)

Values in parentheses are for the assumption of no contribution from E-galaxies below 2000 Å.

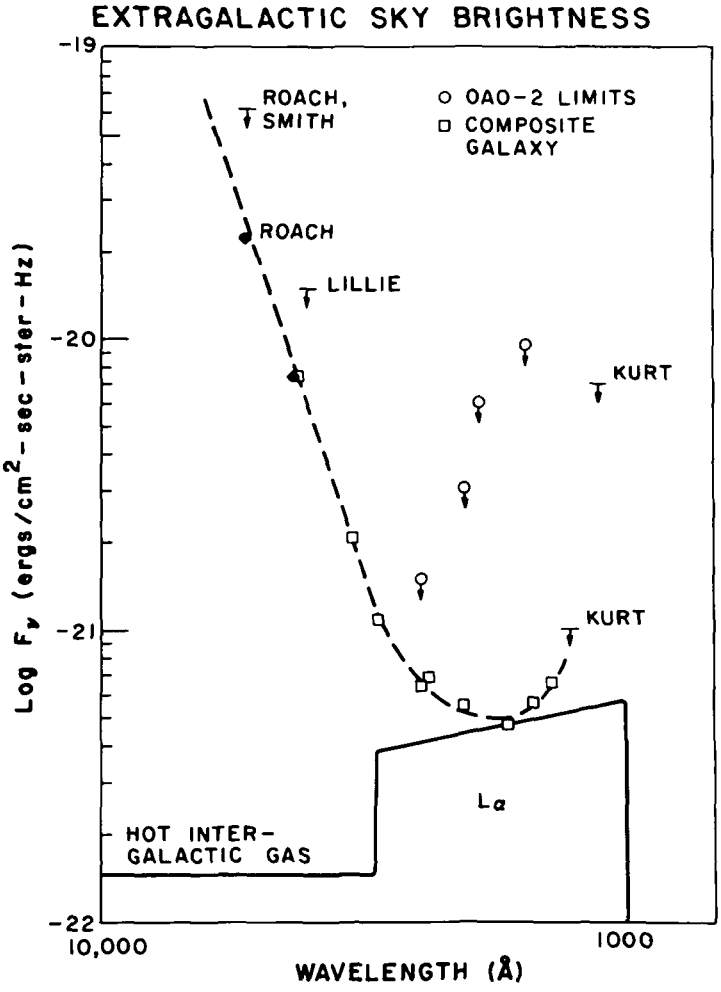

Figure 2.—Upper limits to the extragalactic sky brightness compared with the flux predicted for the hot intergalactic gas and a composite galactic spectrum for a Newtonian universe.

suggest, two orders of magnitude fainter. Thus, the detection of an intergalactic gas will be much more difficult.

3. In both the Milne and Newtonian universes the assumption of an upturn in the spectrum of elliptical galaxies below 2000 Å would lead to a surface brightness for the extragalactic sky which exceeds the upper limits of Kurt and Sunyaev.

It is possible that a rigorous analysis of the 2980 and 3300 Å data from OAO-2 will permit additional limits to the brightness of the extragalactic sky to be set. But it appears that direct measurements of the extragalactic light in the 1000-2000 Å spectral region require an instrument which can

detect a surface brightness of 10^{-22} ergs/cm^2 - sec - ster - Hz. Measurements in the visible and near ultraviolet require instruments which can be carried to the outer part of the solar system so the contribution of the zodiacal light to the LONS may be avoided.

We wish to thank Dr. A. D. Code for the opportunity to participate in the OAO program and the members of the NASA-industry-university team whose efforts led to the success of OAO-2 and provided the data for this study. Support for this research was provided by NASA grant NGR 06-003-179.

REFERENCES

Code, A. D., Houck, T. E., McNall, J. F., Bless, R. C. and Lillie, C. F. 1970, Ap. J. 161, 377.
Code, A. D., Welch, G. A. and Page, T. L. 1972, this volume.
De Vaucouleurs, G. 1949, Ann. Astrophys. 12, 162.
Hayakawa, S., Yamashita, K. and Yoshioka, S. 1969, Astrophys. Space Sci. 5, 493.
Kurt, V. G. and Sunyaev, R. A. 1967, Cosmic Research 5, 496.
_____ 1970, I.A.U. Symposium, No. 36, p. 341.
Lillie, C. F. 1968, Thesis, University of Wisconsin.
_____ 1972, this volume.
McVittie, G. C. and Wyatt, S. P. 1959, Ap. J. 130, 1.
Roach, F. E. and Smith, L. L. 1968, Geophys. J. R. Astr. Soc. 15, 227.
Roach, F. E. 1971, private communication.
Witt, A. N. and Lillie, C. F. 1972, this volume.